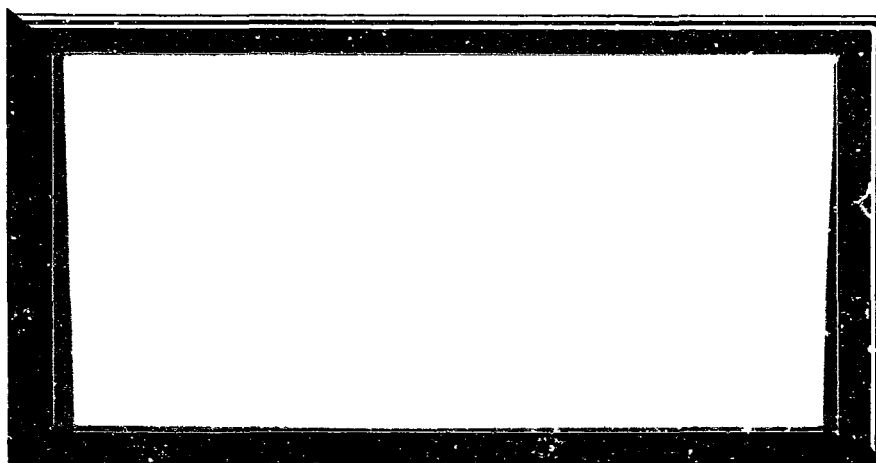


MISSILE AND SPACE DIVISION



GPO PRICE \$ _____

CFSTI PRICE(S) \$ _____

Hard copy (HC) 3.00

Microfiche (MF) .65

ff 653 July 65

N 68-24465

FACILITY FORM 602

(ACCESSION NUMBER)

220
(PAGES)

CS#94684
(NASA CR OR TMX OR AD NUMBER)

(THRU)

1
(CODE)

33
(CATEGORY)

GENERAL  ELECTRIC

FINAL REPORT
IRRADIATION OF THERMAL
CONTROL COATINGS
FEBRUARY 1967 — FEBRUARY 1968

PREPARED FOR
GODDARD SPACE FLIGHT CENTER
GREENBELT, MARYLAND
UNDER CONTRACT No. NAS-5-11001

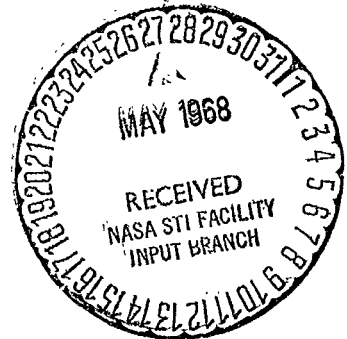
PREPARED BY


JOHN F. SCANNAPIECO, PHYSICIST
MATERIALS DEVELOPMENT AND APPLICATIONS
SYSTEMS AND TECHNOLOGIES

APPROVED BY


DR. A. T. TWEEDIE, MANAGER
MATERIALS DEVELOPMENT AND APPLICATIONS
SYSTEMS AND TECHNOLOGIES

GENERAL  ELECTRIC
MISSILE AND SPACE DIVISION
Valley Forge Space Technology Center
P. O. Box 8555 • Philadelphia, Penna. 19101



PRECEDING PAGE BLANK NOT FILMED.

TABLE OF CONTENTS

Section	Page
LIST OF ILLUSTRATIONS	v
LIST OF TABLES	vi
ABSTRACT	vii
1 INTRODUCTION	1-1
2 TECHNICAL APPROACH TO SIMULATION	2-1
3 FACILITY DESCRIPTION	3-1
4 CALIBRATION OF RADIATION SOURCES	4-1
4.1 Proton and Electron Calibration	4-1
4.2 Near Ultraviolet Calibration	4-5
5 IN-SITU REFLECTANCE MEASUREMENT TECHNIQUE	5-1
5.1 Integrating Sphere	5-1
5.2 Associated Instrumentation	5-1
5.3 Computer Program	5-3
6 EXPERIMENTAL PROGRAM	6-1
7 RESULTS AND ANALYSIS	7-1
7.1 Alzak	7-8
7.2 White Paints	7-11
7.3 Goddard White	7-13
7.4 RTV-602 White	7-13
7.5 Pyromark Standard White	7-14
7.6 Miscellaneous Spacecraft Materials	7-16
7.7 Mylar	7-17
7.8 Lexan.	7-17
8 CONCLUSIONS AND RECOMMENDATIONS	8-1
9 REFERENCES.	9-1

TABLE OF CONTENTS (Cont'd)

Appendix	Page
A FACILITY DESCRIPTION	A-1
A.1 Vacuum and Pumping System	A-1
A.2 Irradiation Sources	A-3
A.3 Turntable System	A-5
A.4 References	A-5
B IN-SITU EMISSOMETER DESIGN, CALIBRATION AND USE	B-1
B.1 Emissometer Design and Operation	B-1
B.2 Detector Element Fabrication and Installation	B-2
B.3 Reference Source Design and Positioning	B-2
B.4 Correlation Measurements as a Function of Temperature	B-6
B.5 Emittance Measurements and Analysis	B-6
C EXAMPLE OF SMOOTHING AND CORRECTION TECHNIQUE	C-1
D COMPILATION OF ALL SPECTRAL REFLECTANCE CURVES USED IN ANALYSIS	D-1
E COMPILATION OF SPECTRAL REFLECTANCE CURVES OF EACH SINGLE SCAN MEASUREMENT FROM THE 945 EUVSH DATA (IN AIR AND VACUUM)	E-1
F COMPILATION OF SPECTRAL REFLECTANCE DATA FROM THE BEKCMAN DK-IL MEASUREMENTS AND FROM THE LEEDS AND NORTHROP HOHLRAUM/13-2 PERKIN-ELMER MEASUREMENTS.	F-1

LIST OF ILLUSTRATIONS

Figure		Page
2-1	Integrated Proton Flux at Geomagnetic Equator as a Function of Energy.	2-2
3-1	Combined Effects Facility	3-1
3-2	Line Drawing of Combined Effects Facility	3-2
4-1	Faraday Cup Positioning	4-2
4-2	2.5 Kev Proton Flux Map	4-3
4-3	3 Kev Electron Flux Map	4-3
4-4	10 Kev Electron Flux Map	4-4
4-5	20 Kev Electron Flux Map	4-4
4-6(a)	Relative Spectral Irradiance	4-7
4-6(b)	Relative Spectral Irradiance	4-7
4-7	Spatial Intensity Plot at Sample Positions	4-9
5-1	Integrating Sphere, Turntable and Monochromator	5-2
5-2	Integrating Sphere and Light Pipe	5-2
5-3	Block Diagram of Digital Acquisition and Reduction System	5-4
5-4	Reflectance Curves Used to Correct for Specular Nature of Alzak	5-7
6-1	Integrated Proton Flux at the Geomagnetic Equator as a Function of Energy.	6-4
7-1	Radiation Degradation of Alzak	7-9
7-2	Radiation Degradation of Alzak	7-10
7-3	Radiation Degradation of White Paints	7-12
7-4	2.5 Kev Proton Irradiation of Pyromark Standard White	7-15
7-5	Radiation Degradation of Mylar	7-18
7-6	Radiation Degradation of Lexan (Etched)	7-19
7-7	Radiation Degradation of Lexan (Dull)	7-19
A-1	Combined Effects Facility	A-2
A-2	Irradiation Sources	A-3
A-3	Turntable Configuration, Side View	A-6
A-4	Turntable Configuration, Top View	A-6
A-5	Photograph of Turntable	A-7
B-1	Schematic of One-Detector Assembly	B-3
B-2	Assembly of Reference Source	B-4
B-3	Variation of Apparent Emissivity with Surface Emissivity at a 15 Degree Included Angle	B-5
B-4	Emissometer, Reference Source and Sample in Measurement Position	B-5
B-5	Infrared Detector Correlation	B-6

LIST OF ILLUSTRATIONS (Cont'd)

Figure		Page
C-1	Reflectance Curve of RTV-602 Run 51667-3	C-1
C-2	SCH/H-37 Before Irradiation in-Air 75 F 82267-15A	C-7

LIST OF TABLES

Table		Page
1-1	List of Samples Investigated	1-3
2-1	Electron Energy Spectrum for 450-Nautical Mile Orbit	2-2
4-1	Average Corpuscular Flux Distribution	4-5
4-2	5 kw HgXe Relative Spectral Irradiance	4-8
4-3	Comparison of Emitted Energy of 5 kw HgXe and the Sun	4-8
5-1	Corrections for Unmeasured Region of Spectrum.	5-6
5-2	Correction for Specular Nature of Alzak	5-8
6-1	Original Sample Matrix	6-2
6-2	Final Sample Matrix	6-3
6-3	Sequence of Reflectance Measurements	6-5
6-4	Coating Composition and Application.	6-6
6-5	Specimens Measured with Conventional In-Air Optical Instruments.	6-7
7-1	Comparison of Smoothed and Unsmoothed Solar Absorptance.	7-2
7-2	Comparison of Smoothed and Unsmoothed Solar Absorptance.	7-3
7-3	Summary of Smooth and Corrected Solar Absorptance	7-4
7-4	Summary of Smoothed and Corrected Solar Absorptance	7-5
7-5	Comparison of Solar Absorptance Values	7-6
7-6	Single Scan Versus Average of Three Scans (In Vacuum)	7-7
7-7	Single Scan Versus Average of Three Scans (In Air)	7-7
7-8	Radiation Degradation of White Paints	7-11

ABSTRACT

This study investigated the effects of those constituents of the space environment which are most damaging to thermal control coatings and which would be experienced by OAO in about one-half year in space. The coatings investigated were primarily Alzak and white paint. The white paints studied were Pyromark Standard White, Goddard 78-2B White, and Grumman RTV 602 White. Other surfaces studied were Lexan, Mylar, solar cells, and microsheet.

The spectral reflectance of these materials was measured while in the vacuum system after exposure to various combinations of ultraviolet radiation, 2.5 keV protons and 3 keV electrons. Measurements were also performed before and after irradiation in air. Most measurements and irradiations were performed at -55°C and $2 \cdot 10^{-7}$ torr. The ultimate radiation exposure of any sample was 945-equivalent ultraviolet sun hours, $5.6 \cdot 10^{14}$ protons cm^{-2} , and $5.8 \cdot 10^{13}$ electrons cm^{-2} . The ultraviolet irradiation was performed at an intensity of nominally 1-equivalent ultraviolet sun hour while the nominal corpuscular fluencies were $8 \cdot 10^{12}$ protons $\text{cm}^{-2} \text{sec}^{-1}$ and $6 \cdot 10^{12}$ electrons $\text{cm}^{-2} \text{sec}^{-1}$.

At the maximum radiation exposure the solar absorptance of Alzak increased by 0.04, while Pyromark Standard White showed an increase of 0.08, as compared to a 0.02 increase in solar absorptance for the other two white paints studied. The solar absorptance of Lexan and Mylar each degraded by at least 0.24. No change could be noted in the reflectance of either the microsheet or the solar cells.

ACKNOWLEDGEMENTS

The author wishes to express his gratitude and appreciation to the following people who have made a significant contribution to the effort described in this report: D. Perry, C. Quaintance, and B. Leach, who performed the radiation exposures and the optical property measurements; S. Babjak for his assistance in making the optical measurement technique operational; and L. Amore for preparing and mounting the thin-film infrared detectors used in the emissometer described in Appendix B.

SECTION 1

INTRODUCTION

The ability of a space vehicle to meet its design goal is inseparably linked with maintaining the temperature of its contents within the relatively narrow design limits where they operate at maximum efficiency. The controlling factor which determines the temperature of the vehicle is the ability of its external surface to exchange energy with its environment. This is determined by the solar absorptance (α_s) and the emittance (ϵ_H) of its external surface. Experimental work to date has shown that it is primarily the solar absorptance, not the emittance, which changes upon radiation.

It has been realized for some time that the space environment degrades most thermal control materials; however, only recently has the magnitude of the difference between space flight and ground based simulation been fully realized. It has recently been shown by a number of independent investigators that "healing" (a regression towards the original state) occurs upon removal of the specimens from vacuum to air. "Healing" caused by annihilation of defects through photolysis and annealing have been known and postulated for some time. "Healing" which occurs upon removal of the specimens from vacuum is generally believed dependent upon the presence of oxygen. Because of this, only simulation utilizing in situ reflectance apparatus should be used, unless it has been clearly shown that the material to be tested does not "heal" upon exposure to air after irradiation.

In order to perform the best simulation possible, synergistic effects should also be considered (i. e., all the parameters of the space environment should be simulated simultaneously). Until recently the majority of space simulation studies performed on thermal control materials consisted of exposing samples to each type of radiation separately and summing the results to predict the combined effects, thereby neglecting synergistic effects. (A synergistic effect is one where the change caused by the sum of each constituent of the space environment acting separately is not the same as the change caused by all of the constituents acting simultaneously.) It should also be noted that the majority of earlier studies computed the change in solar absorptance based on reflectance measurements made in air before and after irradiation, rather than from in situ measurements.

Most of the flight data available on the final control coatings is either on materials other than those of interest here or from vehicles which encountered a drastically different radiation environment (e. g., in 1 hour ATS-B received a greater proton dose than OAO will receive in 1 year).

The primary purpose of this study was to determine the degradation rate expected for coatings contemplated for use on OAO. A list of the materials studied is given in Table 1-1. Also included were backup materials for the white paint and a few miscellaneous materials used, or contemplated for use, in various spacecraft applications. The main coatings of interest were Alzak and Pyromark Standard White. The two white coatings considered as a backup were Goddard White and RTV-602 White (Grumman). All specimens were studied at $-55 \pm 5^{\circ}\text{F}$. Two different thicknesses of the Alzak coatings were studied.

The tests included 945 EUVSH (equivalent ultraviolet sun hours) of near ultraviolet irradiation, performed at an intensity of 1 EUVS (equivalent ultraviolet sun), $5 \cdot 10^{14}$ protons cm^{-2} of 2.5 kev, and $5 \cdot 10^{13}$ electrons cm^{-2} of 3 kev. The nominal dose rates were $8 \cdot 10^{12}$ protons $\text{cm}^{-2} \text{sec}^{-1}$ and $6 \cdot 10^{12}$ electrons $\text{cm}^{-2} \text{sec}^{-1}$. It is believed that the irradiation performed was equivalent to 1 year of electrons, more than 1 year of protons, and 2 to 3 months of near ultraviolet.

Table 1-1. List of Samples Investigated

Material Class	Material Investigated	Number of Samples	Comments
Inorganic	Alzak	13	Manufactured by Alcoa. Nominal thickness of nine samples was 0.175 mils and 0.10 mils on the remaining four samples
White Paints	Pyromark Standard White	3	Manufactured by Tempil Corporation.
	RTV 602 White	3	Grumman formulation
	Goddard 78-2B White	4	Formulated by Dr. J. B. Schutt
Miscellaneous Spacecraft Materials	Lexan (dull)	1	Over polished aluminum
	Lexan (etched)	1	Over polished aluminum
	Mylar	2	Over crinkled aluminized Mylar
	Solar Cells	2	One N/P and one P/N measured as a combination*.
	Microsheet	1	Odd sample geometry (not circular)*.

* Part of the specimen holder (copper) was included in the reflectance measurements made on these samples. This occurred on the solar cells because of the gap where the two cells met, and on the microsheet because the sample geometry could not fill the entire reflectance beam. Because of this, only relative values will be meaningful on these samples.

SECTION 2

TECHNICAL APPROACH TO SIMULATION

The primary constituents of the space environment are (1) ultra high vacuum, (2) near and far ultraviolet radiation, (3) energetic charged particles (primarily electrons and protons), and (4) micrometeoroids. Since all of these constituents are present simultaneously in the space environment, one might deduce that a realistic test should simulate all of them simultaneously. This is partially correct, since synergistic effects have been noted by a number of investigators; however, concern should be confined to synergistic effects from those constituents of the space environment which may affect the critical optical properties (α_s and ϵ_H) of the thermal control coatings used on the external surface of the space vehicle.

Those constituents of the space environment which are most efficient in producing changes in the critical optical properties of thermal control coatings can be qualitatively deduced, if we consider that, in general, it is primarily the outermost layer of the coatings which determines their α_s and ϵ_H . Since a surface phenomenon is being studied, the ultra high vacuum, which determines both the composition and number of particles striking the surface, is important. Similarly, the radiation, which yields the most near-surface interactions (and, therefore, deposited energy), will be more important than the penetrating radiation. The ultraviolet region (below 0.4μ) is both the most damaging and the least penetrating of the solar electromagnetic radiation. The energy deposition per unit path length will increase as the energy of the incident particles decreases. Also, the energy deposition per unit path length is greater for protons than for electrons of equal energy. By considering these facts, together with the energy distribution of charged particles in space, (References 1, 2, and 3), Figure 2-1, and Table 2-1, it is concluded that the low energy protons and low energy electrons are most important (in that order), the heavy ions being neglected because of their extremely low flux. The flux of micrometeoroids is apparently so small that even though they can degrade thermal control coatings, their overall effect can be neglected for most missions.

The intensity of the near ultraviolet irradiation should be kept to approximately 1 equivalent ultraviolet sun, unless reciprocity relationships are available for the coatings to be studied.

A mercury-xenon lamp is used as the ultraviolet radiation source, since it combines a rich ultraviolet spectrum, stability, and reliability with relatively little line spectrum.

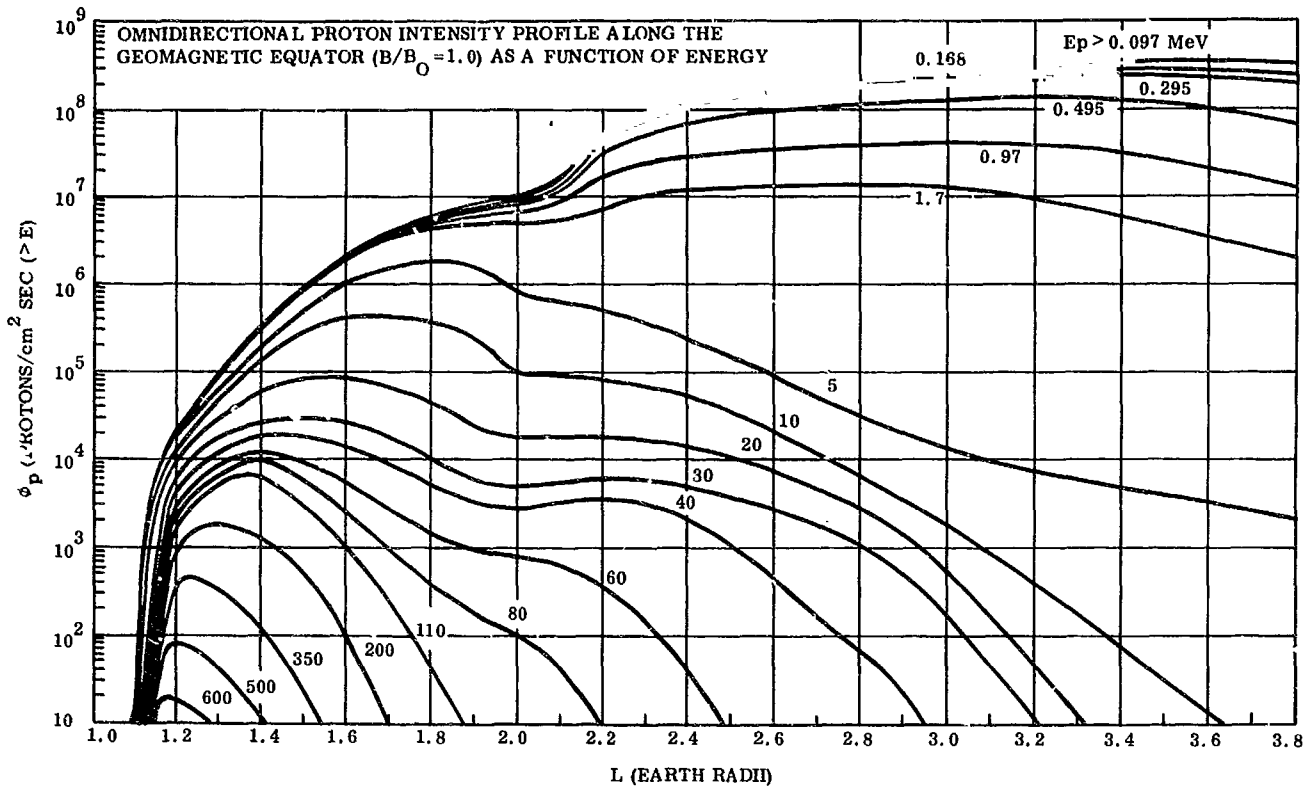


Figure 2-1. Integrated Proton Flux at Geomagnetic Equator as a Function of Energy

Table 2-1. Electron Energy Spectrum for 450-Nautical Mile Orbit (References 1 and 2)

ORBITAL INTEGRATION FOR PROJECTED 1968 ELECTRON ENVIRONMENT									
ORBIT ALTITUDE.. 450 N MI				TOTAL TIME.. 24.HOURS				TIME INTERVAL.. 1.MINUTES	
ENERGY MEV		ORBITAL FLUX 0 DEG		ORBITAL FLUX 30 DEG		ORBITAL FLUX 60 DEG		ORBITAL FLUX 90 DEG	
E1	E2	*E1	E1-E2	*E1	E1-E2	*E1	E1-E2	*E1	E1-E2
0.	0.25	9.17E 09	7.02E 09	4.71E 11	3.94E 11	3.23E 11	2.62E 11	2.65E 11	2.13E 11
0.25	0.50	2.15E 09	1.65E 09	7.72E 10	6.42E 10	6.09E 10	4.60E 10	5.15E 10	3.84E 10
0.50	0.75	4.91E 08	3.79E 08	1.30E 10	1.07E 10	1.49E 10	9.43E 09	1.31E 10	8.13E 09
0.75	1.00	1.13E 08	8.64E 07	2.27E 09	1.85E 09	5.49E 09	2.90E 09	4.98E 09	2.60E 09
1.00	1.25	2.61E 07	2.02E 07	4.13E 08	3.00E 08	2.59E 09	1.20E 09	2.38E 09	1.10E 09
1.25	1.50	5.91E 06	3.86E 06	1.13E 08	3.76E 07	1.39E 09	5.98E 08	1.28E 09	5.52E 08
1.50	1.75	2.05E 06	4.85E 05	7.53E 07	6.55E 06	7.92E 08	3.27E 08	7.25E 08	3.01E 08
1.75	2.00	1.56E 06	3.62E 05	6.87E 07	5.48E 06	4.65E 08	1.84E 08	4.24E 08	1.69E 08
2.00	2.25	1.20E 06	2.59E 05	6.33E 07	4.65E 06	2.81E 08	1.05E 08	2.54E 08	9.65E 07
2.25	2.50	9.41E 05	1.93E 05	5.86E 07	4.05E 06	1.76E 08	6.14E 07	1.58E 08	5.63E 07
2.50	2.75	7.48E 05	1.46E 05	5.46E 07	3.72E 06	1.14E 08	3.60E 07	1.01E 08	3.30E 07
2.75	3.00	6.02E 05	1.15E 05	5.02E 07	3.35E 06	7.85E 07	2.18E 07	6.84E 07	1.99E 07
3.00	3.25	4.87E 05	8.72E 04	4.75E 07	3.05E 06	5.67E 07	1.34E 07	4.86E 07	1.21E 07
3.25	3.50	4.00E 05	7.03E 04	4.44E 07	2.80E 06	4.33E 07	8.45E 06	3.64E 07	7.58E 06
3.50	3.75	3.29E 05	5.56E 04	4.17E 07	2.56E 06	3.48E 07	5.54E 06	2.88E 07	4.91E 06
3.75	4.00	2.74E 05	4.36E 04	3.91E 07	2.36E 06	2.93E 07	3.78E 06	2.39E 07	3.30E 06
4.00	4.25	2.30E 05	3.66E 04	3.67E 07	2.17E 06	2.55E 07	2.71E 06	2.06E 07	2.32E 06
4.25	4.50	1.94E 05	2.96E 04	3.46E 07	2.05E 06	2.28E 07	2.05E 06	1.83E 07	1.72E 06
4.50	4.75	1.64E 05	2.46E 04	3.25E 07	1.88E 06	2.08E 07	1.60E 06	1.66E 07	1.32E 06
4.75	5.00	1.39E 05	2.04E 04	3.06E 07	1.72E 06	1.92E 07	1.31E 06	1.53E 07	1.07E 06
5.00	5.25	1.19E 05	1.70E 04	2.89E 07	1.63E 06	1.78E 07	1.13E 06	1.42E 07	9.08E 05
5.25	5.50	1.02E 05	1.43E 04	2.73E 07	1.53E 06	1.67E 07	1.00E 06	1.33E 07	7.99E 05
5.50	5.75	8.76E 04	1.23E 04	2.57E 07	1.39E 06	1.57E 07	8.71E 05	1.25E 07	6.89E 05
5.75	6.00	7.54E 04	1.04E 04	2.44E 07	1.38E 06	1.48E 07	8.46E 05	1.18E 07	6.67E 05
6.00	6.25	6.49E 04	8.82E 03	2.30E 07	1.21E 06	1.40E 07	7.27E 05	1.11E 07	5.72E 05
6.25	6.50	5.61E 04	7.69E 03	2.18E 07	1.16E 06	1.33E 07	6.93E 05	1.05E 07	5.43E 05
6.50	6.75	4.84E 04	6.44E 03	2.06E 07	1.13E 06	1.26E 07	6.69E 05	1.00E 07	5.23E 05
6.75	7.00	4.20E 04	5.60E 03	1.95E 07	9.94E 05	1.19E 07	5.91E 05	9.48E 06	4.64E 05
7.00		3.64E 04	3.64E 04	1.85E 07	1.85E 07	1.13E 07	1.13E 07	9.02E 06	9.02E 06

SECTION 3 FACILITY DESCRIPTION

The Combined Effects Facility (Figure 3-1), utilized for this study, consisted of an ultrahigh vacuum system, radiation sources for simulation of near ultraviolet radiation and low energy electrons and protons, and in situ optical properties measurement apparatus.

The vacuum system is constructed of 304 stainless steel with a cylindrical liquid nitrogen-cooled shield running the entire length (Figure 3-2). All materials used in the system are capable of 350° F operation without risk of outgassed products from them affecting the samples. The chamber is cryo sorption roughed with sputter ion/titanium sublimation pumping used to obtain ultrahigh vacuum.

The near ultraviolet radiation source is a 5.0 kilowatt mercury-xenon arc lamp. The 2.5 keV protons are produced by accelerating ions from an RF ionized hydrogen plasma. The 3 keV electrons are obtained from a 20 keV electron gun with focus and deflection capability. A



Figure 3-1. Combined Effects Facility

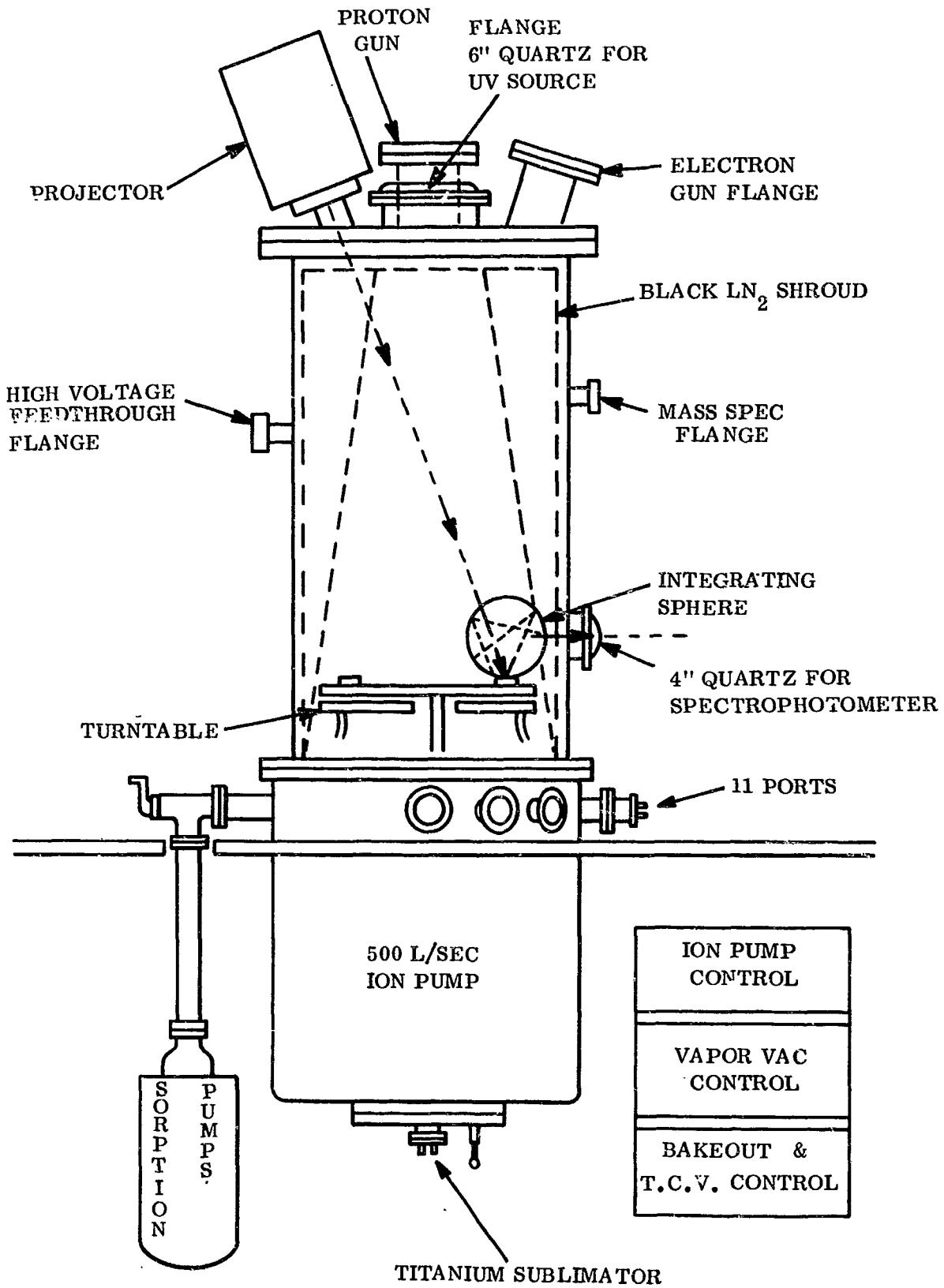


Figure 3-2. Line Drawing of Combined Effects Facility

more detailed description of the vacuum chamber, radiation sources and turntable specimen holder is given in Appendix A.

The in situ optical properties measurements consisted of both spectral reflectance and total normal emittance. The in situ spectral reflectance measurements are performed with a magnesium oxide coated integrated sphere used in the inverted mode. The measurement region (from 0.356 to 2.065 microns) is divided into 54 increments for computation purposes. The monochromator output is electronically integrated and converted to a digital printout which is computer processed for calculation of solar absorptance and plotting of the spectral reflectance. The reflectance measurements are described in greater detail in Section 5. The total normal emittance measurements were attempted in situ with a thin film infrared detector. These measurements were discontinued after the initial measurements because of apparent instability problems. The details of the design and calibration, in addition to the initial measurements performed with this apparatus, are given in Appendix B.

SECTION 4
CALIBRATION OF RADIATION SOURCES

The spatial distribution of the proton and electron flux was measured with a Faraday cup in vacuum. The spatial flux distribution was measured for 2.5 kev protons and for 3, 10, and 20 kev electrons. The energy of the particles was taken as a meter reading of the accelerating voltage. The spatial intensity and spectral distribution of the near ultraviolet radiation was measured in air with a water cooled thermopile.

4.1 PROTON AND ELECTRON CALIBRATION

The proton and electron beams were calibrated separately, using a 1.95 centimeter diameter (3 cm² area) Faraday cup mounted on the turntable as shown in Figure 4-1. The current from the Faraday cup was read with a Kintel 203A Microvolt-ammeter. The formula used to convert the current readings to flux is:

$$\Phi = \frac{i \cos 22 \frac{1}{2}^{\circ}}{q A} \quad (4-1)$$

where

i is the meter reading in amperes (coulombs/second)

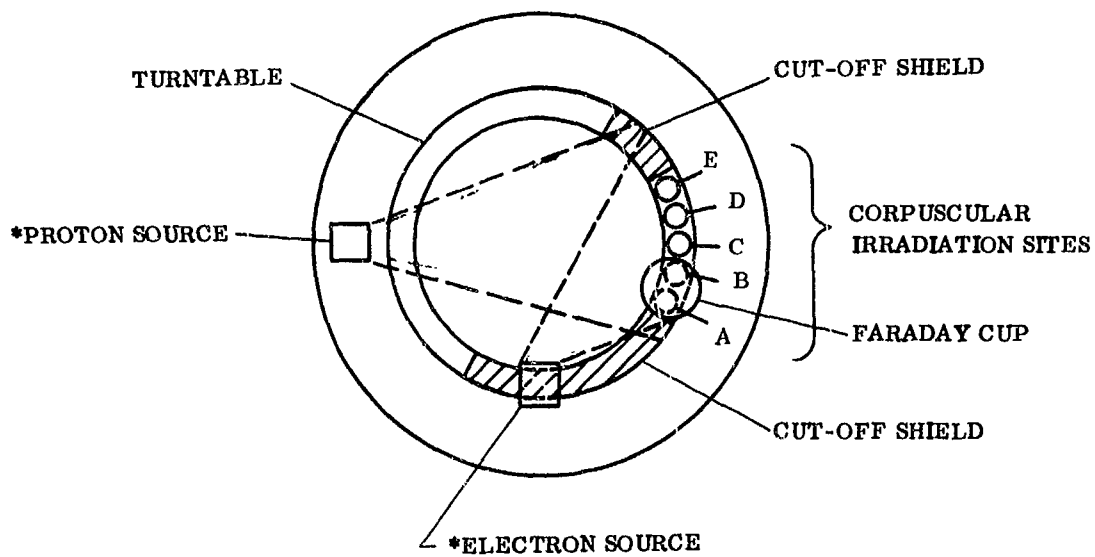
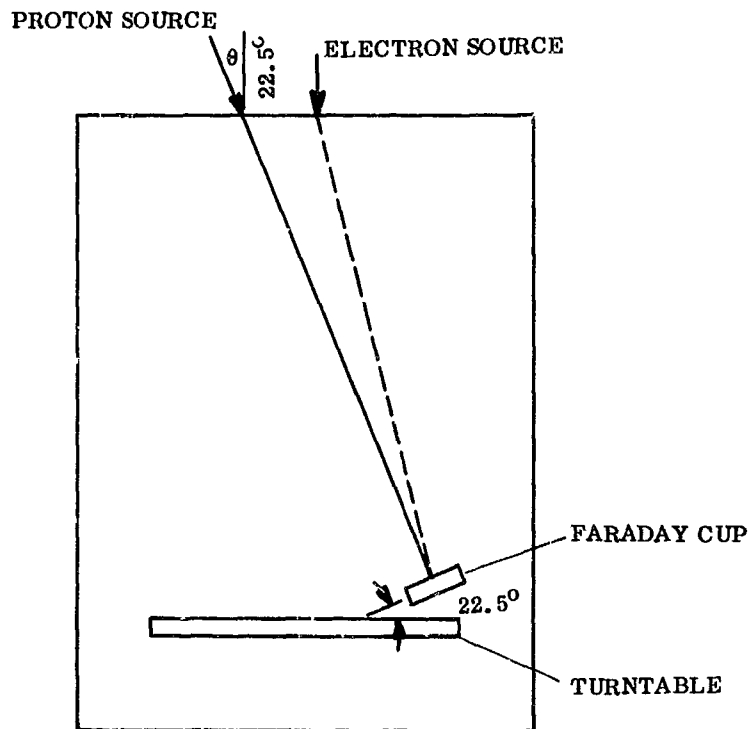
q is the fundamental unit of charge ($1.6 \cdot 10^{-19}$ coulombs per particle)

A is the area of the Faraday cup (3 cm²), and

cos 22 1/2 degrees is used to correct for the angle between the Faraday cup and the sample plane. For this configuration the above formula reduces to:

$$\Phi = 1.92 \cdot 10^{18} i \text{ particles cm}^{-2} \text{ sec}^{-1} \quad (4-2)$$

The proton and electron plots, shown in Figure 4-2 through 4-5 inclusive, were obtained by measurements performed at every 8 degrees around the turntable. The value computed as described above was plotted as that of the bisector of the Faraday cup. The average flux at



*INCLINED $22\ 1/2^\circ$ FROM THE NORMAL TO THE TURNTABLE

Figure 4-1. Faraday Cup Positioning

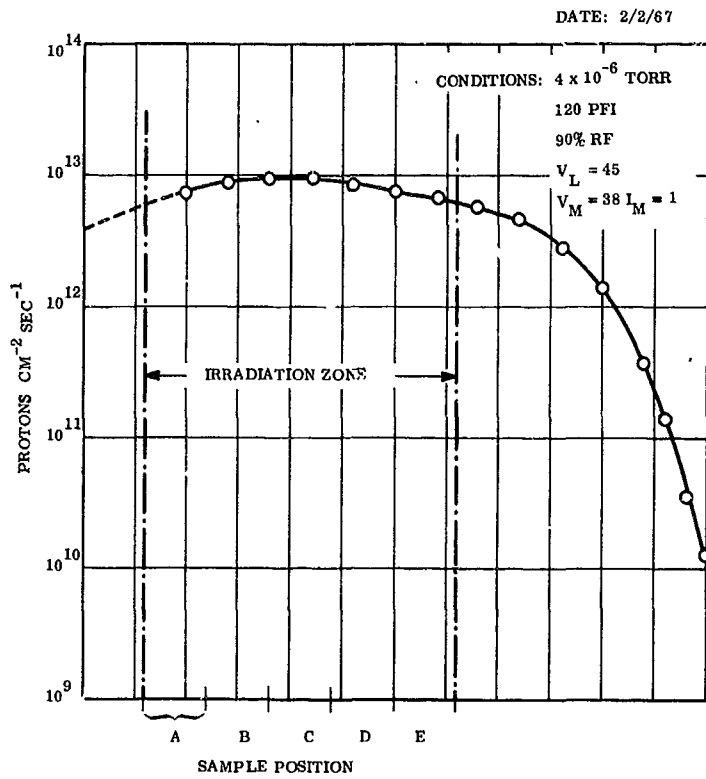


Figure 4-2. 2.5 Kev Proton Flux Map

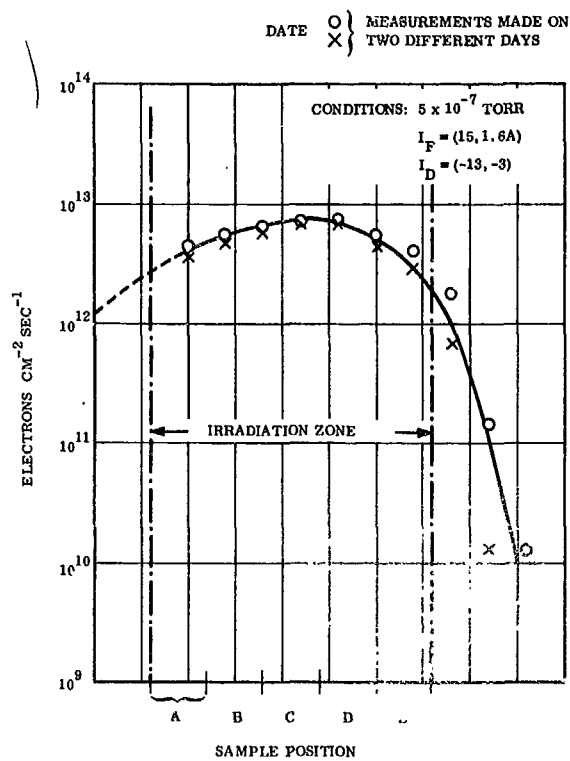


Figure 4-3. 3 Kev Electron Flux Map

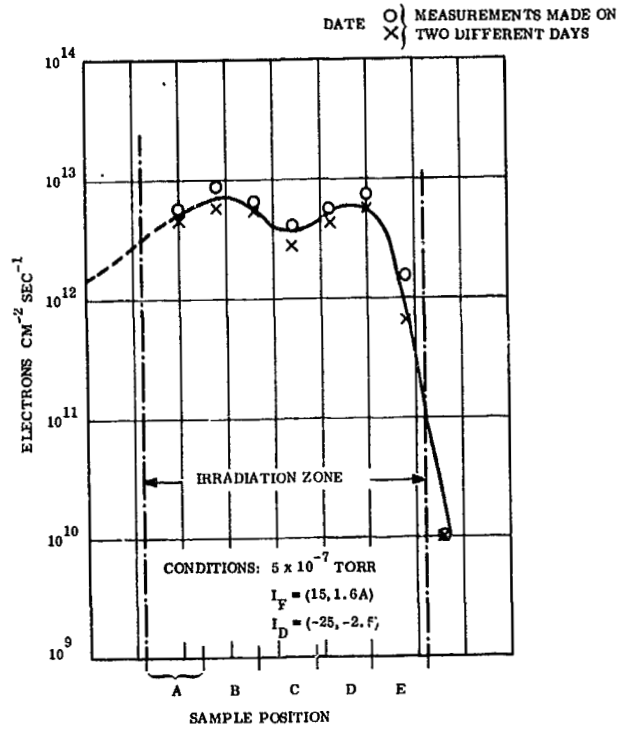


Figure 4-4. 10 Kev Electron Flux Map

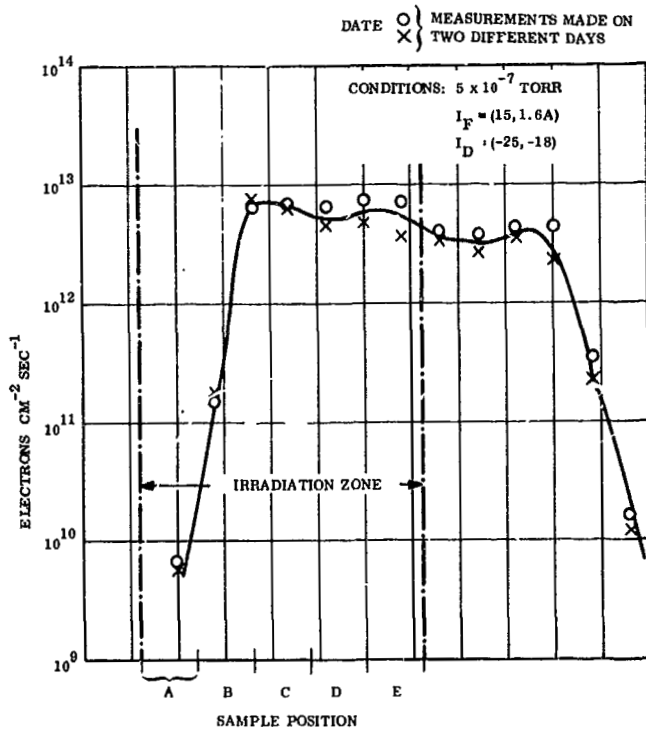


Figure 4-5. 20 Kev Electron Flux Map

each of the five sample sites used for corpuscular irradiation (Figure 4-1) are given in Table 4-1. These values were obtained by averaging the flux over each sample region shown in Figures 4-2 through 4-5. The electron flux plots are the average of two measurements (both sets of points plotted) made on two different days.

Table 4-1. Average Corpuscular Flux Distribution

Corpuscular Radiation Position	Average Flux (Particles cm ⁻² sec ⁻¹)			
	Protons	Electrons		
	2.5 kev	3 kev	10 kev	20 kev
A	$7 \cdot 10^{12}$	$4 \cdot 10^{12}$	$5 \cdot 10^{12}$	$< 10^{10}$
B	$9 \cdot 10^{12}$	$6 \cdot 10^{12}$	$6 \cdot 10^{12}$	$3 \cdot 10^{12}$
C	$9 \cdot 10^{12}$	$7 \cdot 10^{12}$	$4 \cdot 10^{12}$	$6 \cdot 10^{12}$
D	$8 \cdot 10^{12}$	$7 \cdot 10^{12}$	$5 \cdot 10^{12}$	$5 \cdot 10^{12}$
E	$7 \cdot 10^{12}$	$4 \cdot 10^{12}$	$3 \cdot 10^{12}$	$5 \cdot 10^{12}$

The reason measurements were made on two different days was to determine the variation which may be expected due to resetting of the focus and deflection controls. The proton flux map is an average of three measurements made in the same day. The reason it was unnecessary to make these readings on different days is that variation in the proton flux caused by all influencing sources (other than the accelerating voltage) is less than that exhibited in the electron plots for the two sets of measurements.

4.2 NEAR ULTRAVIOLET CALIBRATION

The near ultraviolet spatial intensity was performed with a high intensity eight-junction bismuth-silver thermopile mounted in a water jacketed case. This thermopile has a 60-degree (whole angle) field of view. The spectral calibration of the source was made with the aforementioned thermopile and a set of Eppley band pass filters.

The 5 kw mercury-xenon lamp was fired and allowed to stabilize before all measurements. All measurements were performed at the sample plane with the chamber at atmospheric pressure. The thermopile and filters were shielded whenever measurements were not being made. A Kintel 203A Microvolt-ammeter was used to measure thermopile output.

A continuous plot of the relative spectral distribution of the lamp is given in Figures 4-6a and 4-6b (Reference 4) together with the relative energy of the lamp as measured with the band pass filters. The relative energy of the lamp at the sample plane was computed from the thermopile output with each filter as shown in Equation 4-3.

$$E_R (i) = \frac{V (i)}{k T (i)} \quad (4-3)$$

where

- $E_R (i)$ is the relative energy of the lamp in the wavelength region transmitted by filter i .
- $V (i)$ is the output of the thermopile with filter i in place.
- $T (i)$ is average percent transmittance of the band pass filters over the wavelength region in which they transmit as determined by in-house calibration.
- k is the sensitivity of the thermopile as calibrated by Eppley Laboratories.

Figure 4-6 also shows the relative energy from the lamp (Reference 4) and the sun at zero air mass (Reference 5) integrated over the same regions as the filters transmit. Since the relative spectral irradiance of the lamp at the sample plane is within a few percent of that as reported in Reference 4 for the visible and ultraviolet regions (Table 4-2), the same distribution as reported in Reference 4 (Table 4-3) is used for the energy distribution at the sample plane. As can be readily seen from Table 4-3, the specimens were exposed to about one-half the normal visible and 40 percent of the normal infrared energy for the one EUVs intensity to which they were exposed.

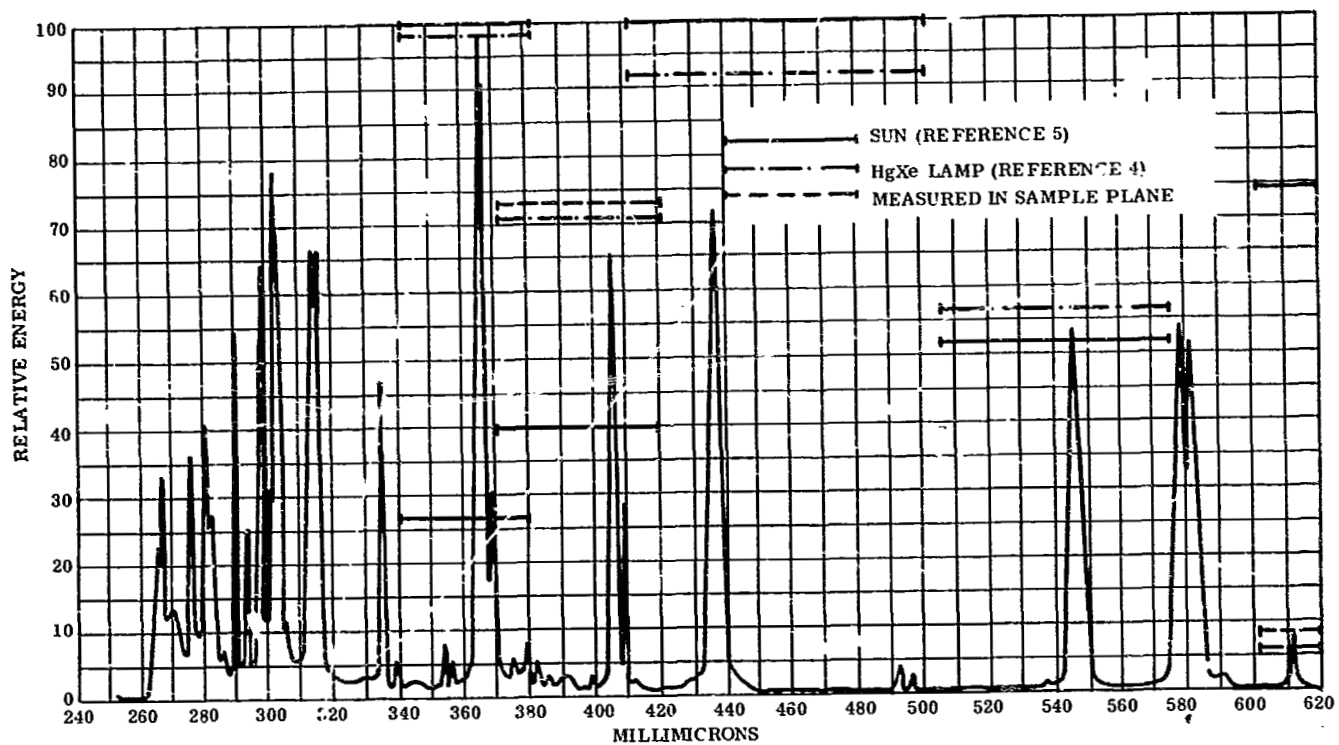


Figure 4-6a. Relative Spectral Irradiance

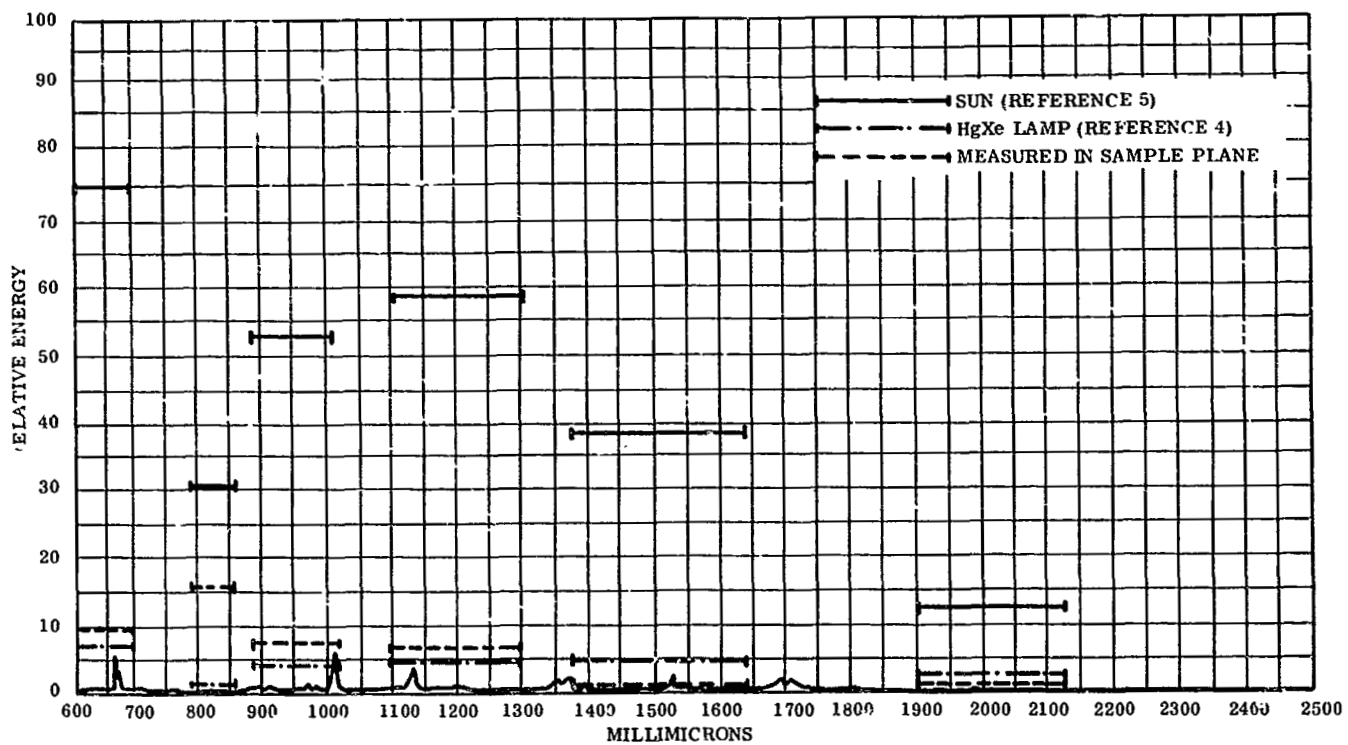


Figure 4-6b. Relative Spectral Irradiance

Table 4-2. 5 kw HgXe Relative Spectral Irradiance

Wavelength Bandpass (mμ)	Relative Spectral Irradiance	
	As Measured in Sample Plane	As Reported in Reference 4
340 - 380	100	100
370 - 420	73.8	71
605 - 690	10.6	7.9
790 - 850	18	1.2
895 - 1020	6.9	4.5
1090 - 1300	6.9	5.7
1375 - 1640	0.29	6.0
1900 - 2125	0.34	2.4

Table 4-3. Comparison of Emitted Energy of 5 kw HgXe and the Sun

Wavelength Region	Percent of Energy	
	HgXe Lamp (Reference 4)	Sun (Reference 5)
Ultraviolet (less than 400 mμ)	19	9
Visible (between 400 and 700 mμ)	41	40
Infrared (above 700 mμ)	40	51

The spatial intensity was obtained by measuring the output from the unfiltered thermopile at various positions on the turntable. This was performed after the lamp was stabilized to an intensity of one EUVS at sample position 11, as determined by Equation 4-4:

$$I(\text{UV}) = \frac{E_L(\text{UV}) V}{k E_S(\text{UV})} \quad (4-4)$$

where

$I(\text{UV})$ is the EUVS intensity

V and k are the same as in equation (4-3), and

$E_S(\text{UV})$ and $E_L(\text{UV})$ are the fraction of energy below 400 millimicrons emitted by the sun and L the lamp respectively. (See Table 4-3.)

The spatial distribution obtained from these measurements is given in Figure 4-7.

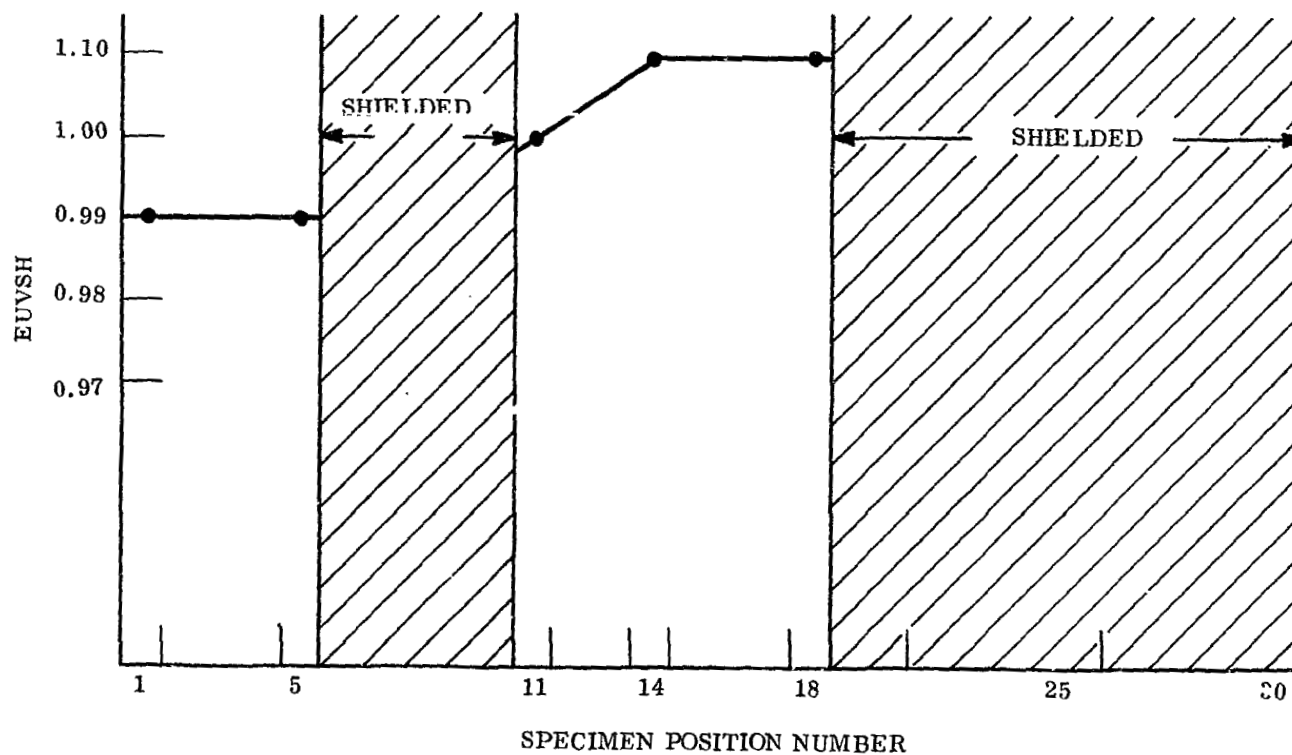


Figure 4-7. Spatial Intensity Plot at Sample Positions

SECTION 5

IN SITU REFLECTANCE MEASUREMENT TECHNIQUE

The reflectance measurement technique will be described in three parts: the integrating sphere, the associated instrumentation, and the computer program for computation and plotting.

5.1 INTEGRATING SPHERE

The integrating sphere has an inside diameter of about 5-1/2 inches, and is coated with magnesium oxide. It is positioned over the turntable so that any sample can be rotated under it for reflectance measurements (Figure 5-1). The integrating sphere is used in the inverted manner ("white" light is put in and the reflected light is put through the monochromator) so that all relatively unstable and unreliable components associated with the reflectance measurements are kept outside the vacuum system. The input source for the reflectance measurements is a 3200^oK tungsten lamp projected through a quartz window. The output from the integrating sphere is channeled through a quartz light pipe and out another quartz window into collecting optics for the monochromator) (Figure 5-2). Twelve specimens are shielded from radiation when the integrating sphere and emissometer (described in Appendix B) are in position over the turntable. The remaining eighteen positions can be irradiated simultaneously or shielded as desired. Samples in the shielded zones can be used as controls, as standards, or rotated into the irradiation zone later in the experiment. The magnesium oxide reference specimen used in these measurements is stored in this zone during irradiations.

5.2. ASSOCIATED INSTRUMENTATION

The associated instrumentation includes a monochromator and a digital data acquisition system. The Perkin-Elmer Model 99 monochromator is used with a photomultiplier tube as a detector in the near ultraviolet and part of the visible spectrum, and with a lead sulfide detector in the remainder of the visible and the near infrared. The output from the monochromator detector is put into the input scanner of the digital acquisition system. The digital acquisition system electronically integrates the monochromator detector output over prespecified

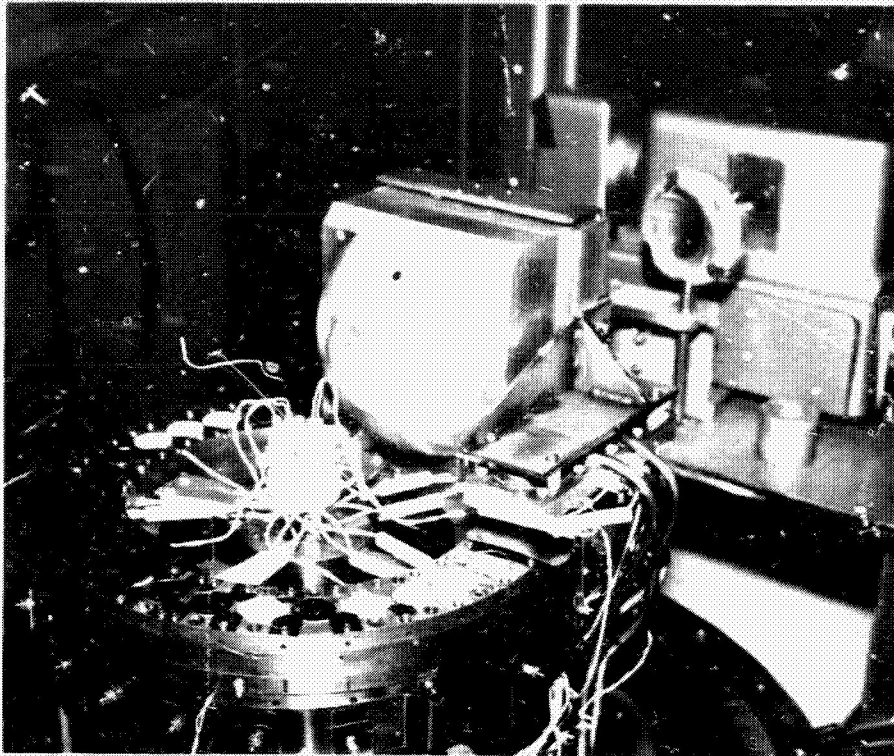


Figure 5-1. Integrating Sphere, Turntable and Monochromator

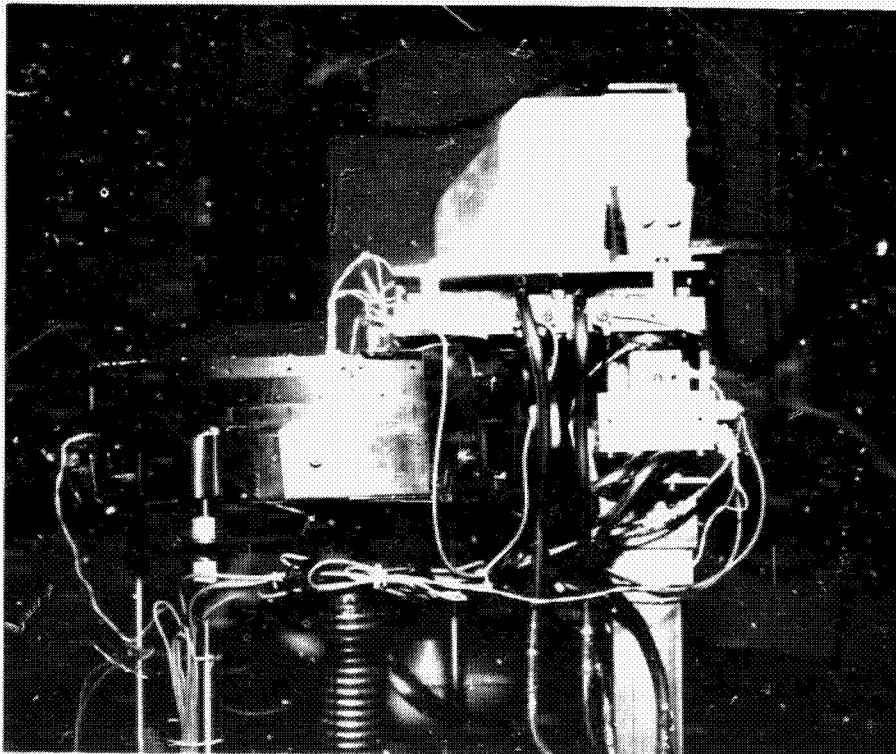


Figure 5-2. Integrating Sphere and Light Pipe

wavelength intervals and prints the value for that interval on digital tape (Figure 5-3). The scanner sends the monochromator signal through the voltage to frequency converter and into the electronic counter. The counter then integrates the output of the voltage to frequency converter over the specified wavelength intervals. The intervals are selected by an actuator connected to the monochromator drum drive, which is used to externally trigger the counter. The counter output is sent to the binary/decimal register, which also receives channel and time information from the digital clock. This data is then printed as a single-line output by the digital recorder.

5.3 COMPUTER PROGRAM

The computer program is then used to convert the digital recorder output to a spectral reflectance plot and an integrated value for the total solar absorptance. The spectral reflectance measurement is presently divided into 54 intervals (from 356 to 2065 millimicrons). The spectral reflectance is measured, using a comparison technique (with a magnesium oxide standard), and computed according to Equation 5-1.

$$R_X(\lambda_i) = \frac{\rho_X(\lambda_i) - \rho_Z(\lambda_i)}{\rho_R(\lambda_i) - \rho_Z(\lambda_i)} R_R(\lambda_i) \quad (5-1)$$

where:

$R_X(\lambda_i)$ is the computed reflectance in the wavelength interval represented by λ_i

$R_R(\lambda_i)$ is the absolute reflectance (References 5 and 6) of the reference (MgO) as measured in air in the wavelength interval represented by λ_i .

and:

$\rho_R(\lambda_i)$, $\rho_X(\lambda_i)$ and $\rho_Z(\lambda_i)$ are the dimensionless values of the reference, sample, and zero readings, respectively, obtained from the digital recorder for the wavelength interval represented by λ_i .

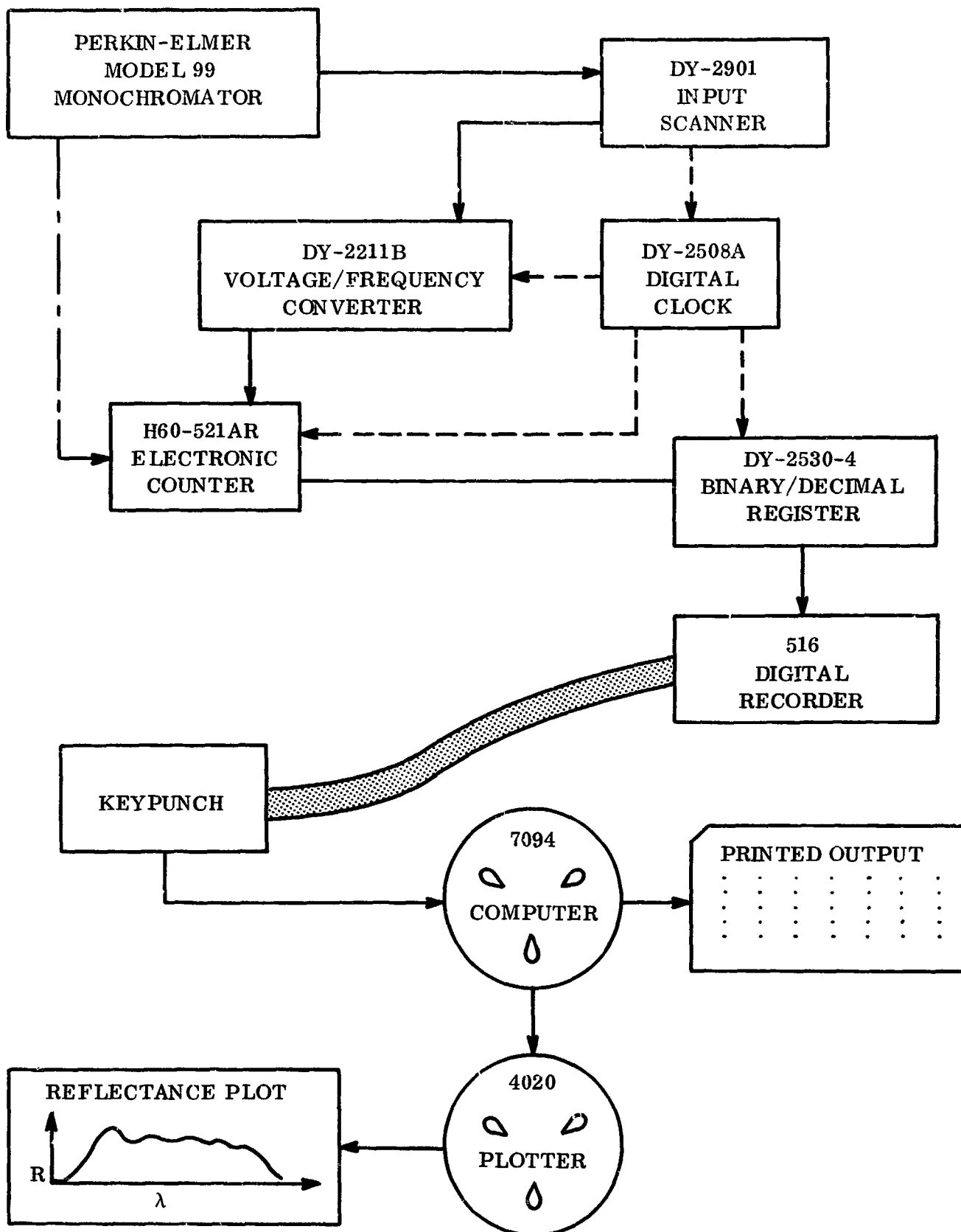


Figure 5-3. Block Diagram of Digital Acquisition and Reduction System

This value is then used in the 4020 plotting routine to produce a spectral reflectance plot.

The solar absorptance is then computed as shown in the following equations:

$$R_S(\lambda_i) = R_X(\lambda_i) J(\lambda_i) \quad (5-2)$$

$$R_S = \sum_{i=1}^{54} R_S(\lambda_i) \quad (5-3)$$

$$\alpha_S = 1 - R_S \quad (5-4)$$

where:

$R_S(\lambda_i)$ is the fractional solar reflectance in the wavelength interval represented by λ_i

R_S is the fractional solar reflectance (as computed based on $J(\lambda_i)$, as defined below)

$J(\lambda_i)$ is fractional energy under the Johnson curve (Reference 7) between 0.356 and 2.065 microns in the wavelength interval represented by λ_i

and:

α_S is the fractional solar absorptance (as computed based on $J(\lambda_i)$, as defined above)

In addition to printing the fractional solar absorptance, the 7090 output also includes the wavelength of computation; the computed absolute reflectance; the computed solar reflectance; the test specimen, reference, and zero readings from the digital recorder; the absolute reflectance of the reference; and the fractional energy in the Johnson curve for each wavelength region, together with the wavelength subscript.

The fractional solar absorptance value computed as described above does not consider the sun's energy outside the region measured; therefore, the computer computed solar absorptance must be manually corrected for these regions. This correction (now added into the computer program) is based on reflectance data obtained in air with a Beckman DK-IL spectrophotometer. The correction is made as described in Appendix C. A

tabulation of the corrections for each material for the unmeasured region of the spectrum is given in Table 5-1. The solar absorptance values given in Section 7 are also corrected for obviously erroneous high and low points (a smoothing of the curves). These corrections are performed manually with the aid of the 7094 output. A specific example of both types of corrections is given in Appendix C. The reflectance curves and their corresponding solar absorptances given in Appendixes D and E are not corrected as described; however, they were used as the basis for corrected values used in all other sections of this report.

Table 5-1. Corrections for Unmeasured Region of Spectrum

Material	Reflectance*		Total Increase in Solar Absorptance
	Below 356 m μ 5.9% of Energy	Above 2065 m μ 4.9% of Energy	
Alzak (.175 mils)	.844	.930	.01
Alzak (.10 mils)	.880	.959	.01
Goddard White	.110	.429	.07
RTV 602 White	.108	.559	.07
Pyromark Standard White	.160	.462	.06
Lexan (etched) over aluminum	.138	.403	.05
Lexan (dull) over aluminum	.117	.417	.06
Mylar over crinkled aluminized Mylar	.275	.300	.05
Solar Cells } Microsheet }	Only change is meaningful because of copper absorption.		

*Based on Beckman DK-IL measurements tabulated in Appendix F.

The specular nature of the Alzak coating results in less light being reflected into the light pipe on the integrating sphere, on the first reflection, than would a diffuse coating with the same reflectance. Since the MgO reference used is a diffuse coating, another correction (in addition to those previously discussed) must be performed. The basis of this correction is a comparison of the reflectance measurements made in the in situ reflectance apparatus (on unirradiated Alzak) in air and vacuum, with a MgO reference, against those made in this apparatus in air with a vapor deposited aluminum reference. Figure 5-4 is a plot of the spectral reflectance of Alzak as measured with a MgO reference and with the vapor deposited aluminum reference in the in situ reflectance apparatus. The MgO reference curve was obtained by using an overlay transparency on each of the before - irradiation Alzak measurements and averaging the result. The corrections at each wavelength and results of the computation are given in Table 5-2.

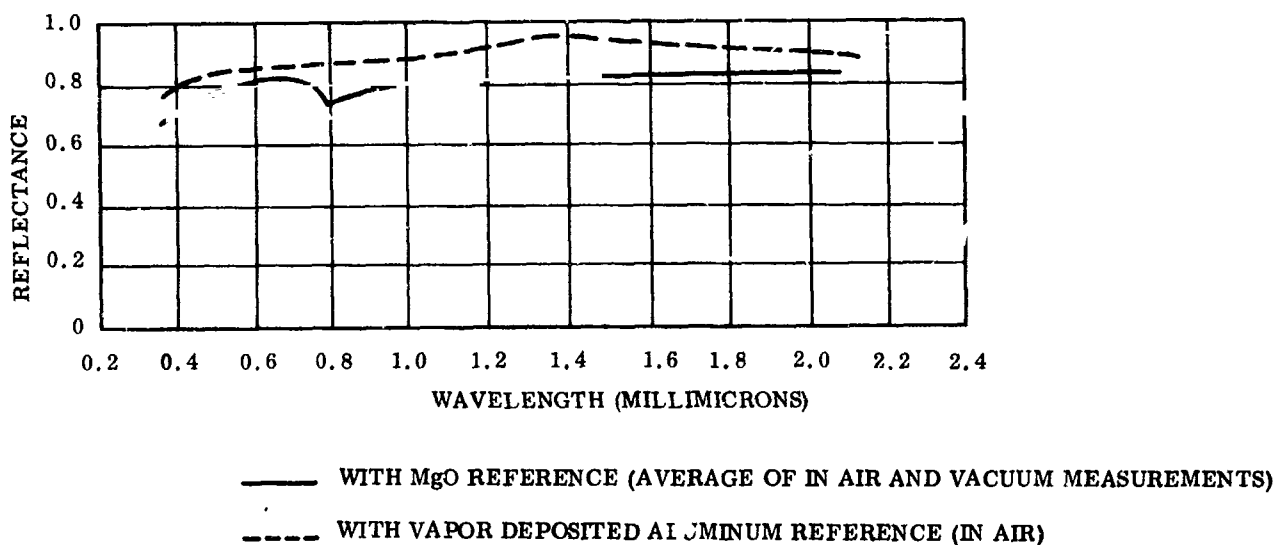


Figure 5-4. Reflectance Curves Used to Correct for Specular Nature of Alzak

Table 5-2. Correction for Specular Nature of Alzak

Wavelength Region ($m\mu$)	Average Fraction Reflectance Difference Between Aluminum and MgO Reference	Fractional Energy in Region	Decrease in Solar Absorption
0.356 — 0.49	0.08	0.170	0.0136
0.49 — 0.55	0.06	0.085	0.0051
0.55 — 0.72	0.04	0.203	0.0080
0.72 — 0.80	0.08	0.071	0.0057
0.80 — 0.87	0.12	0.052	0.0062
0.87 — 0.95	0.10	0.050	0.0050
0.87 — 1.14	0.08	0.092	0.0074
1.14 — 1.26	0.10	0.043	0.0043
1.26 — 1.49	0.13	0.058	0.0075
1.49 — 1.64	0.11	0.028	0.0031
1.64 — 1.80	0.09	0.018	0.0016
1.80 — 2.065	0.07	0.023	0.0016
Total			0.0691

SECTION 6 EXPERIMENTAL PROGRAM

Table 6-1 lists all the samples investigated in this program together with the desired test temperatures and the ultimate radiation levels to which they were to be irradiated. Table 6-2 lists the actual temperatures and ultimate radiation levels to which the specimens were exposed. The reason the temperature was changed was that both temperature extremes desired could not be obtained because of the high thermal contact resistance between the stationary and the fixed part of the specimen turntable. Since the major surface areas of the vehicle are at the colder temperature, it was decided, in conjunction with the contract monitor, to conduct the test at the lowest temperature readily attainable. This temperature was $-55 \pm 5^{\circ}\text{F}$ for both irradiation and optical property measurements. The only exceptions to this was before irradiation (in air and vacuum) and the final in-air measurements which were performed at $+75 \pm 5^{\circ}\text{F}$.

After the initial proton and electron irradiation, $5 \cdot 10^{14}$ protons cm^{-2} (2.5 kev) and $5 \cdot 10^{13}$ electrons cm^{-2} (3 kev), it was decided, in conjunction with the contract monitor, to eliminate all future corpuscular radiation. This decision was based on the fact that even at that low dose the specimens already had been exposed to the equivalent of about one-half year of electrons and over 1 year of protons, while only completing 200 EUVSH of near ultraviolet irradiation. The anticipated dose for this conclusion was based on Table 2-1 (References 1 and 2) and Figure 6-1 (Reference 3). Since the total near ultraviolet irradiation was only 945 EUVSH (about 2 to 3 months in orbit), it was decided not to perform any further corpuscular irradiations. The ultraviolet irradiations were performed at 1 ± 0.1 EUVS. Reflectance measurements were performed at the radiation increments shown in Table 6-3.

All multiple irradiations were performed simultaneously; that is, the samples under electron irradiation were simultaneously irradiated with protons and ultraviolet radiation. The converse is not true, however, since the electron irradiations were of shorter duration than the proton irradiation, which was of shorter duration than the ultraviolet irradiation.

Table 6-1. Original Sample Matrix*

Block No.	Sample**	No.	Temperature (°C)	Radiation (ultimate)		
				UV	Protons	Electrons
Block I	Alzak	1	20	1000 EUVSH	$3 \cdot 10^{17}$ Protons/cm ²	$1 \cdot 10^{17}$ Electrons/cm ² at 3 kev
	Goddard White	2	20			
	RTV 602	3	20	at	at	$1 \cdot 10^{17}$ Electrons/cm ² at 10 kev
	Pyromark***	4	20	1 EUVS	2.5 kev	$1 \cdot 10^{17}$ Electrons/cm ² at 20 kev
Alzak (t ₁)	5	20				
Block II	Alzak	6	To be established during test	None	To be established during test of other materials	To be established during test of other materials
	Alzak	7				
	Goddard White	8				
	Pyromark***	9				
Block III	RTV 602	10				
	Goddard White	11	20	1000 EUVSH at	None	None
	Alzak	12	20			
	Alzak	13	-100	1 EUVS	None	None
	Alzak	19	-100			
MgO	25	20		(Control)		
				(Reflectance Std)		
Block IV	Lexan-1	14	-100	1000 EUVSH	$3 \cdot 10^{17}$ Protons/cm ²	$1 \cdot 10^{17}$ Electrons/cm ² at 3 kev
	Alzak (t ₁)	15	-100			
	Mylar	16	-100	at	at	$1 \cdot 10^{17}$ Electrons/cm ² at 10 kev
	Alzak	17	-100	1 EUVS	2.5 kev	$1 \cdot 10^{17}$ Electrons/cm ² at 20 kev
Lexan-2	18	-100				
Block V	Solar Cell	20	-100	None	$3 \cdot 10^{17}$ Protons/cm ²	$1 \cdot 10^{17}$ Electrons/cm ² at 3 kev
	Alzak (t ₁)	21	-100			
	Mylar	22	-100	at	at	$1 \cdot 10^{17}$ Electrons/cm ² at 10 kev
	Alzak	23	-100	None	2.5 kev	$1 \cdot 10^{17}$ Electrons/cm ² at 20 kev
Microsheet	24	-100				
Block VI	Alzak	26	20	None	$3 \cdot 10^{17}$ Protons/cm ²	$1 \cdot 10^{17}$ Electrons/cm ² at 3 kev
	Goddard White	27	20			
	RTV 602	28	20	at	at	$1 \cdot 10^{17}$ Electrons/cm ² at 10 kev
	Pyromark***	29	20	None	2.5 kev	$1 \cdot 10^{17}$ Electrons/cm ² at 20 kev
Alzak (t ₁)	30	20				

*Refer to Table 6-2 for matrix actually used.

**All Alzak samples were 0.175 mils, except those followed by a (t₁), which were 0.100 mils.

***Pyromark Standard White

Table 6-2. Final Sample Matrix

Block No.	Sample*	No.	UV	Radiation (ultimate)	
				Protons cm ⁻² (2.5 kev)	Electrons cm ⁻² (3 kev)
Block I	Alzak	1	{ 945 EUVSH at 1 EUVS }	4.4 · 10 ¹⁴	3.3 · 10 ¹³
	Goddard White	2		5.6 · 10 ¹⁴	5.0 · 10 ¹³
	RTV 602	3		5.6 · 10 ¹⁴	5.8 · 10 ¹³
	Pyromark**	4		5.0 · 10 ¹⁴	5.8 · 10 ¹³
	Alzak (t ₁)	5		4.4 · 10 ¹⁴	3.3 · 10 ¹³
Block II	Alzak	6	{ None }	{ None }	{ None }
	Alzak	7			
	Goddard White	8			
	Pyromark**	9			
Block III	RTV 602	10	{ 945 EUVSH at 1 EUVS }	{ None }	{ None }
	Goddard White	11			
	Alzak	12			
	Alzak	13			
	Alzak	19			
	MgO	25			
				(Control)	
				(Reflectance Std)	
Block IV	Lexan-1	14	{ 945 EUVSH at 1 EUVS }	4.4 · 10 ¹⁴	3.3 · 10 ¹³
	Alzak (t ₁)	15		5.6 · 10 ¹⁴	5.0 · 10 ¹³
	Mylar	16		5.6 · 10 ¹⁴	5.8 · 10 ¹³
	Alzak	17		5.0 · 10 ¹⁴	5.8 · 10 ¹³
	Lexan-2	18		4.4 · 10 ¹⁴	3.3 · 10 ¹³
Block V	Solar Cell	20	{ None }	4.4 · 10 ¹⁴	3.3 · 10 ¹³
	Alzak (t ₁)	21		5.6 · 10 ¹⁴	5.0 · 10 ¹³
	Mylar	22		5.6 · 10 ¹⁴	5.8 · 10 ¹³
	Alzak	23		5.0 · 10 ¹⁴	5.8 · 10 ¹³
	Microsheet	24		4.4 · 10 ¹⁴	3.3 · 10 ¹³
Block VI	Alzak	26	{ None }	4.4 · 10 ¹⁴	3.3 · 10 ¹³
	Goddard White	27		5.6 · 10 ¹⁴	5.0 · 10 ¹³
	RTV 602	28		5.6 · 10 ¹⁴	5.8 · 10 ¹³
	Pyromark**	29		5.0 · 10 ¹⁴	5.8 · 10 ¹³
	Alzak (t ₁)	30		4.4 · 10 ¹⁴	3.3 · 10 ¹³

*All Alzak samples were 0.175 mils, except those followed by a (t₁), which were 0.100 mils.

**Pyromark Standard White

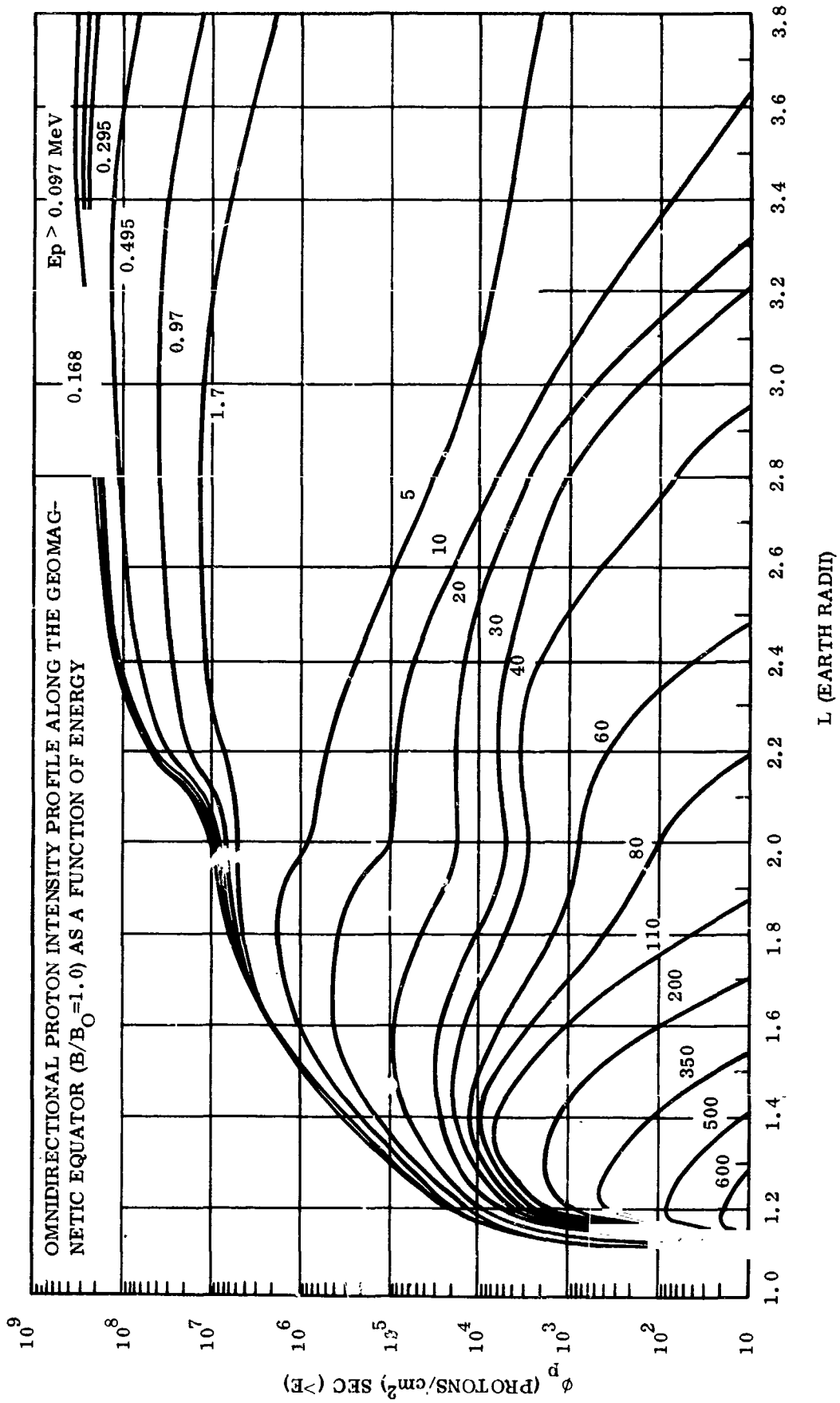


Figure 6-1. Integrated Proton Flux at the Geomagnetic Equator as a Function of Energy

Table 6-3. Sequence of Reflectance Measurements

Measurement Number	Measurement Temperature (°F)	Radiation Exposure		
		Near Ultraviolet (EU VSH)	2.5 keV Protons (p/cm ²)	3 keV Electrons (e/cm ²)
1	75*	None	None	None
2	-55	None	None	None
3	-55	61	None	None
4	-55	200	$5 \cdot 10^{14}$	$5 \cdot 10^{13}$
5	-55	335	$5 \cdot 10^{14}$	$5 \cdot 10^{13}$
6	-55	500	$5 \cdot 10^{14}$	$5 \cdot 10^{13}$
7	-55	714	$5 \cdot 10^{14}$	$5 \cdot 10^{13}$
8	-55	945	$5 \cdot 10^{14}$	$5 \cdot 10^{13}$
9	75*	945	$5 \cdot 10^{14}$	$5 \cdot 10^{13}$

*Measurement performed in air, all others were performed in vacuum.

The composition and preparation of the test specimens are given in Table 6-4. The Alzak samples were cleaned with MEK and wiped with gauze pads immediately before installation in the chamber. The white coatings were cleaned with a mild soap and distilled water and wiped with gauze pads immediately before installation into the chamber. After the initial in-air reflectance measurements the chamber was evacuated to $2 \cdot 10^{-7}$ torr and held there for 24 hours before the initial in-vacuum measurements were performed. Malfunctioning of the Diatron 20B (the analyzing section of the CEC 21-612 Residual Gas Analyzer) resulted in the elimination of the mass spectrometer measurements from the test program. Correction of this problem would have required breaking vacuum and remeasuring the reflectance of the specimens at least in vacuum. Both the absence of pressure bursts and the spectral reflectance measurements obtained prove that there was no deleterious effect due to out-gassed particles from one sample condensing onto other samples during the irradiations. The entire test was performed at $2 \cdot 10^{-7}$ torr, except during the proton irradiation, when the pressure was in the high 10^{-7} torr range. This pressure increase is probably due to atomic hydrogen which enters the chamber through the ion source canal with the protons.

Table 6-4. Coating Composition and Application

Material	Applicable Specifications	Composition
Alzak	Grumman XP-252-TS-26.0 Section 1	Reflective coated bright rolled 1100 aluminum alloy reflector sheet of H-18 temper. The front surface has a high purity aluminum clad for maximum reflectance and is protected by a 0.10 to 0.26 mil anodic oxide coating.
Pyromark Standard White	General Electric Material 171A4199 General Electric Process Specification 171A4200	This is a proprietary coating manufactured by the Tempil Corporation. It is a TiO_2 (rutile) pigment in a Dow Corning methyl-phenyl silicone binder. The binder is probably 805 or 806A.
Goddard 78-2B White	None	Dupont R-960 pigment in General Electric RTV-602 silicone resin in a pigment to binder ratio of 2:1 parts by weight. The R-960 pigment is a silica treated rutile form of TiO_2 . The RTV-602 is a dimethyl siloxane catalyzed with 1.5 to 2.0 percent by weight (of resin) catalyst made of a saturated solution of tetramethyl-ammonium hydroxide in isopropanol. The pigment and resin are blended with toluene to the desired consistency and then the catalyst is added.
Grumman RTV-602 White	Grumman GSS 4 205	This material is composed of 100 parts by weight (pbw) General Electric RTV-602 silicone 240 pbw ZnO from New Jersey Zink (SP-500) and 70 pbw Toluene.

The total normal emittance values obtained with the in situ emittance measurement apparatus were not reproducible and, therefore, discontinued. A description of its construction, calibration, and measurements made are given in Appendix B.

Spectral Reflectance measurements were made, at NASA-Goddard, of all samples tested, except Pyromark Standard White and RTV-602 White, before irradiation. All samples tested were measured after irradiation at NASA-Goddard. One of each of the samples listed in Table 6-5 was measured at General Electric with a Beckman DK-IL spectrophotometer before irradiation. Table 6-5 lists the samples on which spectral emittance measurements were performed with a Leeds and Northrup hohlraum and a Perkin-Elmer 13-2 spectrophotometer. Tables of the spectral reflectance data on samples listed in Table 6-5 are given in Appendix F.

Table 6-5. Specimens Measured with Conventional Air Optical Instruments

Sample Identification	Spectral Solar Absorptance	Spectral Emittance
Alzak* 11 (0.175 mils)	X	X
Alzak* 24 (0.29 mils)	X	X
Alzak* 30 (0.10 mils)	X	X
Goddard White	X	X
RTV-602 White	X	X
Pyromark Standard White	X	X
Lexan (Etched)	Both transmittance and reflectance over polished aluminum.	-
Lexan (Dull)	Both transmittance and reflectance over polished aluminum.	-
Mylar (Shiny side out)	Both transmittance and reflectance over crinkled aluminized Mylar.	-
Microsheet	X	-
Solar Cells	Both N/P and P/N cell	-

*Sample numbers given are NASA-Goddard code numbers.

SECTION 7

RESULTS AND DISCUSSION

A comparison of the solar absorptance based on smoothed and unsmoothed reflectance curves is given in Table 7-1 (Alzak) and Table 7-2 (white paints and miscellaneous spacecraft materials). These values are rounded off to 2 decimal places and are smoothed but uncorrected for the region of the spectrum not measured, as described in Section 5. The values in parentheses are the values before smoothing. If there is no value in parentheses, the solar absorptance did not change upon smoothing. These values are all based on the reflectance curves in Appendix D. The reflectance curves in Appendix D are just as the computer produced them (uncorrected and unsmoothed). A summary of all corrected and smoothed absorptance values obtained are given in Table 7-3 (Alzak) and Table 7-4 (white coatings and miscellaneous spacecraft materials).

The solar absorptance values presented in this report were obtained by placing the Lexan samples over polished aluminum and the Mylar samples over crinkled aluminized Mylar. Table 7-5 compares the solar absorptance values obtained with the in situ apparatus against the Beckman DK-IL measurements (Appendix F) and those obtained at NASA-Goddard. All values in this table are based on in-air measurements. The values from the in situ apparatus are both smoothed and corrected. The Alzak samples are the only ones corrected for specular reflection.

All solar absorptance values from the in situ reflectance apparatus used in this report were obtained as described in Section 5, except as follows:

- a. The measurements made on 4/26/67 (61 EUVSH), 5/2/67 (200 EUVSH plus e and p), and 5/8/67 (335 EUVSH) were reduced manually from a strip chart recording of the monochromator output. This was done by averaging the recorder readings between event markers on the strip chart over the same wavelength regions that the digital acquisition system normally integrates the monochromator output. This data was then computer-processed in the normal manner. The digital data acquisition system was not used in these measurements, since it was inoperative at the time.
- b. The measurements made on 6/6/67 (945 EUVSH) and 6/14/67 (945 EUVSH in air) are based on triple scans, i. e., the measurement described in Section 5 was repeated three times. The reflectance curves (Appendix D) and solar absorptance values for these dates were obtained from a point by point average of the three curves.

Table 7-1. Comparison of Smoothed and Unsmoothed Solar Absorbance⁺

Specimen Number	Thickness	Type Irradiation	Date EUVSH E/cm ² P/cm ²	Solar Absorbance of Alzak (α_s)									
				4/11/67*	4/13/67	4/26/67	5/2/67	5/16/67	5/26/67	6/6/67	6/14/67*		
13		UV		.20 (.21)	.20	.23 (.24)	.23	.23 (.24)	.23 (.24)	.24	.24	.25	.25 (.26)
12		UV		.21 (.22)	.23 (.24)	.22 (.23)	.24 (.25)	.24	.24 (.23)	.24 (.23)	.24	.24	.25
1		UV, E, P		.22 (.23)	.21	.23 (.24)	.22 (.23)	.24	.24 (.22)	.24 (.22)	.24 (.22)	.25	.25
17		UV, E, P		.21 (.22)	.19 (.20)	.24	.24 (.26)	.25 (.24)	.24 (.21)	.24 (.21)	.26	.24	.24 (.25)
5	t**	UV, E, P		.20 (.21)	.19 (.20)	.22	.21 (.22)	.21 (.22)	.21	.21 (.22)	.23 (.22)	.23	.22 (.23)
15	t ₁ **	UV, E, P		.19	.20 (.21)	.20	.20	.20 (.19)	.23 (.22)	.23 (.22)	.23	.23	.23 (.24)
23		E, P		.22 (.23)	.22 (.23)	-	.19	-	-	-	.22	.22	.23 (.24)
26		E, P		.21 (.22)	.18 (.19)	-	.24 (.23)	-	-	-	.21 (.22)	.21 (.22)	.22 (.23)
21	t**	E, P		.18	.21 (.22)	-	.21 (.22)	-	-	-	.20 (.22)	.20 (.22)	.21 (.22)
30	t ₁ **	E, P		.18 (.17)	.19 (.20)	-	.21 (.22)	-	-	-	.21 (.20)	.21 (.20)	.21 (.22)
6		None		.21 (.21)	.20 (.21)	-	.20 (.21)	-	-	-	.22 (.21)	.22	.22
7		None		.21 (.22)	.20	-	.21	-	-	-	.20	.20	.22
19		Control		.18	.21 (.22)	.22 (.23)	.22 (.23)	.19 (.20)	.19	.19	.21 (.22)	.21 (.22)	.21 (.22)

* Measurements made in air; all others made in vacuum.

** The coating of sample thicknesses noted as t₁ are nominally 0.100 mils; all others are nominally 0.175 mils.

() The values in parentheses are the values before smoothing; if no value appears in parentheses then it did not change due to smoothing

+ None of the values in this table are corrected for the regions of the spectrum not measured or for the specular nature of any surface.

Table 7-2. Comparison of Smoothed and Unsmoothed Solar Absorbance[†]

Specimen Number	Material	Irradiation Type	Date	Solar Absorbance of White Paints (α_g)																
				4/11/67*	4/13/67	4/26/67	5/2/67	5/8/67	5/16/67	5/26/67	6/6/67	6/14/67*								
2	Goddard White	UV, E, P	EUVSH																	
11	Goddard White	UV	E/cm ²	.17(.18)	.16	.18	.18	.19	.19	.19	.18	.18	.18	.18	.18	.18	.18	.18	.18	.18
27	Goddard White	E, P	P/cm ²	.15(.14)	.16(.17)	.19(.18)	.19(.18)	.19	.17(.16)	.20(.18)	.13(.12)	.13(.12)	.19(.18)	.13	.19(.18)	.13	.13	.13	.13	.13
8	Goddard White	None		.14	.16(.15)	-	.18(.19)	.16	.16	.15	.20(.23)	.20(.23)	.16	.16	.16	.16	.16	.16	.16	.16
3	RTV 602 White	UV, E, P		.15	.17(.16)	-	.17	.17	.18(.17)	.16	.16(.18)	.16(.18)	.15	.15	.15	.15	.15	.15	.15	.15
28	RTV 602 White	UV, E, P		.12	.12	.14	.15	.15	.17(.19)	.15	.15(.14)	.15(.14)	.14	.14	.14	.14	.14	.14	.14	.14
10	RTV 602 White	E, P		.12	.12	-	.13(.14)	.13	.13	.13	.14	.14	.14	.14	.14	.14	.14	.14	.14	.14
4	PyromarkStd. White	None		.10	.11(.12)	-	.11(.12)	.10	.10	.13	.16(.17)	.16(.17)	.13	.13	.13	.13	.13	.13	.13	.13
29	PyromarkStd. White	UV, E, P		.18(.17)	.18(.19)	.22	.25	.26(.25)	.26(.25)	.26(.25)	.26(.25)	.26	.26	.26	.26	.26	.26	.26	.26	.26
9	PyromarkStd. White	E, P		.18	.18	-	.20(.21)	.22(.23)	.22(.23)	.19(.18)	.20(.21)	.20(.21)	.20	.20	.20	.20	.20	.20	.20	.20
		None		.20	.15	-	.18	.21	.21	.19	.22(.24)	.22(.24)	.20	.20	.20	.20	.20	.20	.20	.20
Solar Absorbance of Miscellaneous Spacecraft Materials (α_R)																				
14	Lexan (Etched)	UV, E, P		.28	.29	.25(.27)	.50(.49)	-	-	.51(.50)	.50	.50	.50	.50	.50	.50	.50	.50	.50	.50
18	Lexan (Dull)	UV, E, P		.24	.24	.42(.44)	.51	-	-	.52(.48)	.48(.46)	.48(.46)	.48	.48	.48	.48	.48	.48	.48	.48
16	Mylar	UV, E, P		.29	.30(.31)	.24	.43	-	-	.45(.44)	.47(.45)	.47(.45)	.45	.45	.45	.45	.45	.45	.45	.45
22	Mylar	E, P		.29	.34	-	.33	-	-	-	.29(.28)	.29(.28)	.32	.32	.32	.32	.32	.32	.32	.32
20	Solar Cells	E, P		.83	.82	-	.81	-	-	-	-	-	.79	.79	.79	.79	.79	.79	.79	.79
24	Microsheet	E, P		.46	.46(.47)	-	.44	-	-	-	-	-	.43	.43	.43	.43	.43	.43	.43	.43

* Measurements made in air; all others made in vacuum.

** Reflectance curve appears to be similar to that of polished aluminum (Lexan probably slipped off polished aluminum substrate).

*** Sample slipped off table; no measurement performed.

() The values in parentheses are the values before smoothing, if no value appears in parentheses then it did not change due to smoothing.

+ None of the values in this table are corrected for the regions of the spectrum not measured or for the specular nature of any surface.

Table 7-3. Summary of Smooth and Corrected Solar Absorbance

Specimen Number	Thickness	Type Irradiation	Date EUVSH E/cm ² P/cm ²	Solar Absorbance of Alzak (α_s)									
				4/11/67*	4/13/67	4/26/67	5/2/67	5/16/67	5/26/67	6/6/67	6/14/67*		
13		UV	.14	.14	.17	.17	.17	.17	.17	.18	.19	.19	.19
12		UV	.15	.17	.16	.13	.18	.18	.18	.18	.18	.18	.19
1		UV, E, P	.16	.15	.17	.16	.18	.18	.19	.18	.19	.19	.19
17		UV, E, P	.15	.13	.18	.18	.19	.17	.20	.17	.20	.18	.18
5	t_1^{**}	UV, E, P	.14	.13	.16	.15	.15	.15	.17	.15	.17	.16	.16
15	t_1^{**}	UV, E, P	.13	.14	.14	.14	.14	.17	.17	.17	.17	.17	.17
23		E, P	.16	.16	-	.13	-	-	.16	-	.16	.17	.17
26		E, P	.15	.12	-	.18	-	-	.15	-	.15	.16	.16
21	t_1^{**}	E, P	.12	.15	-	.15	-	-	.14	-	.14	.15	.15
30	t_1^{**}	E, P	.12	.13	-	.15	-	-	.15	-	.15	.15	.15
6		None	.15	.14	-	.14	-	-	.16	-	.16	.16	.16
7		None	.15	.14	-	.15	-	-	.15	-	.14	.16	.16
19		Control	.12	.15	.16	.16	.16	.13	.13	.13	.15	.15	.15

* Measurements made in air; all others made in vacuum

** The coating of sample thicknesses noted as t_1 are nominally 0.100 mils; all others are nominally 0.175 mils.

Table 7-4. Summary of Smoothed and Corrected Solar Absorbance

Specimen Number	Material	Date EUVSH E/cm ² Irradiation P/cm ²	Solar Absorbance of White Paints (α _g)										
			4/11/67*	4/13/67	4/26/67	5/2/67	5/8/67	5/16/67	5/26/67	6/6/67	6/14/67*		
2	Goddard White	UV, E, P	.24	.23	.25	.25	.26	.25	.25	.25	.25	.25	.24
11	Goddard White	UV	.22	.23	.26	.26	.24	.27	.27	.27	.27	.26	.25
27	Goddard White	E, P	.21	.23	.25	.25	.23	.22	.22	.22	.27	.23	.23
8	Goddard White	None	.22	.24	.24	.24	.25	.23	.23	.23	.23	.22	.22
3	RTV 602 White	JV, E, P	.19	.19	.21	.22	.24	.22	.22	.22	.22	.21	.21
28	RTV 602 White	E, P	.19	.19	.20	.20	.20	.20	.20	.20	.21	.21	.20
10	RTV 602 White	None	.17	.18	.18	.18	.17	.20	.20	.20	.23	.20	.18
4	Pyromark Std. White	UV, E, P	.24	.24	.28	.31	.32	.32	.32	.32	.32	.32	.27
29	Pyromark Std. White	E, P	.24	.24	.24	.26	.28	.25	.25	.26	.26	.26	.23
9	Pyromark Std. White	None	.26	.21	.24	.24	.27	.25	.25	.28	.28	.26	.25
Solar Absorbance of Miscellaneous Spacecraft Materials (α _g)													
14	Lexan (Etched)	UV, E, P	.33	.34	.29	.55	.55	.56	.56	.55	.55	.57	.54
18	Lexan (Dull)	UV, E, P	.30	.30	.48	.57	.57	.58	.58	.54****	.54****	**	***
16	Mylar	UV, E, P	.34	.35	.29	.48	.48	.50	.50	.52	.52	.59	.50
22	Mylar	E, P	.34	.39	.39	.3f	.3f	-	-	.34	.34	.37	.38
20	Solar Cells	E, P	.83	.82	.81	.81	.81	-	-	-	-	.79	.84
24	Microsheet	E, P	.46	.46	.44	.44	.44	-	-	-	-	.43	.44

*Measurements made in air; all others made in vacuum.

**Reflectance curve appears to be similar to that of polished aluminum (Lexan probably slipped off polished aluminum substrate).

***Sample slipped off table; no measurement performed.

**** No correction made since a part of reflectance included that of copper, because of sample geometry.

***** This sample was probably partially off the polished aluminum substrate even at this time.

Table 7-5. Comparison of Solar Absorptance Values

Material	Solar Absorptance (in air)		
	In Situ* Apparatus	Beckman** DK-IL	NASA-Goddard*
Alzak (.175 mils)	.15	.16	.15
Alzak (.100 mils)	.13	.15	.14
Goddard White	.22	.19	.21
RTV 602 White	.18	.18	+
Pyromark Standard White***	.25	.22	+
Mylar (shiny side out) over crinkled aluminized Mylar	.34	.31	.31
Lexan (etched) over polished aluminum	.33	.34	++
Lexan (dull) over polished aluminum	.30	.30	++

++Transmission and reflectance measurements made only on Lexan at NASA-Goddard before testing.

+ Unavailable for measurement at NASA-Goddard before testing.

* Based on an average of all samples measured before irradiation in air, except for Alzak where in vacuum measurements before irradiation were also used.

**Based on measurement of one sample.

***A solar absorptance of 0.25 rather than 0.22 is considered more normal for Pyromark Standard White.

In addition to plotting the average reflectance from the three scans, separate plots of each of the three scans were also made (Appendix E). A compilation of the solar absorptance obtained in each separate scan and from the point-by-point averaging of the three scans is given in Table 7-6 (for 945 EUVSH data in vacuum) and in Table 7-7 for 945 EUVSH data in air). All values in both these tables are both unsmoothed and uncorrected (just rounded off to 2 decimal places). All values which deviate from the average by more than ± 0.01 are put in parentheses. Analysis of these two tables shows that only 9 out of the 168 scans made deviate by more than ± 0.01 from the average value for any given sample. Of these nine, four are exaggerated by rounding off from 3 to 2 decimal places. Based on this, it is

Table 7-6. Single Scan Versus Average of Three Scans (in vacuum)

Sample Identification	Sample Number	Solar Absorbance* in vacuum after 945 EUVSH, 5.10 ¹⁴ P/cm ² , and 5.10 ¹³ E/cm ²	
		Each Scan Computed Separately	Computed as the Average of Three
Alzak	13	.25	.25
Alzak	12	.24	.24
Alzak	1	.24	.24
Alzak	17	.27	.26
Alzak	5	.22	.22
Alzak	15	.22	.23
Alzak	23	.22	.22
Alzak	26	.22	.22
Alzak	21	.22	.22
Alzak	30	.20	.20
Alzak	6	.22	.21
Alzak	7	.20	.20
Alzak	19	.22	.22
Alzak	2	.18	.18
Alzak	11	.17	.18
Goddard White	27	.15	.16
Goddard White	3	.14	.14
Goddard White	8	.15	.15
RTV 602 White	28	.13	.13
RTV 602 White	10	.12	.13
Pyromark White	4	.27	.26
Pyromark White	29	.19	.20
Pyromark White	9	.20	.20
Lexan (Etched)	14	.50	.50
Lexan (Dull)	18	Lexan slipped, polished aluminum exposed	
Mylar	16	.51	.52
Mylar	22	.31	.32
Solar Cells	20	.79	.79
Microsheet	24	.42	.43

() Value deviates from the average by more than ± .01
* Unsmoothed and uncorrected

Table 7-7. Single Scan Versus Average of Three Scans (in air)

Sample Identification	Sample Number	Solar Absorbance* in air after 945 EUVSH, 5.10 ¹⁴ P/cm ² , and 5.10 ¹³ E/cm ²	
		Each Scan Computed Separately	Computed as the Average of Three
Alzak	13	.26	.26
Alzak	12	.24	.25
Alzak	1	.25	.25
Alzak	17	.24	.25
Alzak	5	.22	.23
Alzak	15	.23	.24
Alzak	23	.23	.24
Alzak	26	.22	.23
Alzak	21	.21	.22
Alzak	30	.21	.22
Alzak	6	.22	.22
Alzak	7	.21	.22
Alzak	19	.21	.22
Alzak	2	.16	.17
Alzak	11	.18	.18
Goddard White	27	.15	.16
Goddard White	3	.14	.14
RTV 602 White	28	.13	.13
RTV 602 White	10	.13	.13
Pyromark White	4	.20	.21
Pyromark White	29	.16	.17
Pyromark White	9	.17	.18
Lexan (Etched)	14	.49	.50
Lexan (Dull)	18	Sample slipped or table no measurement performed	
Mylar	16	.44	.45
Mylar	22	.32	.33
Solar Cells	20	.83	.84
Microsheet	24	.43	.44

() Value deviates from the average by more than ± .01
* Unsmoothed and uncorrected

believed that most of the values obtained are reproducible and self-consistent to ± 0.01 , and all values are reproducible and self-consistent to ± 0.02 . The smoothed values should be even more reproducible and self-consistent. It is believed that an analysis based on the spread in measurements actually performed (such as that above) is more meaningful and accurate than a theoretical analysis which considers the stability of each component of the measurement system separately to establish the theoretical reproducibility of the total system. It should be noted that the one factor not considered in the analysis presented is proper sample positioning under the integrating sphere (a theoretical analysis would not consider this either).

It should be obvious that the aforementioned analysis does not establish the accuracy of the solar absorptance values obtained with the in situ reflectance apparatus. Based on the comparison of values obtained with two other systems (Table 7-5), it appears that the agreement is very good for some materials and fair in the case of Mylar (shiny side out), where no adjustment was made for the specular nature of its surface. The question of the accuracy of the measurements made with the in situ reflectance apparatus should not hinder the usefulness of the data, however, since any desired correction in the initial value stated can be applied to all values listed for the material of interest (a linear translation of the curve along the solar absorptance axis). What is most important is that the reported change in solar absorptance for each radiation exposure listed is believed to be accurate to ± 0.01 and certainly accurate to ± 0.02 (as illustrated by the values listed in Tables 7-6 and 7-7).

The following is an analysis of the data on each material category and each coating, separately.

7.1 ALZAK

The solar absorptance of Alzak as a function of radiation dose is given in Figure 7-1. The two different thickness coatings are plotted separately. The initial solar absorptance values for Figure 7-1 are based on an average of all initial measurements made on each thickness of Alzak (Table 7-5). The values at each radiation level are based on an average of

the ultraviolet and the combined electron, proton, and ultraviolet irradiated samples listed in Table 7-3 (for each thickness).

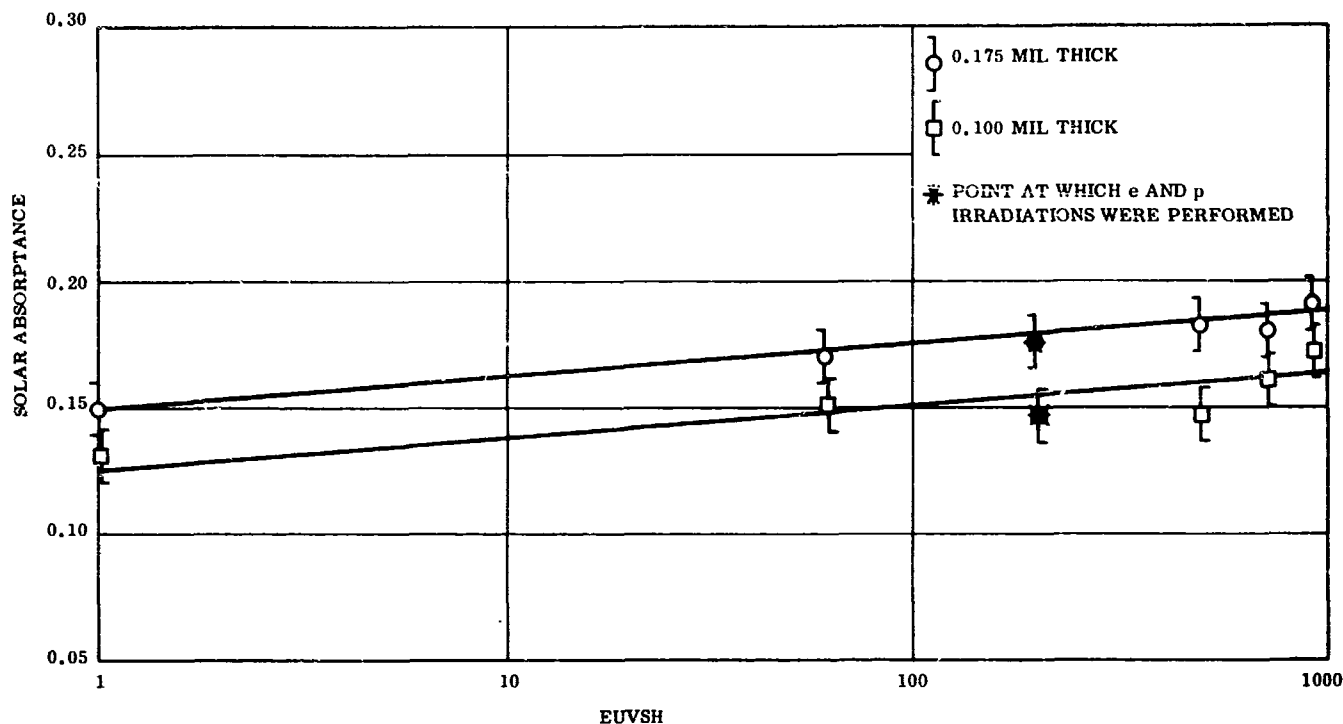


Figure 7-1. Radiation Degradation of Alzak

The reason the samples irradiated with ultraviolet radiation alone are combined with those which also experienced electron and proton irradiation is that no significant difference could be detected, due to the addition of the corpuscular irradiation (see Table 7-3). As can be seen from Figure 7-1, both thicknesses of Alzak appear to exhibit about the same incremental change in solar absorptance for each radiation level. Figure 7-2 is a plot of the incremental change in the solar absorptance of Alzak as a function of radiation exposure. The result is that the thicker Alzak coating has a higher solar absorptance, but the thinner coating exhibits a greater percent of change in solar absorptance. The most desirable thickness of Alzak must then be determined by thermal design, since there will now be a tradeoff between maximum desired solar absorptance (or temperature) and maximum tolerable change in solar absorptance during the mission lifetime (or maximum) temperature change during flight). The fact that this incremental change in the solar absorptance of Alzak is independent of thickness probably means that all the degradation (for the type of

irradiation to which these samples were exposed) was caused by changes which occurred at least within the first 0.100 mils of the coatings. The degradation (change in solar absorptance) due to electron and proton irradiation only, (based on the values presented in Table 7-3) is 0.01 for the 0.175-mil Alzak coating and 0.02 for the 0.100-mil Alzak coating.

Based on the spectral reflectance curves in Appendix D and the average values of solar absorptance presented in Tables 7-6 and 7-7, it appears that the Alzak coatings do not heal when exposed to air after irradiation.

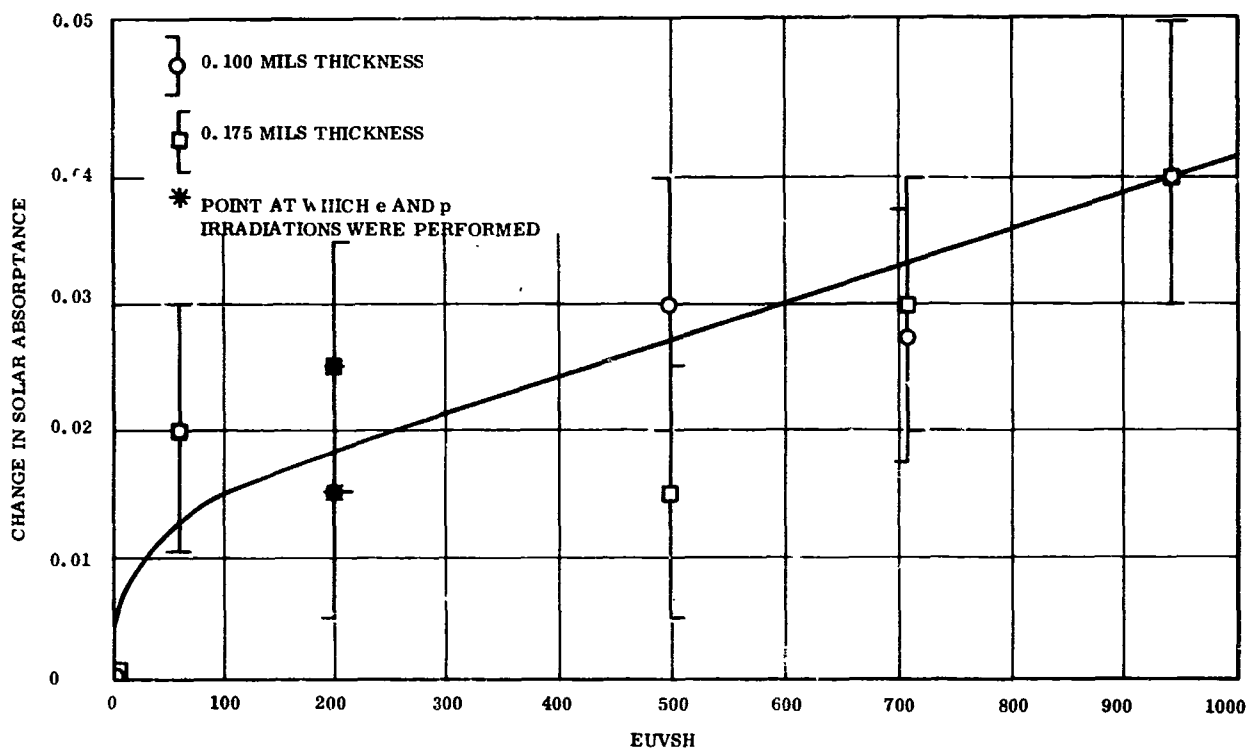


Figure 7-2. Radiation Degradation of Alzak

The use of overlays (as described in Section 5 for correction of the specular nature of Alzak) on the Alzak curves in Appendix D revealed the following:

- a. It was observed that the 0.175-mil samples irradiated both with ultraviolet only and with the combination of corpuscular and ultraviolet irradiation exhibited the following spectral reflectance changes:

1. After 61 EUVSH there was a general decrease in the reflectance below 0.8 microns and an increase in the radius of curvature of the absorption edge out to 0.6 microns.
 2. The rounding of the absorption edge continued until it reached 0.8 microns after 714 EUVSH. It remained like this for the duration of the test.
- b. The 0.100-mil samples exhibited a similar general decrease in reflectance below 0.8 microns, but the rounding of the absorption edge only was observed below 0.7 microns. It appears that the electron and proton irradiation at the 200 EUVSH radiation level may have healed the rounding of the absorption edge on samples 5 and 15. The absorption edge was rounded again at the next measurement (after 500 EUVSH).

7.2 WHITE PAINTS

The change in solar absorptance as a function of radiation dose for all the white paints is given in Figure 7-3. The initial solar absorptance values for Figure 7-3 are based on only the in-vacuum measurements. The values at each radiation level are based on one sample, except for Goddard White, where the sample that received only ultraviolet and the sample that received both ultraviolet and corpuscular radiation were averaged. These are the values listed in Table 7-4 except as stated in the following discussion of each white paint. Table 7-8 shows that Pyromark Standard White exhibited the greatest change in solar absorptance and the greatest percent of change of any of the white paints. RTV 602 White and Goddard White displayed the same incremental change in solar absorptance; therefore, RTV-602 White had a slightly higher percent of change in solar absorptance than Goddard White, since its initial value was lower.

Table 7-8. Radiation Degradation of White Paints

Material	Increase in Solar Absorptance	
	Increment	Percentage
Goddard White	0.02	8.7
RTV 602 White	0.02	10.5
Pyromark Standard White	0.08	33

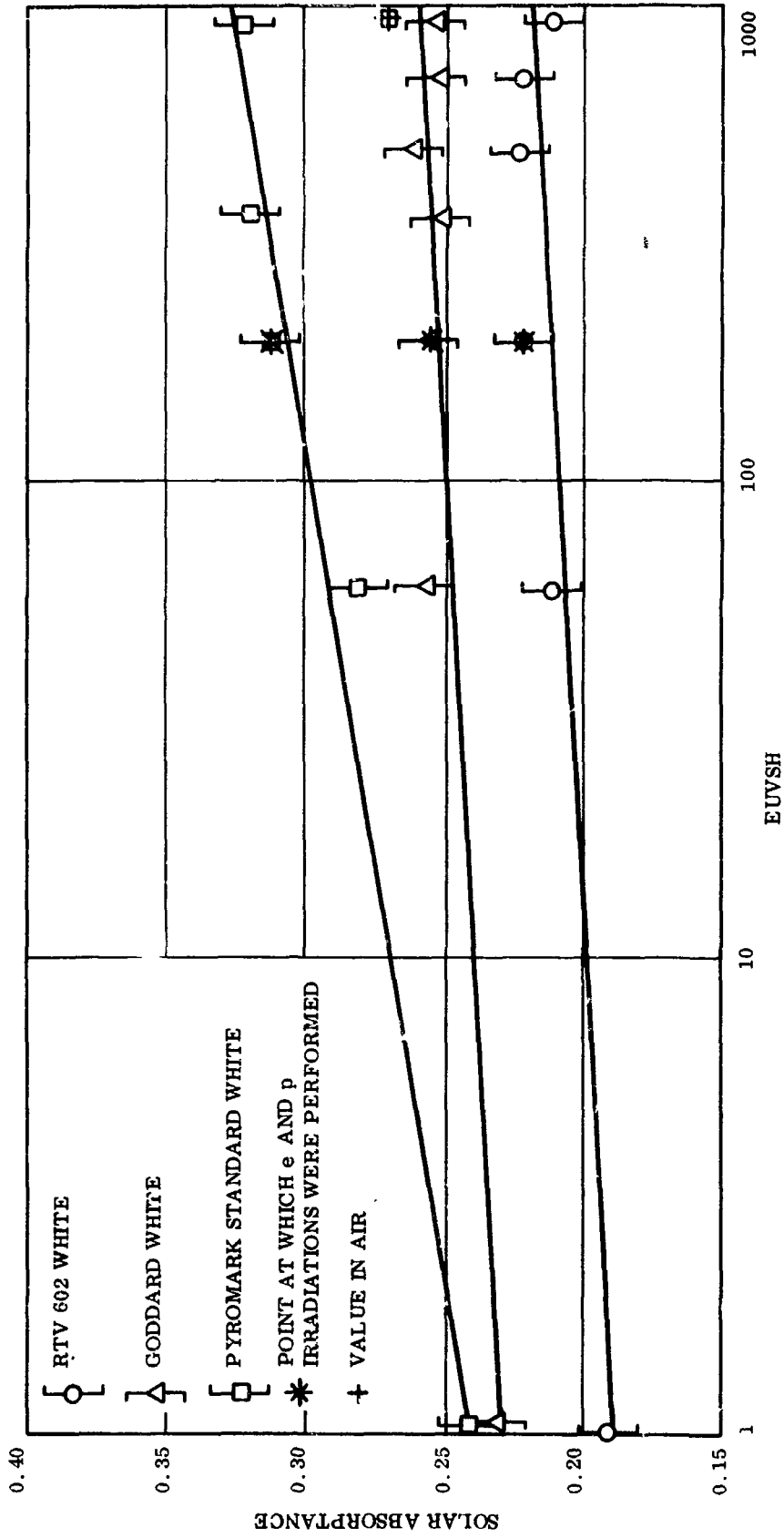


Figure 7-3. Radiation Degradation of White Paints

7.3 GODDARD WHITE

The value of the solar absorptance in Figure 7-3 at 714 EUVSH is based only on Sample 4. The value of Sample 11 was not used to obtain the average value for this point because its reflectance curve exhibited an abnormally high reflectance, from 0.6 micron to 1.0 micron, which is not corrected for by a simple smoothing of the curve. The reason this is not corrected by the smoothing process is because of the large wavelength region which it encompasses. The erroneous reflectance curve obtained is almost certainly due to improper sample positioning.

Virtually all the degradation due to ultraviolet irradiation occurred within the first 61 EUVSH. The degradation was exhibited as a general decrease in the reflectance below 0.8 micron. There was no change in the sharpness of the absorption edge. No change could be noted in this coating due to the electron and proton bombardment. Analysis of the absorption edge and the reflectance below 0.8 microns of the spectral reflectance curves in Appendix D shows that this coating did heal slightly (about 0.01 solar absorptance increase) when exposed to air after irradiation.

7.4 RTV-602 WHITE

The value for the solar absorptance at 335 EUVSH is missing because its reflectance curve exhibited an abnormally low reflectance in the wavelength region between 0.8 and 1.4 microns which does not get compensated for in the normal smoothing process. This erroneous plot is probably due to an improper sample positioning for the reflectance measurement.

Virtually all of the degradation due to ultraviolet radiation occurred within the first 200 EUVSH, and was due, primarily, to a decrease in reflectance below 0.6 micron. There was no change in the shape of the absorption edge, as determined with overlays as described earlier. No healing was noted when this material was exposed to air after irradiation. The proton and electron irradiation produced less than a 0.02 change in the solar absorptance.

7.5 PYROMARK STANDARD WHITE

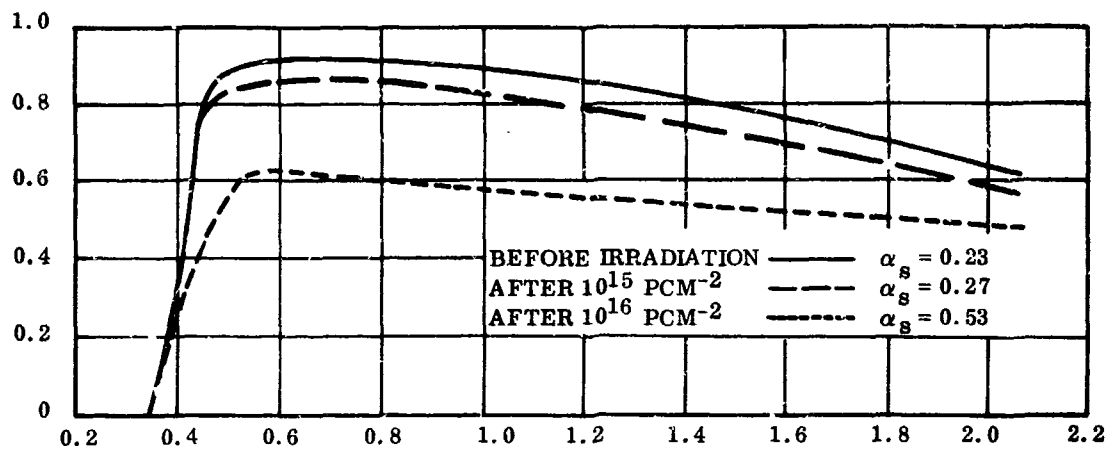
By 335 EUVSH the degradation to this material appeared to reach a threshold. The change in the reflectance curve was primarily below 1.0 micron after 61 EUVSH, and the absorption edge became rounded back to 0.6 micron. The reflectance curve decreased out to 1.6 microns as the degradation continued. The electron and proton irradiation caused less than a 0.02 change in solar absorptance.

The solar absorptance of this material exhibited noticeable healing when exposed to air after irradiation. The healing was exhibited by an increase in reflectance in the entire wavelength region where degradation was noted, including a reduction of the radius of curvature of the absorption edge.

Two samples of Pyromark Standard White were exposed to 2.5 keV protons with reflectance measurements performed after 10^{14} , 10^{15} , and 10^{16} p cm⁻². There was no significant change after the 10^{15} p cm⁻² dose; however, after 10^{16} p cm⁻² a change in solar absorptance of 0.20 and 0.28 was noted on the two specimens (Figure 7-4.) This means that the solar absorptance of Pyromark Standard White was between 0.44 and 0.52, after exposure to 10^{16} p cm⁻² of 2.5 keV. Although this data may seem irrelevant, since it is not expected that OAO will receive even one tenth of this dose in one year of flight, it becomes important when the following facts are considered:

- a. To date, virtually all space flight coating experiments have shown that the coatings degrade more in space than they do in ground simulation.
- b. A very recent preliminary investigation by Babjak and Goldis at General Electric has shown that Pyromark Standard White degradation due to 15 keV electrons is not dependent on total measured incident dose (when different dose rates are used), but is dependent on total irradiation time. Based on this work, it has been shown that the variation in total dose (performed at different flux levels) for an equivalent change in reflectance can vary by at least as much as 450. This can be

SPECIMEN
NO. 28



SPECIMEN
NO. 29

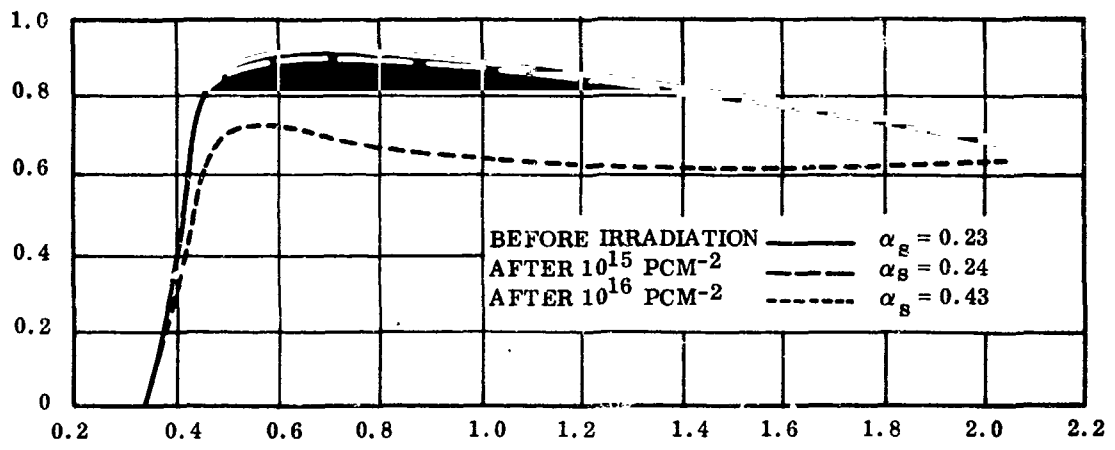


Figure 7-4. 2.5 Kev Proton Irradiation of Pyromark Standard White

due either to space charge buildup and/or reaction rate limitation*. If it is primarily space charge buildup which is responsible, this effectively means that the flux measured with a Faraday cup over the sample is much greater than the flux which the sample actually receives. The actual difference in the measured flux and the flux incident on the sample can be experimentally determined.

- c. Although it is true that the lower energy particles deposit more energy per unit path length traversed than the higher energy particles, and that the flux of lower energy particles in space is much greater than that of the higher energy particles, one must consider the following details of a coating to determine the proper simulation:
 1. The effect of coating thickness on the solar absorption
 2. The range of corpuscular radiation (especially protons) in the coating and the incremental energy deposited by each type particle and energy in the critical region of the coating

The approximations used in selecting 2.5 kev protons and 3 kev electrons could feasibly result in as much as a factor of two between the actual dose and the equivalent dose for simulation of a continuous energy spectrum (space) with the "mono-energetic" laboratory simulation.

- d. The accuracy to which the anticipated orbital radiation dose is known (for low energy particles).

The combination of the aforementioned three unknowns could account for a factor of 1000 or more between the proper equivalent dose and the reported measured dose. This could bring the measured 10^{16} p cm⁻² dose down to an equivalent 10^{13} p cm⁻² dose, in which case the resultant 0.20 to 0.28 degradation in the solar absorptance of Pyromark Standard White becomes very meaningful. It should also be noted that both of these samples healed appreciably when exposed to air after irradiation.

7.6 MISCELLANEOUS SPACECRAFT MATERIALS

Based on the measurements listed in Table 7-2 and the fact that both the solar cells and the microsheet could move slightly (since they were not single piece circular samples), no detectable change occurred in either of these samples due to the electron and proton irradiation to which they were exposed.

* A paper is being prepared for publication.

7.7 MYLAR

The reported reflectance measurements were obtained with the shiny side of the 14-mil Mylar facing out, with aluminized crinkled Mylar behind it. No change was detected in this material due to corpuscular radiation. The ultraviolet degradation of this material was quite severe, as noted in Figure 7-5, and did not appear to reach a degradation threshold even after 945 EUVSH. The value after 61 EUVSH was not plotted in Figure 7-5, since it is obvious from the shape of the absorption edge in the reflectance curve that the wrong specimen was under the integrating sphere, for the region of the spectrum measured with the phototube. The degradation consisted primarily of a rounding of the absorption edge out to 1.0 micron and a slight decrease in the reflectance above 1.0 micron (originally the absorption edge was rounded out to 0.7 micron). Upon exposure to air at the end of the test a large amount of healing was noted (see Figure 7-5). Virtually all the degradation above 1.0 micron was healed, and an increase in the slope of the absorption edge was also noted, although it remained rounded out to 1.0 micron.

7.8 LEXAN

The Lexan samples (one etched and one dull) were measured over polished aluminum. Lexan exhibited about the same degree of degradation as Mylar; however, it degraded faster initially and then almost leveled off after 500 EUVSH (Figures 7-6 and 7-7). The value of the etched Lexan at 61 EUVSH was not used since it is evident from the spectral reflectance curve that the wrong sample was under the integrating sphere during this measurement (based on the shape of the absorption edge).

During the measurements after 945 EUVSH, the dull Lexan sample slipped off its polished aluminum substrate, as evidenced by the spectral reflectance curve and a later visual observation; therefore, there is no data presented after 714 EUVSH for this sample. The ultraviolet degradation consisted primarily of a sloping of the absorption edge out to about 1.1 microns. Originally the absorption edge was very sharp at about .47 micron. Although it is not so obvious as in the case of Mylar, it appears that some healing occurred upon exposure of Lexan to air at the end of the test. This consisted of a slight increase in the slope of the absorption edge, so that it started falling off at 1.0 rather than 1.1 microns.

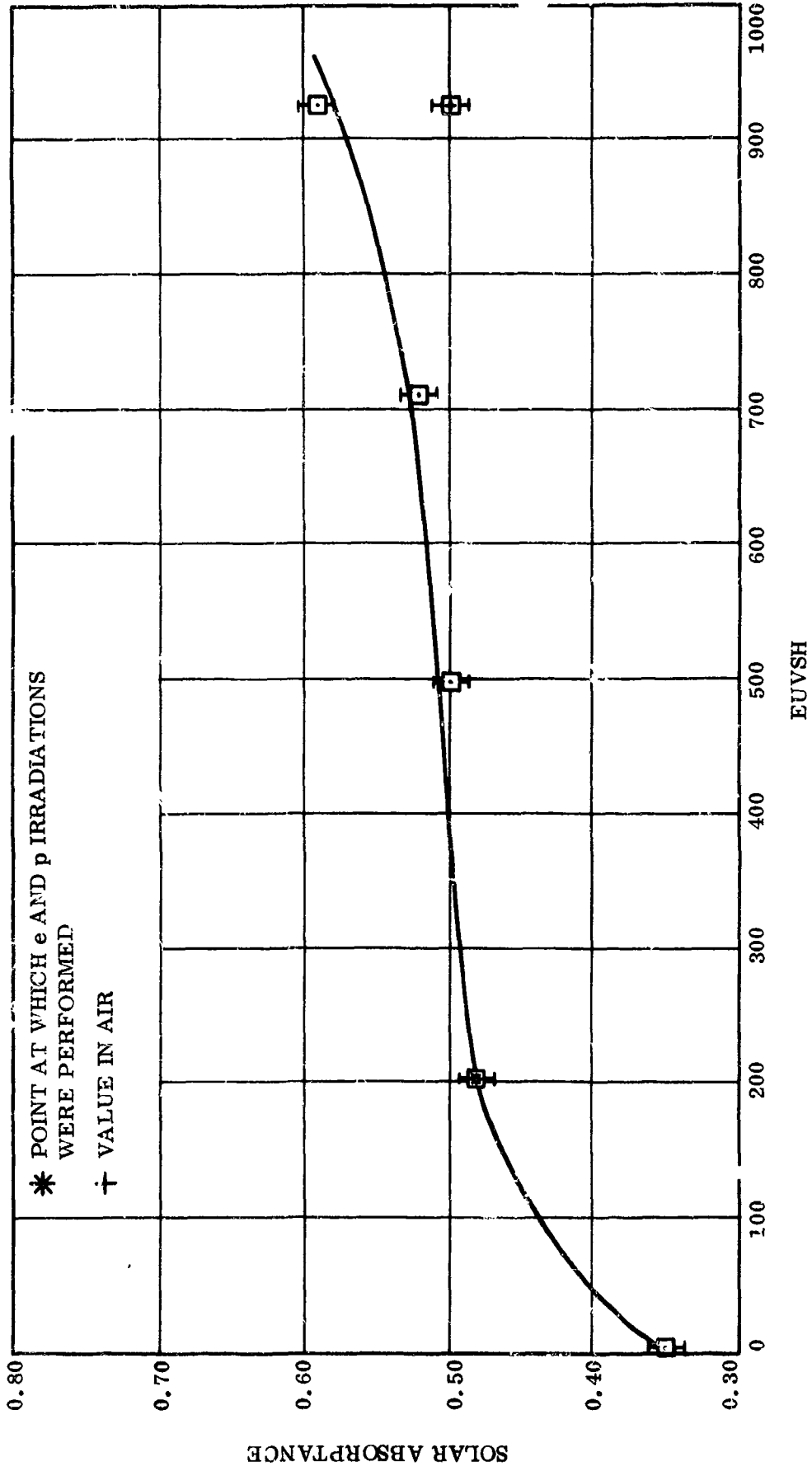


Figure 7-5. Radiation Degradation of Mylar

Although no significant change was noticed due to the corpuscular radiation after 200 EUVSH, it cannot be said that, by itself, the incident corpuscular radiation would not cause any damage (since an appreciable degradation had already occurred even after 61 EUVSH).

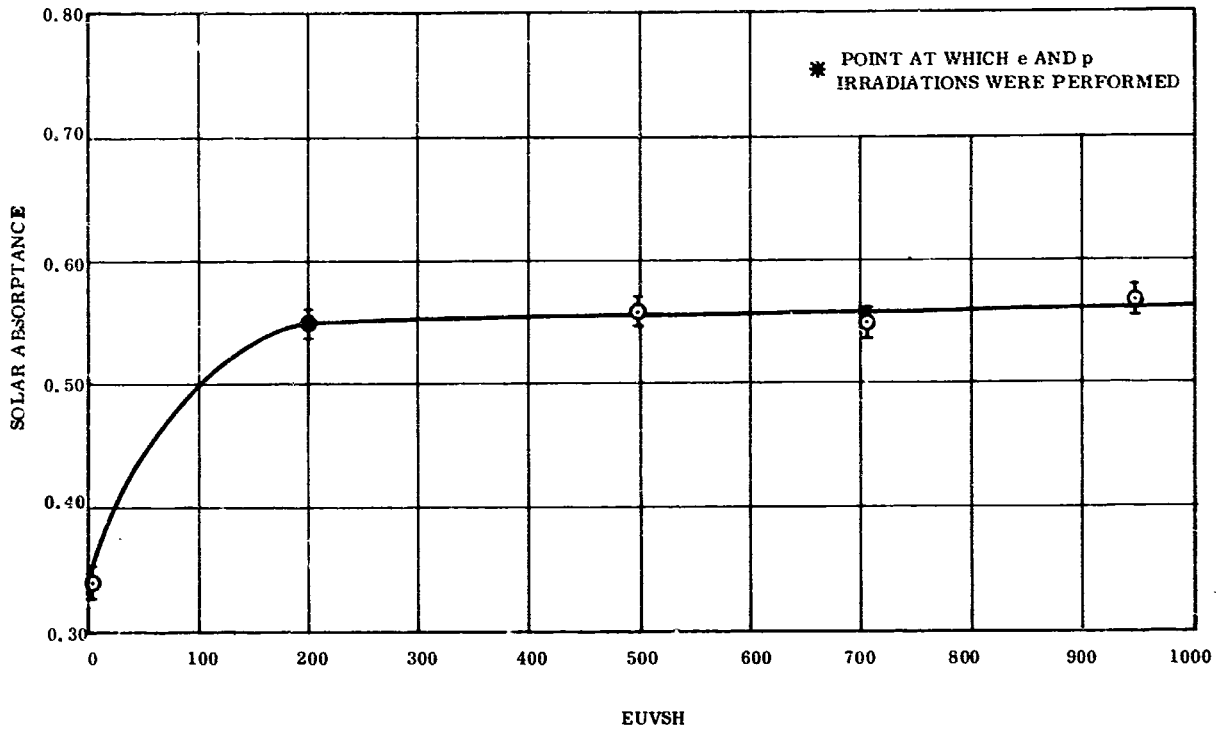


Figure 7-6. Radiation Degradation of Lexan (Etched)

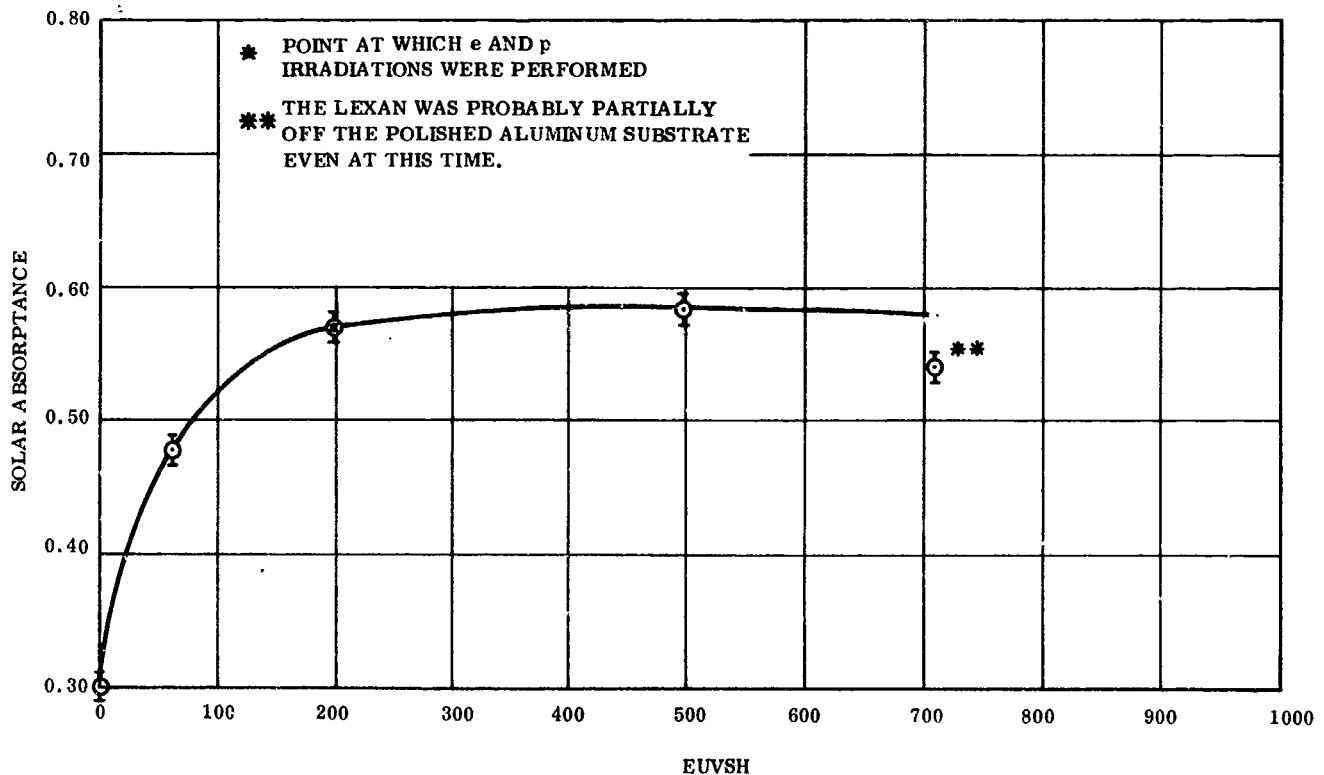


Figure 7-7. Radiation Degradation of Lexan (Dull)

SECTION 8
CONCLUSIONS AND RECOMMENDATIONS

Mylar and Lexan degrade severely and rapidly under ultraviolet radiation (over 50 percent increase in solar absorptance in 945 EUVSH). No change in solar absorptance was detected due to $5 \cdot 10^{13} \text{ e cm}^{-2}$ and $5 \cdot 10^{14} \text{ p cm}^{-2}$, with either the microsheet or the solar cells.

The change in solar absorptance of Alzak after 945 EUVSH was about 0.04 for both the 0.100 mil and the 0.175 mil samples. The electron and proton irradiation caused between a 0.01 and 0.02 change in solar absorption. The combination of corpuscular radiation with the ultraviolet did not result in a degradation which was the sum of the two separately. In fact, it appears that the corpuscular radiation may have healed some of the ultraviolet degradation.

Pyromark Standard White experienced the greatest degradation of all the white paints studied. The following conclusions and recommendations, although based on other studies, are presented since, it is believed they are essential facts which must be considered in order to decide whether or not a specific coating will be satisfactory for a particular space vehicle mission.

Virtually all correlations between ground and flight data have shown that coatings appear to degrade more in space than in the supposedly equivalent ground-based simulation. It is believed that a recent electron irradiation study performed at General Electric will help to elucidate at least a major part of this discrepancy. It has been shown, under experiment, that the change in reflectance is independent of the measured dose rate, if families of constant irradiation times rather than constant total doses are plotted. Although this experiment, in itself, is not conclusive, it reinforces the suspicion that either a space charge buildup or reaction rate limitation can explain the major discrepancy between ground and flight data. A space charge on the sample will appreciably reduce the flux incident on the sample from that measured. In addition to this uncertainty, the establishment of the dose of monoenergetic particles which should be used to properly simulate the continuous energy spectrum of

space should be experimentally and theoretically justified. Also, the definition of the space radiation environment (especially for the lower energy particles) should be better defined.

It is recommended that the measured dose rate dependence, monoenergetic simulation, and definition of the space environment, (and especially the dose rate dependence) be re-analyzed before a decision is made on which coatings should and should not be used in any mission.

SECTION 9
REFERENCES

1. Vette, J.I., Models of the Trapped Radiation Environment, Volume I: Inner Zone Protons and Electrons, NASA SP-3024, 1966.
2. Vette, J.I., Lucero, A.B., and Wright, J.A., Models of the Trapped Radiation Environment, Volume II: Inner and Outer Zone Electrons, NASA SP-3024, 1966.
3. Galbraith, T.L., paper presented at the American Geophysical Union Meeting, September 1-3, 1965.
4. "Report on an Examination of Spectral Emission Characteristics of Xenon and Mercury Xenon Short Arc Lamps," Eppley Laboratory Incorporation, July 1962; also personal communication with R. Barrett.
5. Middleton, E.E.K., and Sanders, C.L., J. Opt. Soc. Am., Vol 41, pp 419-424, 1951.
6. Sanders, C.L., and Middleton, E.E.K., J. Opt. Soc. Am., Vol 43, p 58, 1953.
7. Johnson, F.S., Satellite Environmental Handbook, Stanford University Press, 1961.

APPENDIX A FACILITY DESCRIPTION

The Combined Effects Facility (Figure A-1) simultaneously combines the radiation components of the space environment which are believed to produce the greatest changes in the optical properties of thermal control materials. The system holds thirty specimens, of which 21 can be irradiated simultaneously, each receiving various combinations of radiation. The solar absorptivity is determined from in situ reflectance measurements obtained with an integrating sphere in the vacuum system, while the total normal emittance is measured in situ with a thin film infrared detector. The specimen temperature during irradiation can be held constant or cycled between -100°F and $+350^{\circ}\text{F}$.

A.1 VACUUM AND PUMPING SYSTEM

The basic chamber is constructed of Type 304SS and has eight 2-3/4-inch feedthrough ports around the 22-inch diameter base. The bell proper has nine ports for accommodating the radiation sources, mass spectrometer, and optical windows for reflectance measurement, in addition to an access port. A rough vacuum is obtained by stage pumping with three molecular-sieve sorption pumps from atmosphere to 10^{-3} torr or less. These pumps are first baked out and desorbed to the atmosphere at approximately 150°C , then capped and chilled with liquid nitrogen for use when needed. The three sorption pumps provide two-stage pumping to approximately 1 micron with the third unit held in reserve for the bakeout period.

Sputter ion, titanium sublimation, and cryosorption pumping are used to obtain ultra high vacuum. With a 300°C bakeout, the system has been pumped down to 10^{-11} torr, as measured with a cold cathode trigger gauge. The sputter ion triode pump is rated at 500 liters/second, with no impedance between the pump and the chamber. The titanium sublimation filament used for getter pumping is rated at 5000 liters/second with a total of four filaments which can be used sequentially. The cryosorption pumping is performed by an inner aluminum cylindrical shroud, cooled with liquid nitrogen and having a low-emissivity outer surface and a carbon-black anodized inner surface. Electrophoretically deposited carbon was used to avoid problems associated with sublimation of organic coatings at high temperatures.

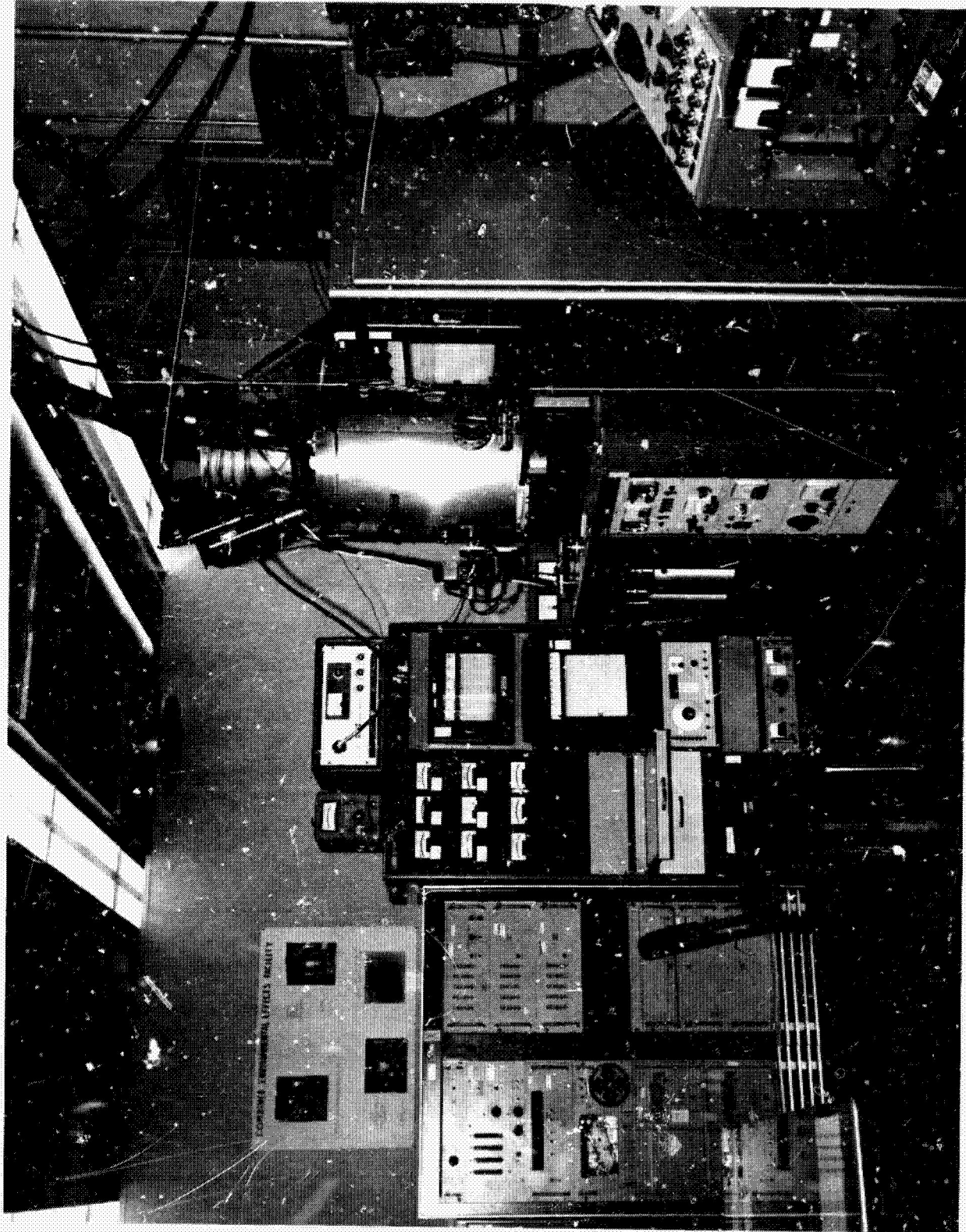


Figure A-1. Combined Effects Facility

This type of pumping system, coupled with close attention to construction materials (such as all-metal seals to eliminate organic outgassing contamination), produces an extremely clean oil-free system, which is needed to perform a valid evaluation of control coatings.

A.2 IRRADIATION SOURCES

A.2.1 NEAR ULTRAVIOLET RADIATION

Near ultraviolet radiation is produced with a high pressure mercury xenon arc lamp (either 2.5 or 5 kw, depending on the desired intensity). The lamp is mounted in a water-cooled housing (Figure A-2) and is cooled with a gaseous nitrogen flow, which also helps to reduce the ozone buildup in the housing. A front surface aluminized spherical reflector is used to increase the lamp output, which is projected through the 6-inch quartz window in the top of the chamber. The intensity on the sample plane can be varied from 1 to 6 EUVS*.

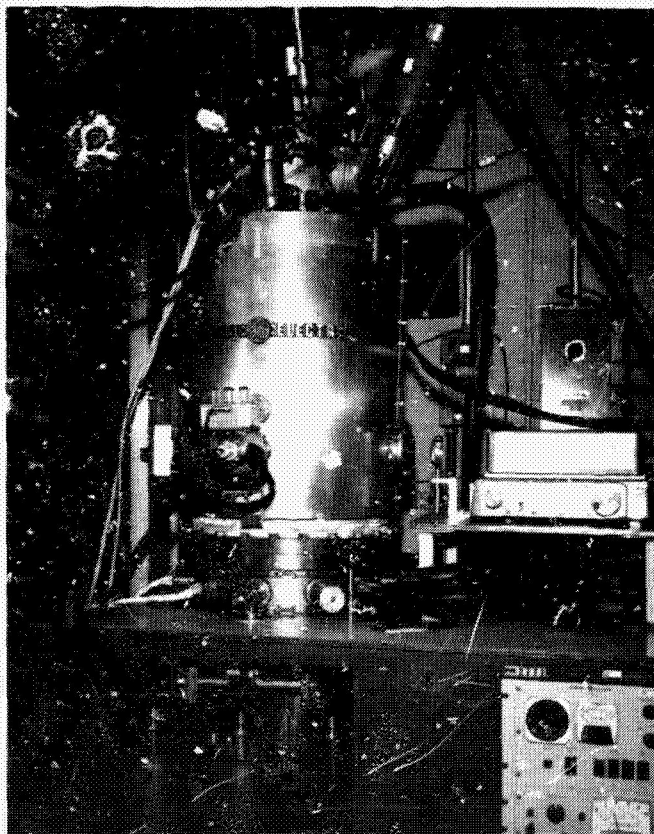


Figure A-2. Irradiation Sources

*Equivalent Ultraviolet Suns, defined as the total integrated energy below 400 millimicrons at zero air mass, as defined by the Johnson curve (Reference A-1). The reason the intensity is defined by the 400 millimicron cutoff is that, in general, photons with wavelengths longer than this do not have sufficient energy to cause degradation (Reference A-2).

The HgXe lamp was chosen as the ultraviolet source for a number of reasons:

- a. It produces a relatively continuous spectrum, due to the high pressure band broadening and xenon component.
- b. It has a sufficient amount of energy in the visible to preclude the possibility that photolytic healing would occur in space but not under simulation
- c. It combines a rich source of ultraviolet with long lamp life and troublefree operation.

A.2.2 FAR ULTRAVIOLET IRRADIATIONS

Far ultraviolet irradiations are performed with a hydrogen lamp designed and built in the Missile and Space Division of General Electric. The spectral irradiance of this lamp is between 1100 and 2000 Angstroms, and produces an intensity of about 5 suns in that wavelength region, at the sample plane. The lamp is composed of a Pyrex tube mounted in a stainless steel flange with a lithium fluoride window sealed to the end. The spectrum is produced by energizing the hydrogen with a microwave generator and initiating the discharge with a Tesla coil. When used, this source replaces either the electron or the proton gun.

Although the total energy in the electromagnetic spectrum between 1100 and 2000 Å is small, it is still important to simulate, since it may cause reactions which will not occur with near ultraviolet irradiation. This is because a 2000 Å photon can only cause reactions which require less than 6 ev directly, whereas an 1100 Å photon can directly cause reactions requiring up to almost 11 ev.

A.2.3 THE PROTON IRRADIATIONS

The proton irradiations can be performed at energies up to 5 kev. The proton gun (Figure A-2) ionizes hydrogen, admitted into the source through a palladium leak, with an rf oscillator. These protons are then accelerated through an orifice with a high voltage power supply. The average proton flux at the sample plane is 8.10^{12} protons $\text{cm}^{-2} \text{sec}^{-1}$ at an energy of 2.5 kev. The proton flux approximately doubles with each 1000-volt increment, from about 1.0 kev. In comparison to other positive ion sources, the rf ion source has the important feature of a high ratio of atomic hydrogen ions to molecules. Two factors contribute to this

figure of merit: (1) low atomic recombination rate and (2) ion focusing at the canal entrance. Low atomic recombination is achieved by the choice of materials inside the plasma region; the discharge vessel is Pyrex glass, all electrodes are aluminum, and the probe insulator is sapphire. The purpose of the probe electrode insulator is to shape the plasma boundary; thus, the "emitted ions" are effectively focused into the canal entrance.

A.2.4 LOW ENERGY ELECTRON IRRADIATIONS

Low energy electron irradiations are performed with the electron gun shown in Figure A-2. This assembly has 300 milliampere and 20 keV capability. The beam assembly is composed of a filament, bias cup, X-Y deflection coils, and beam focusing coils. The electron flux of 3 keV electrons at the sample plane is nominally 6×10^{12} electrons $\text{cm}^{-2} \text{sec}^{-1}$.

A.3 TURNTABLE SYSTEM

The turntable (Figures A-3, A-4, and A-5) accommodates thirty samples simultaneously. The specimens are 0.906 inch in diameter and 0.063 inch thick and are held in contact with the rotating heat exchange block by spring clips. The turntable is composed of two sections: one which is stationary and used for support and establishing a heat sink at the lowest specimen temperature, and the other for rotating the specimens in and out of irradiation and optical property measurement zones, as well as for maintaining the desired specimen temperatures. The segment heater sections make it possible to obtain five different irradiation temperatures simultaneously on each of six specimens. The hollow drive shaft provides more than adequate accommodations for specimen temperature and radiation sensor leads. This design combines faster and more economical irradiation with greater thermal control and monitoring capability. The split table concept, stationary and rotating sections, provides reliability through simplicity, and is ideal for incorporation with an integrating sphere and emissometer for in situ optical property measurements, as well as a number of other important in situ property measurements.

A.4 REFERENCES

A-1 Johnson, F.S., Satellite Environmental Handbook, Stanford University Press, 1961.

A-2 Schexnayder, C.J., Jr., "Tabulated Values of Bond Dissociation Energy, Ionization Potentials, and Electron Affinities for Some Molecules Found in High-Temperature Reactions," NASA Technical Note D-1791, May 1963.

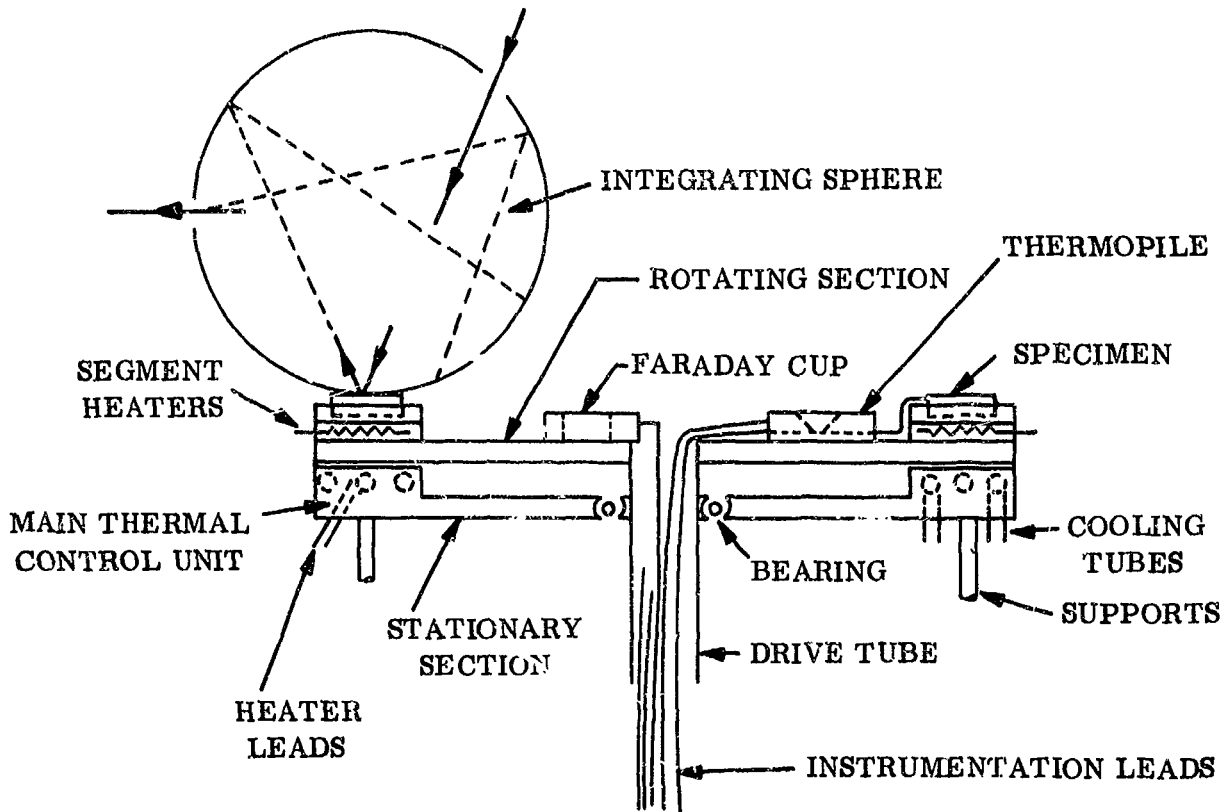


Figure A-3. Turntable Configuration, Side View

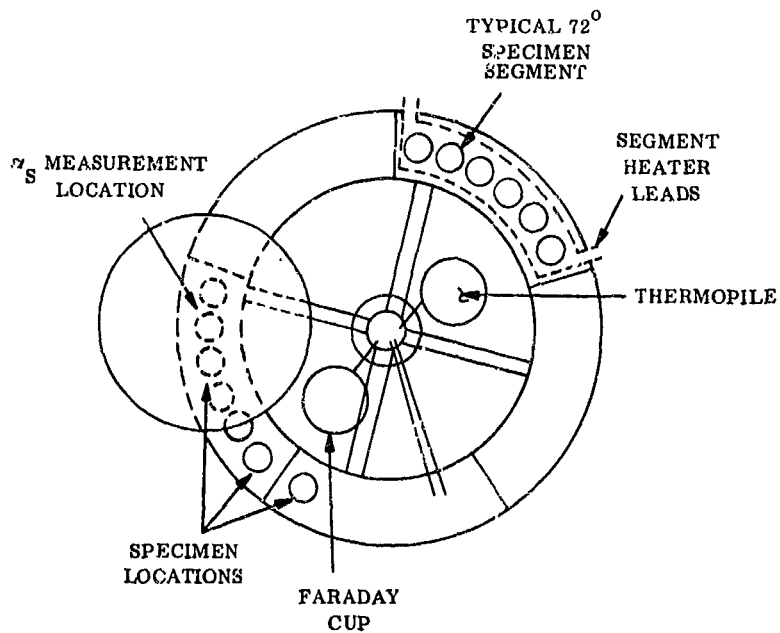


Figure A-4. Turntable Configuration, Top View

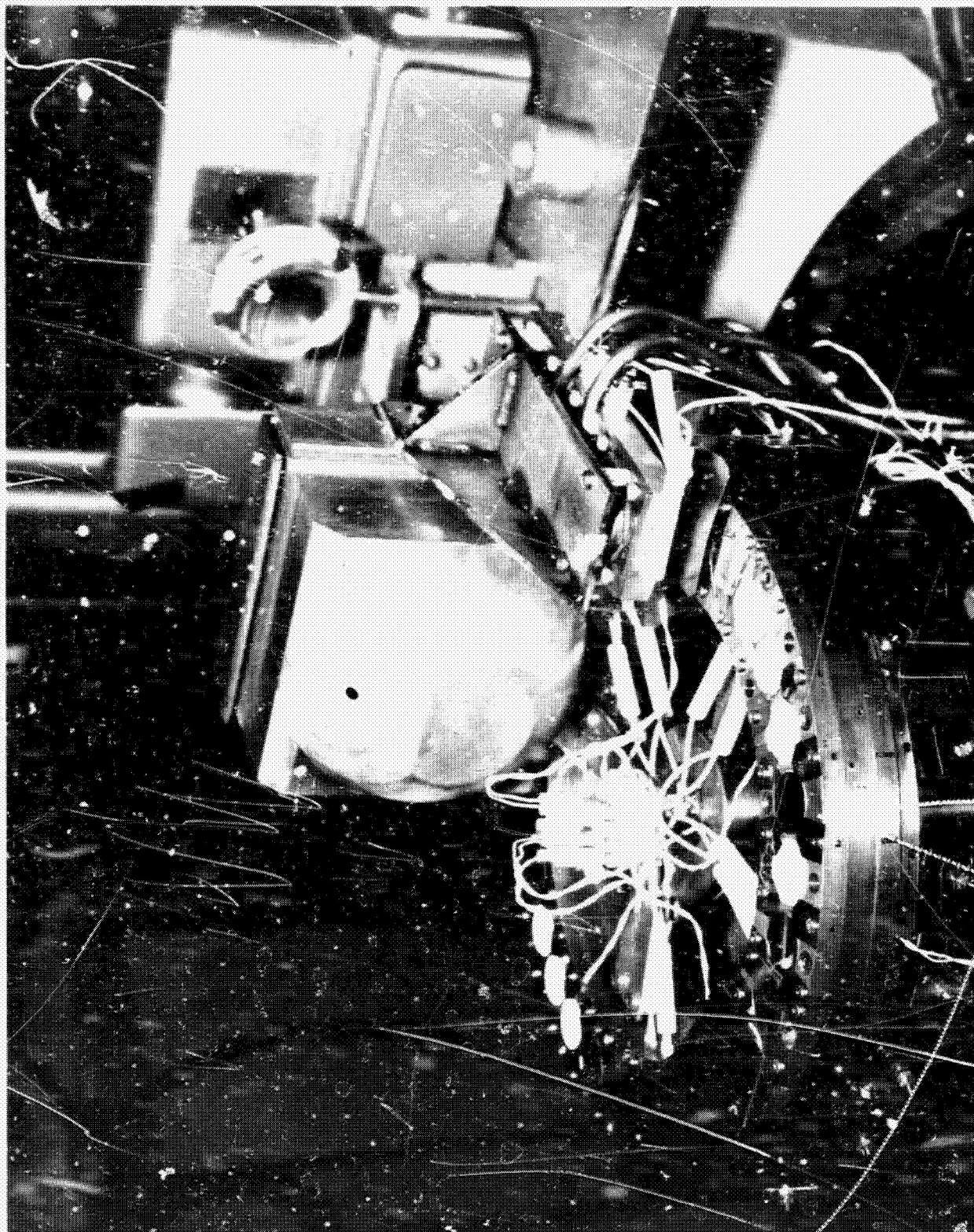


Figure A-5. Photograph of Turntable

APPENDIX B
IN SITU EMISSOMETER DESIGN, CALIBRATION, AND USE

The total in situ emissometer is composed of two main parts: detectors and reference source. The total emittance is determined by a comparative technique with one detector positioned over the specimen, while the other one is over a reference body. The infrared detectors used are vapor deposited onto a thin plastic film. A V-grooved reference body is used to minimize errors due to shifts in the reference source.

The detectors were correlated against each other as a function substrate temperature while observing the same infrared source, but were not tested before use against known standards because of scheduling difficulties. When used in the actual test the results were not reproducible and did not produce results which corresponded to the known emittance values of the samples measured. Since correction of this problem, regardless of its cause, would have required the vacuum system to be opened (a time consuming operation after evacuation), the emittance measurements were discontinued.

B.1 EMISSOMETER DESIGN AND OPERATION

The total emittance is measured with an emissometer composed of two thin film 17 junction tellurium-gold IR detectors, made at the Missile and Space Division of General Electric. The two IR detectors have the same sensitivity (except for some small variation, $k(T)$, which is a function of the specular distribution of the incident flux and the reference junction), and are mounted in the same temperature controlled housing. One looks at the specimen to be measured while the other looks at a blackbody reference held at the same temperature as the sample being measured. Since both detectors and radiators are in identical situations (temperature, solid angle subtended, etc.), the total normal emittance of the specimen is given simply by:

$$\epsilon(T) = \frac{V_x}{V_r} k(T) \quad (B-1)$$

where:

$\epsilon(T)$ is the total emittance at temperature T ,

V_x and V_r are the outputs of the IR detectors over the specimen and black body reference respectively,

and:

$k(T)$ is the correction factor for the dissimilarity between the two IR detectors at a reference junction temperature T and a specimen temperature obtained from the correlation chart.

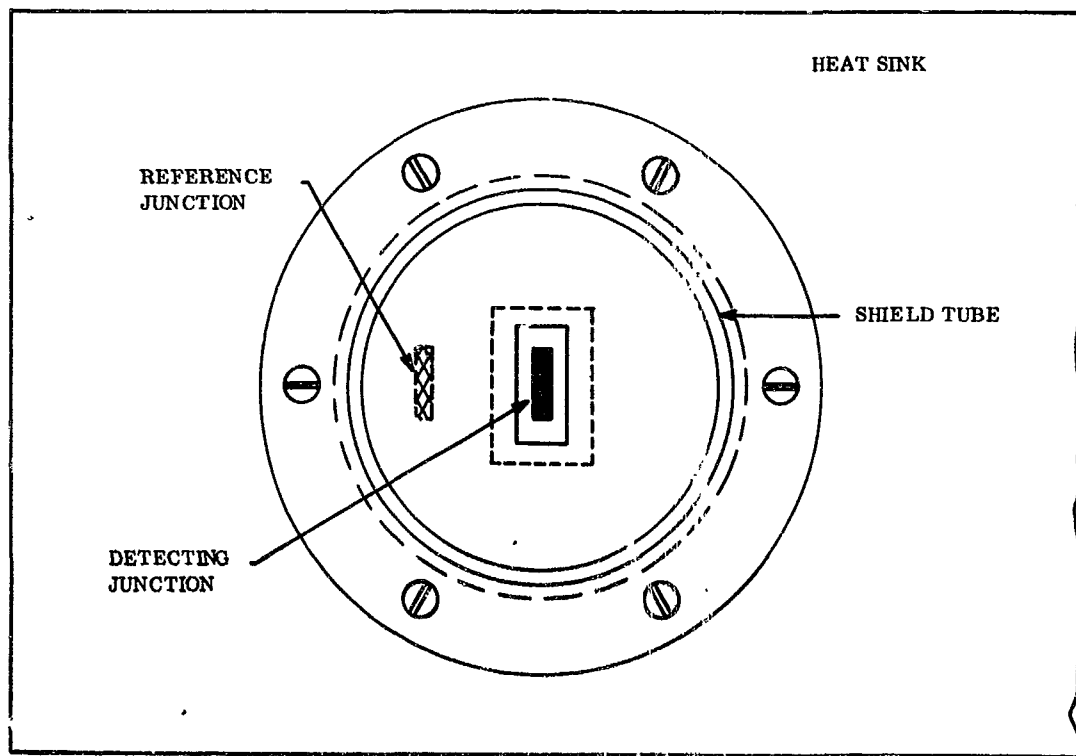
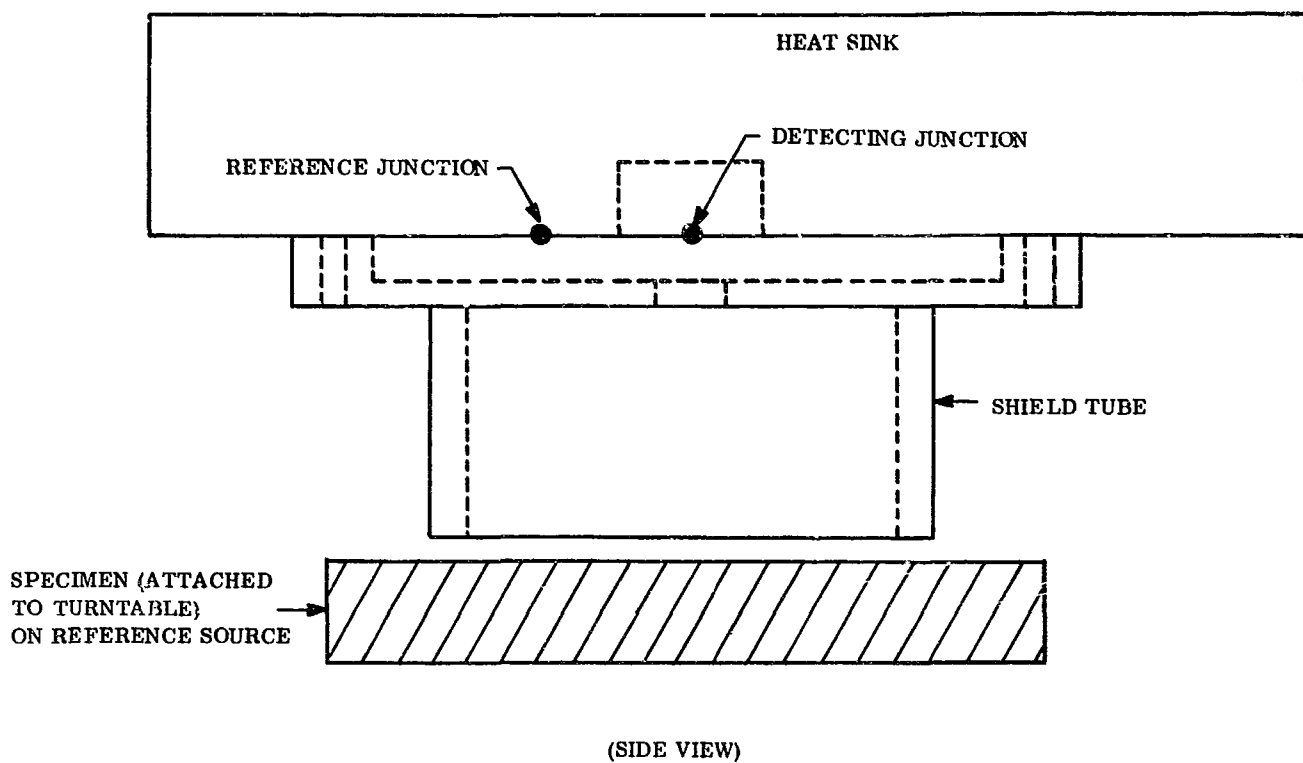
The correction factor $k(T)$ is obtained by dividing the output of the detector usually positioned over the black body reference by that of the detector normally over the specimen when they are in identical positions over the same radiator. If for each reference junction temperature this measurement is performed as a function of specimen temperature the resulting temperature dependent correction factor $k(T)$ is obtained. This correction factor will be good for all materials which are approximately gray bodies (that is, a material whose emitted energy has about the same specular distribution as a black body at the same temperature).

B. 2 DETECTOR ELEMENT FABRICATION AND INSTALLATION

The 17-junction tellurium-gold detectors are each composed of two sets of junctions. The set which views the specimen or reference source is placed over a hole in the heat sink plate (Figure B-1), while the other set is attached thermally to the heat sink plate. A shield tube is then placed over the set of detector junctions which views the sample, so that other than the sample or reference source, they see only liquid nitrogen-cooled surfaces.

B. 3 REFERENCE SOURCE DESIGN AND POSITIONING

A V-grooved reference source is used to minimize changes in its apparent emissivity due to changes which may occur to the emissivity of the coating used on its surface. The source material selected was sulfuric acid anodized aluminum prepared the same as Specimen Number 65 in Reference B-1. This produced an actual surface emittance of



VIEW FROM SAMPLE SIDE WITH SAMPLE REMOVED

Figure B-1. Schematic of One-Detector Assembly

0.71 when measured as described in Appendix F. The reference source was composed of a number of 0.125-inch thick sheets of aluminum which were machined, polished, anodized and assembled, as shown in Figure B-2. The anodize process was selected as a compromise between high emittance and freedom of outgassing condensables, when in thermal vacuum. By machining each "blade" separately the problem associated with having a "flat" at the bottom of the V-groove, rather than a sharp angle, was eliminated. Based on Figure B-3, from Reference B-2, the apparent emissivity of the resulting reference source was 0.97. As can be seen in Figure B-3, even large changes in the surface emissivity of the blades cause only small changes in the apparent emissivity of the reference source. This source was then mounted under one of the infrared detectors as shown in Figure B-4. During measurement the reference source is maintained at the same temperature as the sample which is positioned under the other infrared detector.

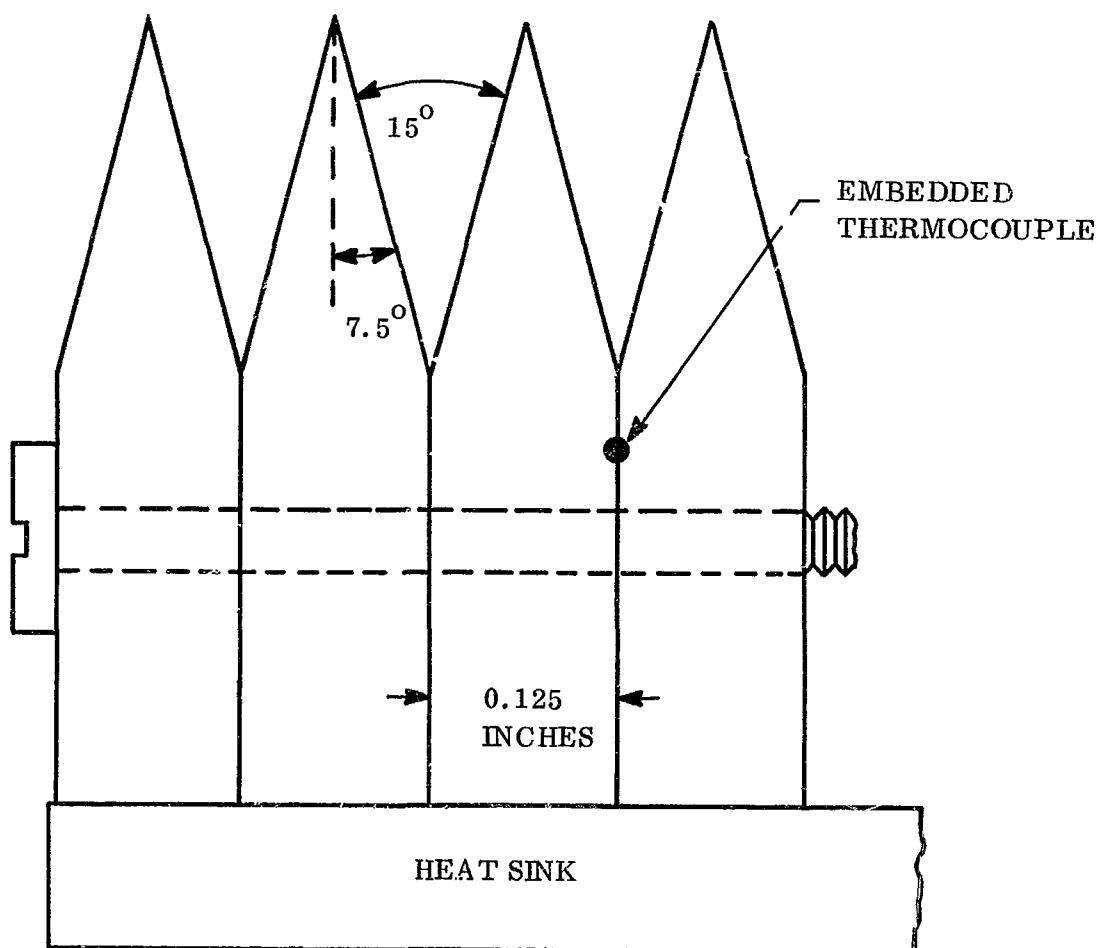


Figure B-2. Assembly of Reference Source

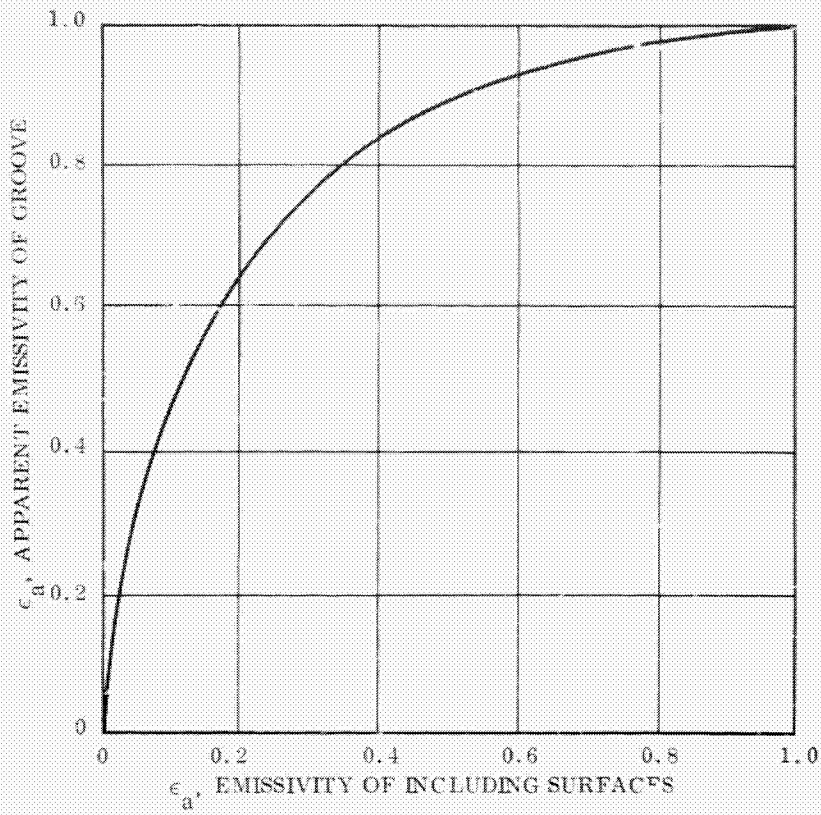


Figure B-3. Variation of Apparent Emissivity with Surface Emissivity at a 15° Included Angle

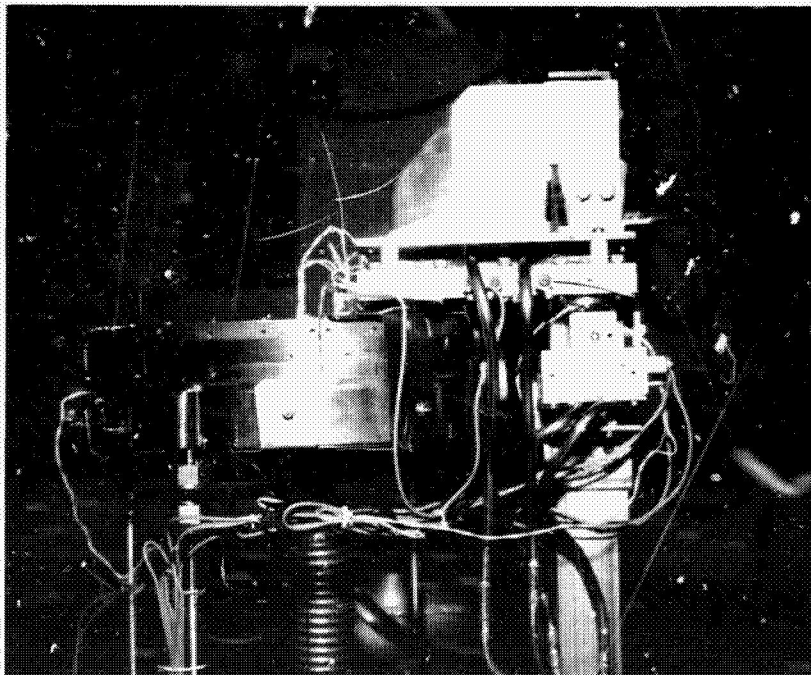


Figure B-4. Emissometer, Reference Source and Sample in Measurement Position

B. 4 CORRELATION MEASUREMENTS AS A FUNCTION OF TEMPERATURE

The emissometer was placed over a gray body whose temperature was the same under each infrared detector. The millivolt output of each detector was then measured as a function of the gray body temperature, while the emissometer heat sink temperature (the same as the temperature of the reference junctions) was held constant at -250°F (161°K). Figure B-5 is the plot resulting from this correlation measurement.

To obtain $k(T)$ for Equation B-1, from Figure B-5, the output of the reference source detector is divided by that of the specimen detector at whatever temperature the specimen and reference body are being measured.

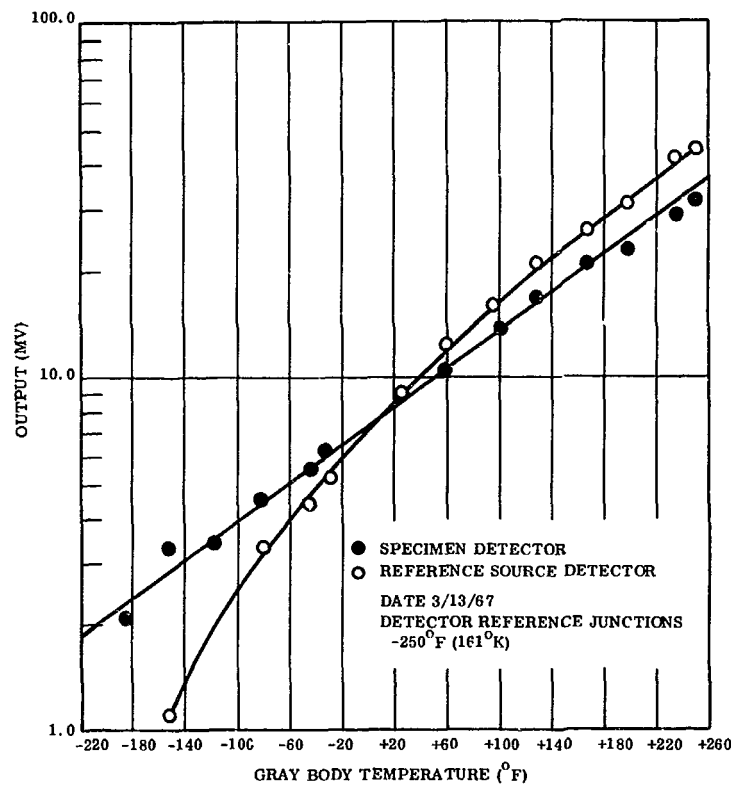


Figure B-5. Infrared Detector Correlation

B. 5 EMITTANCE MEASUREMENTS AND ANALYSIS

The first in situ emittance measurements performed were on a 0.175-mil Alzak coating as a function of temperature. The data obtained is listed in Table B-1. The computed emittance for this table was obtained according to Equation B-1, except that the resultant value was multiplied by 0.97 to account for the fact that our reference source was not a true black body.

Table B-1. Emittance of Alzak In Situ as a Function of Temperature

Temperature (°F)	Detector Outputs (mv)		k(T)	Computed Emittance
	Specimen	Reference Source		
-88	3.8	3.4	0.70	0.76
-58	3.2	3.0	0.80	0.83
-35	5.2	3.7	0.88	1.2
-10	5.0	4.5	0.94	1.0
+15	5.5	5.0	1.0	1.1
+40	6.7	7.0	1.1	1.0
+68	9.4	8.2	1.1	1.2

Tables B-2 and B-3 list the detector outputs for measurements of the specimens made in vacuum before irradiation. The k(T) for these tables was obtained from Figure B-5. The computed emittance shown in these tables was obtained the same way as that shown in Table B-1.

The values of the computed emittance in Table B-1, B-2, and B-3 immediately indicate two problems: (1) there are emittance values greater than 1, a physically impossible situation and (2) the reproducibility of the measured value is inconsistent for the same material, even when measured on the same day at the same temperature.

The source of the first problem, computed emittance of greater than 1, is probably caused by inaccuracies in the computed apparent emittance of the reference source. This problem in itself is not grave, since it can either be calibrated out or the device can be used on a comparative basis.

The source of the second problem is probably due to instability in the temperature of the reference source blades and/or the detector reference junctions. This is obvious from the variations seen in the reference source detector output, while it is supposedly at a constant temperature. These variations were probably the result of two items: (1) the control thermocouple could not be located at the detector reference junctions in the emissometer or on the emitting surfaces of the reference source and (2) the temperature was maintained with an on/off controller which alternated between opening a liquid nitrogen valve and powering infrared radiant heaters. No attempt was made to rectify either of these problems since that would have resulted in an unacceptable slip in schedule.

Table B-2. Emittance of Specimens In Situ Before Irradiation at -65°F

Specimen	Specimen Number	Detector Output (mv)		Computed Emittance
		Specimen	Reference Source	
Goddard White	27	5.8	3.3	1.4
	27	4.2	2.7	1.2
	2	5.0	3.5	1.1
	2	5.0	3.0	1.3
RTV-602 White	28	4.5	3.4	1.0
	28	4.3	2.8	1.2
	3	5.4	3.1	1.3
	3	5.2	3.0	1.3
Pyromark Standard White	29	5.1	3.4	1.2
	29	5.0	2.8	1.4
	4	3.7	3.0	0.92
	4	3.9	3.0	1.0
Alzak (t_1)	5	5.3	2.9	1.4
	5	5.4	3.0	1.4
	30	5.1	3.4	1.2
	30	4.9	2.9	1.3
	21	5.0	3.4	1.2
	21	5.0	2.8	1.4
Alzak	1	5.0	3.4	1.2
	1	5.0	2.8	1.4
	6	5.0	2.8	1.4
	6	5.0	3.0	1.3
	26	5.0	2.8	1.4
	26	5.0	3.0	1.3
	17	5.8	3.3	1.4
	17	4.2	2.7	1.2
	19	5.1	3.4	1.2
	19	5.0	2.8	1.4
23	5.4	3.1	1.3	
23	5.2	3.0	1.3	

Table B-3. Emittance of Specimens In Situ Before Irradiation at -80°F

Specimen	Specimen Number	Detector Outputs (mv)		Computed Emittance
		Specimen	Reference Source	
Pyromark Standard White	29	3.2	5.0	0.46
	4	3.0	4.0	0.54
	9	3.2	5.5	0.41
Alzak (t_1)	30	2.8	3.4	0.59
	5	2.6	2.7	0.69
	15	2.8	4.8	0.41
Alzak	1	2.5	3.8	0.47
	6	2.9	3.5	0.59
	7	3.0	3.6	0.59
	12	3.2	4.0	0.57
	13	3.1	4.8	0.47
	17	3.0	4.1	0.52
Goddard White	19	3.2	3.9	0.59
	2	3.0	4.0	0.54
	8	3.2	4.0	0.57
RTV-602 White	11	3.0	4.2	0.51
	3	3.0	4.0	0.54
	10	3.0	3.6	0.59

REFERENCES

- B-1. Janssen, J.E., Torborg, R.H., Luck, J.R., and Schmidt, R.N., "Normal Spectral Reflectance of Anodized Coatings on Aluminum, Magnesium, Titanium, and Beryllium, ASD Technical Report 61-147, September 1961.
- B-2. Psarounakis, J., "Apparent Thermal Emissivity from Surfaces with Multiple V-Shaped Grooves, " AIAA Journal, Vol 1, No. 8, August 1963.

APPENDIX C

EXAMPLE OF SMOOTHING AND CORRECTION TECHNIQUE

The smoothing consists of drawing the most probable line through the computer plotted spectral reflectance curve as shown in Figure C-1. This consists of splitting the neighboring high and low points and following the smooth points to produce a curve with a small rate of change in slope (except at the absorption edge). The 7094 computer is then used to determine the corrections required for each interval in which the hand drawn curve is appreciably different than the computer plotted spectral reflectance. Table C-1 is a copy of the 7094 output for the curve shown in Figure C-1.

The symbols at the top of Table C-1 are the same as those given in Section 5, except that in Section 5:

$$J(\lambda_i) = \frac{E(\lambda_i)}{\sum_{i=1}^{54} E(\lambda_i)} \quad (C-1)$$

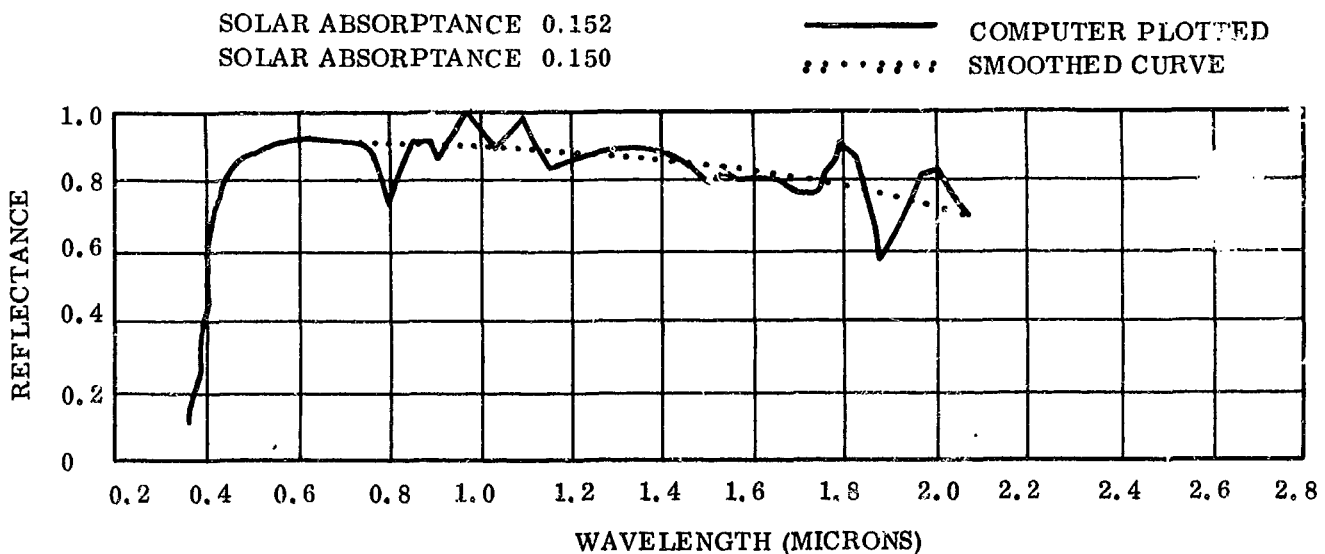


Figure C-1. Reflectance Curve of RTV 602 Run 51667-3

Table C-1. 7094 Output

RTV 602 5X10E14P 5X10E13E 500EUVSH IN VAC -55F 5-16-63

i	λ_i	$R_x(\lambda_i)$	$R_B(\lambda_i)$	$R_T(\lambda_i)$	$R_S(\lambda_i)$	$R_C(\lambda_i)$	$R_Z(\lambda_i)$	$R_I(\lambda_i)$	$E(\lambda_i)$
NO.	LAMBDA	REFLECTANCE	SOLAR RFL.	TEST SAMPLE	MG O SAMPLE	ZERO READING	MG O STANDARD	ENERGY IN REGION	
1	0.363	0.09181	0.00061	41.00000	60.00000	39.00000	0.96400	0.59000	
2	0.370	0.17012	0.00122	44.00000	72.00000	38.00000	0.96450	0.64000	
3	0.377	0.20083	0.00149	48.00000	86.00000	38.00000	0.96500	0.66000	
4	0.385	0.22594	0.00178	53.00000	102.00000	38.00000	0.96570	0.70000	
5	0.392	0.2772	0.00241	74.00000	130.00000	38.00000	0.96640	0.75000	
6	0.400	0.34627	0.00454	106.00000	158.00000	38.00000	0.96700	0.77000	
7	0.408	0.44811	0.00735	155.00000	213.00000	36.00000	0.96770	1.01000	
8	0.416	0.58392	0.00795	207.00000	292.00000	36.00000	0.96850	1.10000	
9	0.424	0.78754	0.00990	277.00000	331.00000	36.00000	0.97000	1.12000	
10	0.428	0.72934	0.00409	130.00000	167.00000	15.00000	0.97000	0.50000	
11	0.432	0.78924	0.00461	155.00000	186.00000	15.00000	0.97000	0.52000	
12	0.441	0.81086	0.01147	451.00000	529.00000	38.00000	0.97000	1.26000	
13	0.450	0.83785	0.01279	578.00000	659.00000	40.00000	0.97000	1.36000	
14	0.461	0.84273	0.01646	731.00000	830.00000	43.00000	0.97270	1.74000	
15	0.472	0.86096	0.01624	935.00000	1042.00000	41.00000	0.97330	1.68000	
16	0.486	0.87981	0.02193	1201.00000	1312.00000	41.00000	0.97370	2.22000	
17	0.500	0.88527	0.02047	1515.00000	1646.00000	42.00000	0.97400	2.06000	
18	0.515	0.89386	0.02107	1892.00000	2037.00000	44.00000	0.97400	2.10000	
19	0.530	0.89099	0.02000	2327.00000	2514.00000	45.00000	0.97400	2.00000	
20	0.546	0.80654	0.02381	2806.00000	2981.00000	45.00000	0.97370	2.34000	
21	0.555	0.90625	0.01282	1292.00000	1373.00000	21.00000	0.97360	1.26000	
22	0.564	0.91330	0.01189	1449.00000	1449.00000	23.00000	0.97300	1.16000	
23	0.585	0.91766	0.02926	3404.00000	3573.00000	59.00000	0.97250	2.84000	
24	0.606	0.92867	0.02836	3292.00000	3415.00000	59.00000	0.97150	2.72000	
25	0.630	0.92642	0.03099	2770.00000	2880.00000	58.00000	0.97050	2.98000	
26	0.658	0.92258	0.03480	1853.00000	1934.00000	49.00000	0.96900	3.36000	
27	0.688	0.91867	0.03424	956.00000	1001.00000	44.00000	0.96750	3.52000	
28	0.723	0.91494	0.03615	412.00000	432.00000	39.00000	0.96580	3.52000	
29	0.763	0.89731	0.03717	187.00000	198.00000	39.00000	0.96400	3.69000	
30	0.808	0.87200	0.02768	104.00000	127.00000	35.00000	0.96250	3.41000	
31	0.860	0.91044	0.04272	102.00000	106.00000	34.00000	0.96080	4.18000	
32	0.887	0.90891	0.01877	45.00000	45.00000	10.00000	0.96000	1.84000	
33	0.914	0.86071	0.01662	39.00000	42.00000	14.00000	0.95940	1.72000	
34	0.970	1.00156	0.03643	105.00000	102.00000	25.00000	0.95800	1.24000	
35	1.030	0.87715	0.03013	123.00000	133.00000	22.00000	0.95700	3.06000	
36	1.094	0.97224	0.03394	155.00000	154.00000	37.00000	0.95600	3.11000	
37	1.150	0.83103	0.02415	154.00000	184.00000	39.00000	0.95480	2.59000	
38	1.223	0.87108	0.02425	132.00000	204.00000	38.00000	0.95350	2.48000	
39	1.298	0.88411	0.02193	205.00000	220.00000	39.00000	0.95200	2.21000	
40	1.368	0.88584	0.01810	208.00000	223.00000	38.00000	0.95000	1.82000	
41	1.434	0.86703	0.01499	159.00000	206.00000	37.00000	0.95000	1.54000	
42	1.502	0.78594	0.01262	160.00000	189.00000	32.00000	0.95150	1.43000	
43	1.537	0.81940	0.00580	4.00000	73.00000	13.00000	0.95100	0.63000	
44	1.572	0.80061	0.00566	34.00000	74.00000	15.00000	0.95050	0.63000	
45	1.638	0.71619	0.00953	155.00000	174.00000	28.00000	0.94950	1.04000	
46	1.692	0.75827	0.00664	160.00000	195.00000	31.00000	0.94900	0.78000	
47	1.743	0.76498	0.00541	136.00000	188.00000	33.00000	0.94820	0.63000	
48	1.788	0.91087	0.00552	155.00000	162.00000	35.00000	0.94700	0.54000	
49	1.832	0.86128	0.00445	144.00000	157.00000	35.00000	0.94450	0.46000	
50	1.880	0.57682	0.00311	107.00000	156.00000	34.00000	0.94150	0.48000	
51	1.920	0.67102	0.00271	102.00000	133.00000	31.00000	0.94100	0.36000	
52	1.964	0.80768	0.00335	99.00000	111.00000	27.00000	0.94170	0.37000	
53	2.012	0.82629	0.00362	93.00000	104.00000	27.00000	0.94200	0.39000	
54	2.065	0.70446	0.00361	34.00000	41.00000	15.00000	0.94200	0.38000	

TOTAL SOLAR ABSORPTIVITY = 0.415298

The smoothing correction is made by determining the change in reflectance, $\Delta R_x(\lambda_i)$ (this can be either positive or negative), and the corresponding change in solar reflectance, $\Delta R_s(\lambda_i)$, for each wavelength interval requiring correction. According to Section 5 this is given by:

$$\Delta R_s(\lambda_i) = \frac{\Delta R_x(\lambda_i)}{R_x(\lambda_i)} R_s(\lambda_i) \quad (C-2)$$

for $R_s(\lambda_i) \neq 0$.

If $R_x(\lambda_i)$ is zero, then the correction must be made according to:

$$\Delta R_s(\lambda_i) = \Delta R_x(\lambda_i) J(\lambda_i) \quad (C-3)$$

The correction to the fractional solar absorptance is then given by:

$$\Delta \alpha_s = - \sum_{i=1}^{54} \Delta R_s(\lambda_i), \quad (C-4)$$

where the minus sign converts from differential solar reflectance to differential solar absorptance. Table C-2 lists the wavelength increments, the computed reflectance, the computed solar reflectance and the differential corrections required for reflectance and solar reflectance in each wavelength increment, based on Figure C-1 and Table C-1. This correction is only for smoothing the curve. As can be seen in Table C-2, the net correction in total solar absorptance from smoothing this curve is -0.002, which does not change the value of the solar absorptance when rounded off to two decimal places. Tables 7-1 and 7-2 list the smoothed value of the solar absorptance; therefore, 0.15 appears in Table 7-2 for RTV-602 Sample 3 after 500 EUVSH. Note that there is no value in parentheses, since the solar absorptance when rounded off to two decimal places did not change due to smoothing of this curve.

Table C-2. Corrected 7094 Output for RTV-602 Run 51667-3

Wavelength (i)	Reflectance $R(\lambda_i)$	Differential Reflectance $\Delta R(\lambda_i)$	Solar Reflectance $R_x(\lambda_i)$	Differential Solar Reflectance $\Delta R_x(\lambda_i)$
0.363	0.092	-	0.001	-
0.370	0.170	-	0.001	-
0.377	0.201	-	0.001	-
0.385	0.226	-	0.002	-
0.392	0.377	-	0.002	-
0.400	0.546	-	0.005	-
0.408	0.648	-	0.007	-
0.416	0.644	-	0.008	-
0.424	0.788	-	0.010	-
0.428	0.729	-	0.004	-
0.432	0.789	-	0.005	-
0.441	0.811	-	0.011	-
0.450	0.838	-	0.013	-
0.461	0.843	-	0.016	-
0.472	0.861	-	0.016	-
0.486	0.880	-	0.022	-
0.500	0.885	-	0.020	-
0.515	0.894	-	0.021	-
0.550	0.891	-	0.020	-
0.546	0.907	-	0.024	-
0.555	0.906	-	0.013	-
0.564	0.913	-	0.012	-
0.585	0.918	-	0.030	-
0.606	0.929	-	0.028	-
0.630	0.926	-	0.031	-
0.658	0.923	-	0.035	-
0.688	0.919	-	0.034	-
0.723	0.915	-	0.036	-
0.763	0.897	-	0.037	-
0.808	0.723	+ .18	0.028	+ .0069
0.860	0.910	-	0.043	-
0.887	0.909	-	0.019	-
0.914	0.861	+ .04	0.017	+ .0008
0.970	1.002	- .12	0.036	- .0044
1.030	0.877	-	0.030	-
1.094	0.972	- .09	0.034	- .0031
1.150	0.831	+ .05	0.024	+ .0015
1.228	0.871	+ .01	0.024	+ .0003
1.298	0.884	-	0.022	-
1.368	0.886	-	0.018	-
1.434	0.867	-	0.015	-
1.502	0.786	+ .02	0.013	+ .0003
1.537	0.819	-	0.006	-
1.572	0.801	-	0.006	-
1.638	0.816	-	0.010	-
1.692	0.758	+ .05	0.007	+ .0004
1.743	0.765	+ .03	0.005	+ .0002
1.788	0.911	- .12	0.006	- .0007
1.832	0.861	- .09	0.004	- .0005
1.880	0.577	+ .18	0.003	+ .0010
1.920	0.671	+ .07	0.003	+ .0003
1.964	0.808	- .06	0.003	- .0003
2.012	0.826	- .10	0.004	- .0004
2.065	0.704	-	0.003	-
Net Change in Total Solar Reflectance				+ 0.0023

The correction for the ends of the spectrum not measured is based on the reflectance measurements given in Appendix F, and the spectral radiance of the sun at zero air mass. (Reference A-1). The end corrections are made in accordance with the following equations:

$$\Delta R_s = R_x(\text{UV}) J(\text{UV}) + R_x(\text{IR}) J(\text{IR}) \quad (\text{C-5})$$

where:

ΔR_s is the change in the total solar reflectance (always positive) and

$R_x(\text{UV})$ and $R_x(\text{IR})$ are the reflectance below 0.356 micron and above 2.065 microns, respectively, as given in Appendix F.

$J(\text{UV})$ and $J(\text{IR})$ are the fractional energies under the Johnson curve (Reference A-1)

below 0.356 micron and above 2.065 microns, respectively.

$$J(\text{UV}) = 0.059$$

$$J(\text{IR}) = 0.049$$

Since the $J(\lambda_i)$ in the computer program considers only the region of the spectrum measured (89.08 percent), compensation must be made for this when the rest of the spectrum is considered. The corrected total solar reflectance will be given by:

$$R_s(\text{corrected}) = 0.89 R_s + \Delta R_s \quad (\text{C-6})$$

where R_s is given by Equation 5-3 and ΔR_s by Equation C-5.

Since:

$$R_s = 1 - \alpha_s \quad (\text{C-7})$$

(as given in Equation 5-4), Equation C-6 becomes:

$$R_s \text{ (corrected)} = 0.89 - 0.89 \alpha_s + \Delta R_s \quad (\text{C-8})$$

The total corrected solar absorptance is, therefore, computed as follows:

$$\alpha_s \text{ (corrected)} = 0.11 + 0.89 \alpha_s - \Delta R_s \quad (\text{C-9})$$

The α_s in Equation C-9 is given in Tables 7-3 and 7-4.

The correction for RTV-602 white is now given as an example. From Equation C-5.:

$$\Delta R_s = 0.108 \times 0.059 + 0.559 \times 0.049 \quad (\text{C-10})$$

$$\Delta R_s = 0.033$$

where R_x (UV) = 0.108 and R_x (IR) = 0.559, as given in Table 5-1. The uncorrected solar absorptance, used in Equation C-9, is obtained by averaging the in-air (before irradiation) solar absorptance values listed in Table 7-2 (for white paints and miscellaneous materials) and the in air and in-vacuum (before irradiation) solar absorptance values listed in Table 7-1 (for Alzak). The average value for RTV-602 white is 0.113, which when substituted into Equation C-9 gives a corrected solar absorptance (rounded to two decimal places), of:

$$\alpha_s \text{ (corrected)} = 0.11 + 0.89 \times 0.113 - 0.033 \quad (\text{C-11})$$

$$\alpha_s \text{ (corrected)} = 0.18$$

The correction for the solar absorptance listed in Table 5-1 for RTV-602 white, therefore, is 0.07 as determined from the following equation:

$$\alpha_s = \alpha_s \text{ (corrected)} - \alpha_s \text{ (uncorrected)} \quad (\text{C-12})$$

The solar absorptance values for RTV-602 white in Table 7-4 were obtained by adding 0.07 to their corresponding value in Table 7-2. The remainder of the values in Table 7-2 are corrected in a similar manner to obtain the values presented in Table 7-4. The corrections for all materials are listed in Table 5-1. The values for Alzak in Table 7-1 are corrected to those listed in Table 7-3 by using the correction listed in Table 5-1 together with that listed in Table 5-2, which compensates for the specular nature of Alzak.

It should be noted for future reference that measurements performed after 22 August 1967 will not require smoothing as described herein. This is because a seven fold increase in sensitivity in the lead sulfide detector was obtained by replacing the lead sulfide cell and re-aligning the monochrometer optics.

An example of the spectral reflectance curves presently being obtained is given in Figure C-2. Modifications are presently being performed on the computer program so that the value printed above the spectral reflectance curve by the computer will include the correction for the region of the spectrum not measured. It should also be noted that corrections for specular samples should not be necessary in the future since a vapor deposited aluminum mirror is being used as a reference for specular materials.

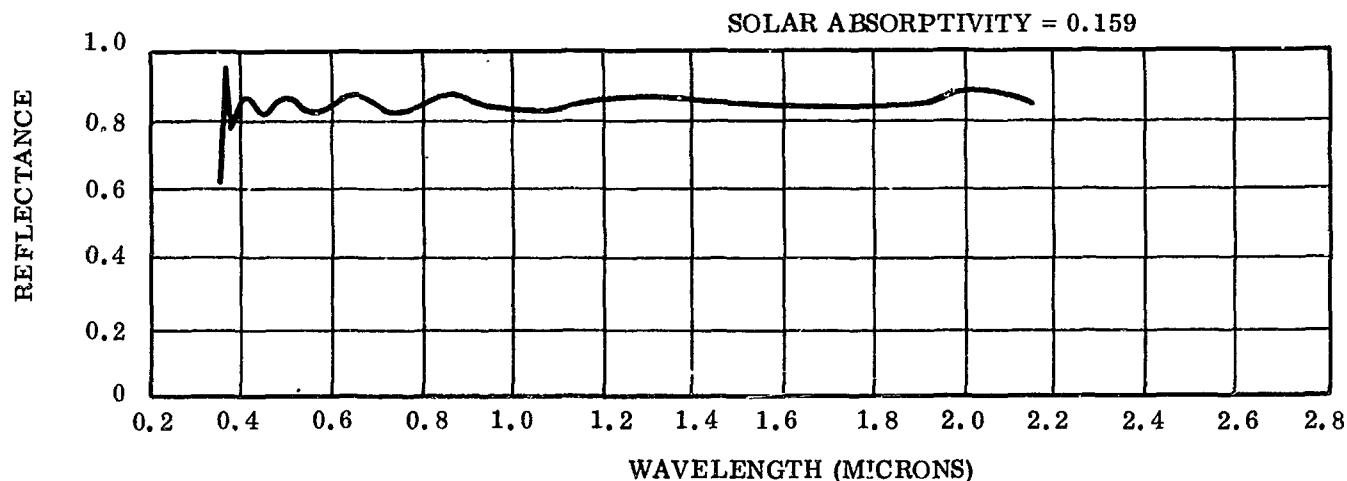


Figure C-2. SCH/H-37 Before Irradiation in-air 75F 82267-15A

APPENDIX D
COMPILATION OF ALL SPECTRAL REFLECTANCE CURVES USED IN ANALYSIS

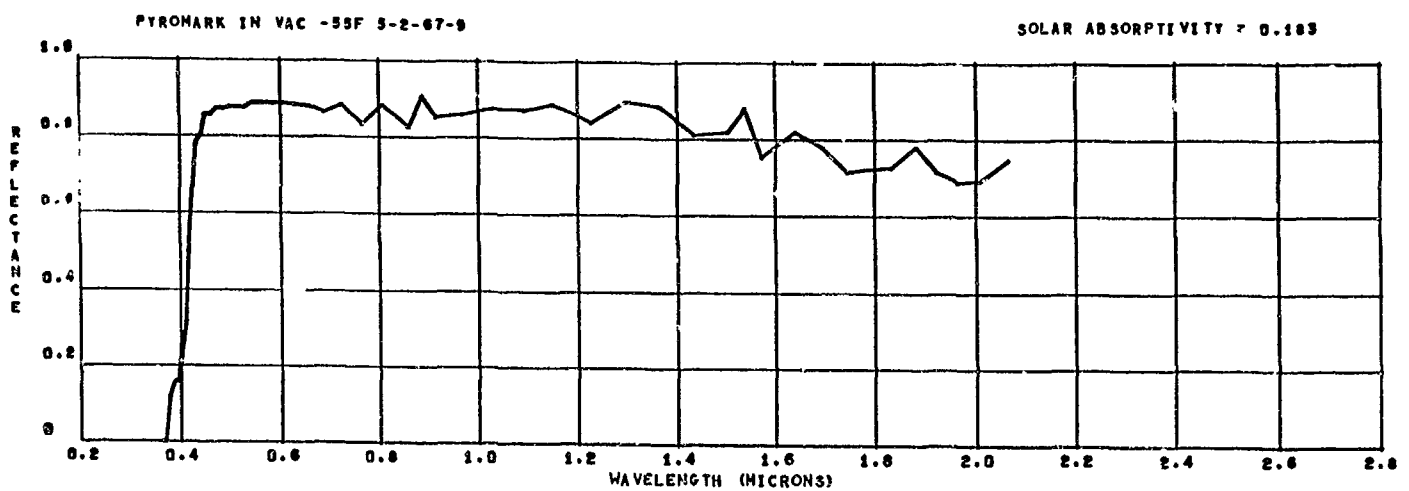
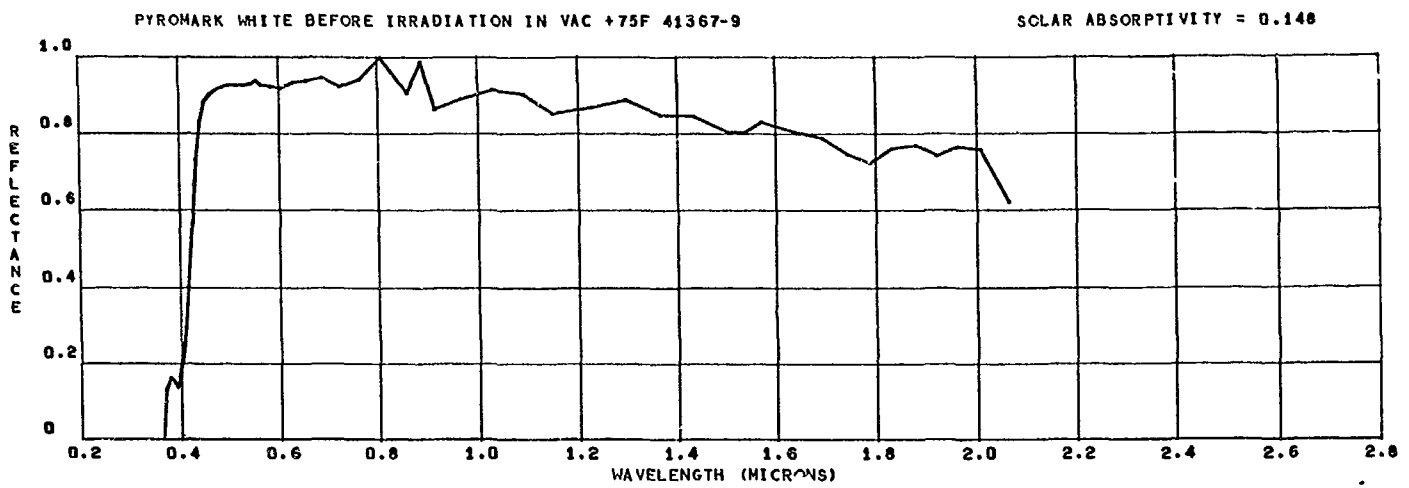
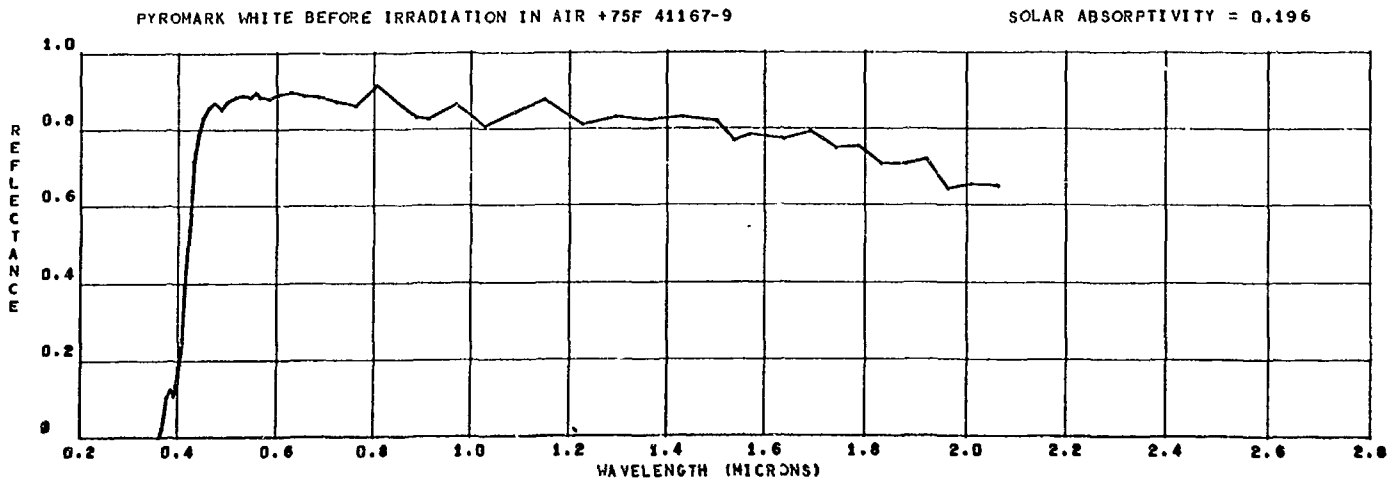
This appendix lists all the spectral reflectance curves obtained in this program in the order described in Table D-1. These curves were obtained as described in Sections 5 and 7 of this report. All the curves have the same abscissa and ordinate scale. The solar absorptance printed above each graph on the right side is the value obtained by the computer and, therefore, is both unsmoothed and uncorrected. The computer printed title above each graph on the left gives the sample identification, the total radiation exposure of the sample, the pressure environment and temperature at which the measurement was performed, and a code number. The digits before the dash in the code numbers give the date the measurement was performed, the digits after the dash gives the specimen number as used in the tables throughout this report (e. g. , 41167-9 indicates the measurement was performed on 11 April 1967, and that the specimen number was nine). The corpuscular irradiation is abbreviated as follows: $5 \times 10^{14}P$ represents $5 \cdot 10^{14}$ protons cm^{-2} , and $5 \times 10^{13}E$ represents $5 \cdot 10^{13}$ electrons cm^{-2} .

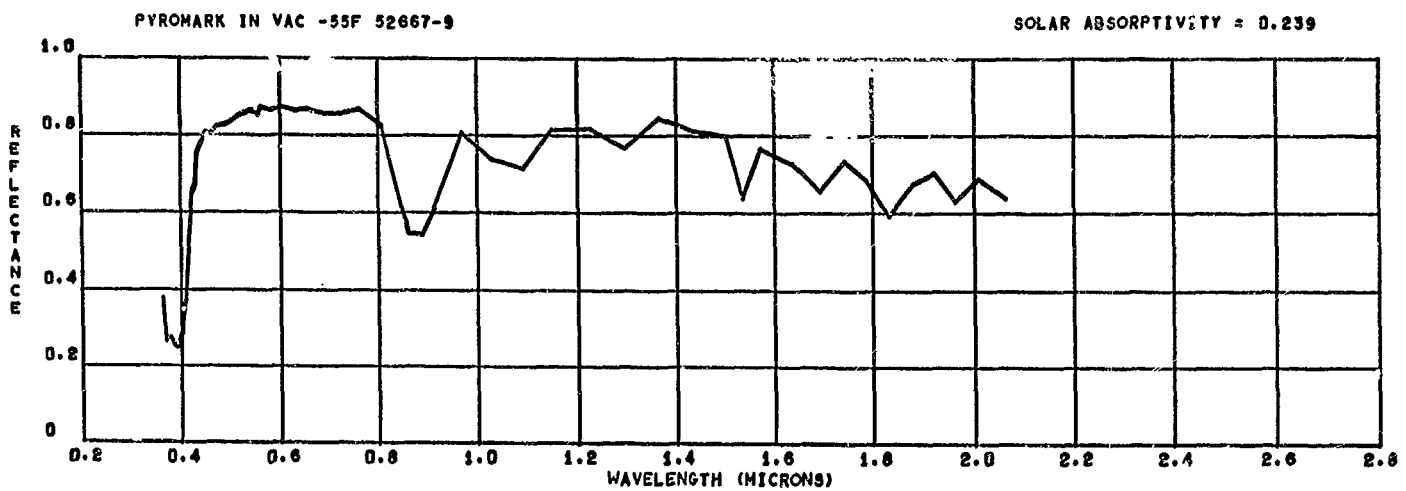
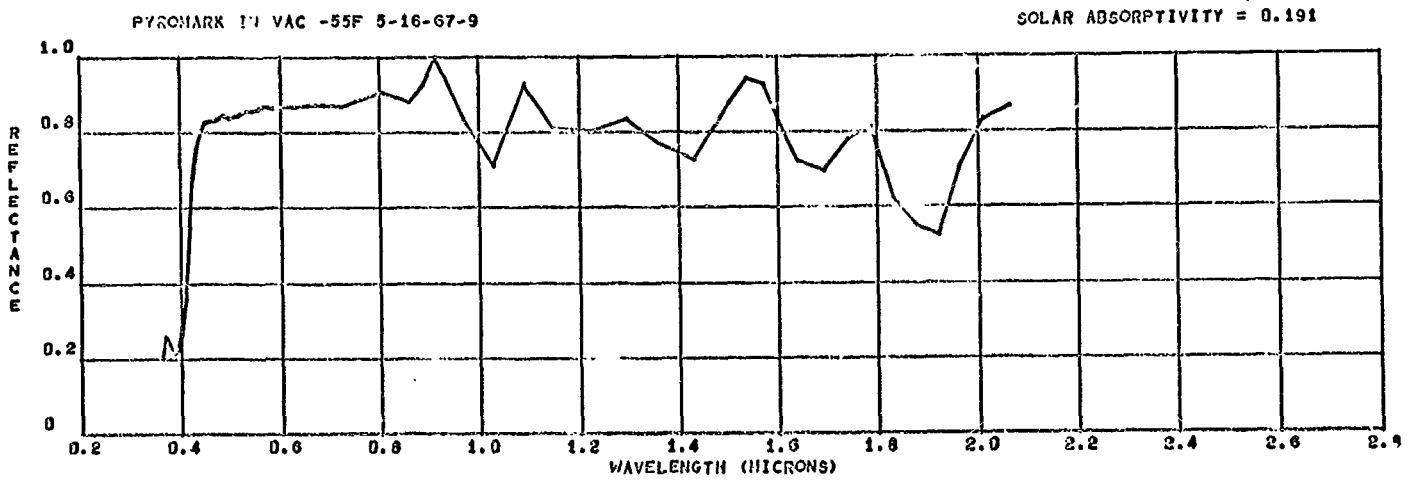
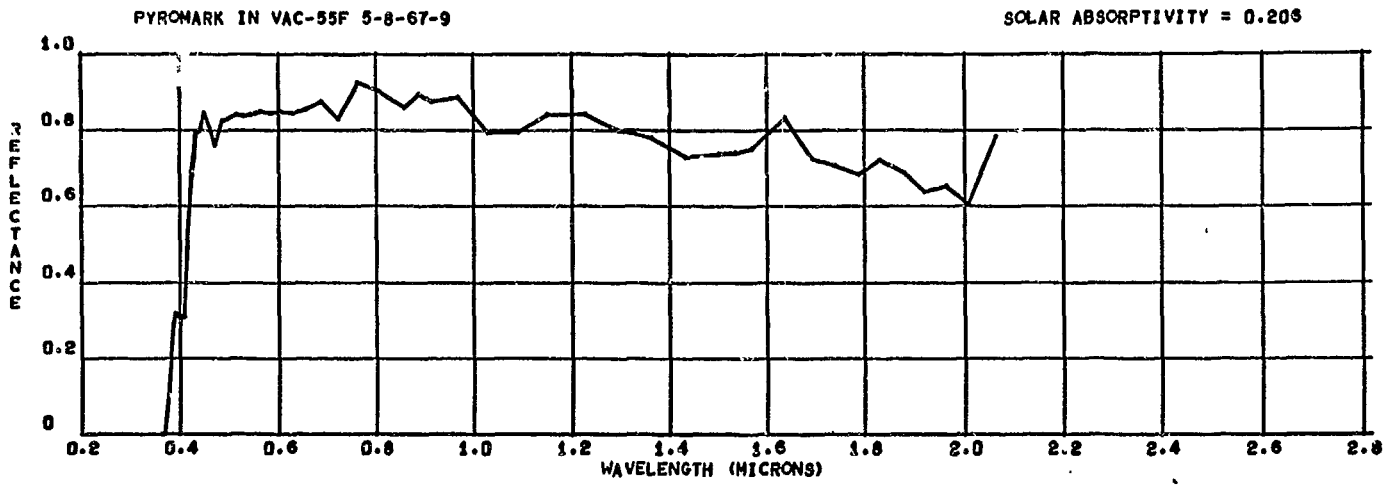
Table D-1. Index of Reflectance Measurements in Appendix D

Material	Specimen Number	Type Irradiation	Page
Pyromark Std White	9	None	D-3
Pyromark Std White	29	F and P	D-6
Pyromark Std White	4	UV, E, and P	D-9
Goddard White	8	None	D-12
Goddard White	27	E and P	D-15
Goddard White	2	UV, E, and P	D-18
Goddard White	11	UV	D-21
RTV 602 White	10	None	D-23
RTV 602 White	28	E and P	D-27
RTV 602 White	3	UV, E, and P	D-30
Alzak	19	None	D-33
Alzak	6	None	D-36
Alzak	7	None	D-38
Alzak	21*	E and P	D-40
Alzak	23	E and P	D-42
Alzak	26	E and P	D-44
Alzak	30*	E and P	D-46
Alzak	1	UV, E, and P	D-48
Alzak	17	UV, E, and P	D-51
Alzak	5*	UV, E, and P	D-53
Alzak	15*	UV, E, and P	D-57
Alzak	12	UV	D-59
Alzak	13	UV	D-63
Lexan (etched)	14	UV, E, and P	D-66
Lexan (dull)	18	UV, E, and P	D-69
Mylar	16	UV, E, and P	D-72
Mylar	22	E, and P	D-75
Solar Cells	20	E, and P	D-77
Microsheet	24	E and P	D-79

*

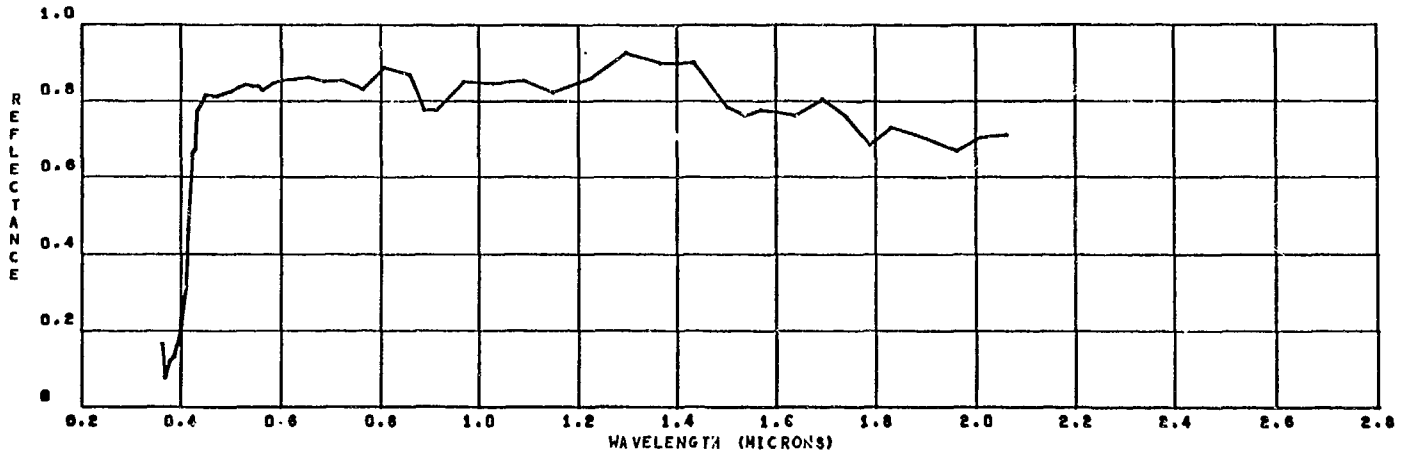
*Indicates 0.10 mils, all others are 0.175 mils thick





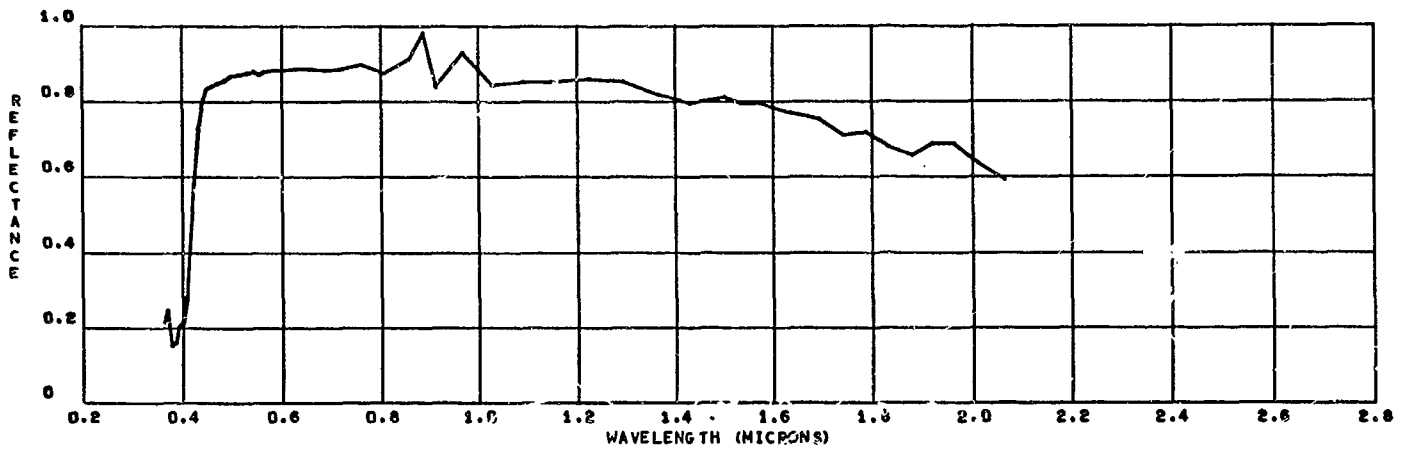
PYROHARK IN VAC -53F 6667-9

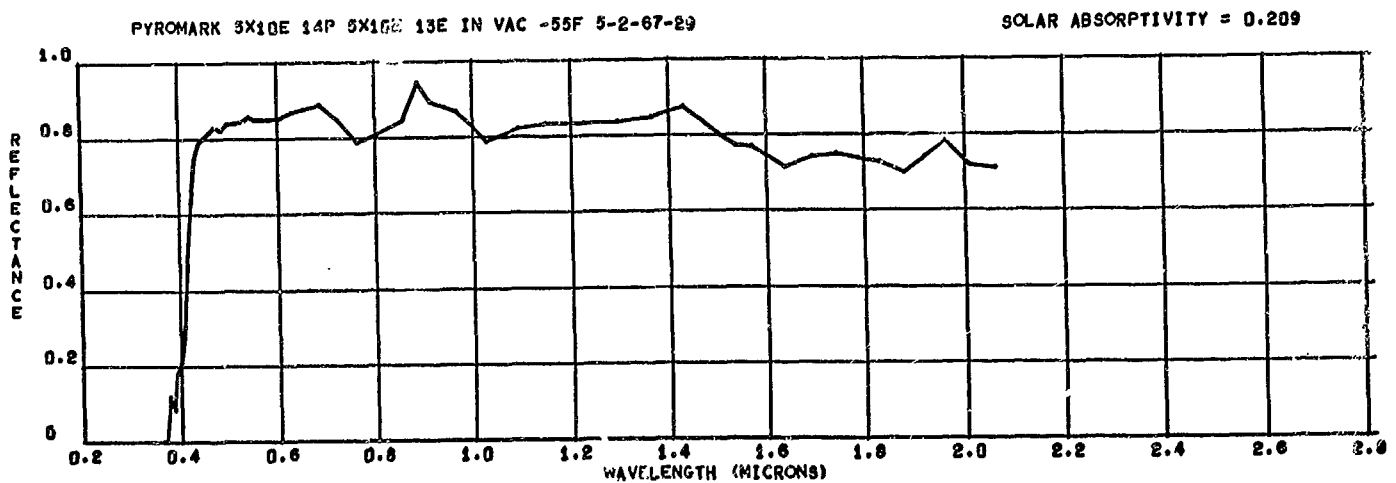
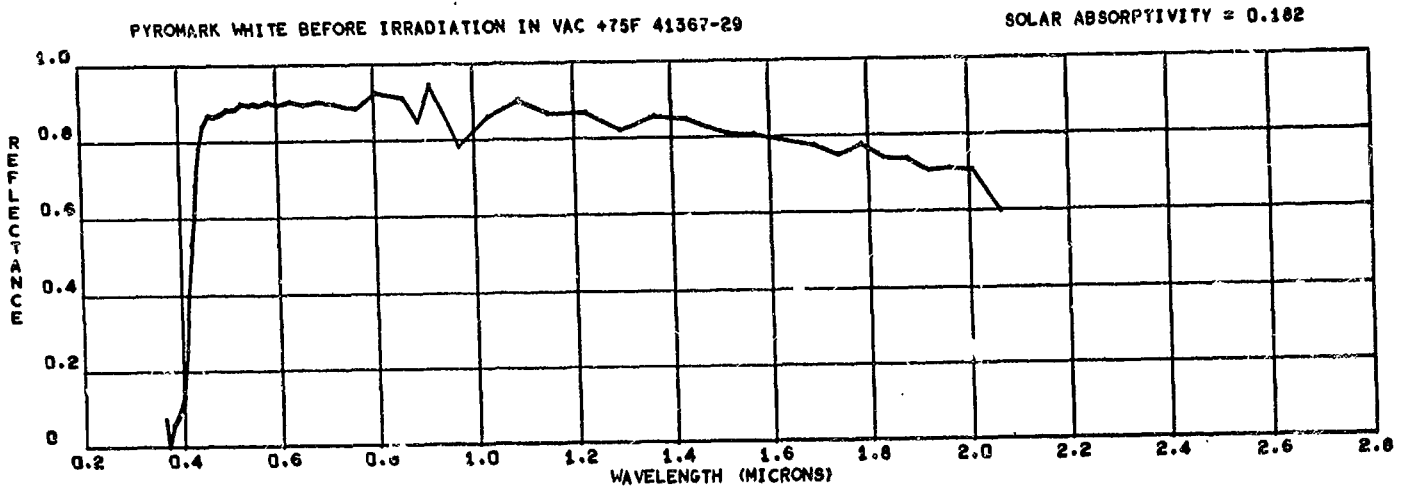
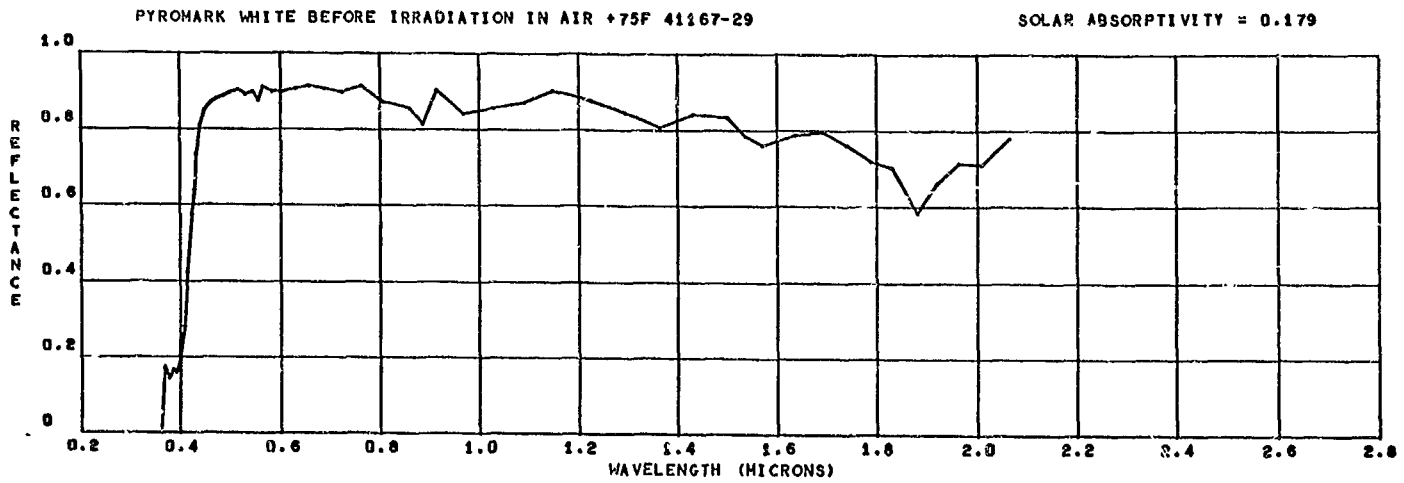
SOLAR ABSORPTIVITY = 0.204

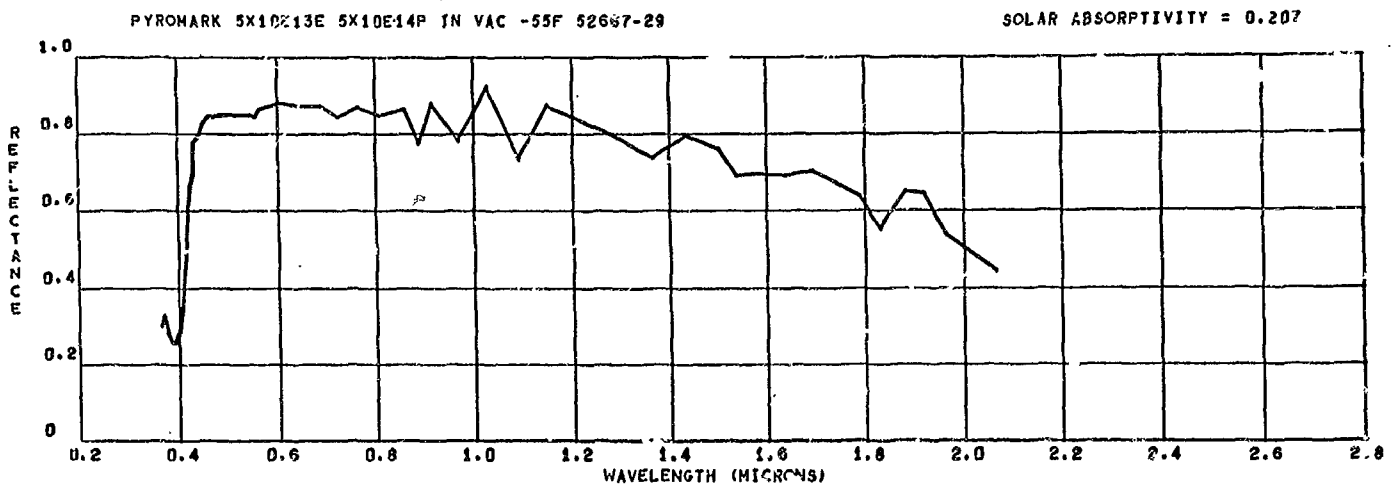
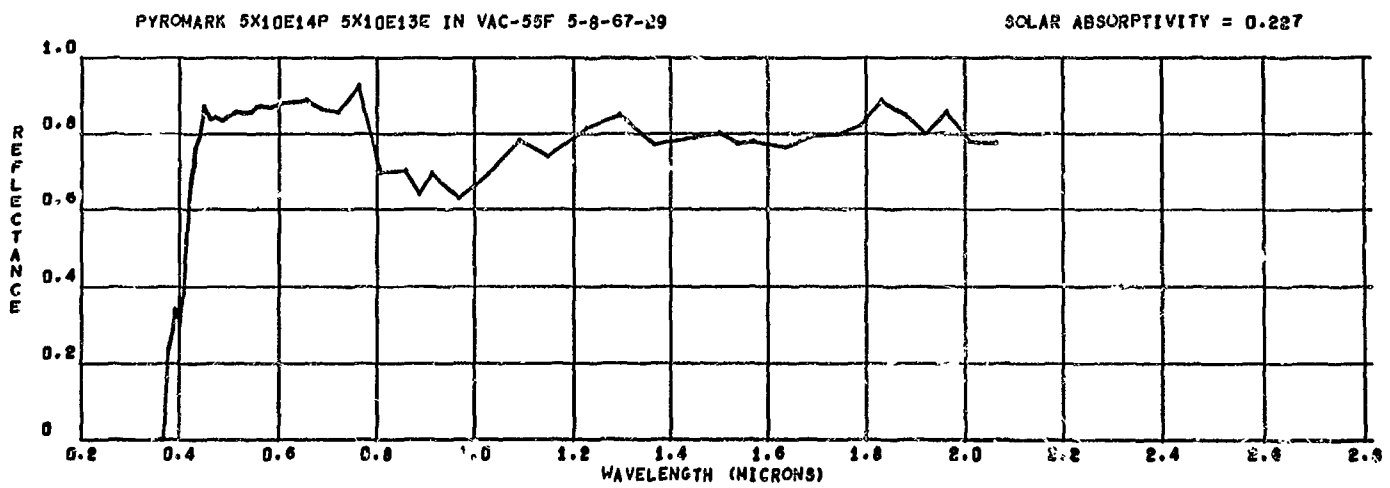
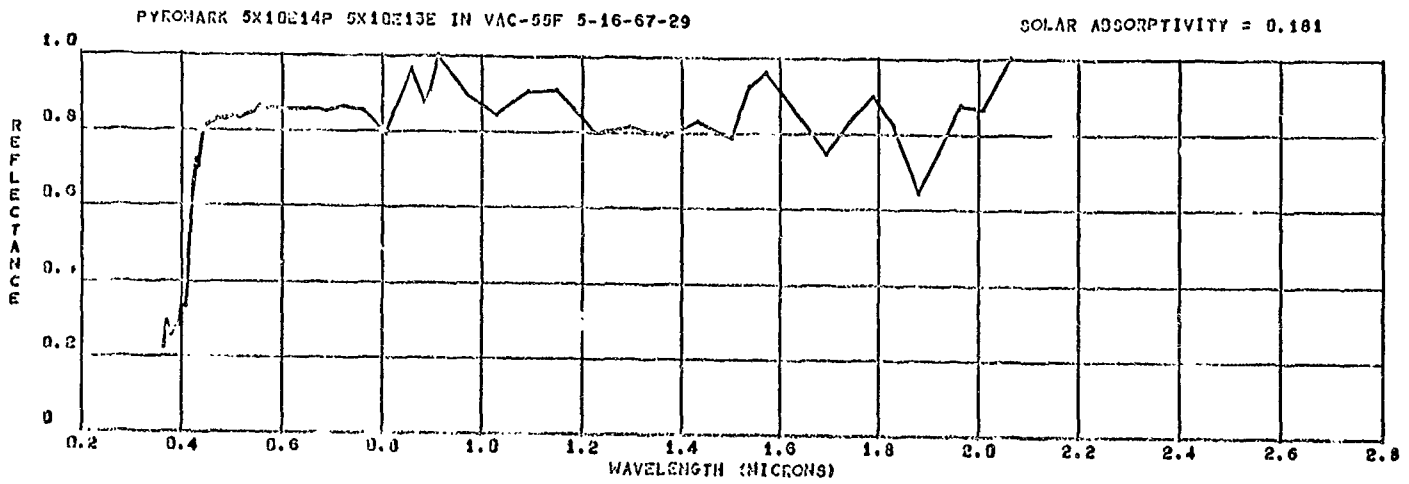


PYROHARK IN AIR 61467-9

SOLAR ABSORPTIVITY = 0.182

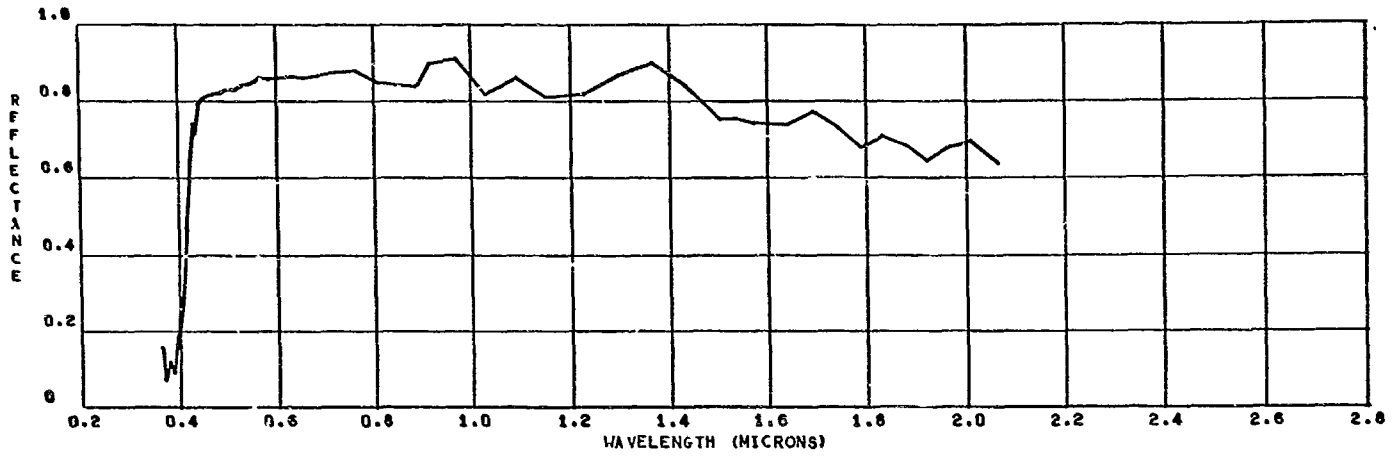






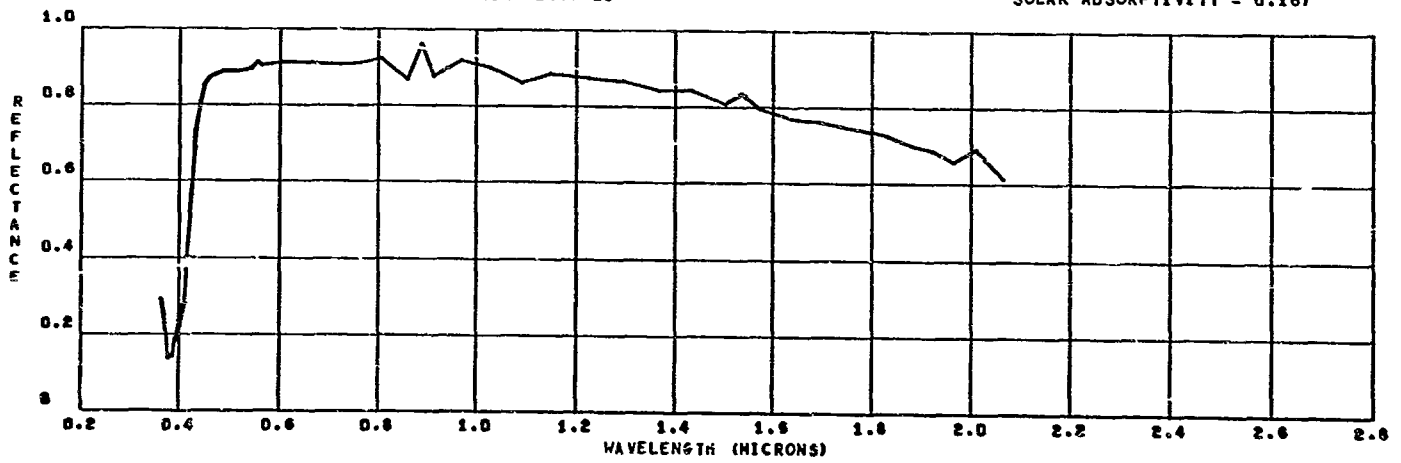
PYROMARK 5X10E13E 5X10E14P IN VAC -55F 6667-29

SOLAR ABSORPTIVITY = 0.203



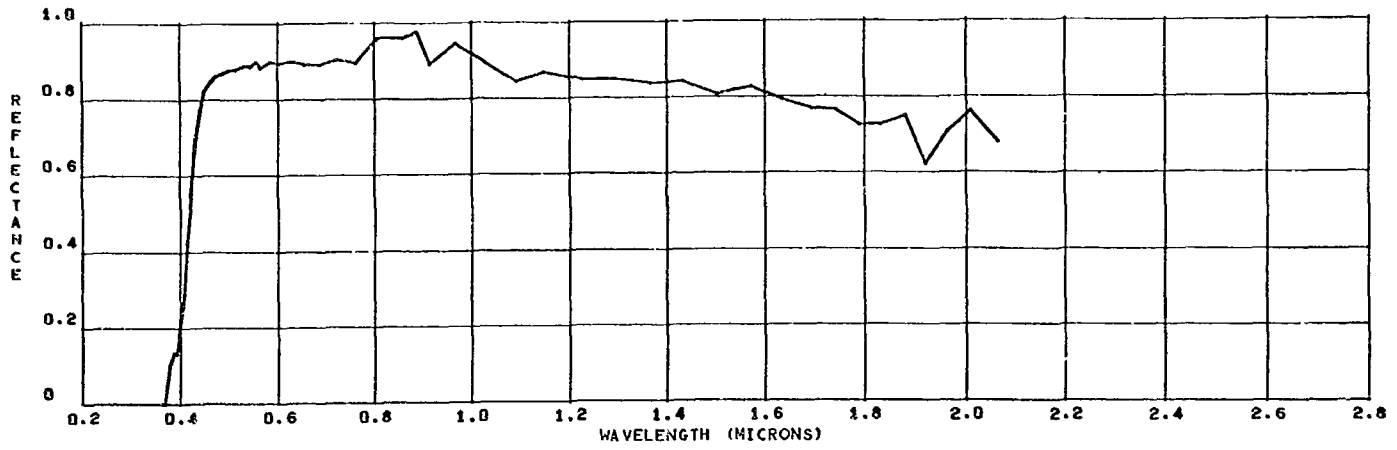
PYROMARK 5X10E13E 5X10E14P IN A.R 61467-29

SOLAR ABSORPTIVITY = 0.167



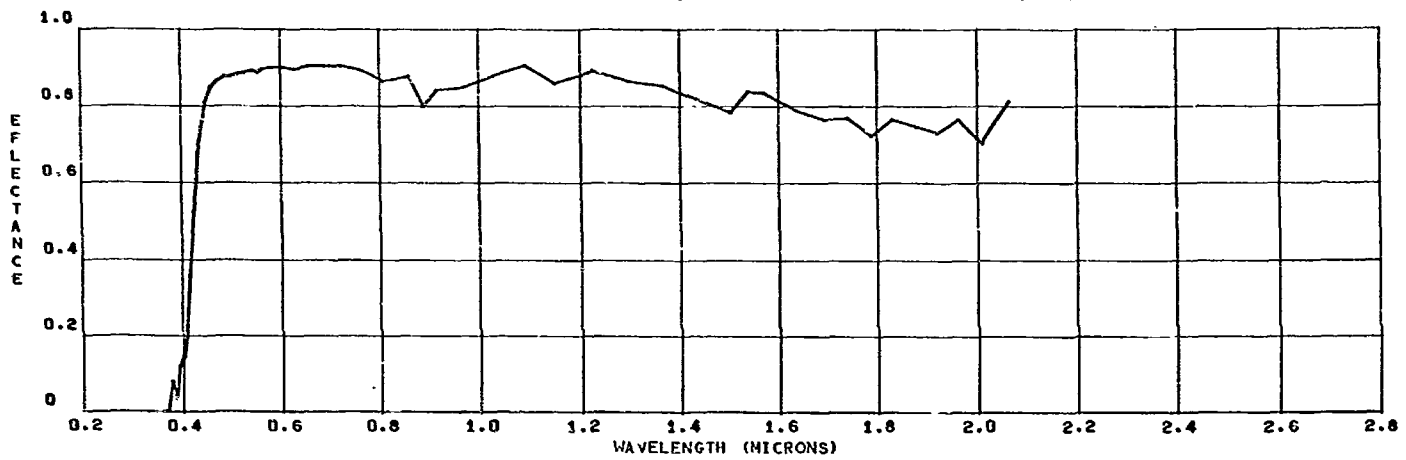
PYROMARK WHITE BEFORE IRRADIATION IN AIR +75F 41167-4

SOLAR ABSORPTIVITY = 0.171



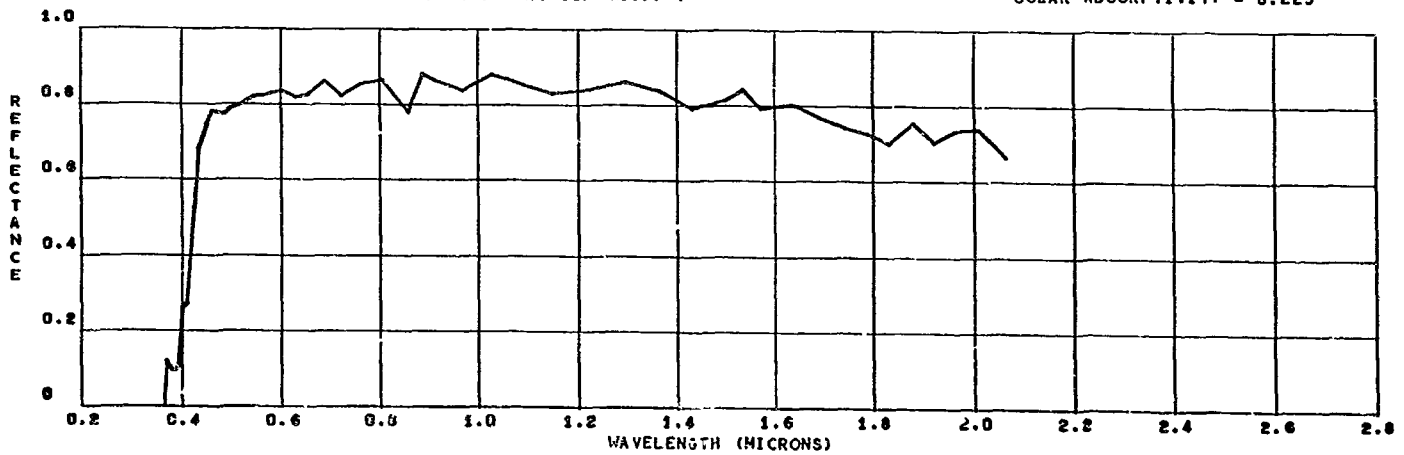
PYROMARK WHITE BEFORE IRRADIATION IN VAC +75F 41367-4

SOLAR ABSORPTIVITY = 0.187



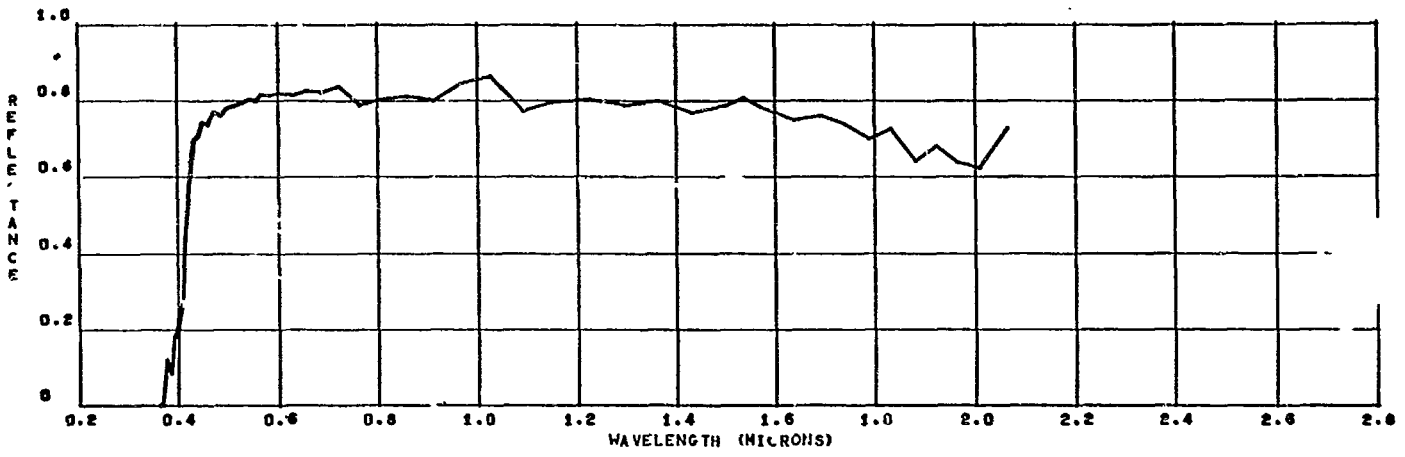
PYROMARK WHITE AFTER 61 EUVSH IN VAC-55F 42667-4

SOLAR ABSORPTIVITY = 0.225



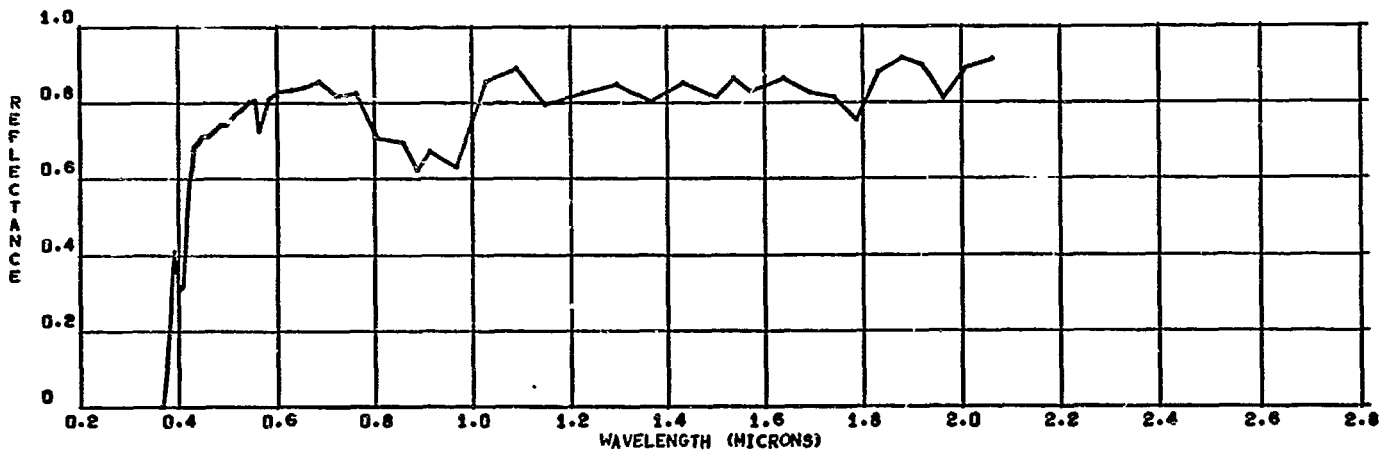
PYROMARK 5X10E 14P 5X10E 13E 200EUVSH IN VAC -55F 5-2-67-4

SOLAR ABSORPTIVITY = 0.246



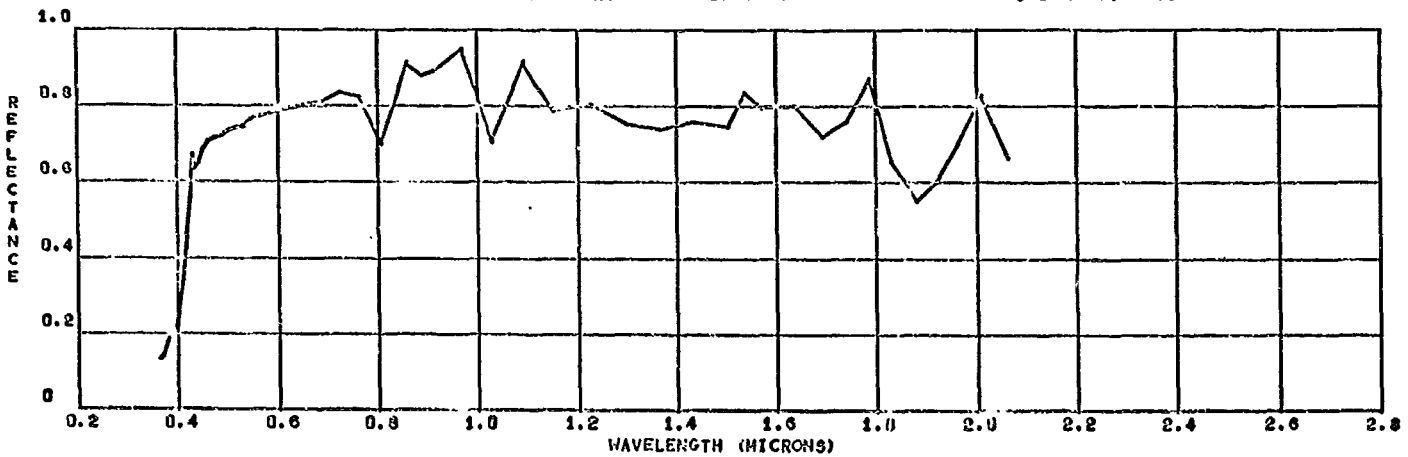
PYROMARK 5X10E14P 5X10E13E 335 EUVSH IN VAC-55F 5-8-67-4

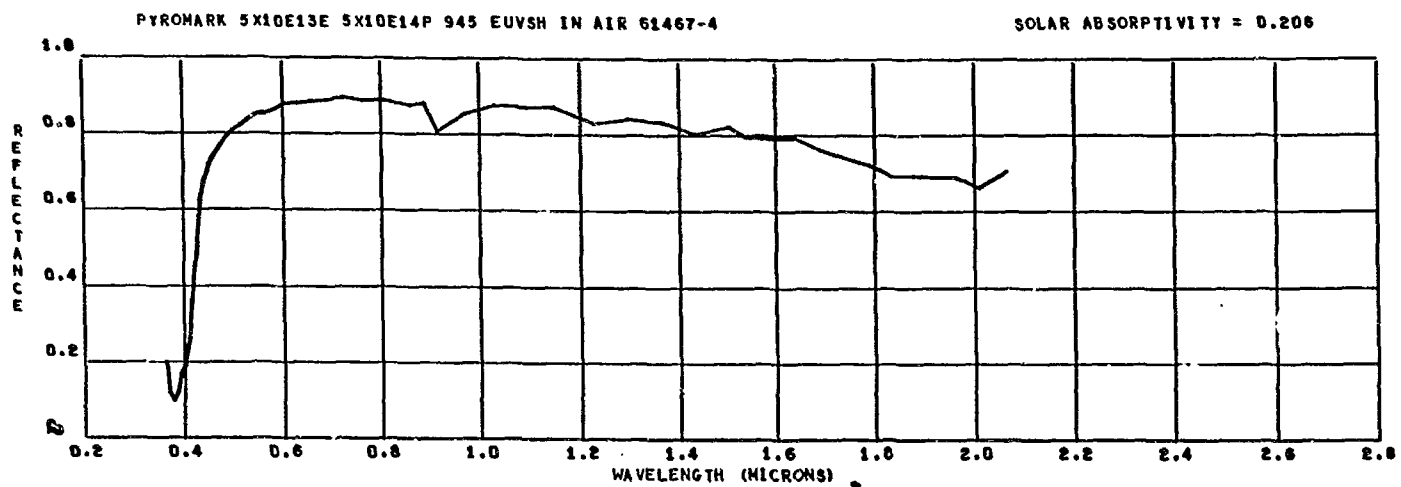
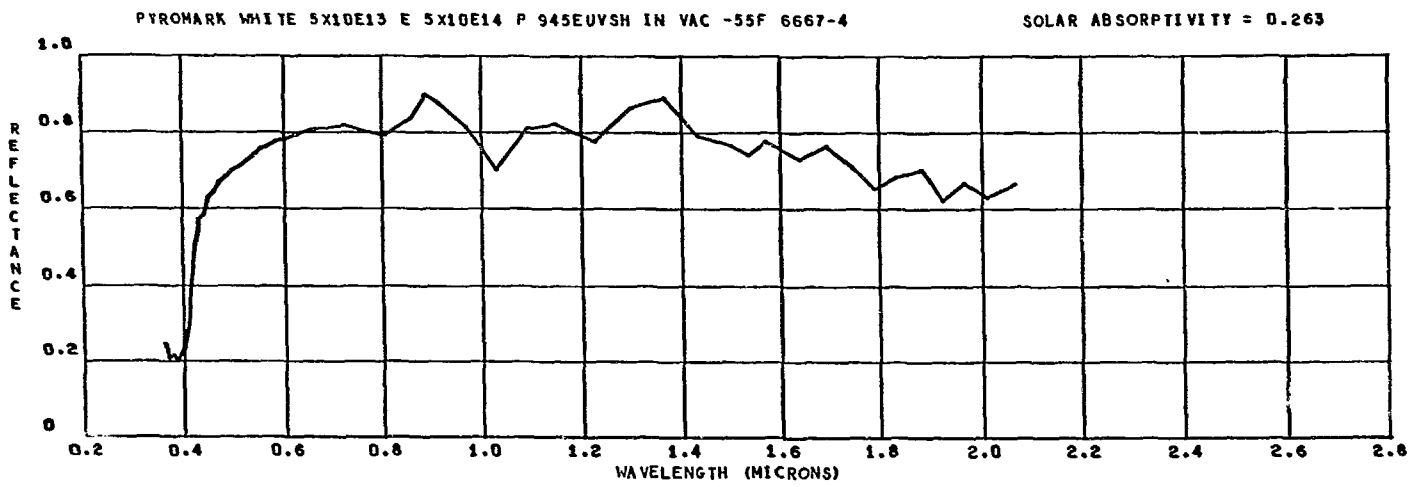
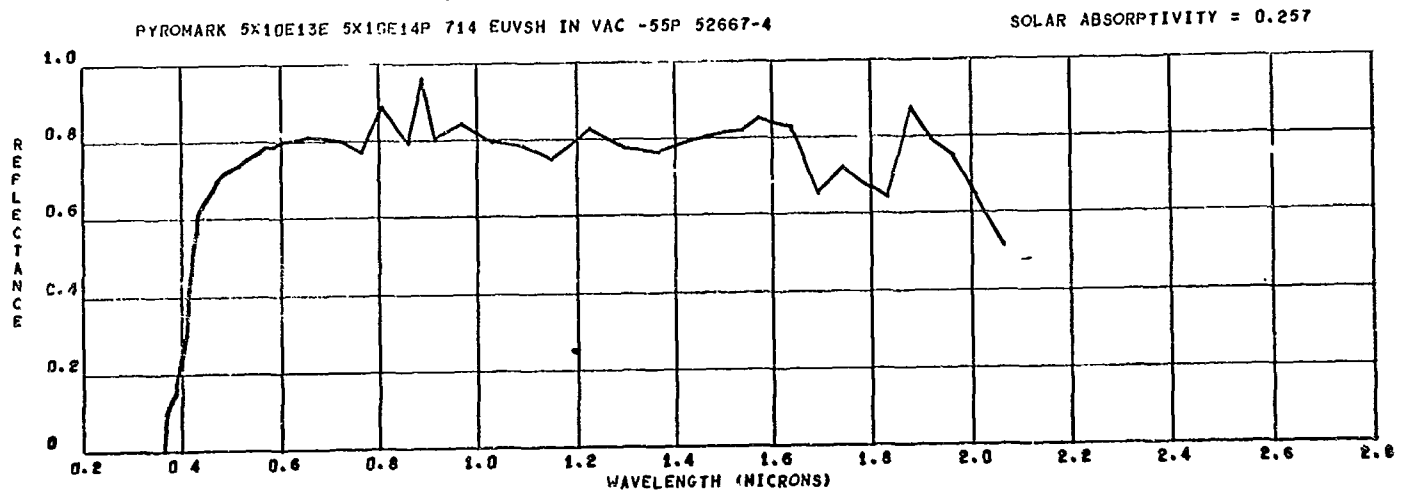
SOLAR ABSORPTIVITY = 0.249

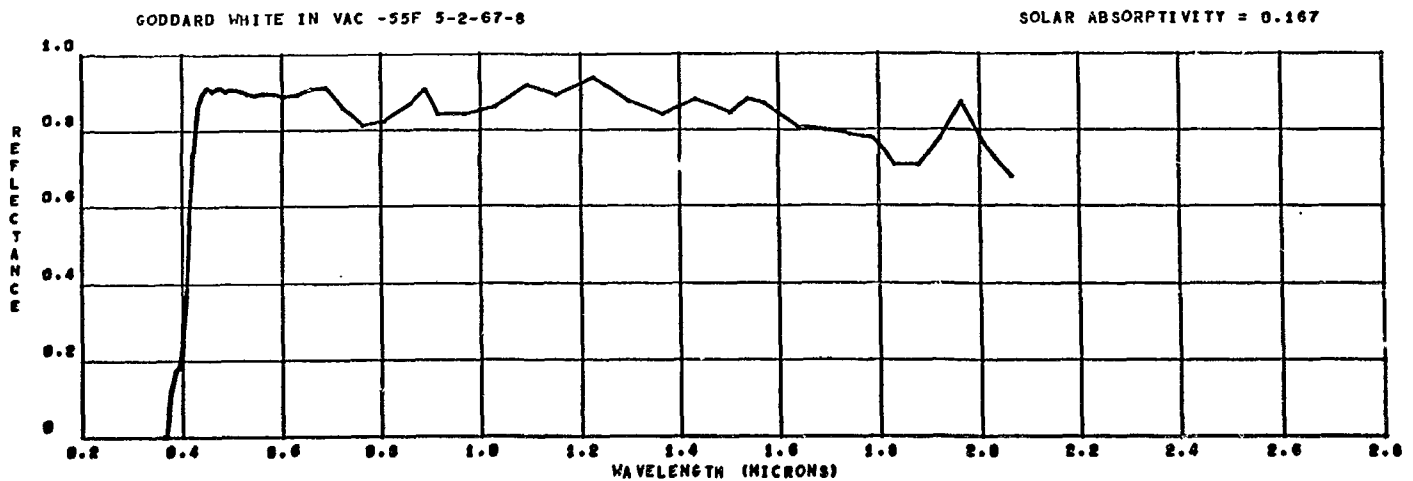
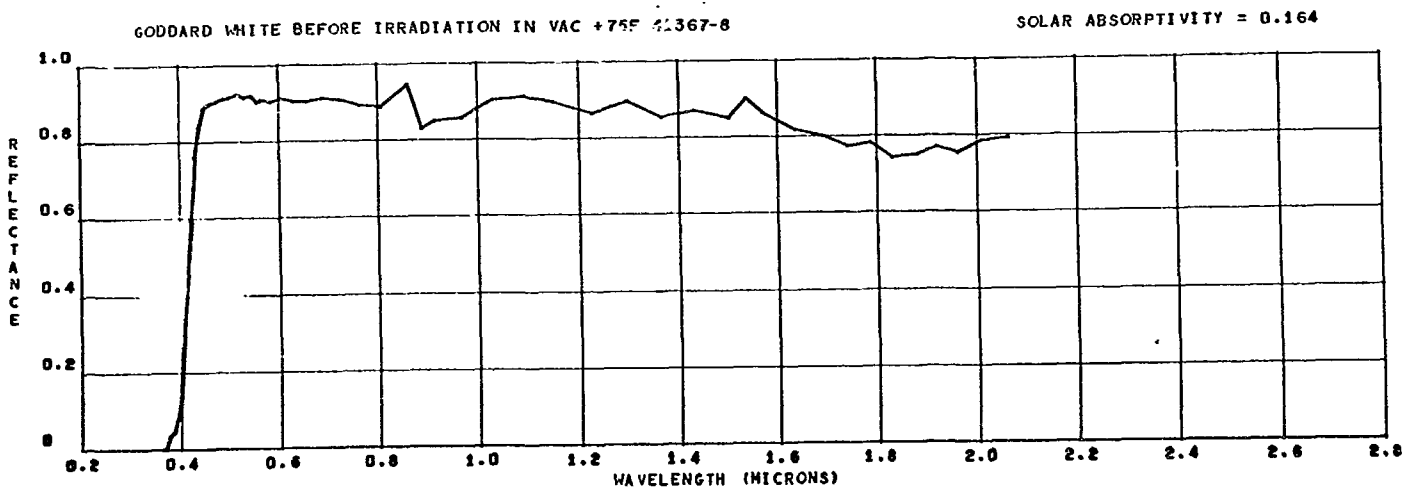
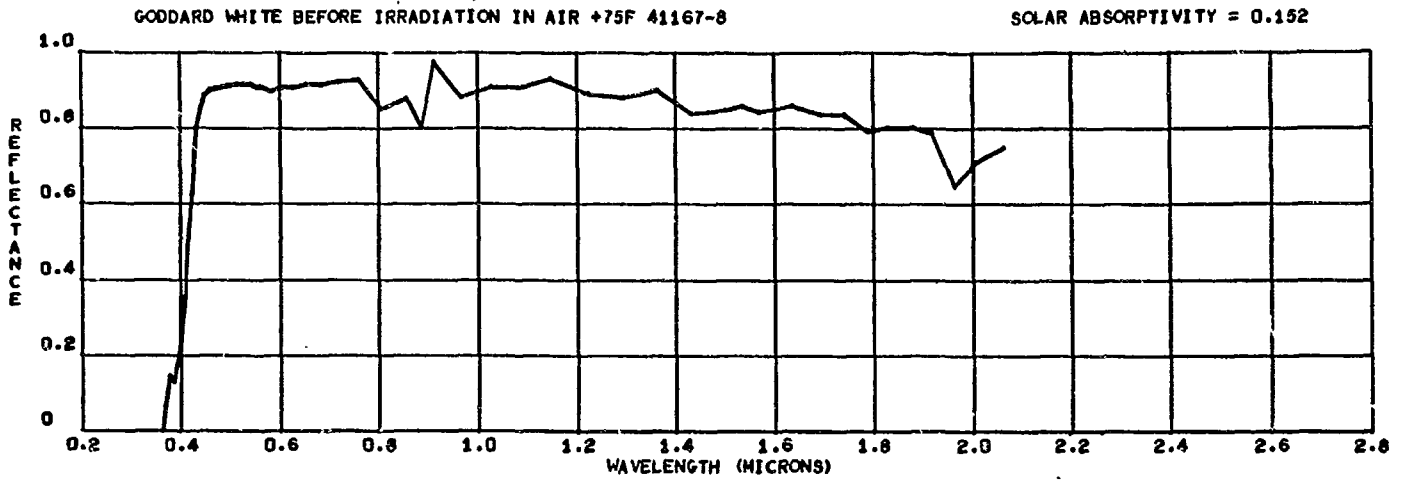


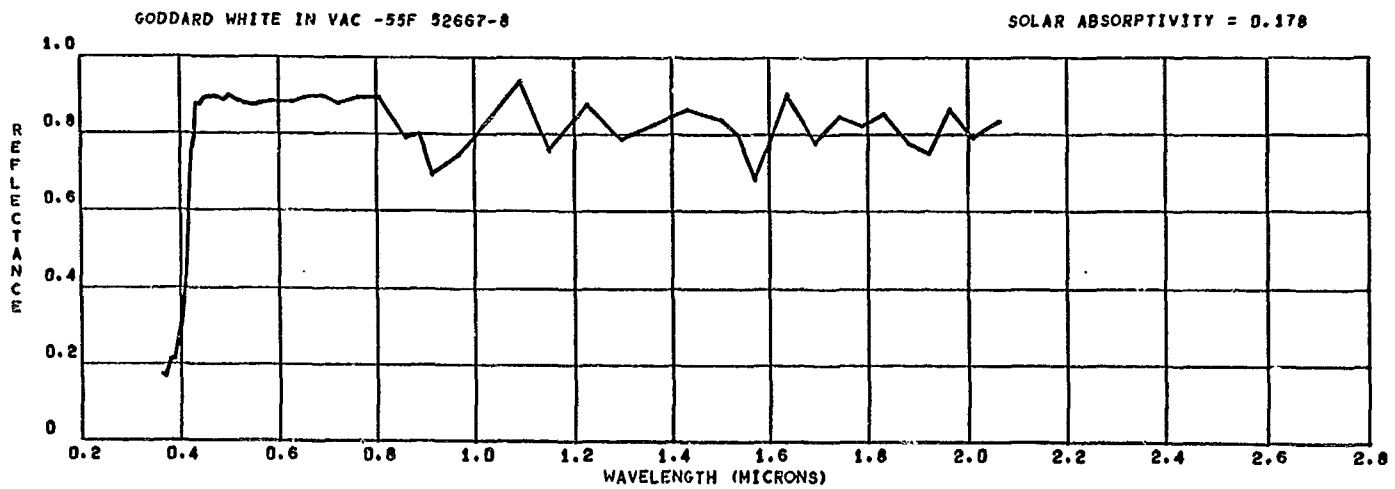
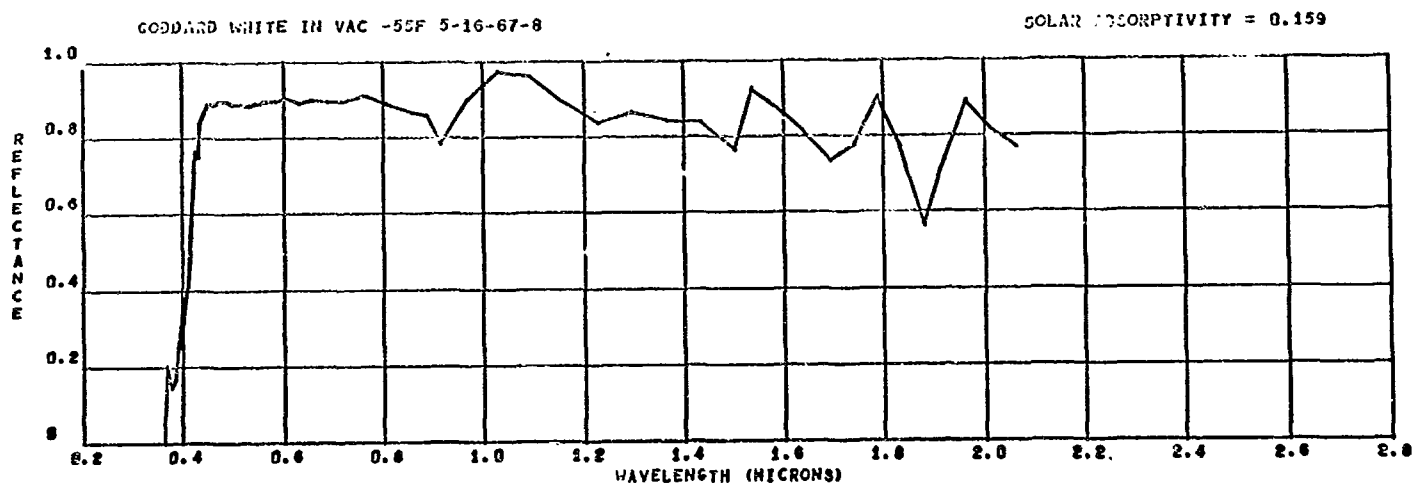
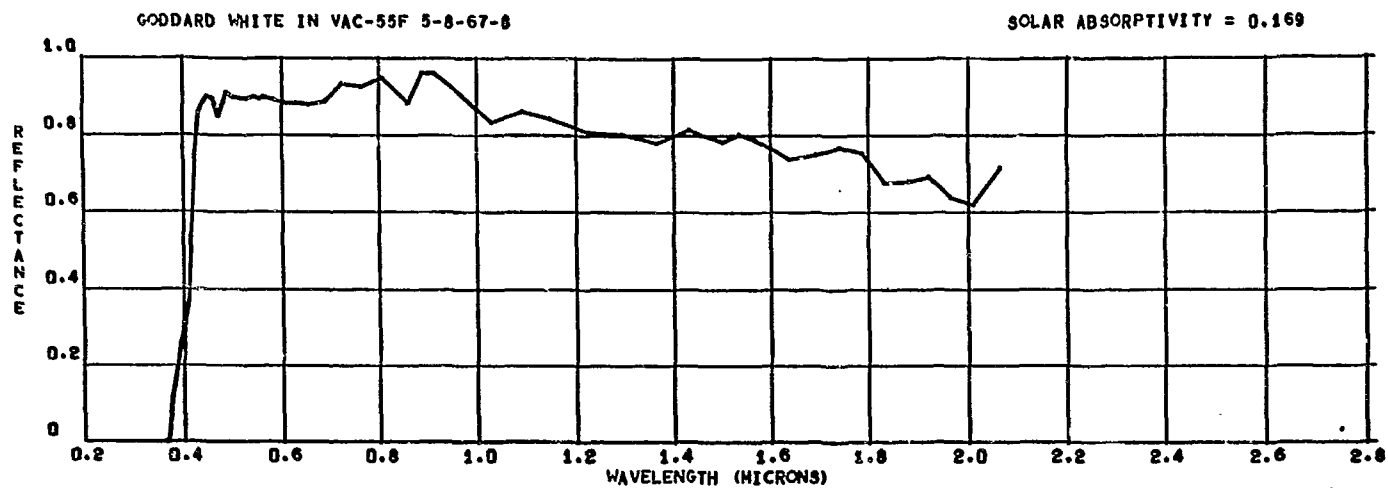
PYROMARK 5X10E14P 5X10E13E 500EUVSH IN VAC -55F 5-16-67-4

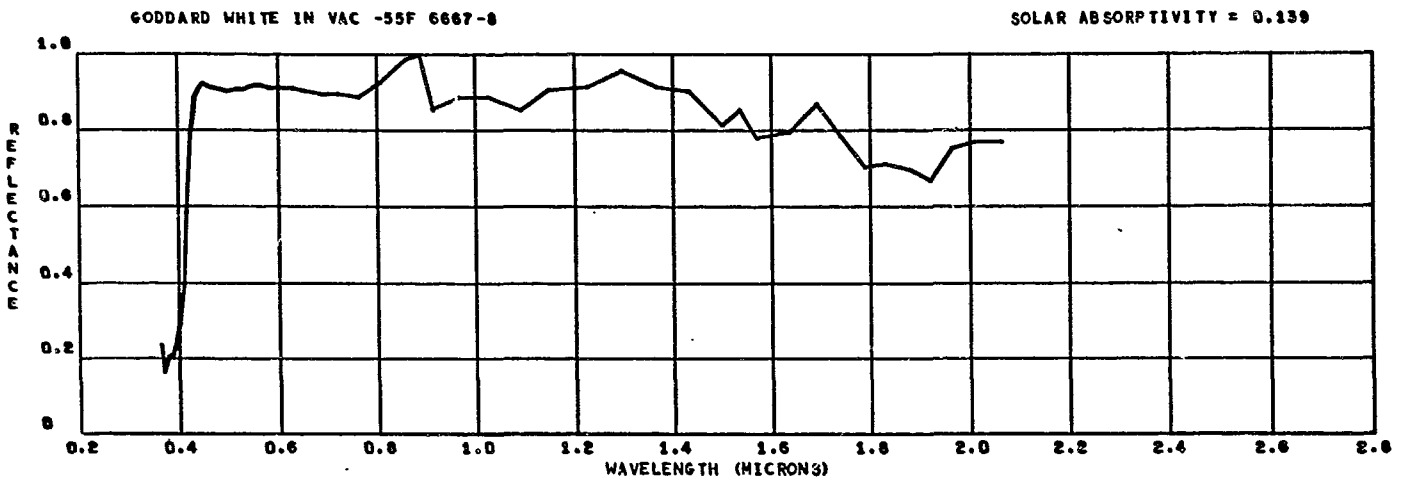
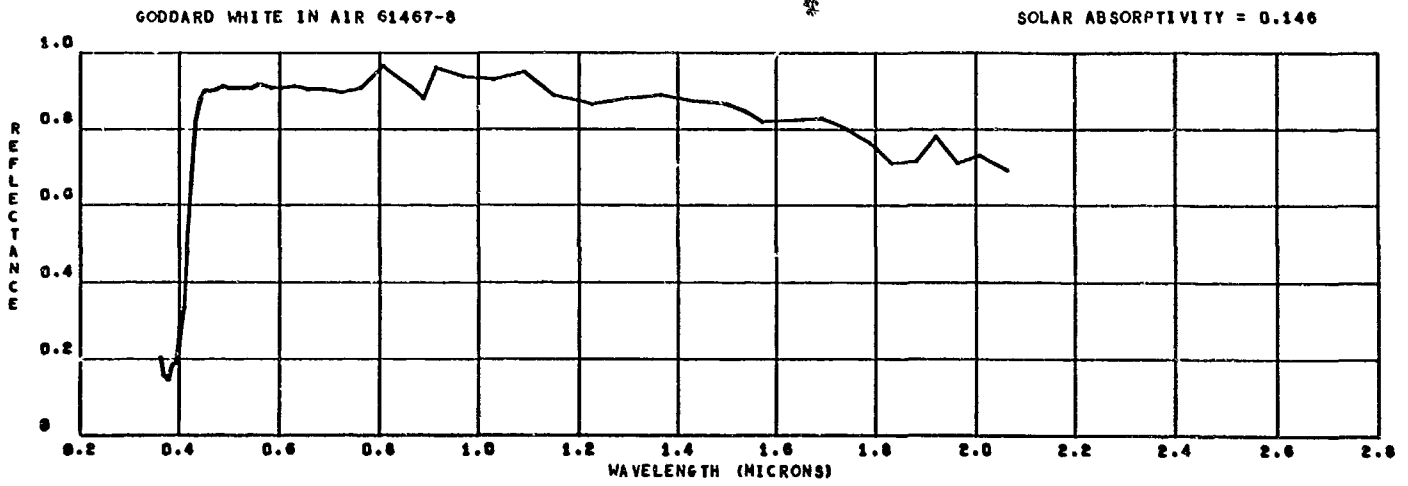
SOLAR ABSORPTIVITY = 0.249

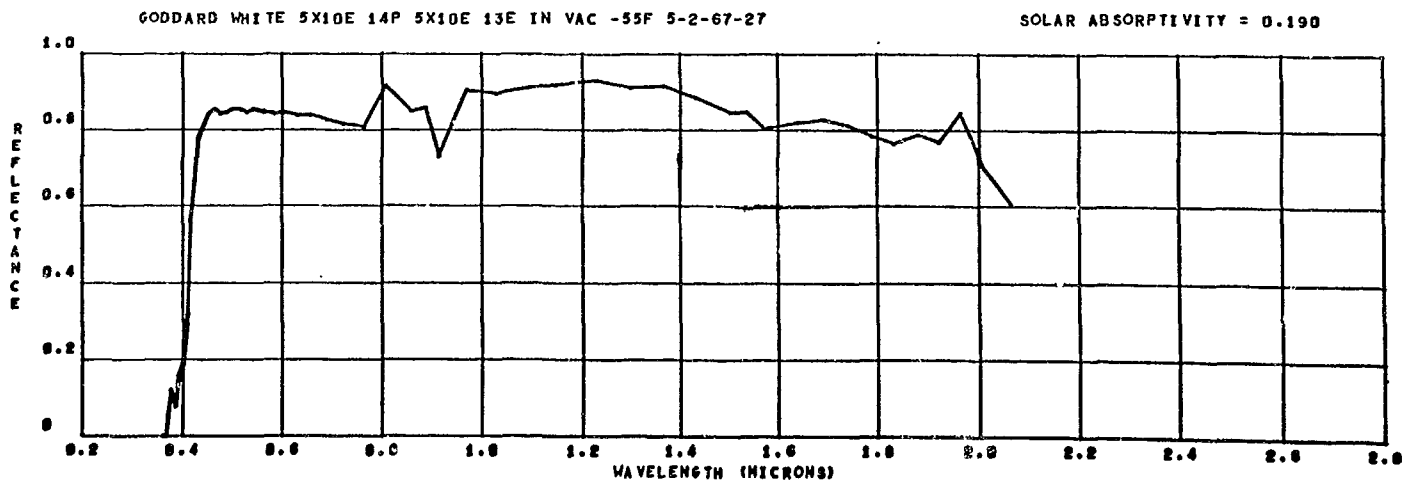
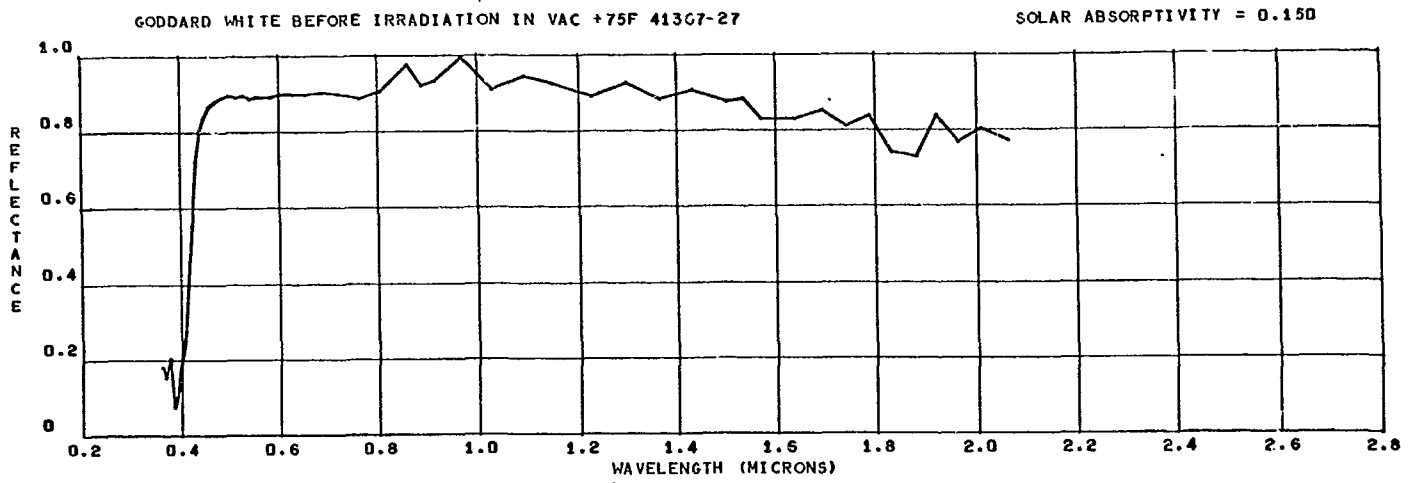
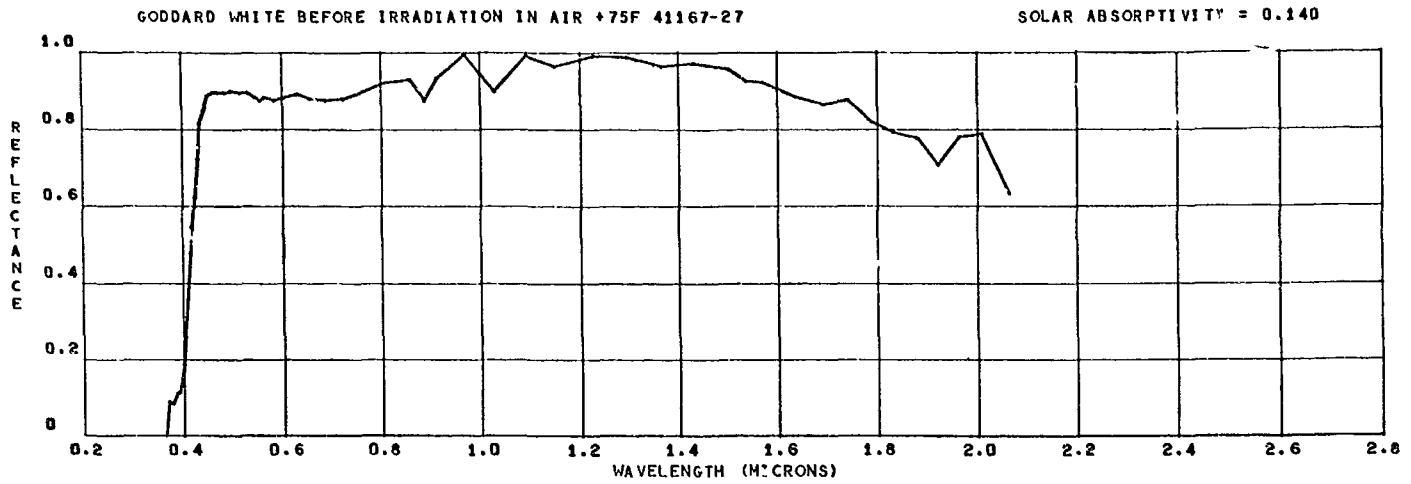


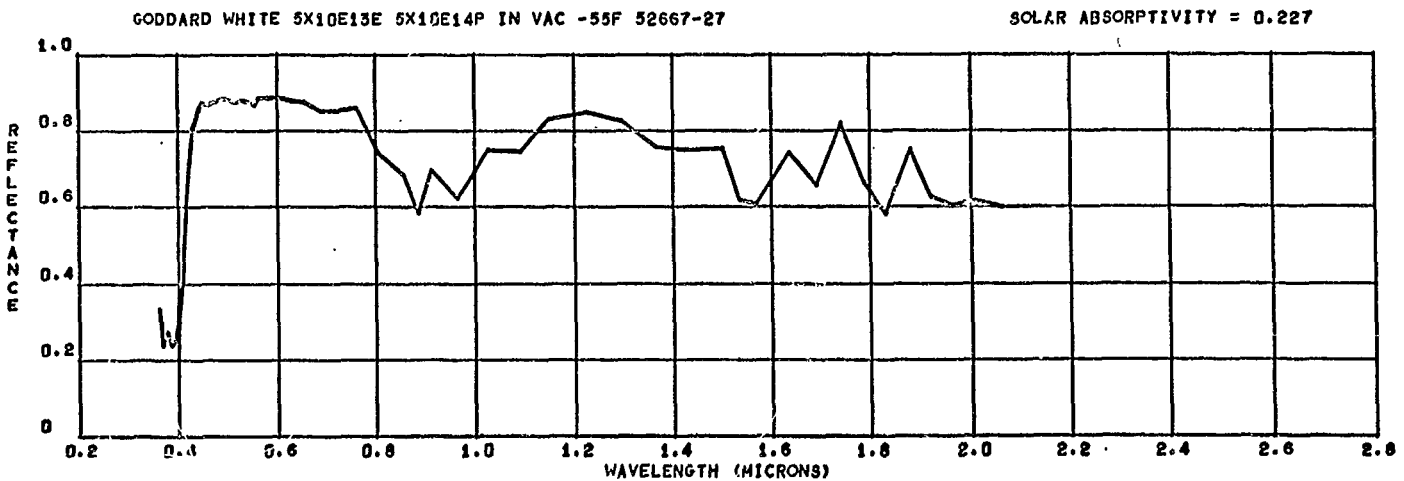
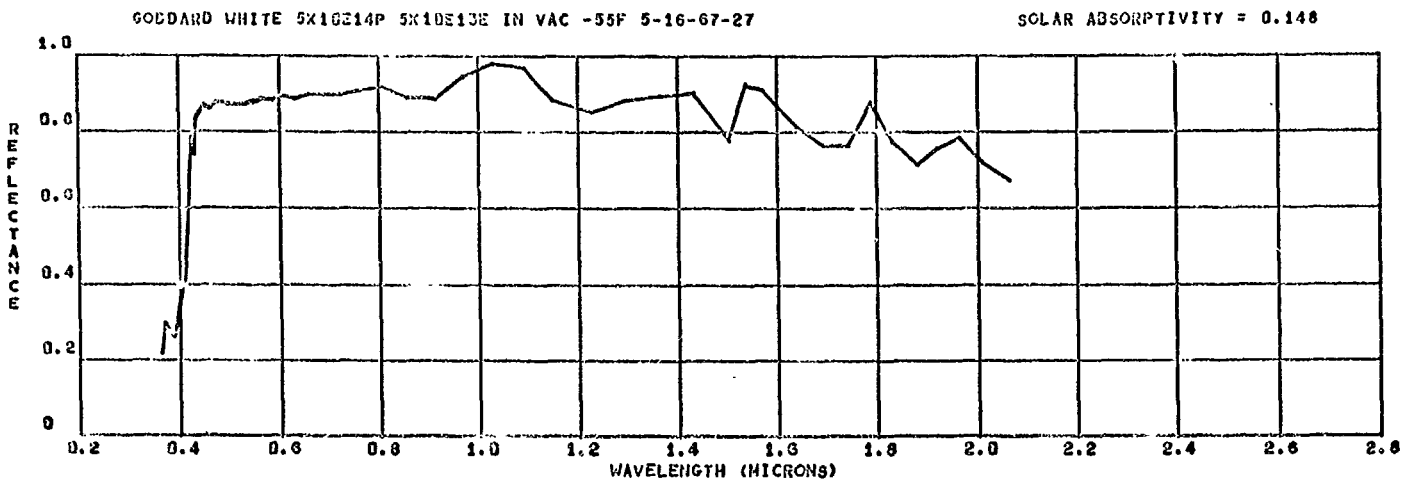
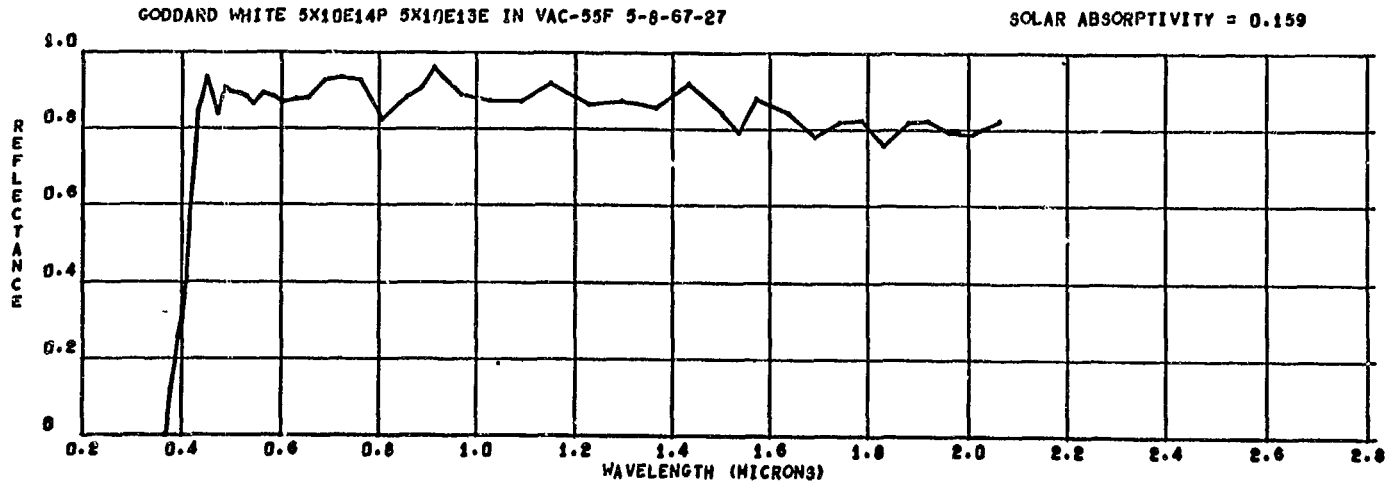


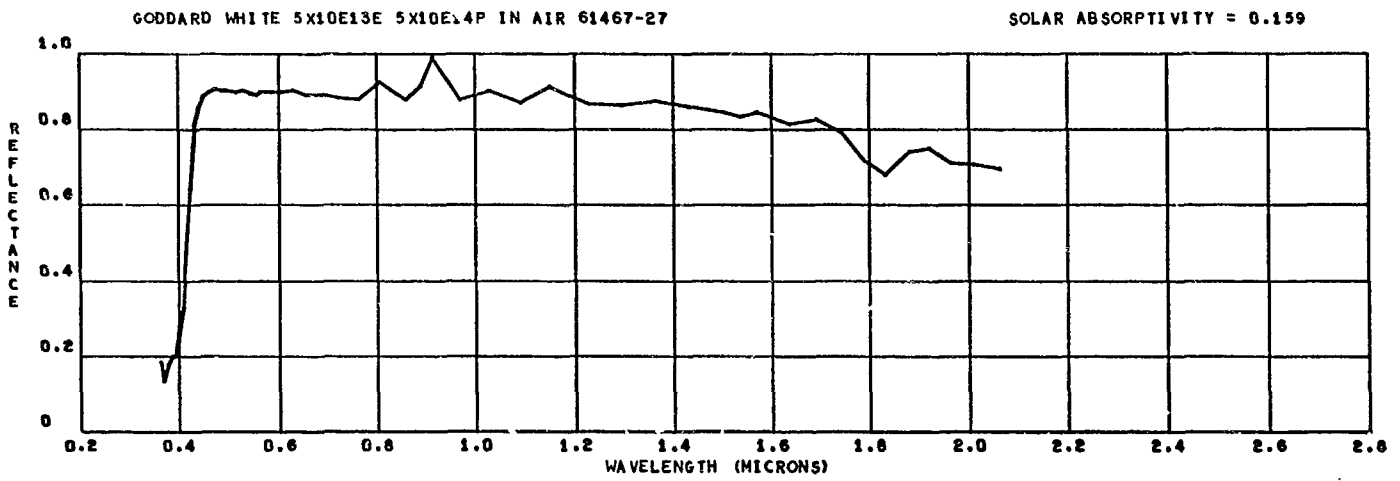
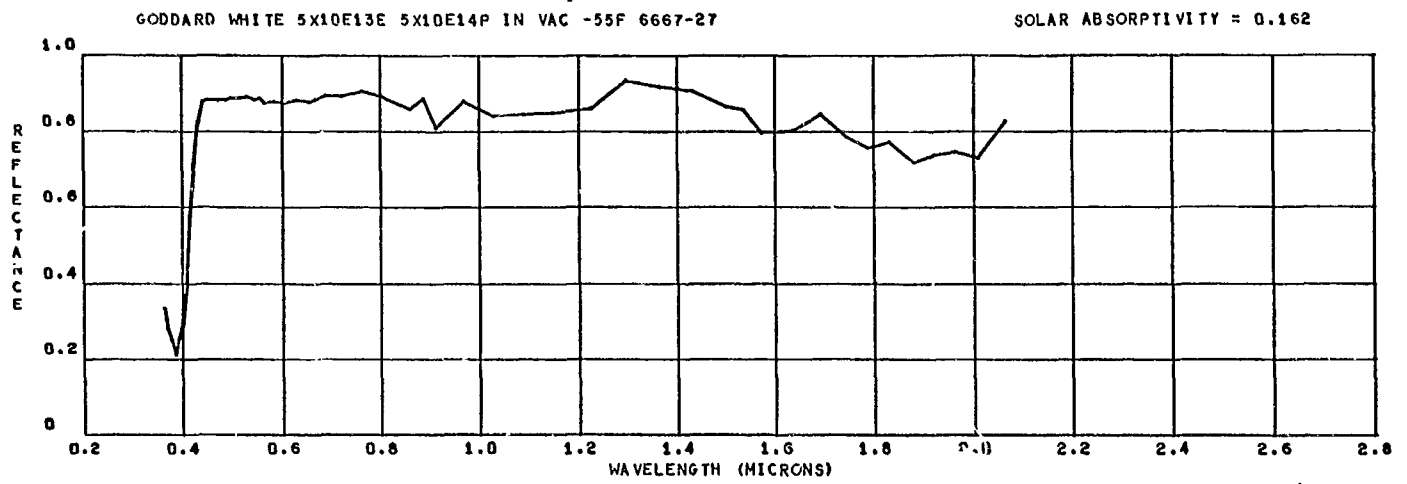


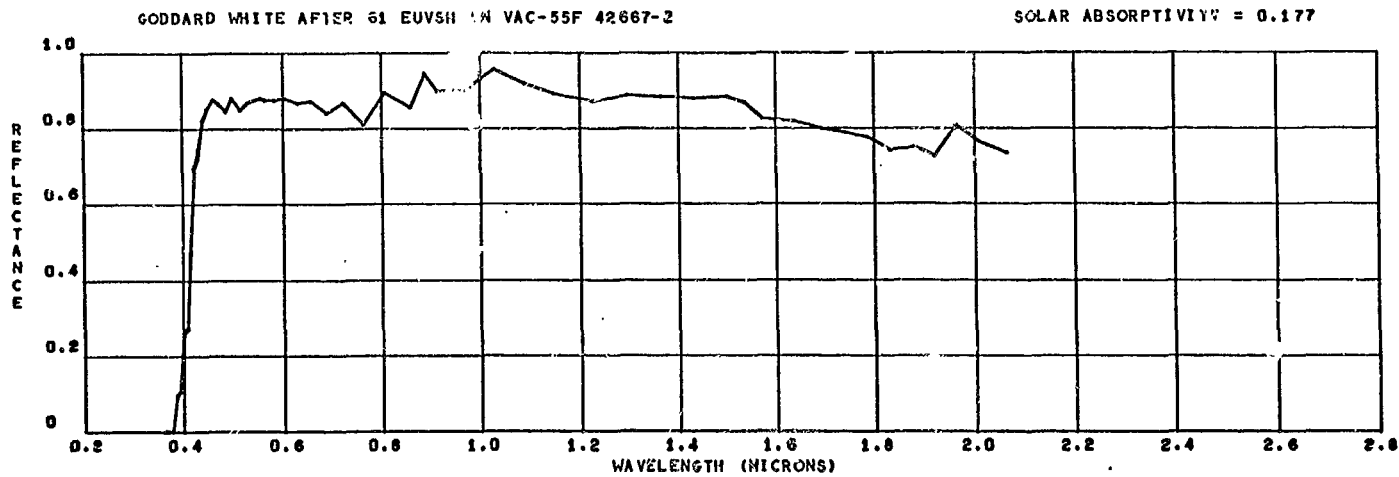
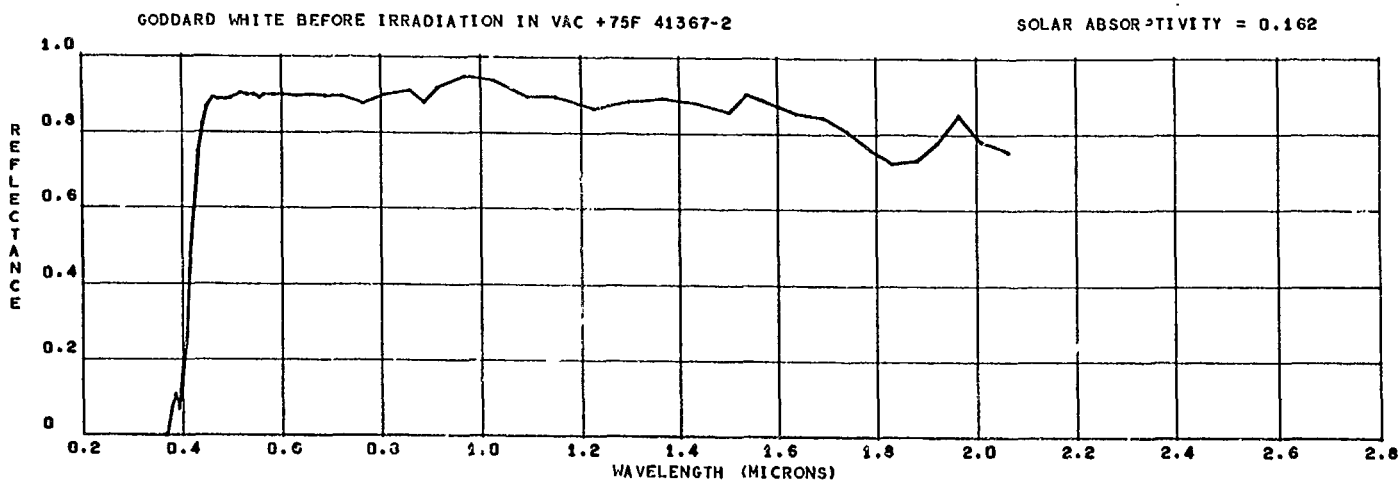
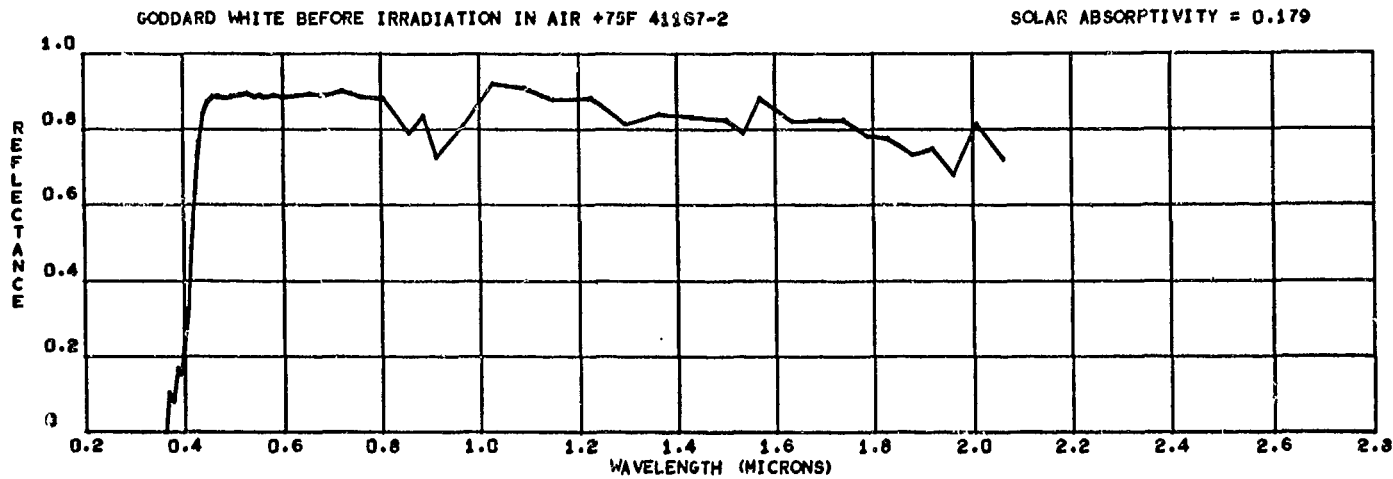


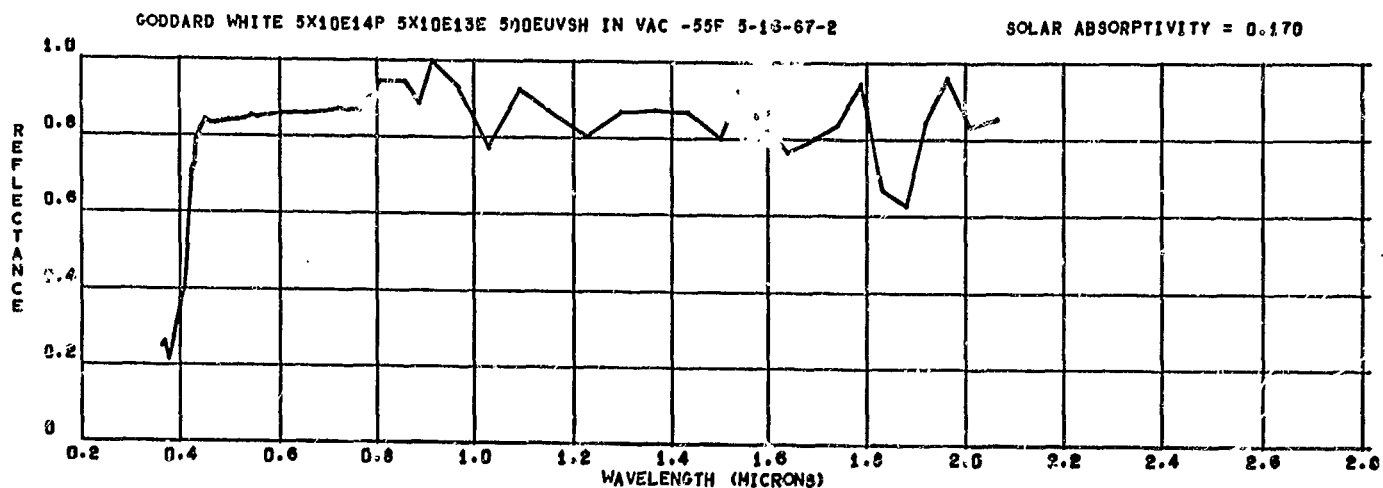
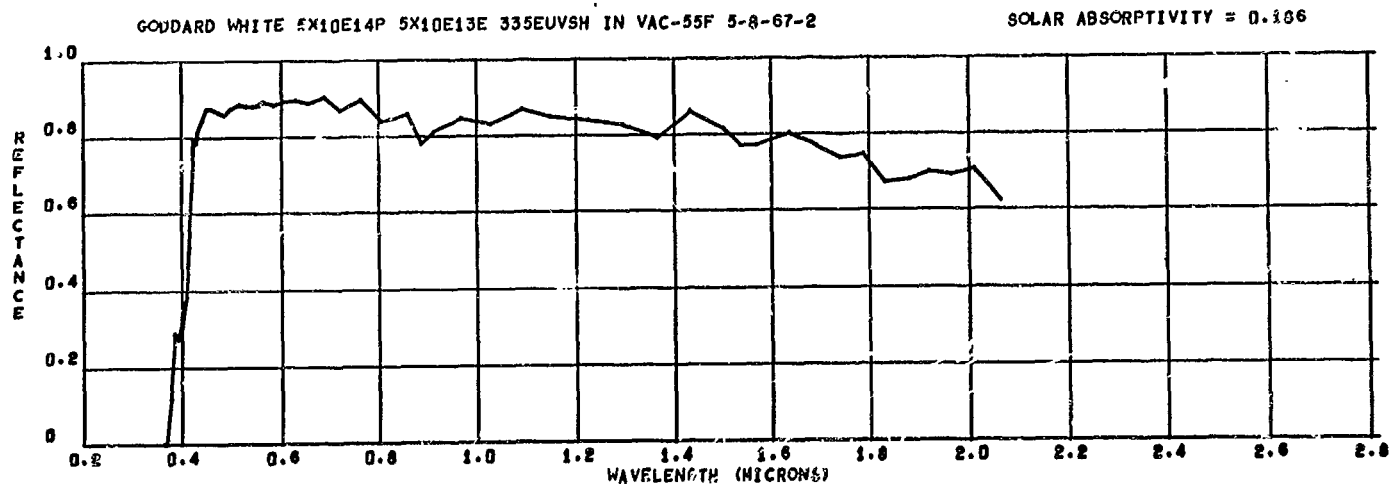
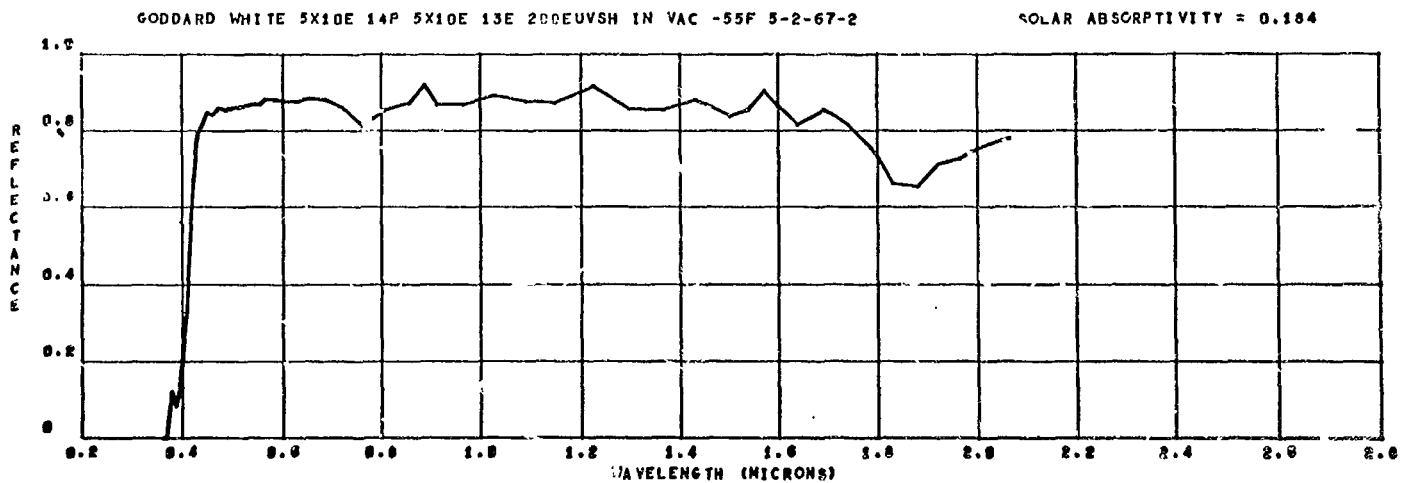


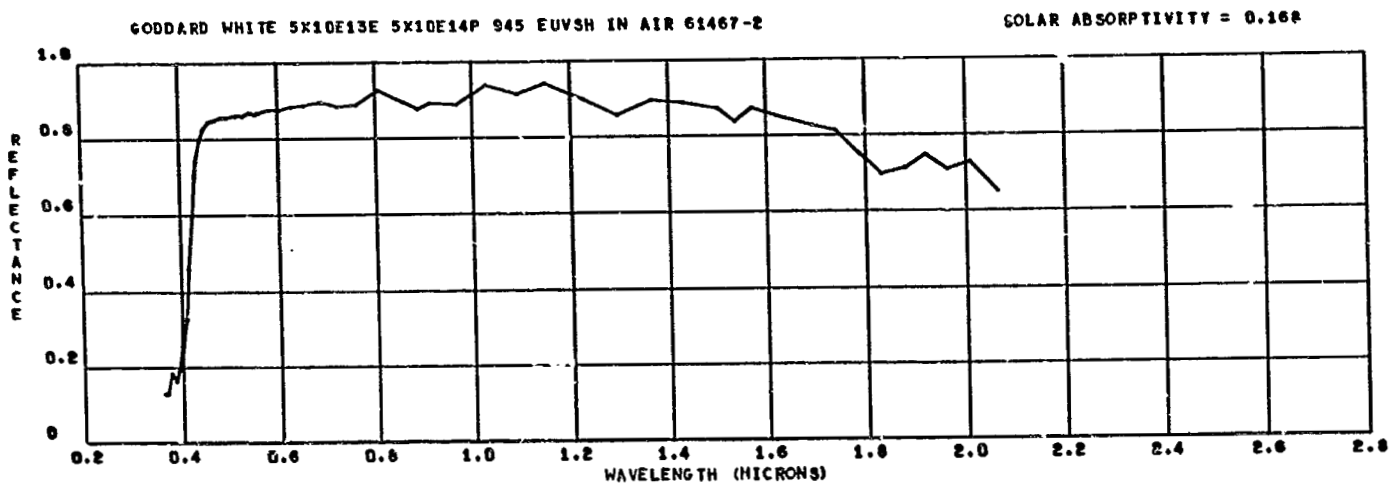
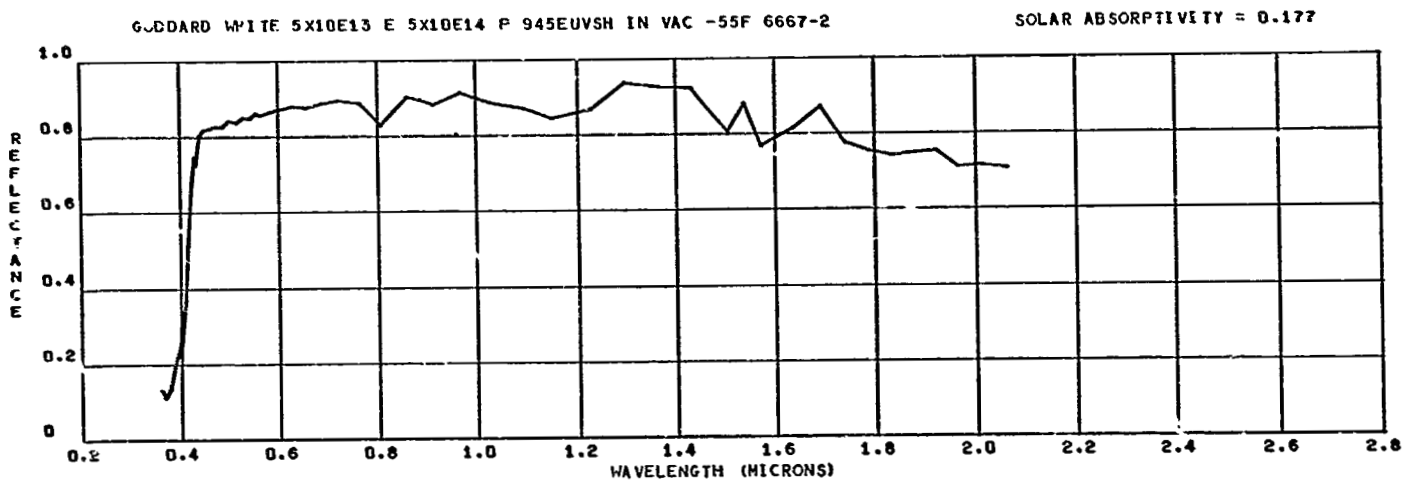
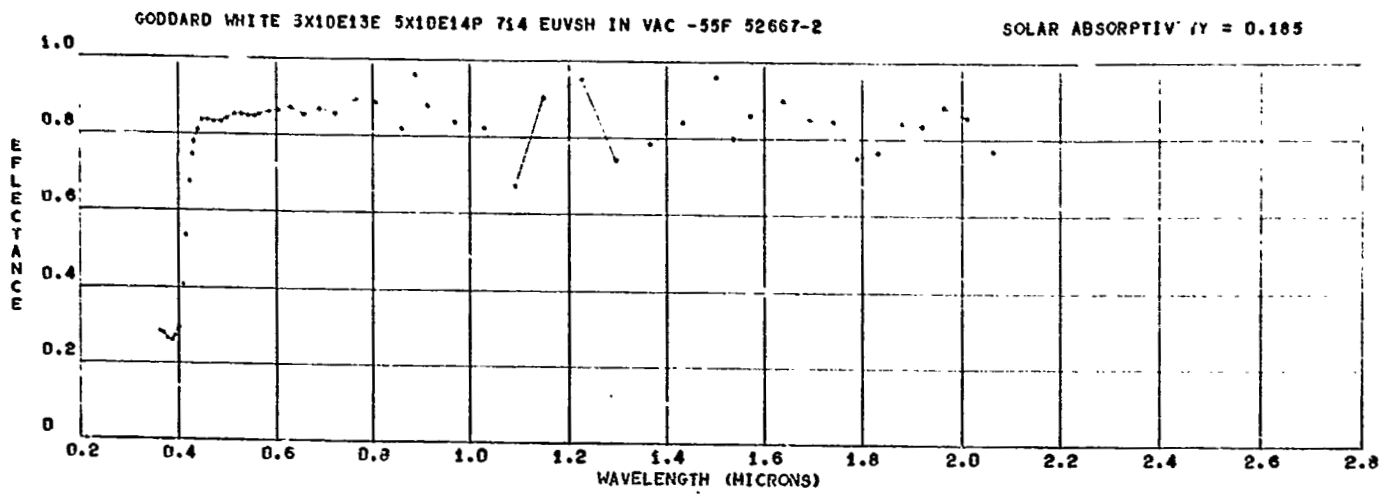


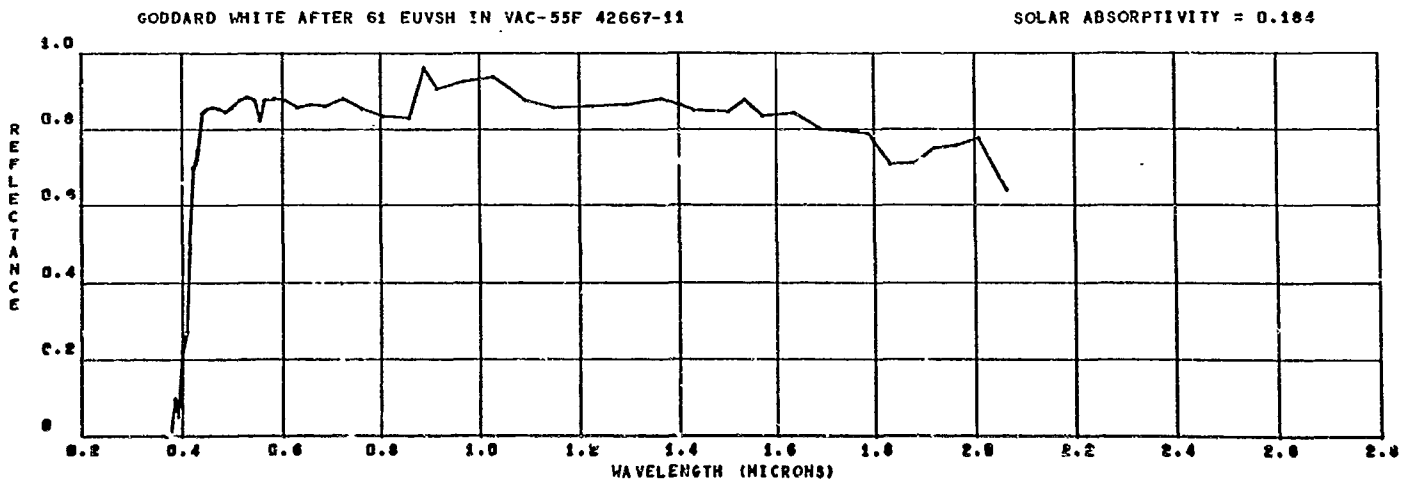
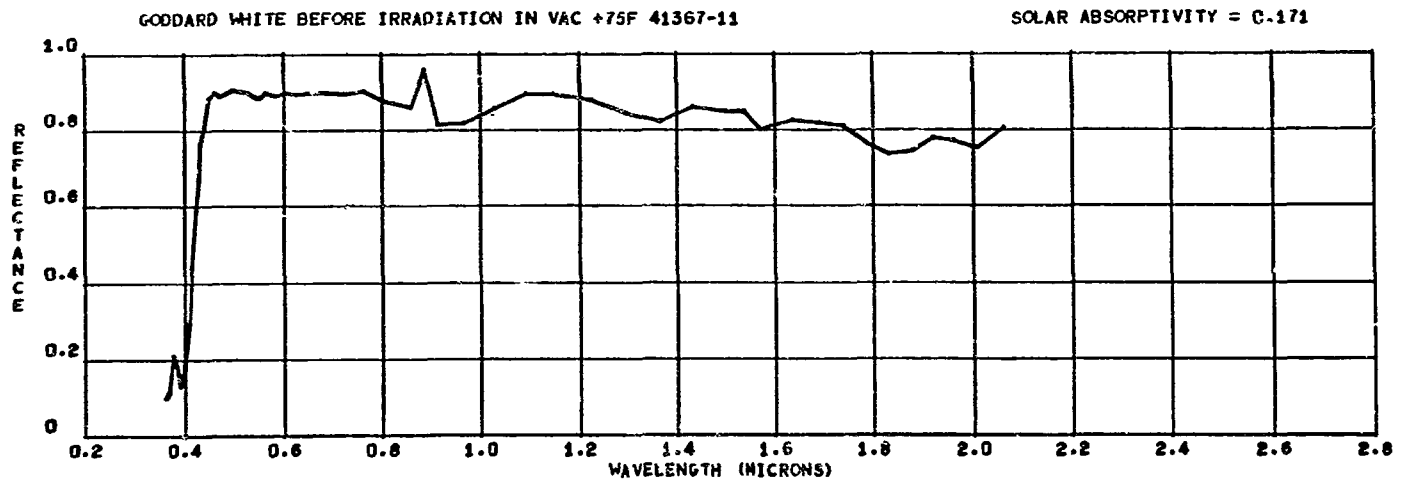
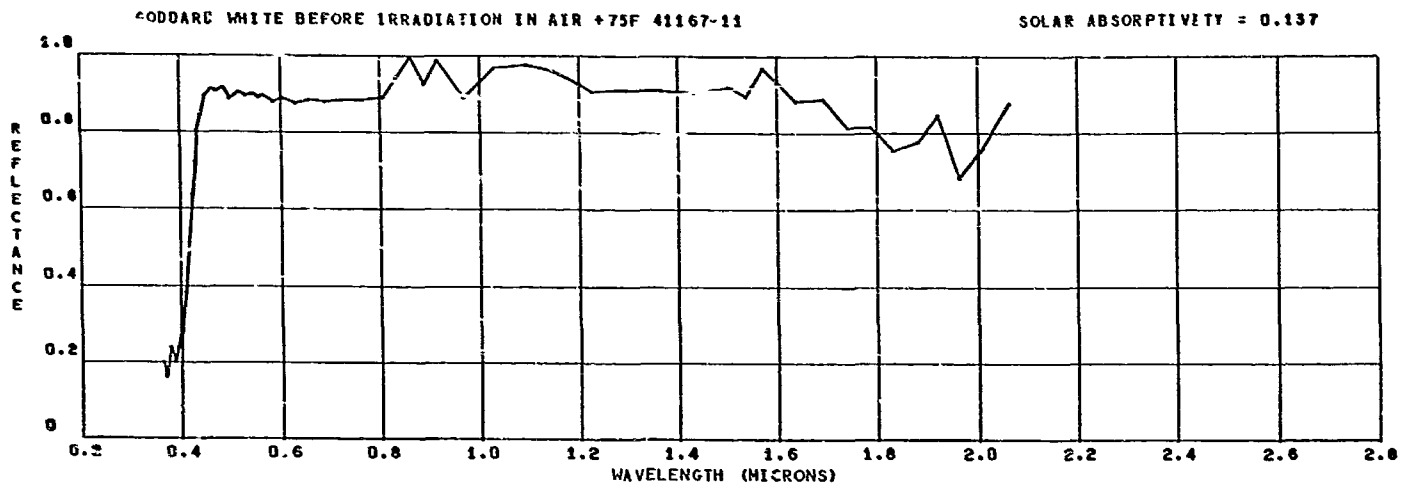






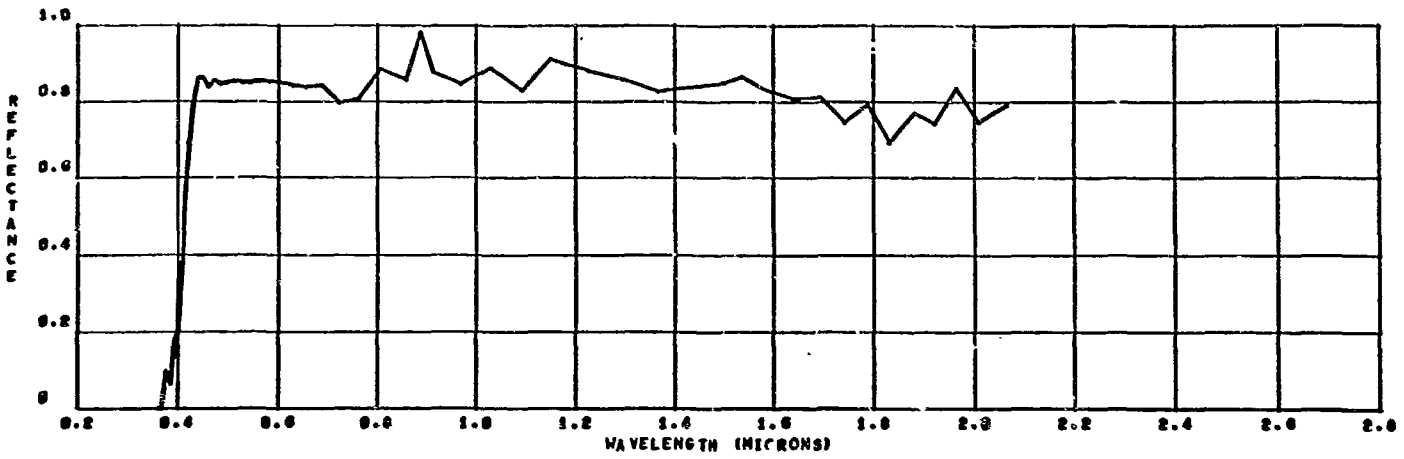






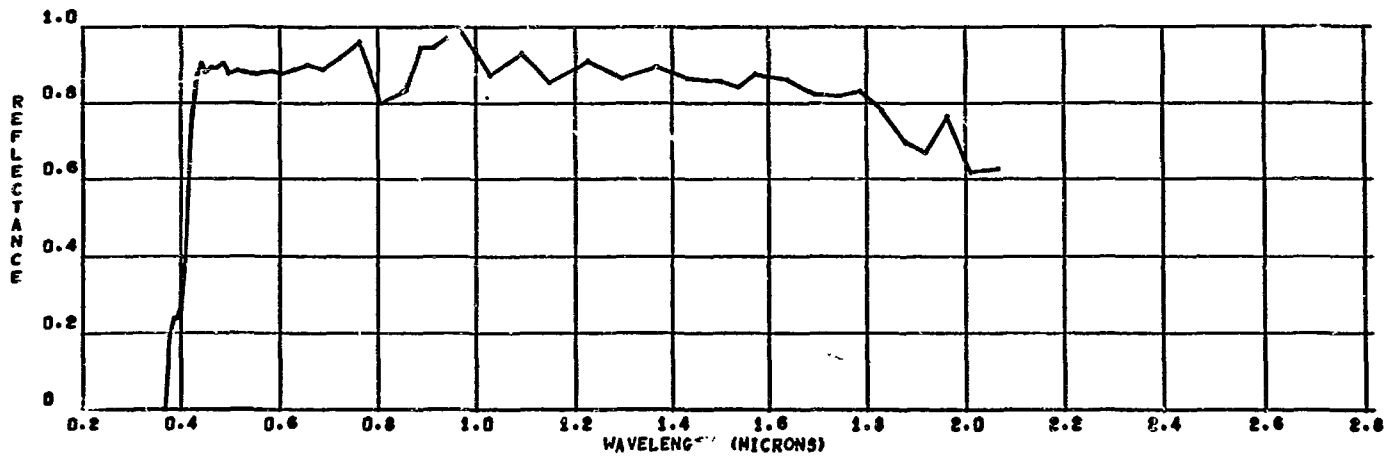
GODDARD WHITE 200EUVSH IN VAC -55F 5-2-67-11

SOLAR ABSORPTIVITY = 0.193



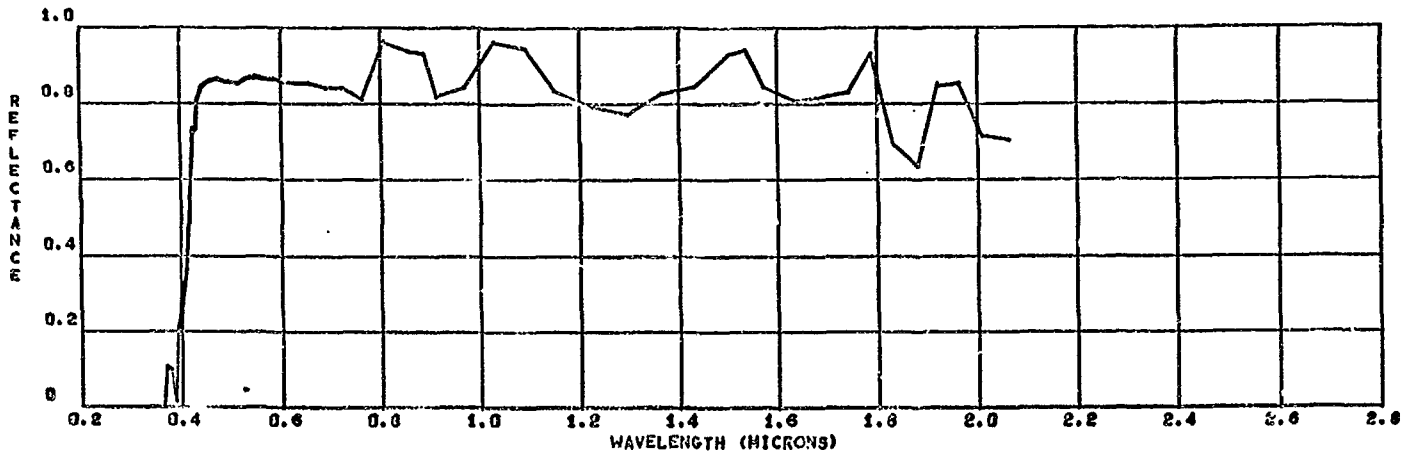
GODDARD WHITE 335 EUVSH IN VAC-55F 5-8-67-11

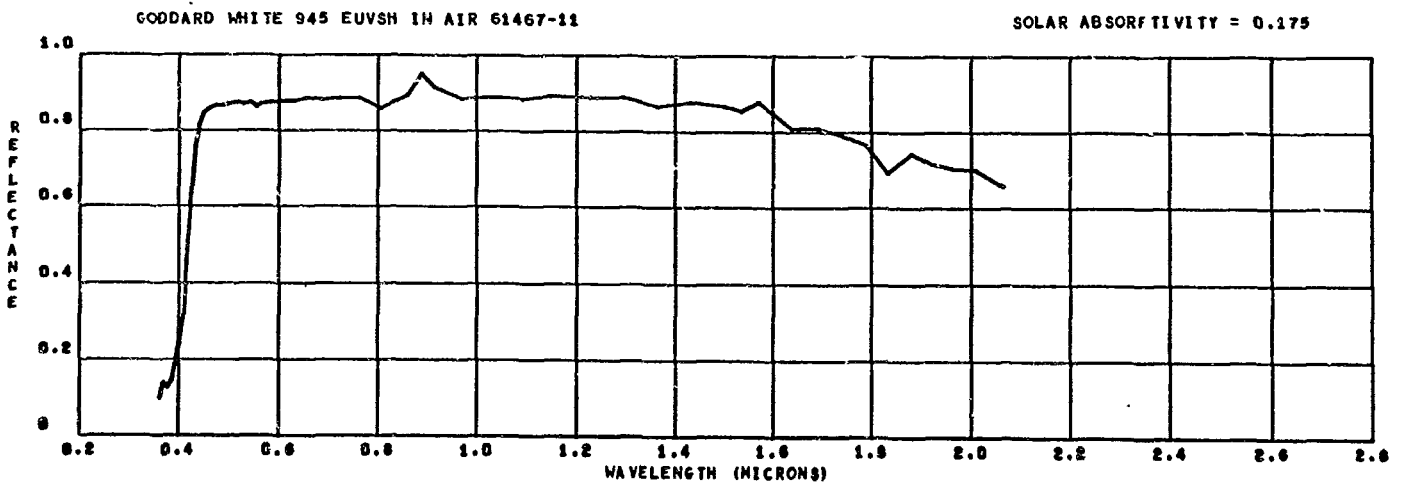
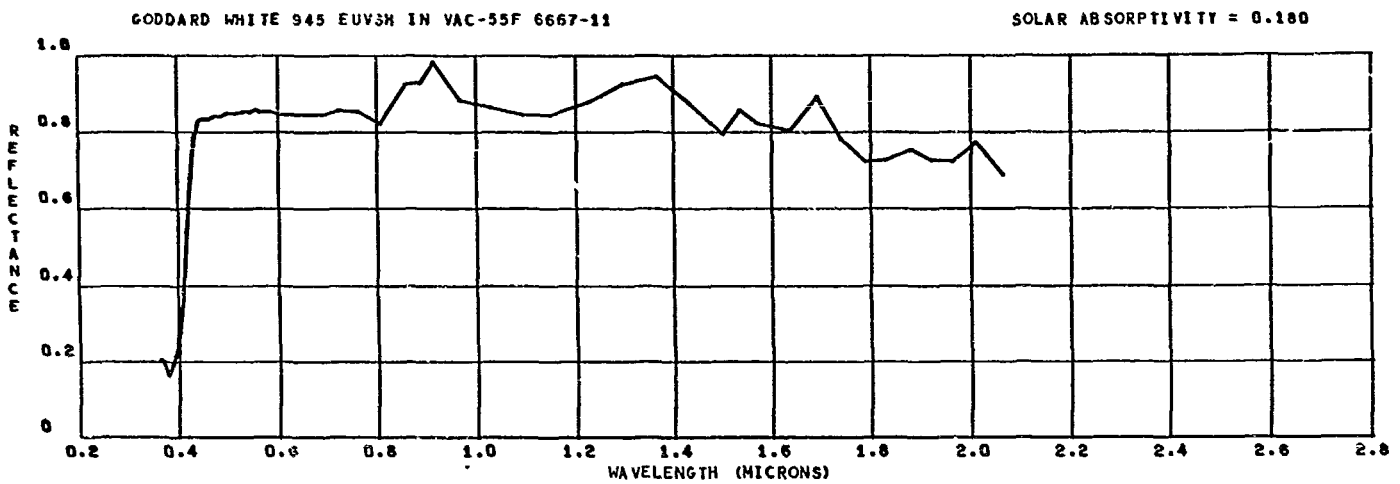
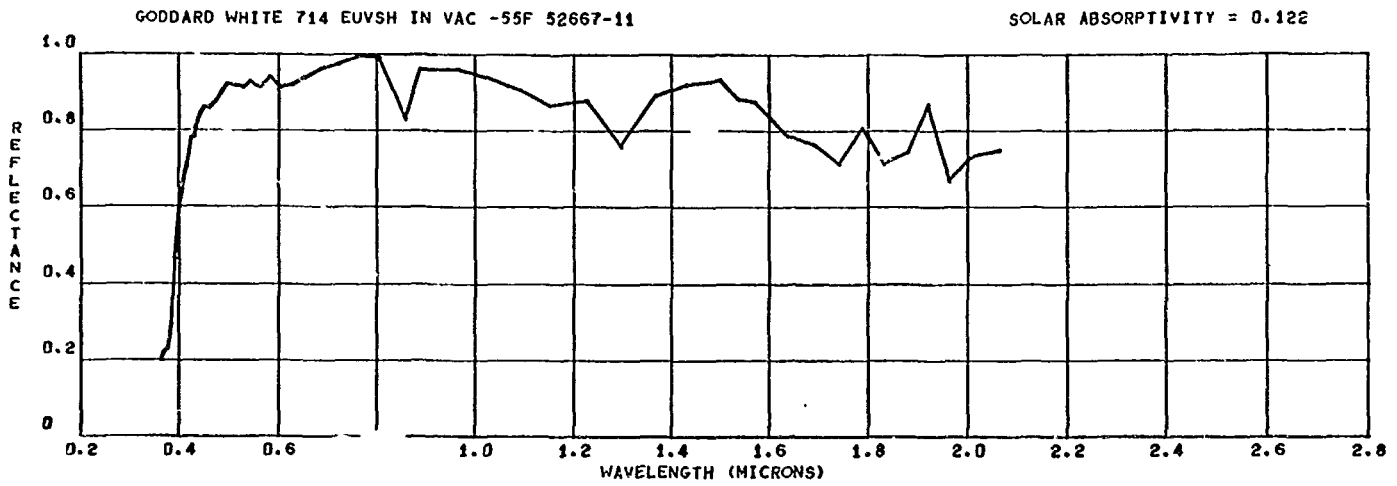
SOLAR ABSORPTIVITY = 0.156

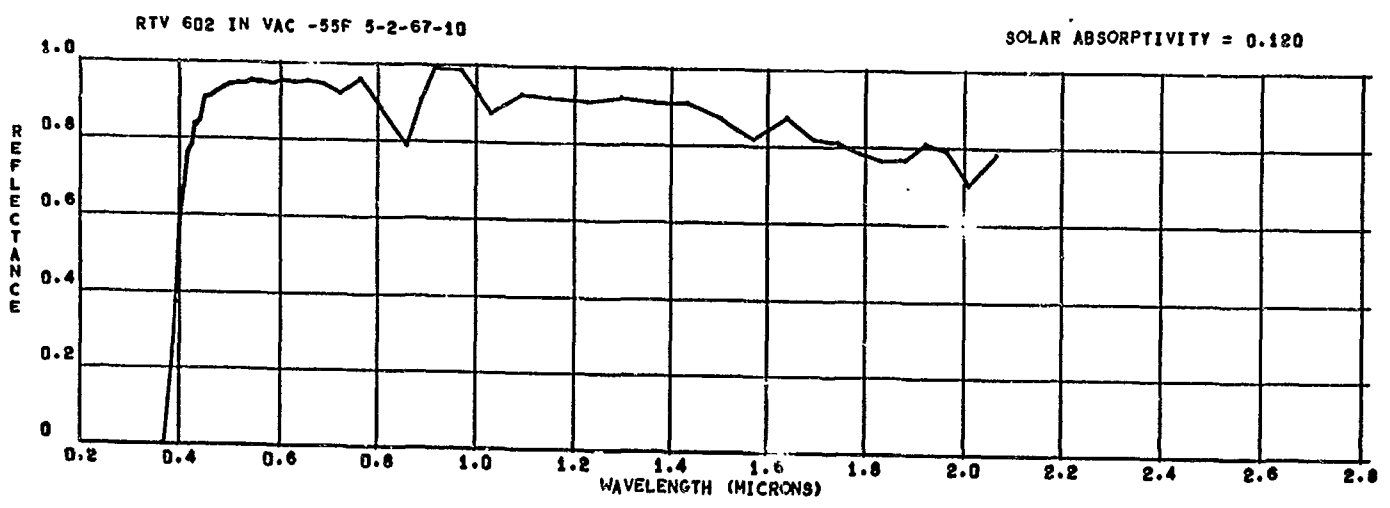
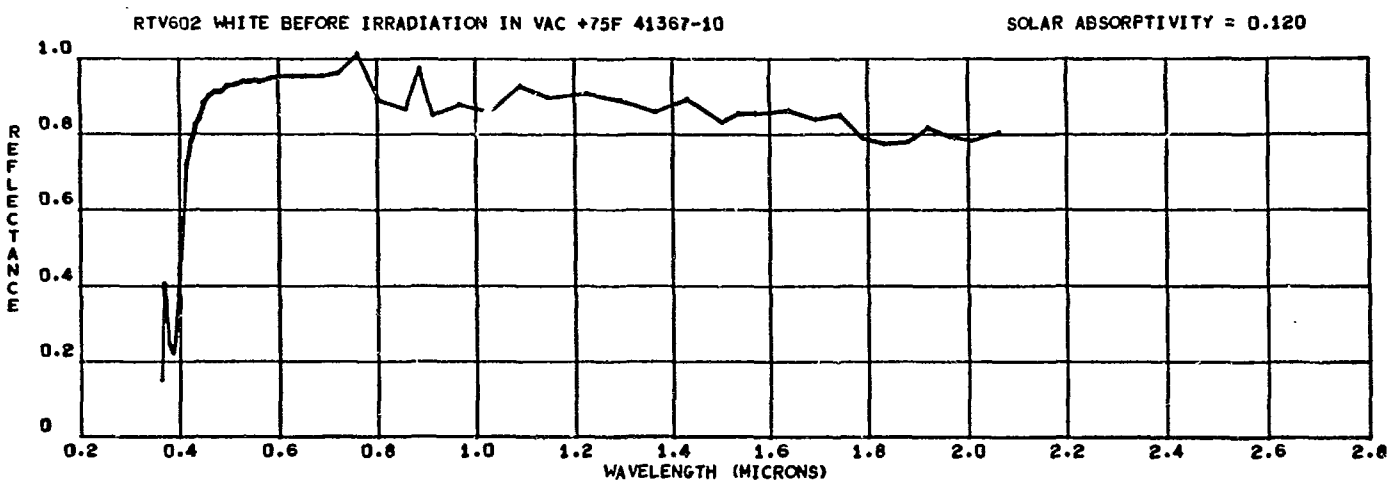
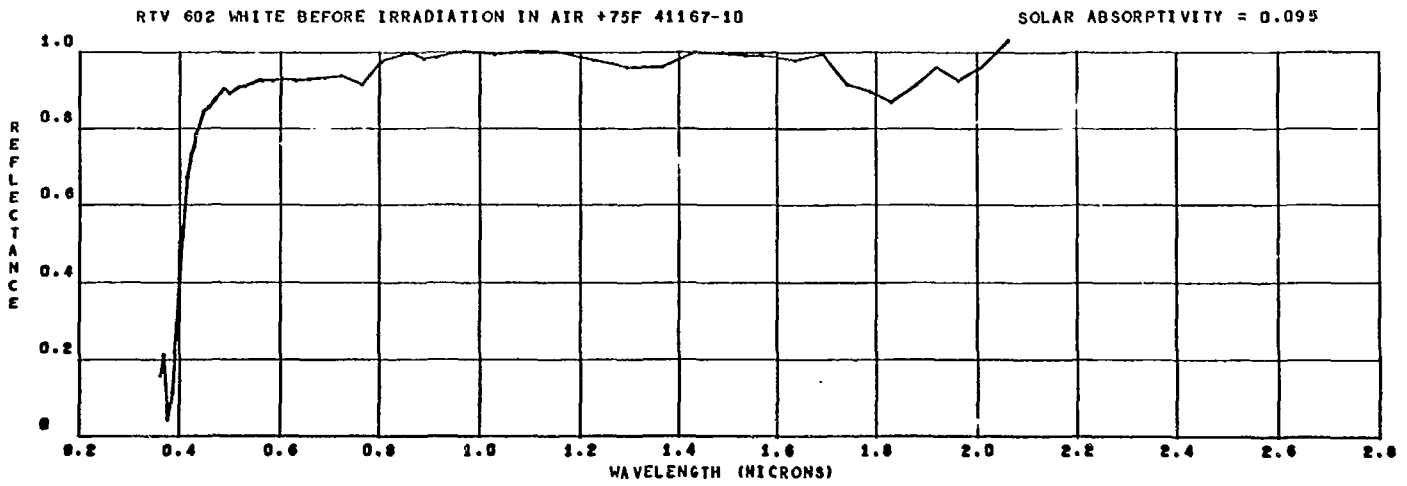


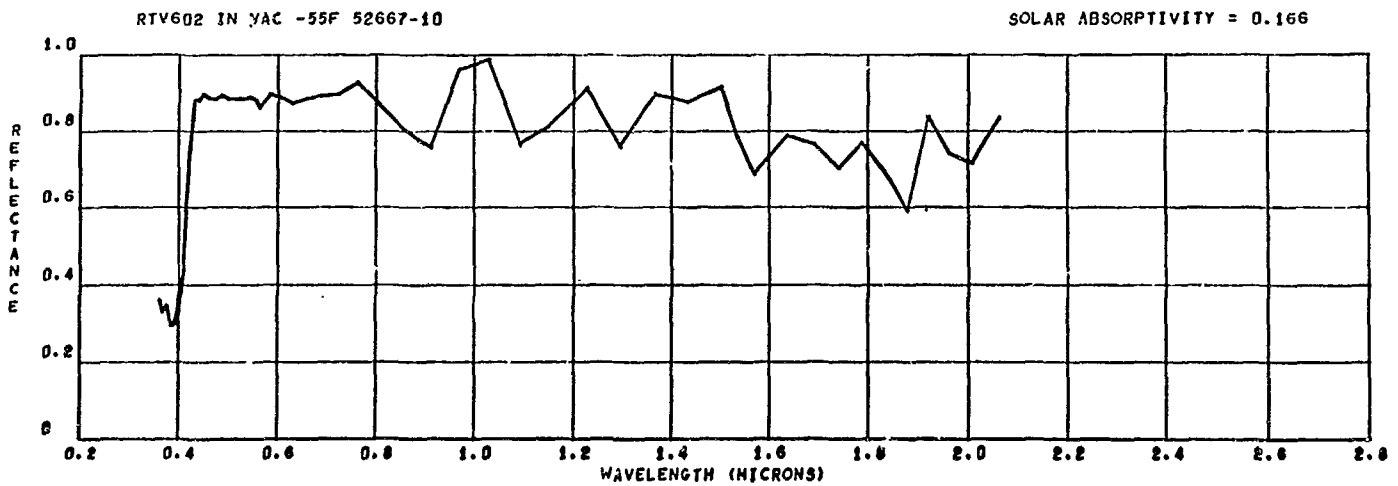
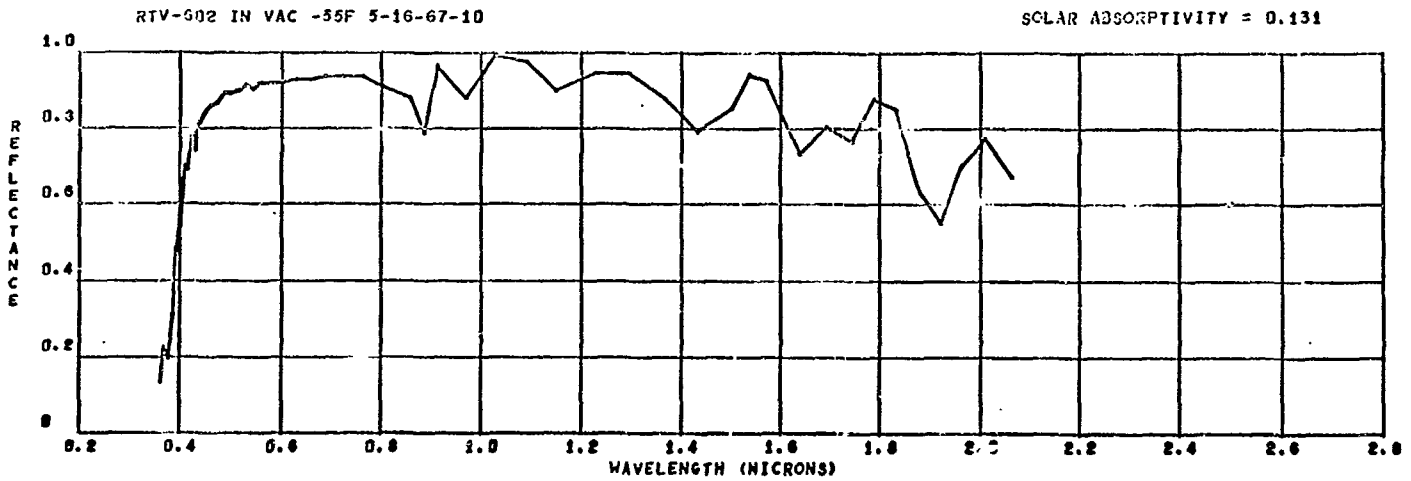
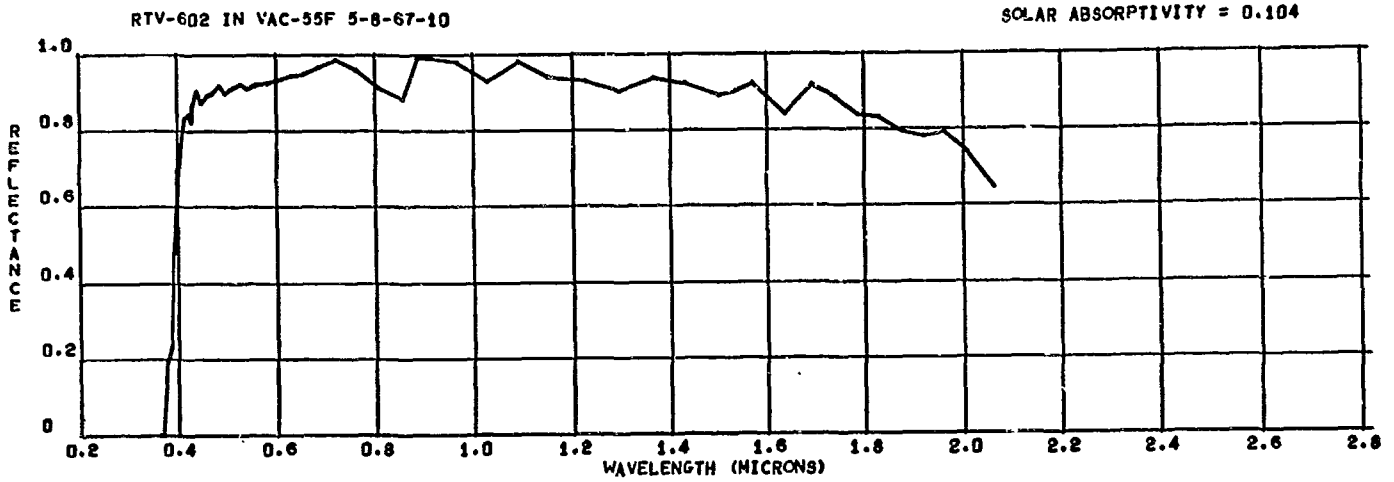
GODDARD WHITE 500EUVSH IN VAC -55F 5-16-67-11

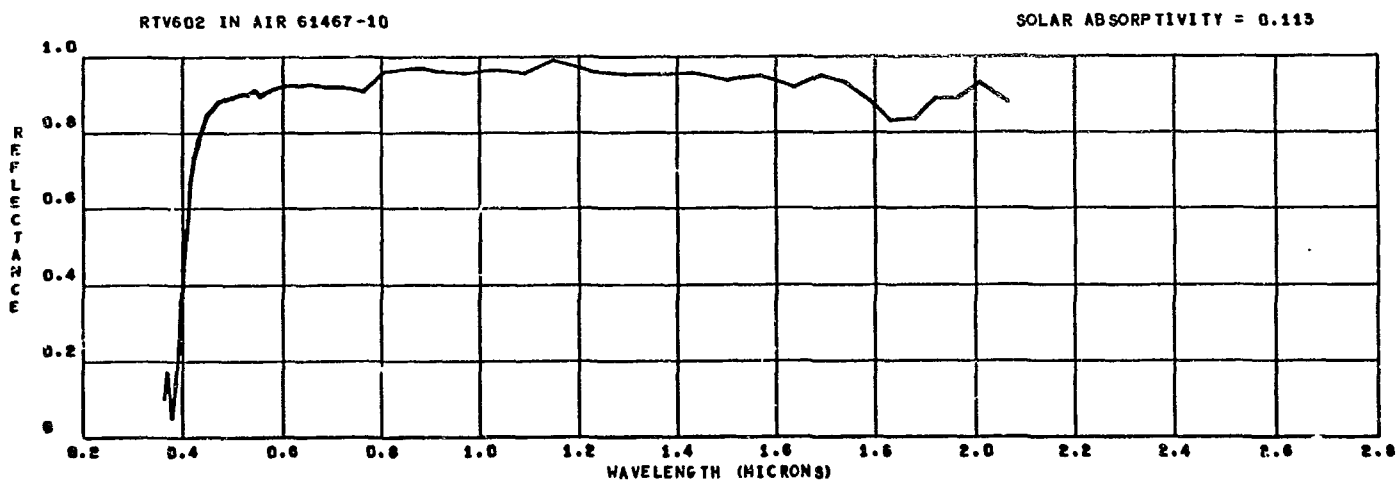
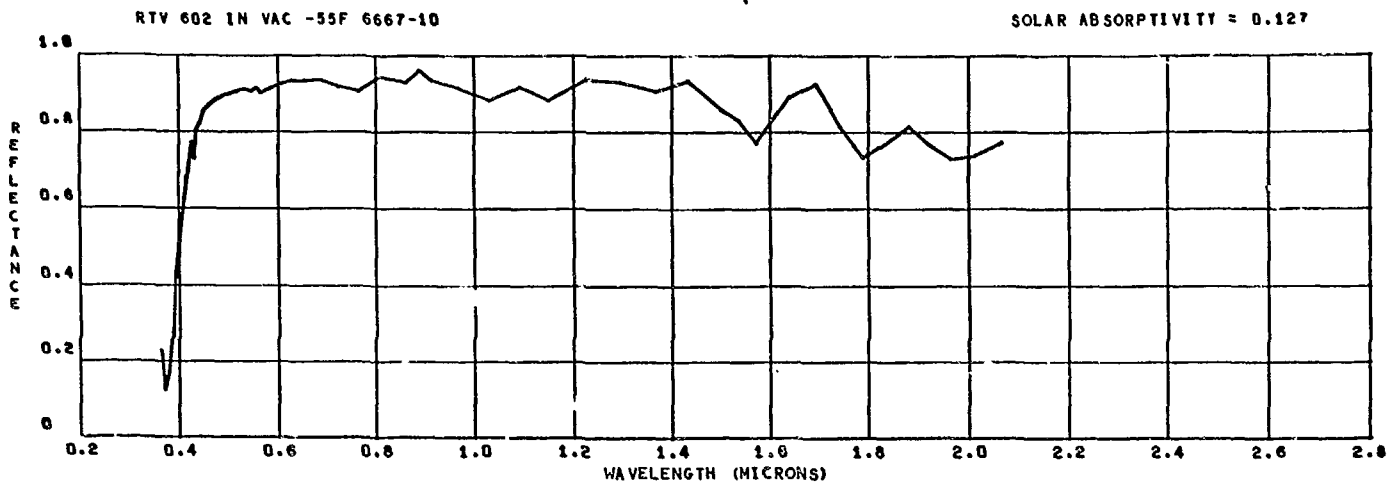
SOLAR ABSORPTIVITY = 0.180

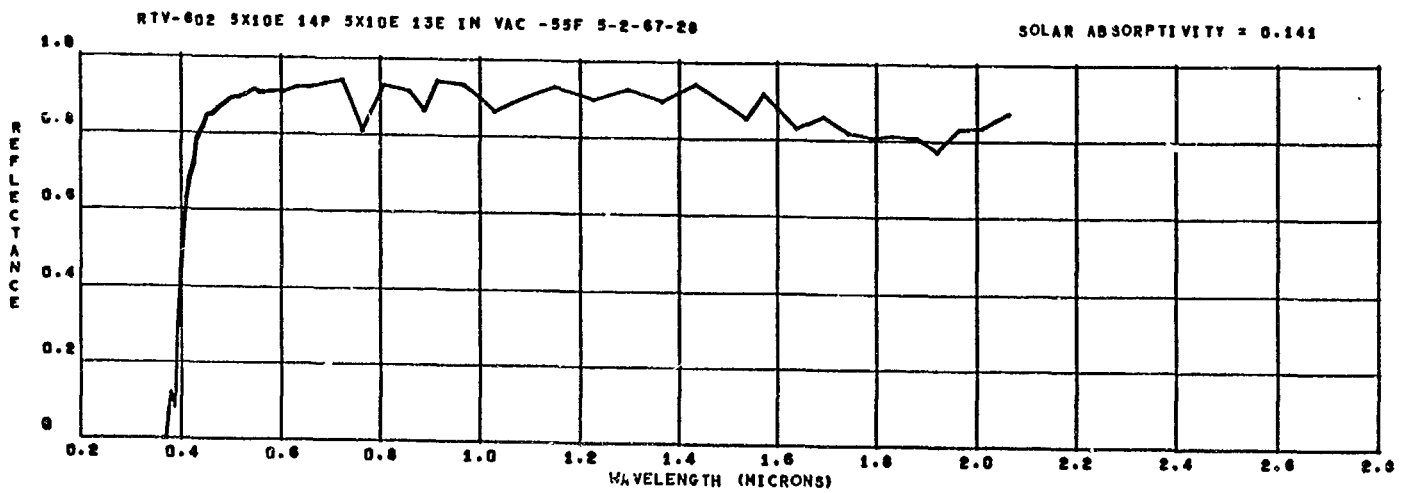
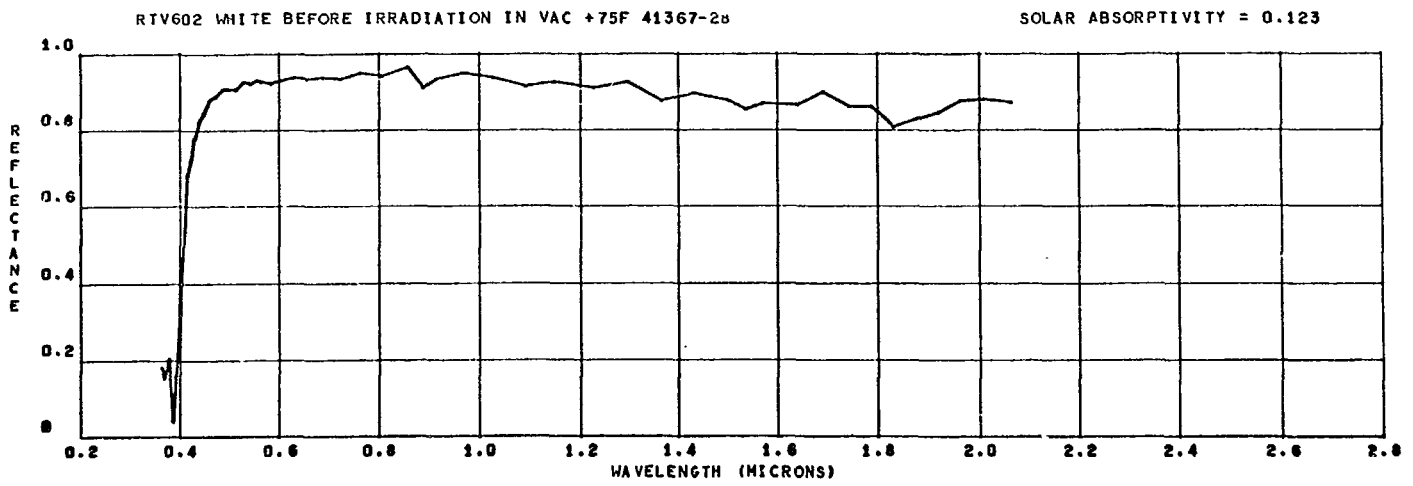
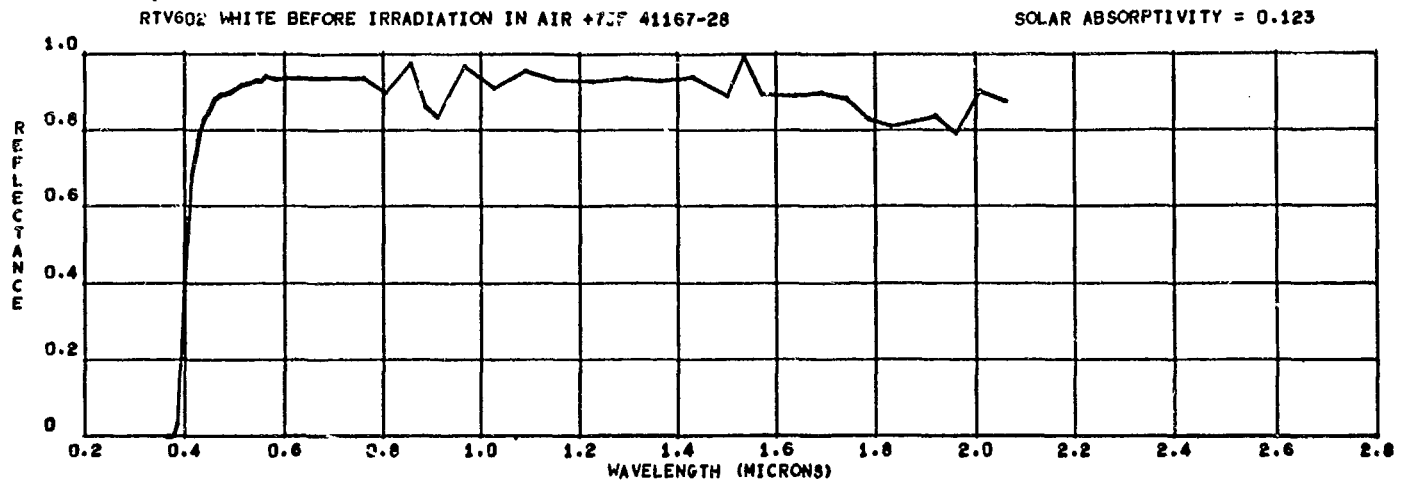


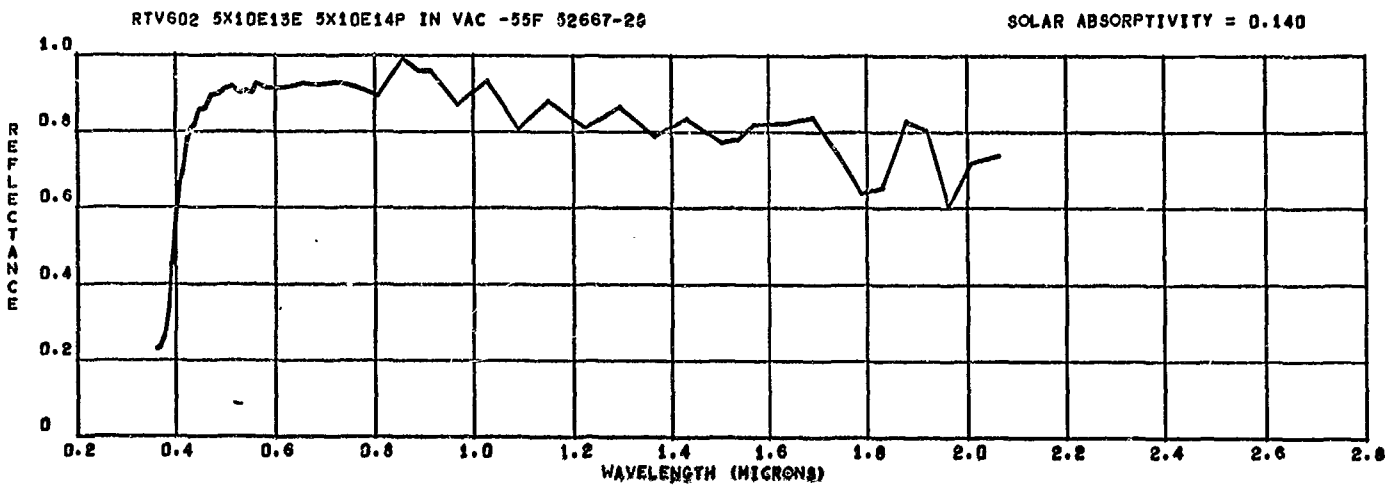
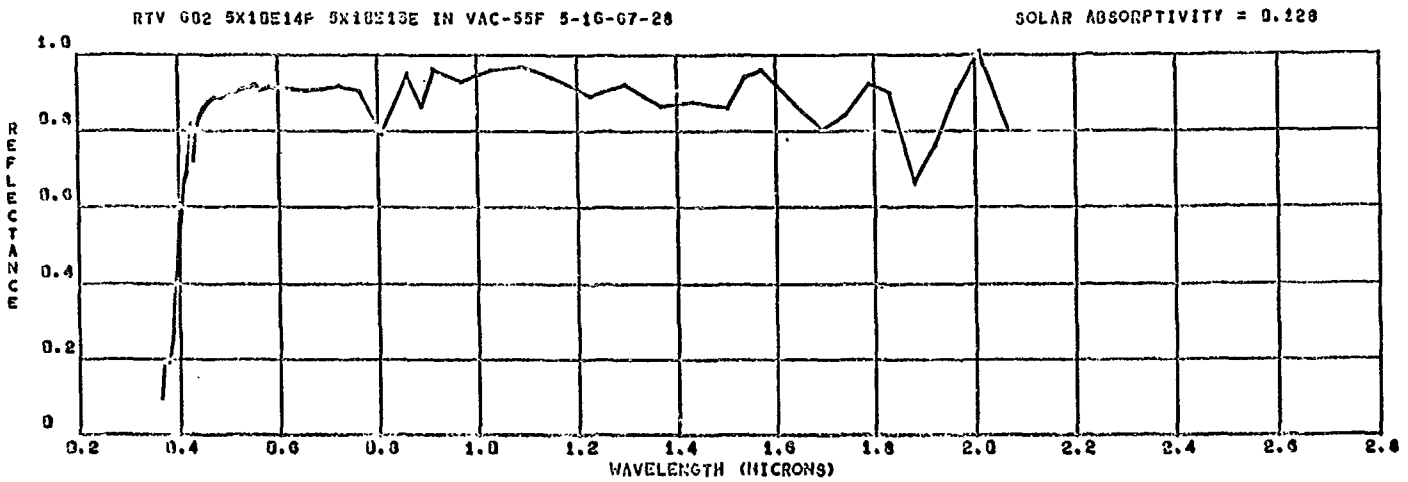
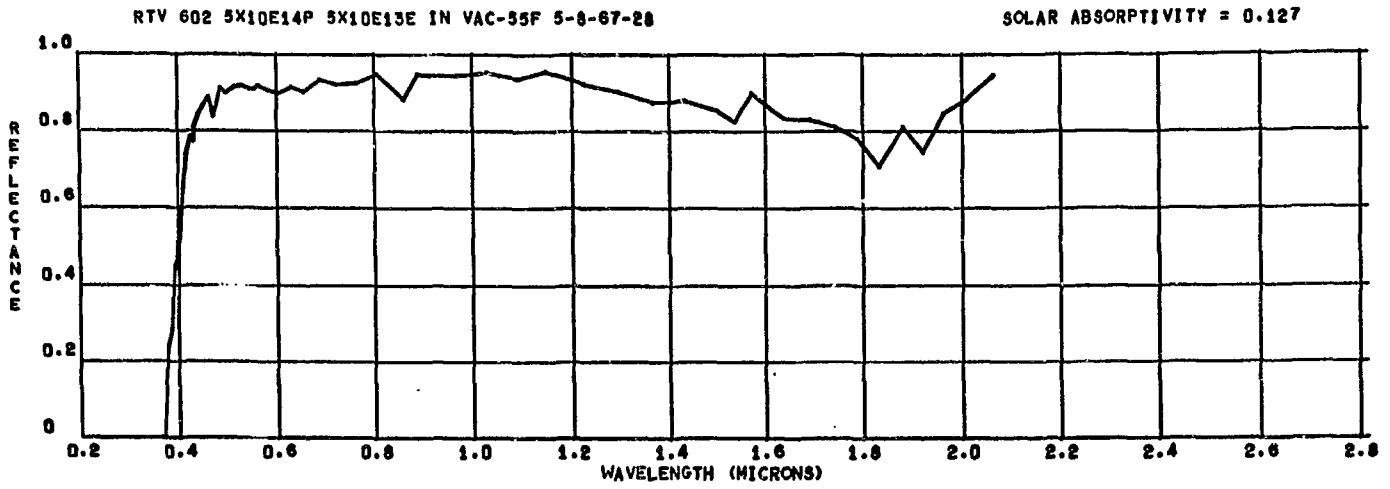






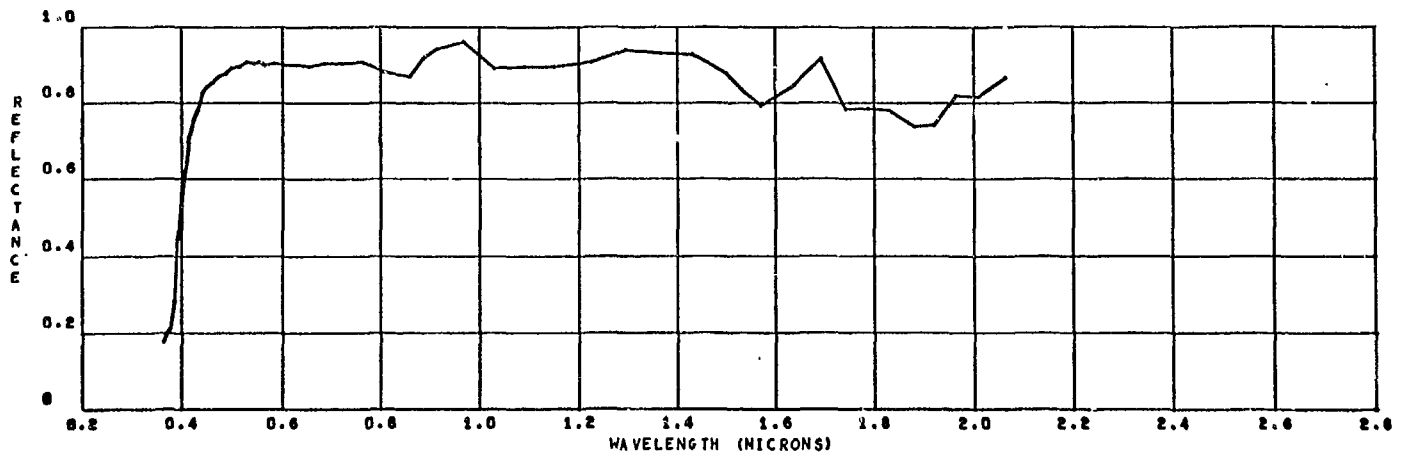






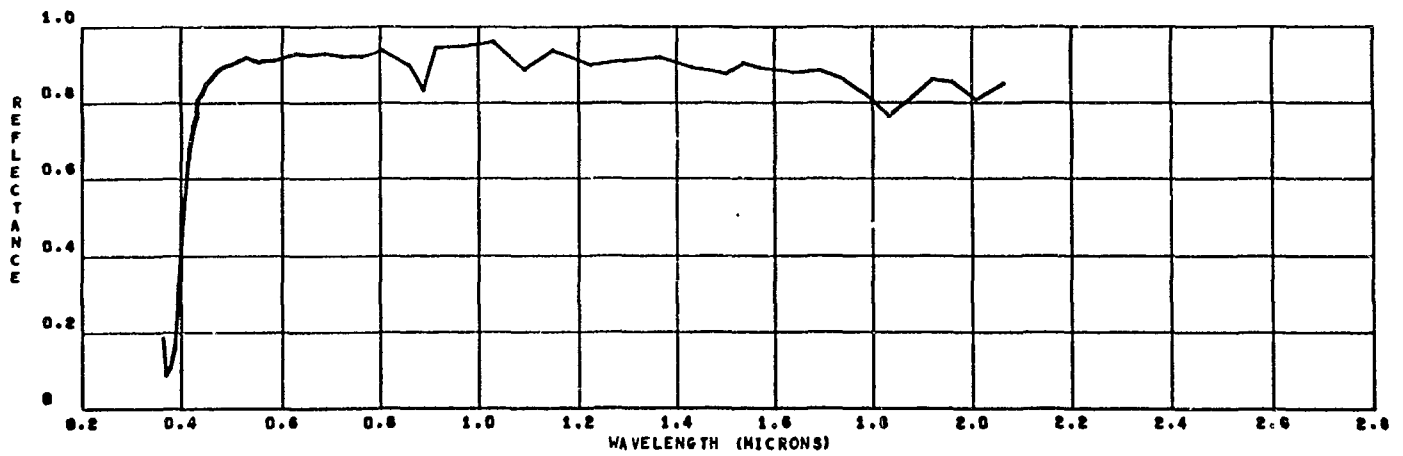
RTV 602 5X10E13E 5X10E14P IN VAC -55F 6667-28

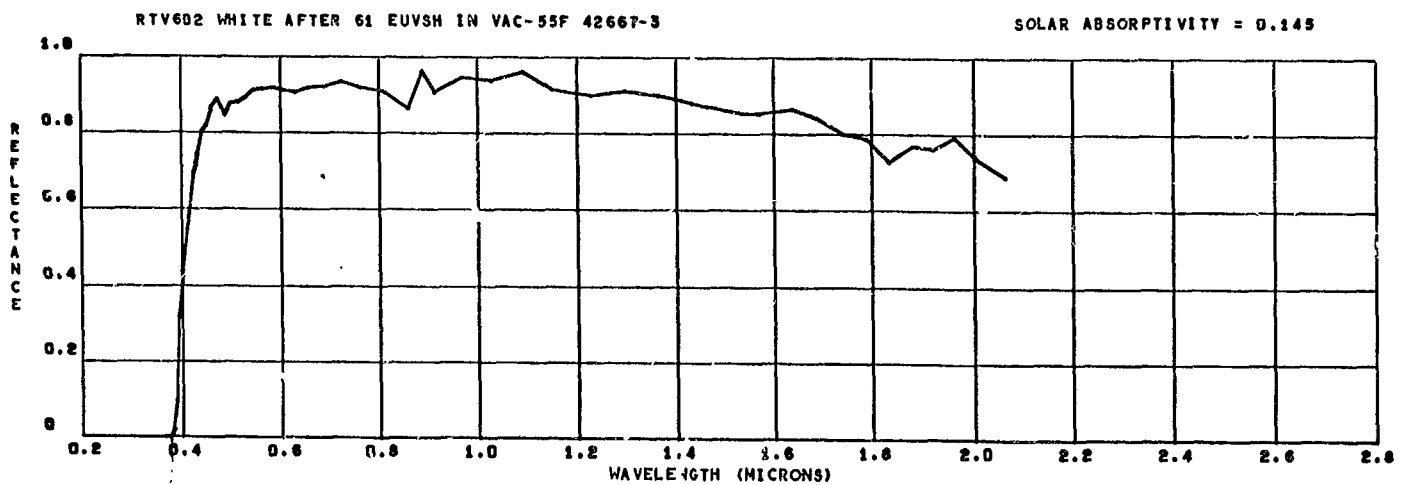
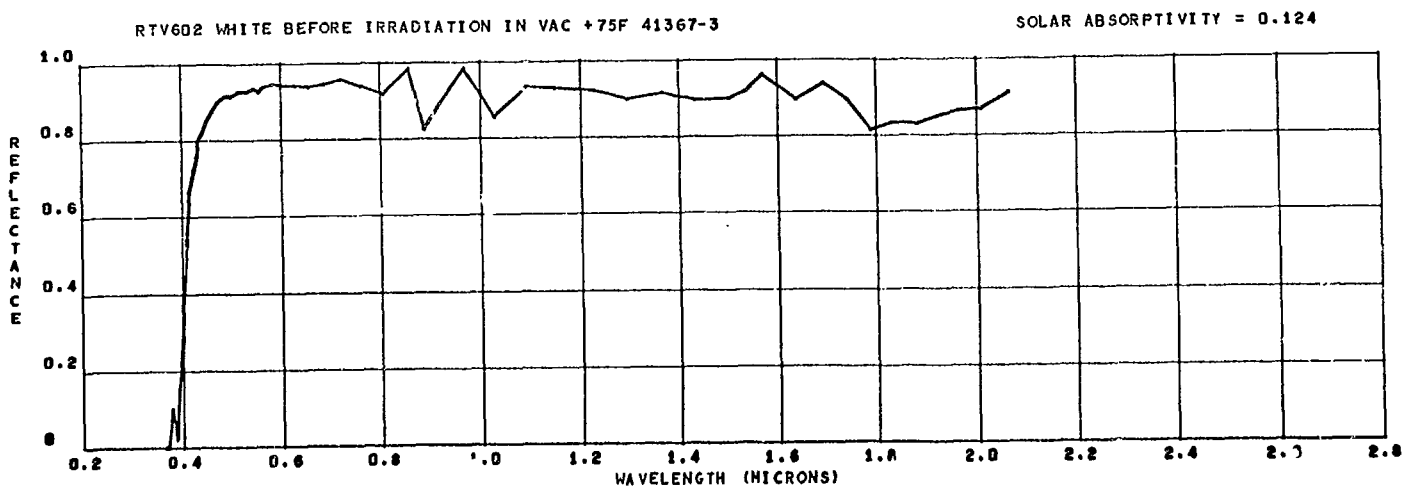
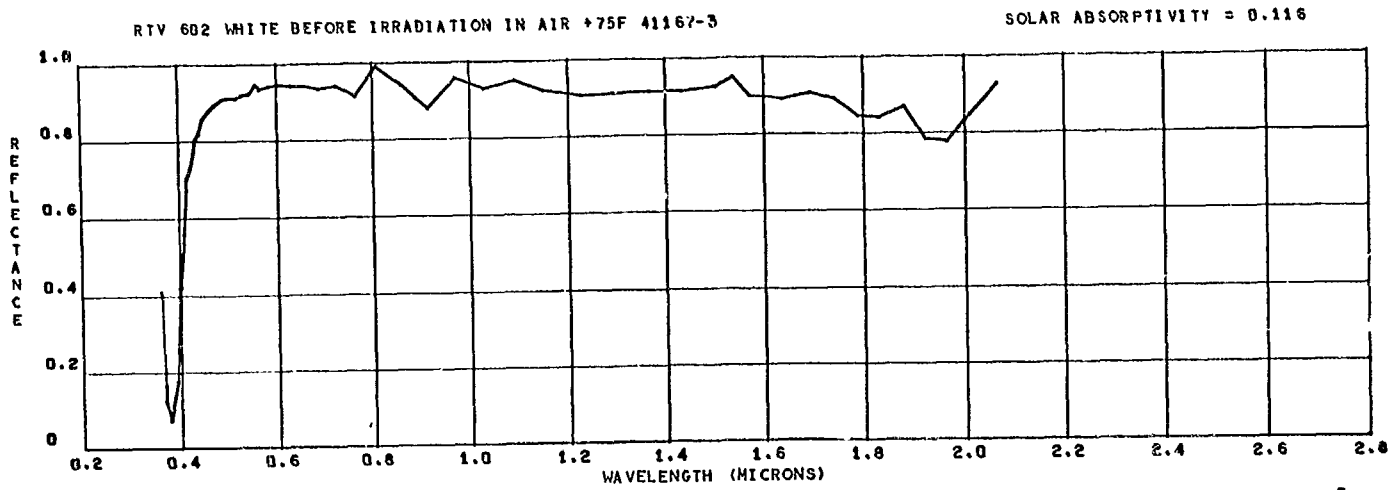
SOLAR ABSORPTIVITY = 0.138

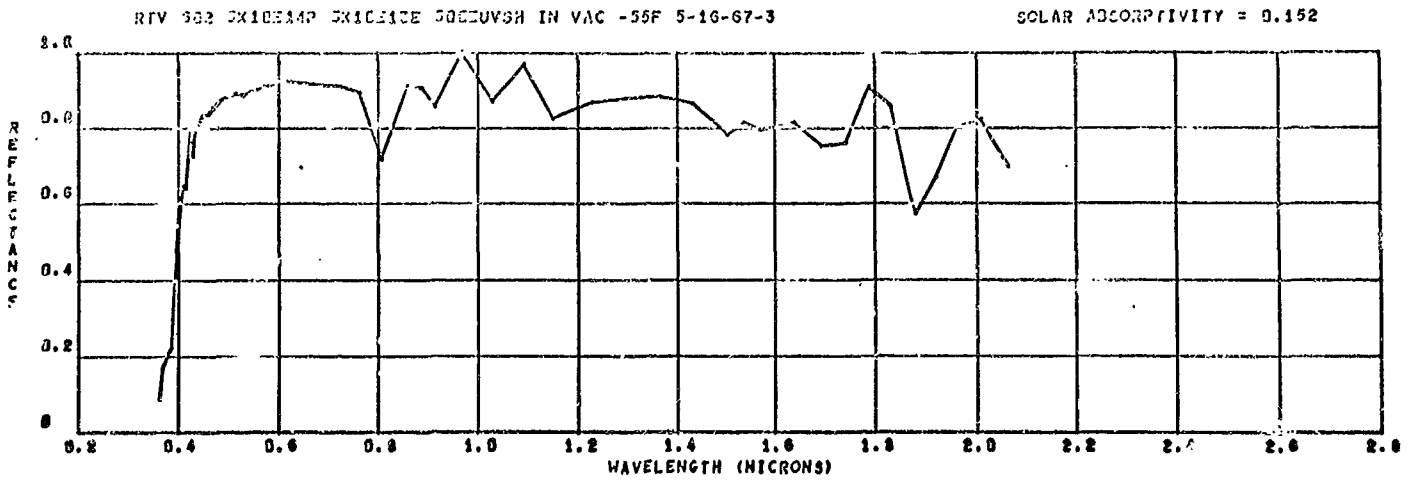
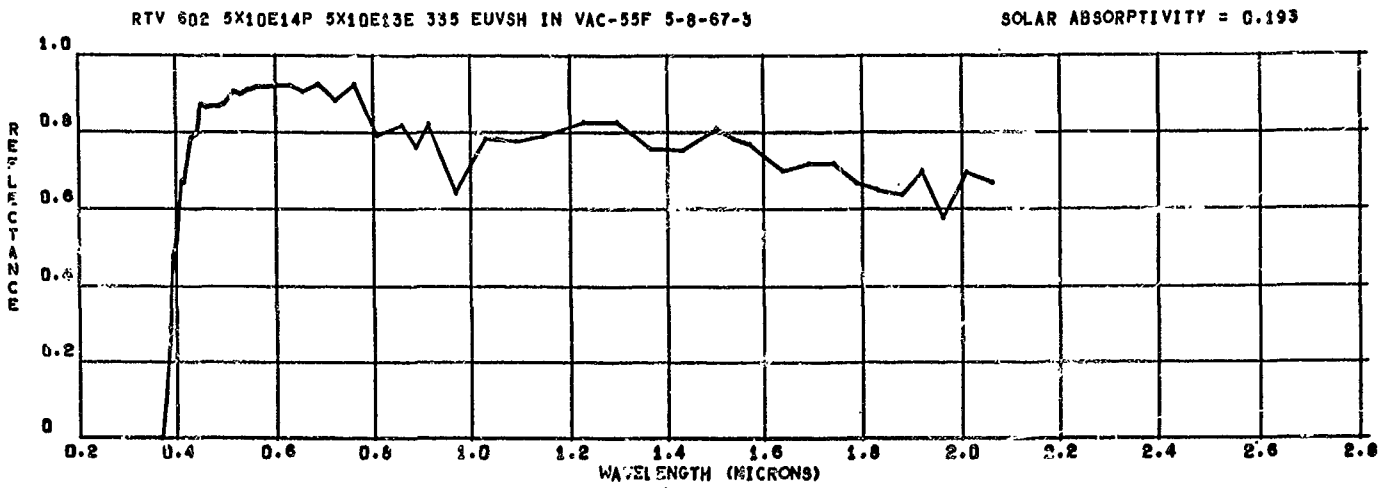
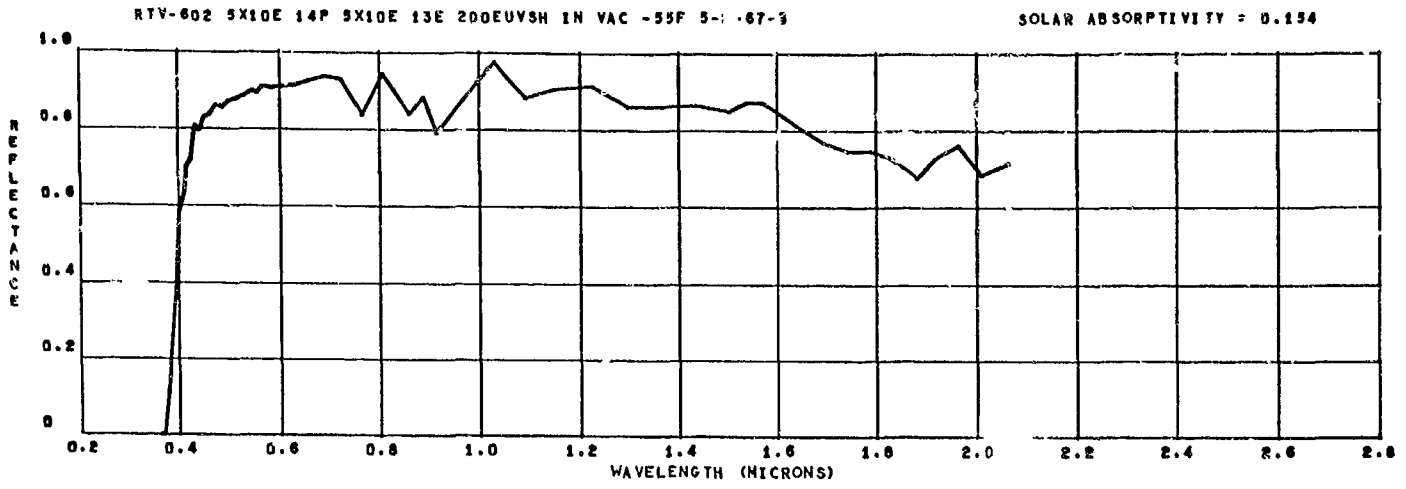


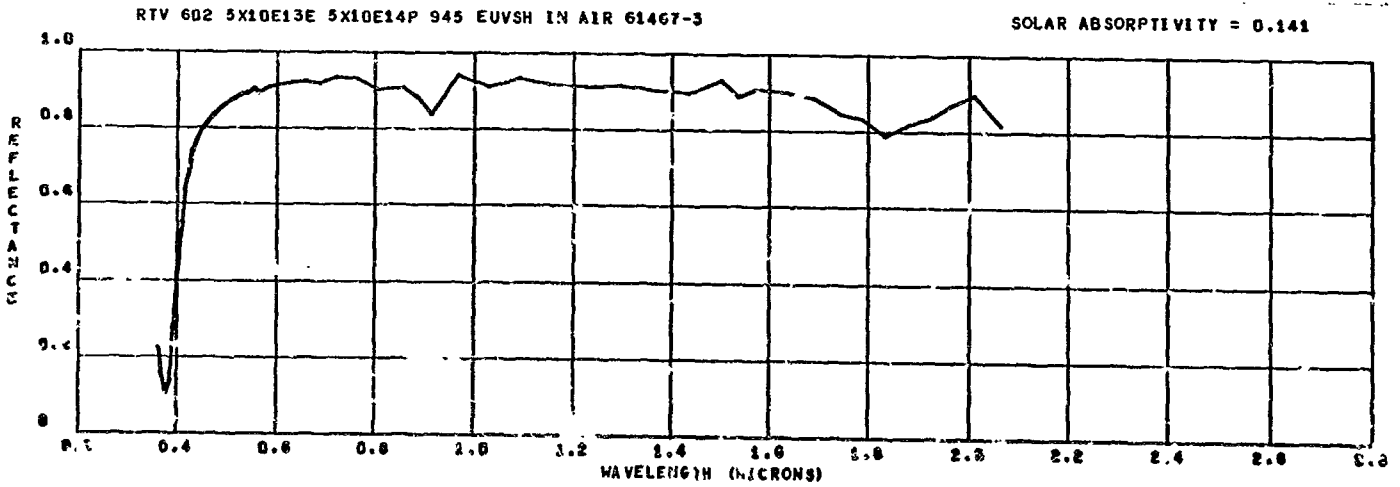
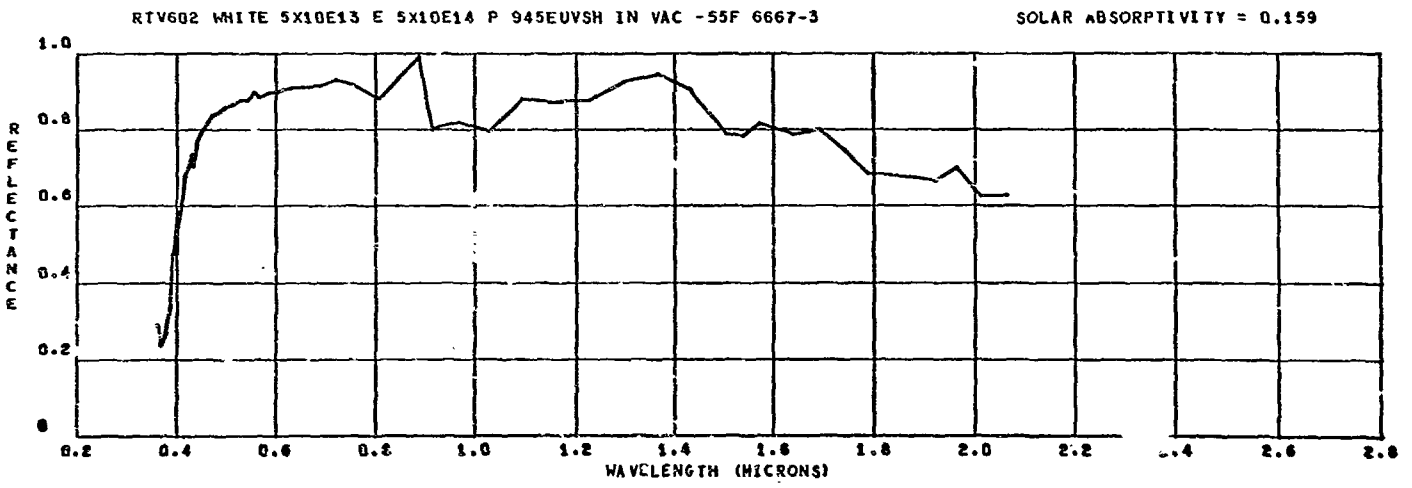
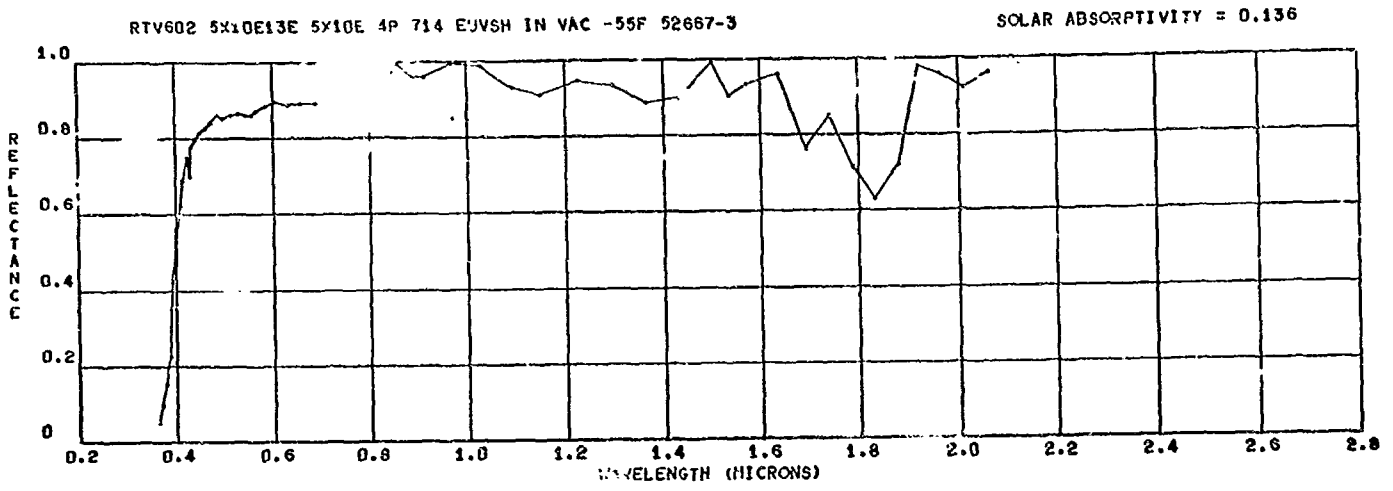
RTV 602 5X10E13E 5X10E14P IN AIR 61467-28

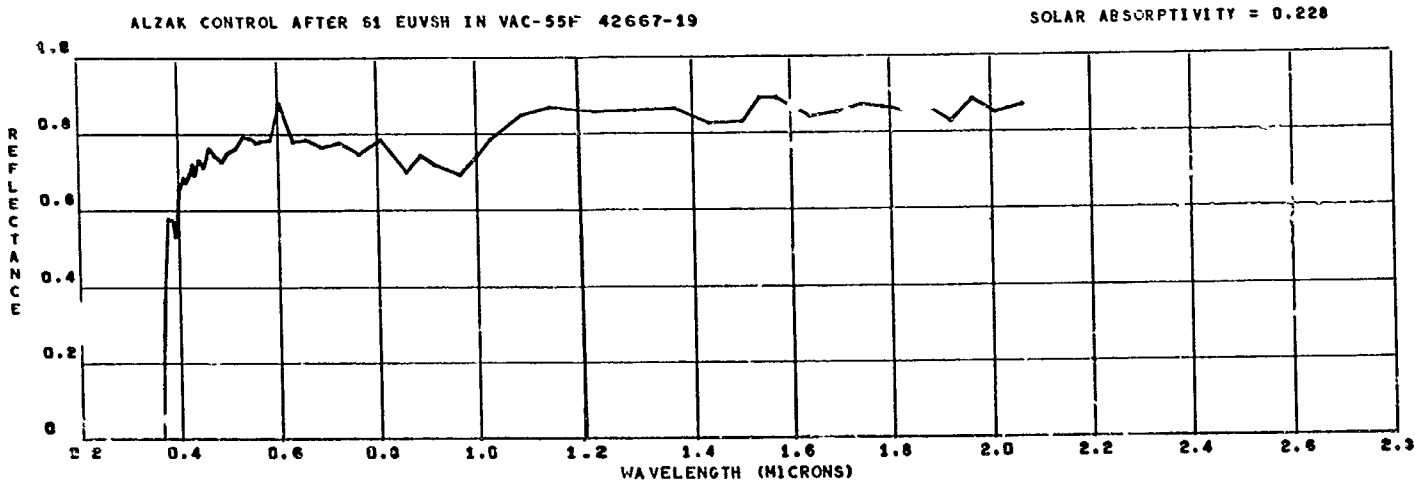
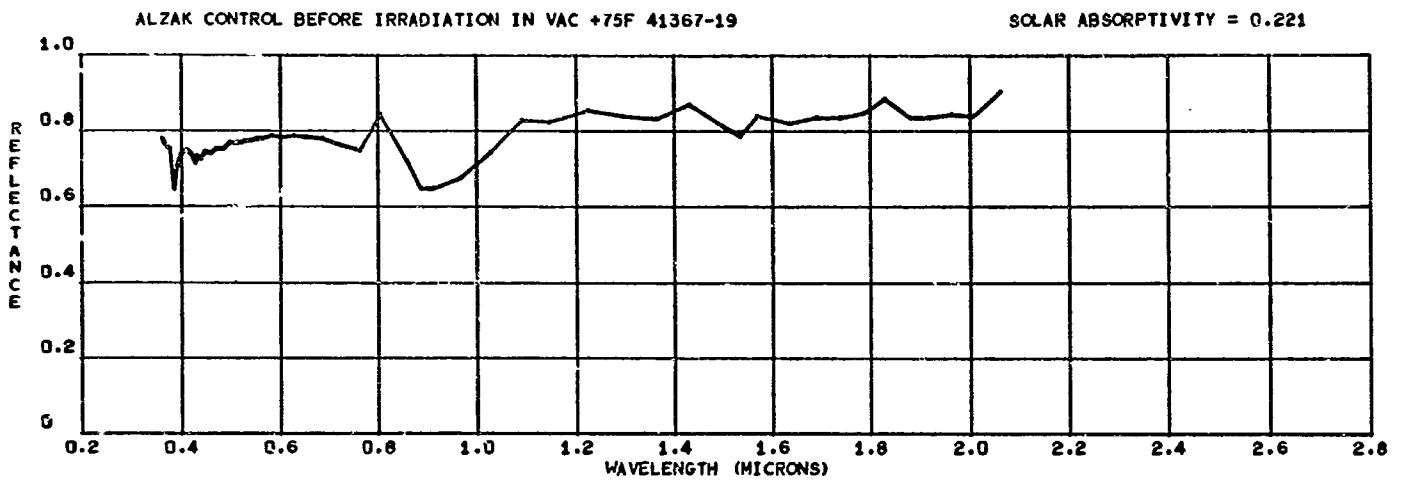
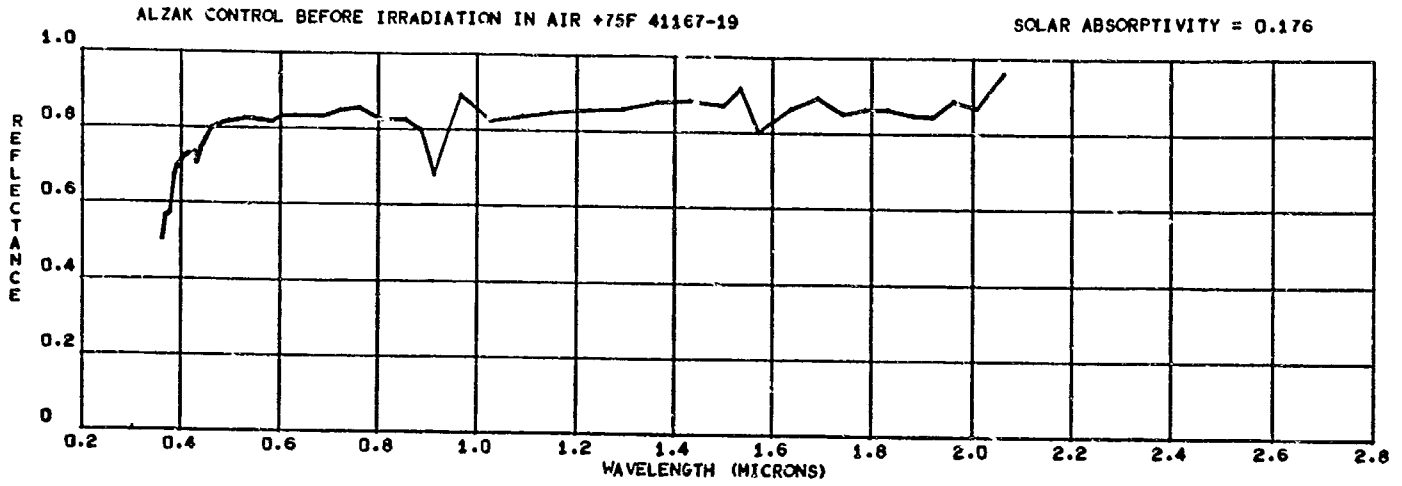
SOLAR ABSORPTIVITY = 0.130

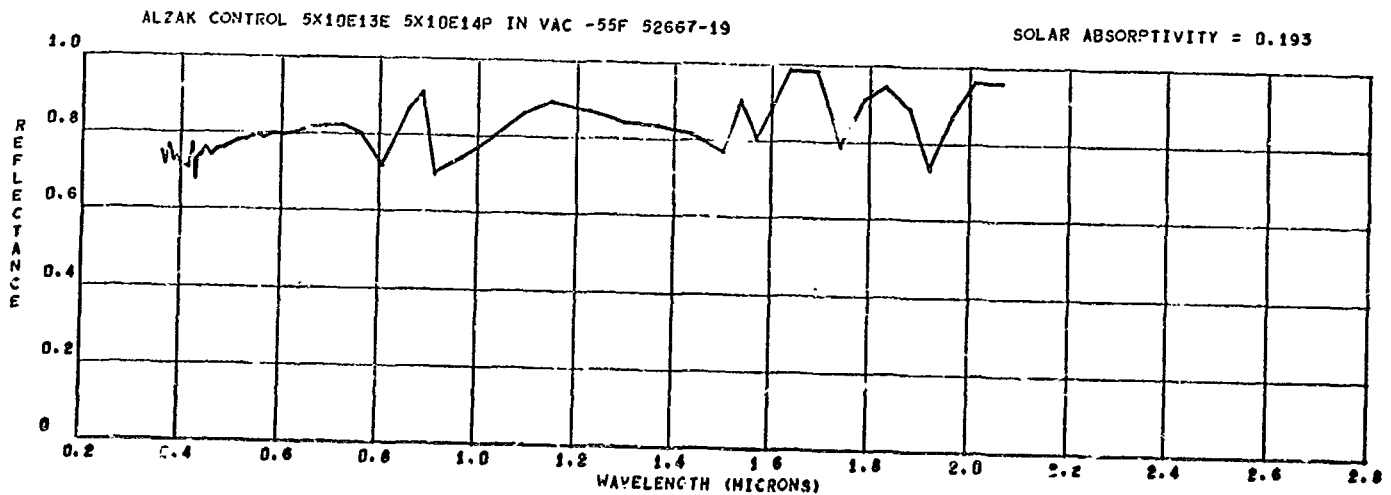
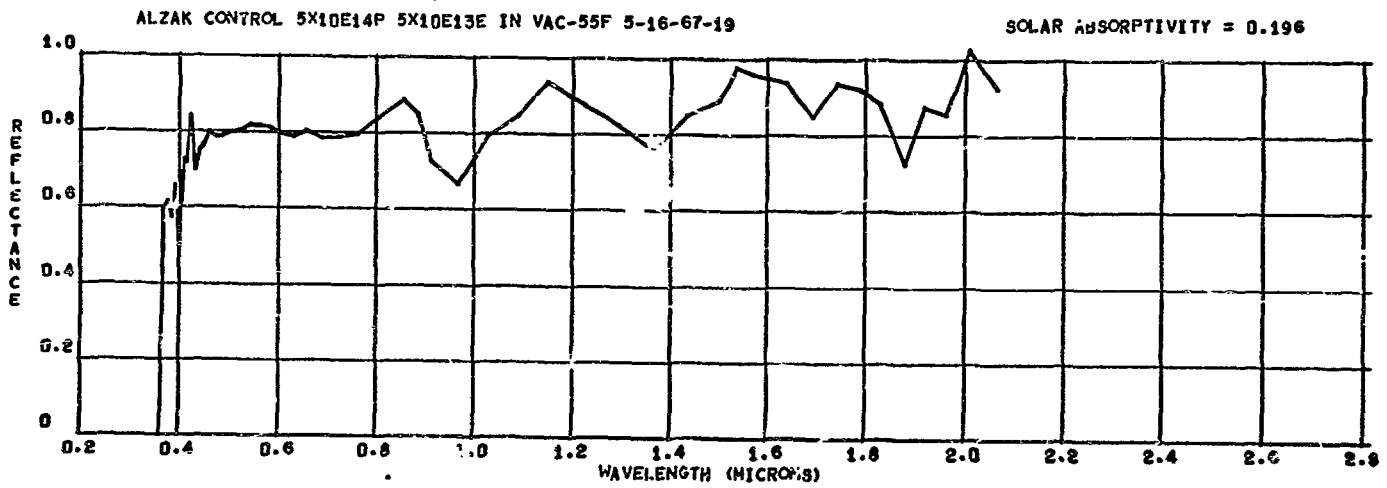
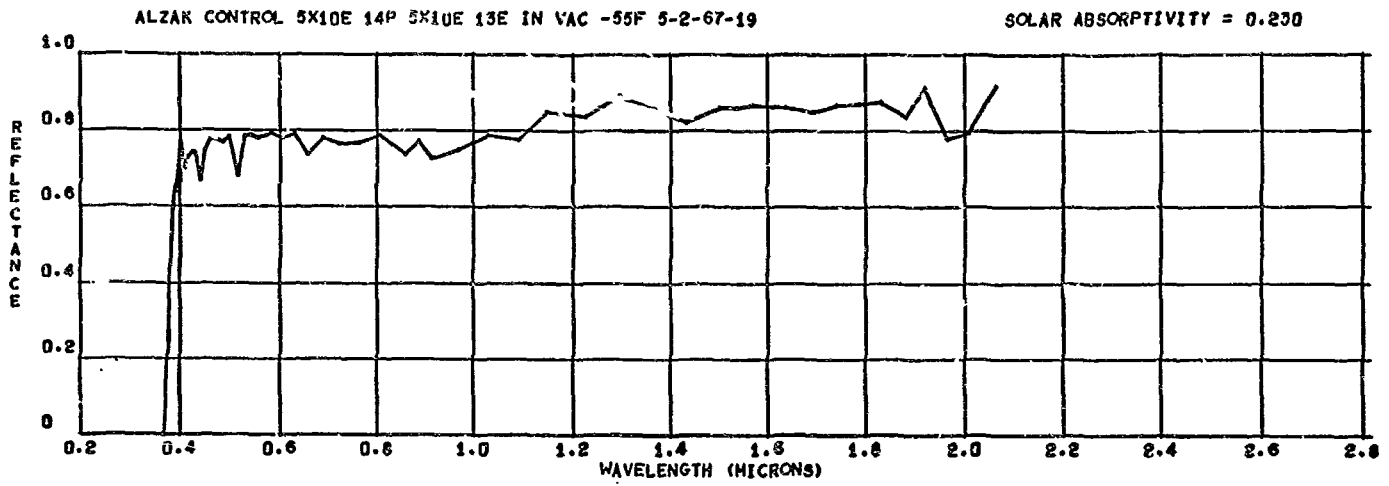


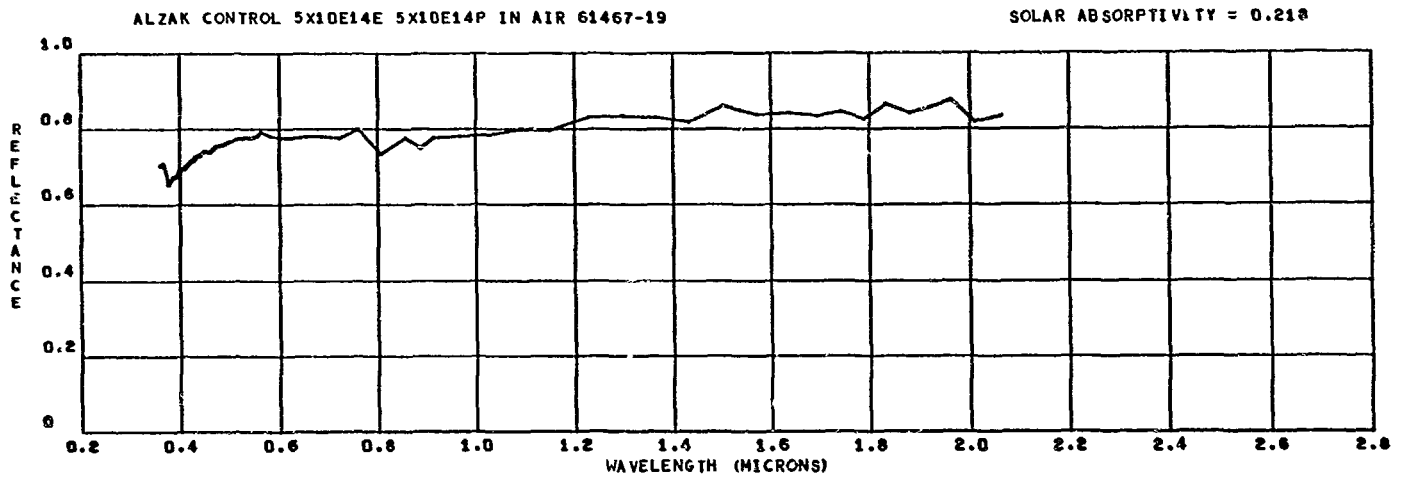
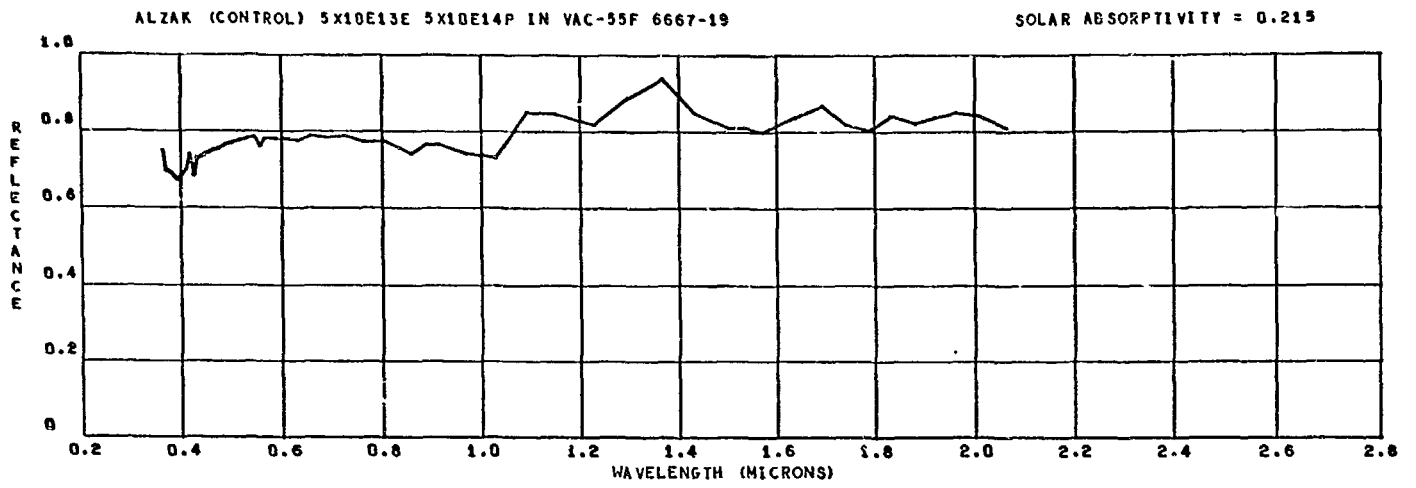


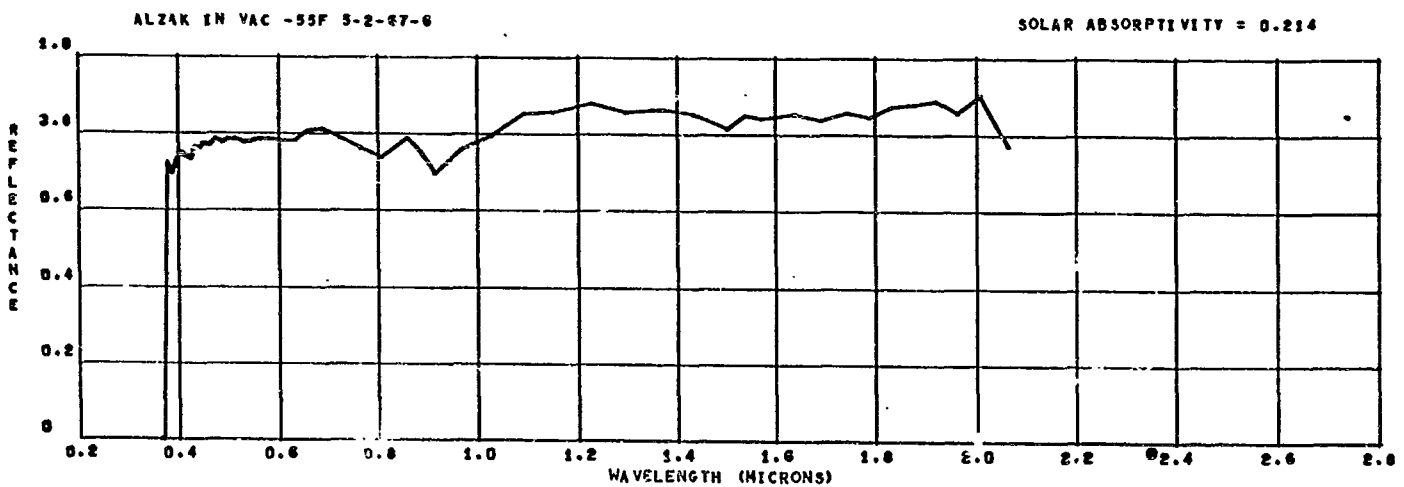
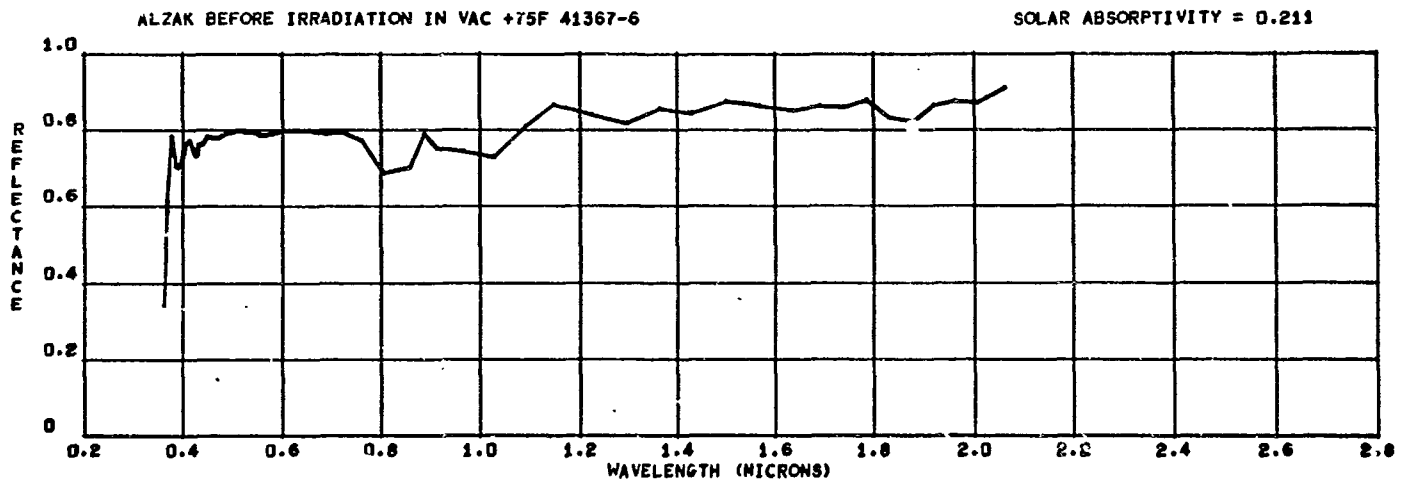
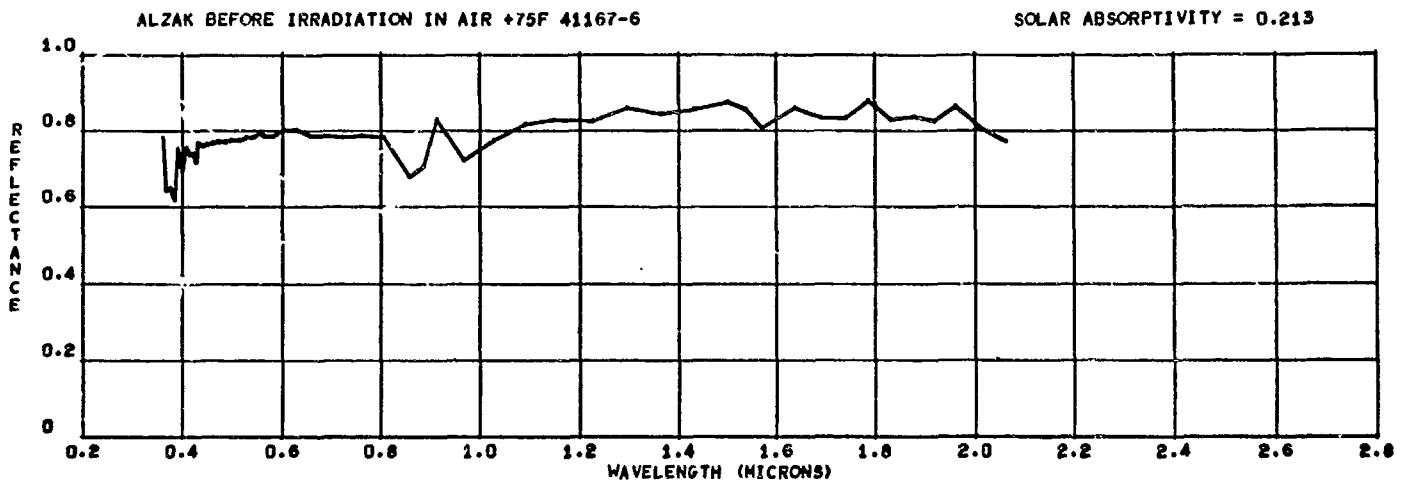


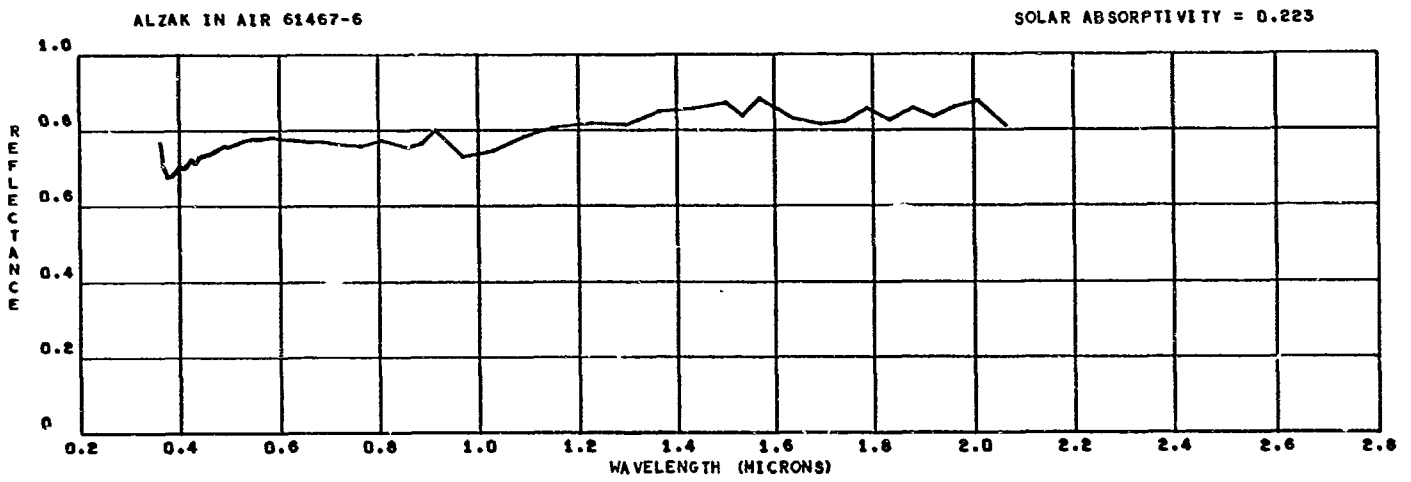
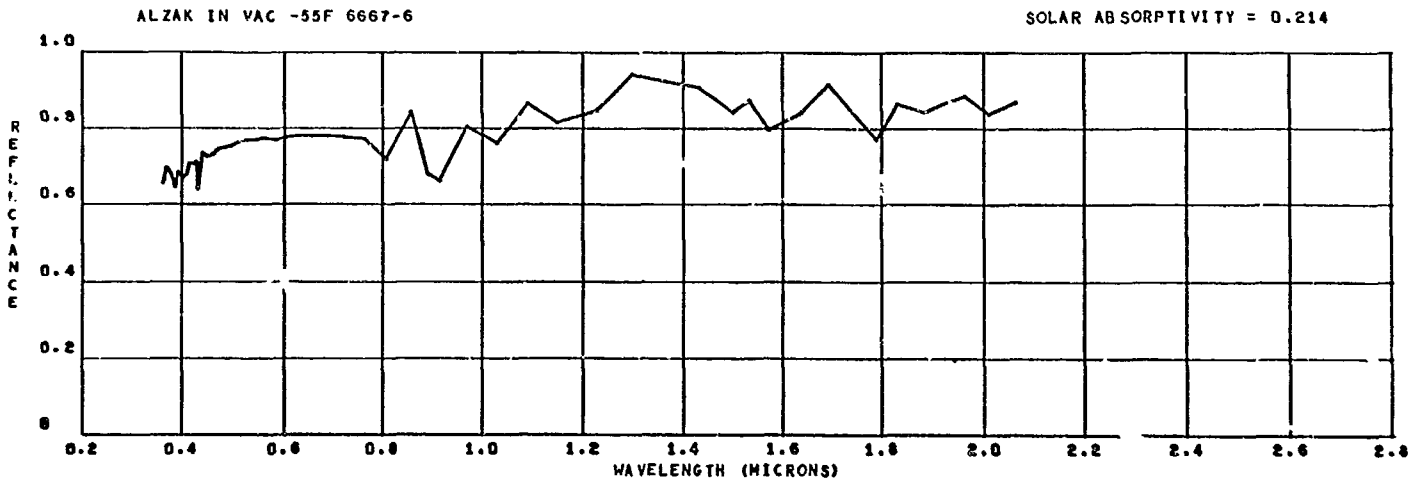


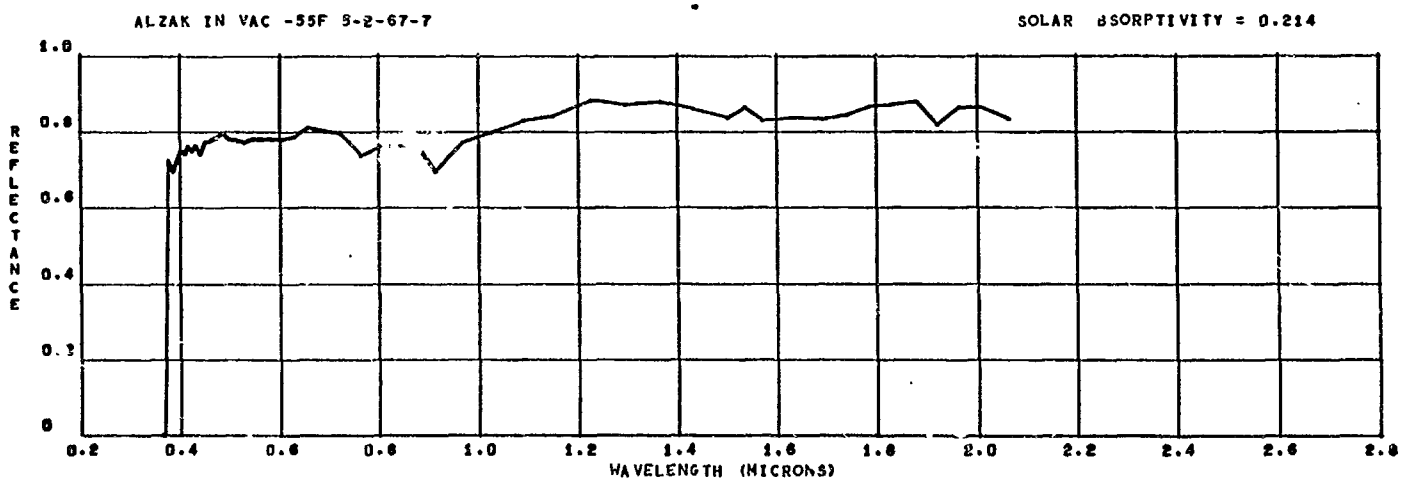
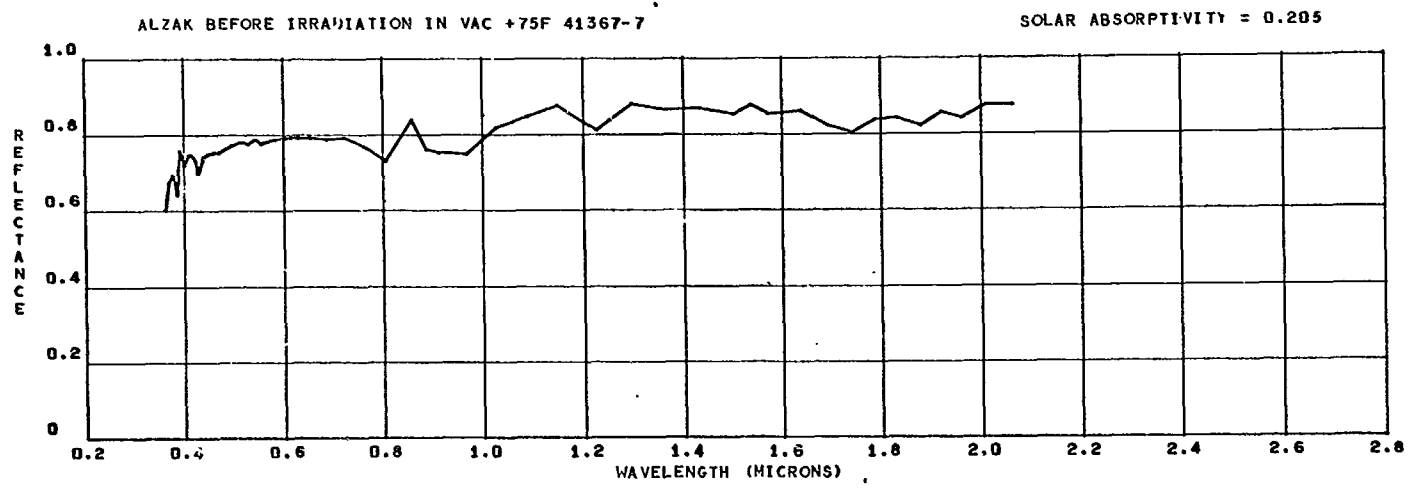
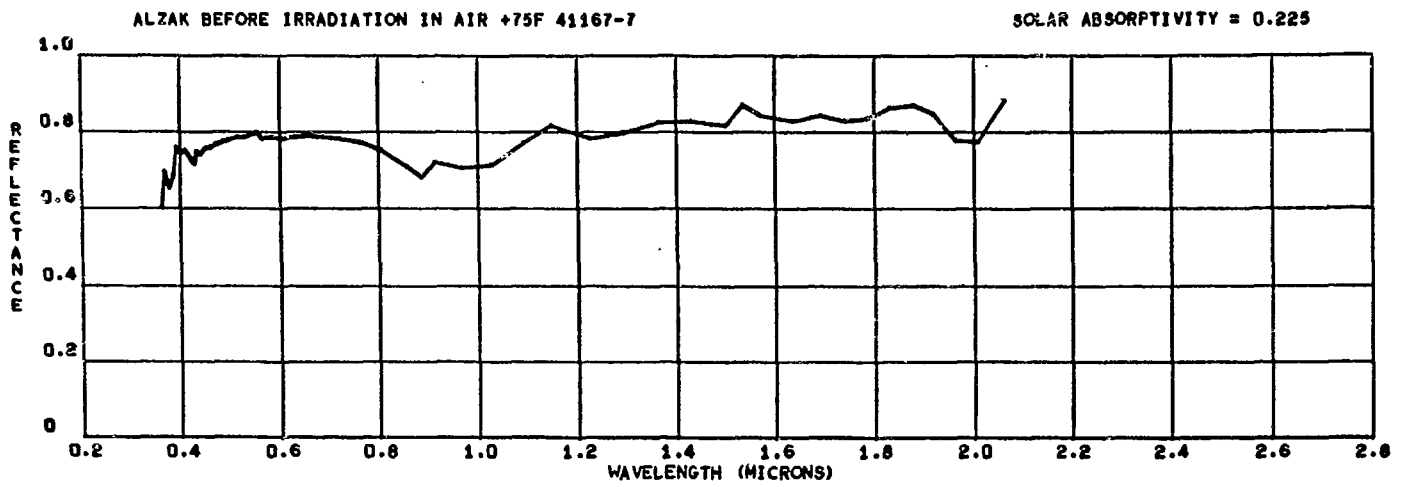


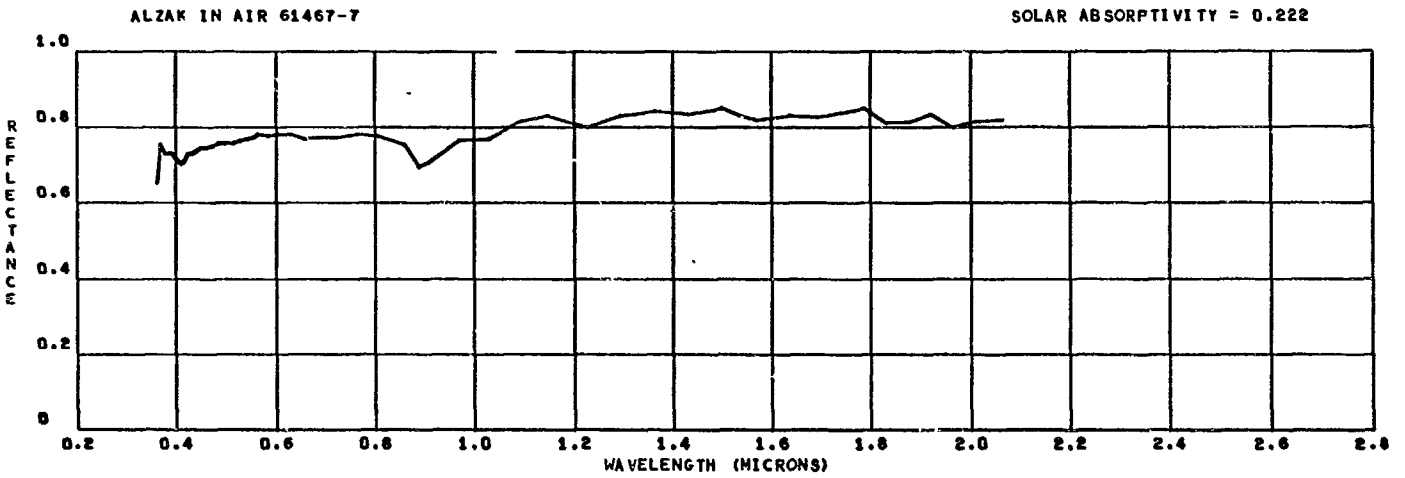
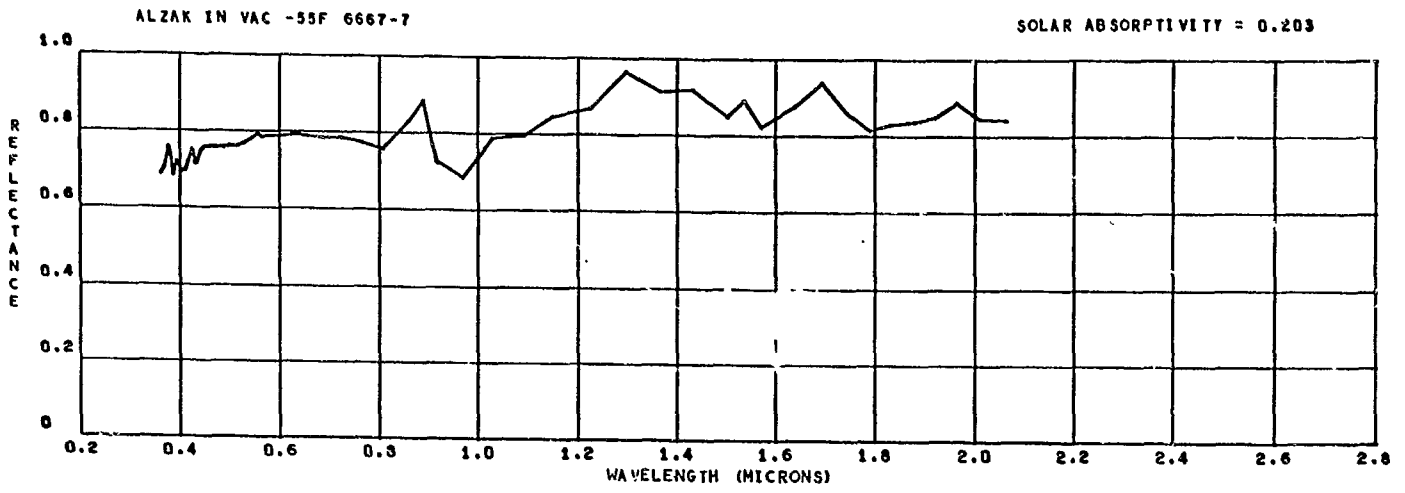


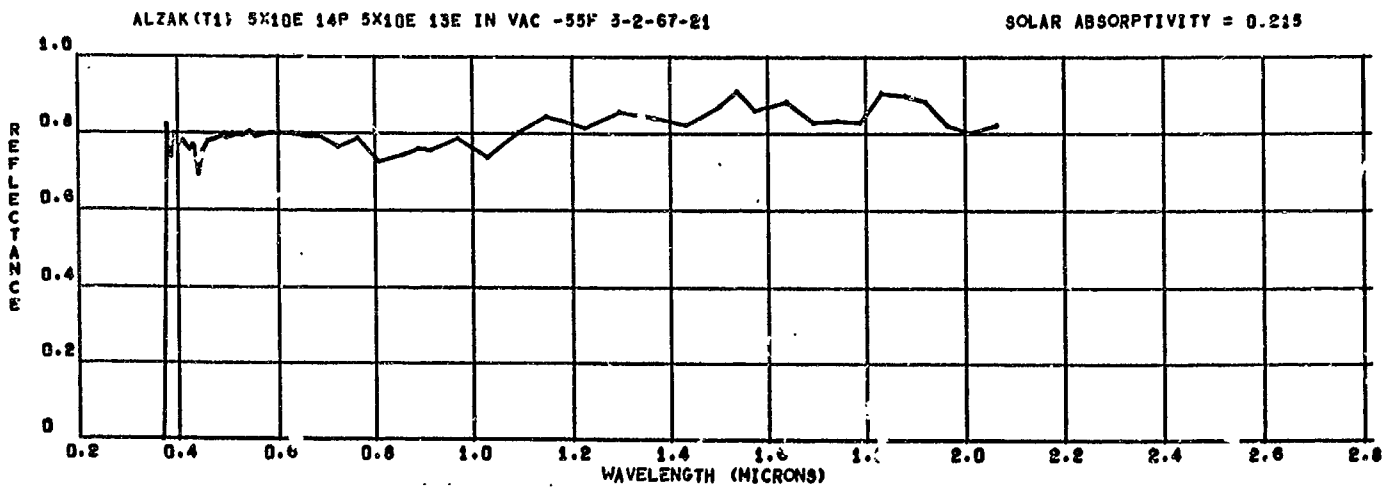
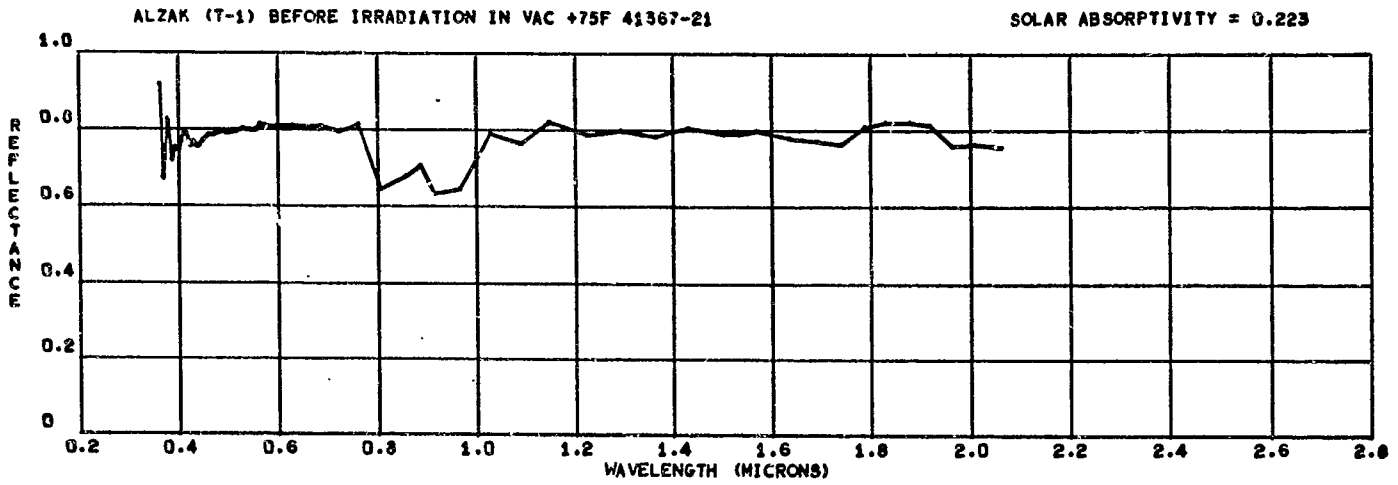
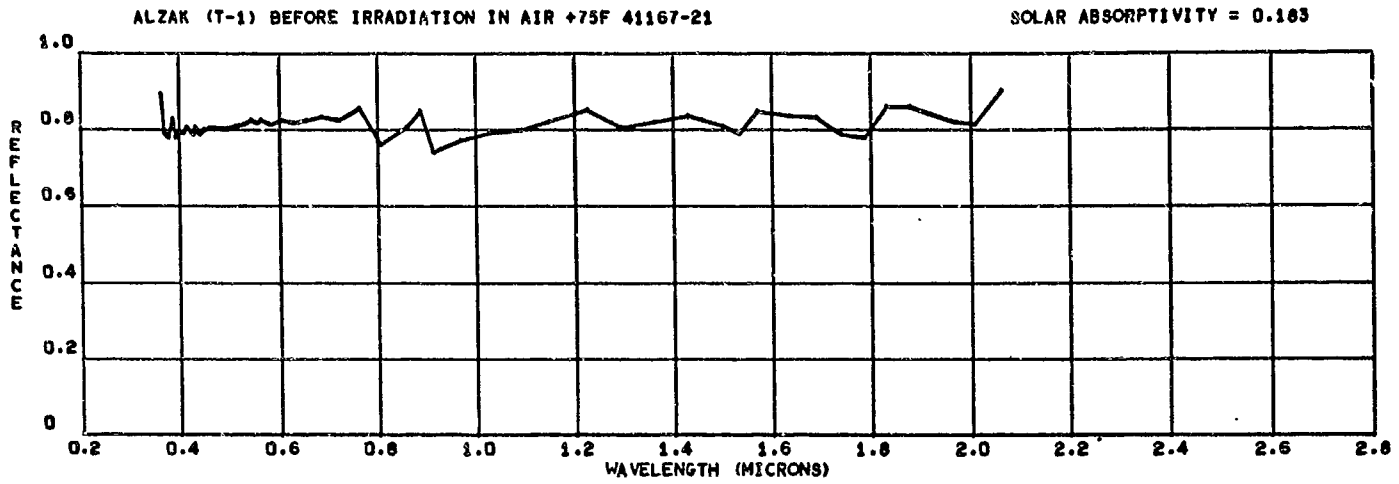






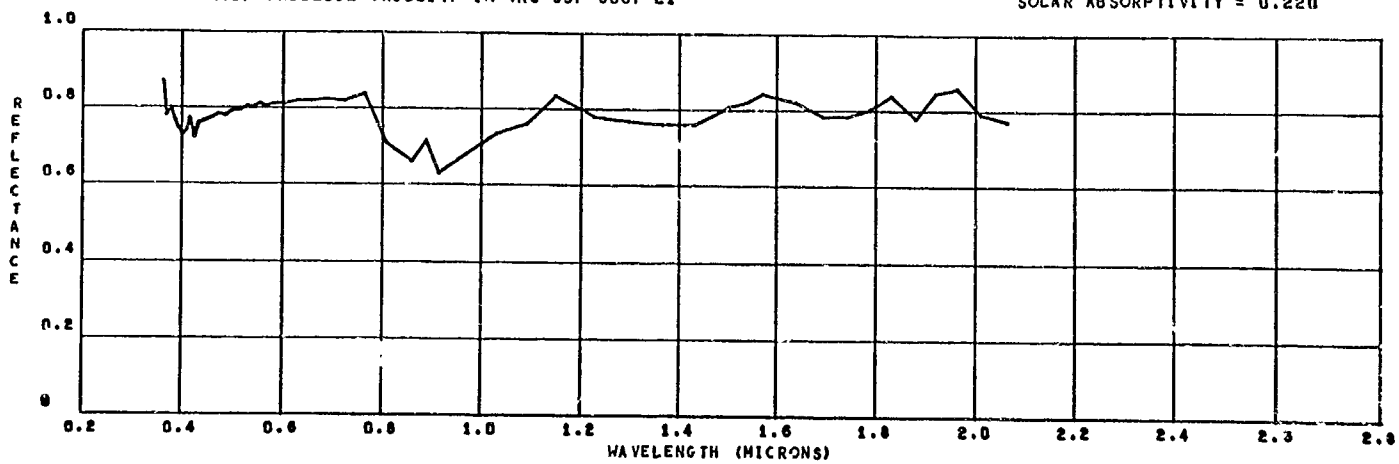






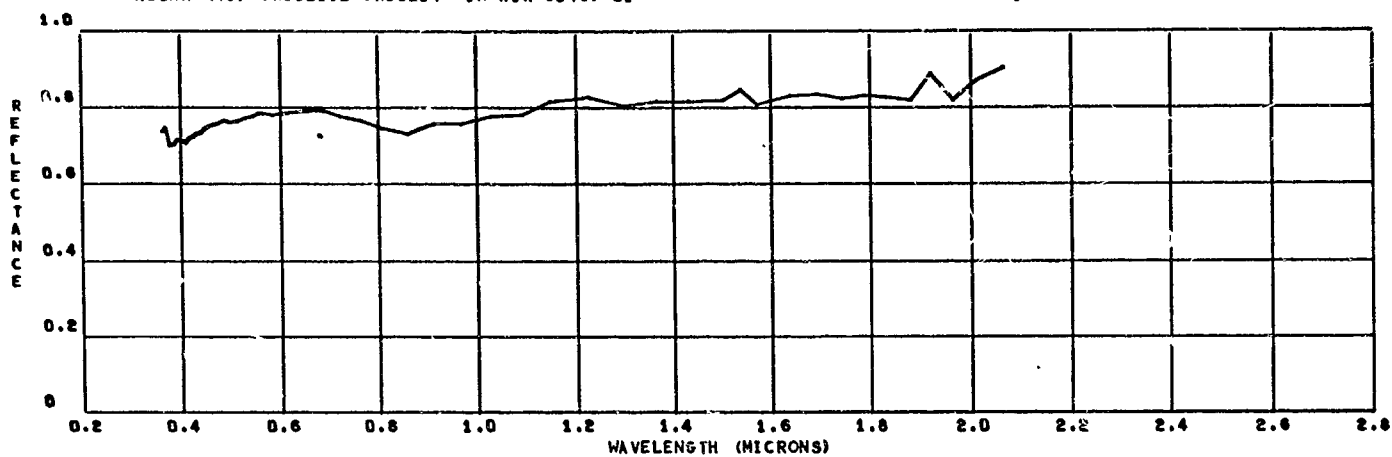
ALZAK (T1) 5X10E13E 5X10E14P IN VAC-55F 6667-21

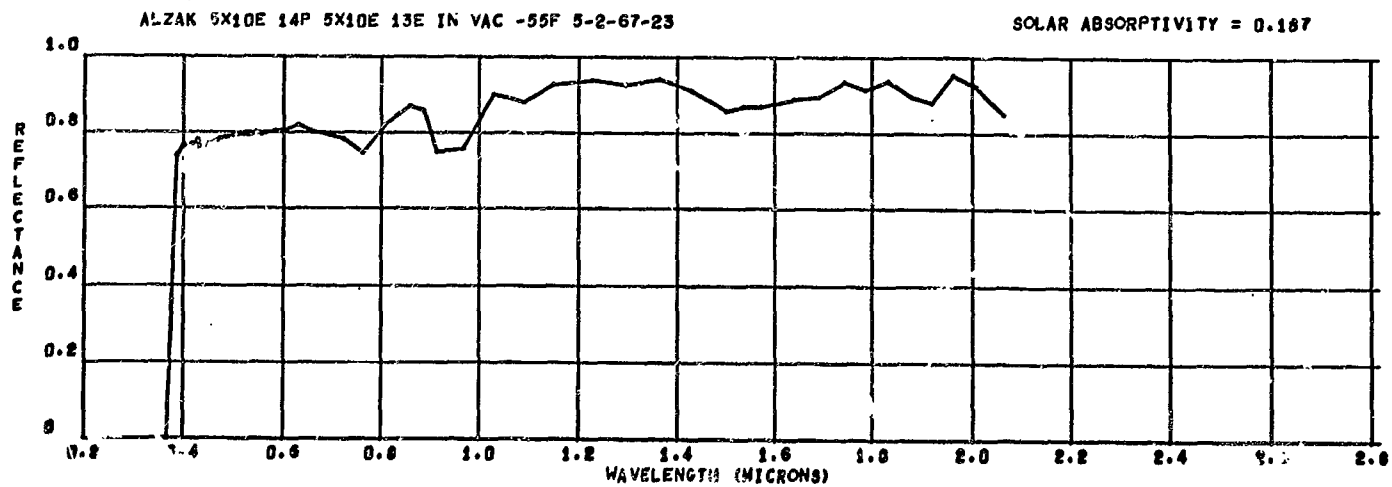
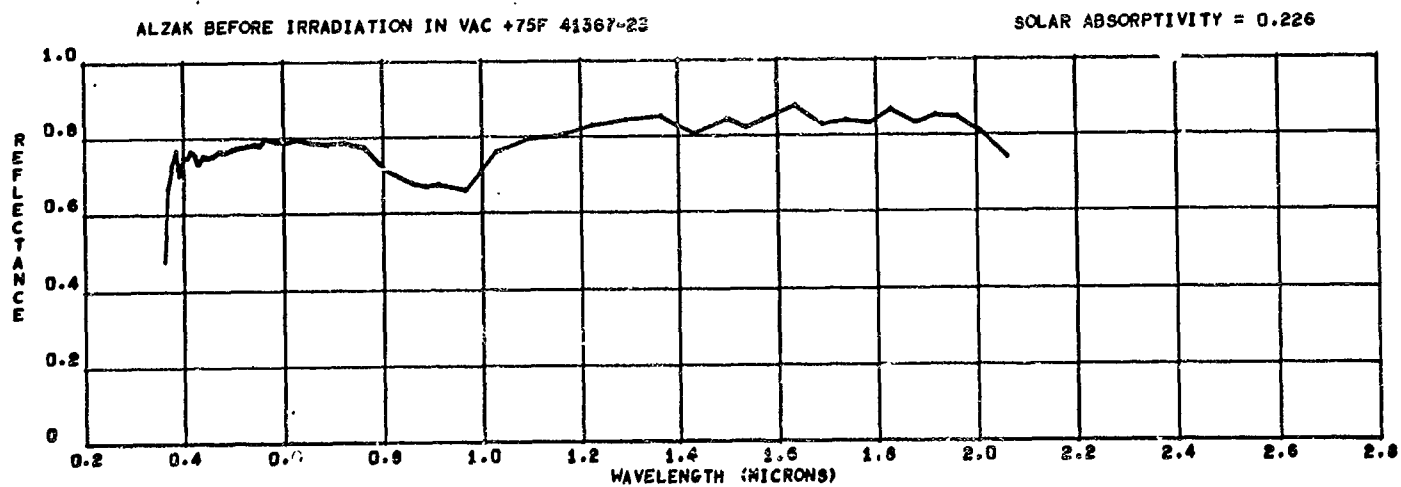
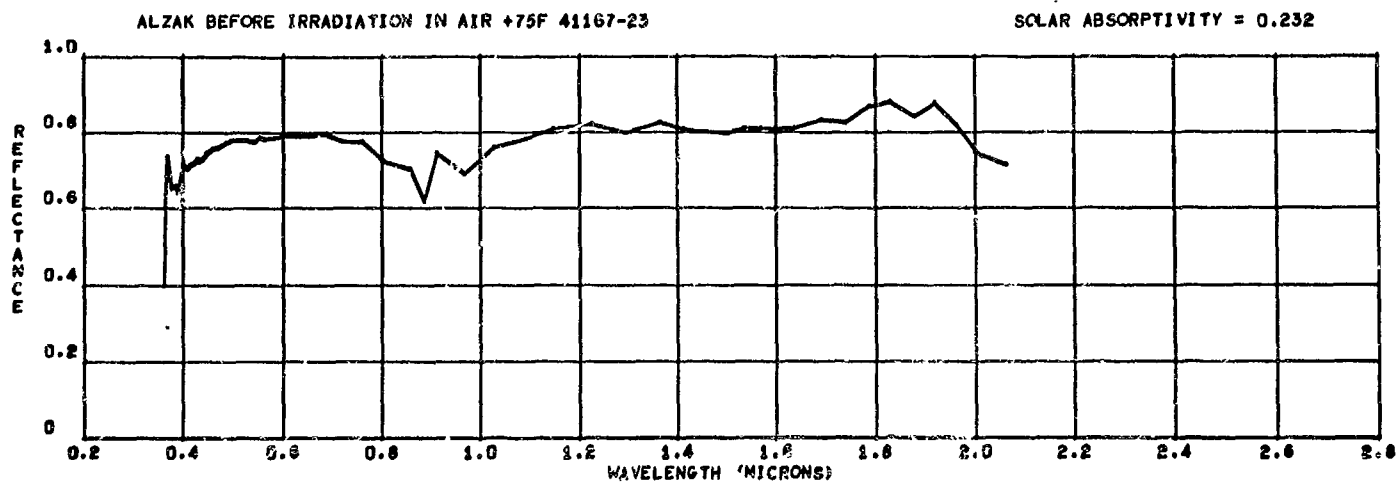
SOLAR ABSORPTIVITY = 0.220

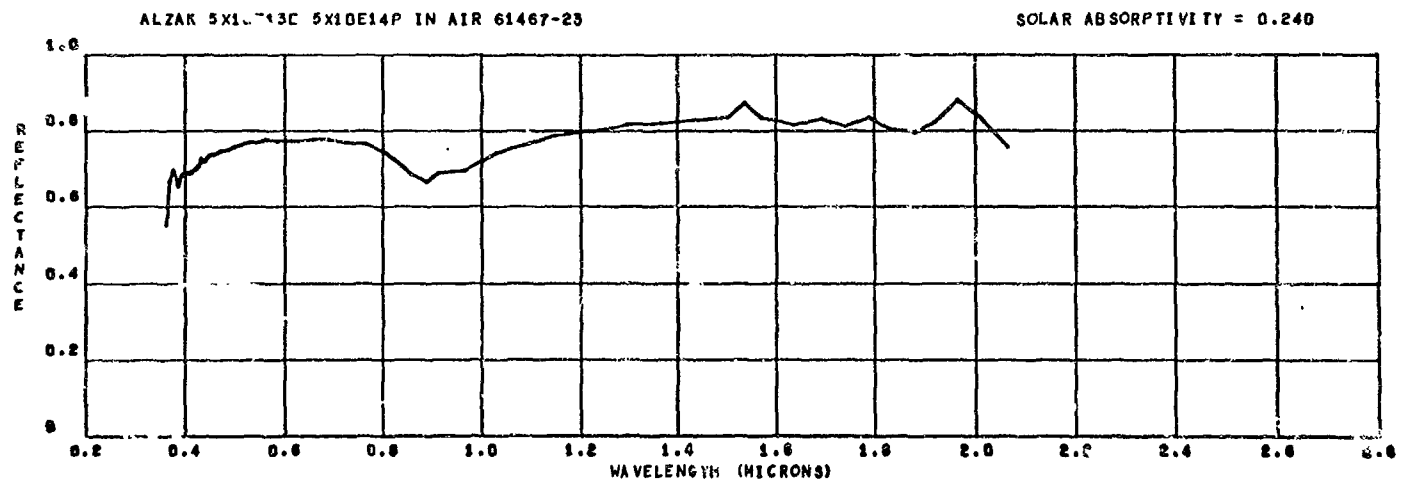
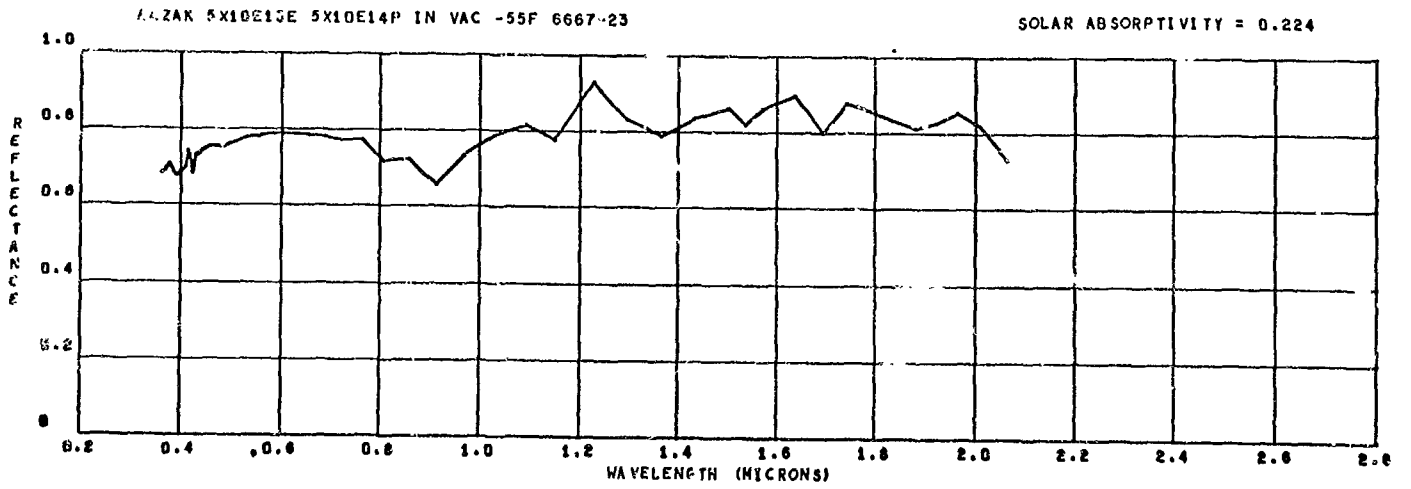


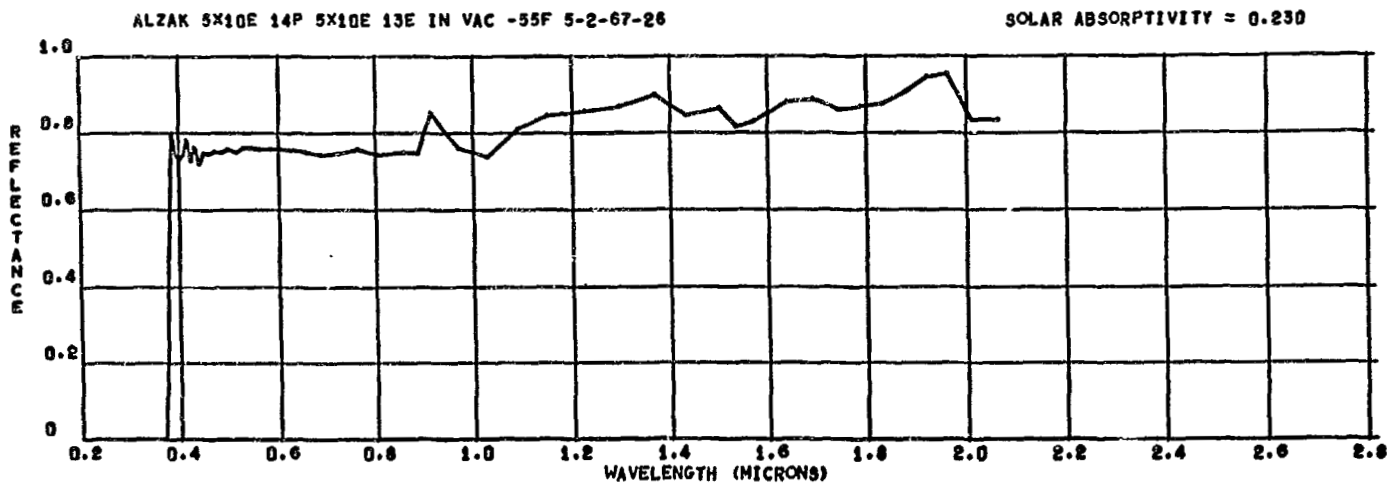
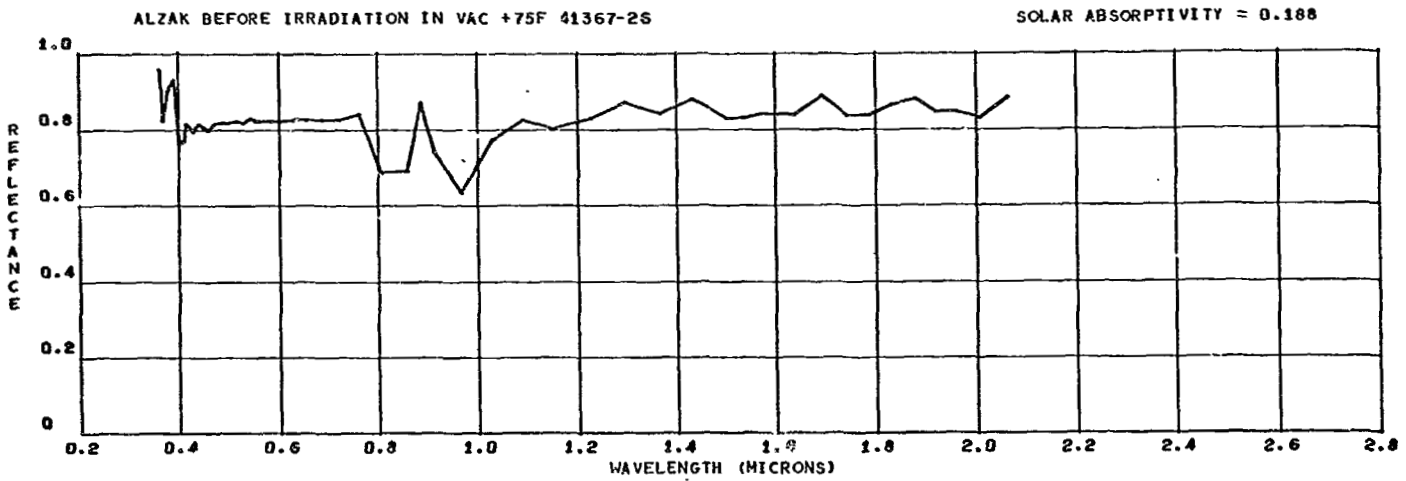
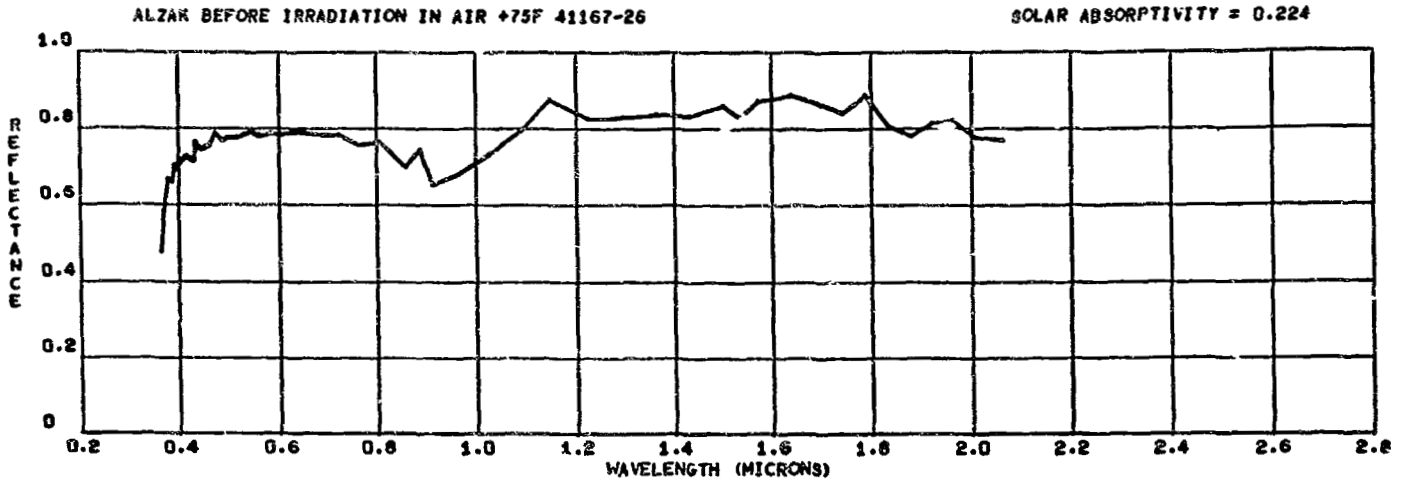
ALZAK (T1) 5X10E13E 5X10E14P IN AIR 61467-21

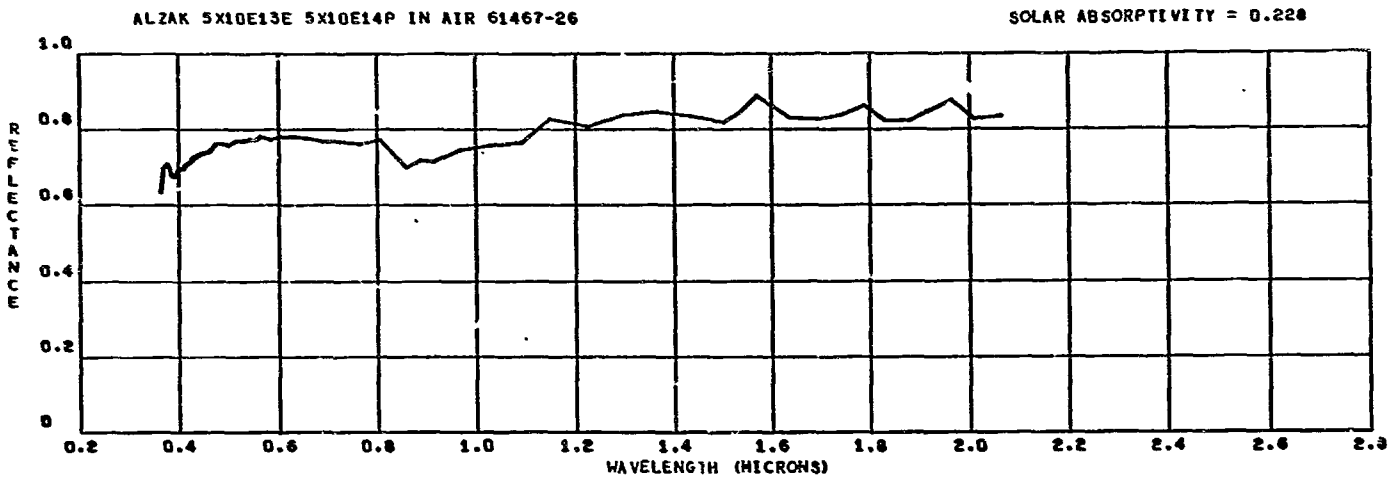
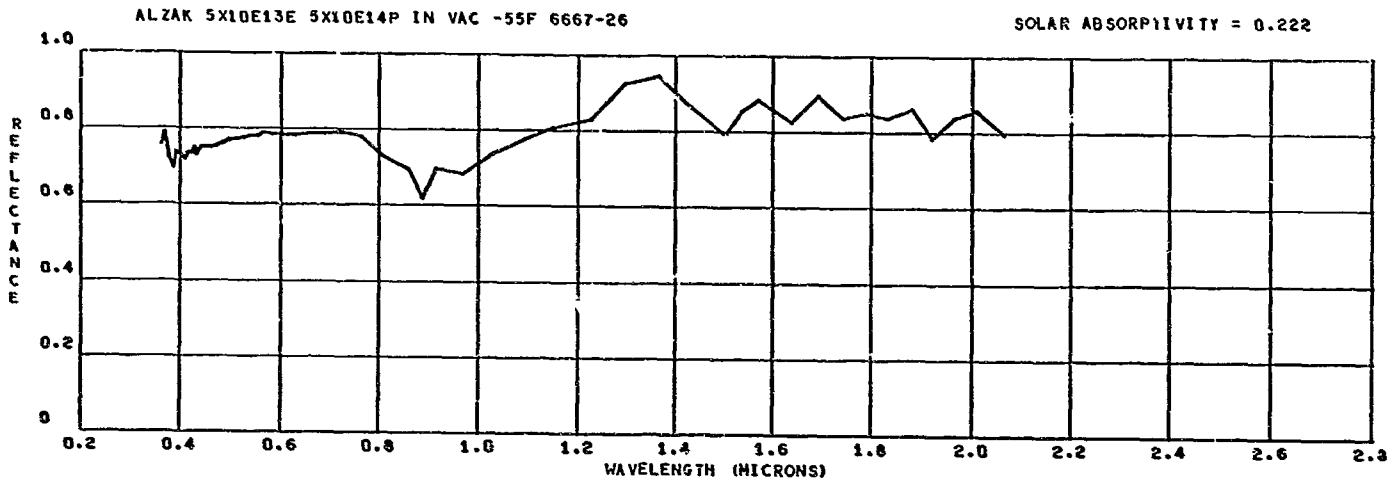
SOLAR ABSORPTIVITY = 0.221





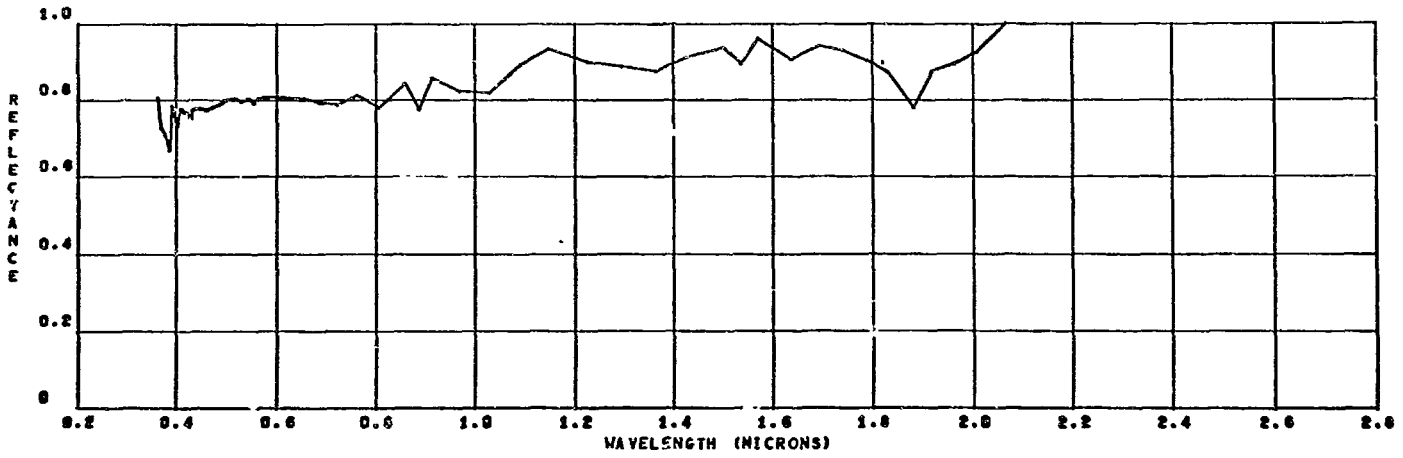






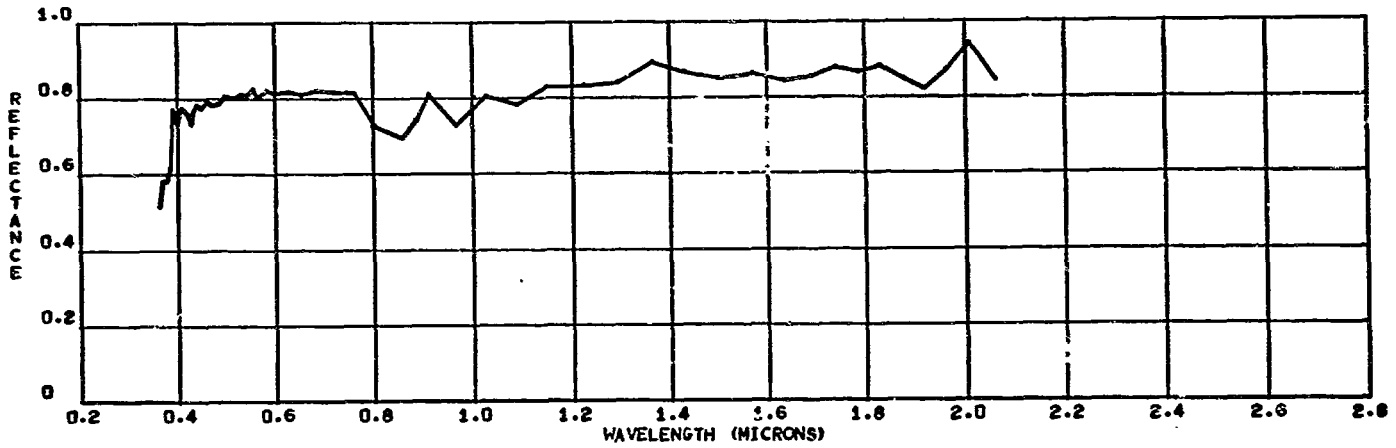
ALZAK (T-1) BEFORE IRRADIATION IN AIR +75F 1167-30

SOLAR ABSORPTIVITY = 0.173



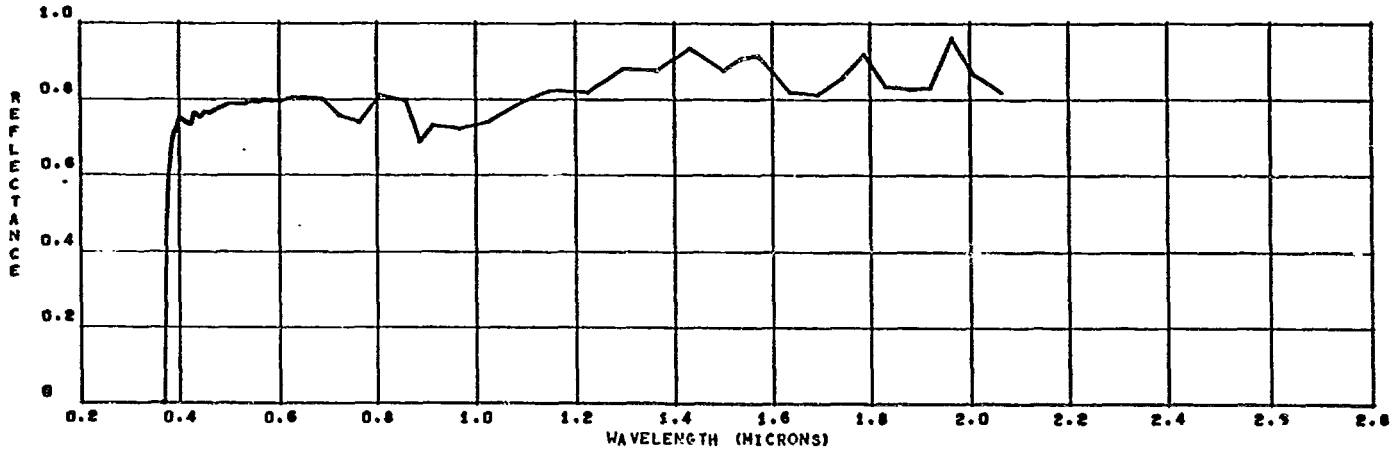
ALZAK (T-1) BEFORE IRRADIATION IN VAC +75F 41367-30

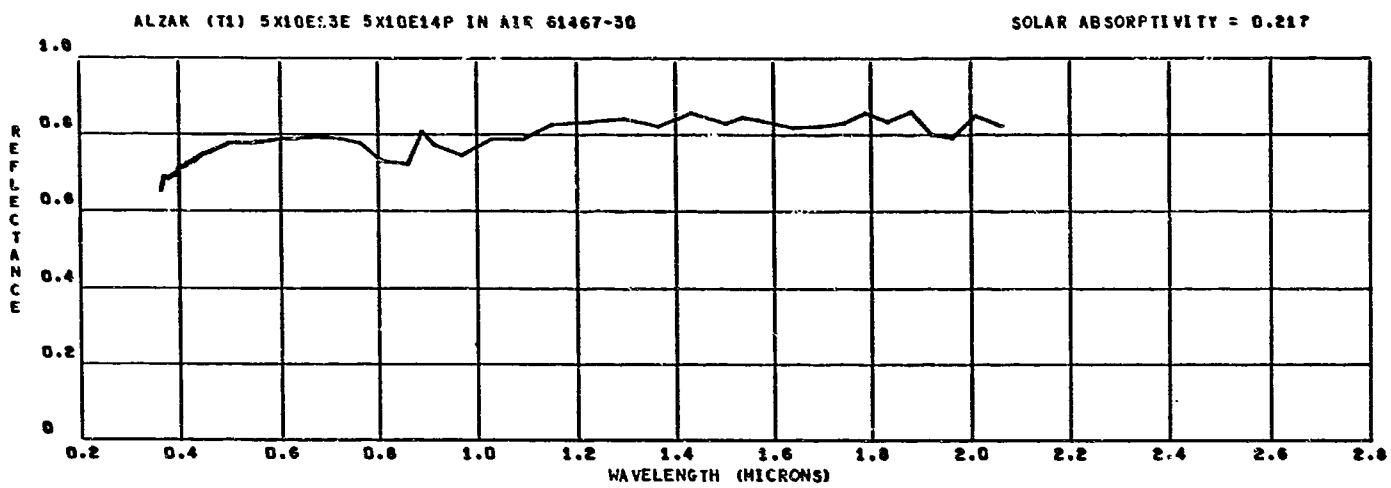
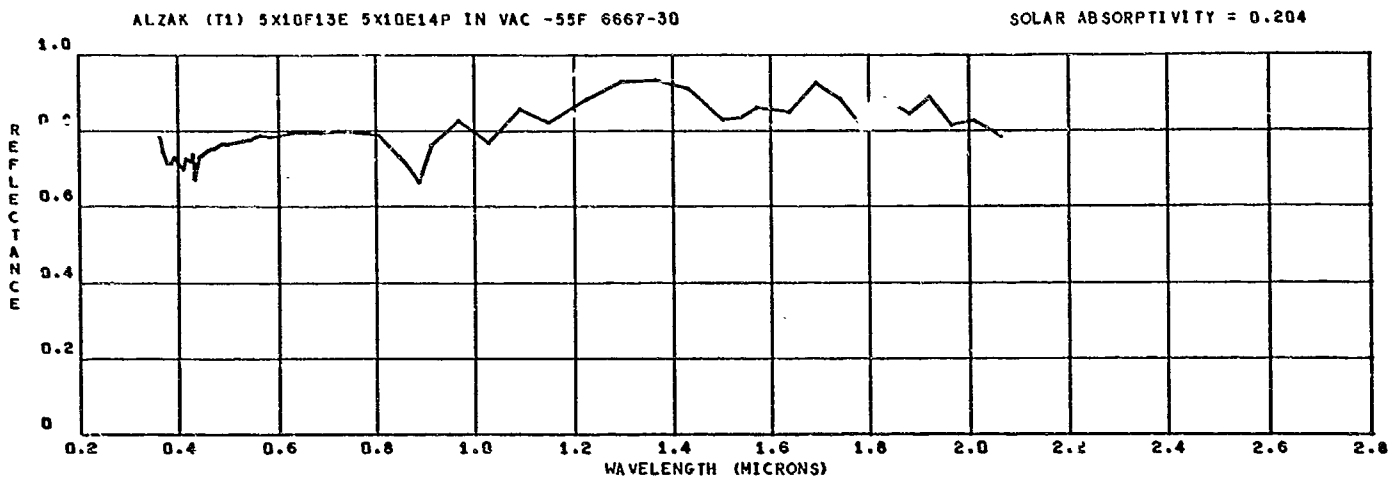
SOLAR ABSORPTIVITY = 0.201



ALZAK (T1) 5X10E 14P 5X10E 13E IN VAC -55F 5-2-67-30

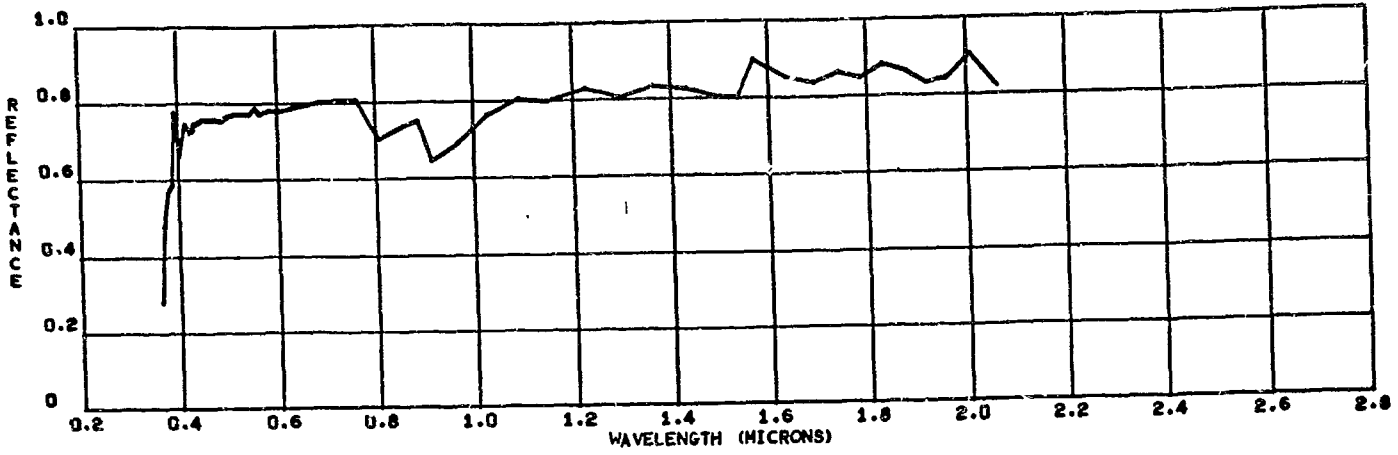
SOLAR ABSORPTIVITY = 0.217





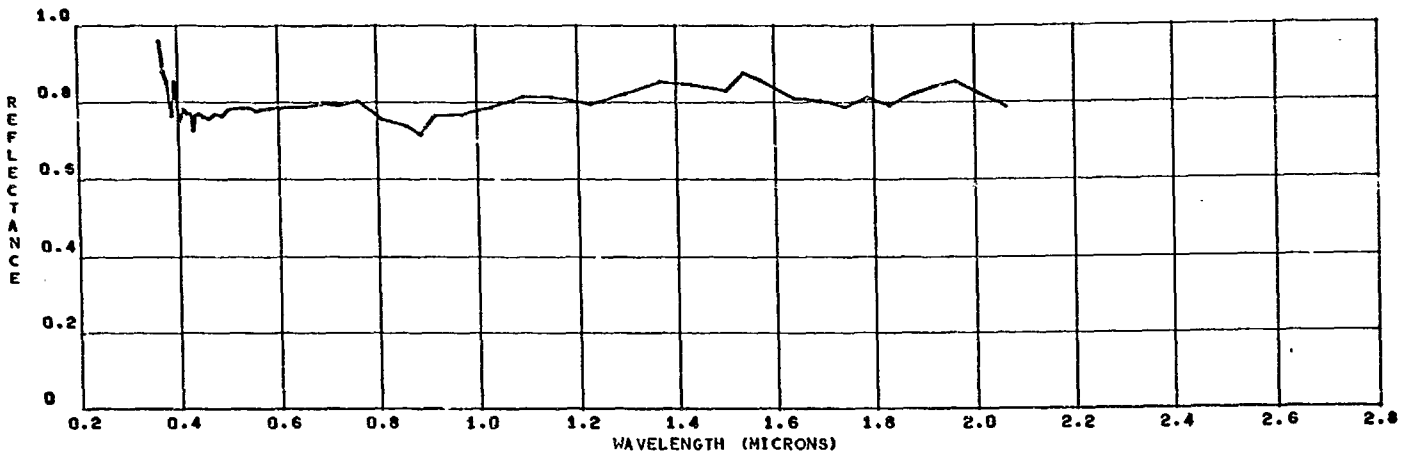
ALZAK BEFORE IRRADIATION IN AIR +75F 41167-1

SOLAR ABSORPTIVITY = 0.227



ALZAK BEFORE IRRADIATION IN VAC +75F 41367-1

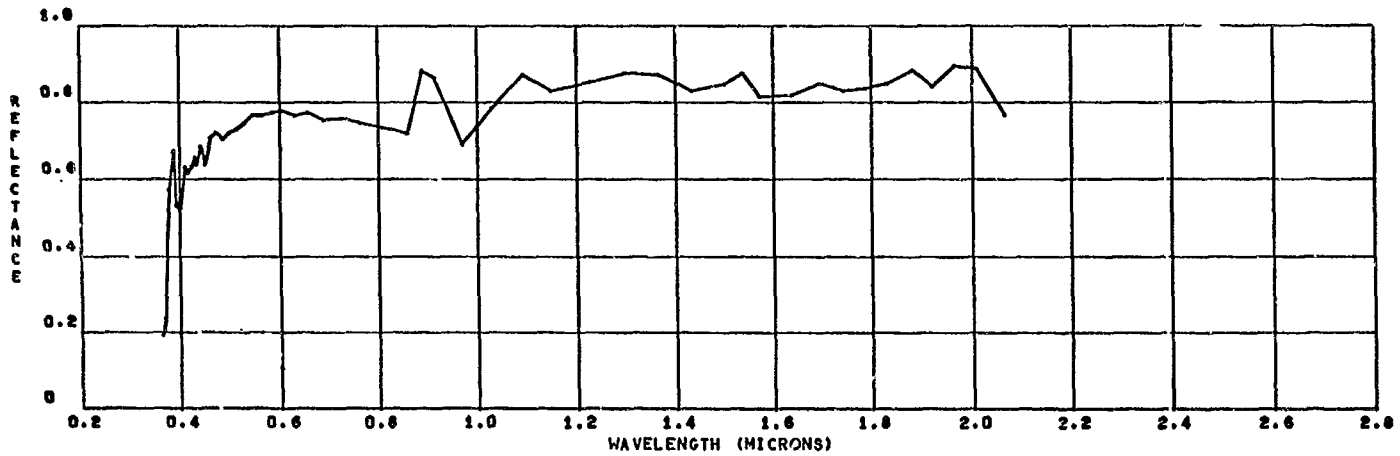
SOLAR ABSORPTIVITY = 0.207



6

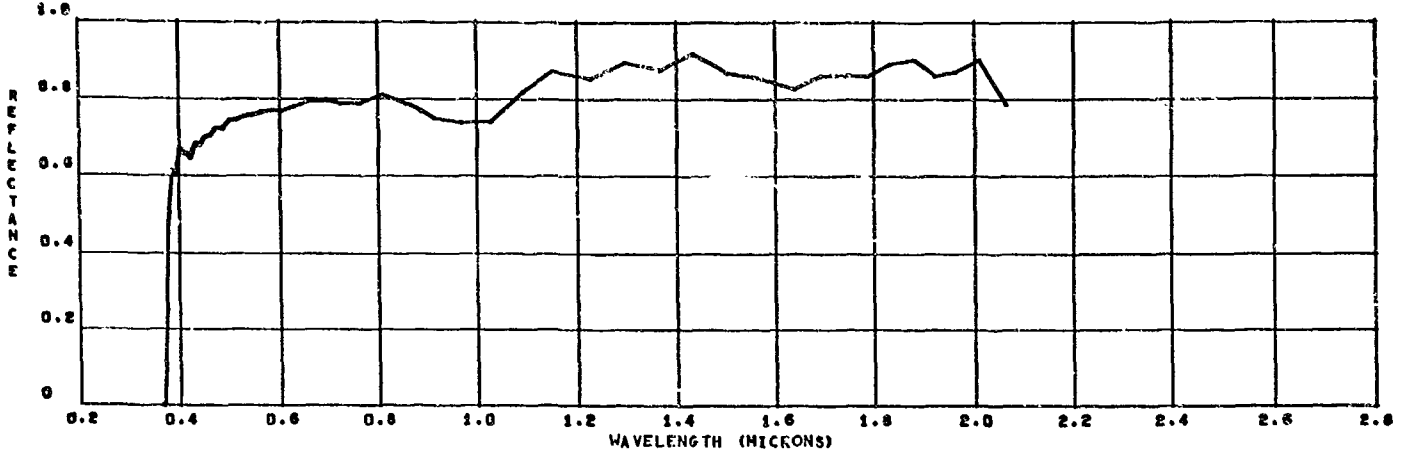
ALZAK AFTER 61 EUVSH IN VAC-55F 42667-1

SOLAR ABSORPTIVITY = 0.240



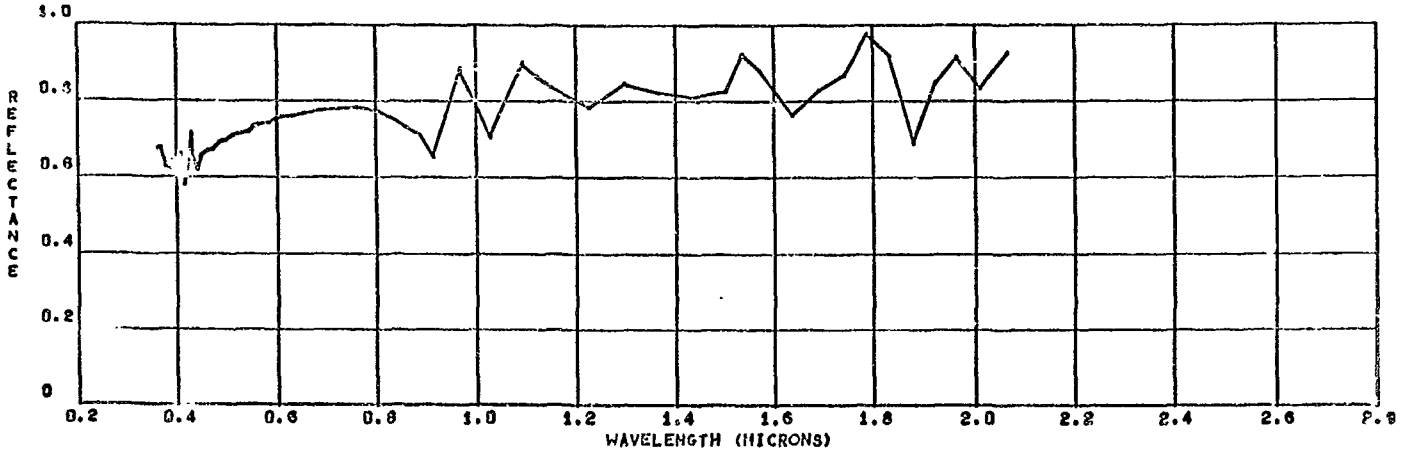
ALZAK 5X10E 14P 5 (10E 13E 200EUVSH IN VAC -55F 5-2-67-1

SOLAR ABSORPTIVITY = 0.229



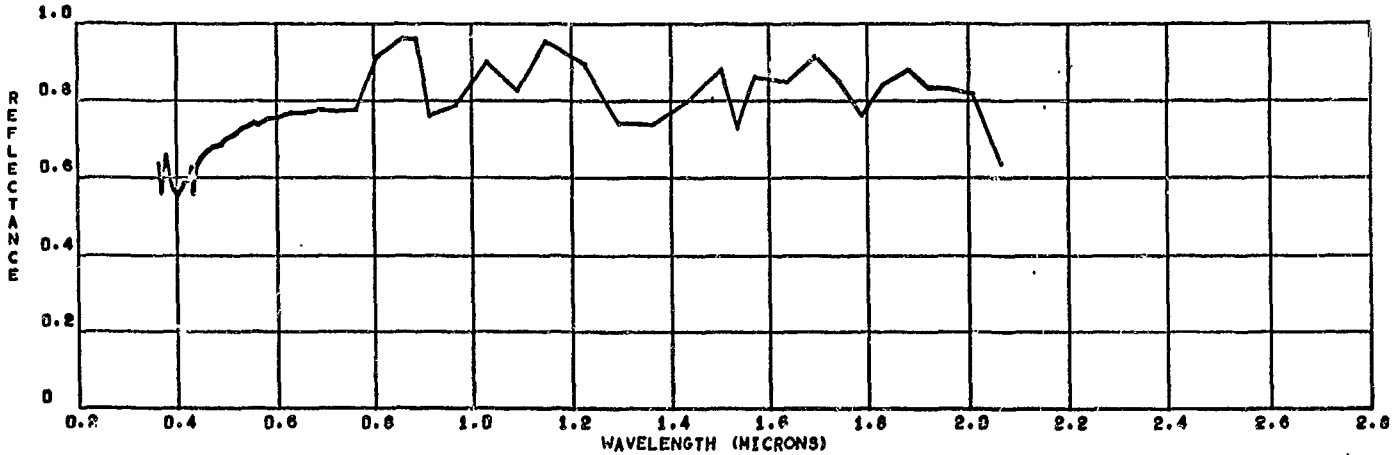
ALZAK 5X10E14P 5X10E13E 50CEUVSH IN VAC -55F 5-16-67-1

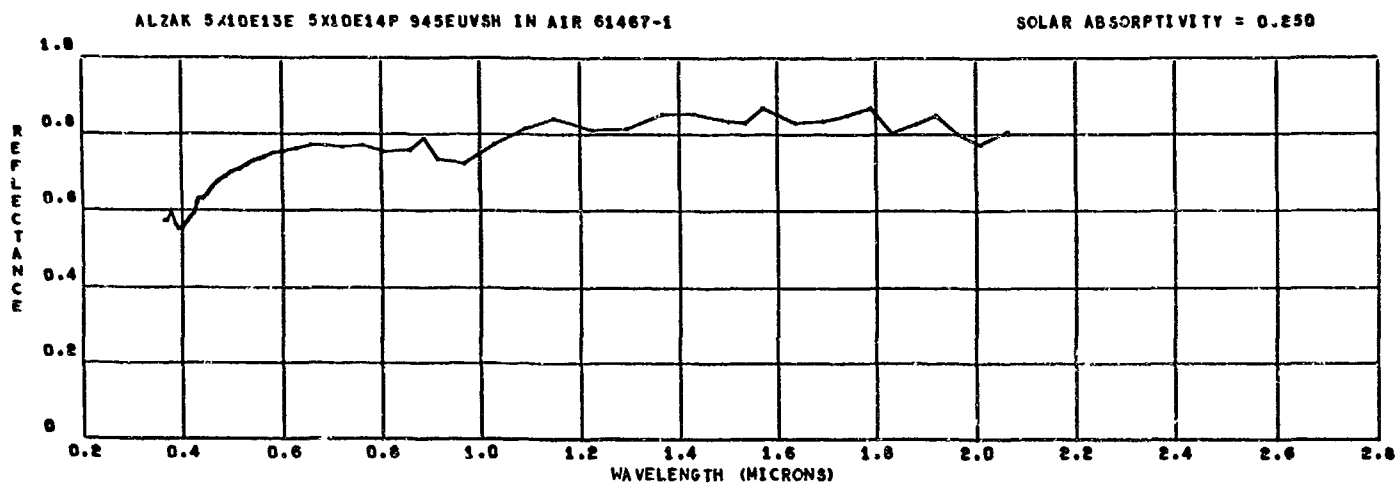
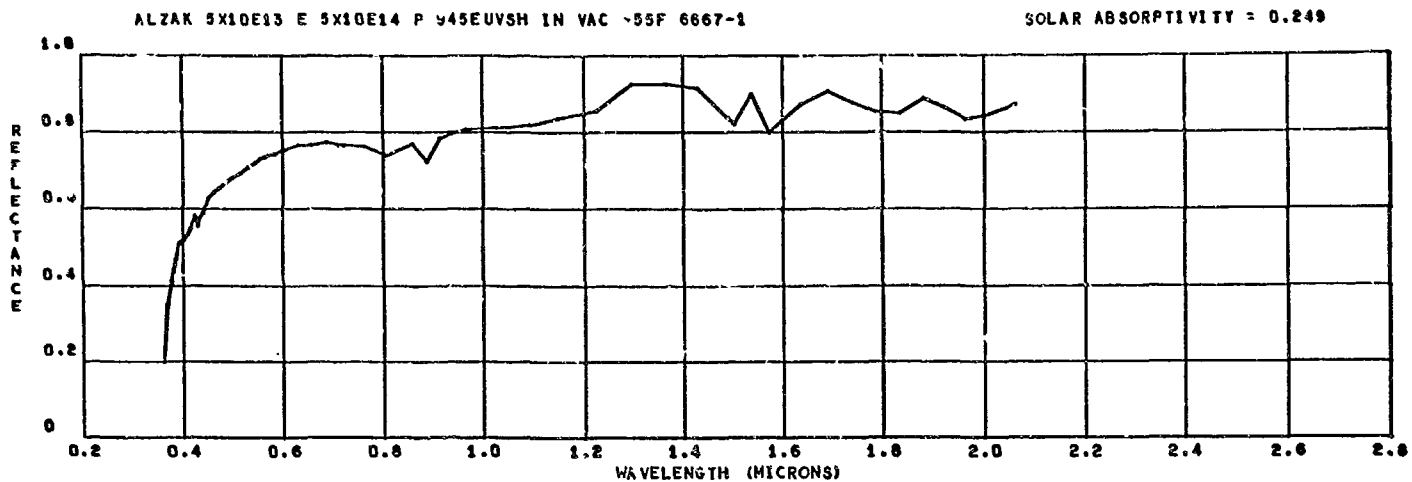
SOLAR ABSORPTIVITY = 0.240

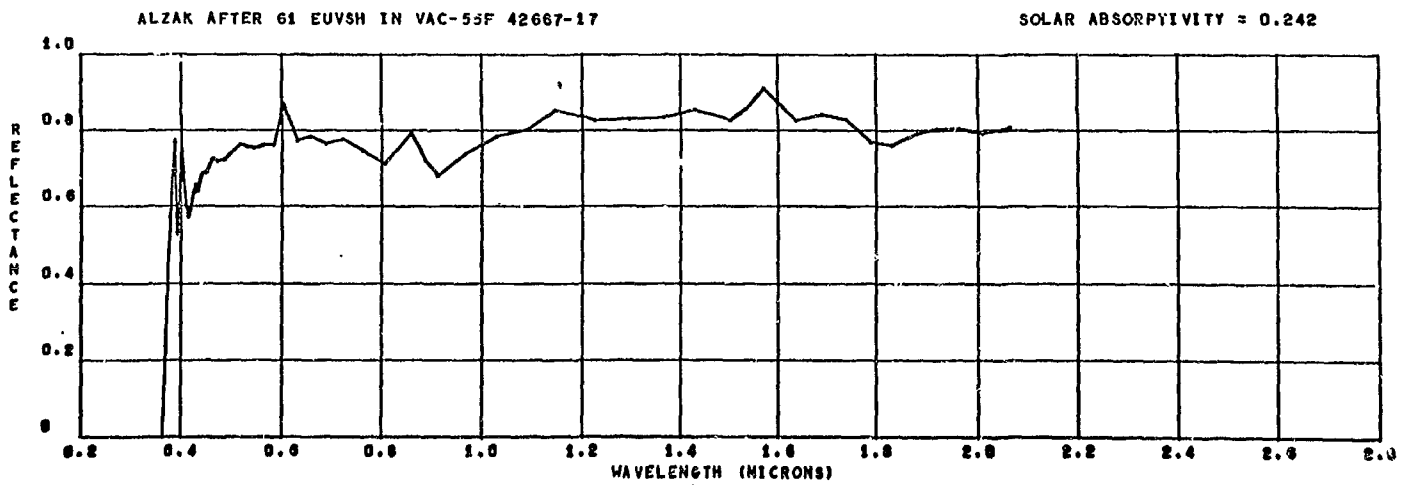
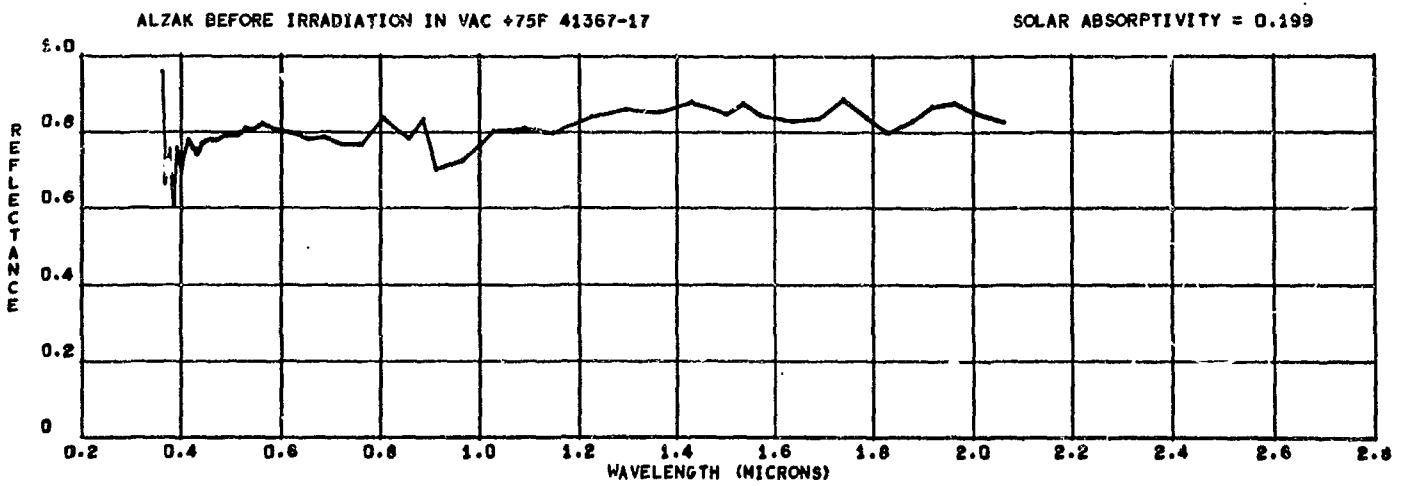
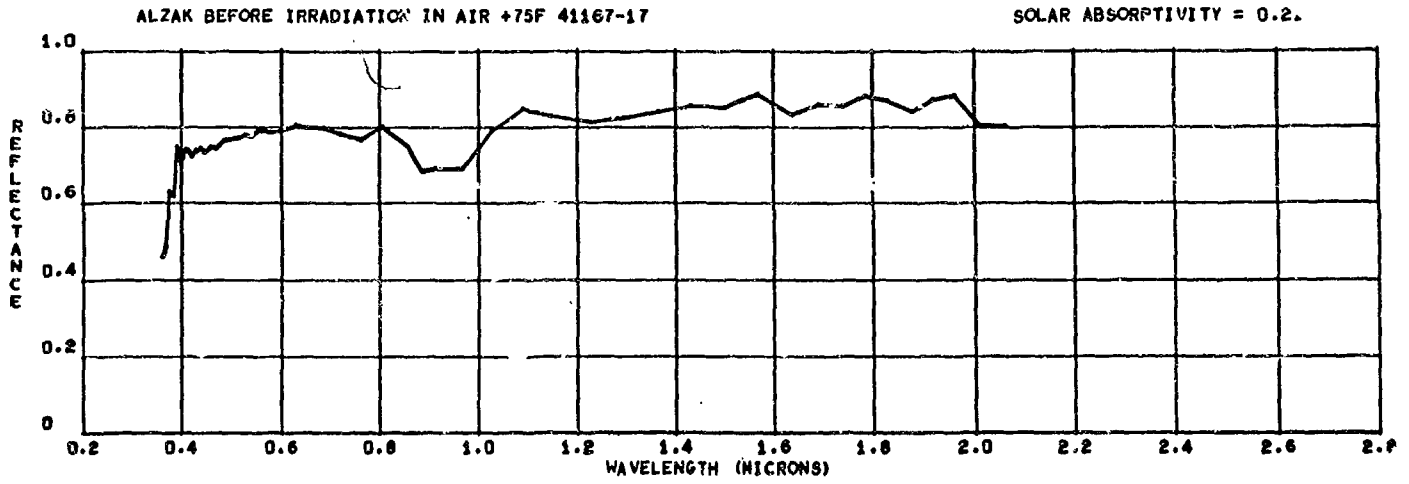


ALZAK 5X10E13E 5X10E14P 714 EUVSH IN VAC -55F 52667-1

SOLAR ABSORPTIVITY = 0.219

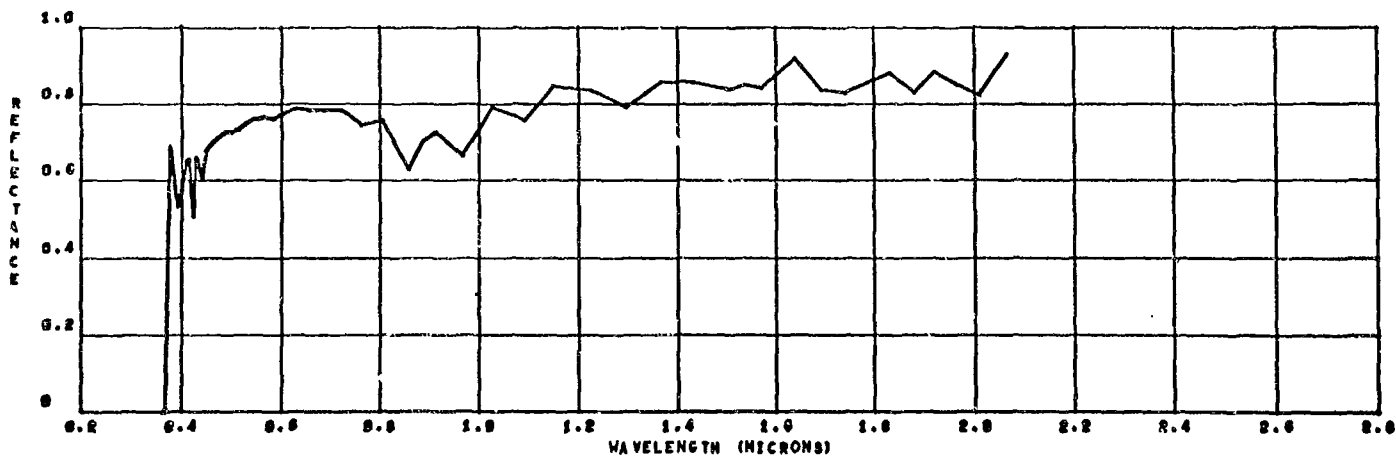






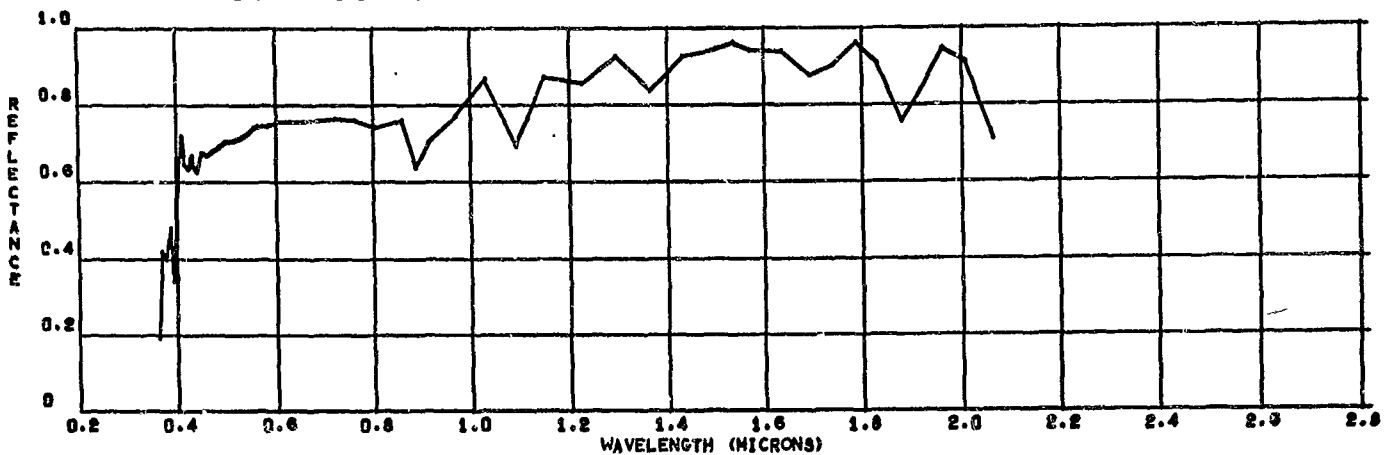
ALZAK 5X10E 14P 5X10E 13E 200EUVSH IN VAC -55F 5-2-67-17

SOLAR ABSORPTIVITY = 0.256



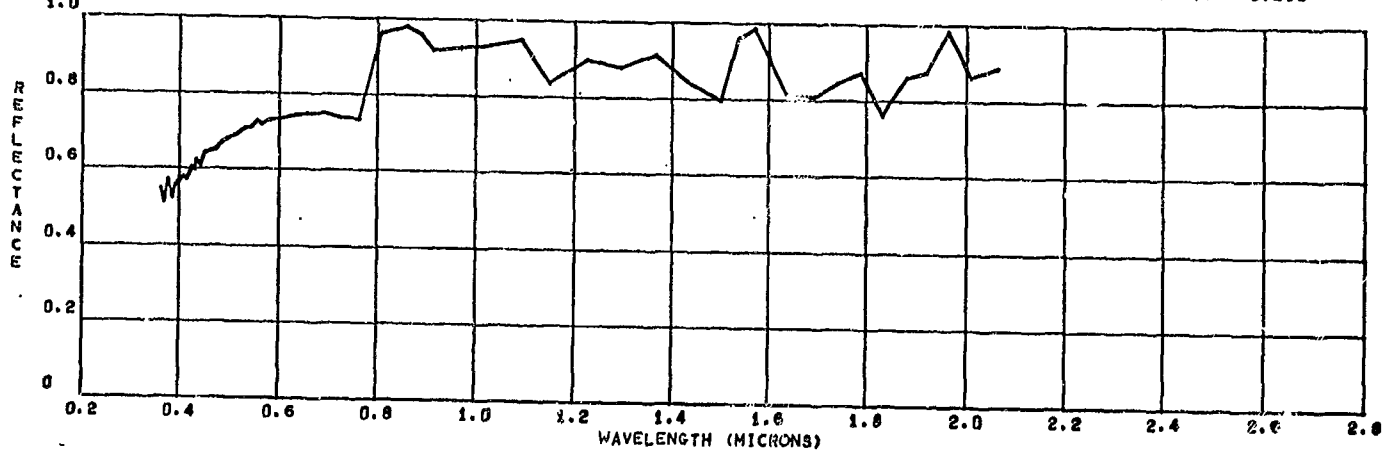
ALZAK 5X10E14P 5X10E13E 500 EUVSH IN VAC-55F 5-16-67-17

SOLAR ABSORPTIVITY = 0.244



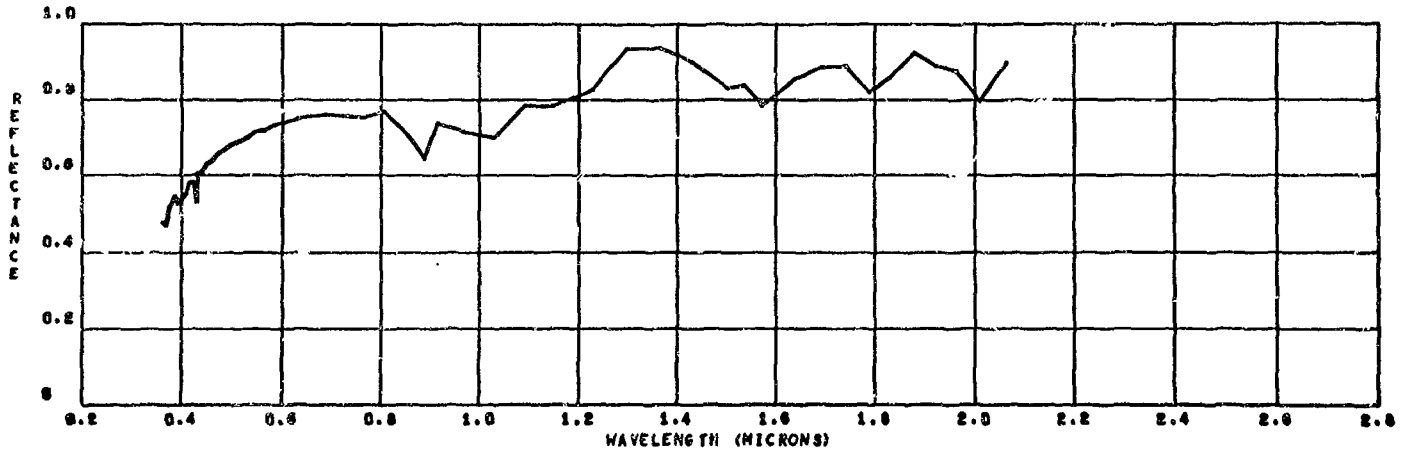
ALZAK 5X10E13E 5X10E14P 714 EUVSH IN VAC -55F 52667-17

SOLAR ABSORPTIVITY = 0.210



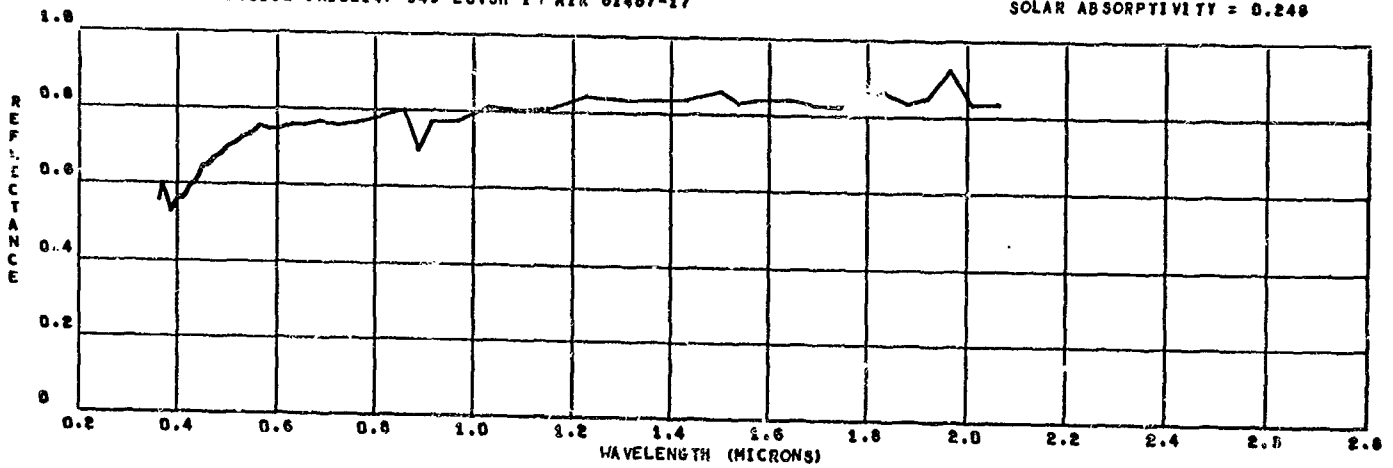
ALZAK 5X10E13E 5X10E14P 945 EUVSH IN VAC-55F 6667-17

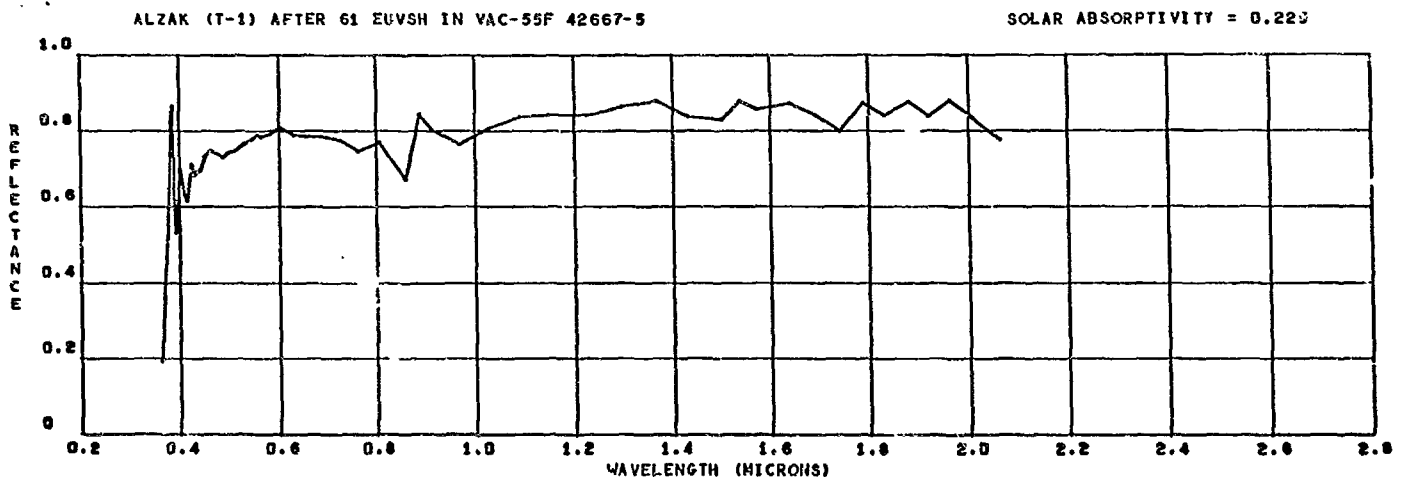
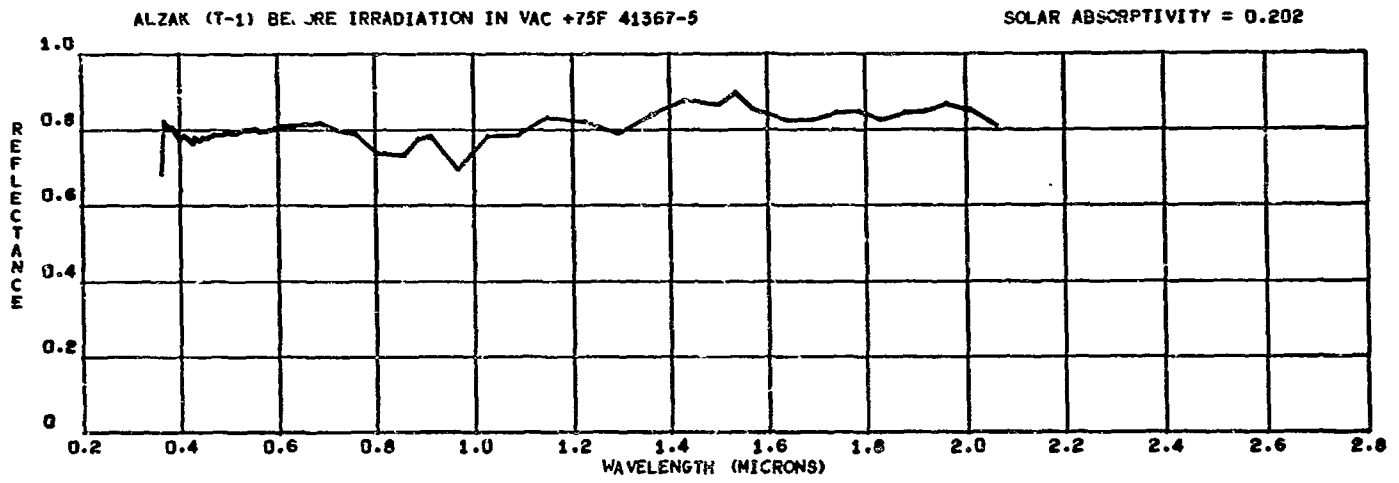
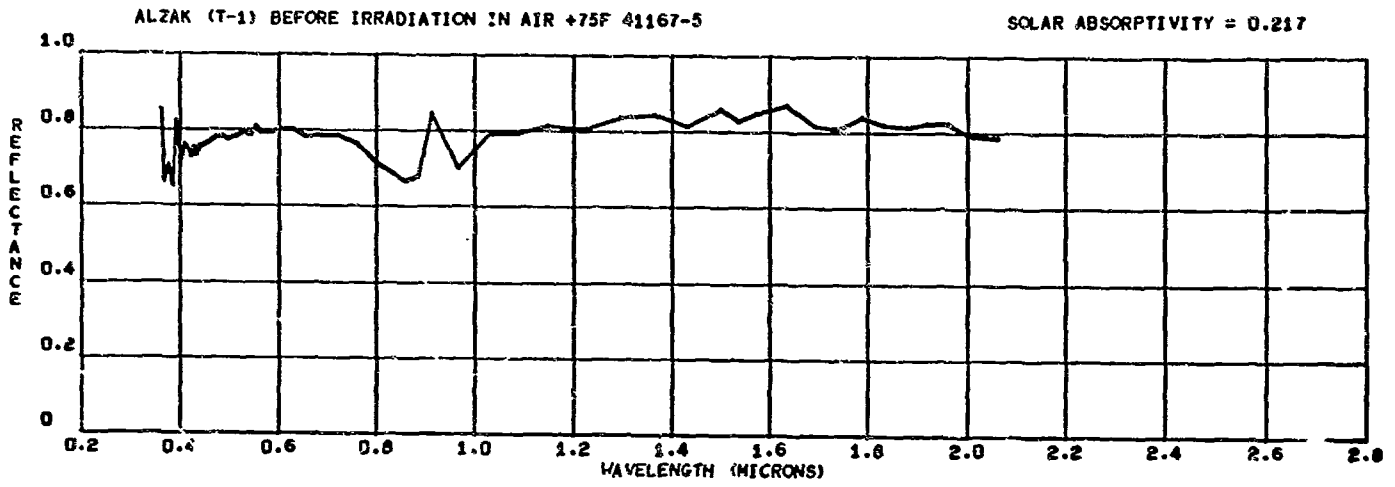
SOLAR ABSORPTIVITY = 0.263



ALZAK 5X10E13E 5X10E14P 945 EUVSH IN AIR 61467-17

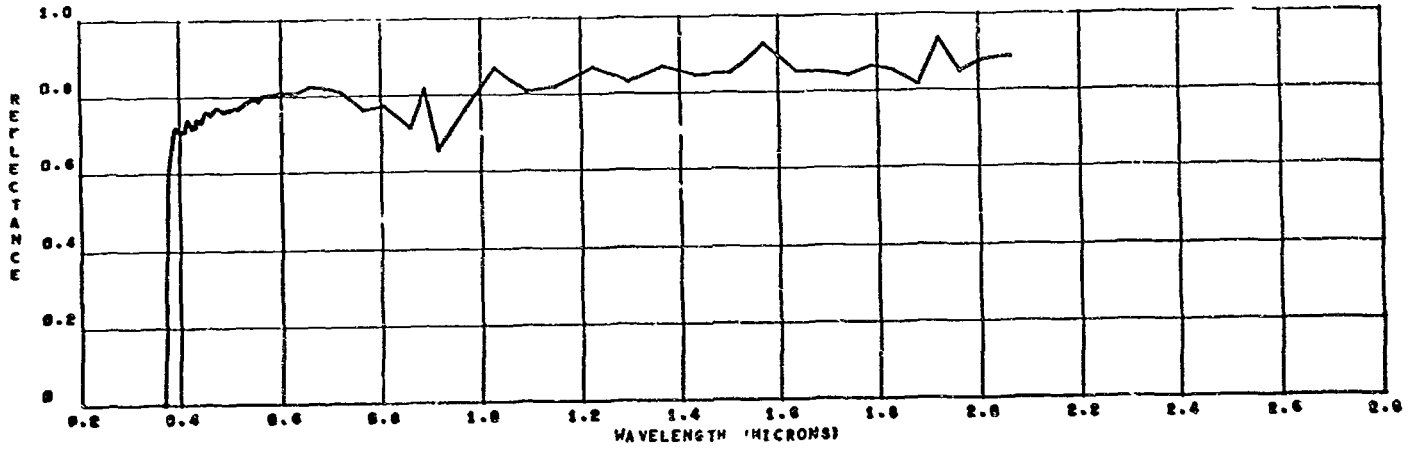
SOLAR ABSORPTIVITY = 0.246





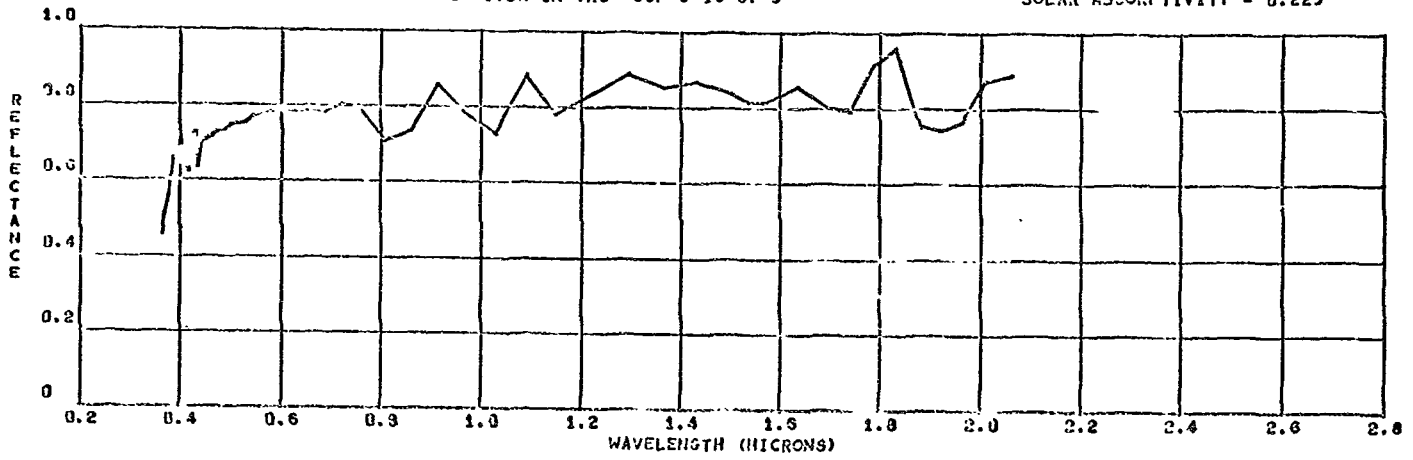
ALZAK(T1) 5X10E 14P 5X10E 13E 200EUVSH IN VAC -55F 5-2-67-5

SOLAR ABSORPTIVITY = 0.219



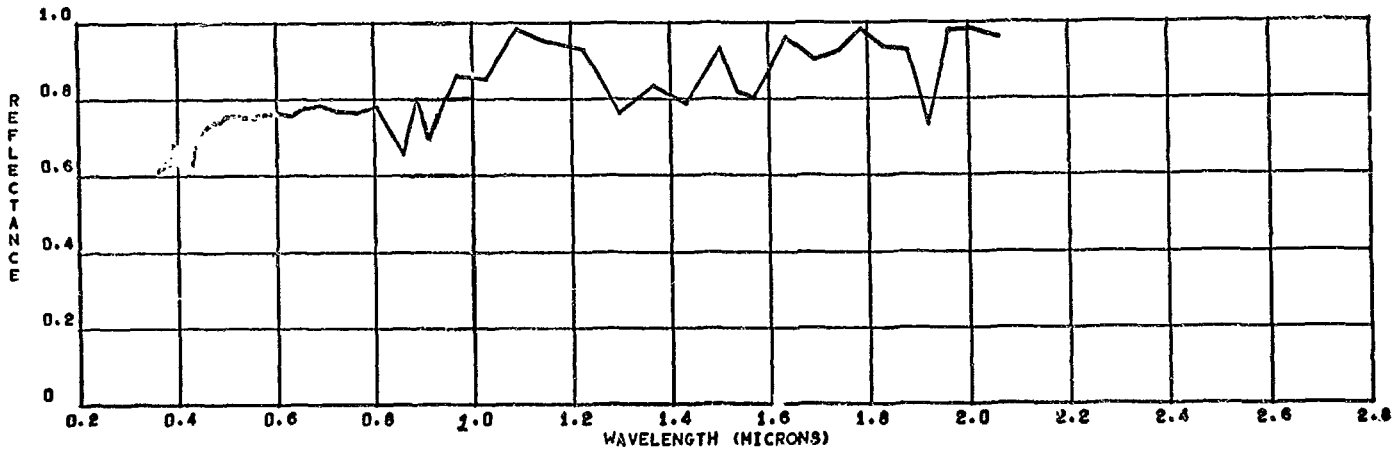
ALZAK(T1) 5X10E14P 5X10E13E EUVSH IN VAC -55F 5*16*67*5

SOLAR ABSORPTIVITY = 0.225



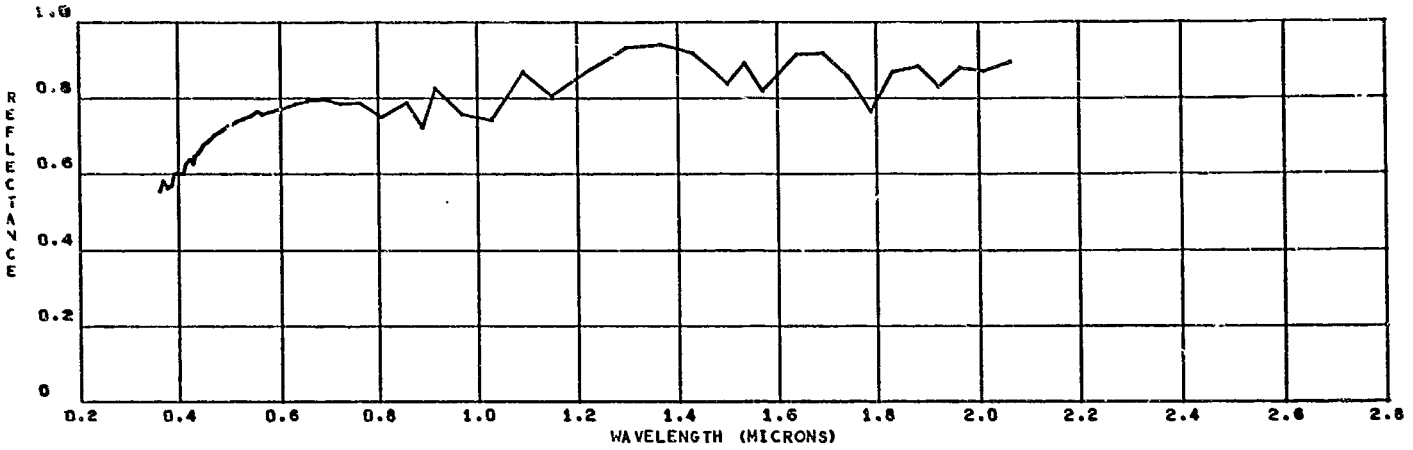
ALZAK(T1) 5X10E13E 5X10E14P 714 EUVSH IN VAC -55F 52667-5

SOLAR ABSORPTIVITY = 0.211



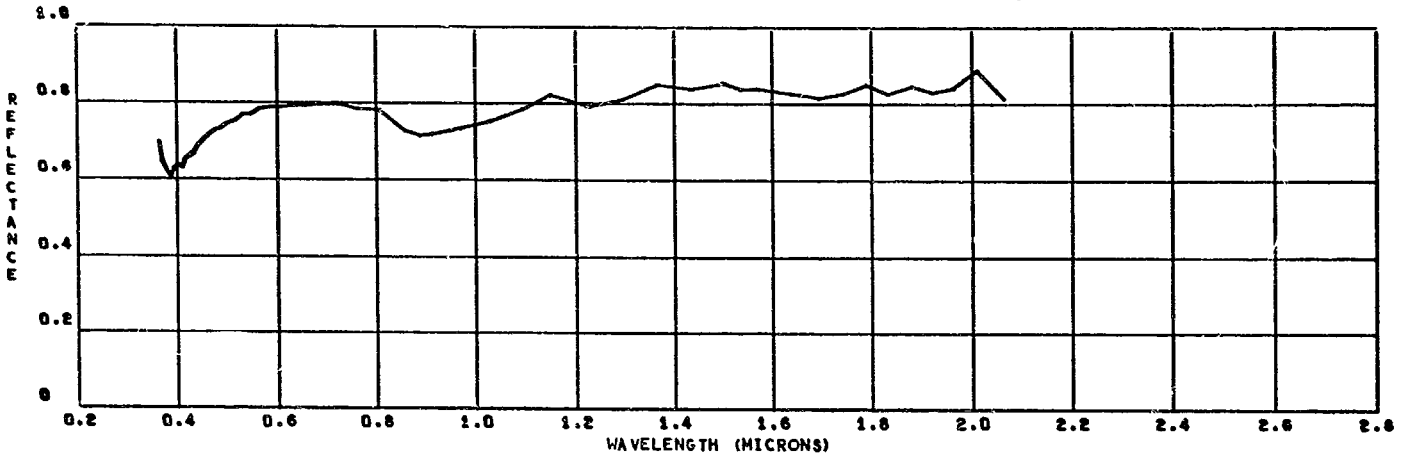
ALZAK (T1) 5X10E13E 5X10E14P 945EUVSH IN VAC -55F 6667-5

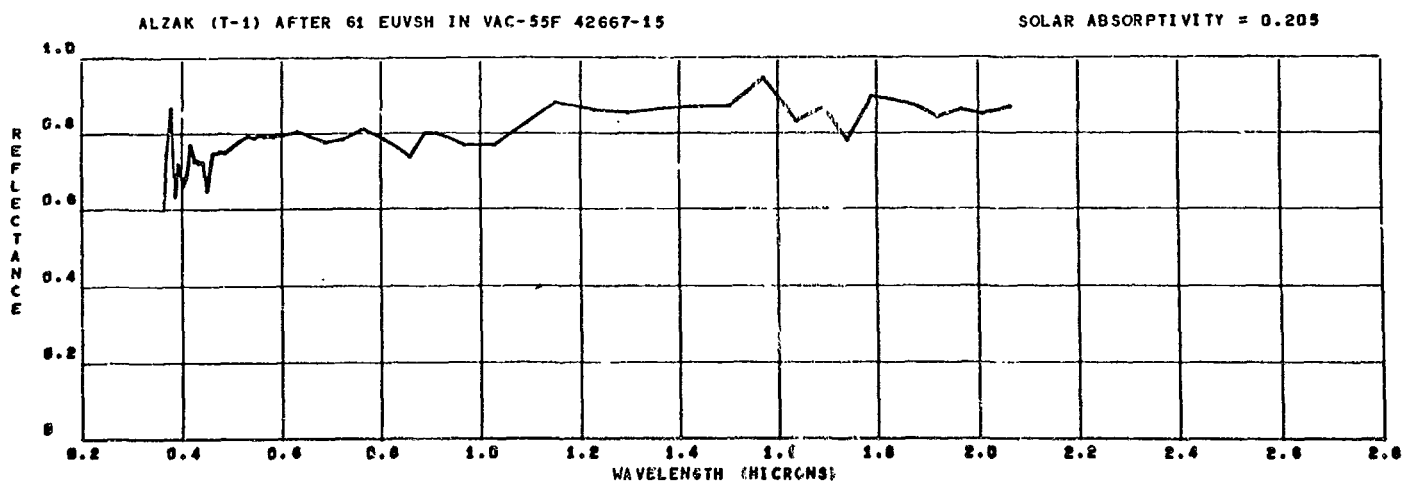
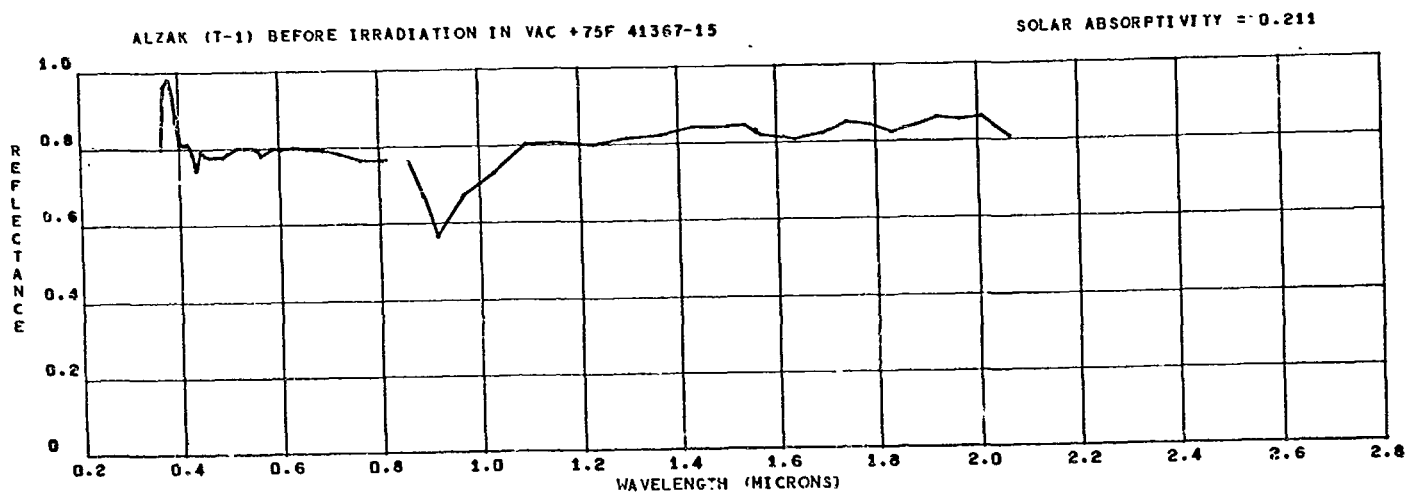
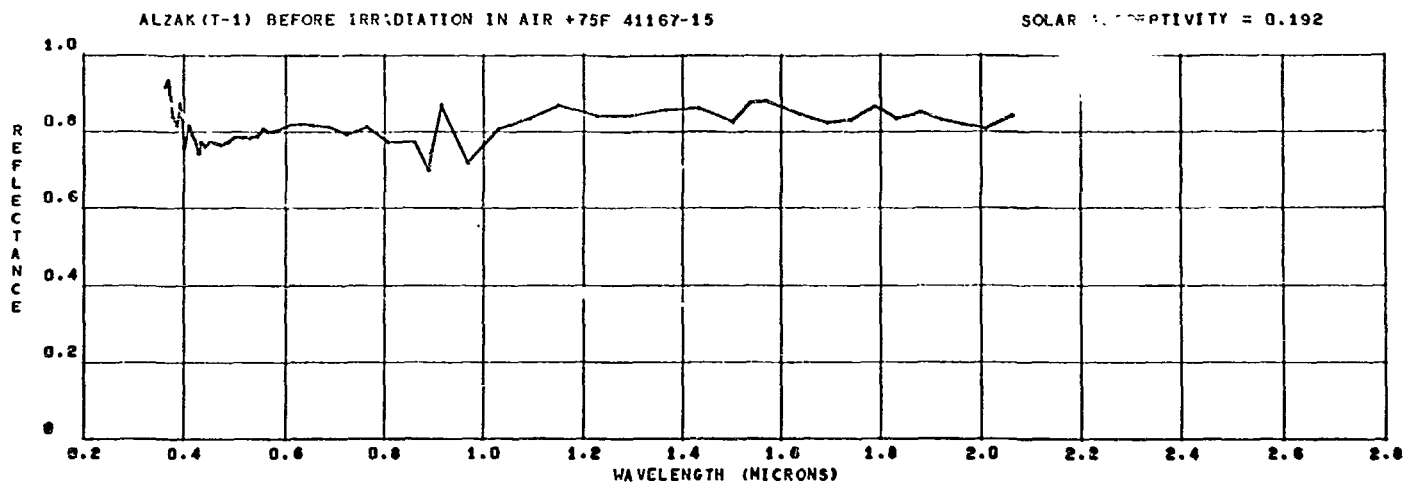
SOLAR ABSORPTIVITY = 0.223

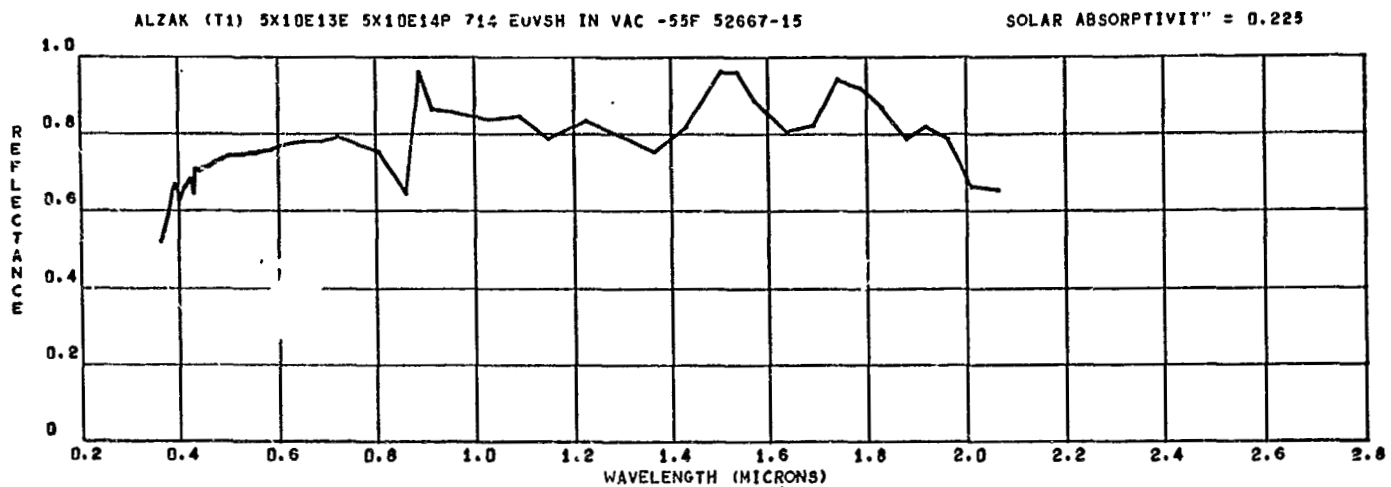
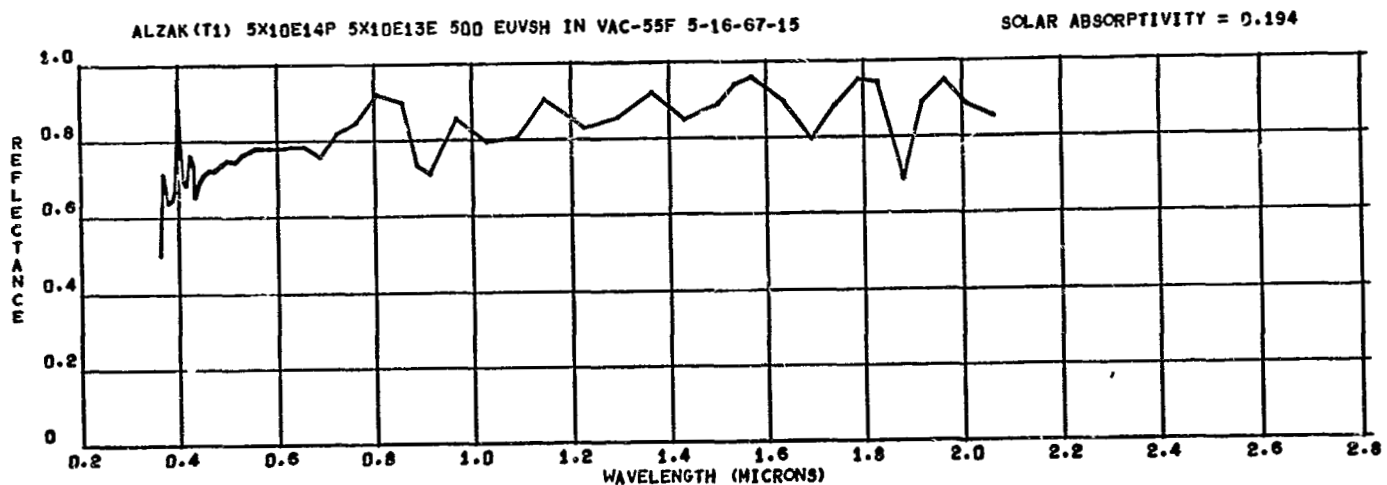
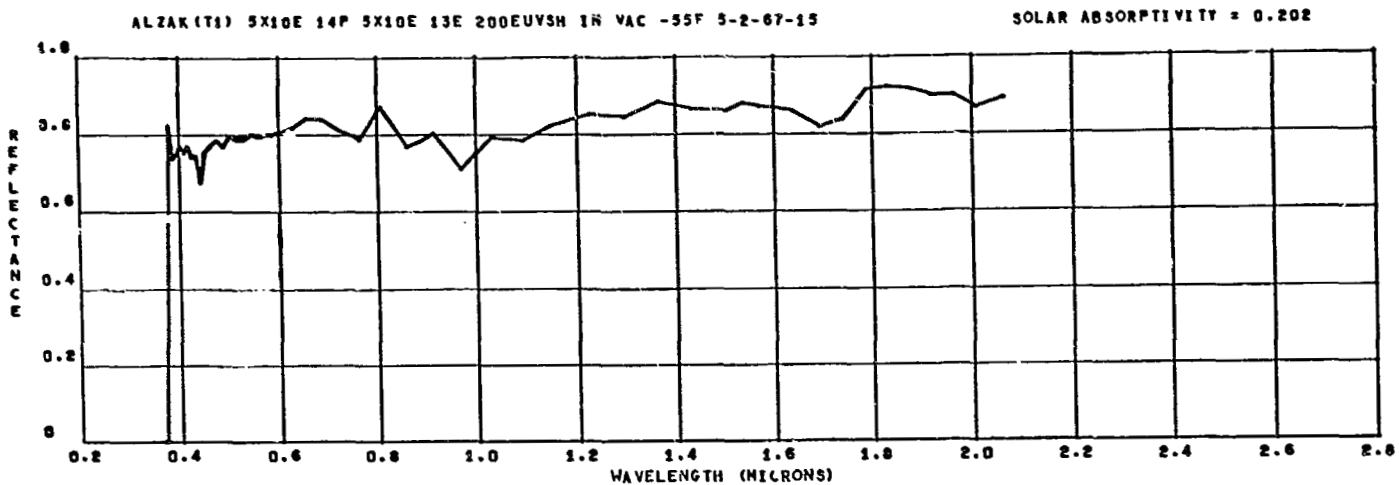


ALZAK (T1) 5X10E13E 5X10E14P 945 EUVSH IN AIR 61467-5

SOLAR ABSORPTIVITY = 0.231

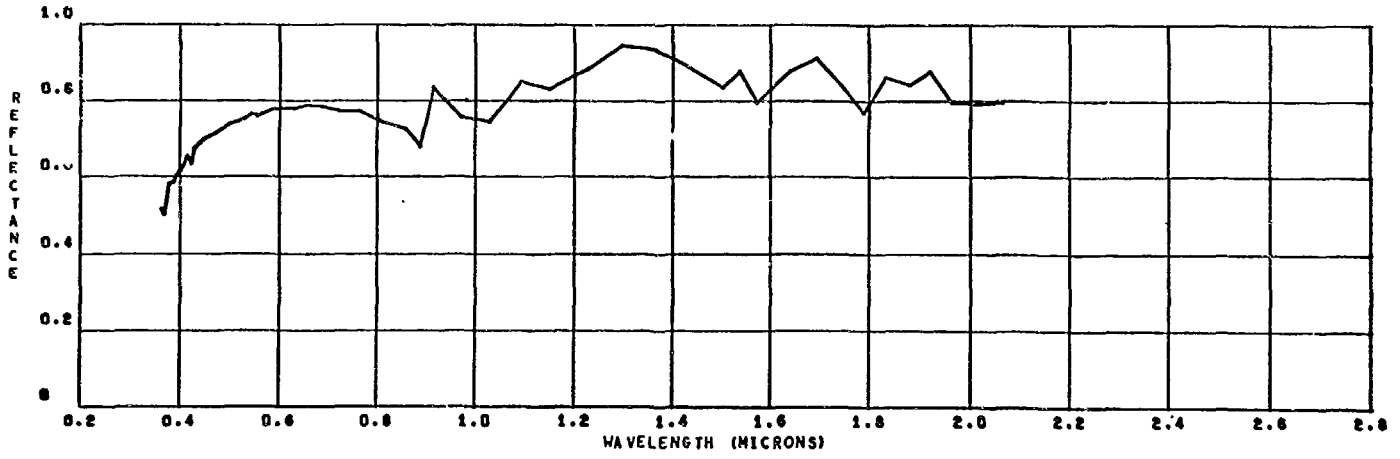






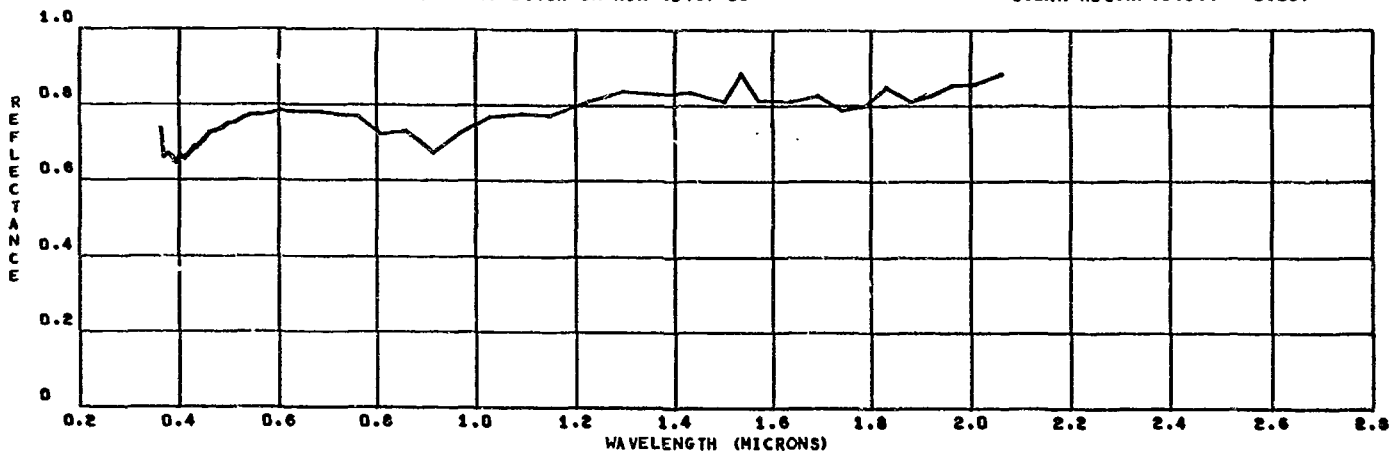
ALZAK (T1) 5X10E13E 5X10E14P 945 EUVSH IN VAC-55F 60-7-15

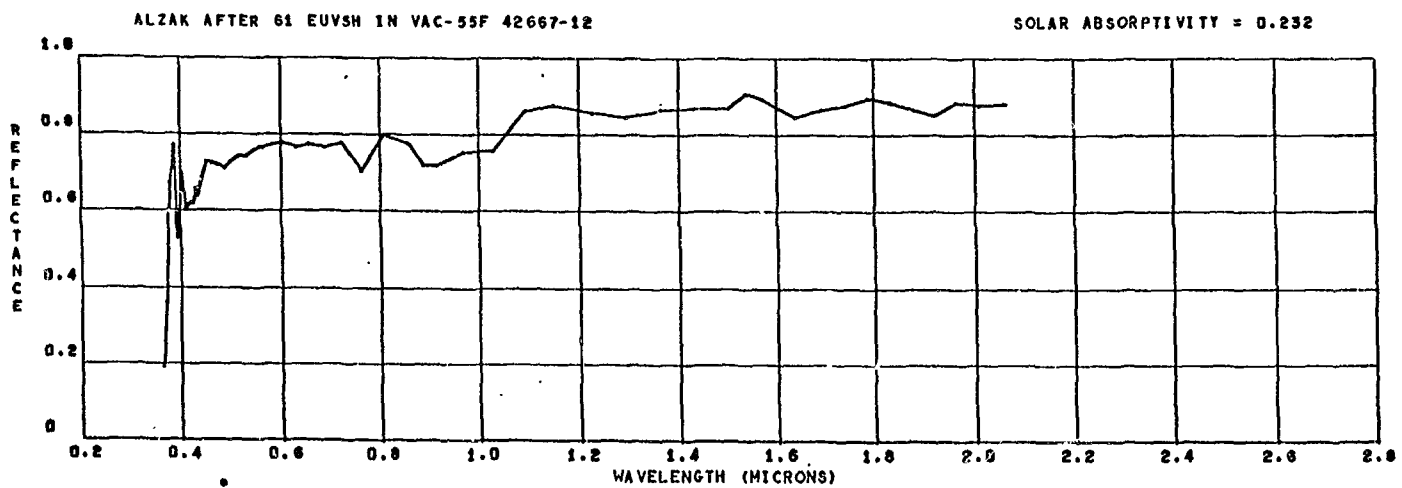
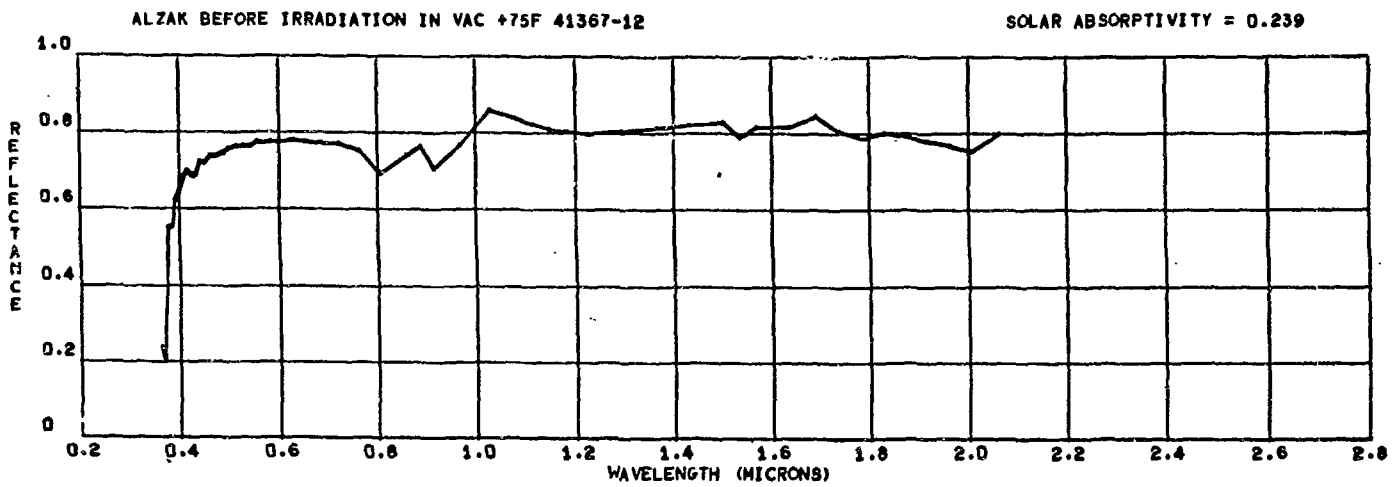
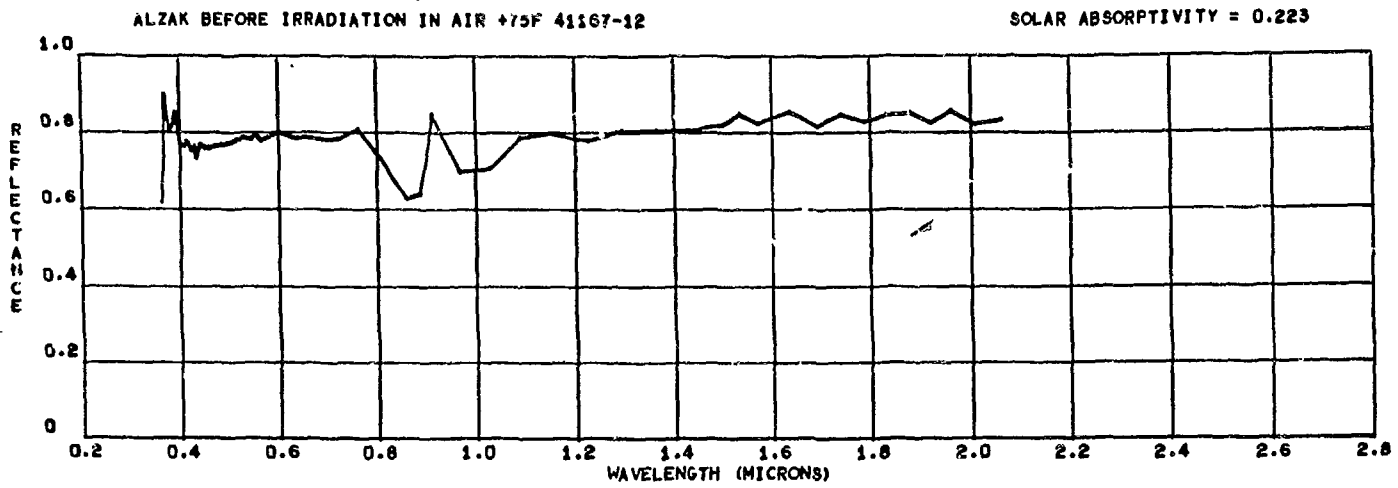
SOLAR ABSORPTIVITY = 0.227



ALZAK (T1) 5X10E13E 5X10E14P 945 EUVSH IN AIR 61467-15

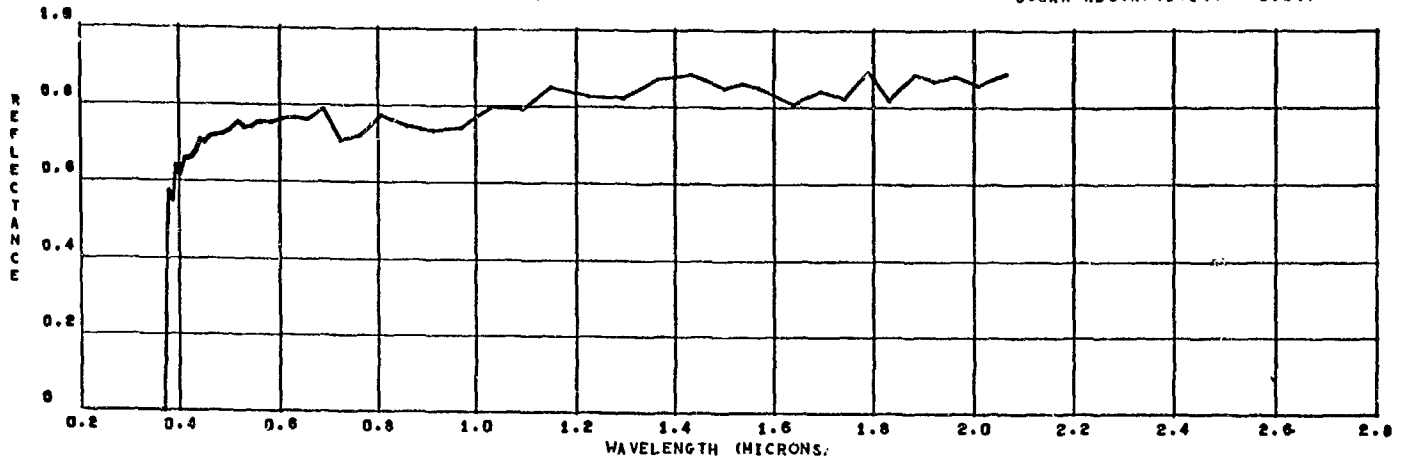
SOLAR ABSORPTIVITY = 0.237





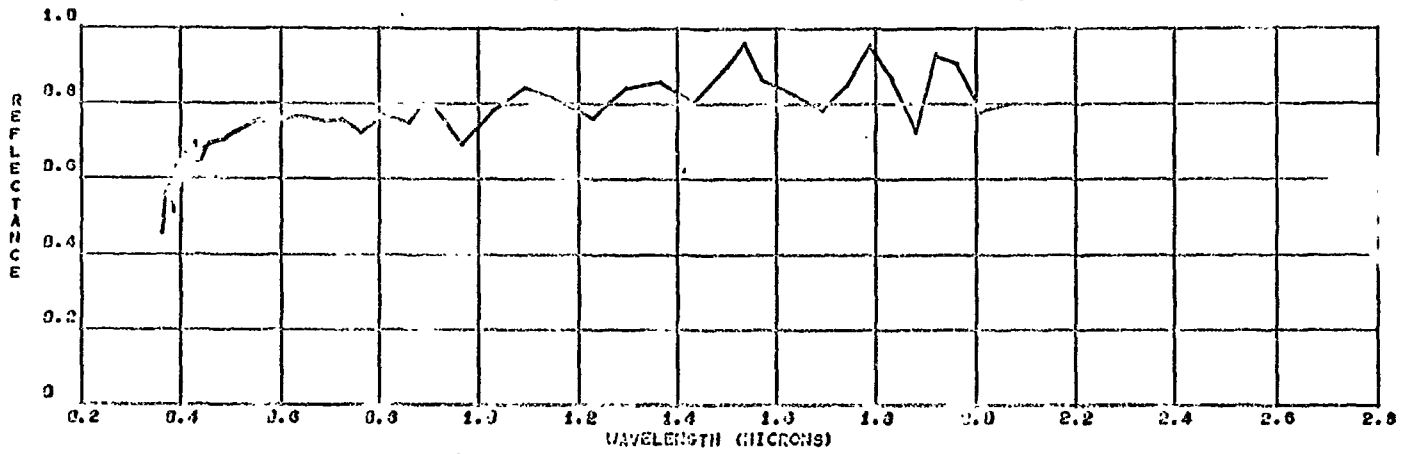
ALZAK 200EUVSH IN VAC -55F 5-2-67-12

SOLAR ABSORPTIVITY = 0.247



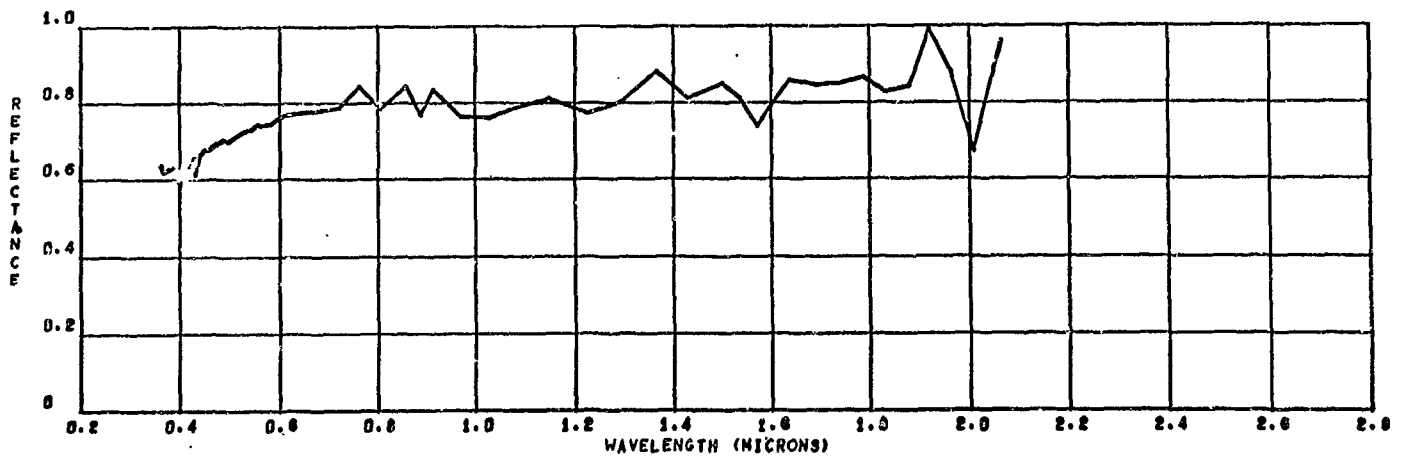
ALZAK 500EUVSH IN VAC -55F 5-16-67-12

SOLAR ABSORPTIVITY = 0.244



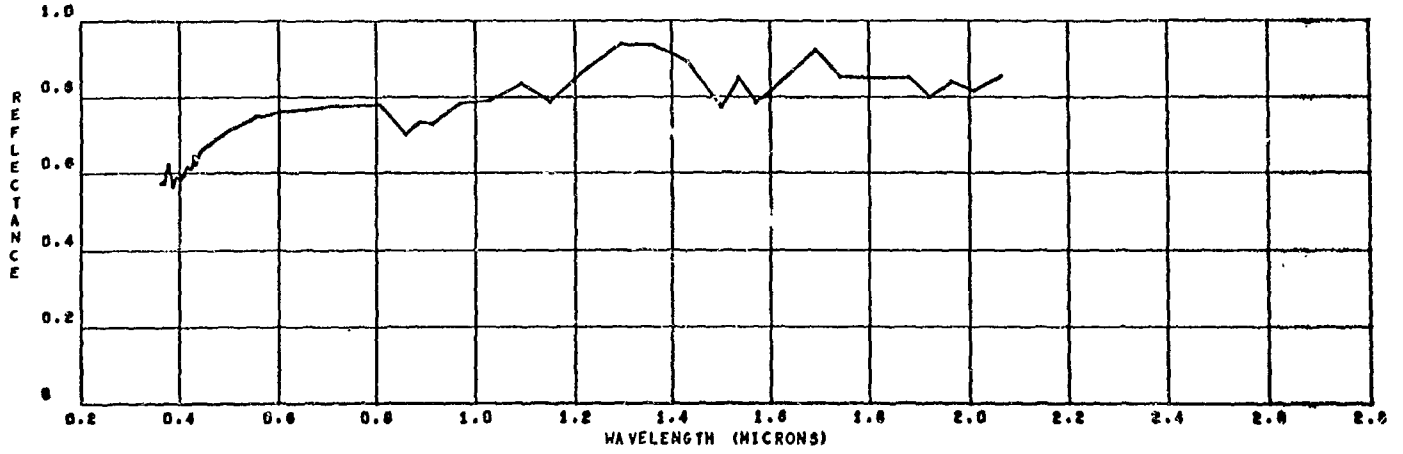
ALZAK 714 EUVSH IN VAC -55F 52667-12

SOLAR ABSORPTIVITY = 0.253



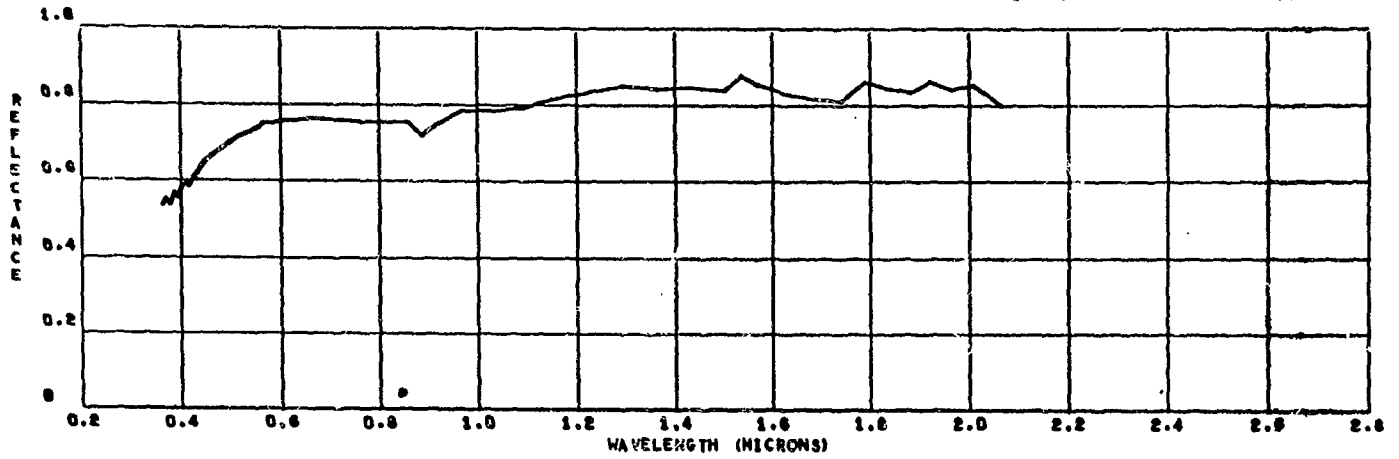
ALZAK 945EUVSH IN VAC -55F 6667-12

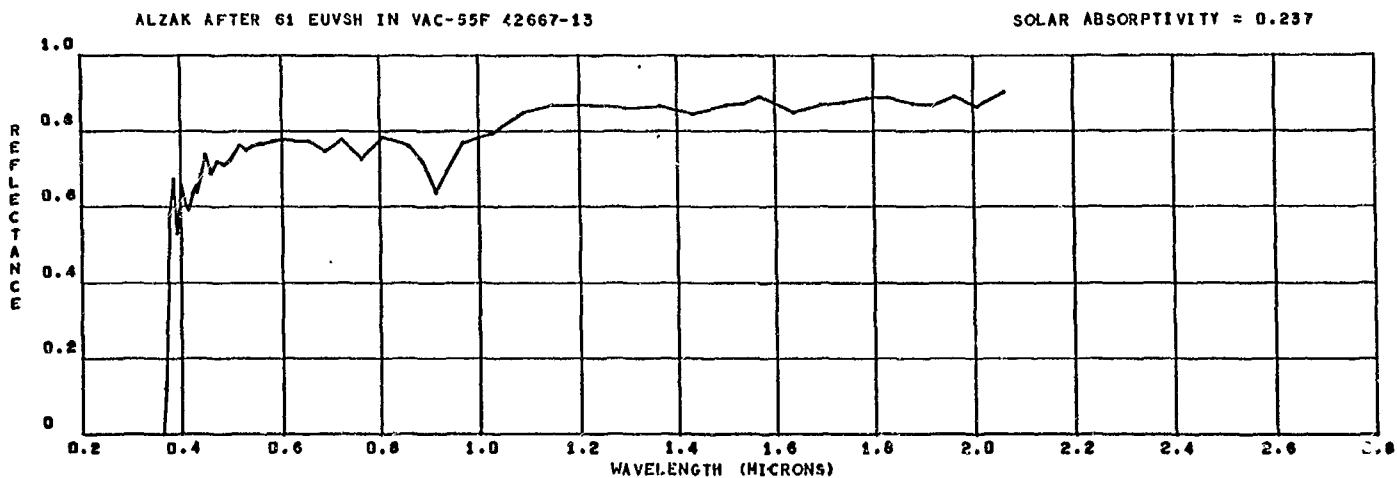
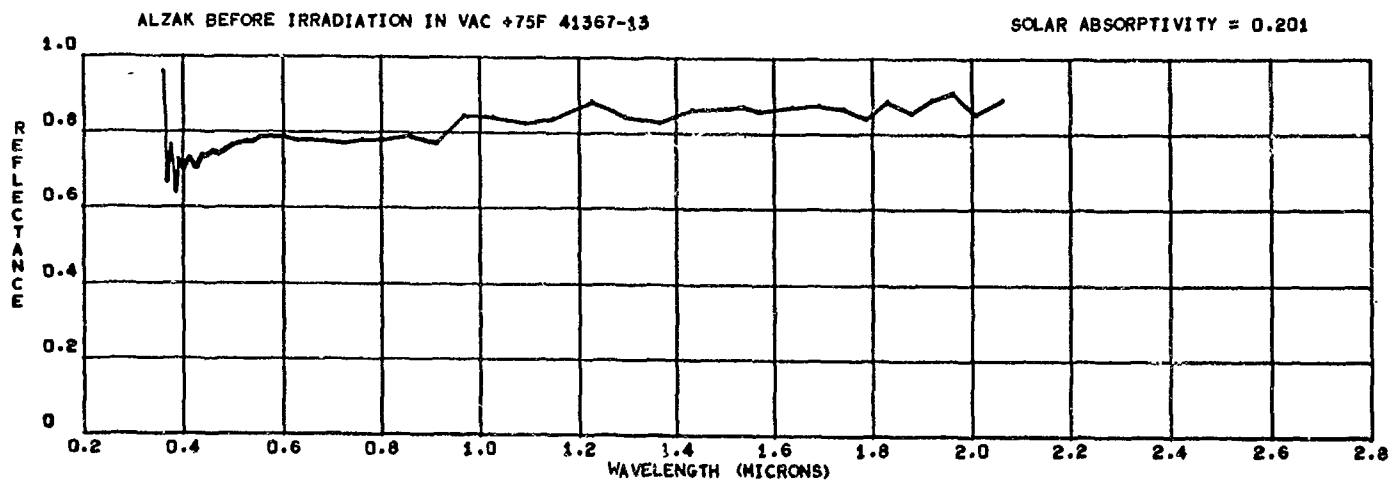
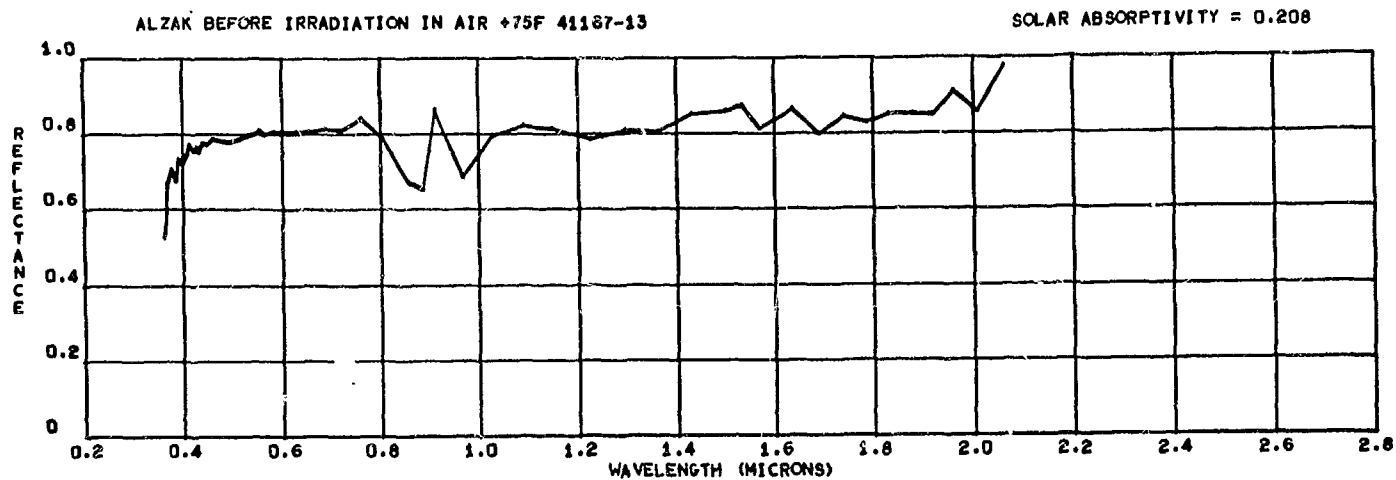
SOLAR ABSORPTIVITY = 0.237



ALZAK 945 EUVSH IN AIR 61467-12

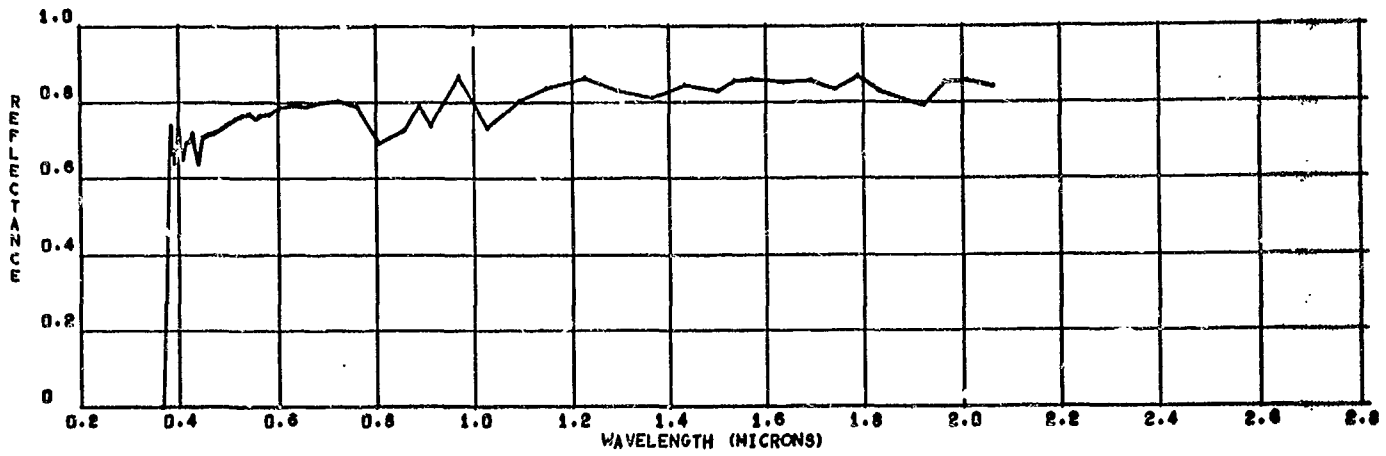
SOLAR ABSORPTIVITY = 0.249





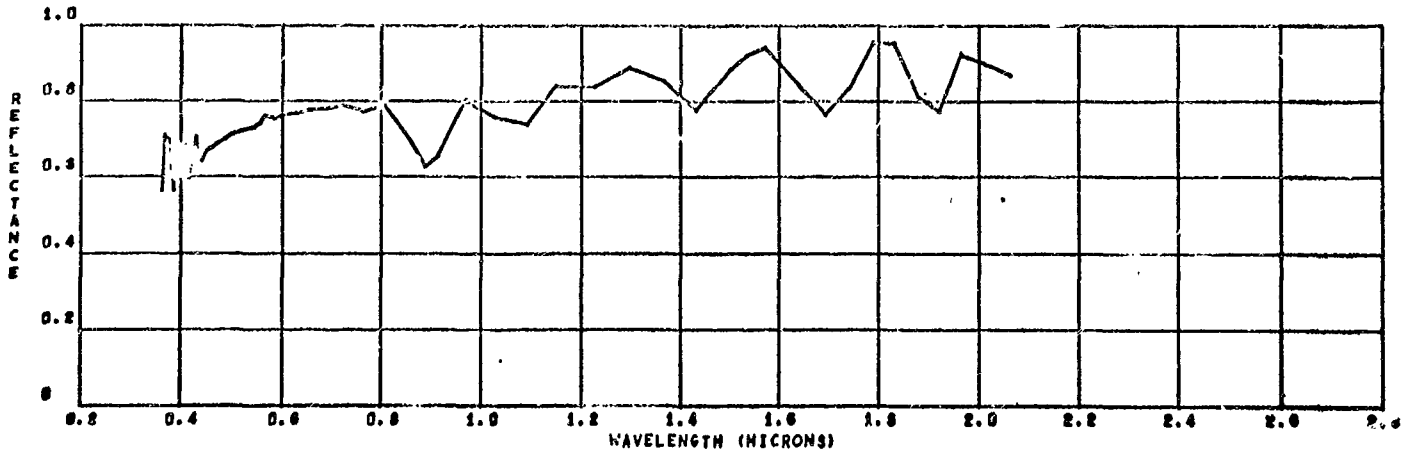
ALZAK 200EUVSH IN VAC -55F 5-2-67-13

SOLAR ABSORPTIVITY = 0.234



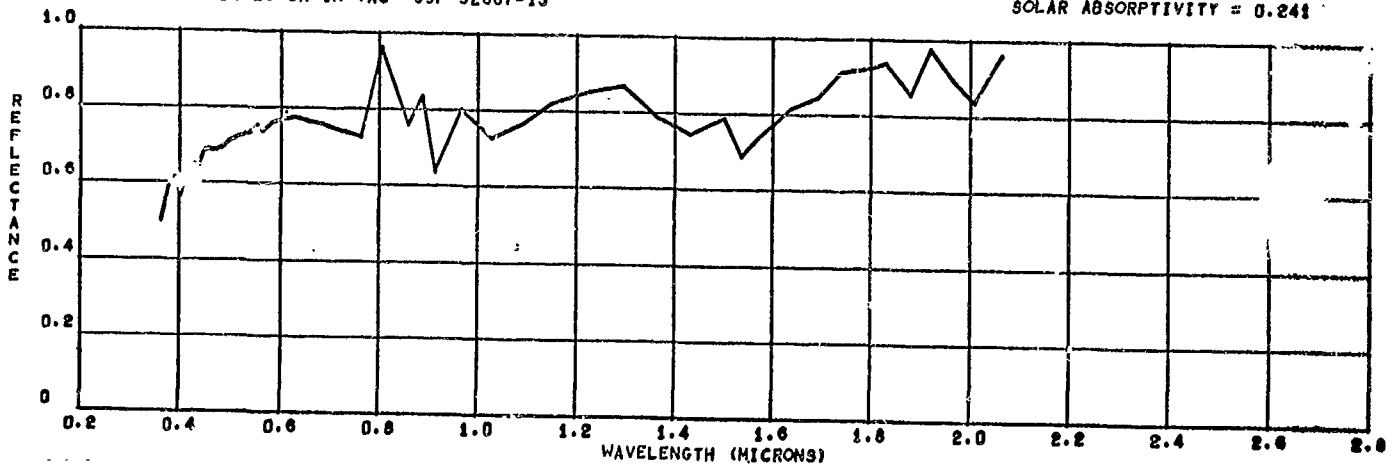
ALZAK 500 EUVSH IN VAC-55F 5-16-67-13

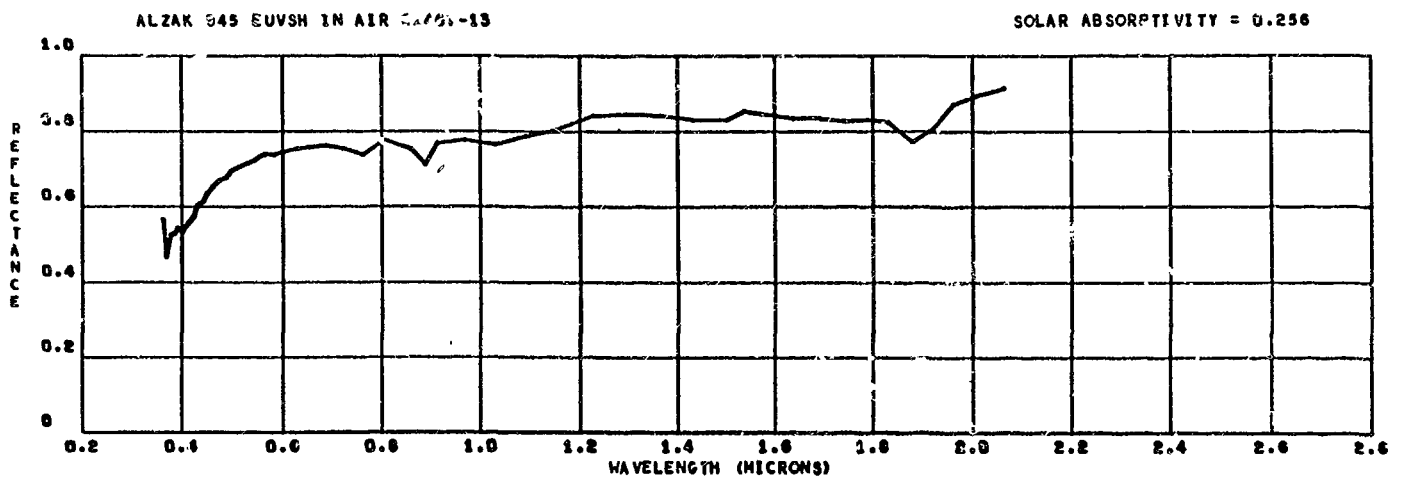
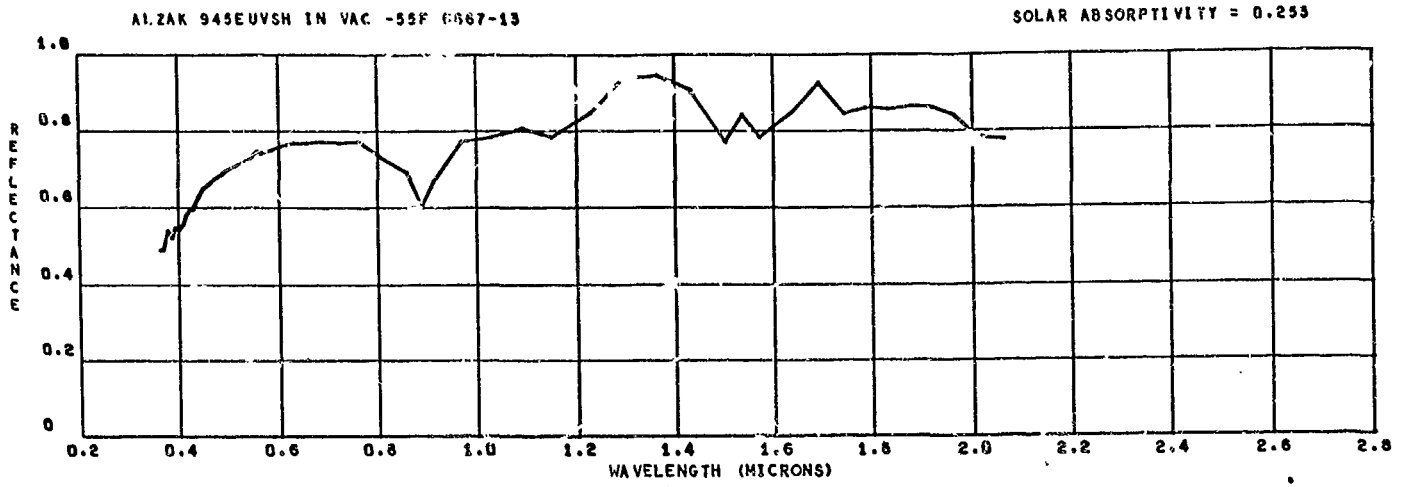
SOLAR ABSORPTIVITY = 0.241

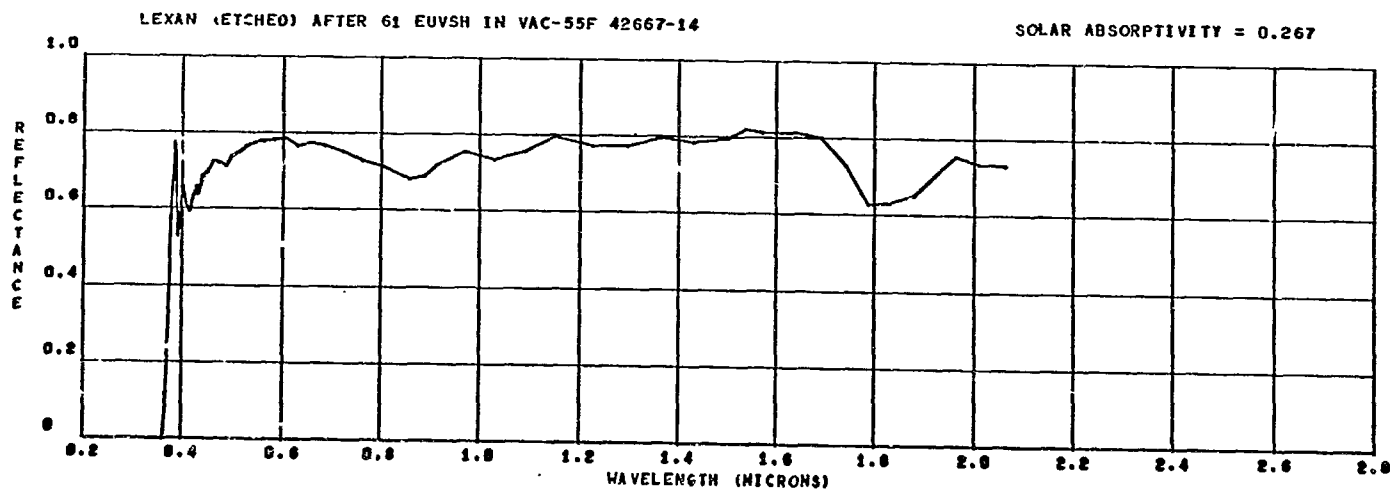
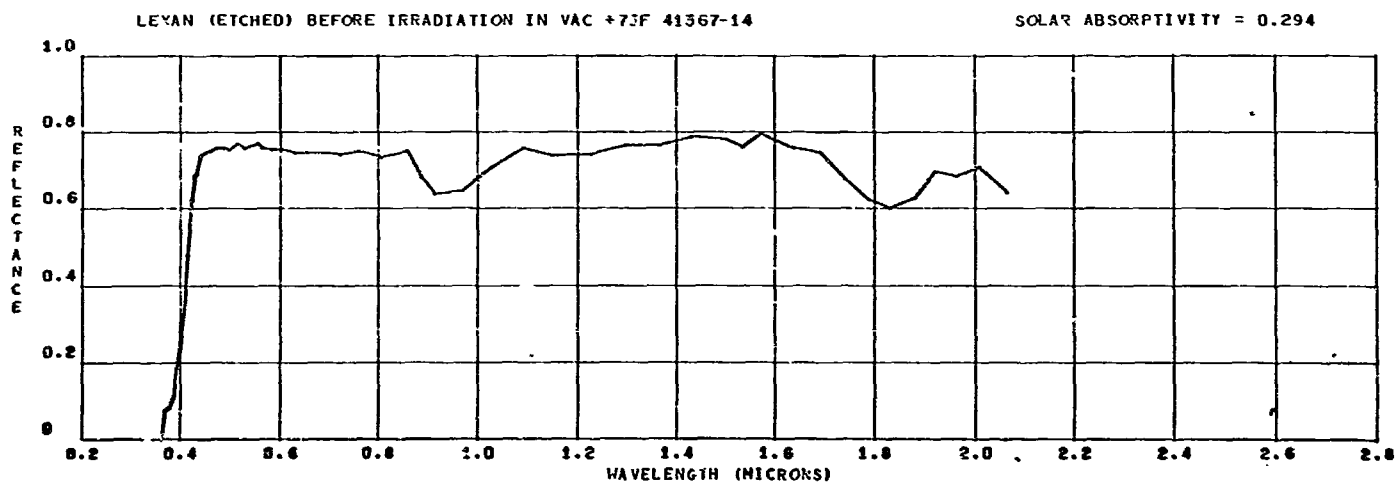
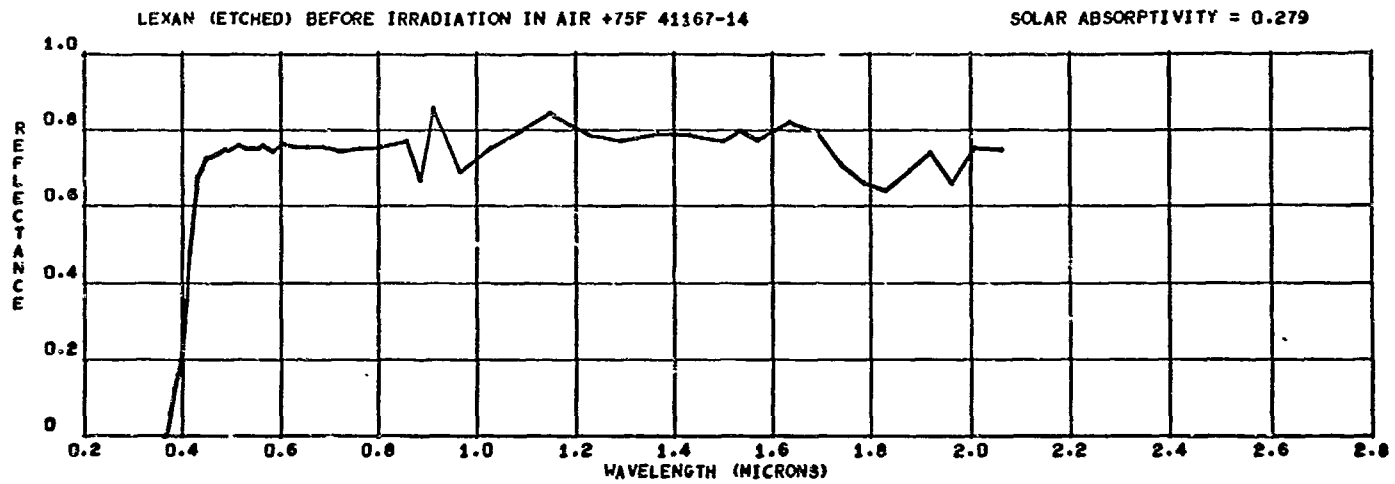


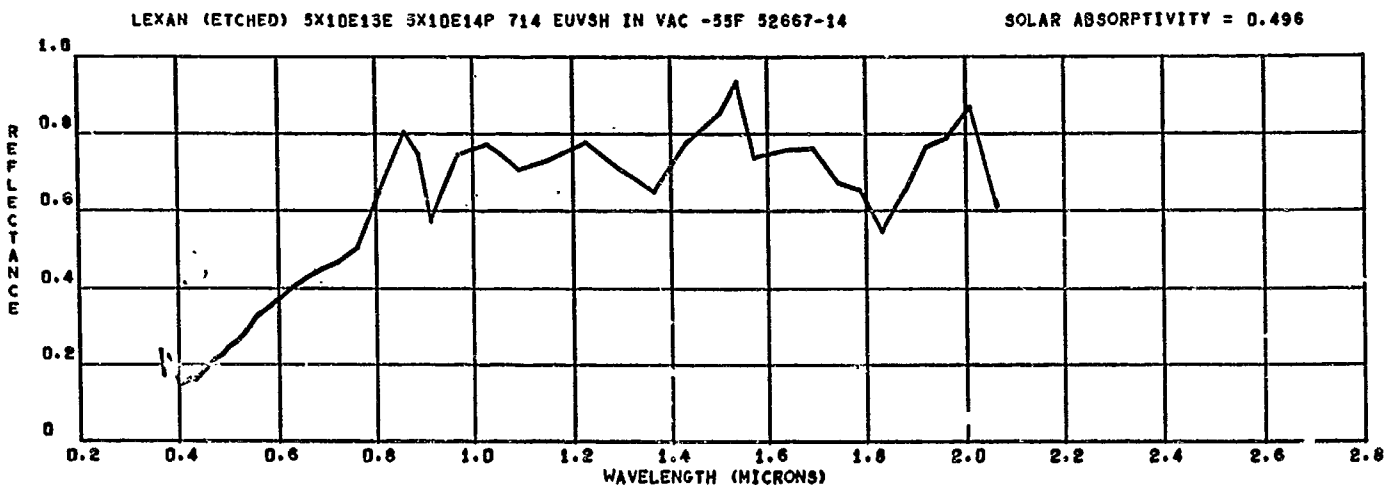
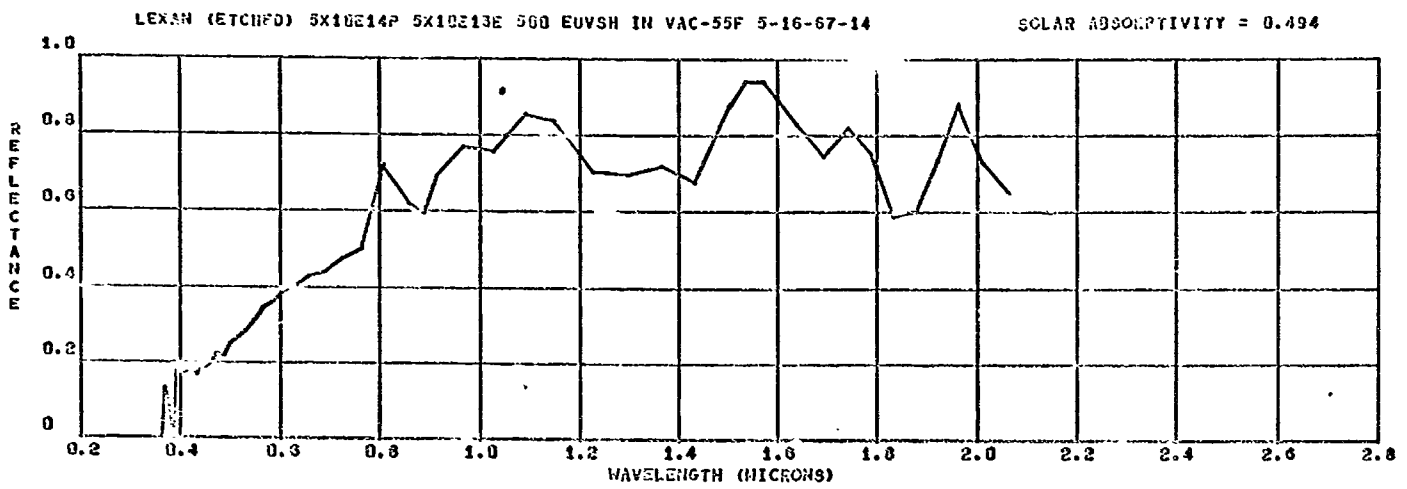
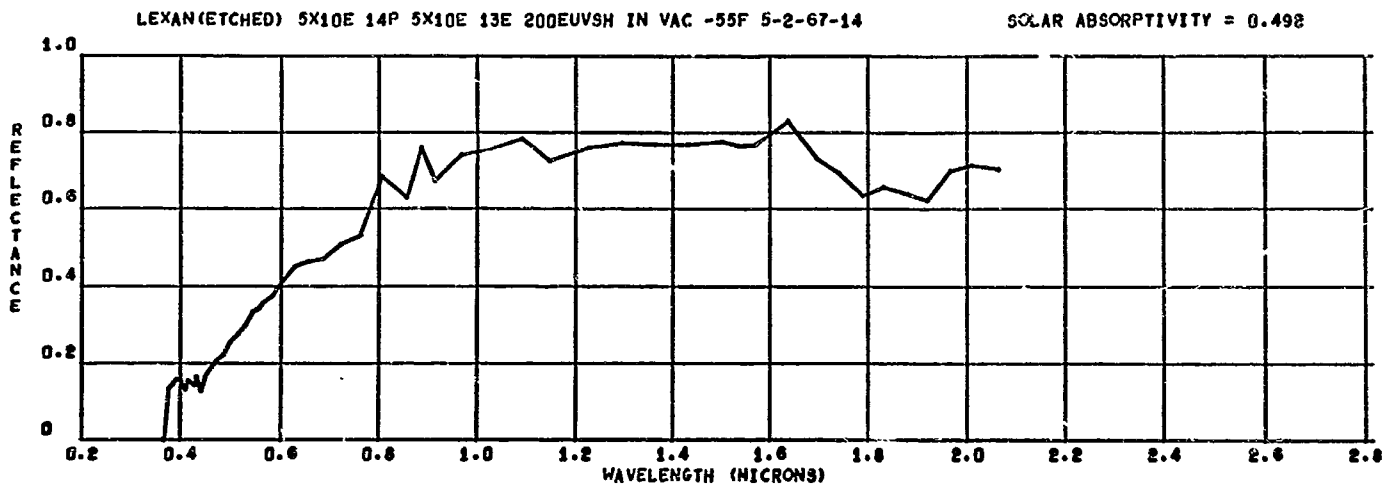
ALZAK 714 EUVSH IN VAC -55F 52667-13

SOLAR ABSORPTIVITY = 0.241



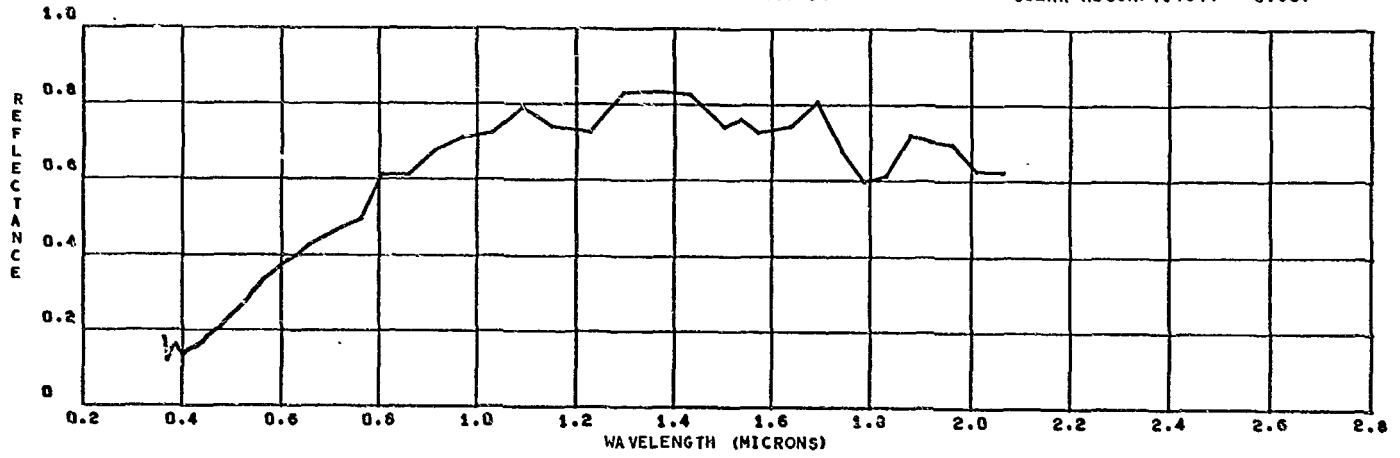






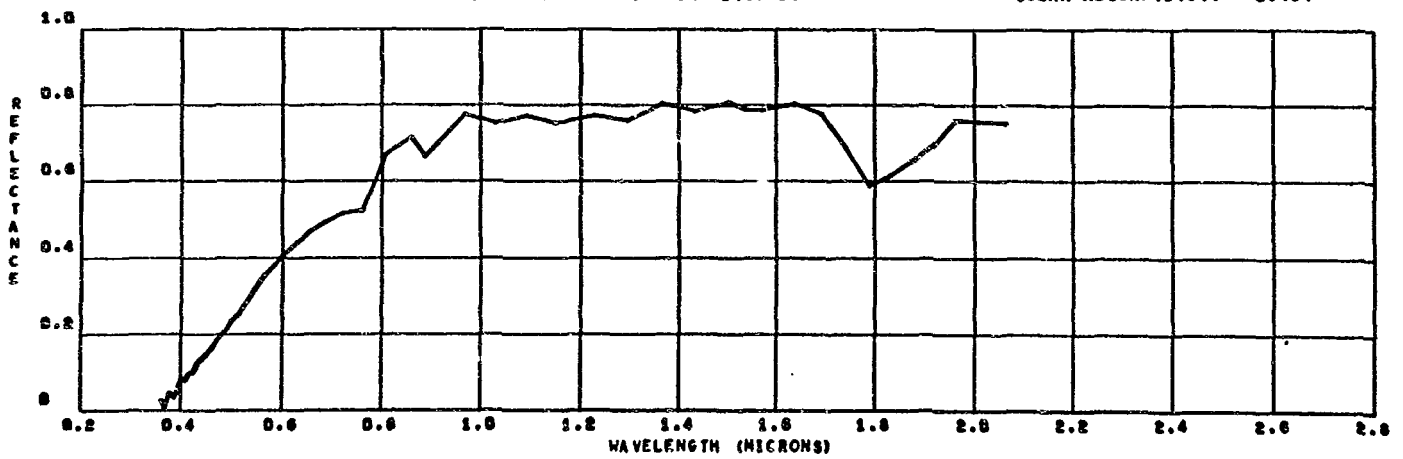
LEXAN (ETCHED) 5X10E13E 5X10E14P 945 EUVSH IN VAC-55F 6667-14

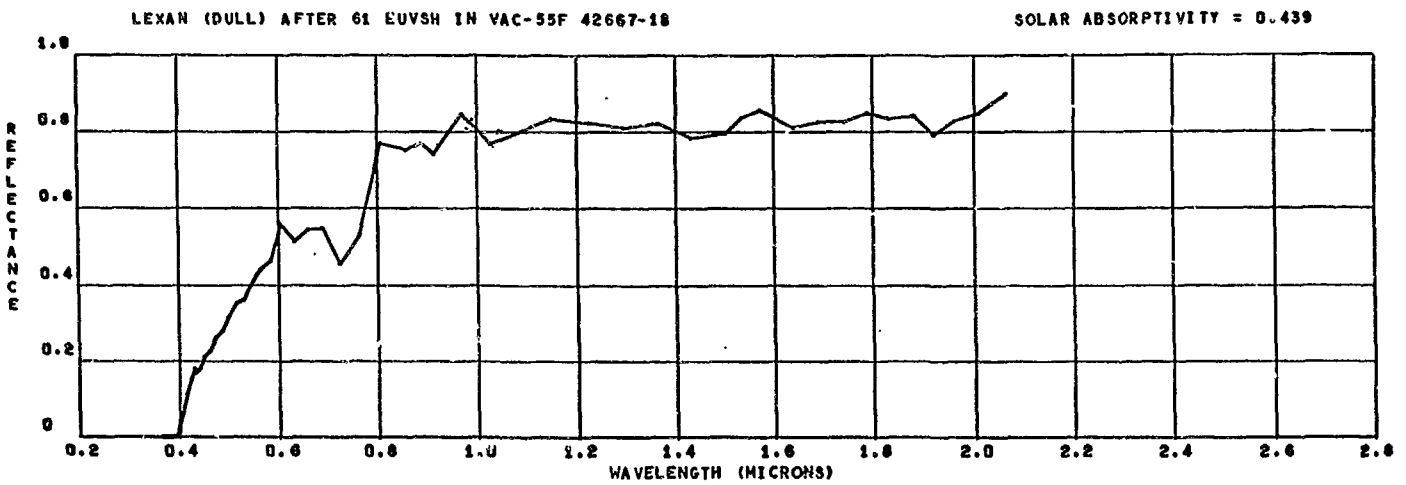
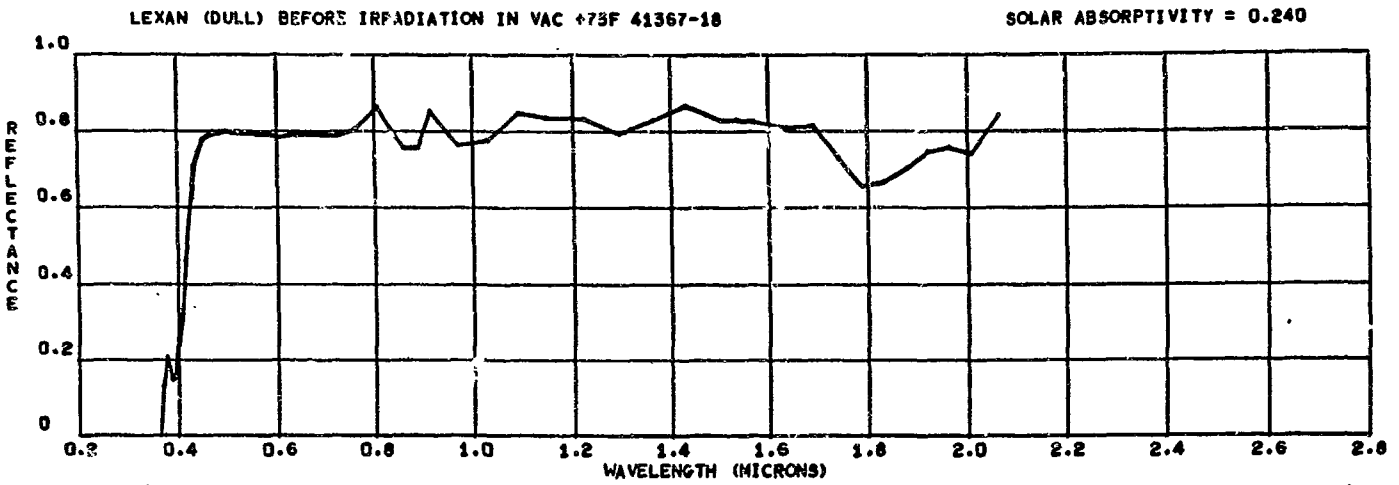
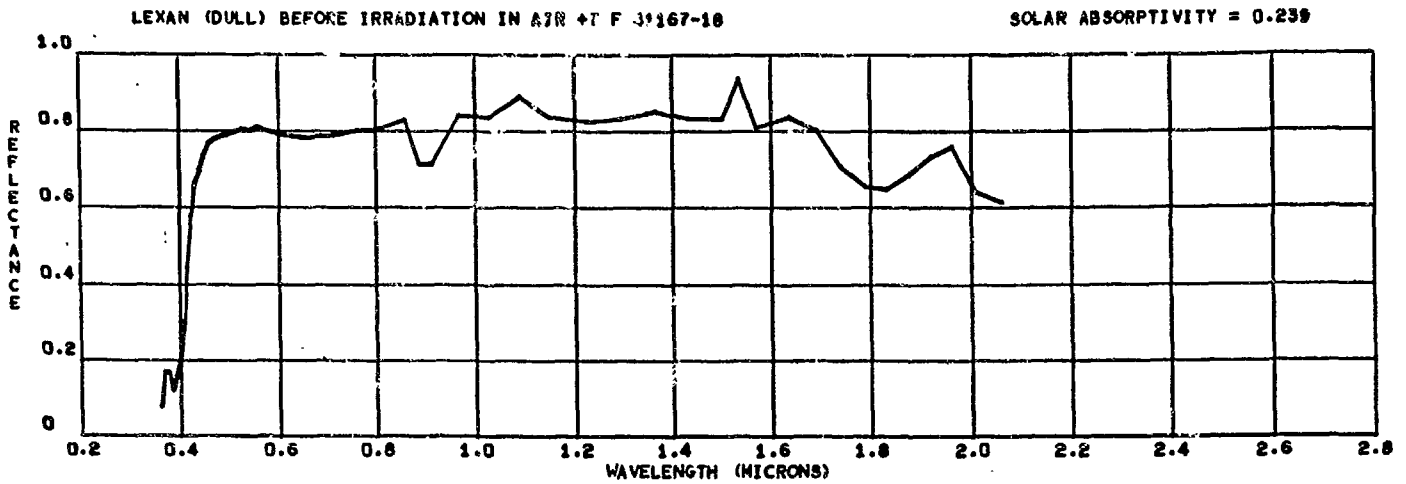
SOLAR ABSORPTIVITY = 0.507

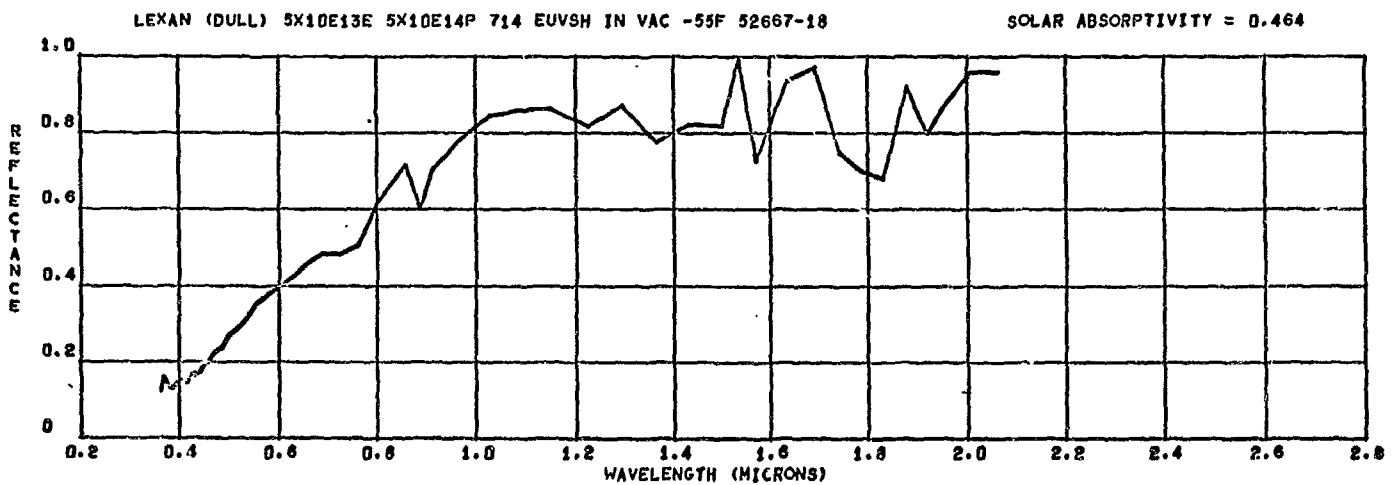
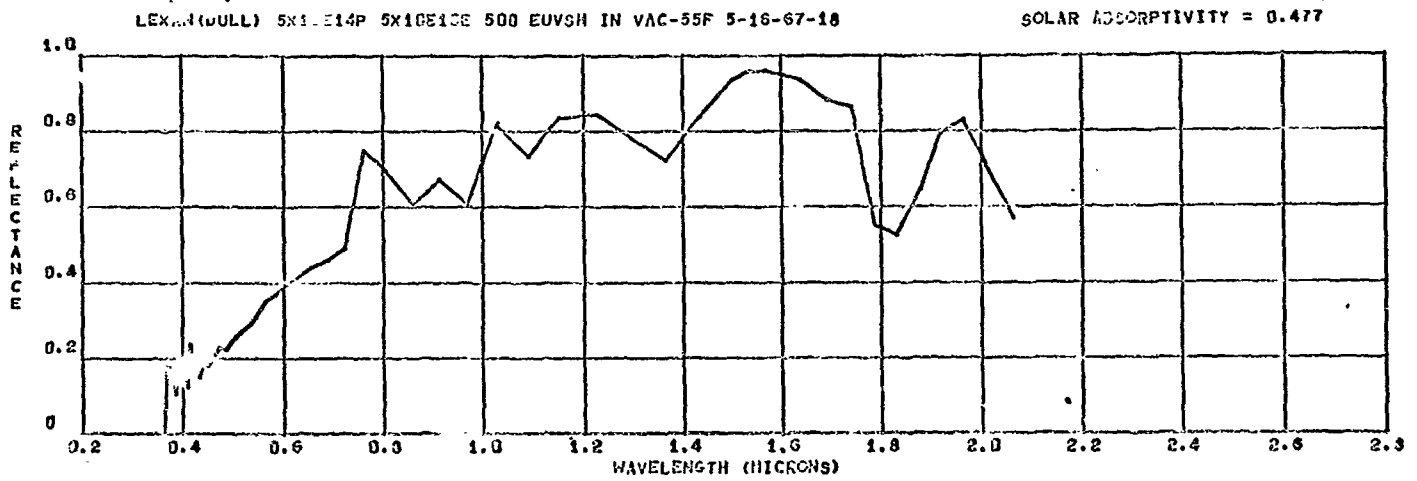
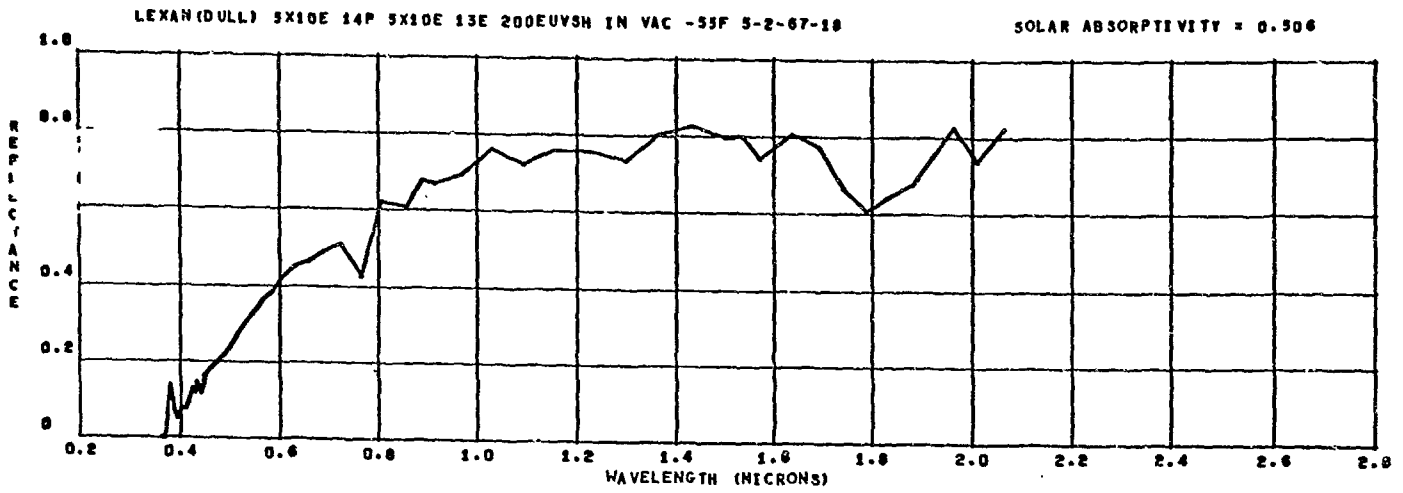


LEXAN (ETCHED) 5X10E13E 5X10E14P 945 EUVSH IN AIR 61467-14

SOLAR ABSORPTIVITY = 0.494

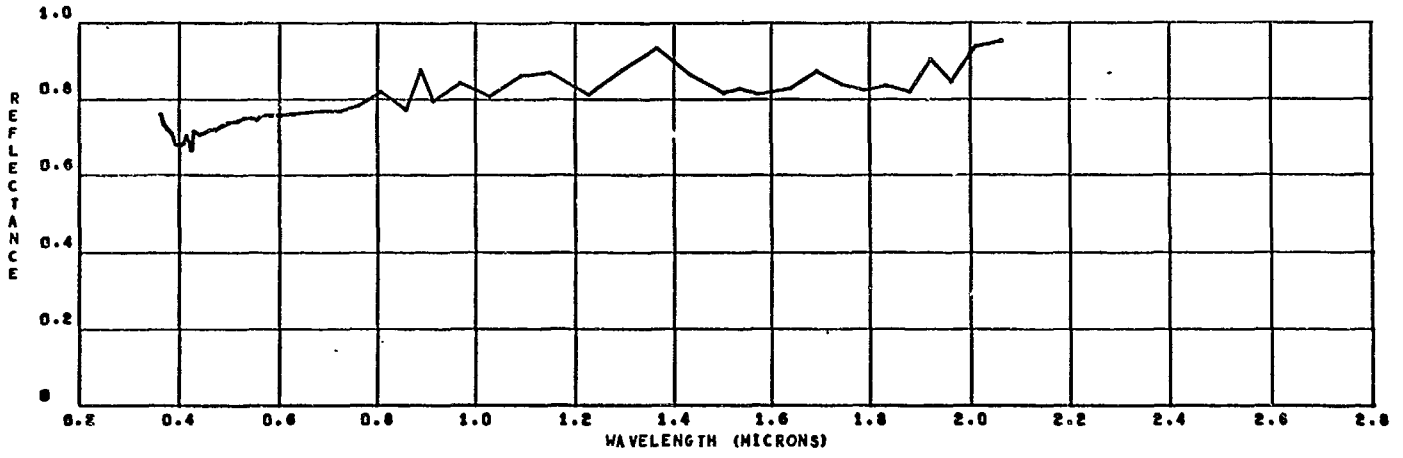


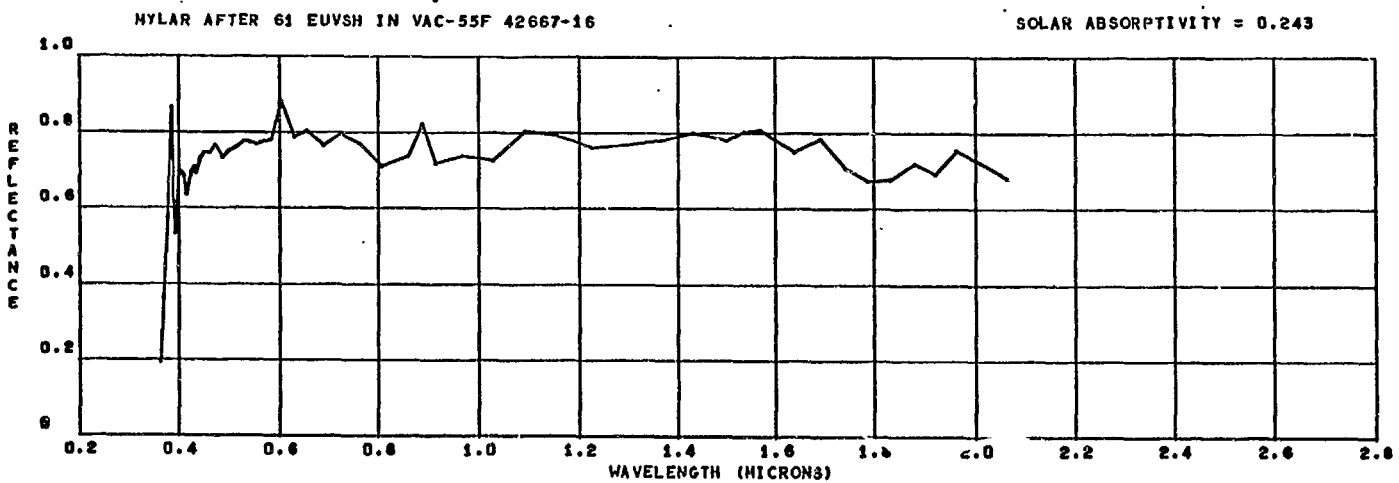
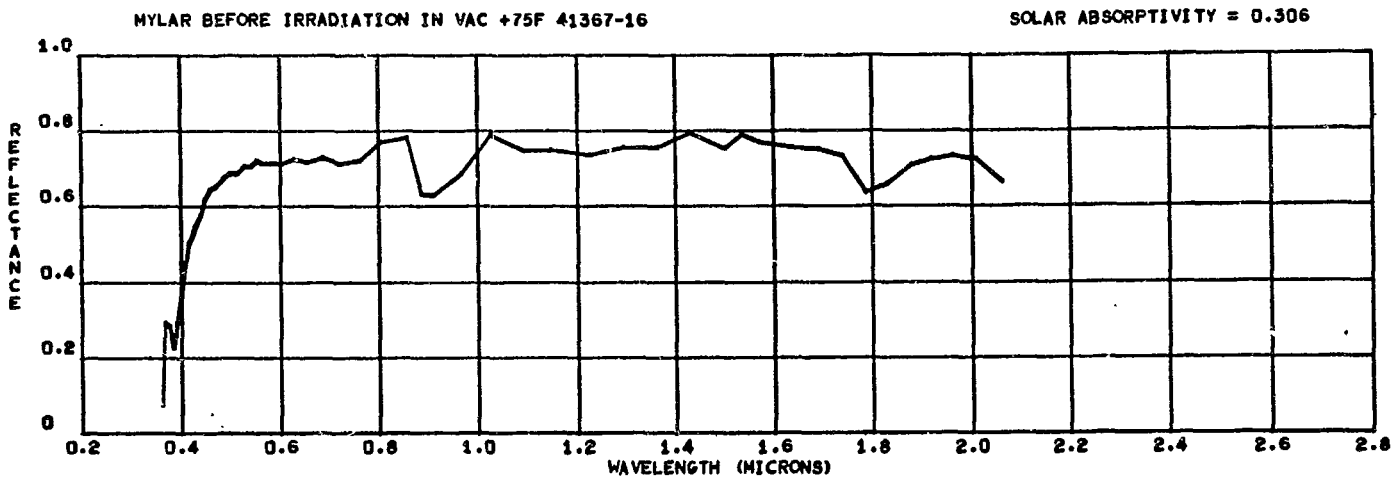
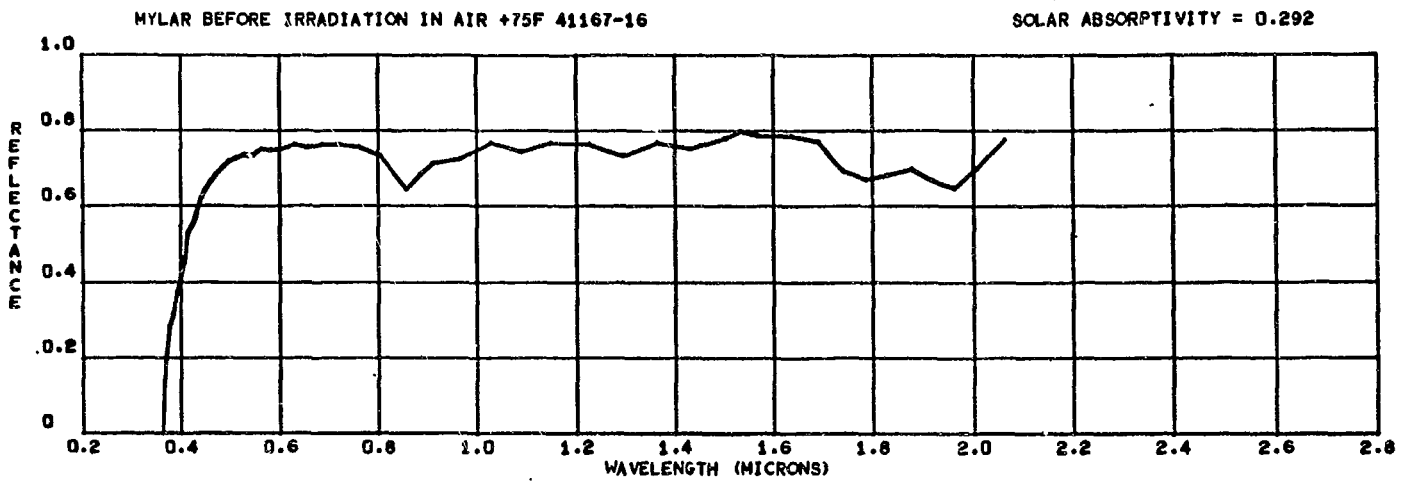


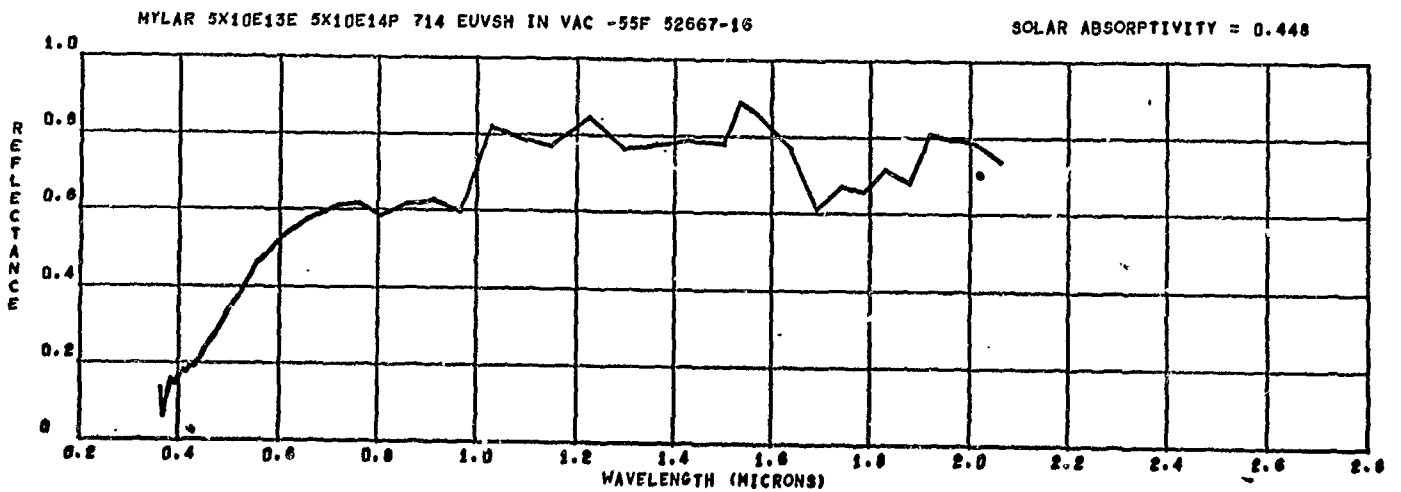
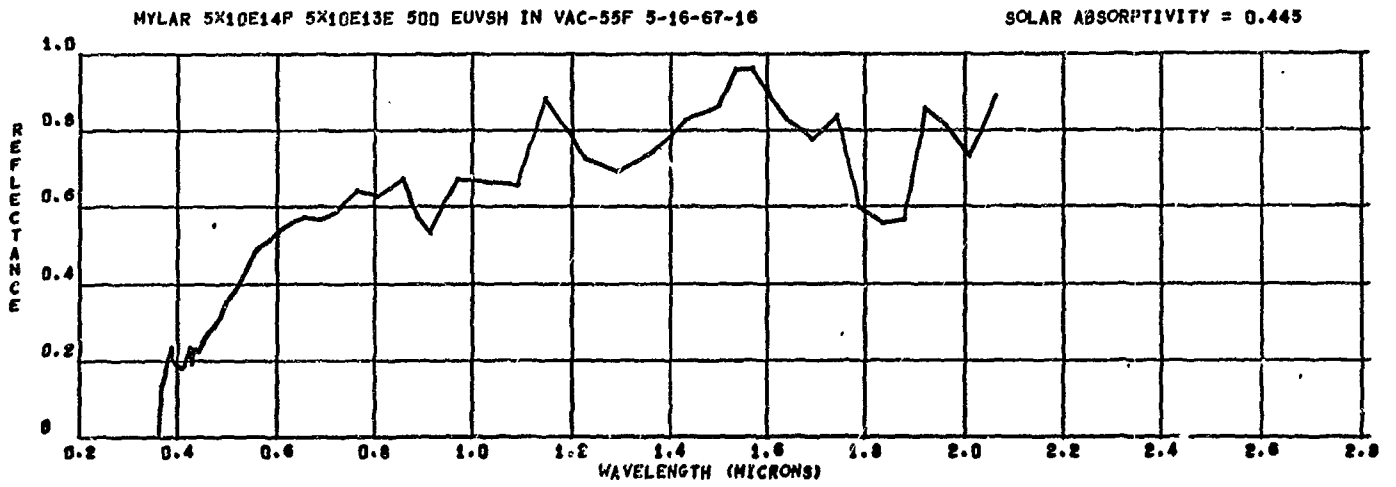
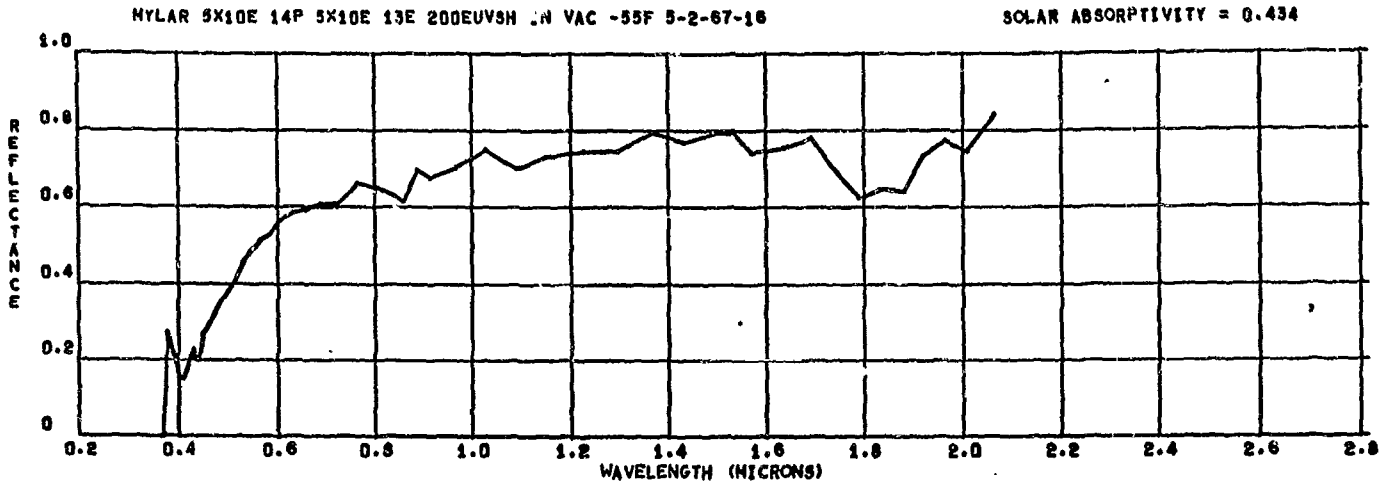


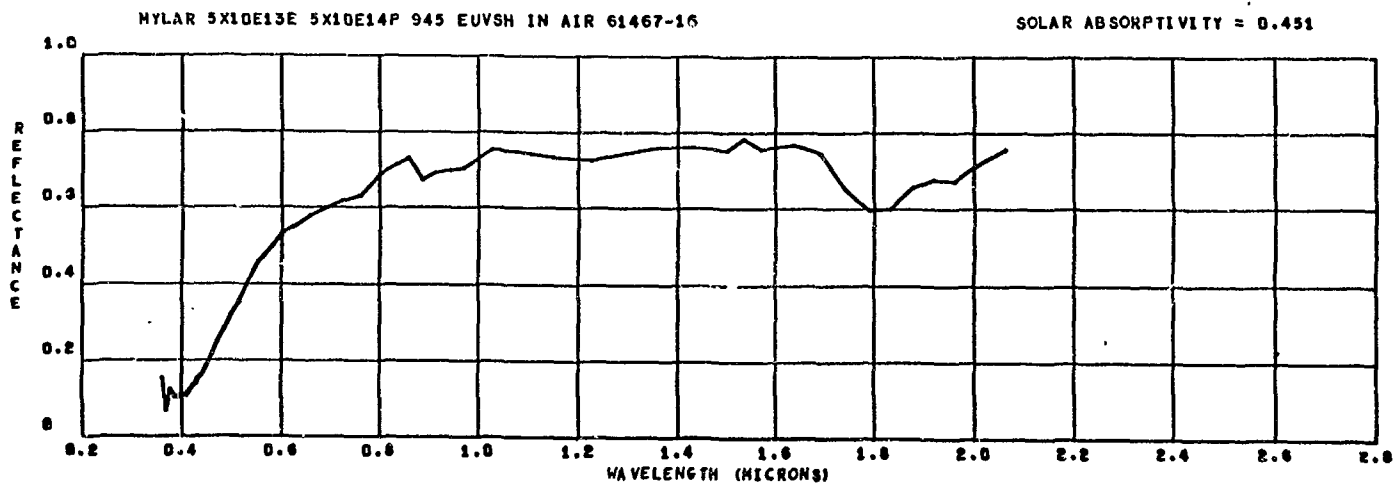
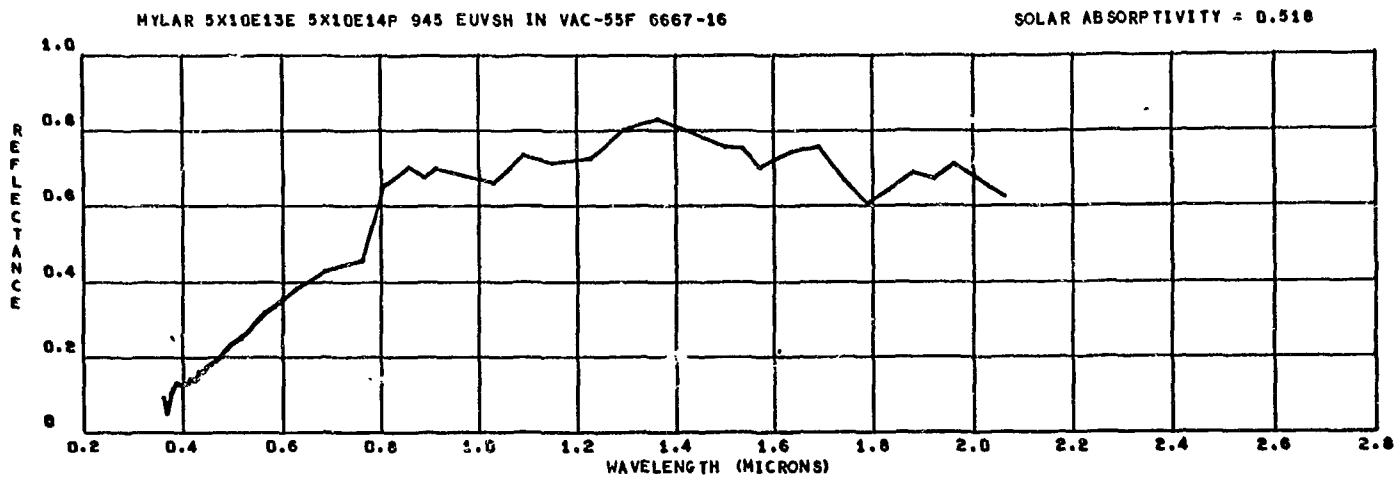
LEXAN (DULL) 5X10E13E 5X10E14P 945 EUVSH IN VAC-55F 6667-18

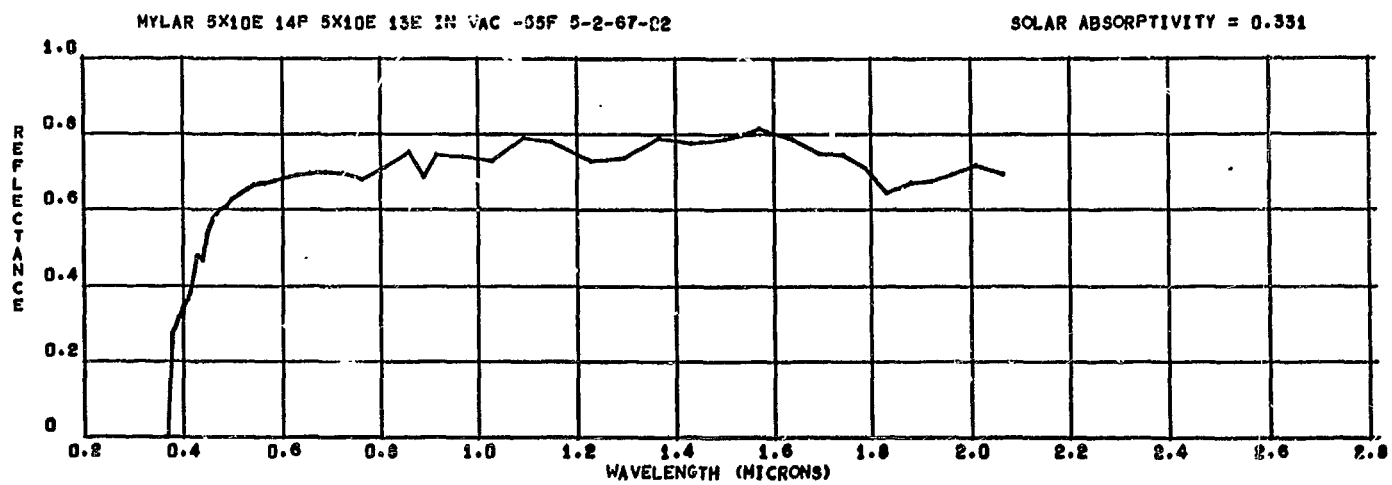
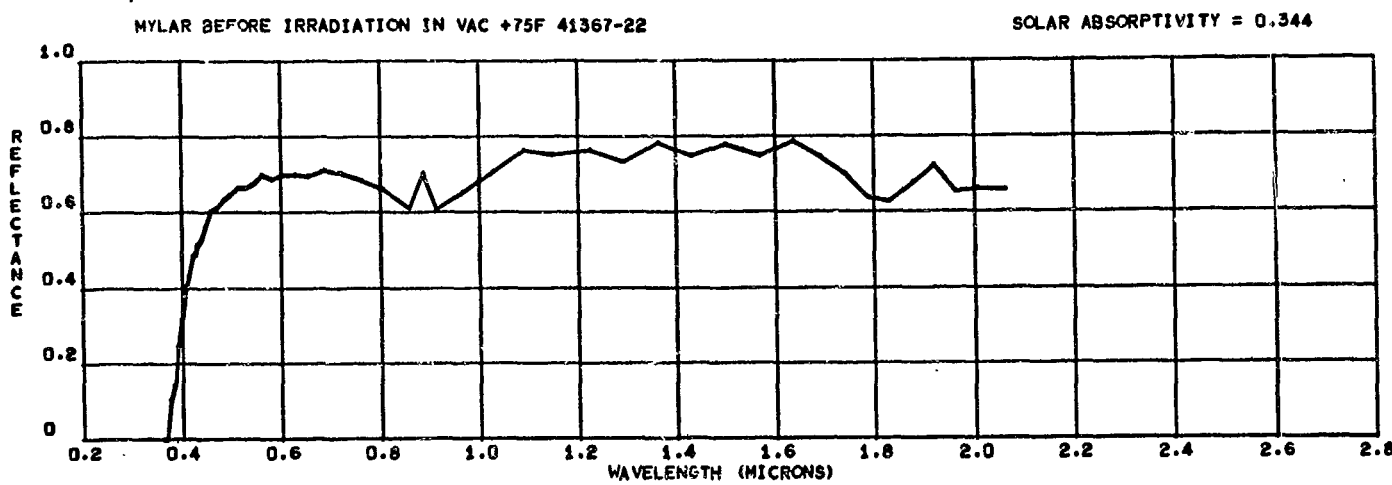
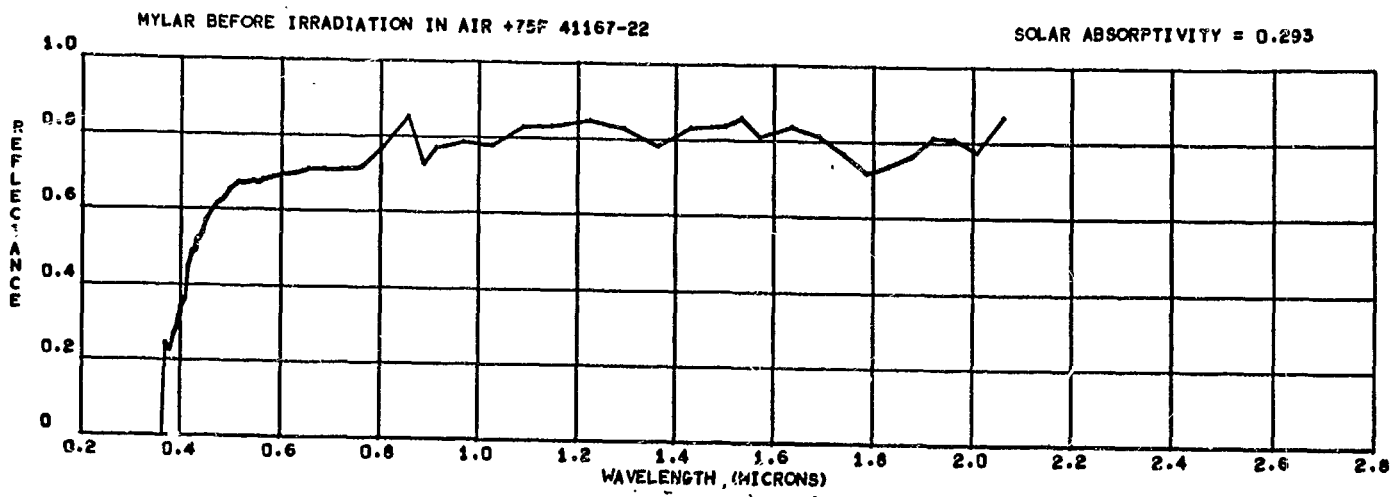
SOLAR ABSORPTIVITY = 0.211

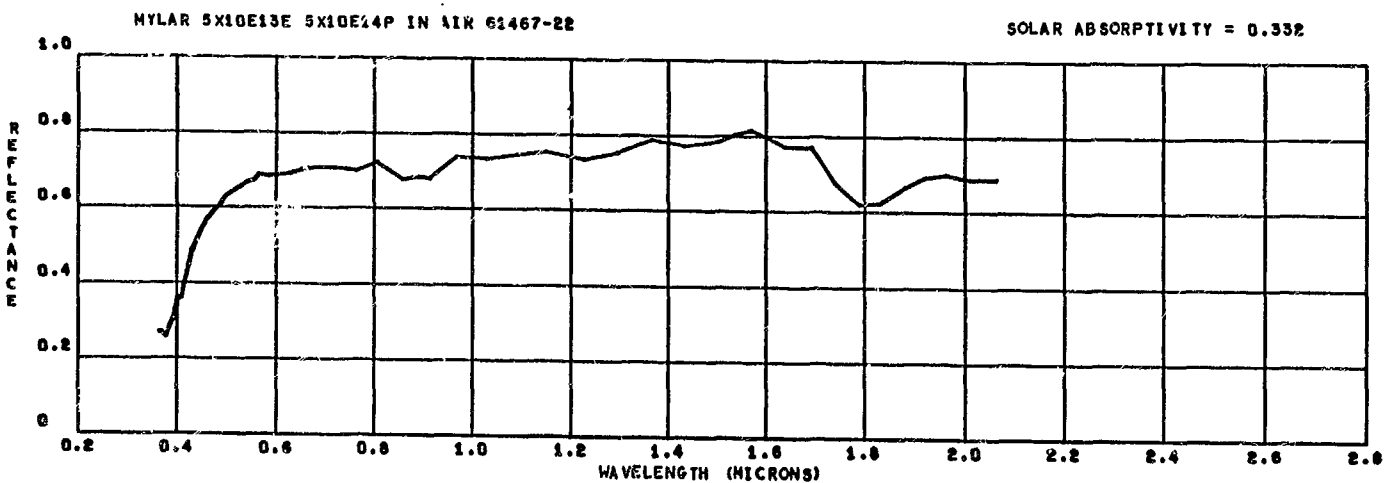
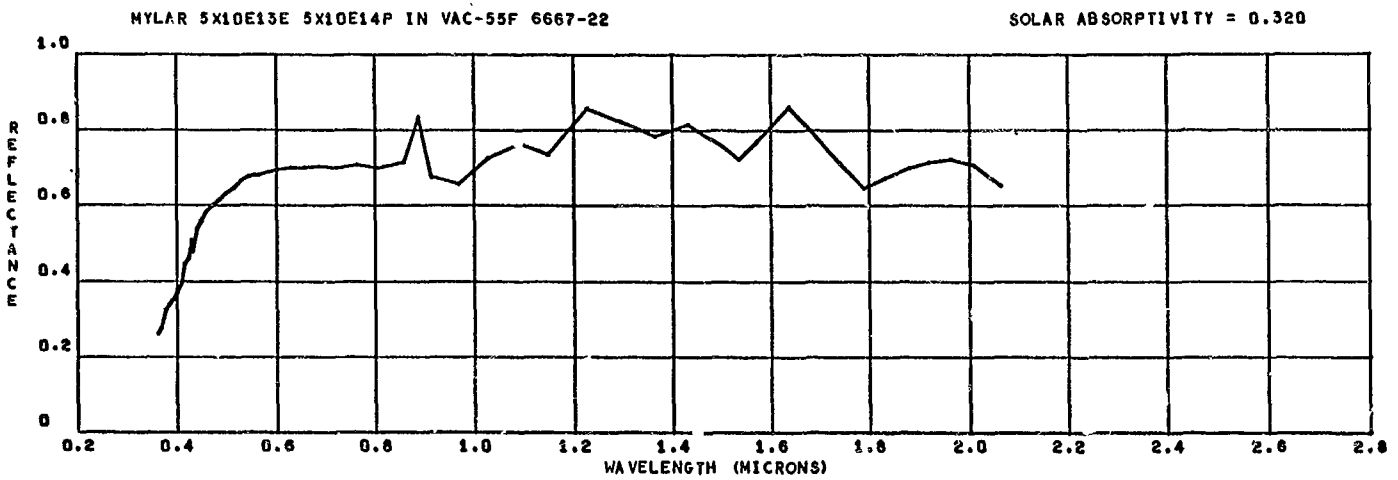
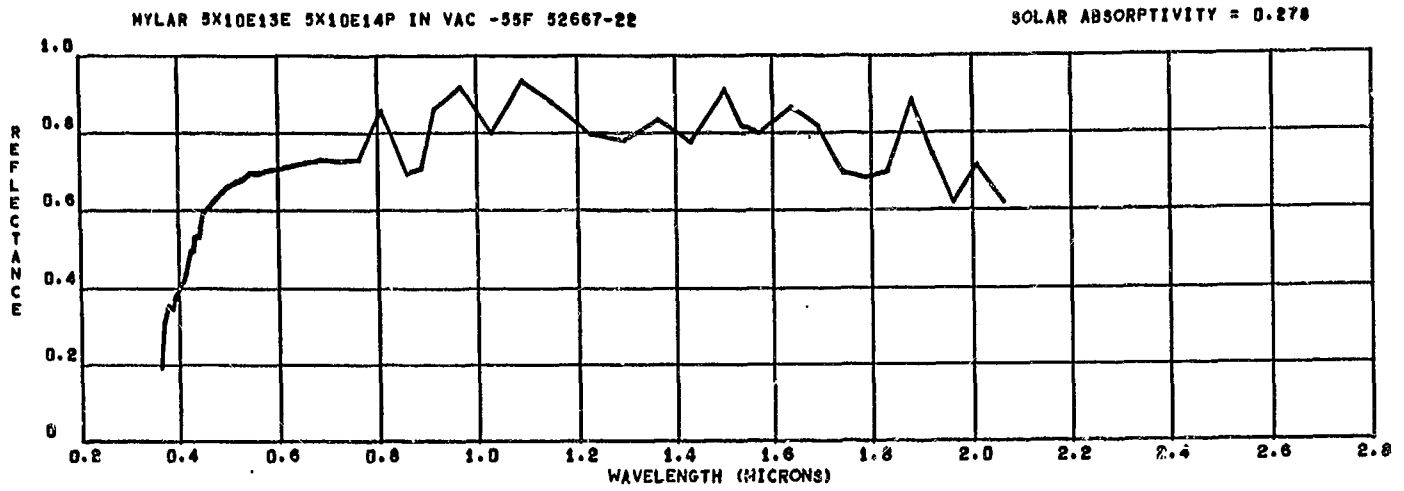






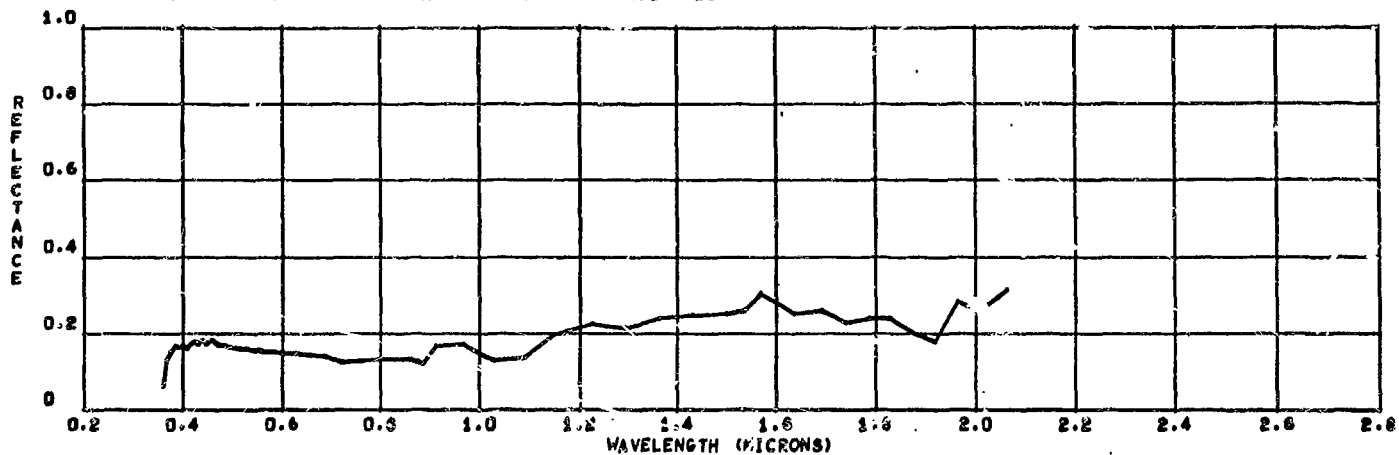






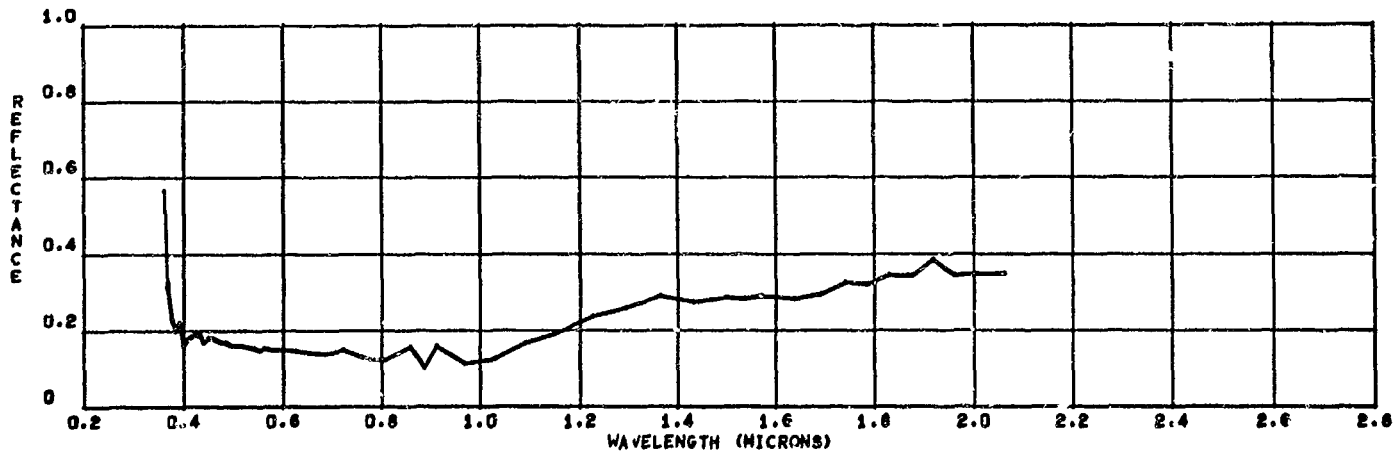
SOLAR CELLS BEFORE IRRADIATION IN AIR +75F 41167-20

SOLAR ABSORPTIVITY = 0.829



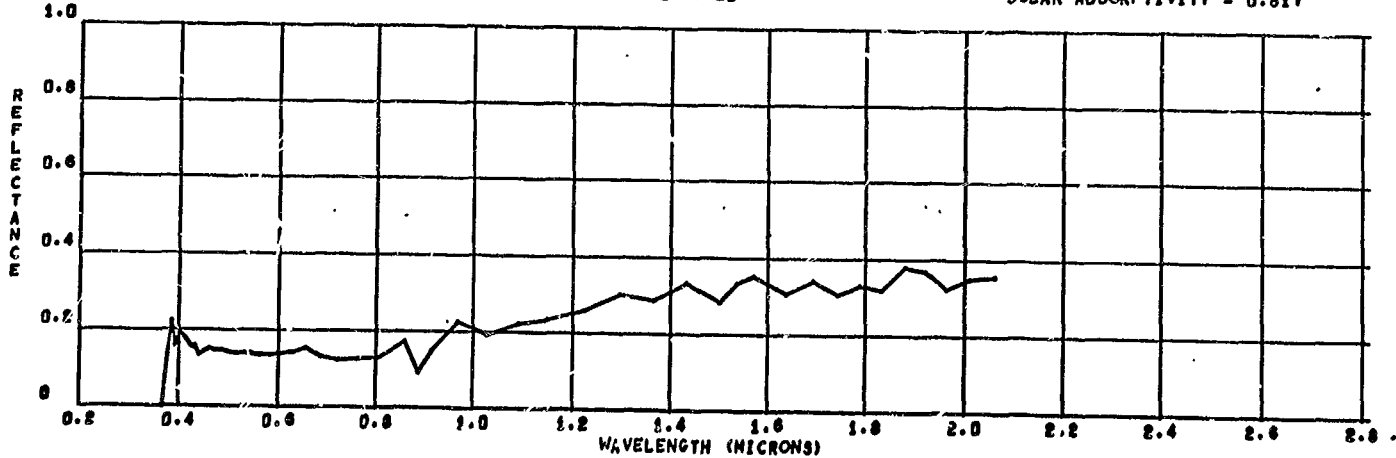
SOLAR CELLS BEFORE IRRADIATION IN VAC +75F 41367-20

SOLAR ABSORPTIVITY = 0.816



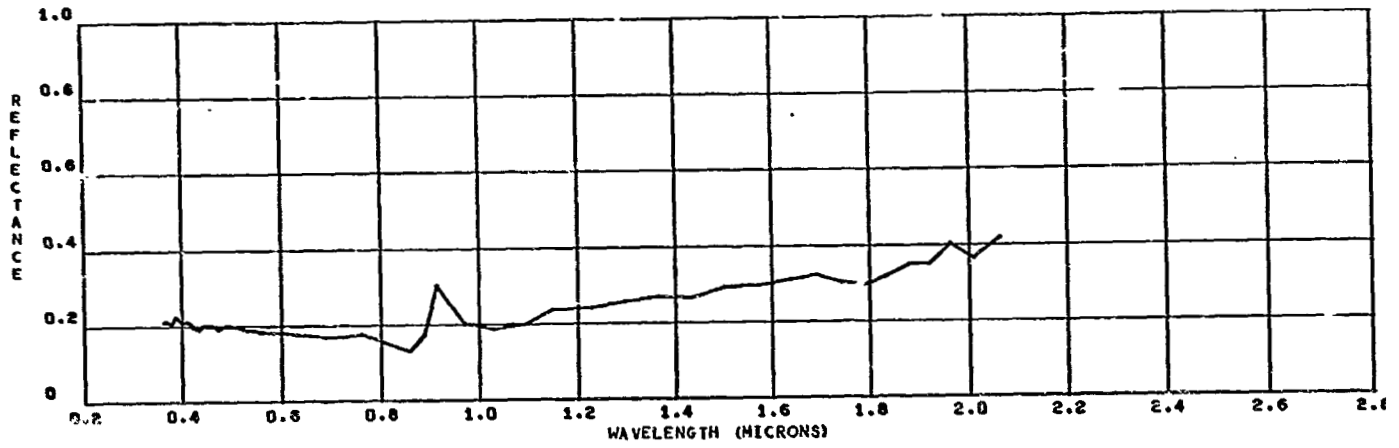
SOLAR CELLS 5X10E 14P 5X10E 13E IN VAC -55F 5-2-67-20

SOLAR ABSORPTIVITY = 0.817



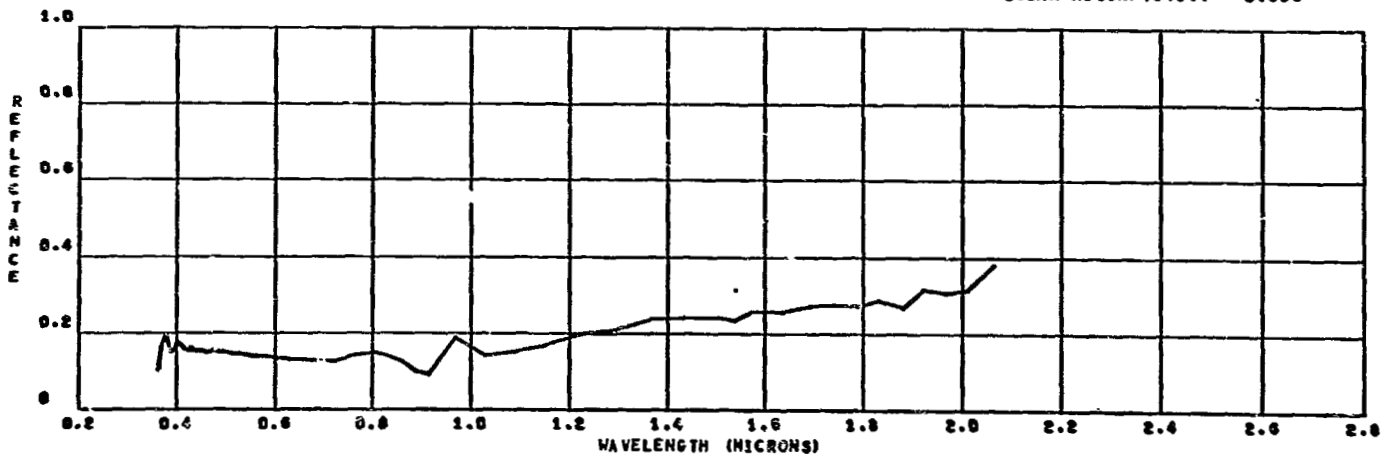
SOLAR CELLS 5X10E13E 5X10E14P IN VAC-55F 6667-20

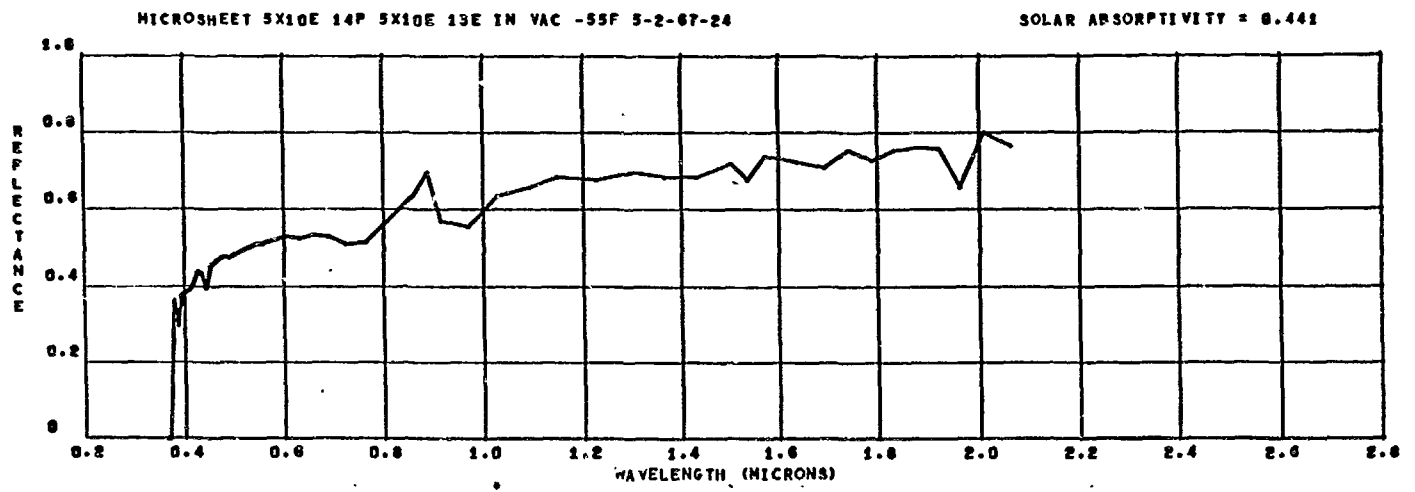
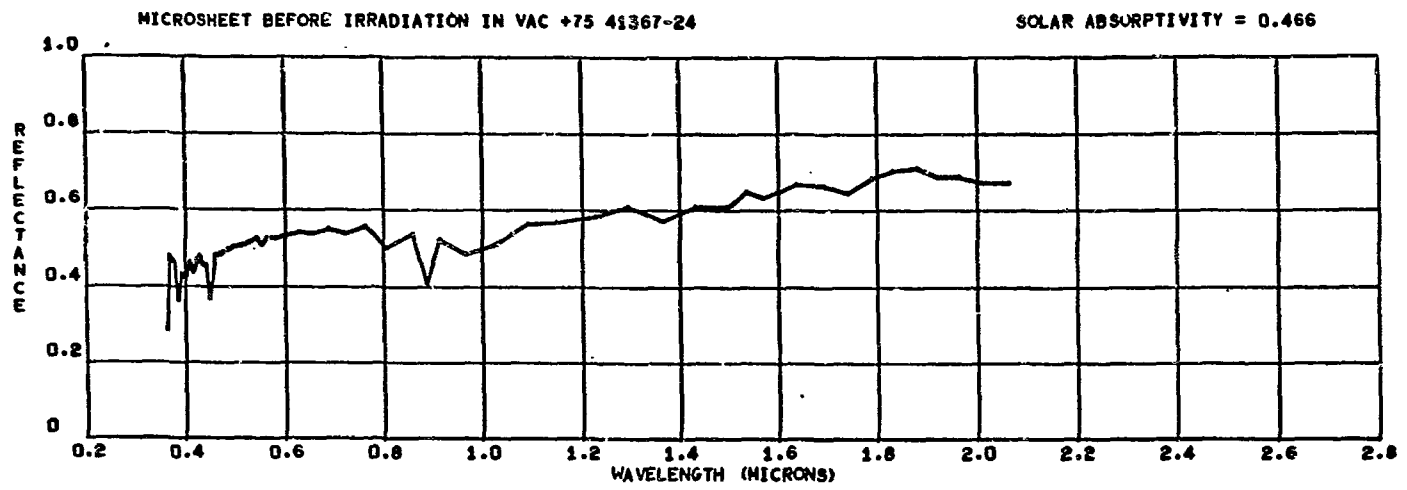
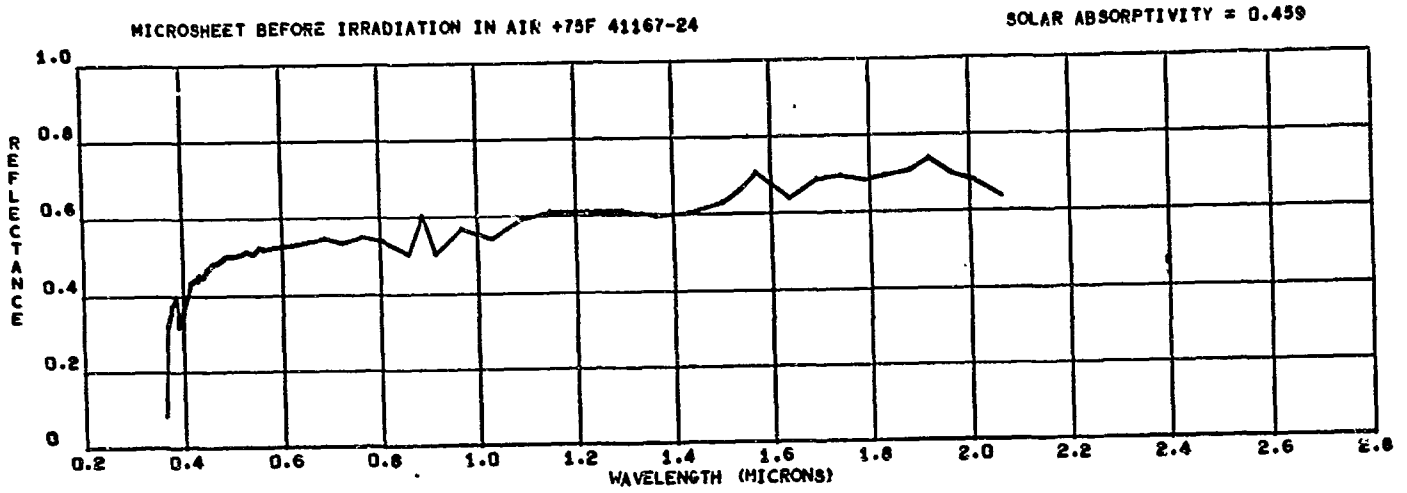
SOLAR ABSORPTIVITY = 0.791



SOLAR CELLS 5X10E13E 5X10E14P IN AIR 61467-20

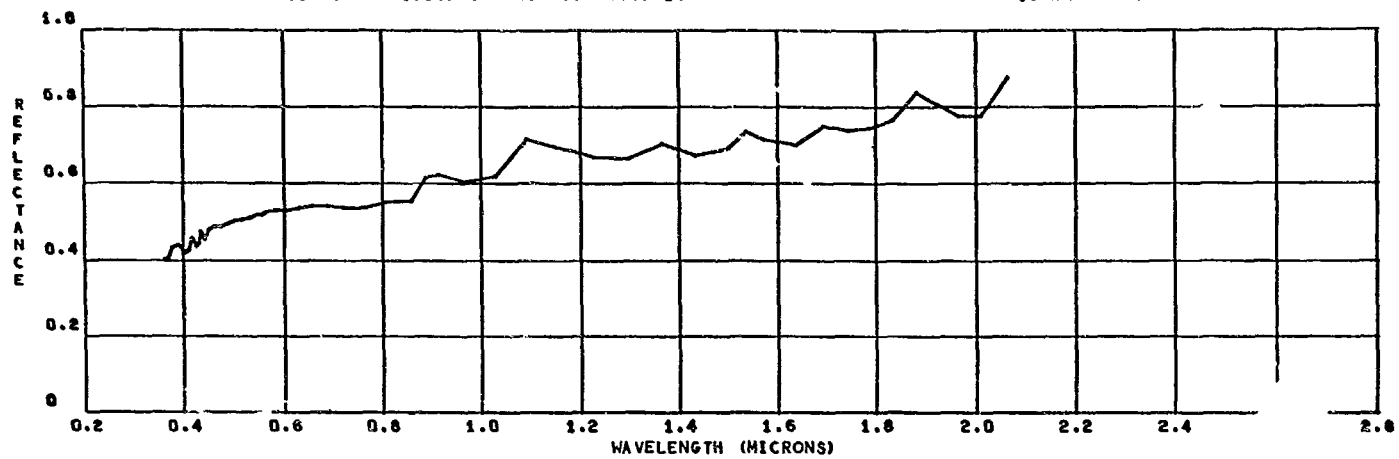
SOLAR ABSORPTIVITY = 0.836





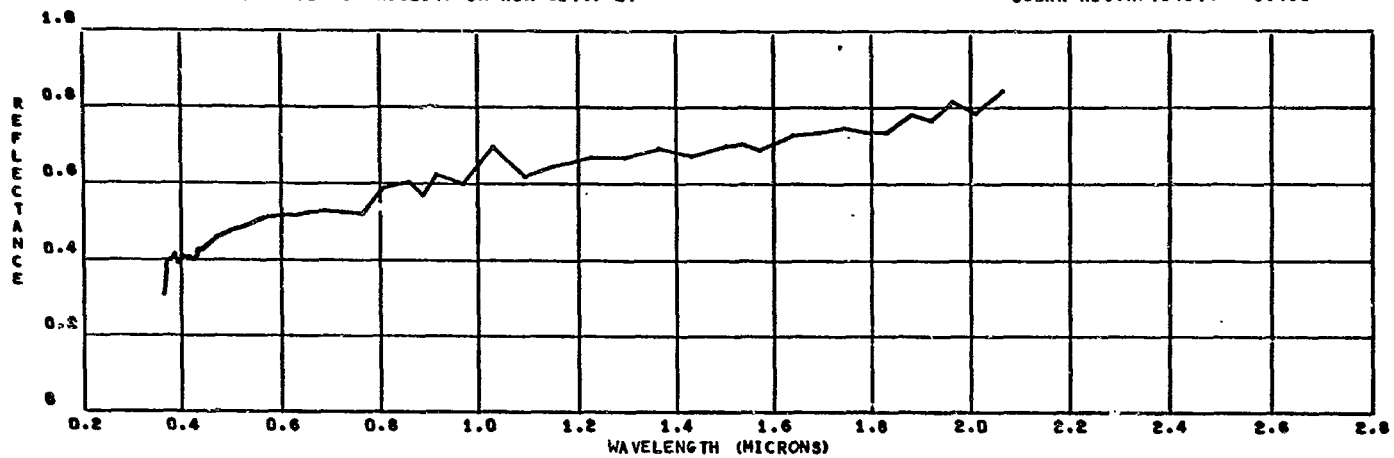
MICROSHEET 5X10E13E 5X10E14P IN VAC -55F 6667-24

SOLAR ABSORPTIVITY = 0.426



MICROSHEET 5X10E13E 5X10E14P IN AIR 61467-24

SOLAR ABSORPTIVITY = 0.436

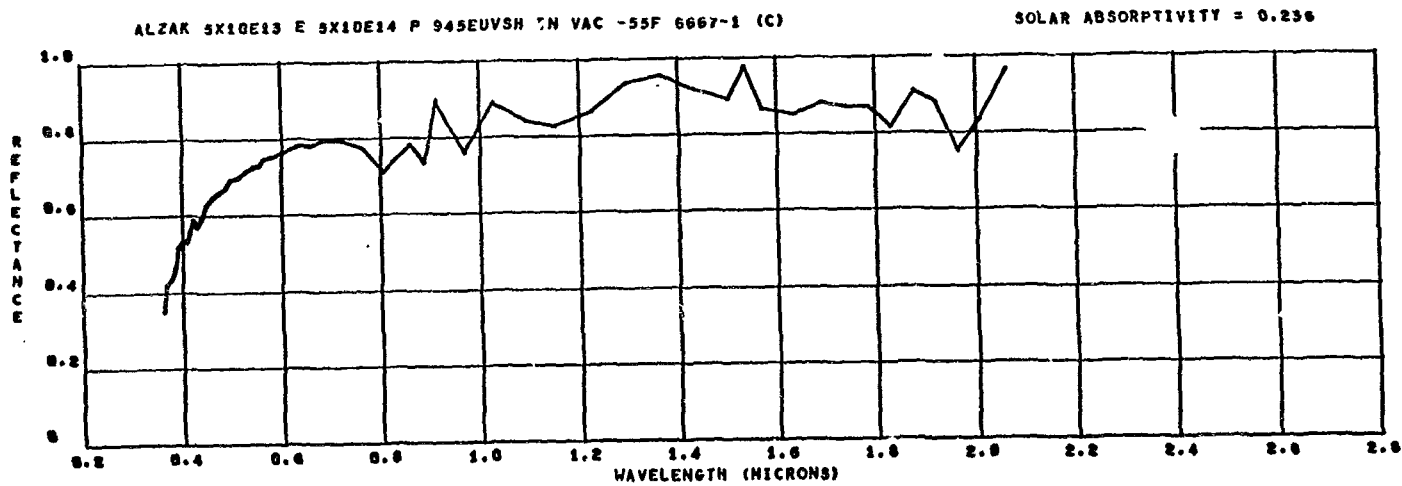
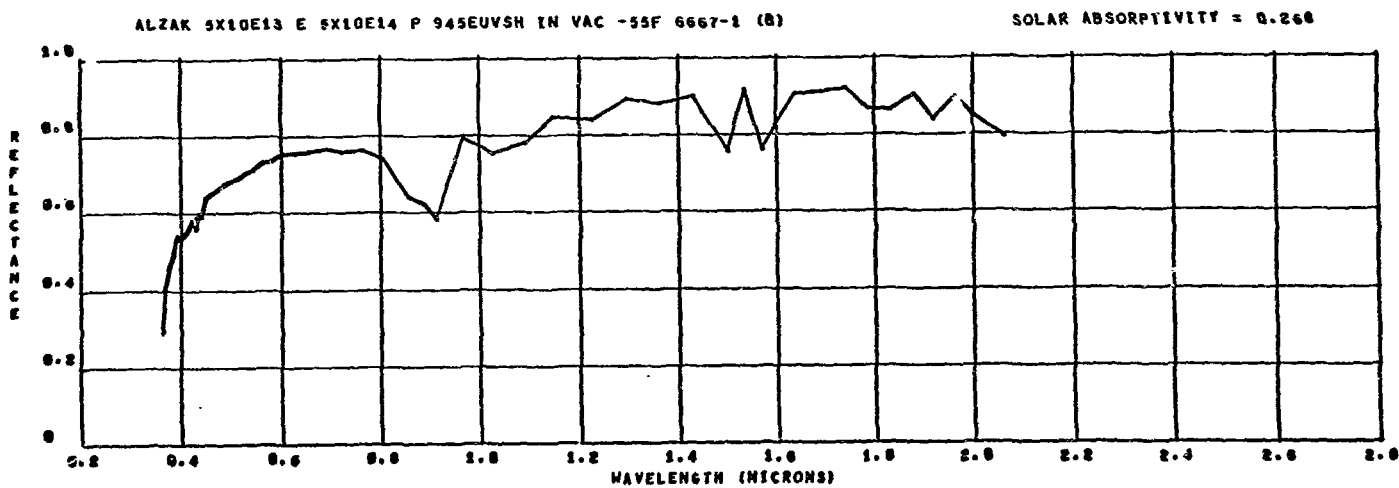
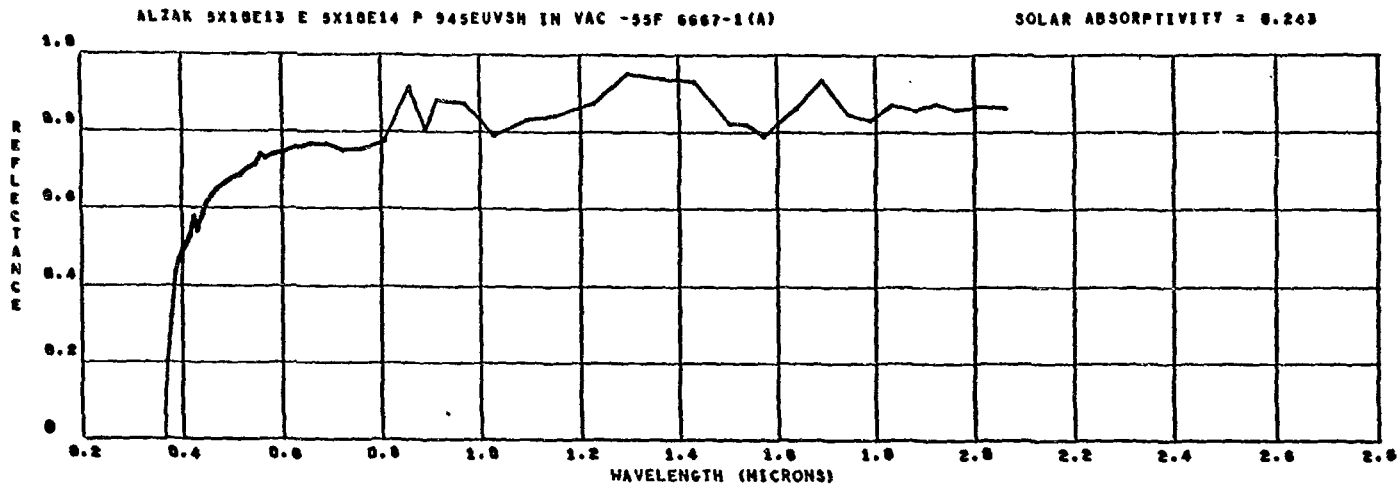


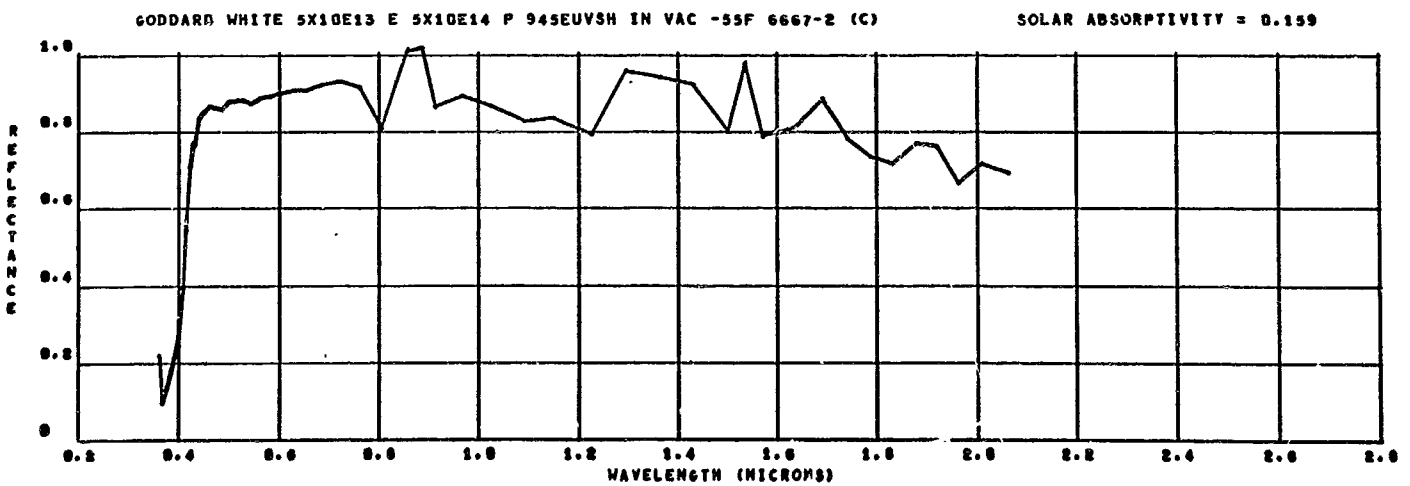
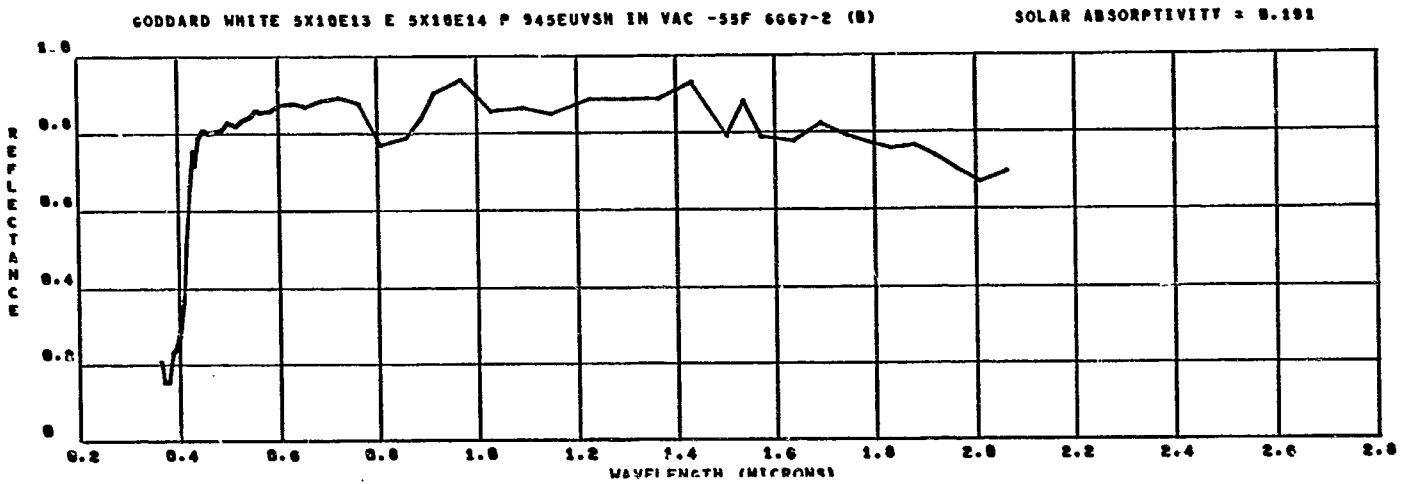
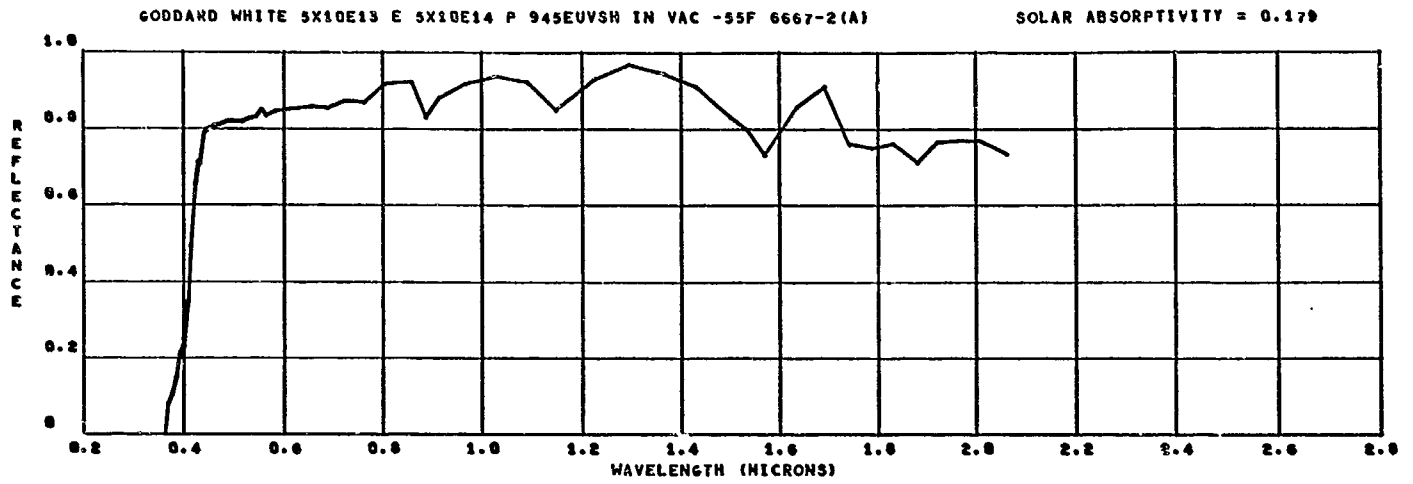
APPENDIX E

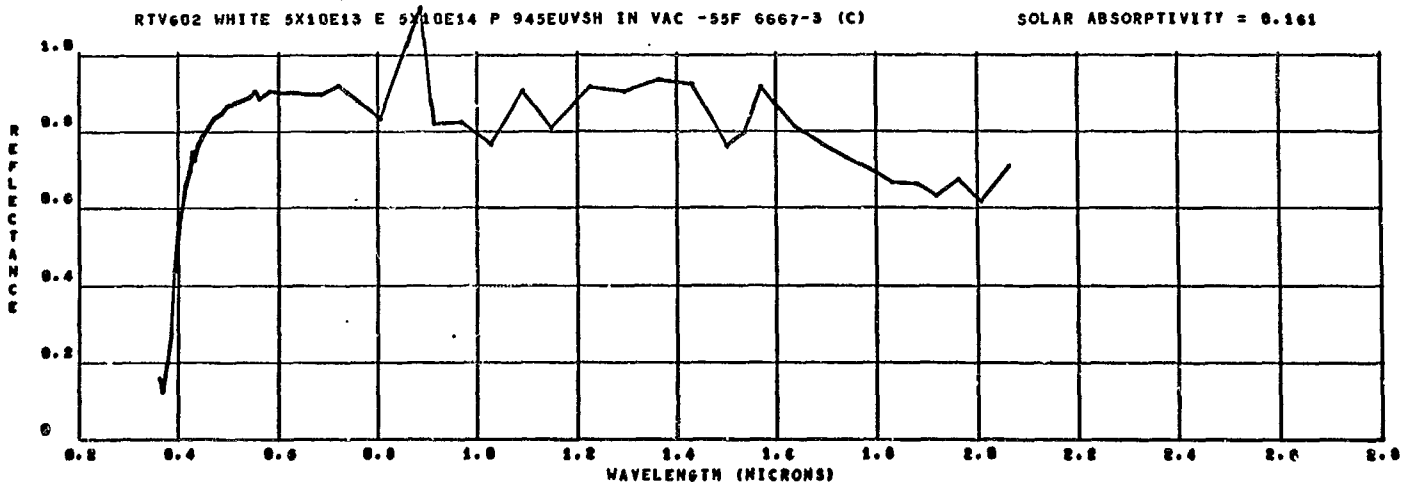
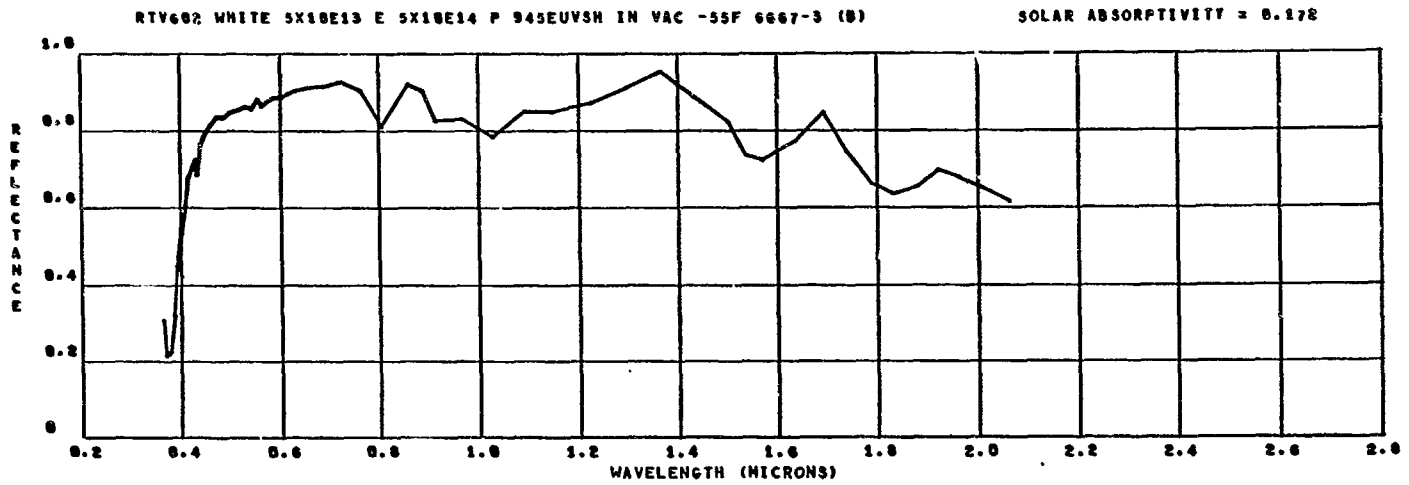
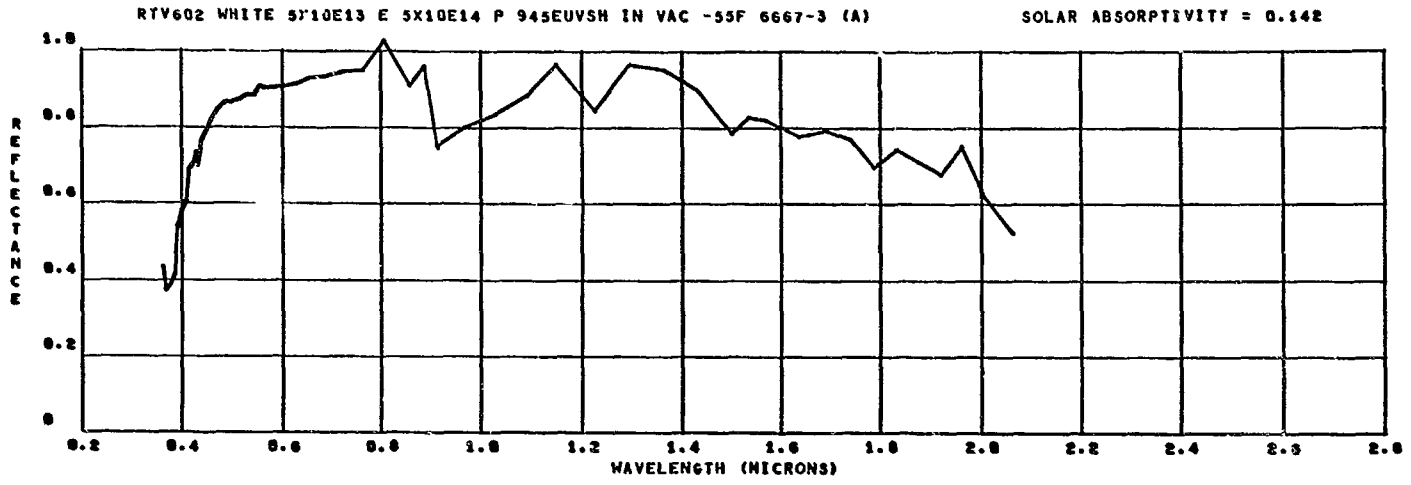
COMPILATION OF SPECTRAL REFLECTANCE CURVES OF EACH SINGLE SCAN MEASUREMENT FROM THE 945 EUVSH DATA (IN AIR AND VACUUM)

This appendix lists the single scan spectral reflectance curves obtained after 945 EUVSH in air and vacuum. The point by point average of these was used to obtain the corresponding curves presented in Appendix D. The same nomenclature as described for the spectral reflectance curves in Appendix D is applicable to those presented in this appendix.

The three curves for each single scan of each sample are all on the same page. The curves are in numerical order according to specimen number, with the in vacuum set first (starting on page E-2) and the in air set next (starting on page E-31). The randomness of the curves above 0.7 micron is due to the low signal to noise ratio obtained with the lead sulfide cell. The average of three measurements did help this problem, as can be seen by comparing corresponding curves in Appendices D and E. This problem has now been solved, as described in Appendix C, without the need for triplicate measurements. An example of the spectral reflectance curves now being obtained is given in Figure C-2.

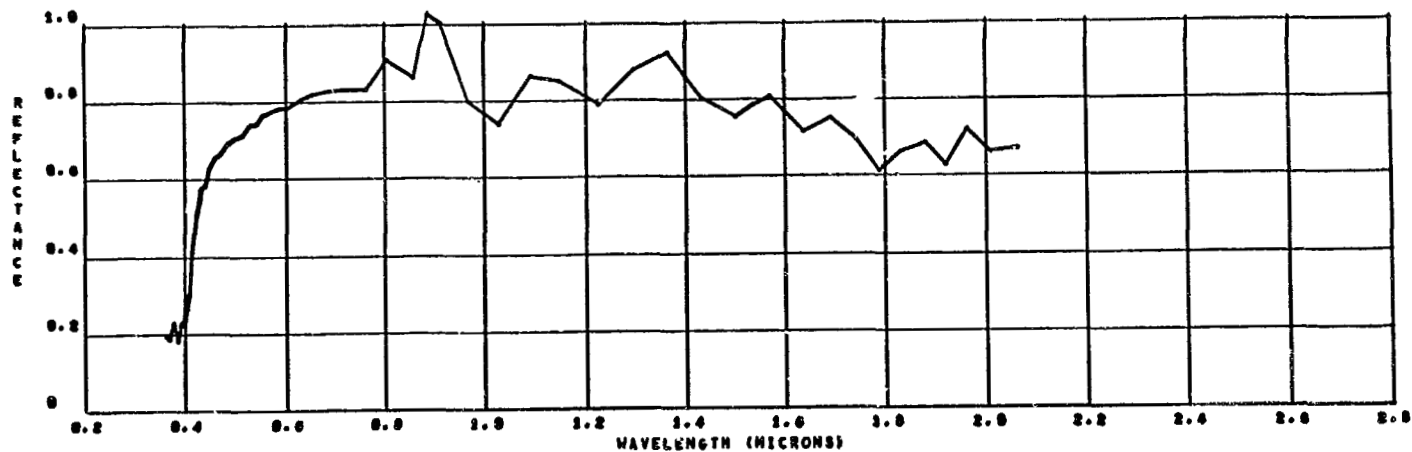






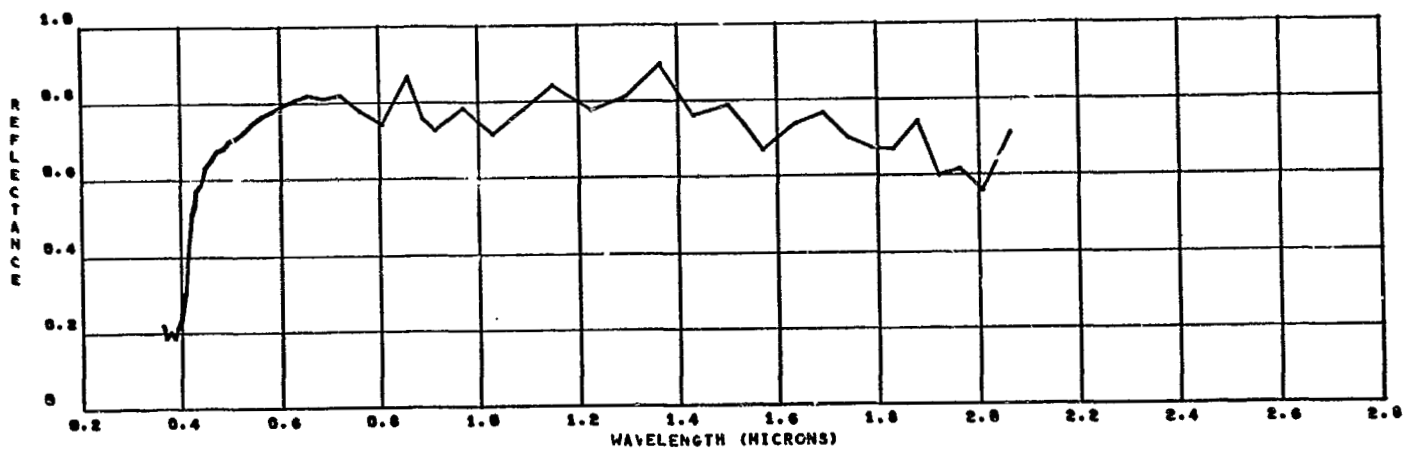
PYROMARK WHITE 5X10E13 E 5X10E14 P 945EUVSH IN VAC -55F 6667-4 (A)

SOLAR ABSORPTIVITY = 0.245



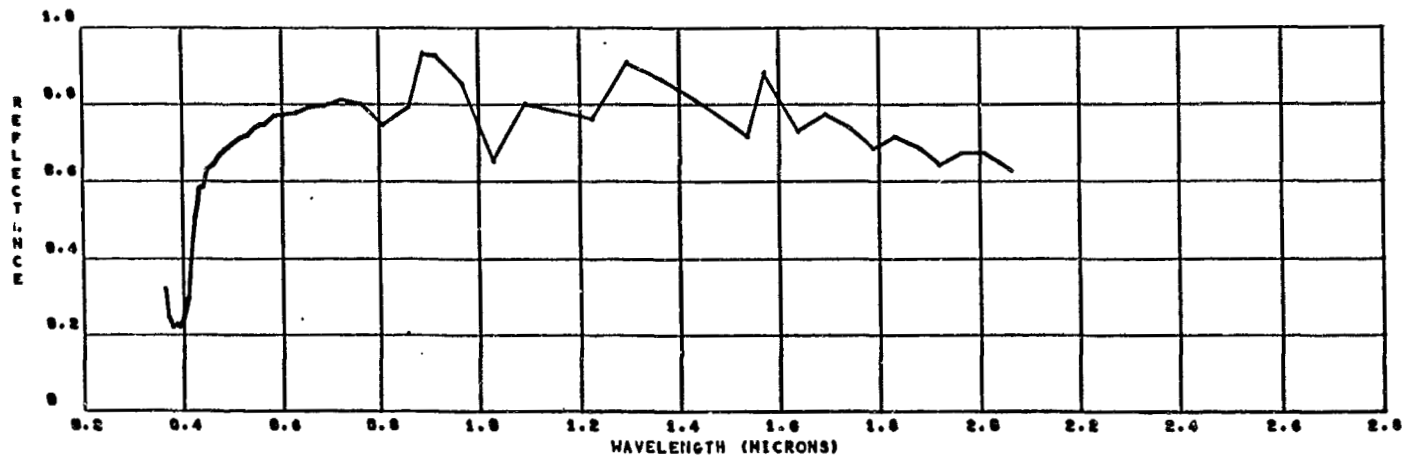
PYROMARK WHITE 5X10E13 E 5X10E14 P 945EUVSH IN VAC -55F 6667-4 (B)

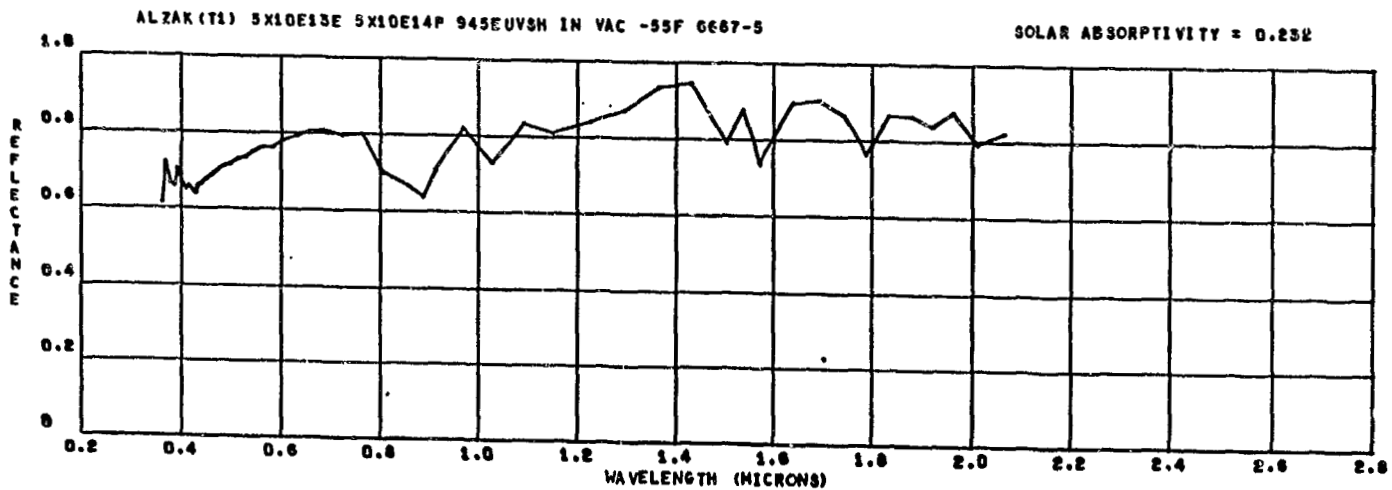
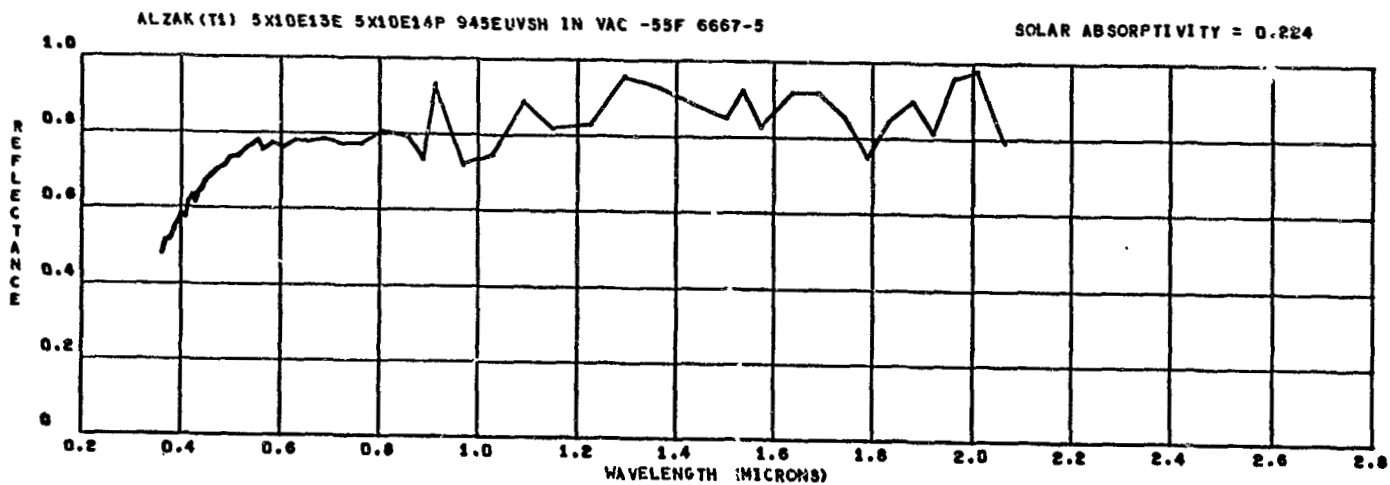
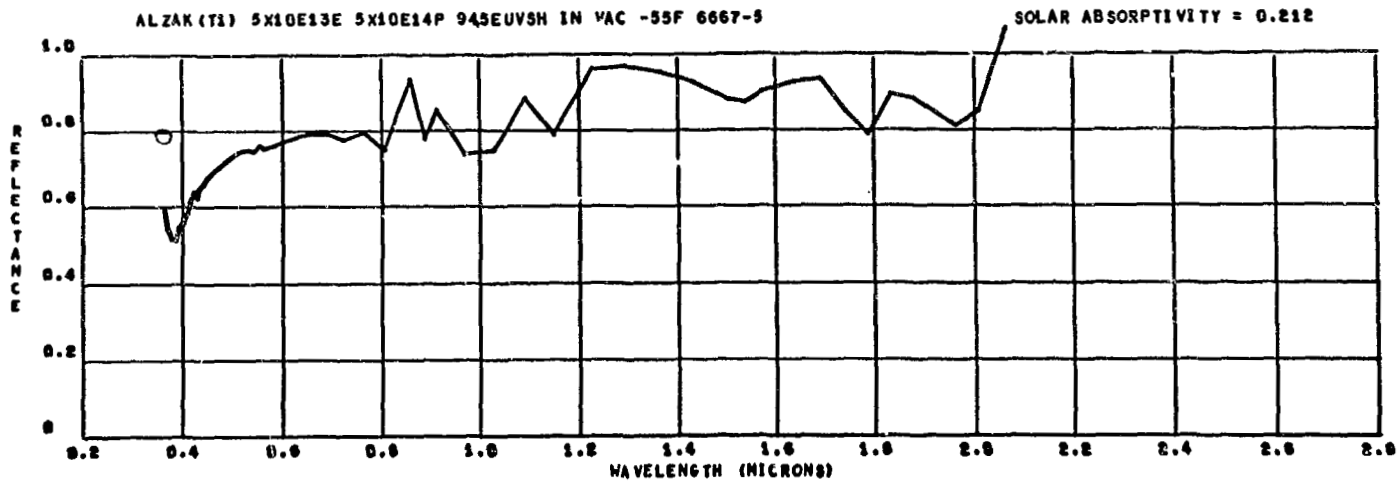
SOLAR ABSORPTIVITY = 0.274

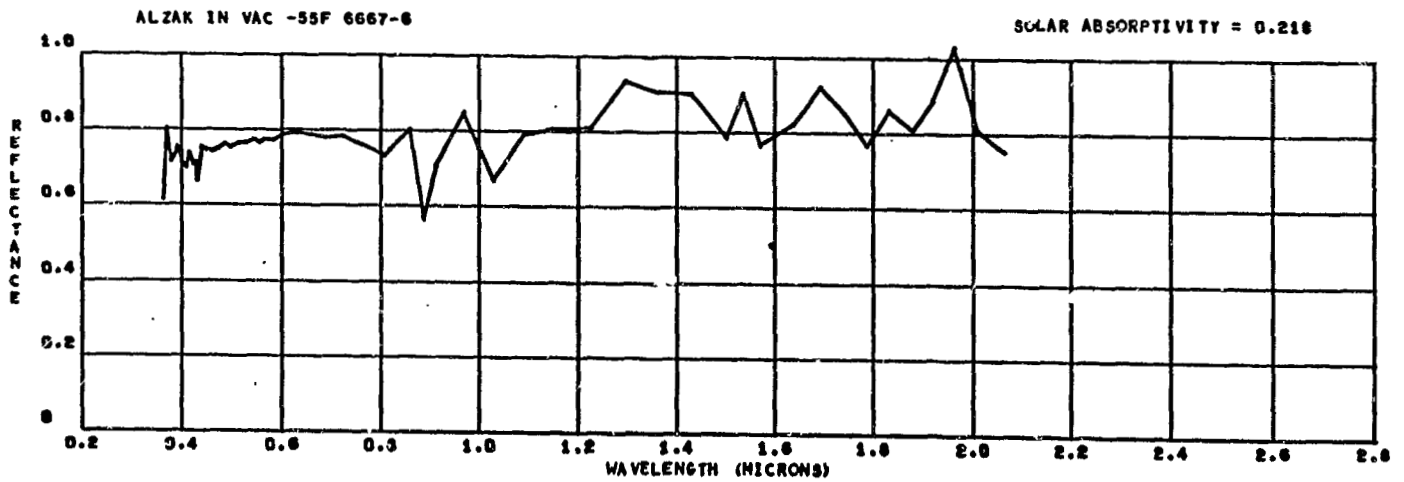
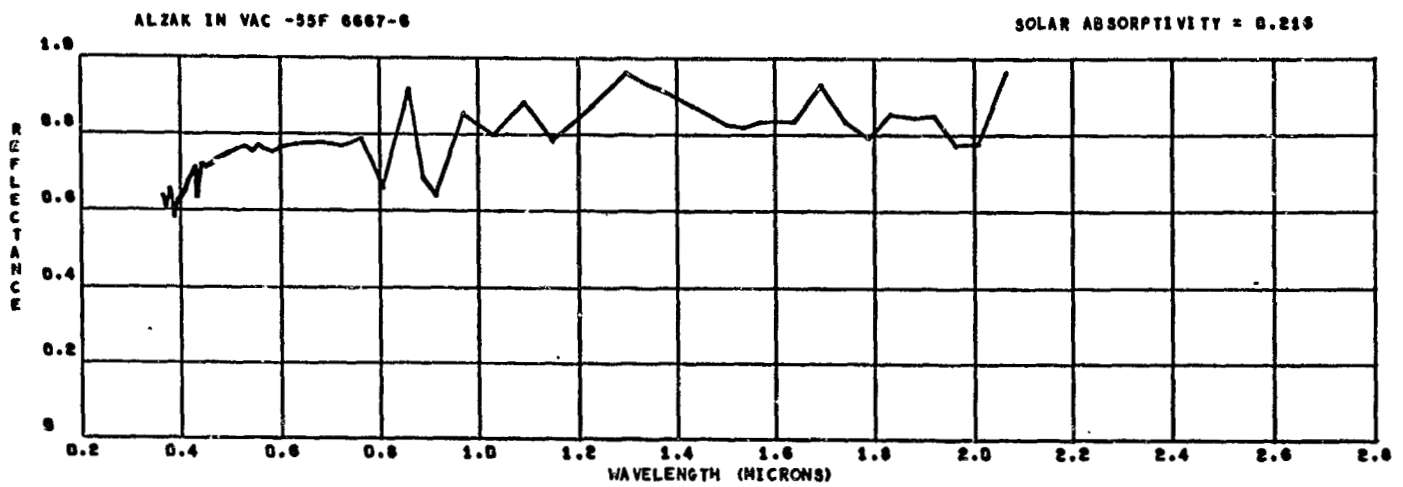
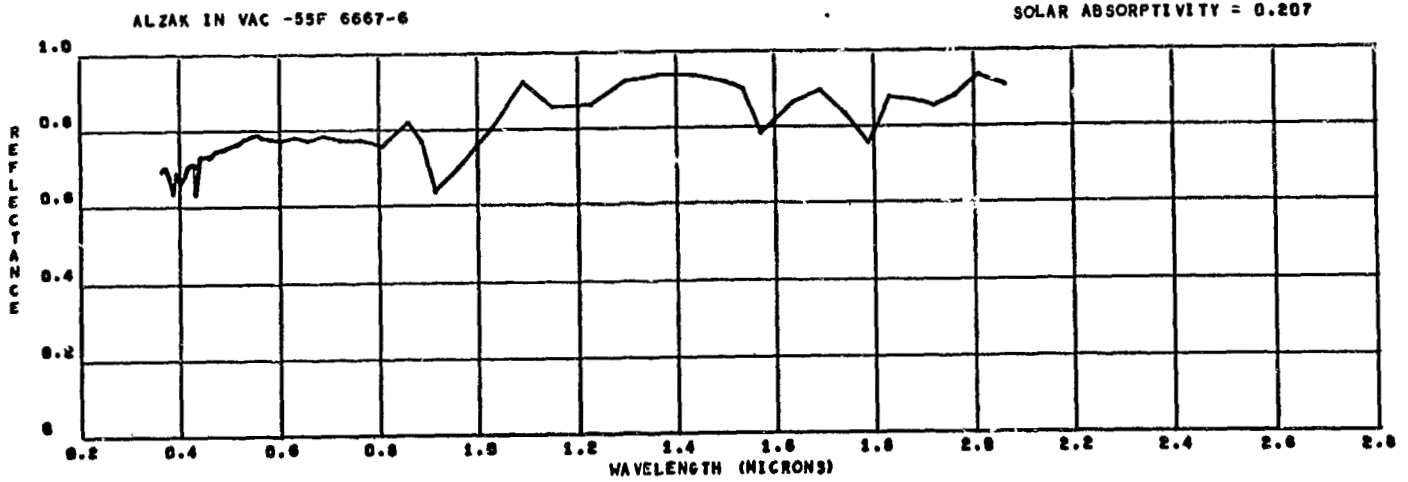


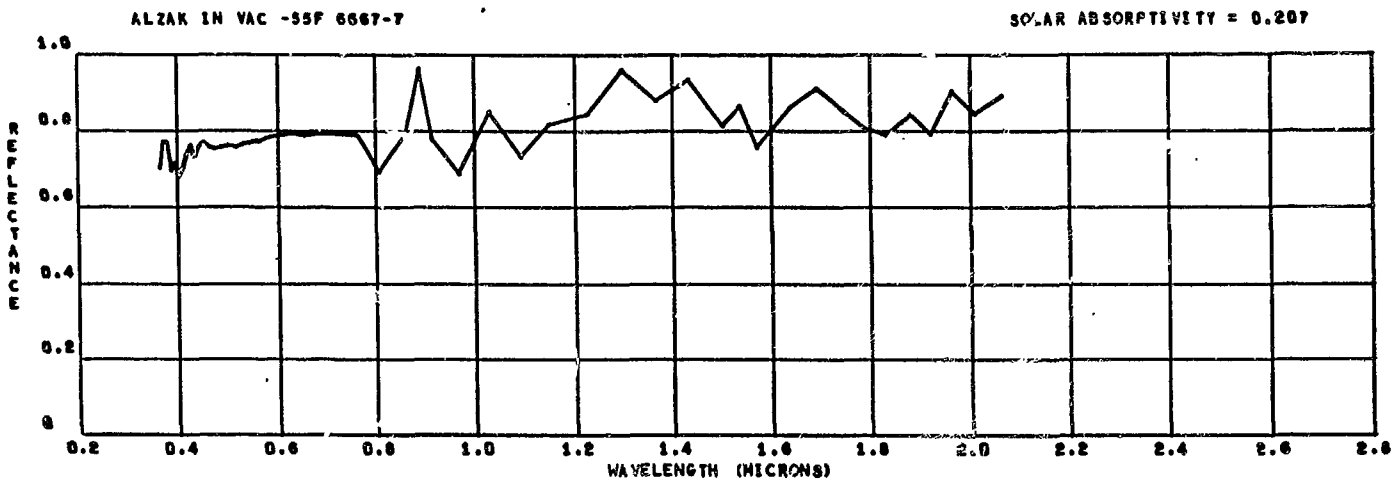
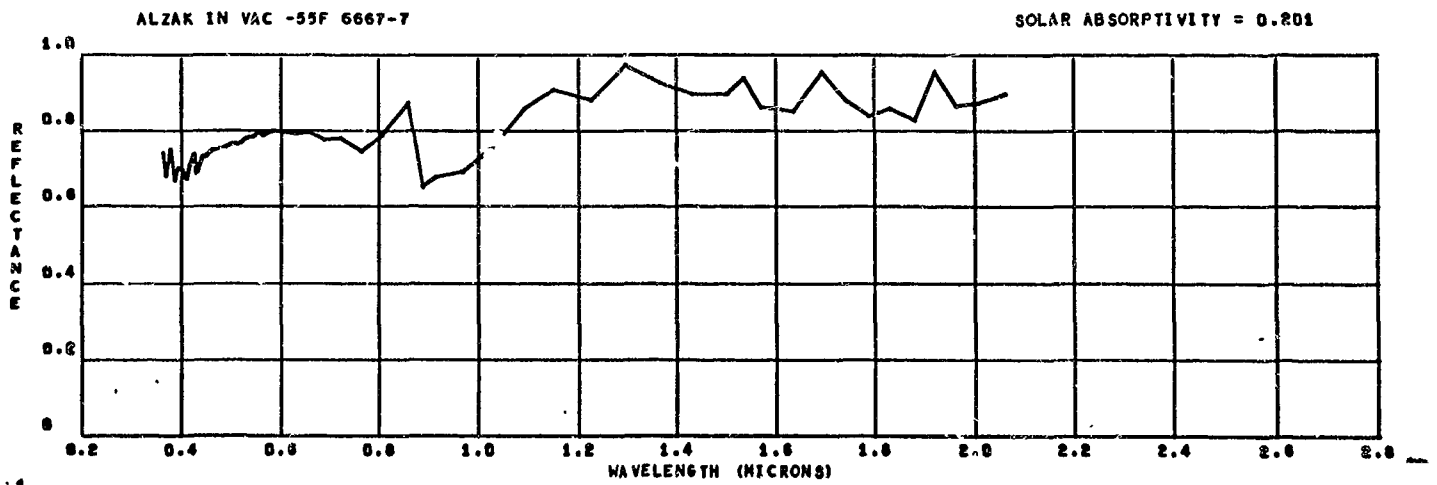
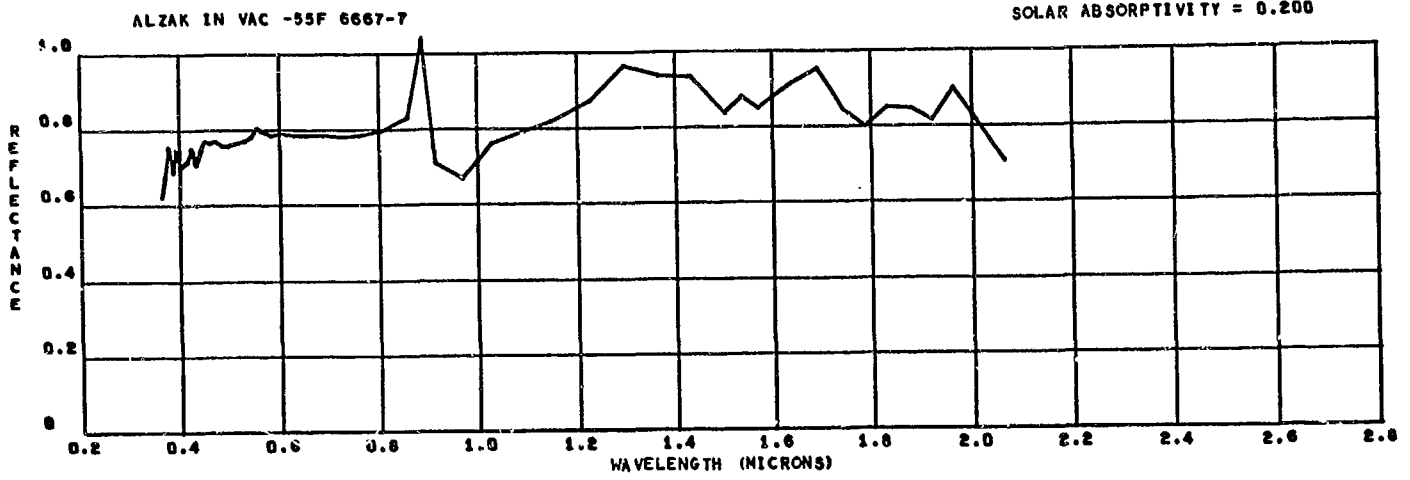
PYROMARK WHITE 5X10E13 E 5X10E14 P 945EUVSH IN VAC -55F 6667-4 (C)

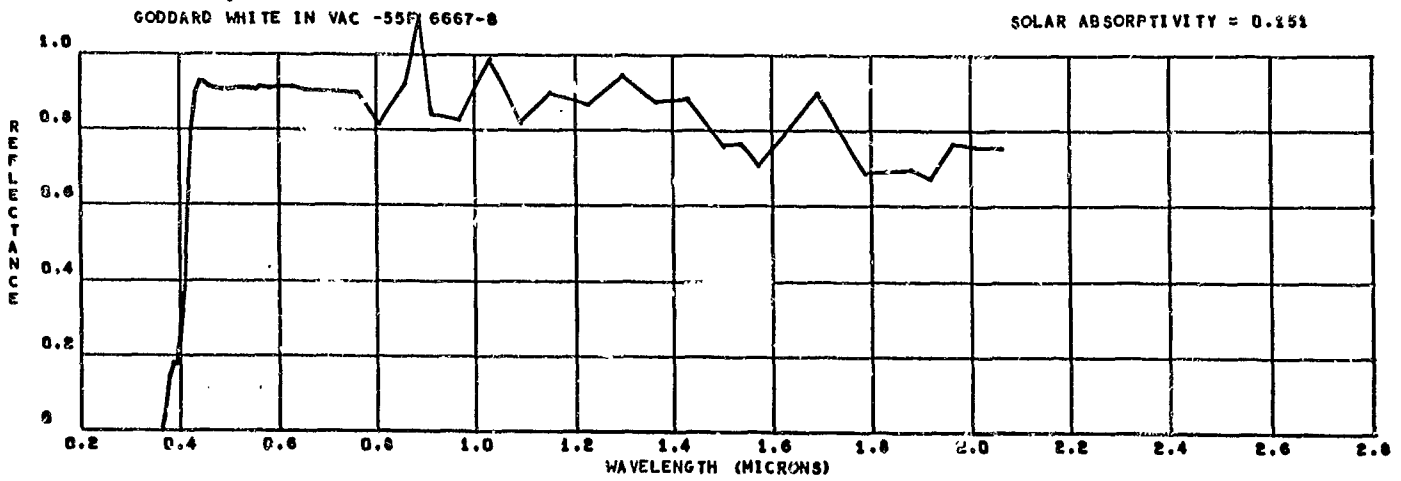
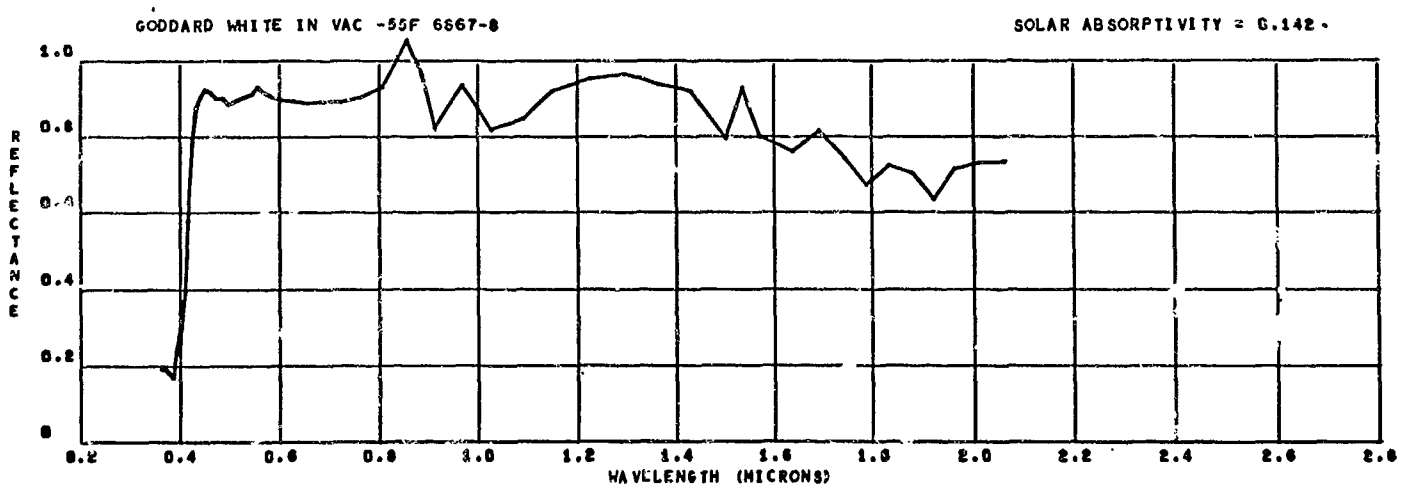
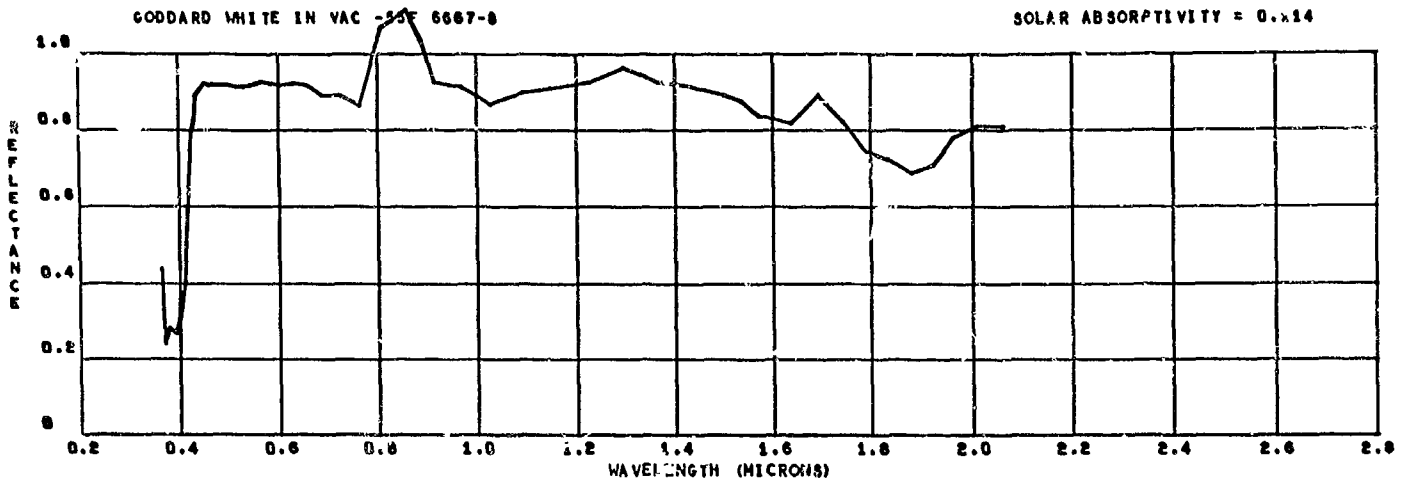
SOLAR ABSORPTIVITY = 0.260

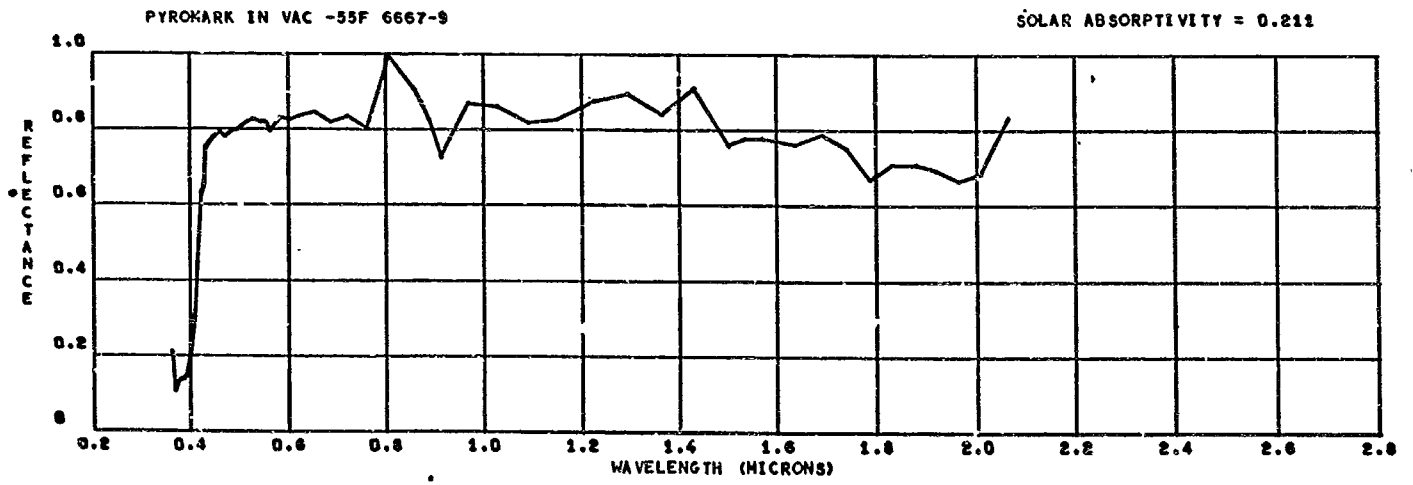
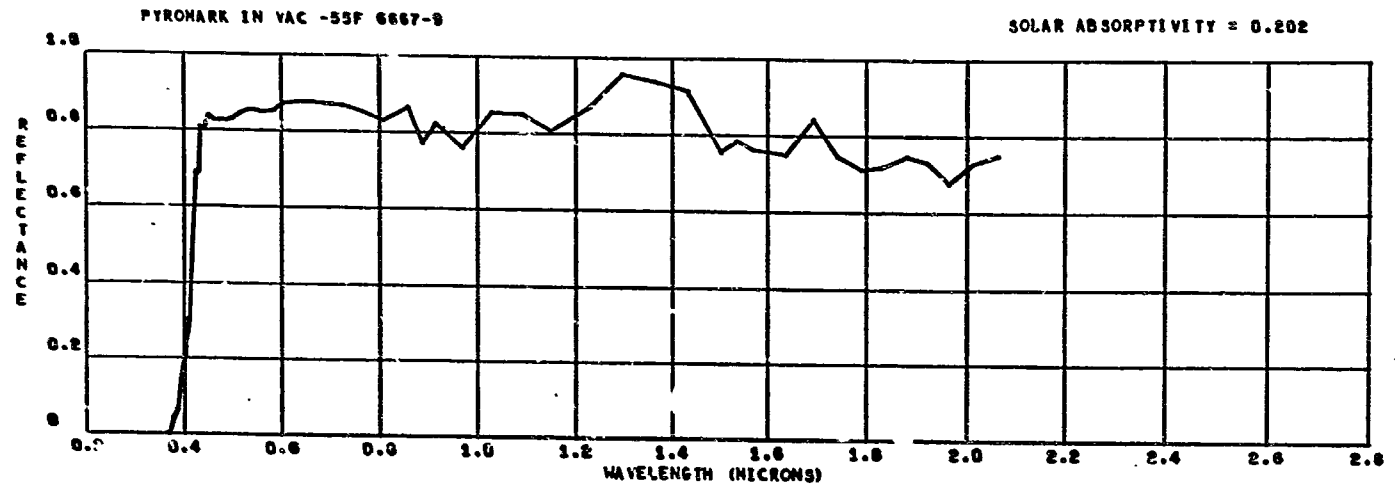
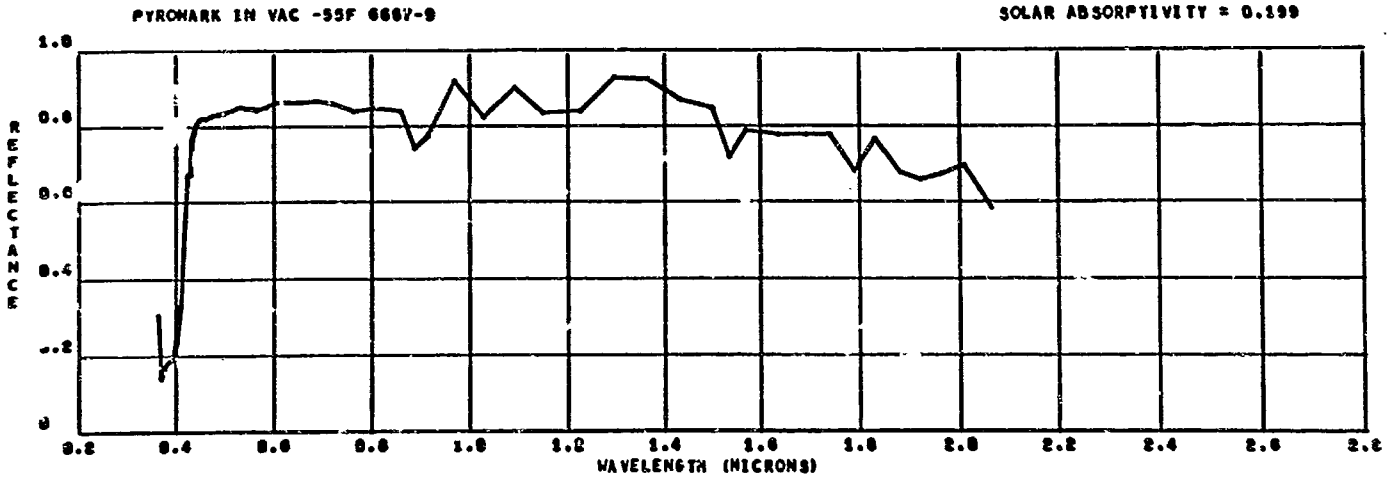


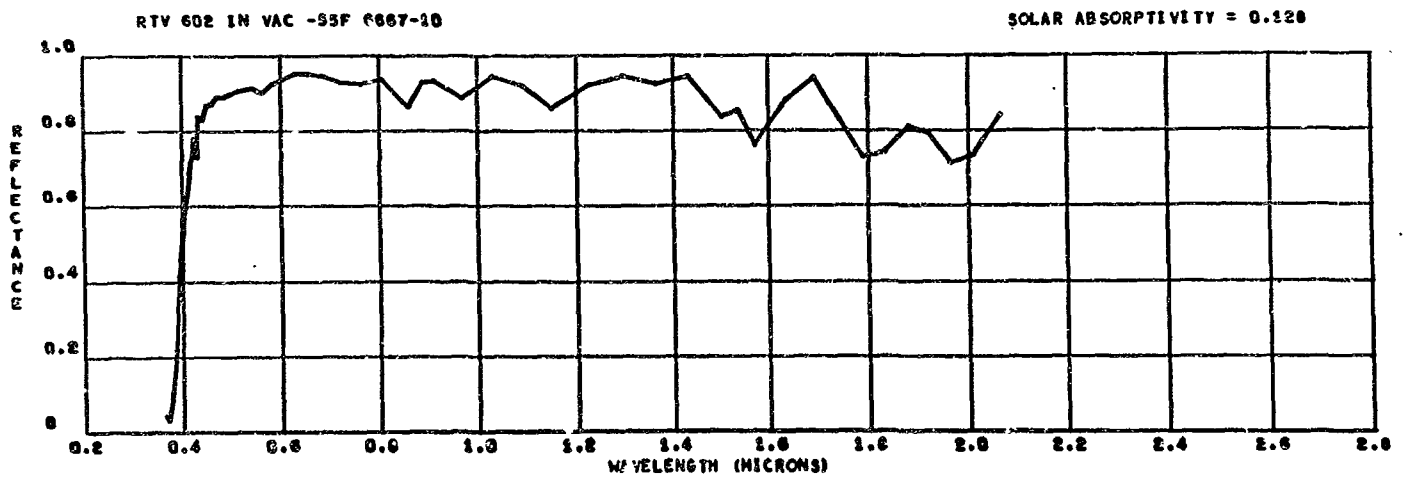
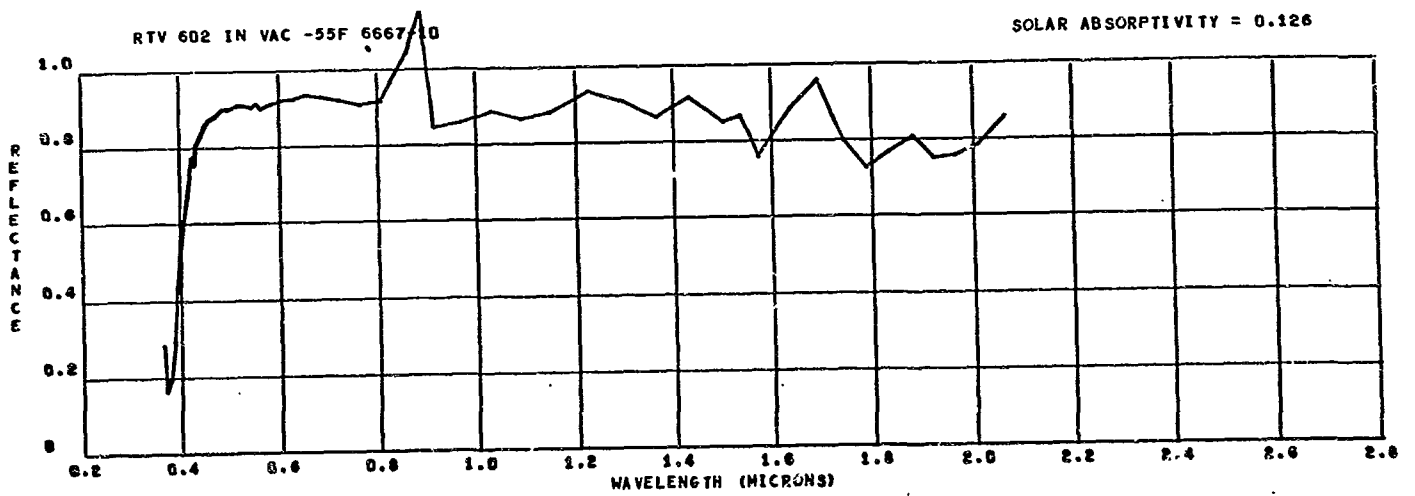
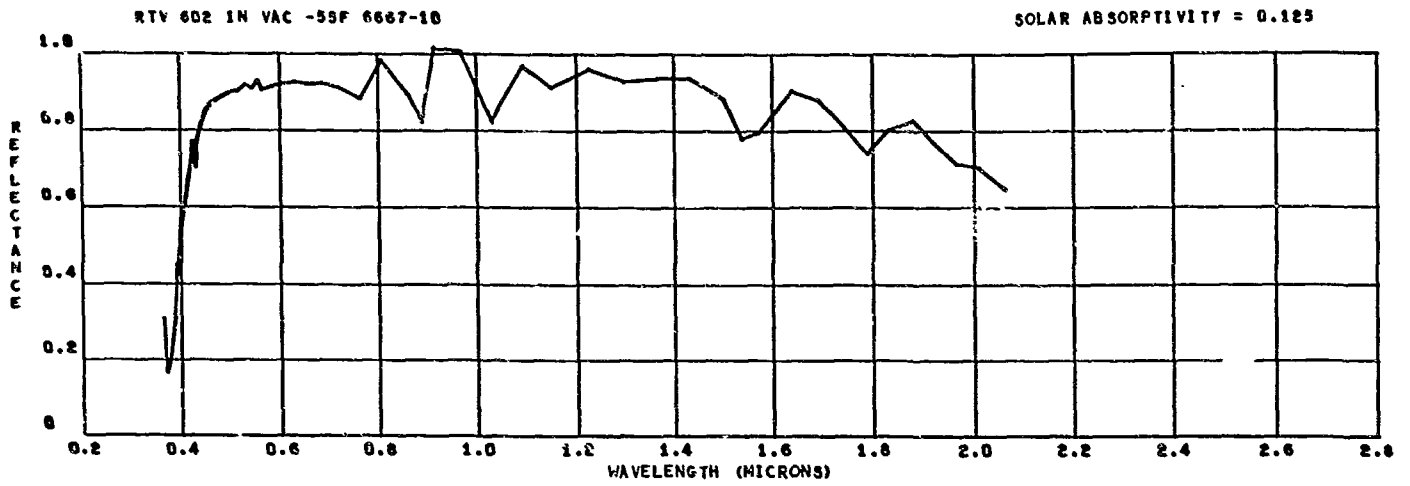


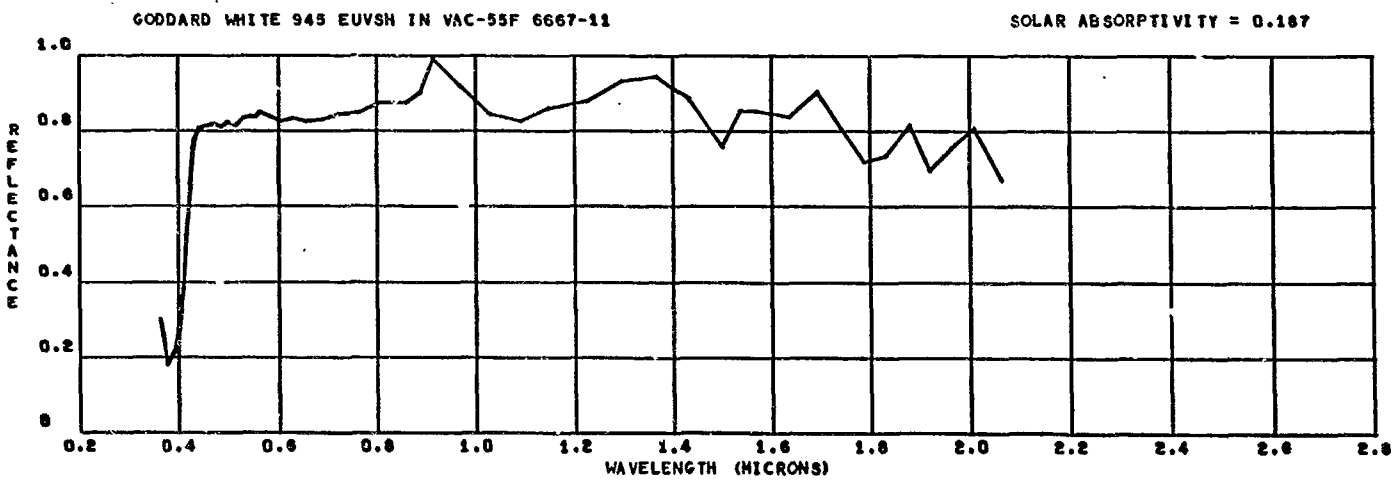
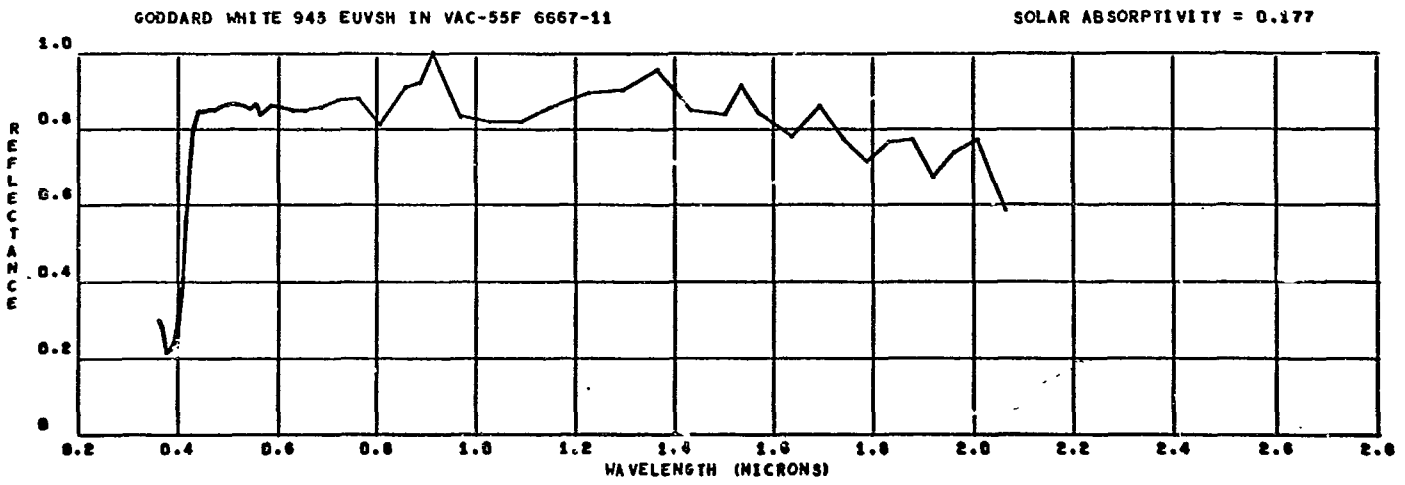
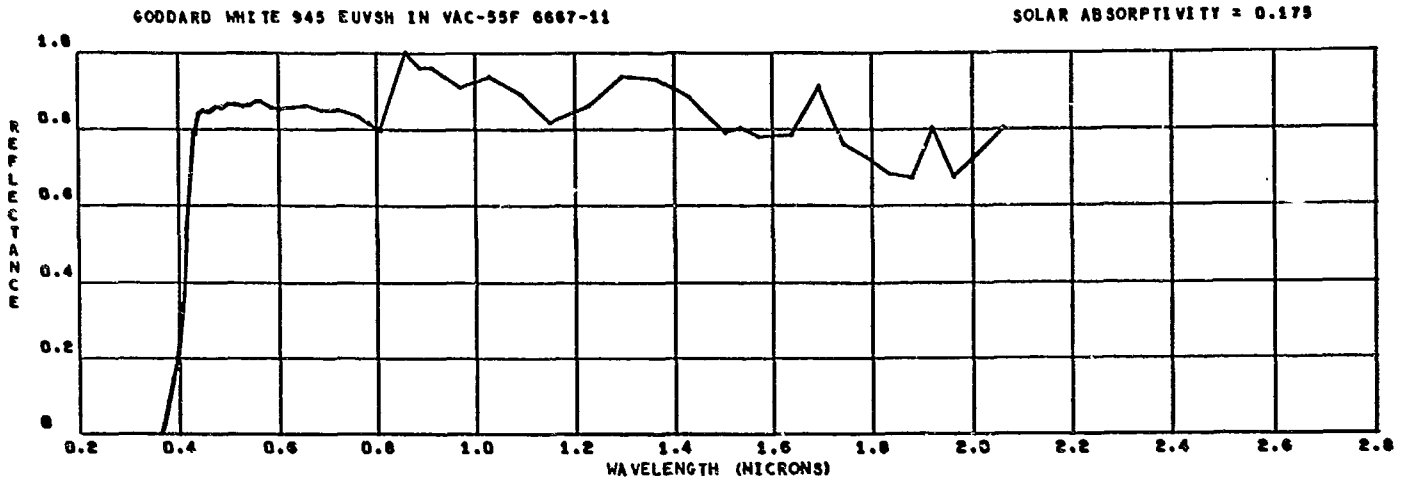


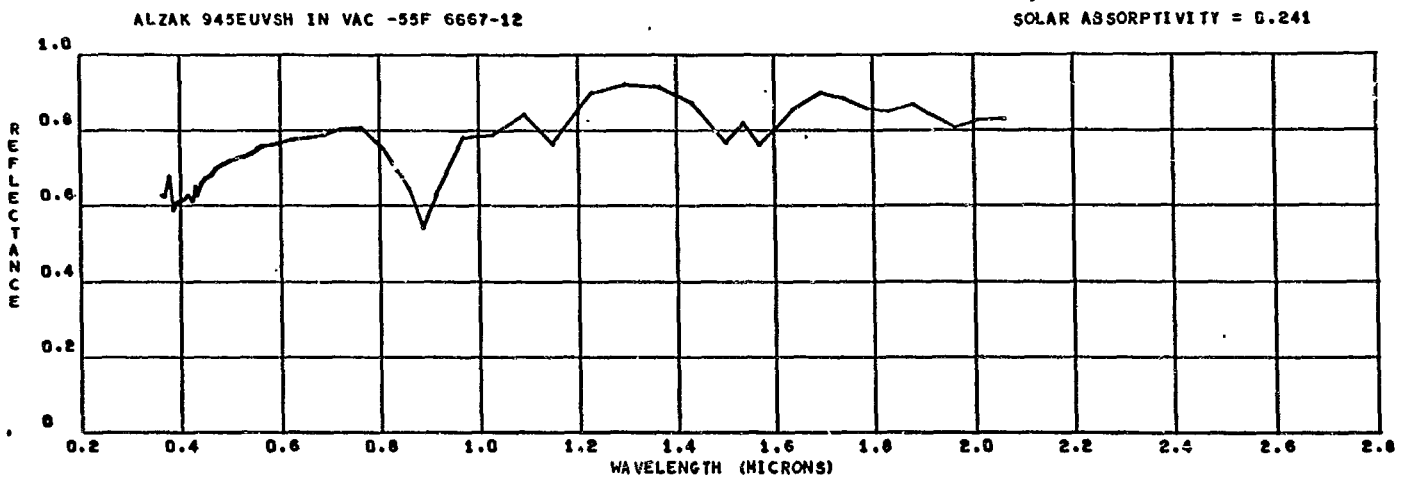
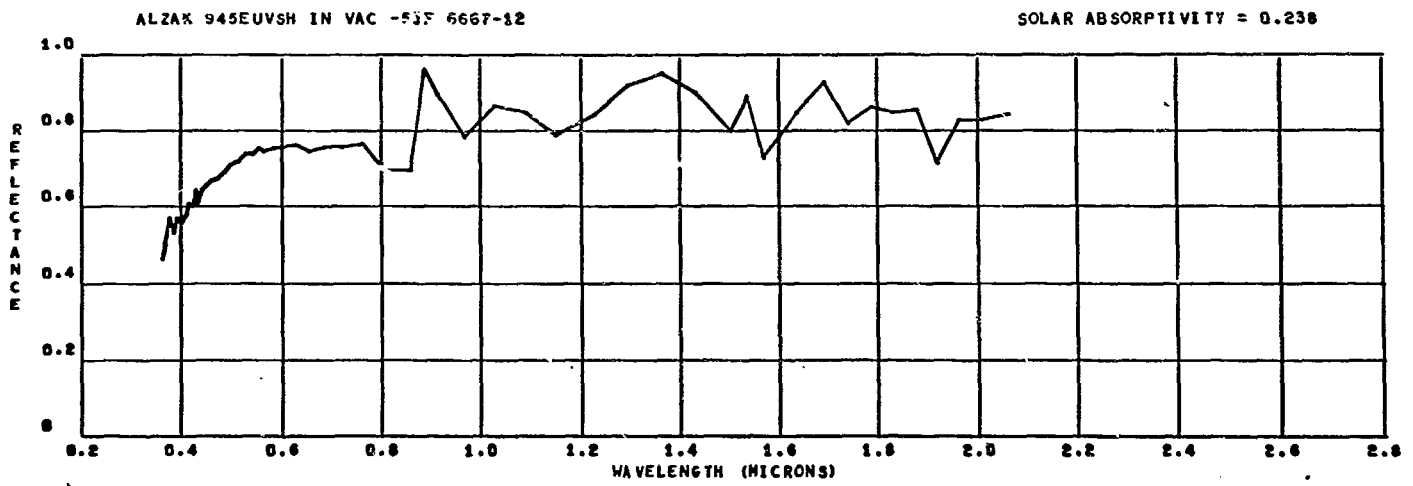
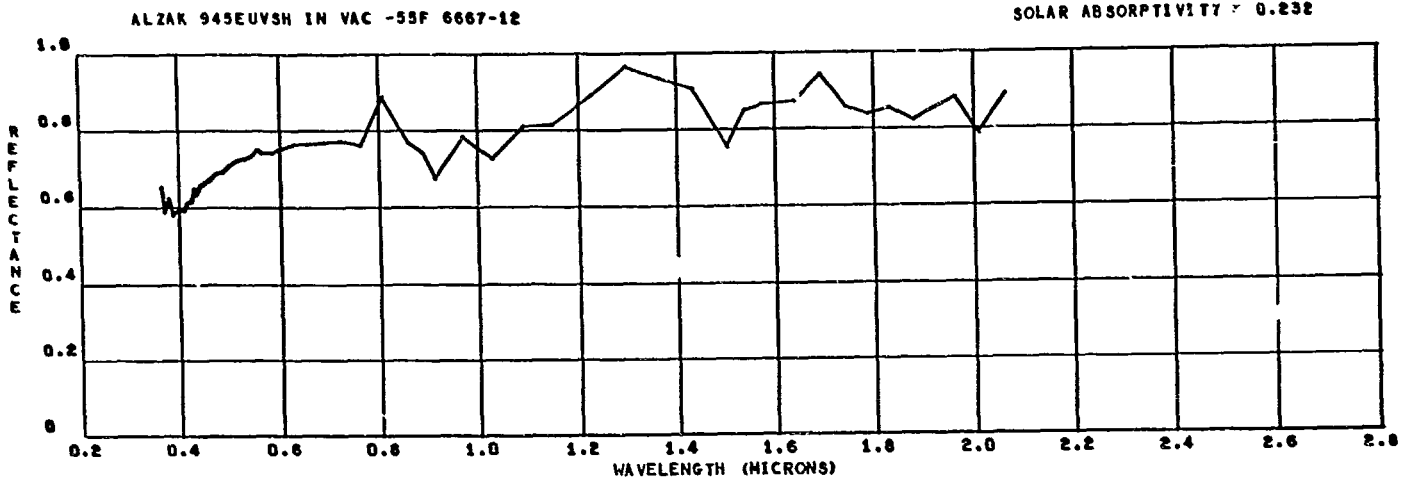


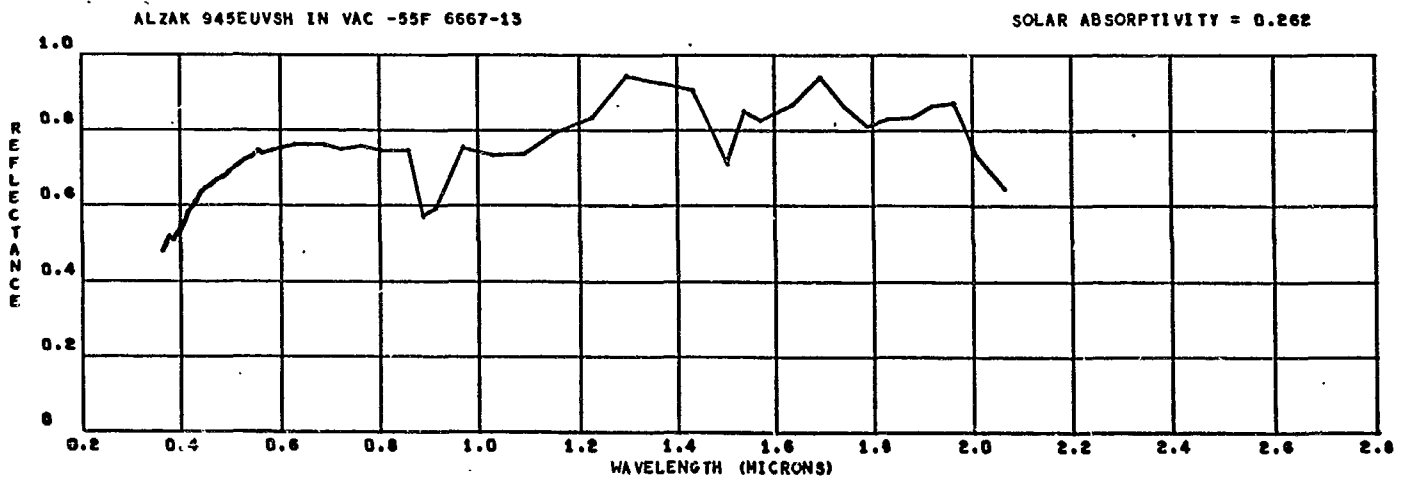
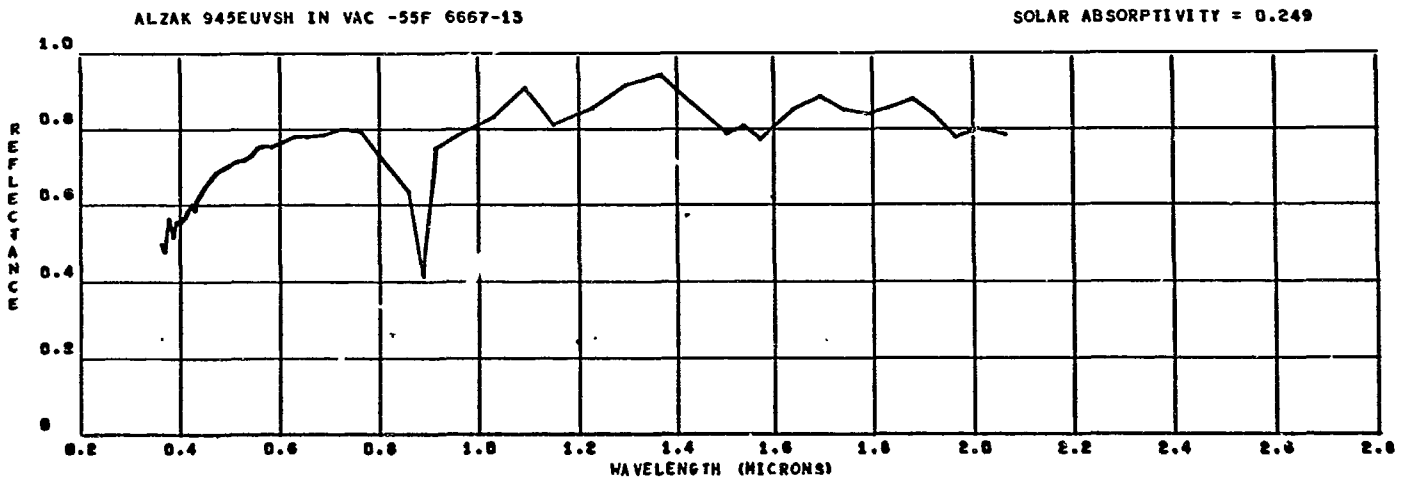
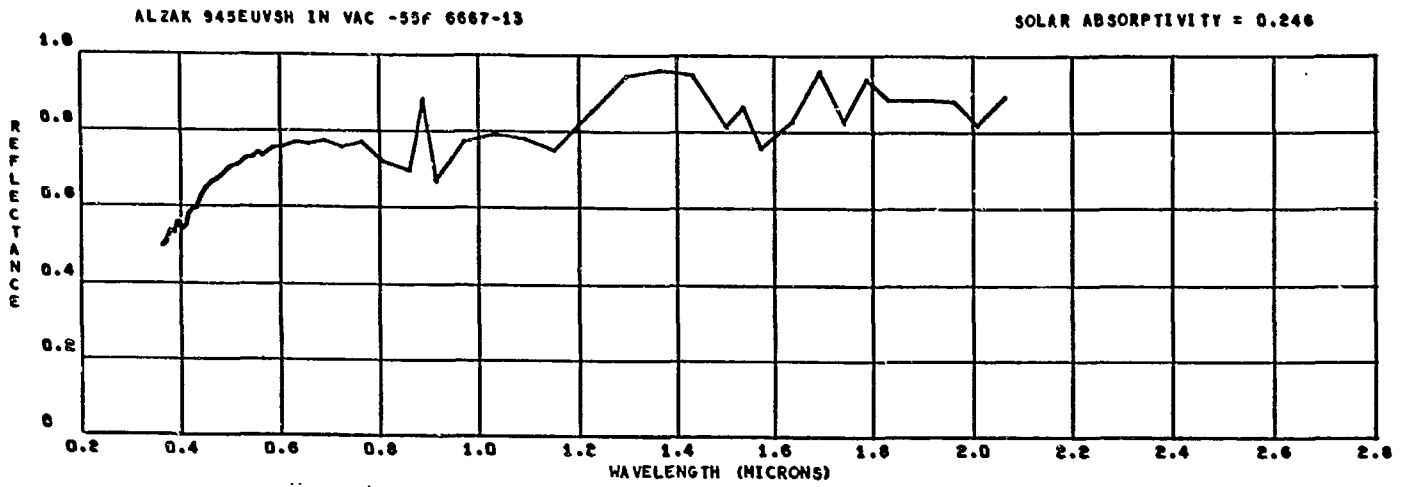


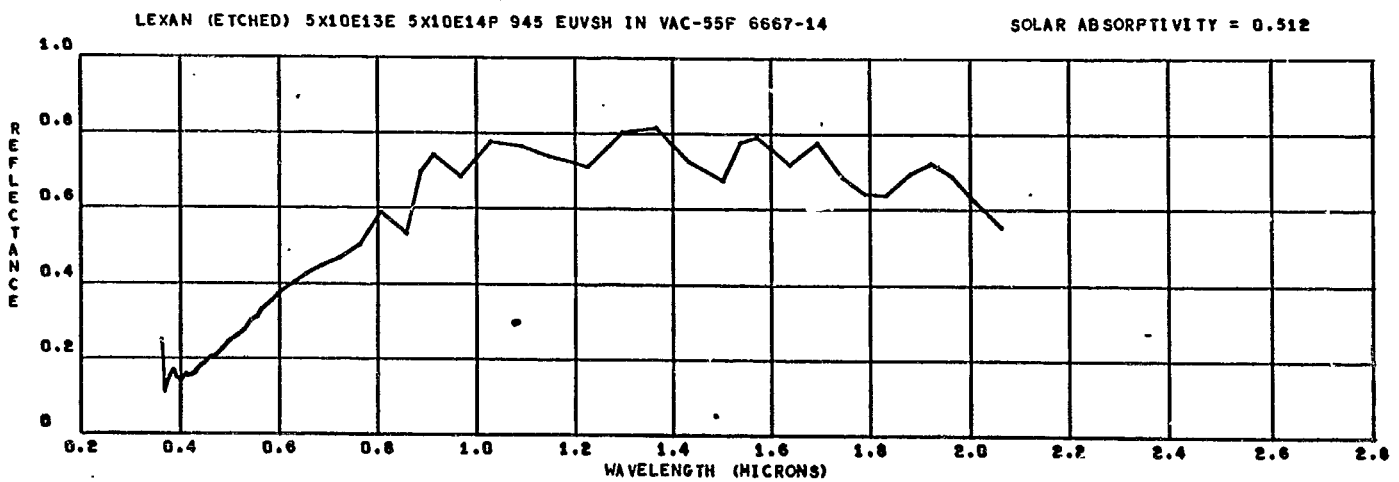
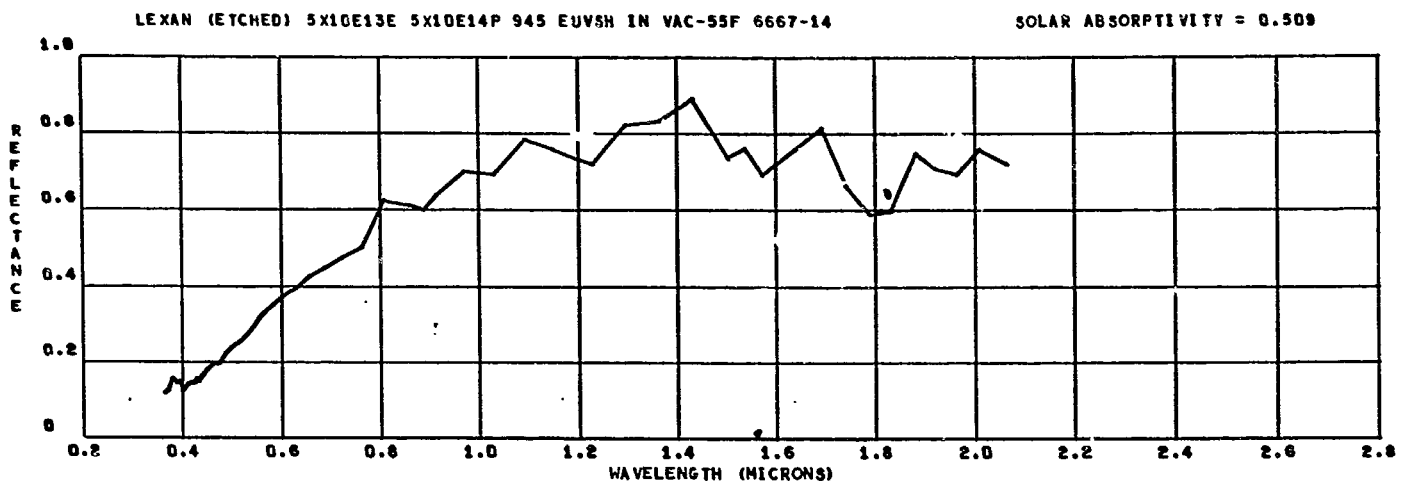
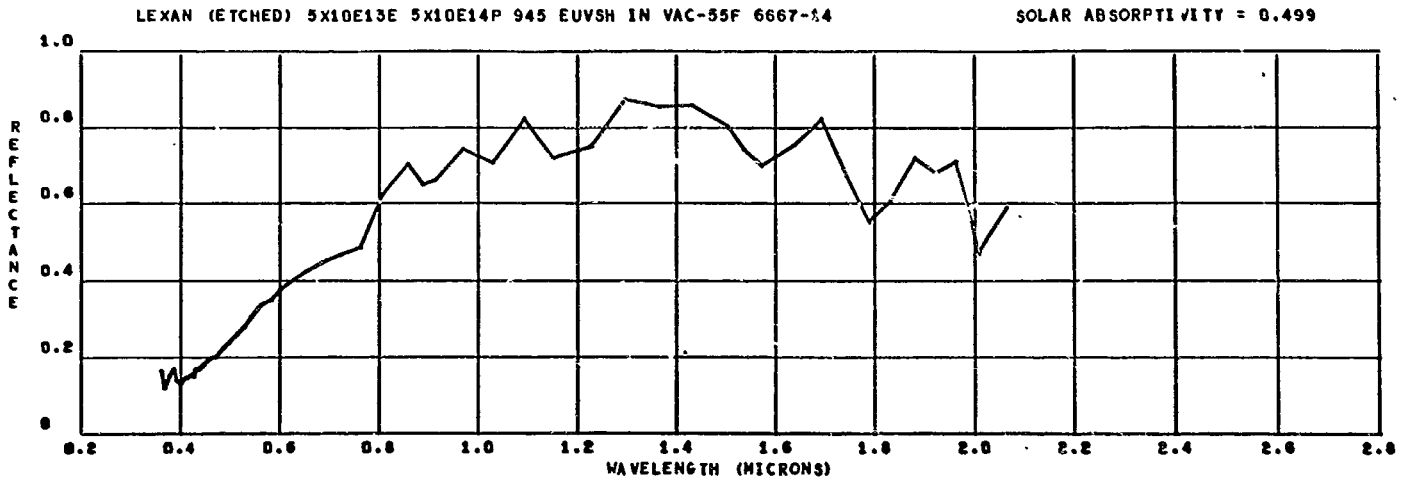


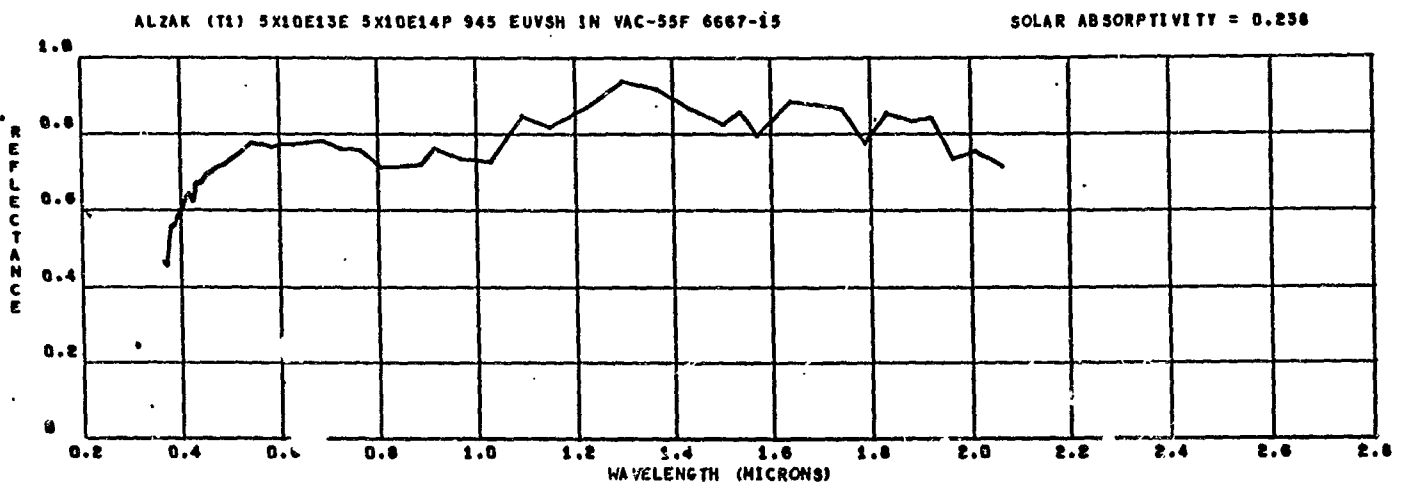
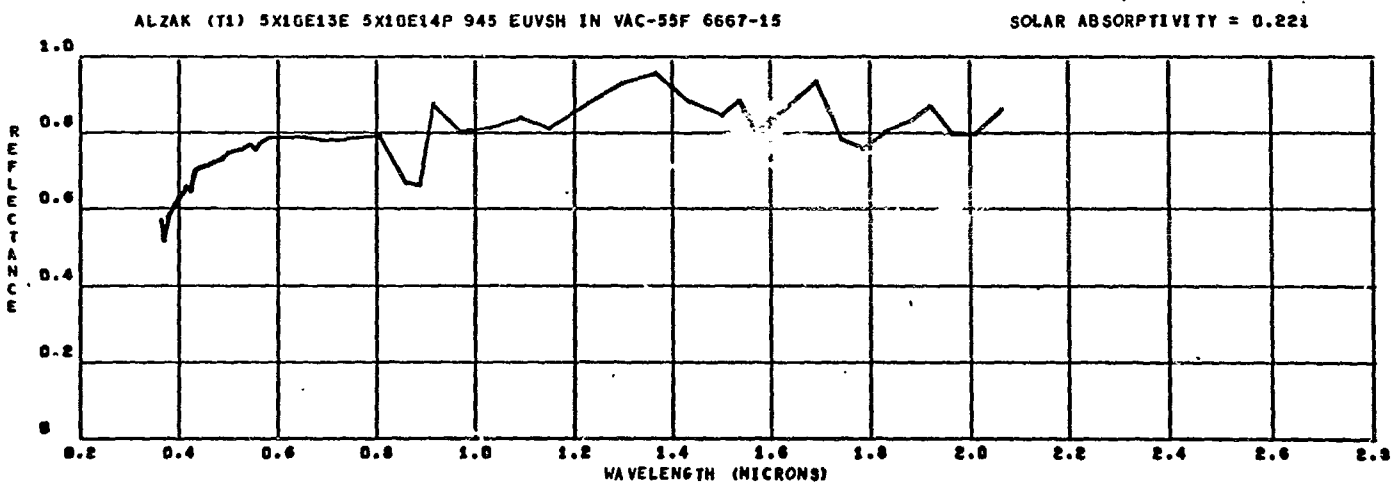
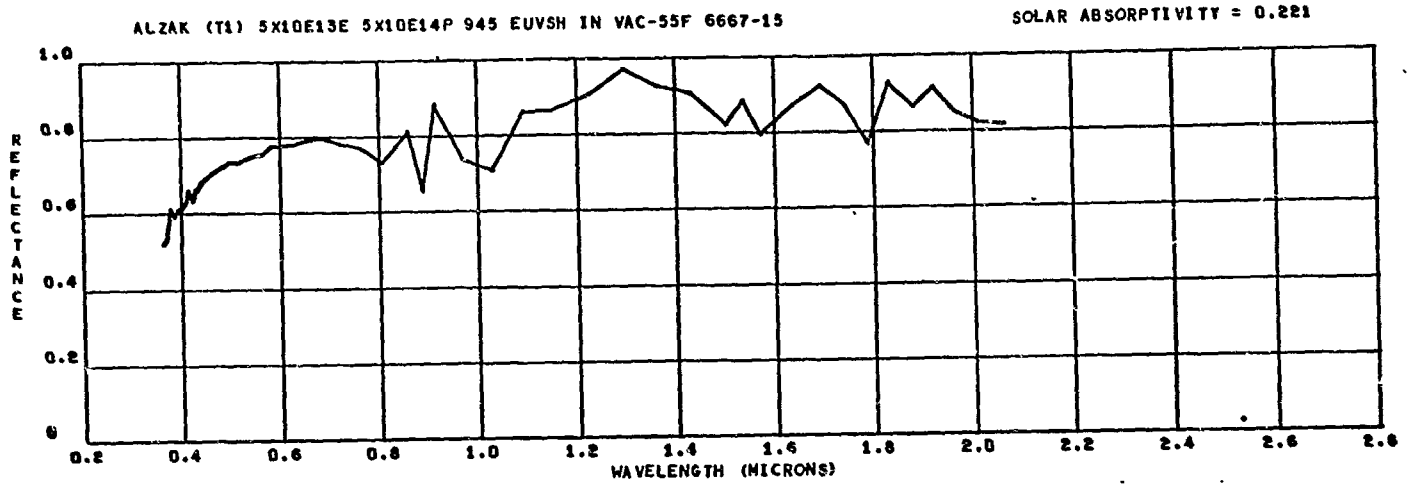


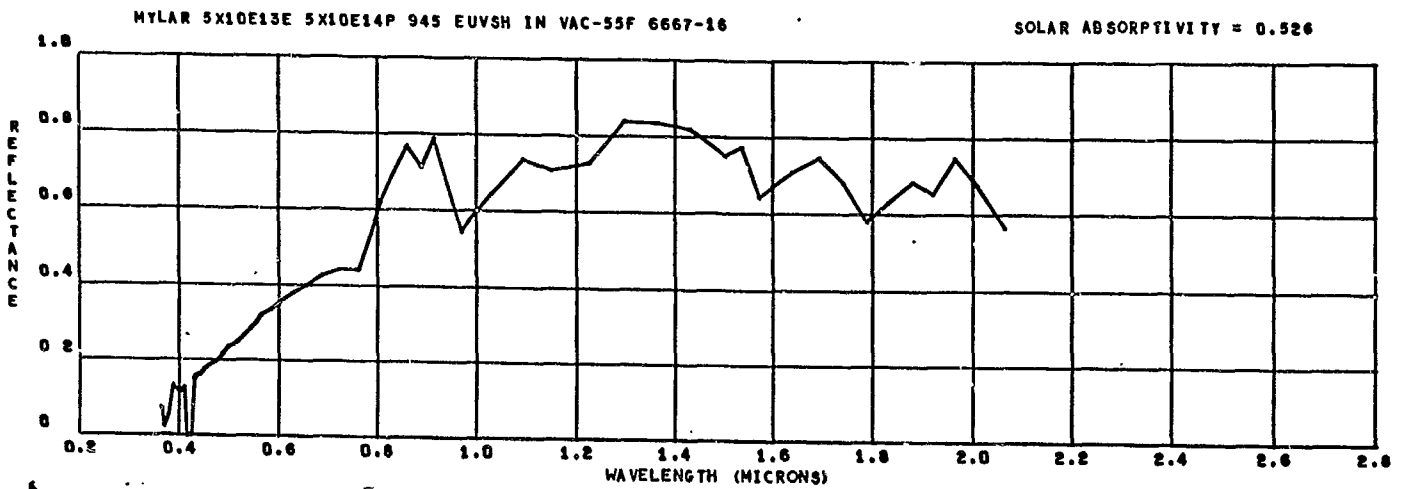
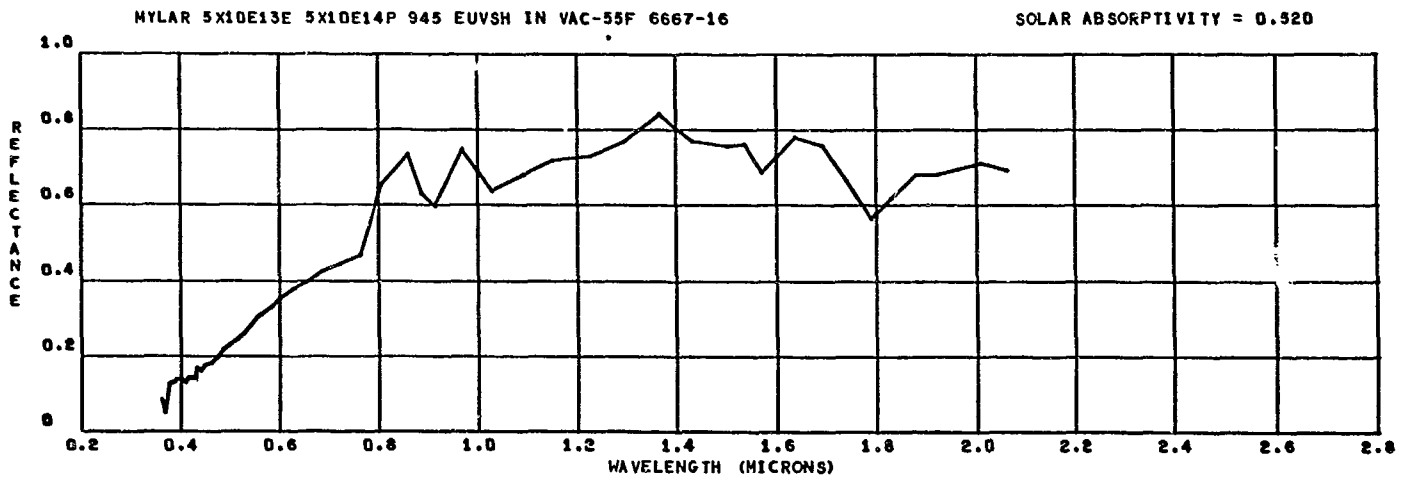
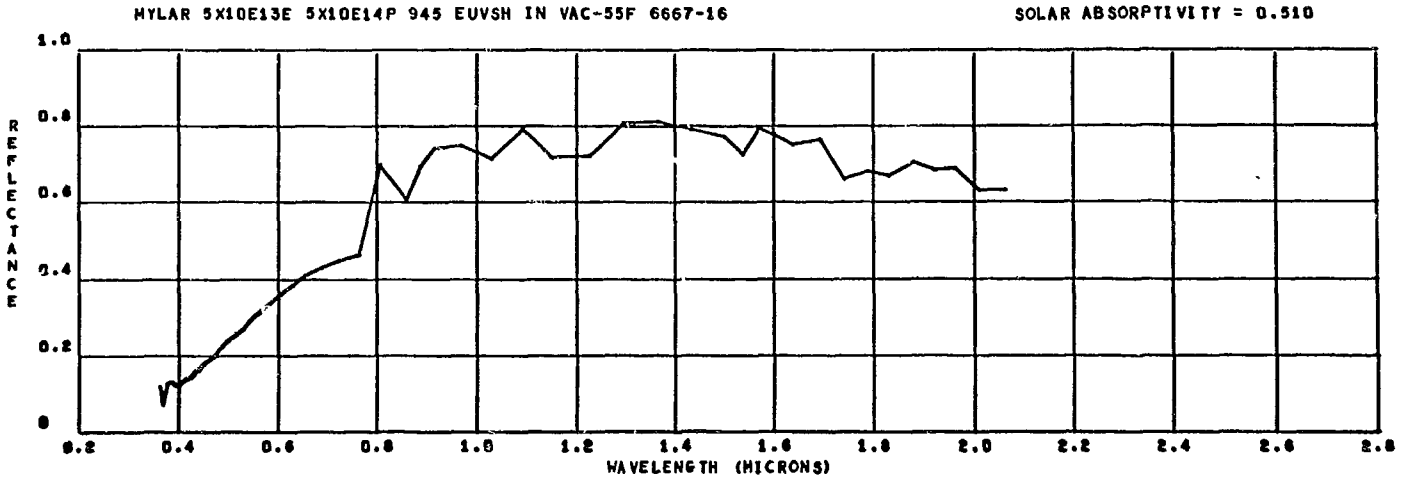


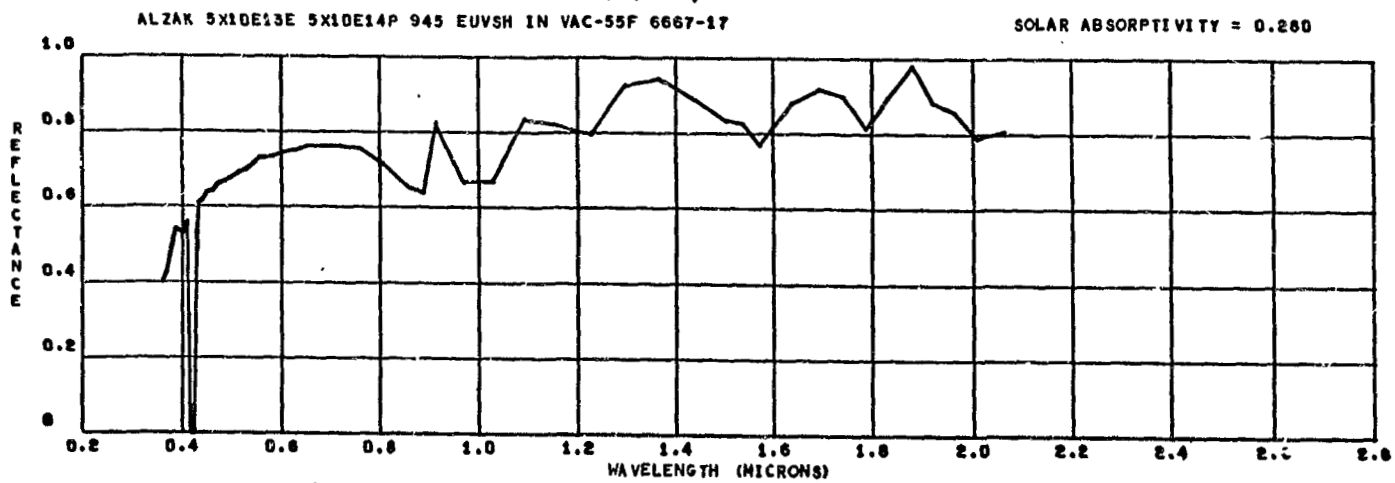
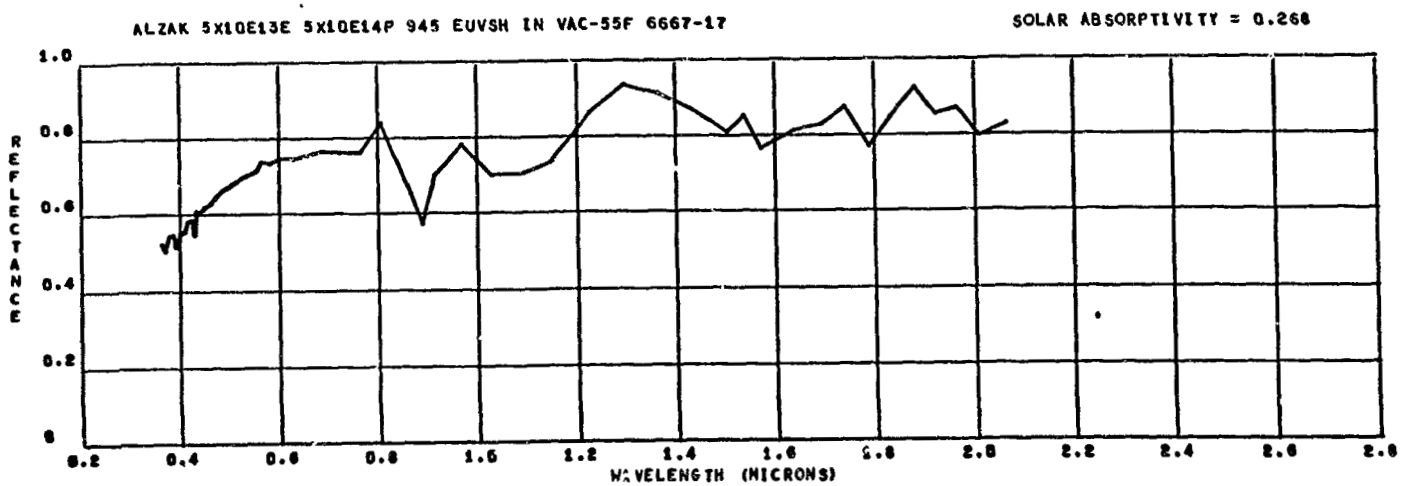
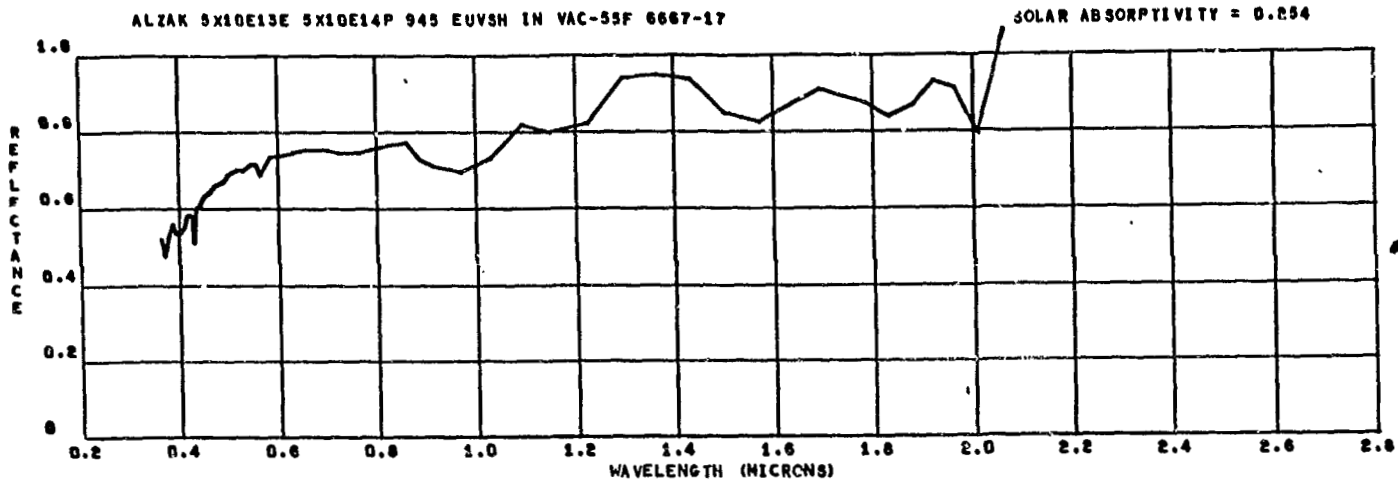






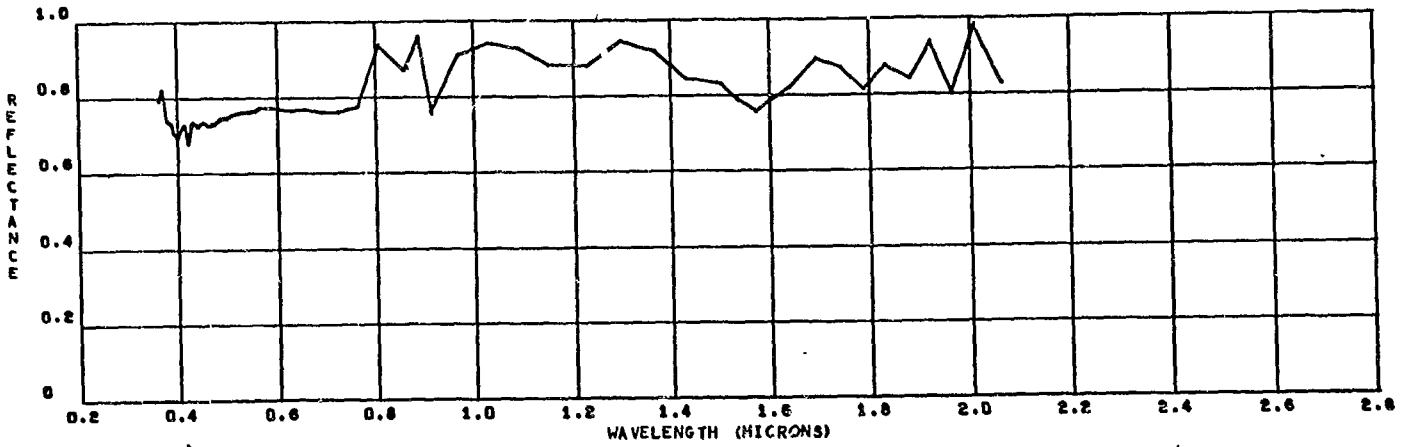






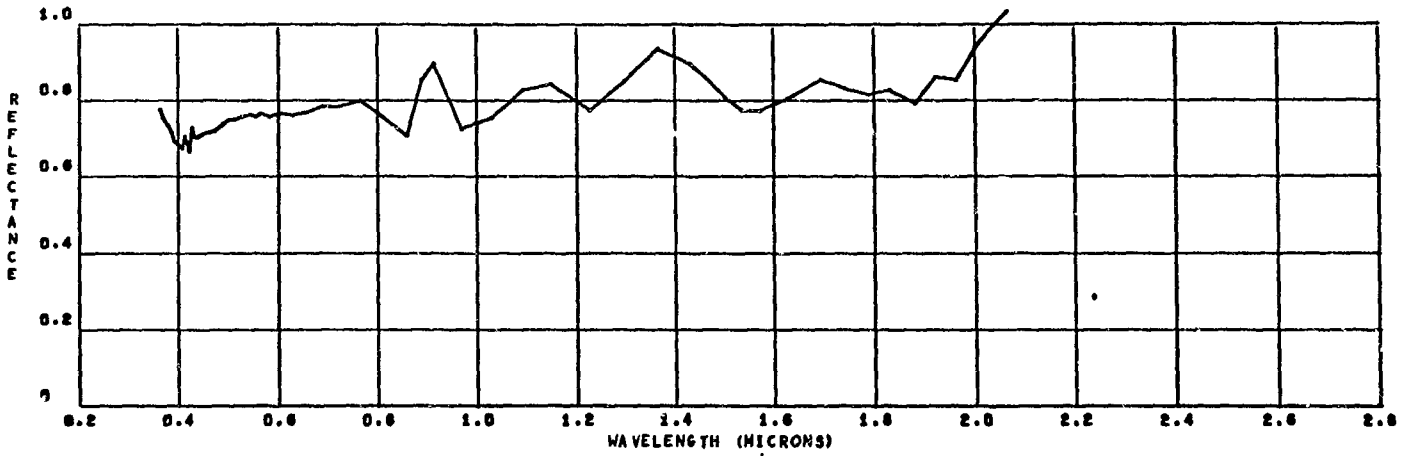
LEXAN (DULL) 5X10E13E 5X10E14P 945 EUVSH IN VAC-55F 6667-18

SOLAR ABSORPTIVITY = 0.182



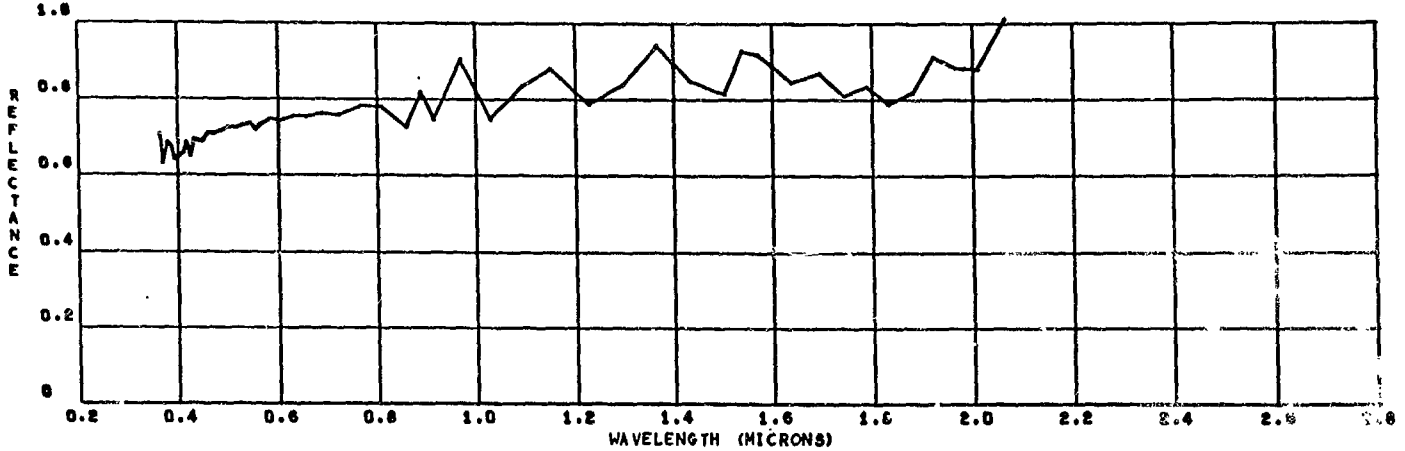
LEXAN (DULL) 5X10E13E 5X10E14P 945 EUVSH IN VAC-55F 6667-18

SOLAR ABSORPTIVITY = 0.221



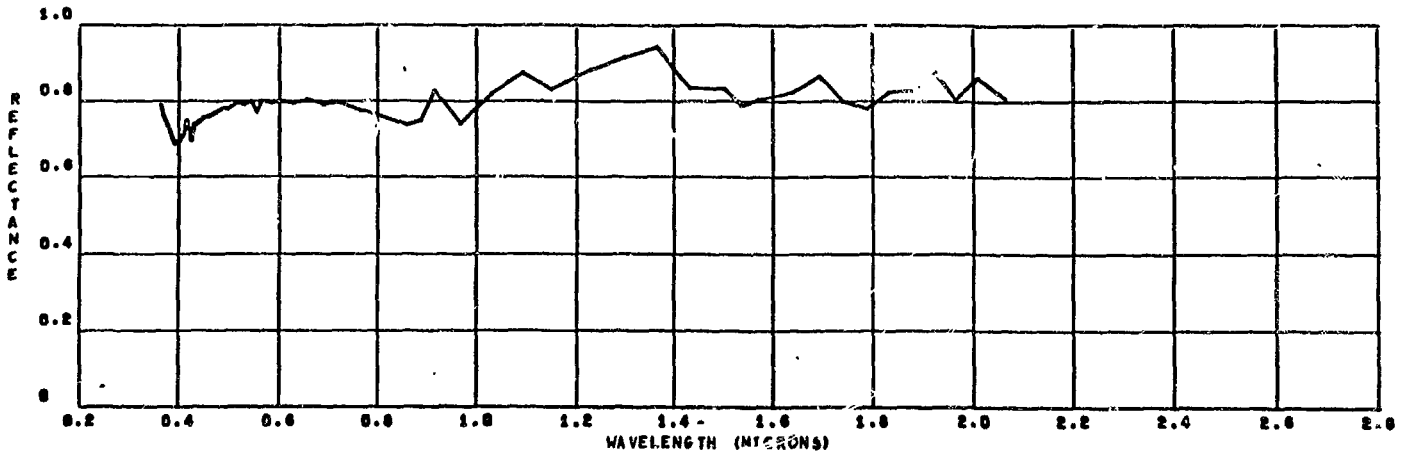
LEXAN (DULL) 5X10E13E 5X10E14P 945 EUVSH IN VAC-55F 6667-18

SOLAR ABSORPTIVITY = 0.227



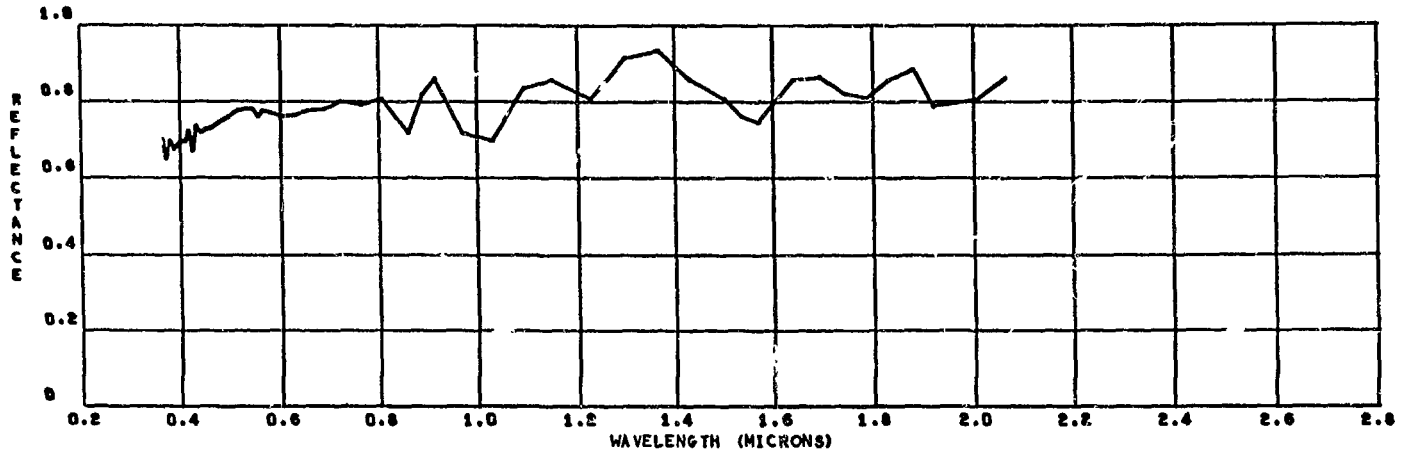
ALZAK (CONTROL) 5X10E13E 5X10E14P IN VAC-55F 6667-19

SOLAR ABSORPTIVITY = 0.202



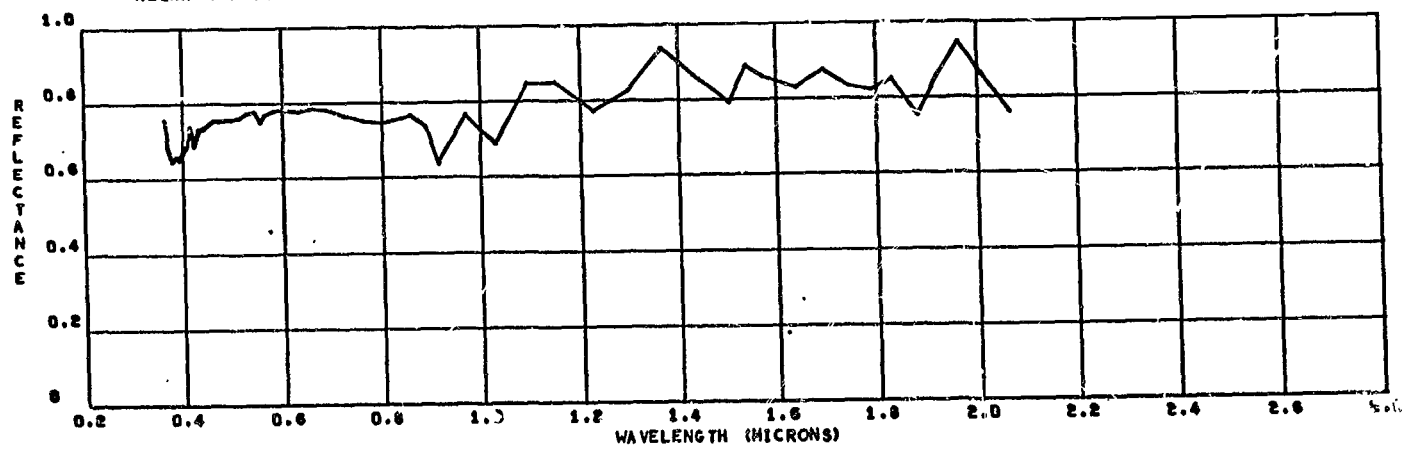
ALZAK (CONTROL) 5X10E13E 5X10E14P IN VAC-55F 6667-19

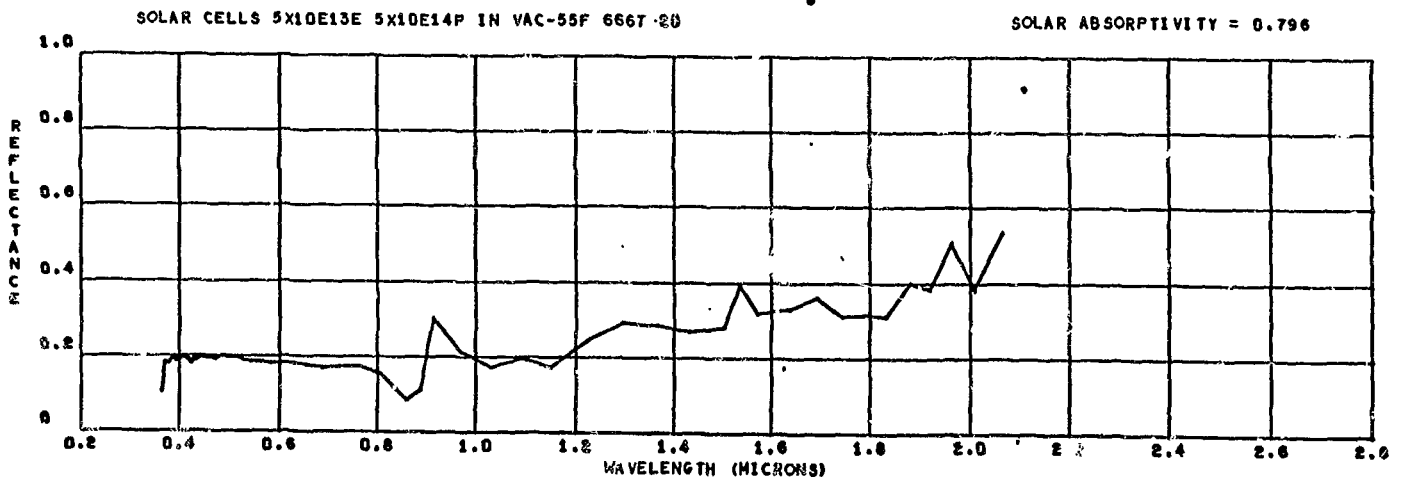
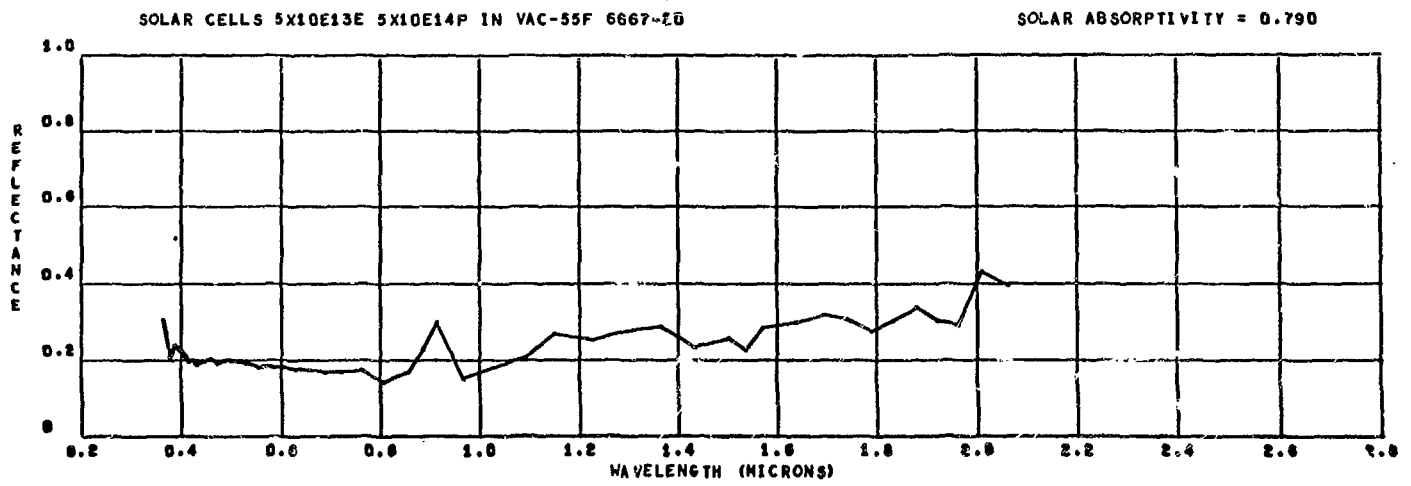
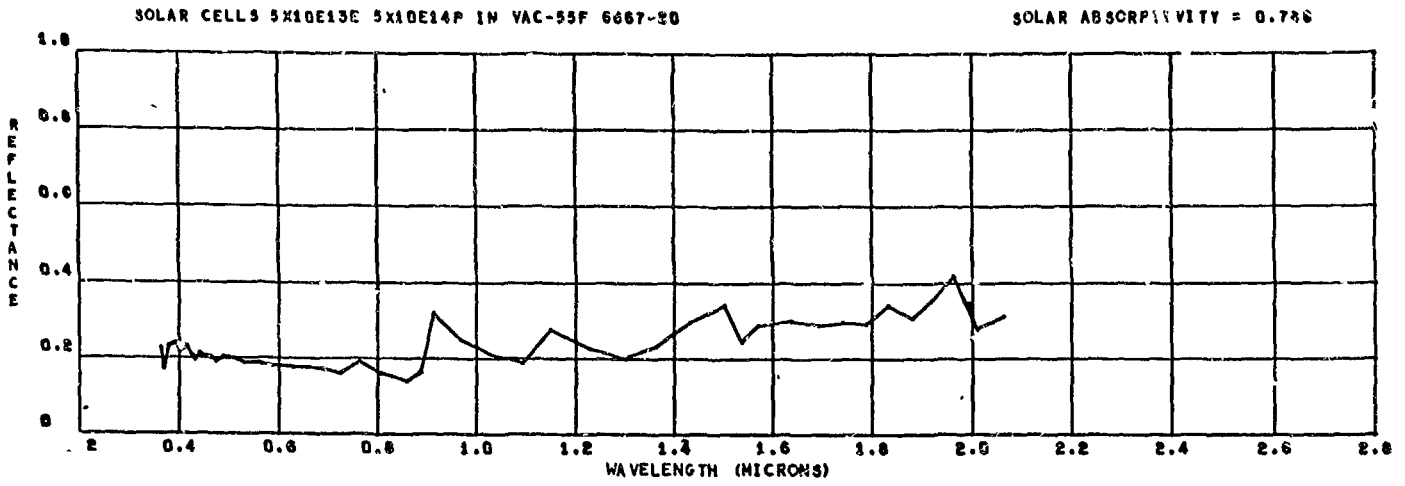
SOLAR ABSORPTIVITY = 0.210

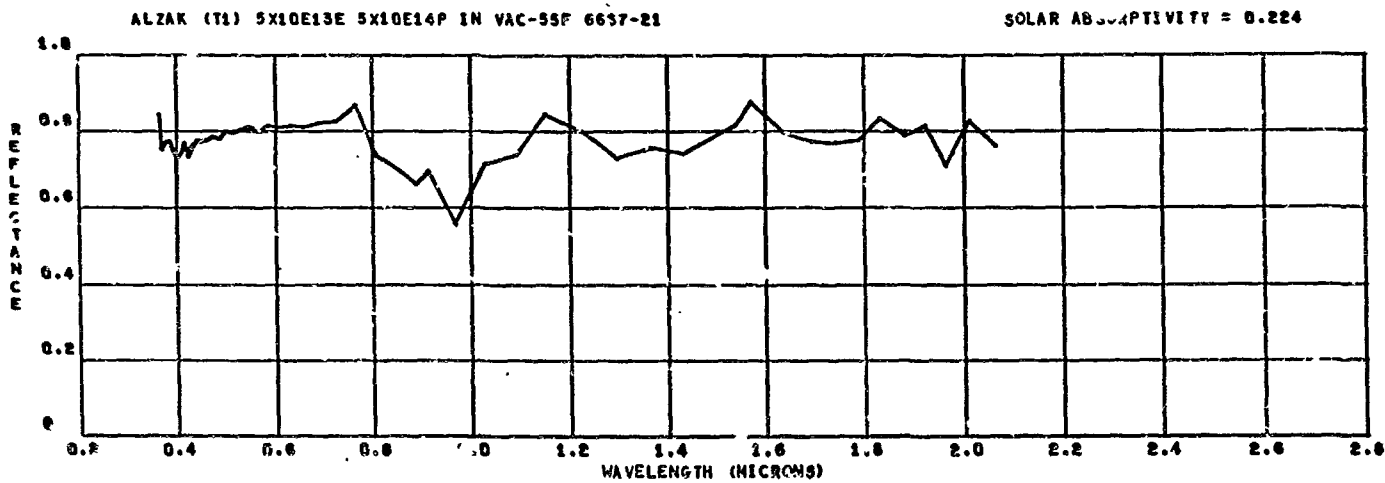
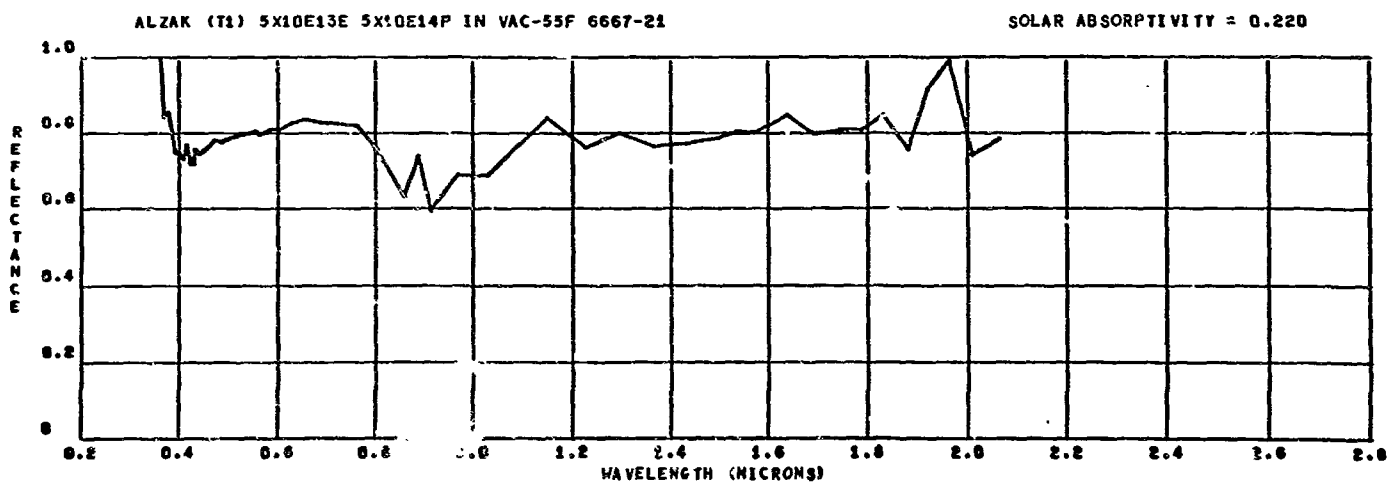
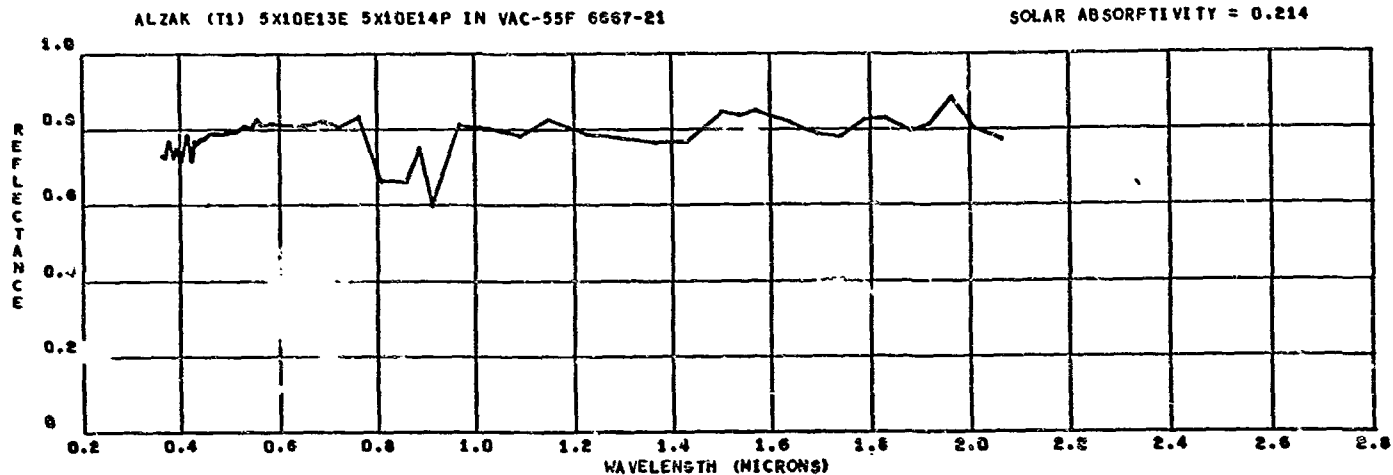


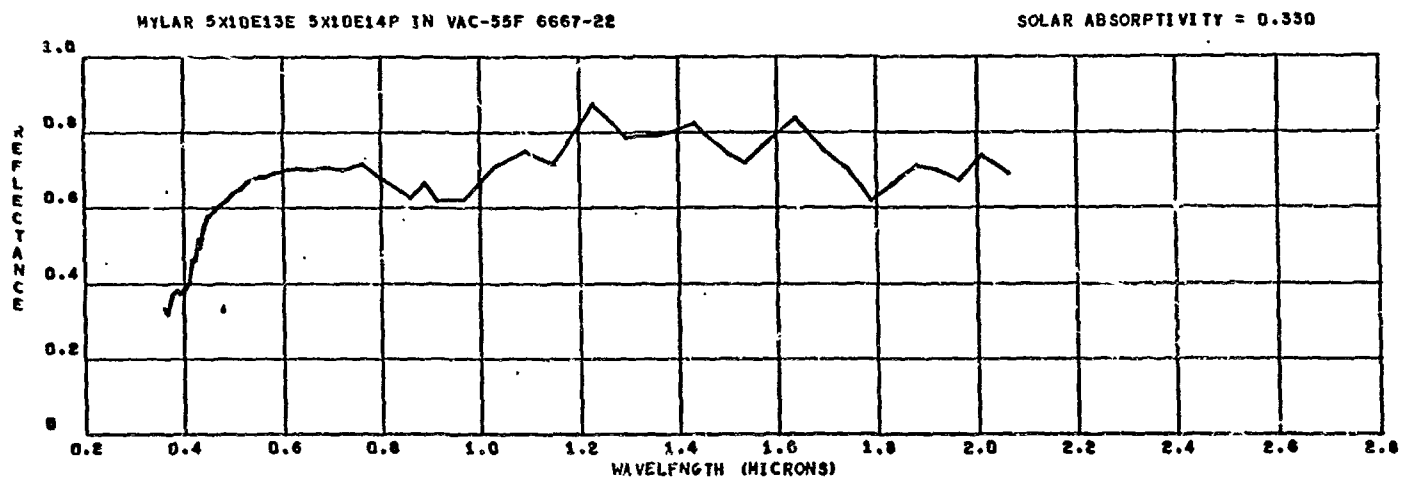
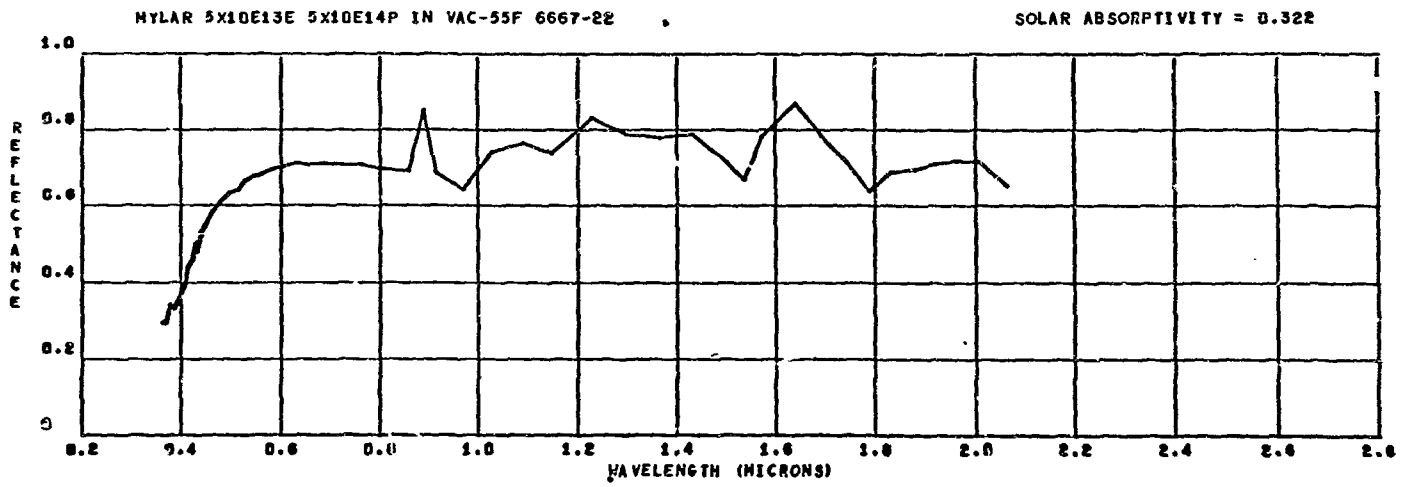
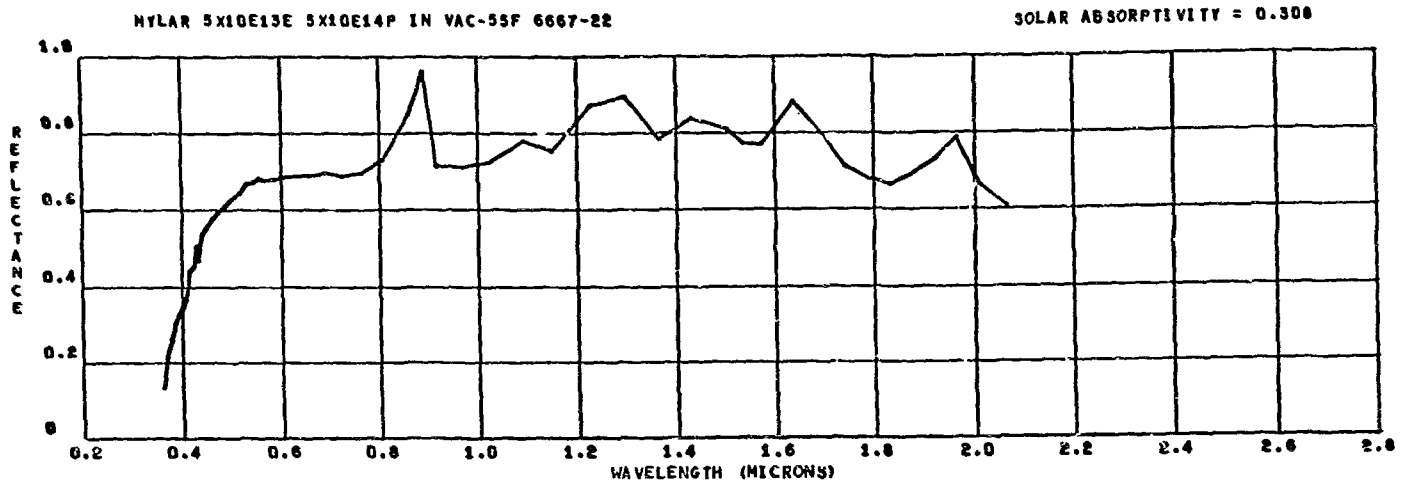
ALZAK (CONTROL) 5X10E13E 5X10E14P IN VAC-55F 6667-19

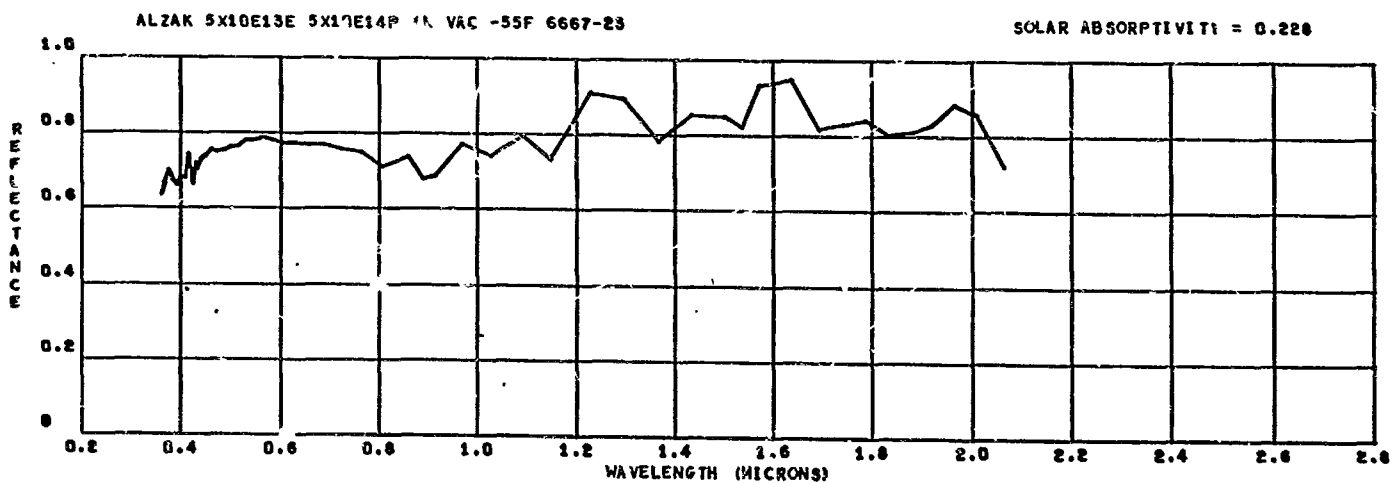
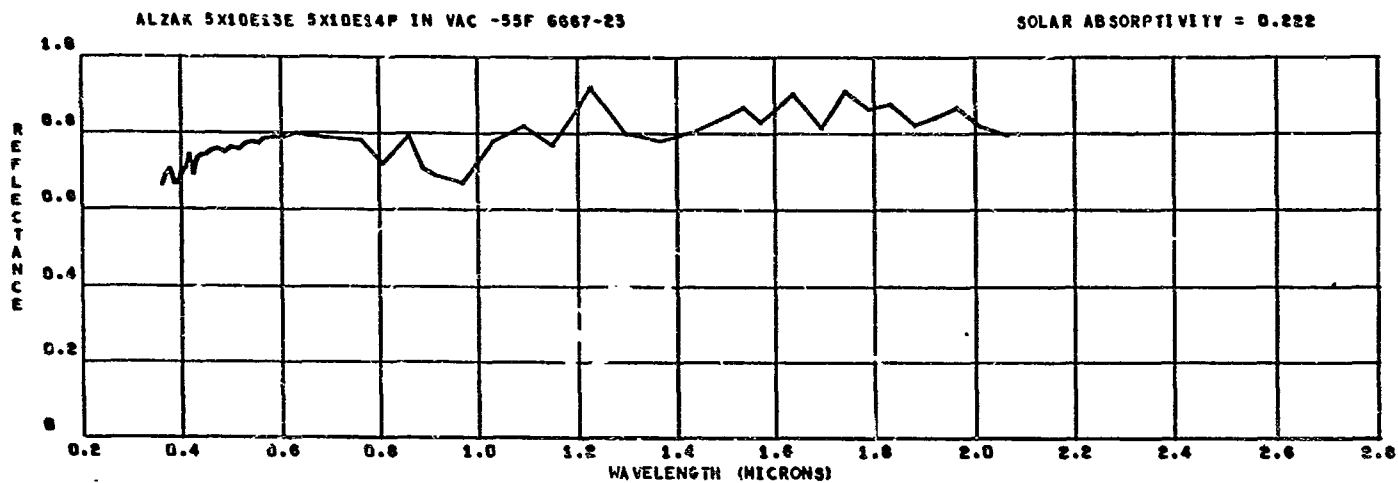
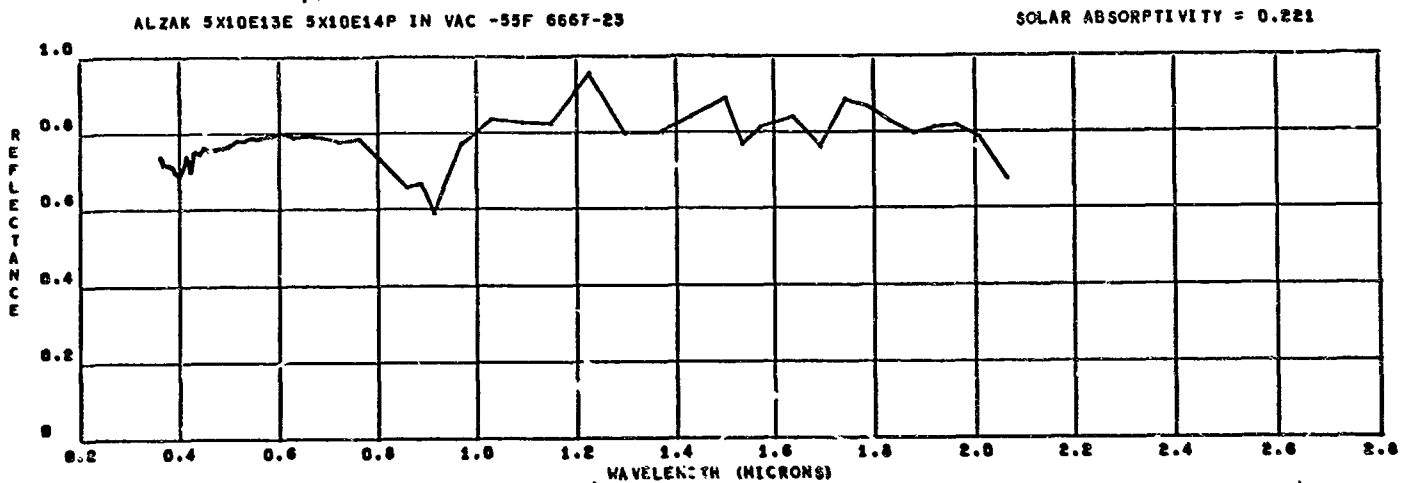
SOLAR ABSORPTIVITY = 0.225

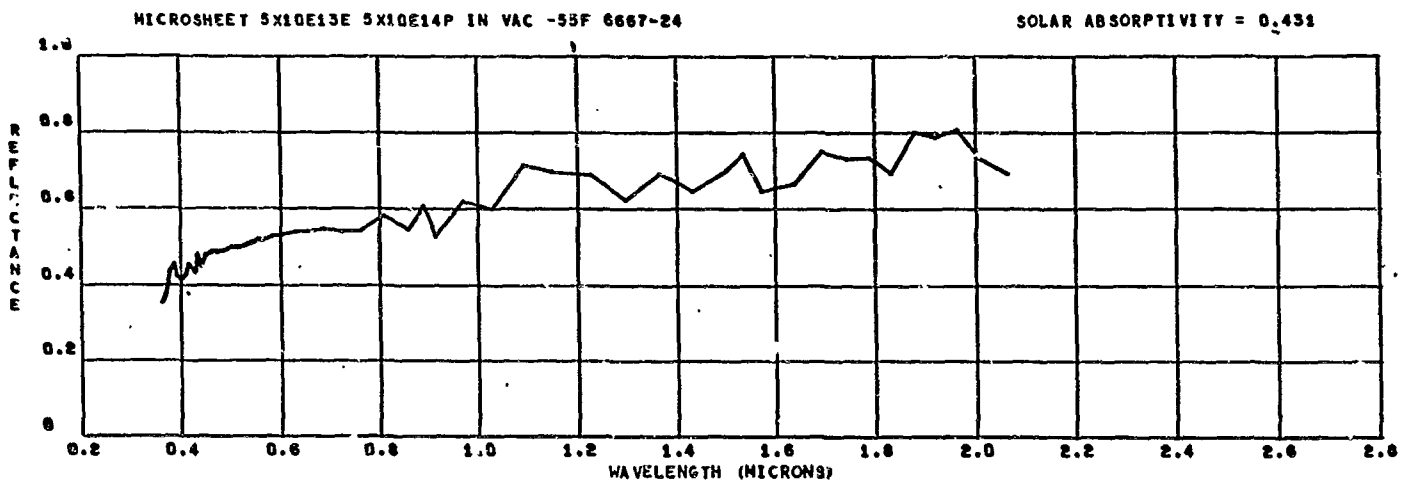
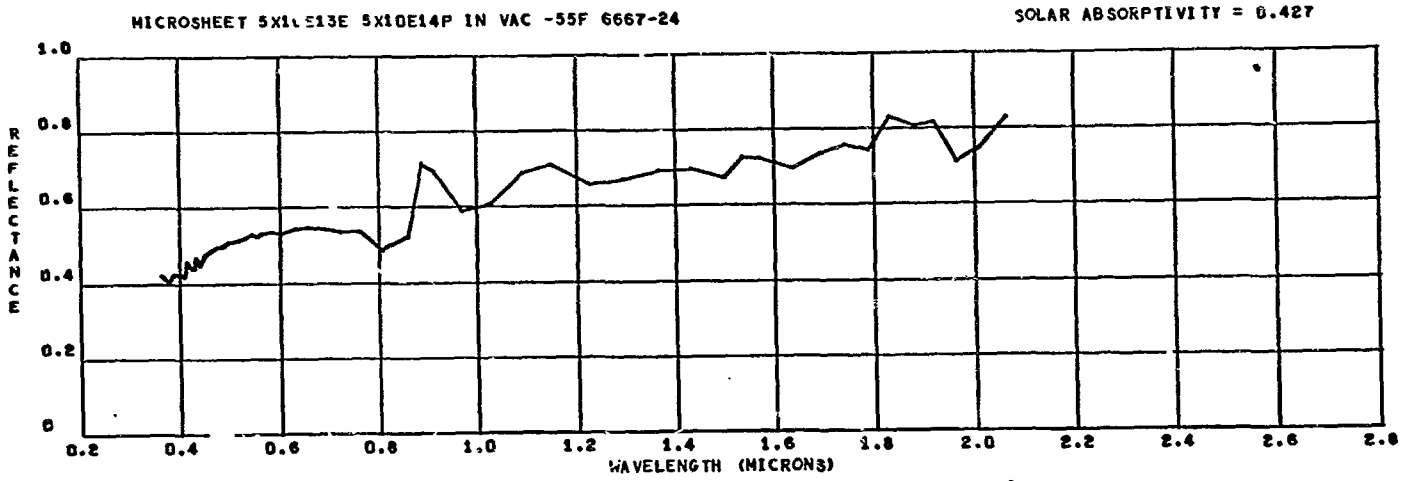
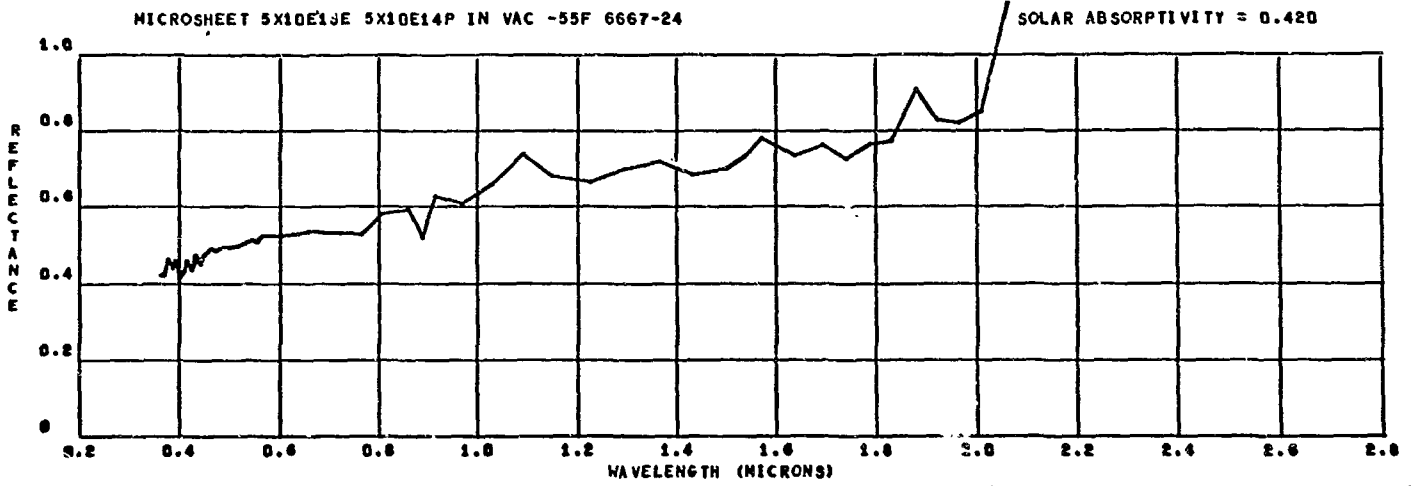


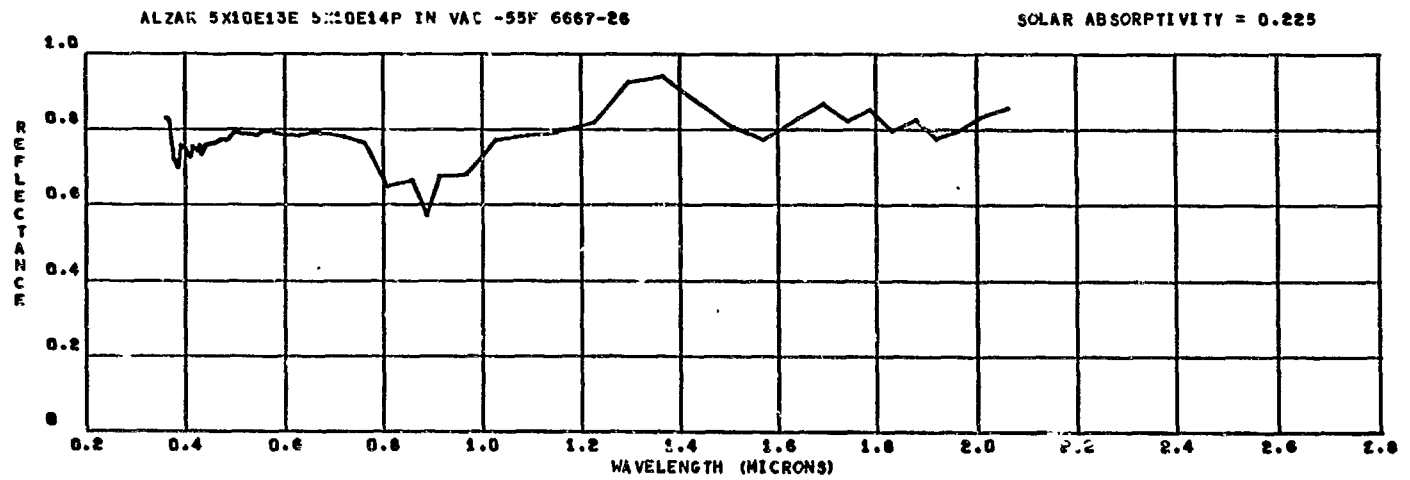
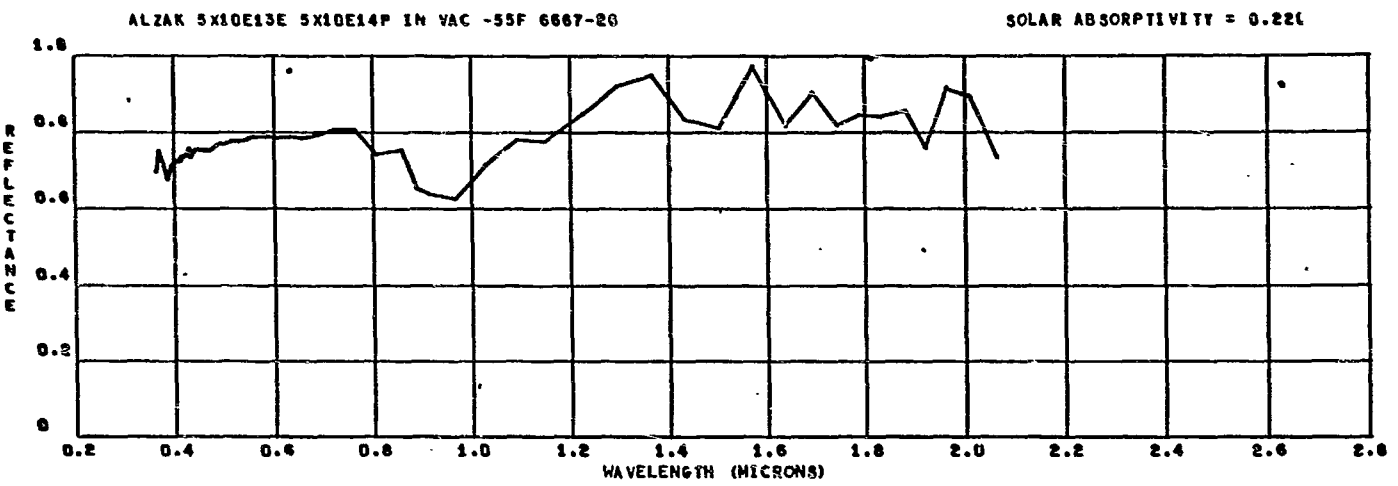
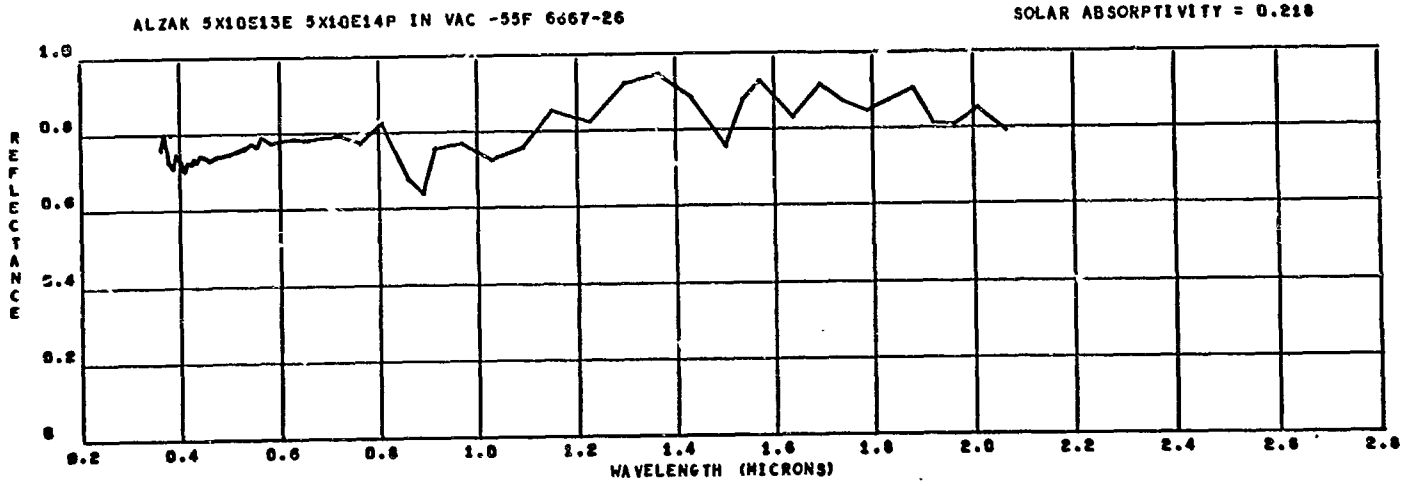






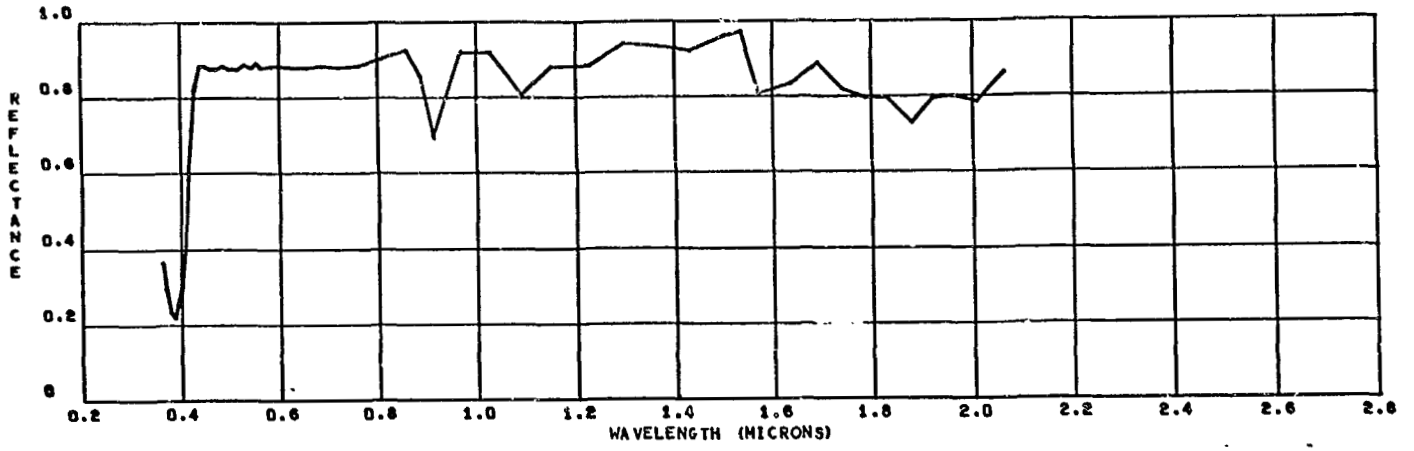






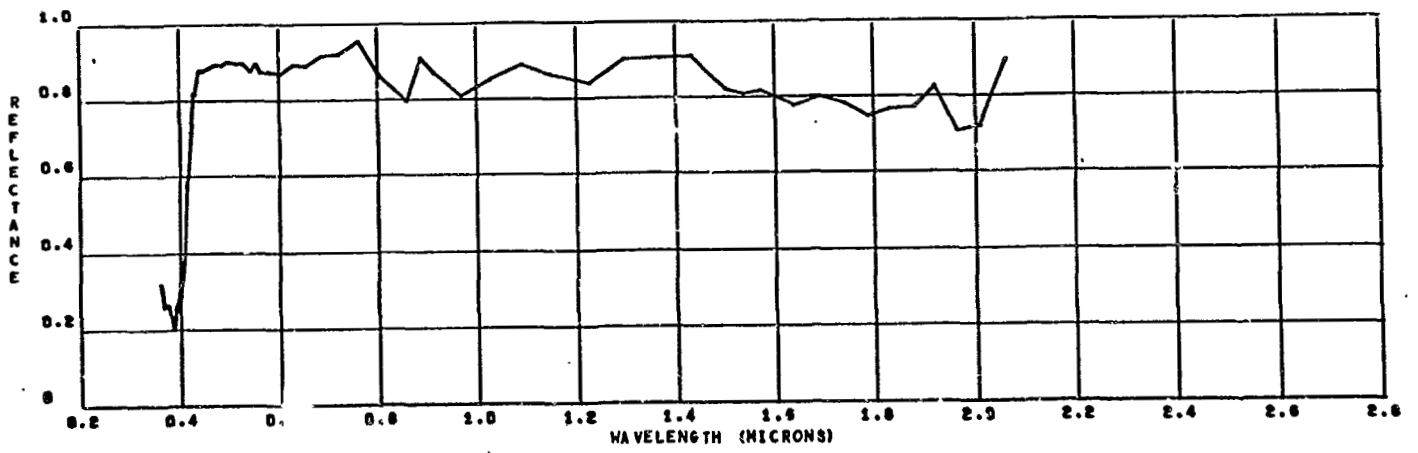
GODDARD WHITE 5X10E13E 5X10E14P IN VAC -55F 6667-27

SOLAR ABSORPTIVITY = 0.153



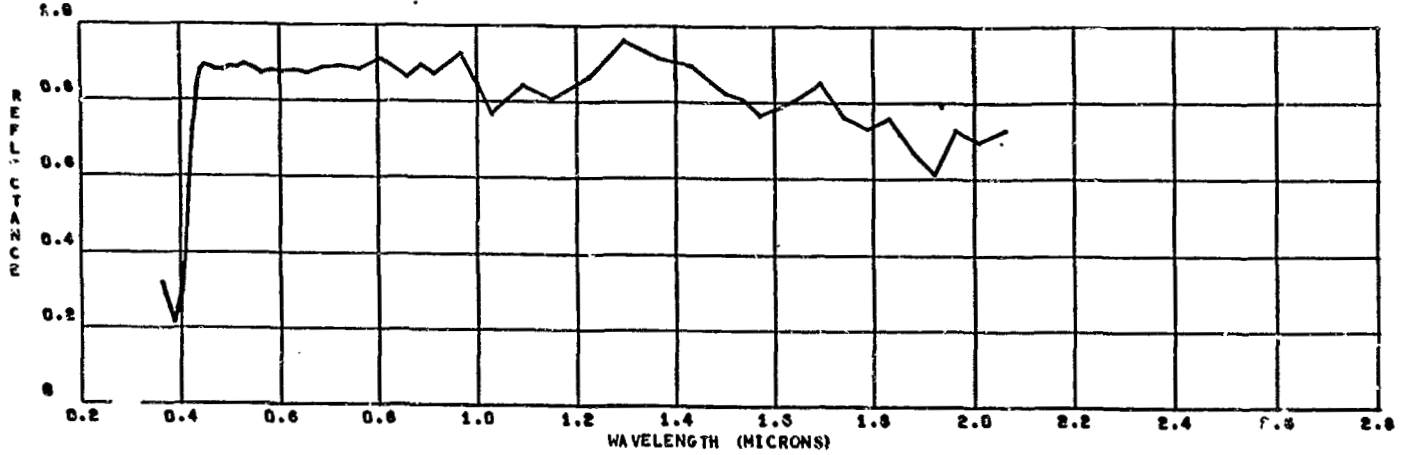
GODDARD WHITE 5X10E13E 5X10E14P IN VAC -55F 6667-27

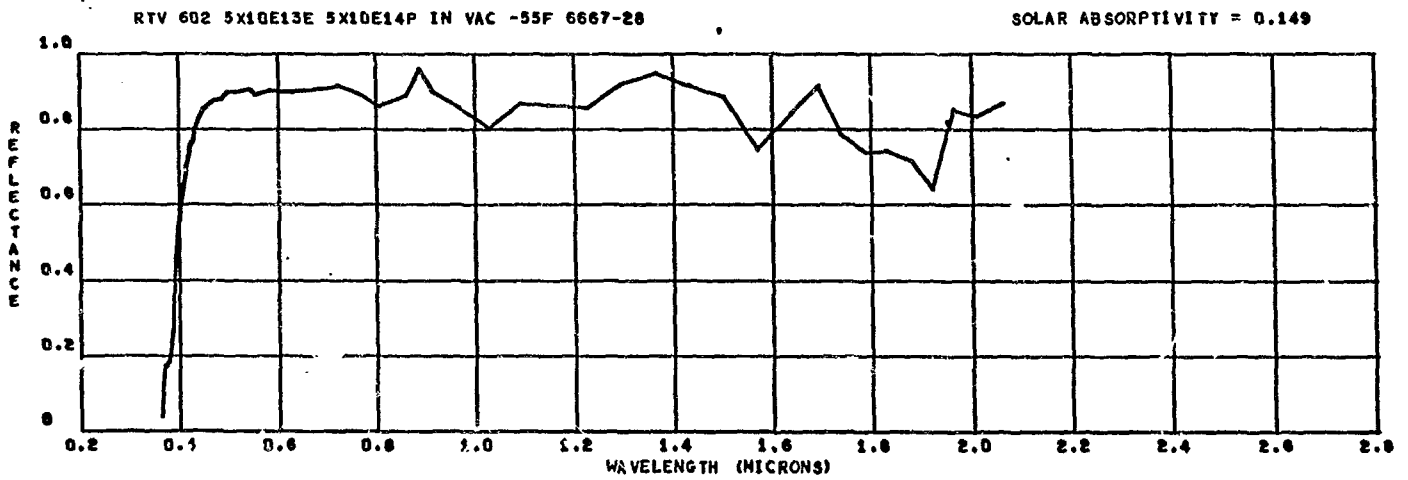
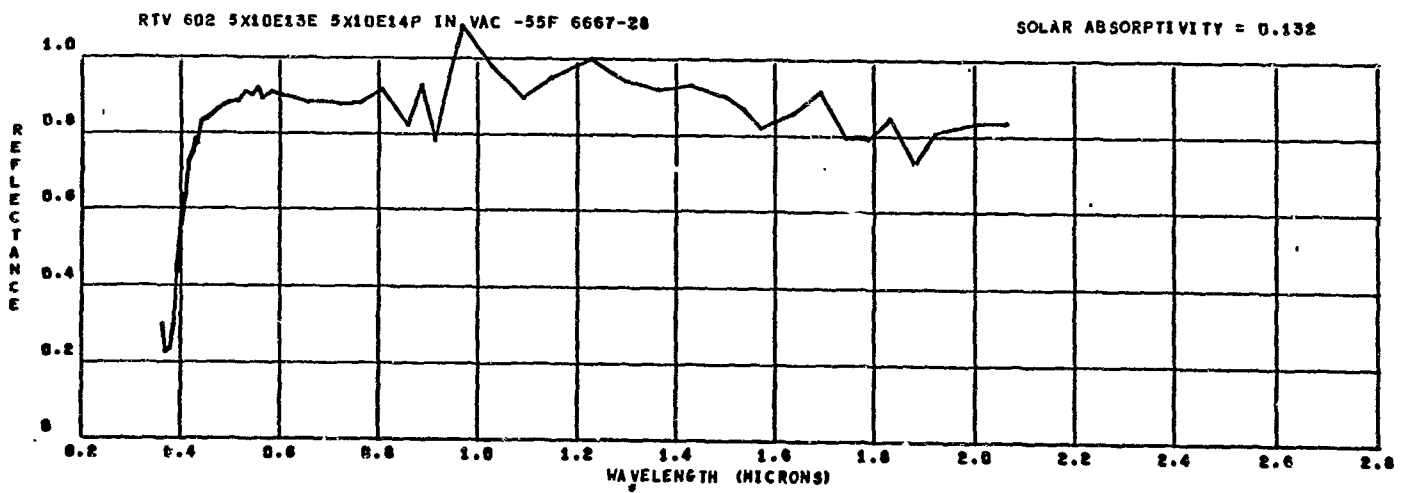
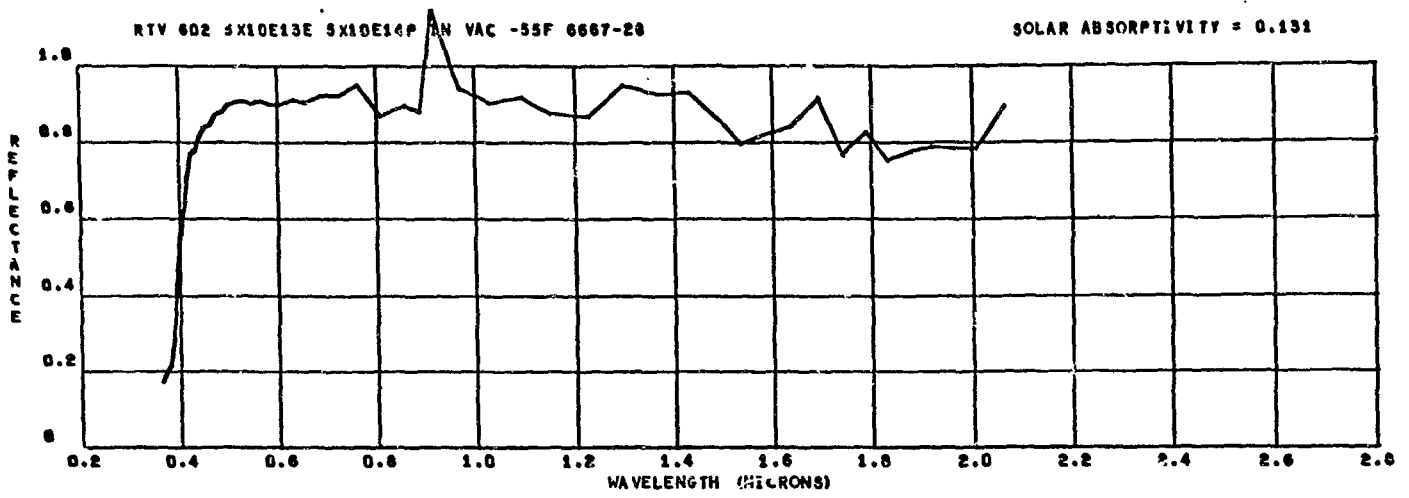
SOLAR ABSORPTIVITY = 0.164

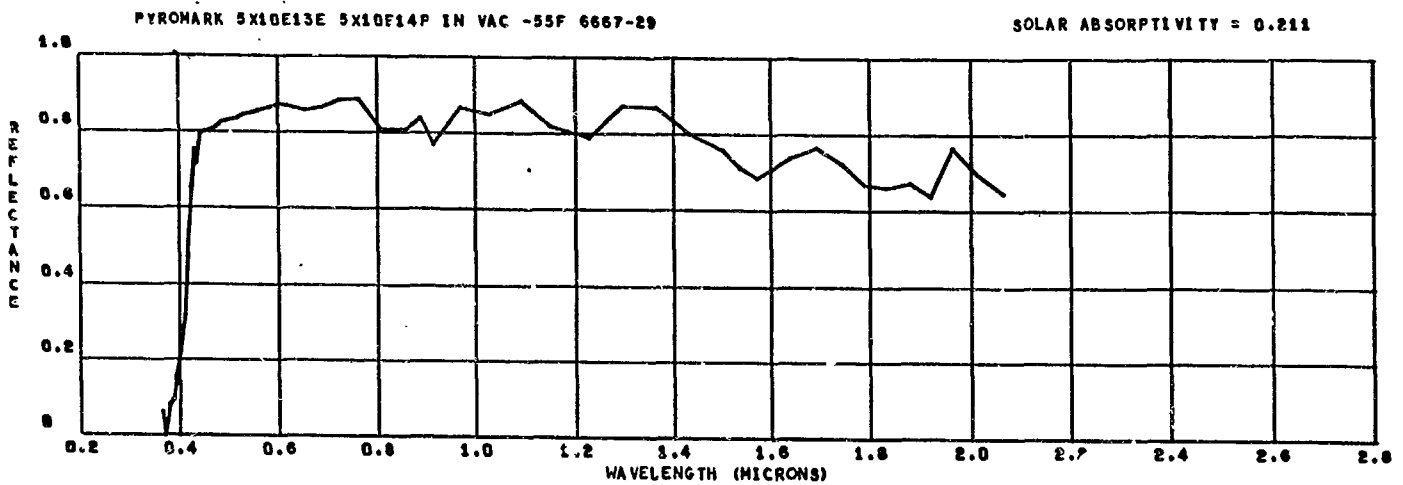
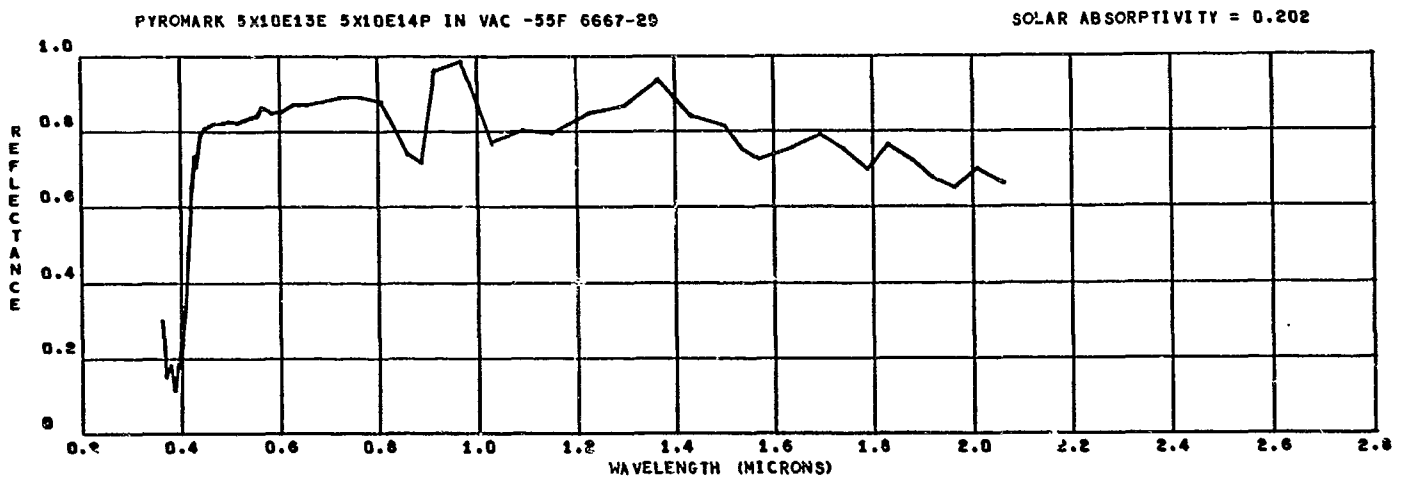
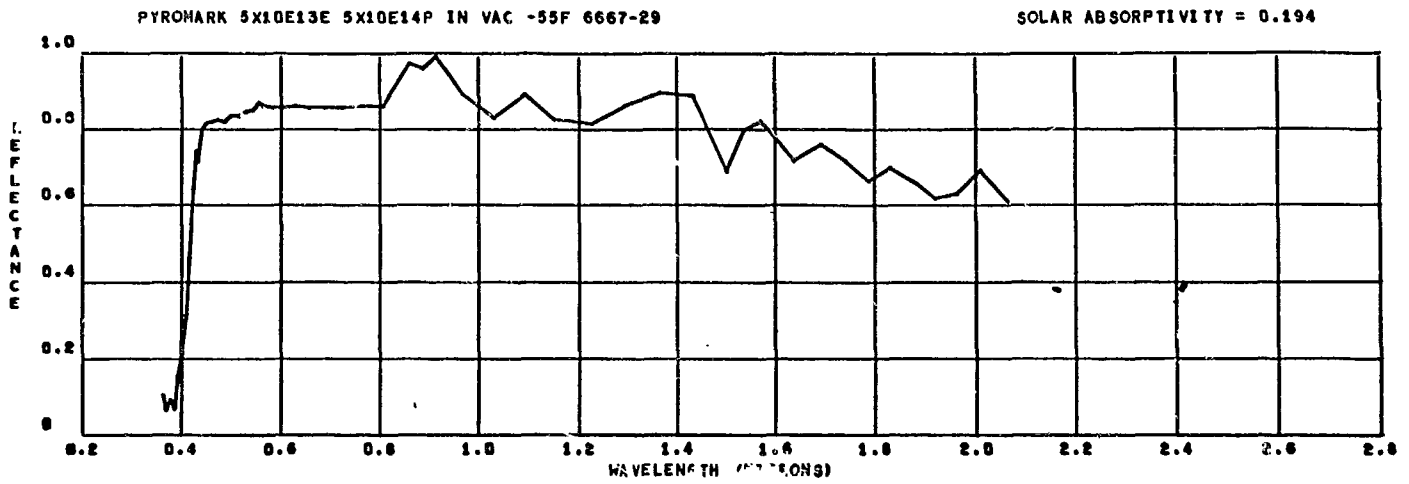


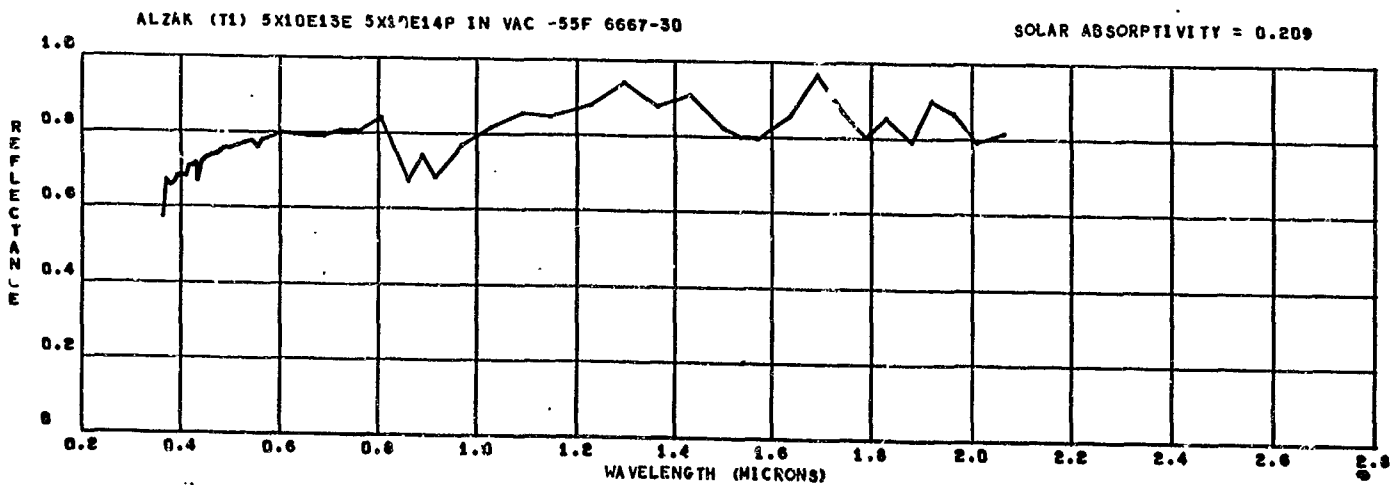
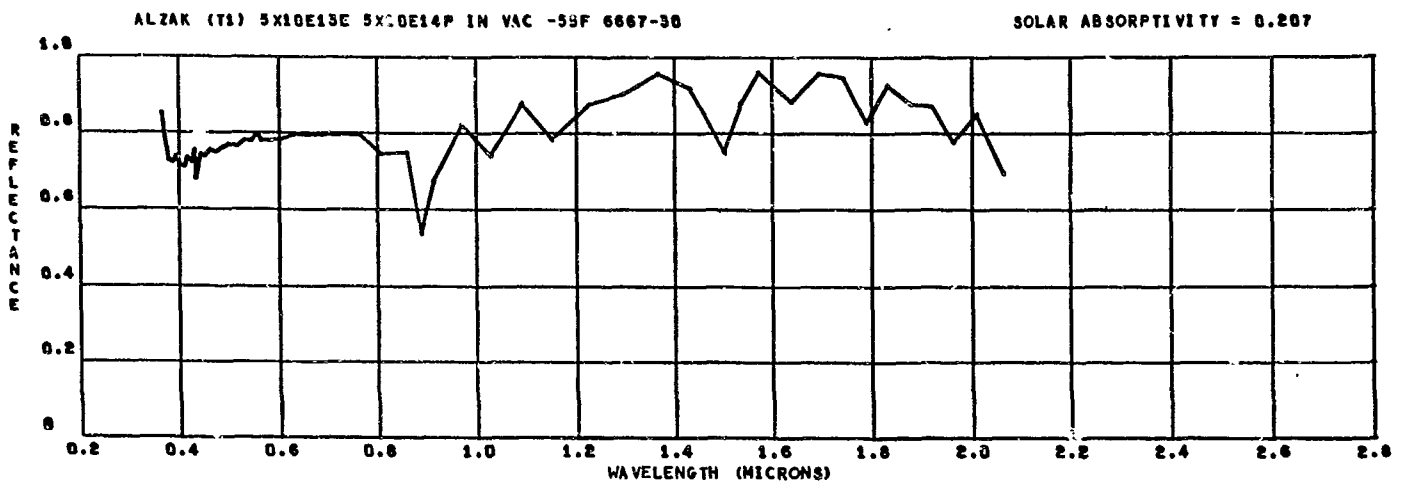
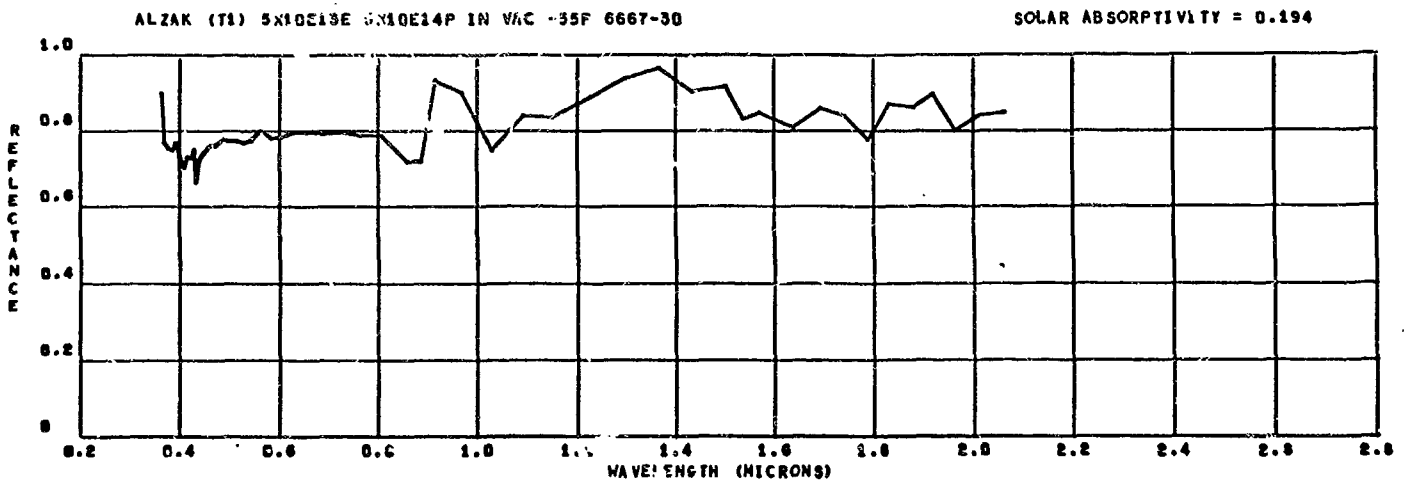
GODDARD WHITE 5X10E13E 5X10E14P IN VAC -55F 6667-27

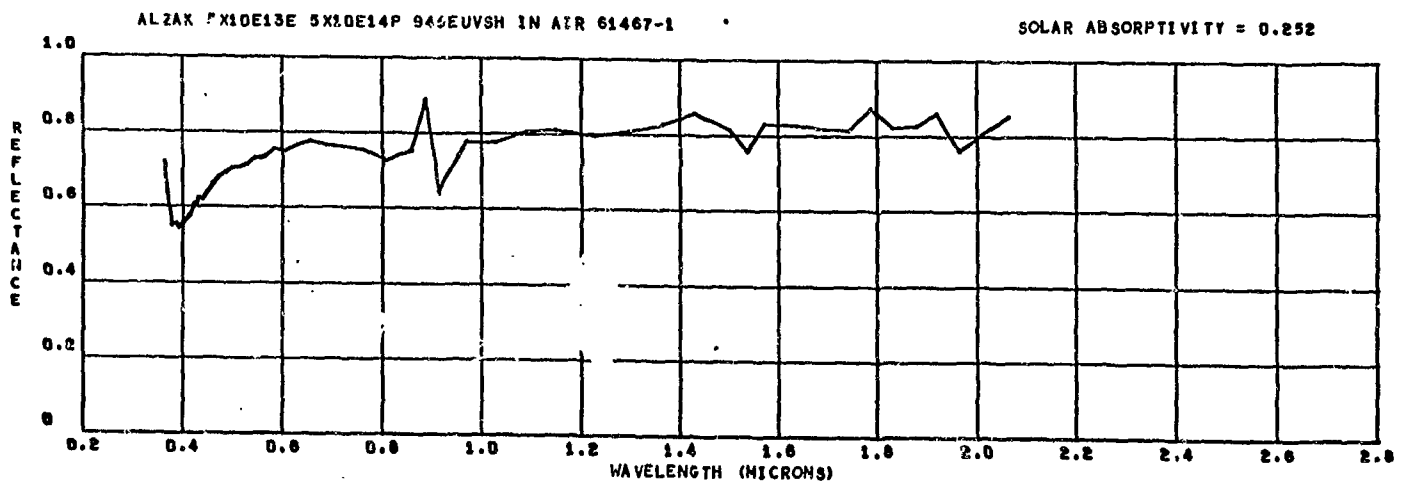
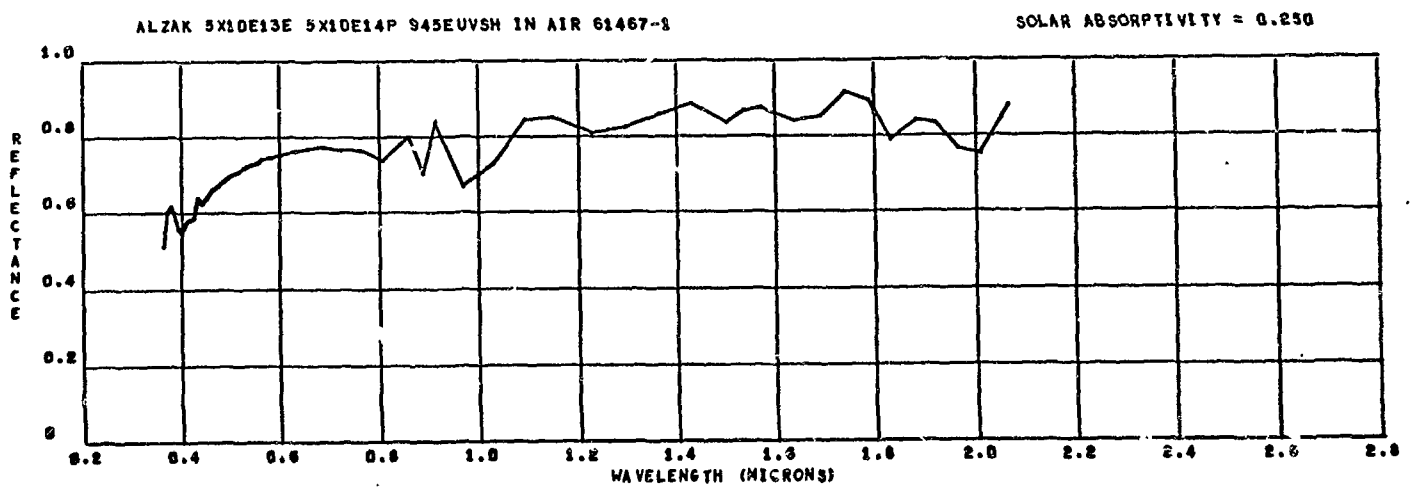
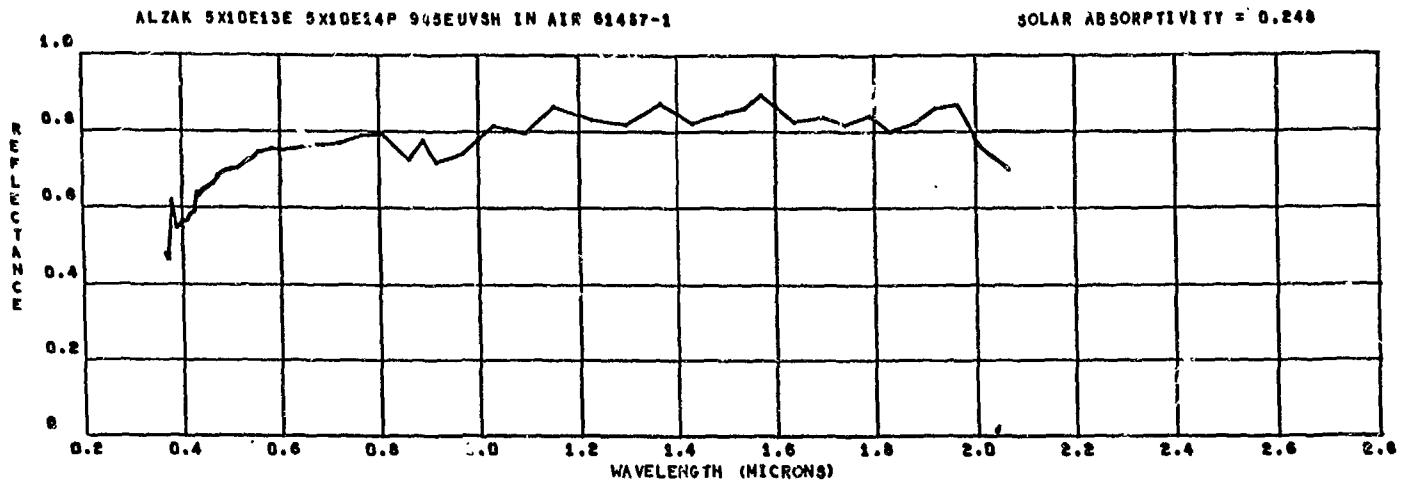
SOLAR ABSORPTIVITY = 0.166

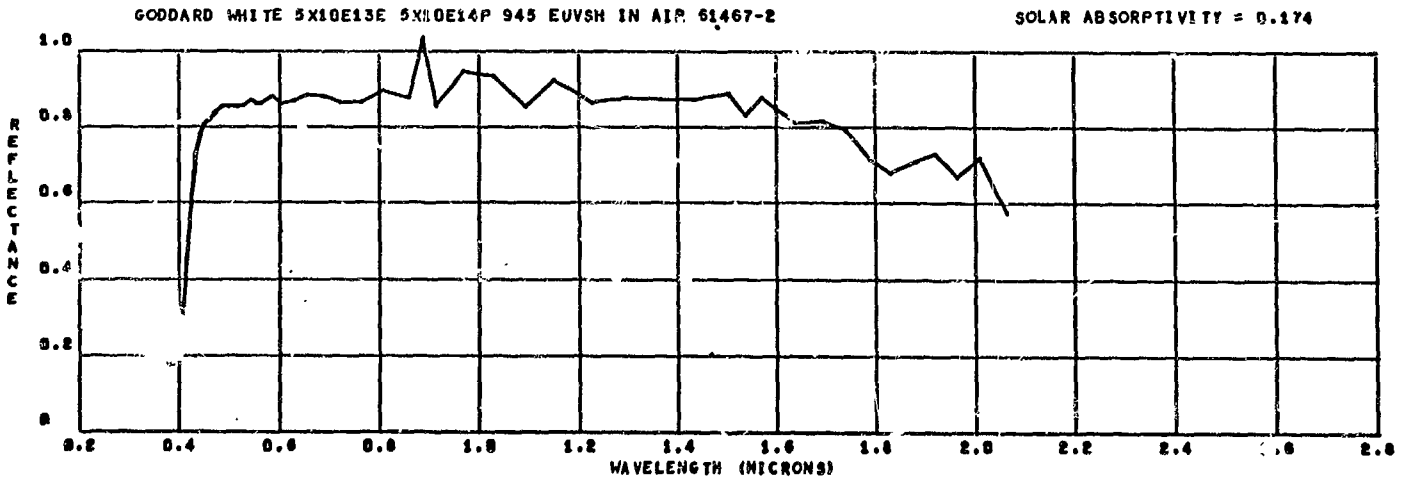
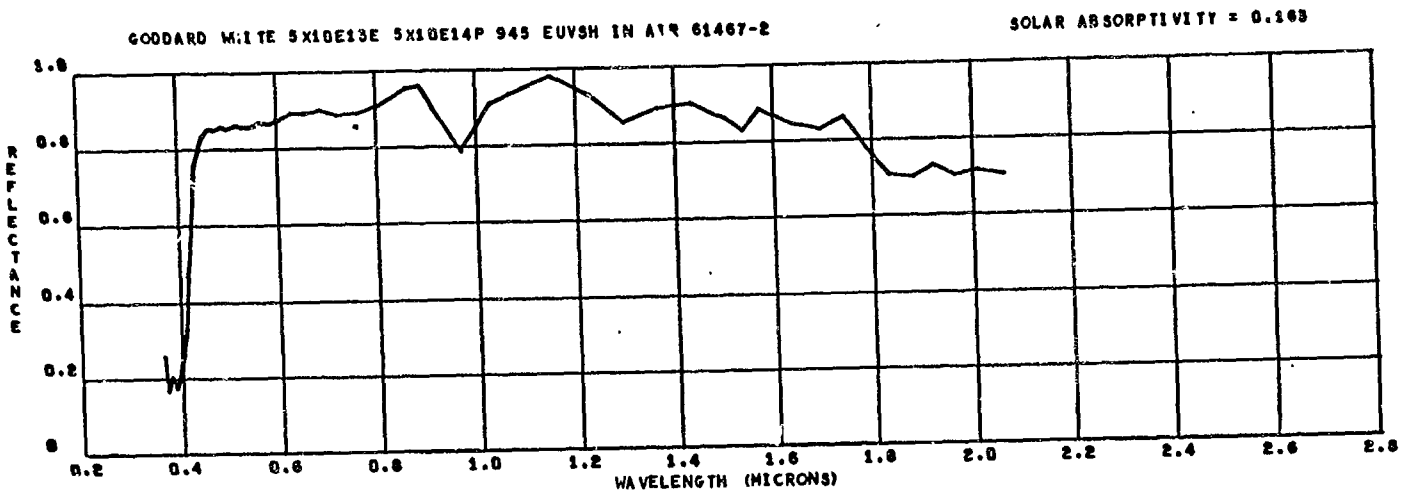
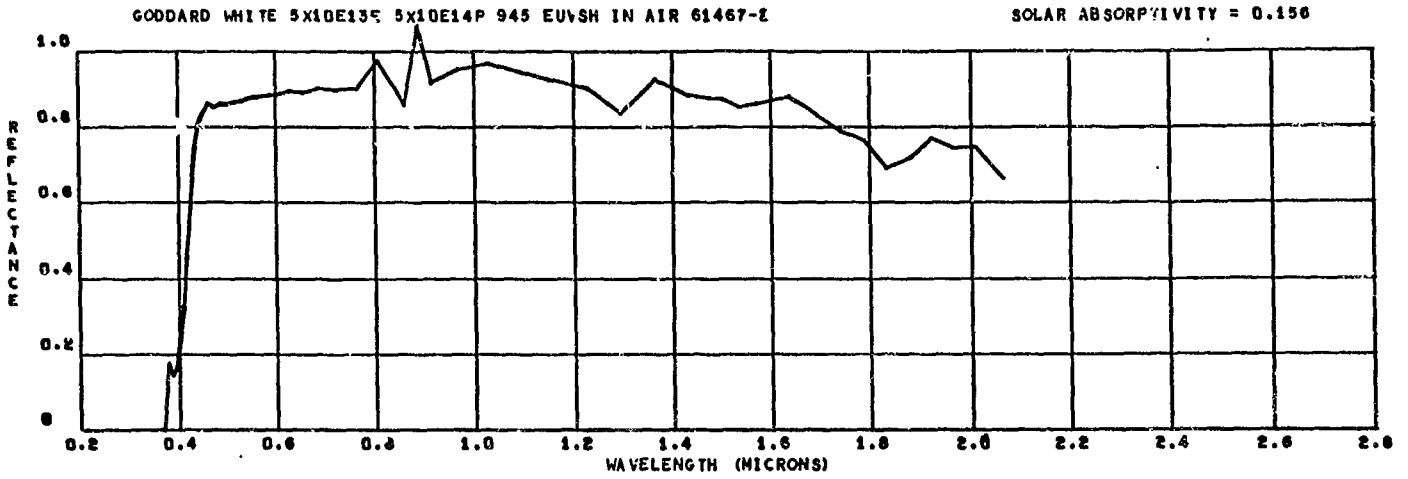


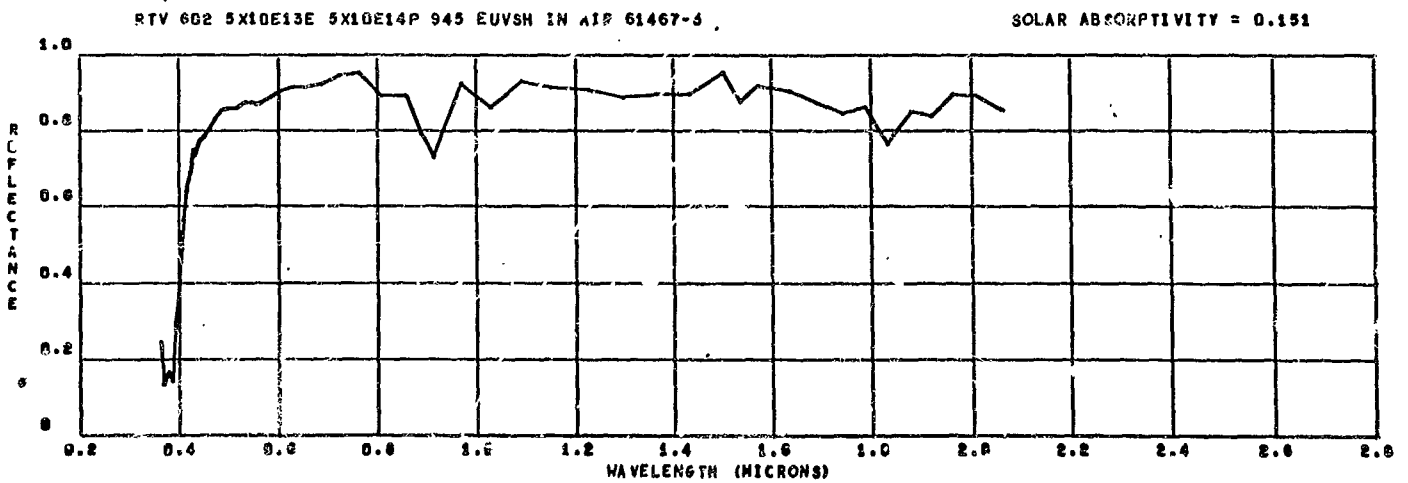
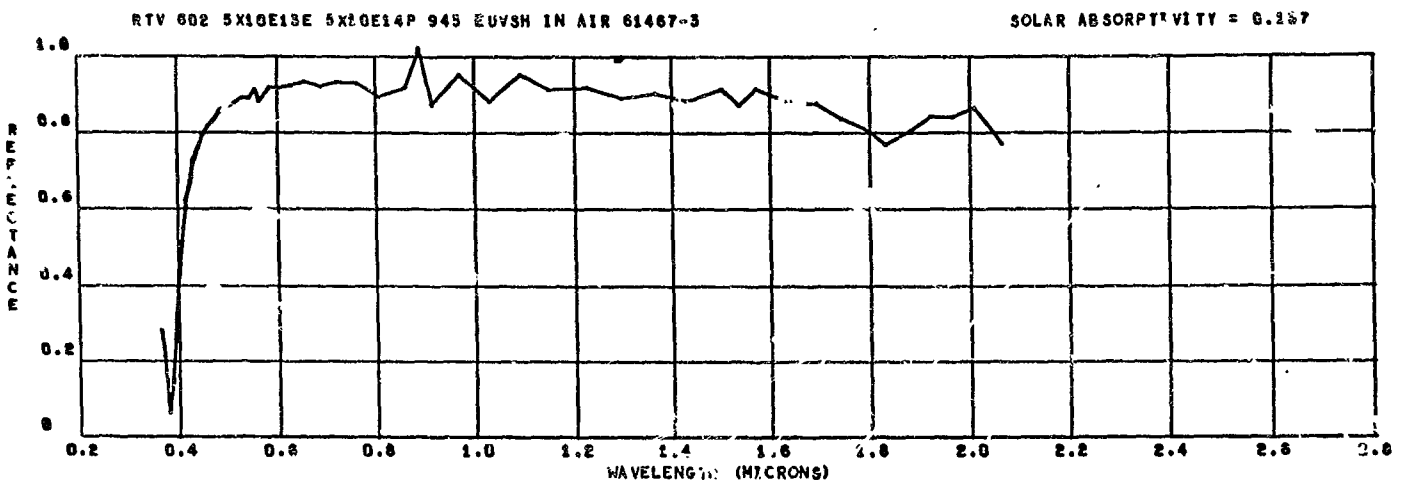
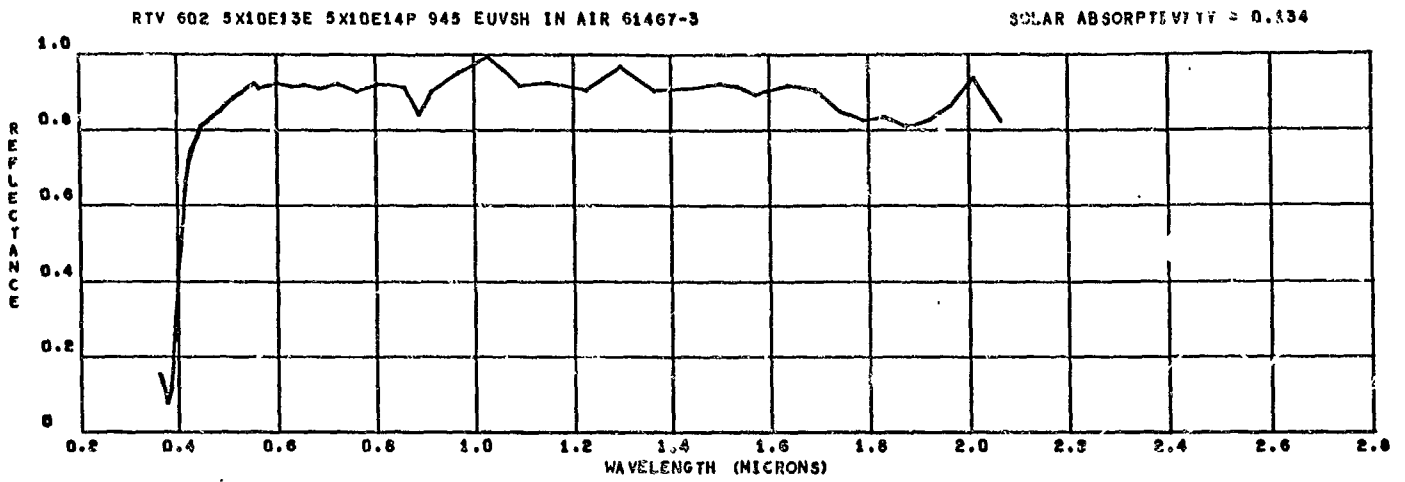


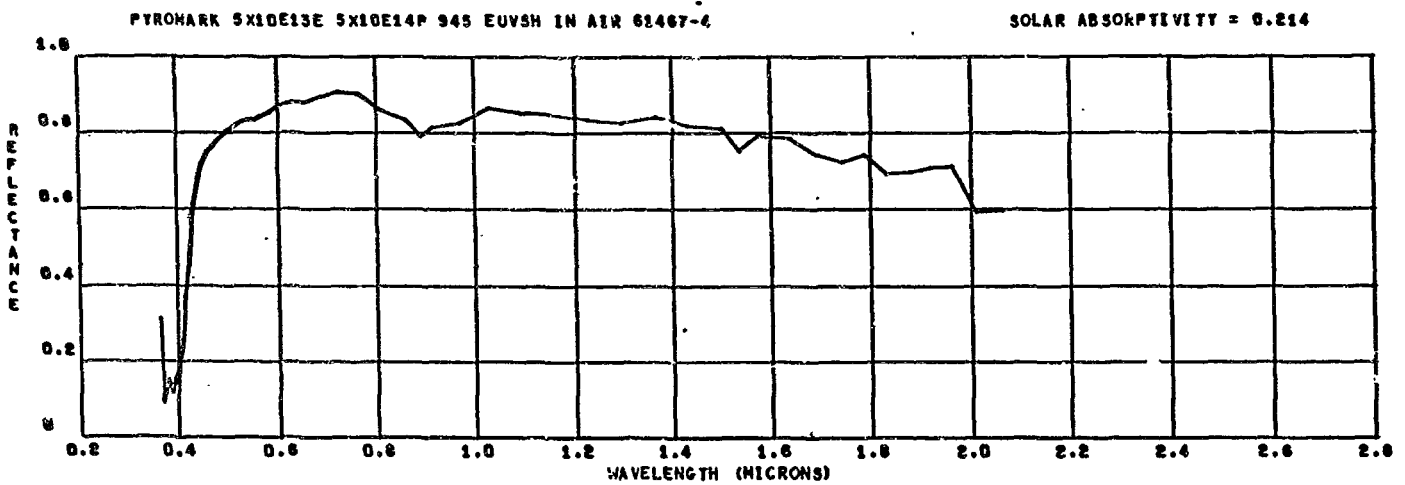
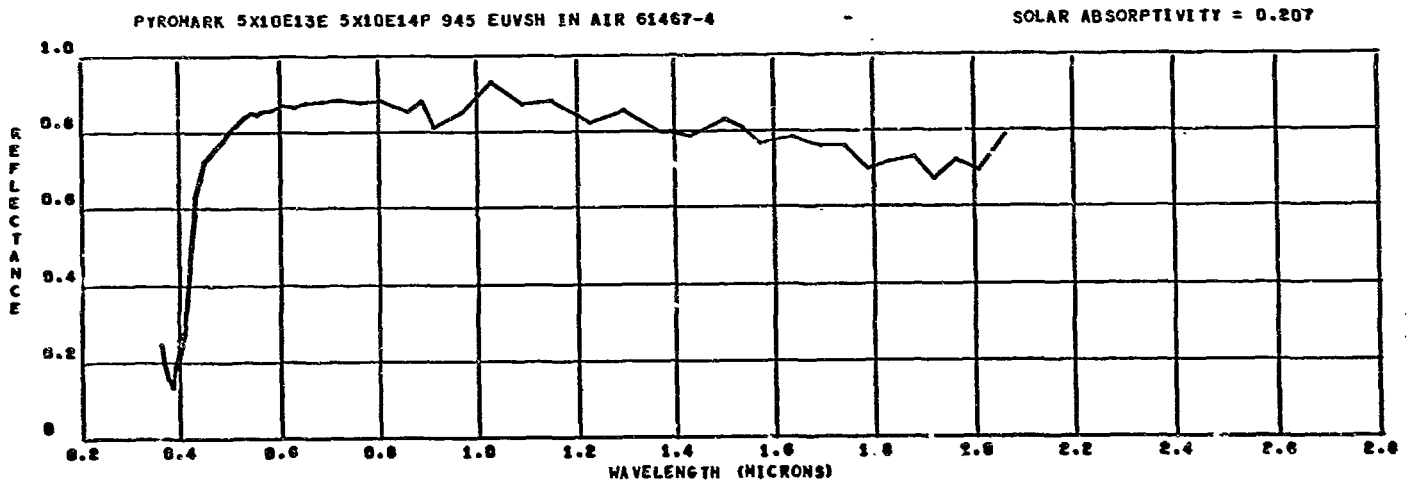
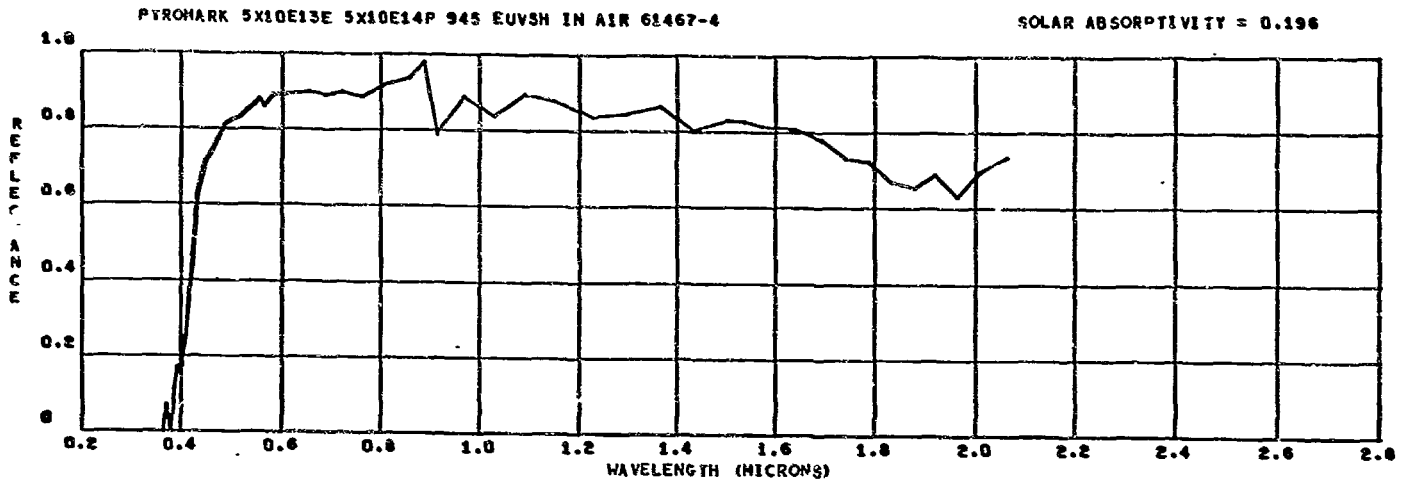






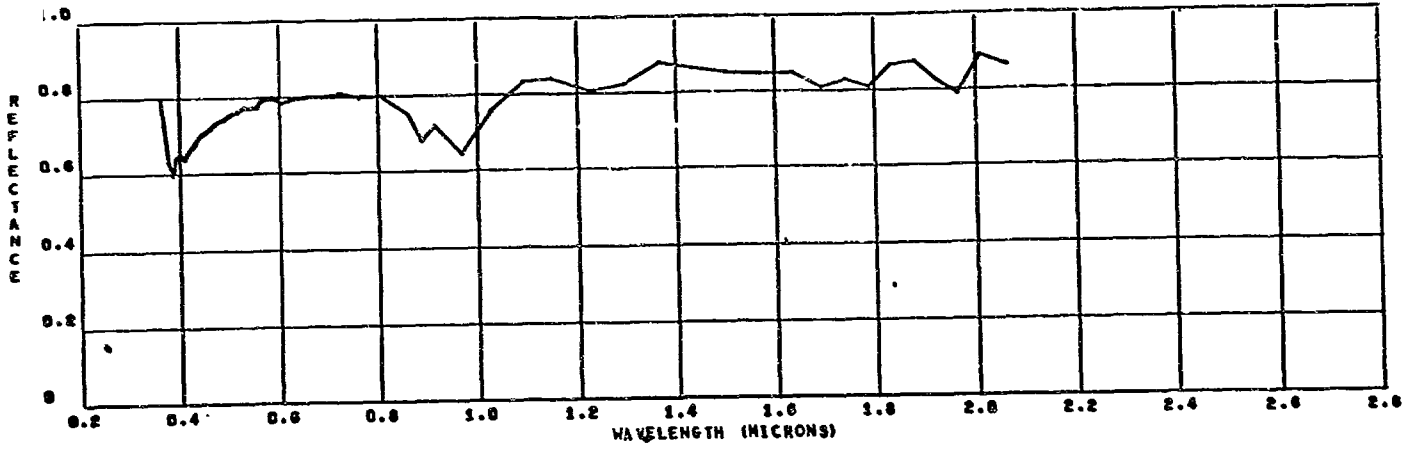






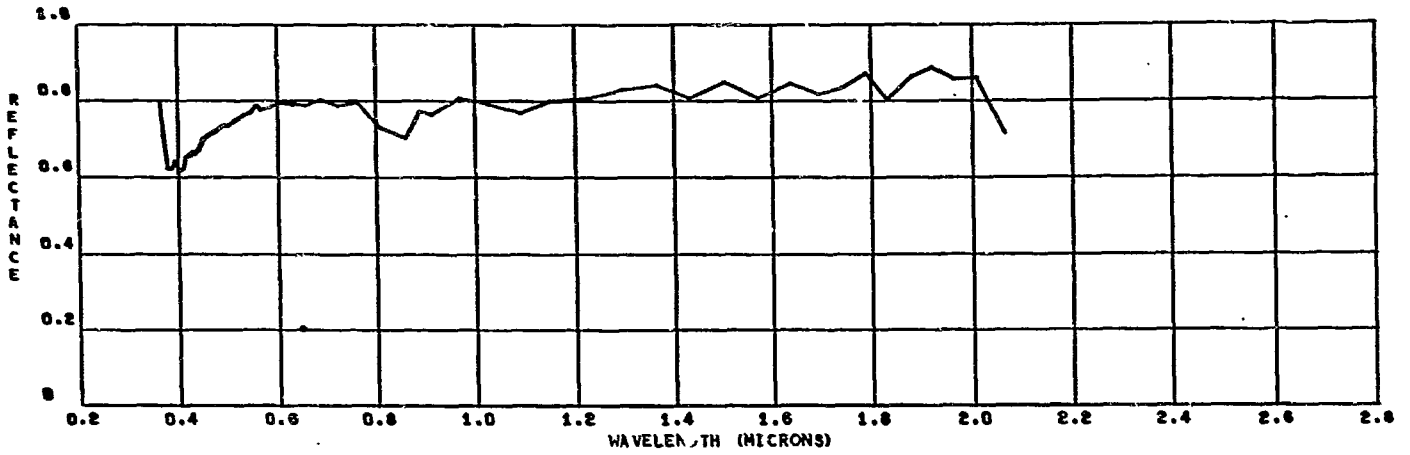
ALZAK (T1) 5X10E13E 5X10E14P 945 EUVSH IN AIR 61467-5

SOLAR ABSORPTIVITY = 0.224



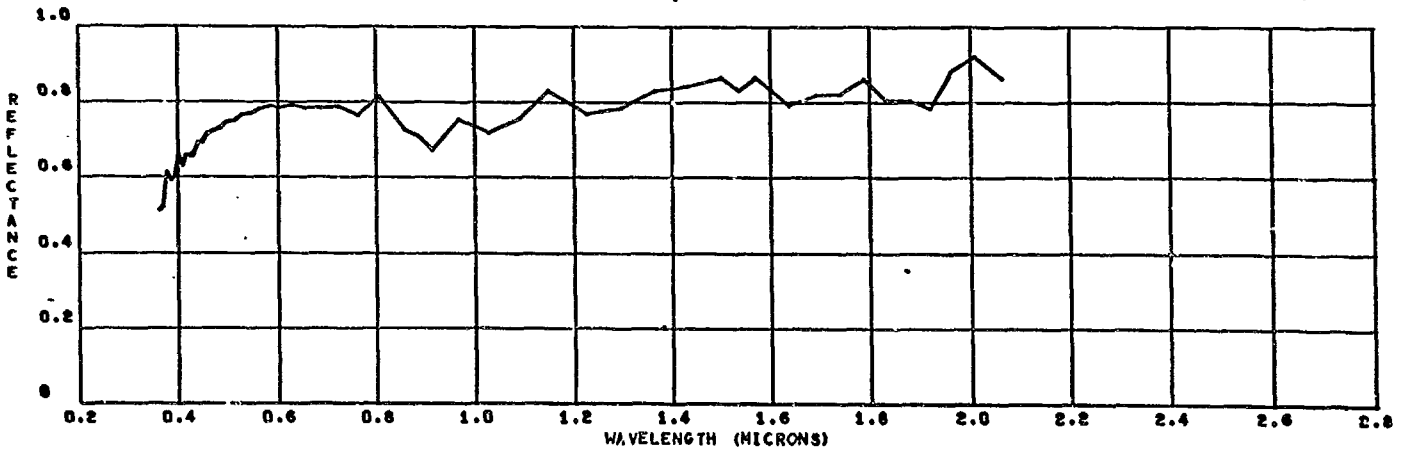
ALZAK (T1) 5X10E13E 5X10E14P 945 EUVSH IN AIR 61467-5

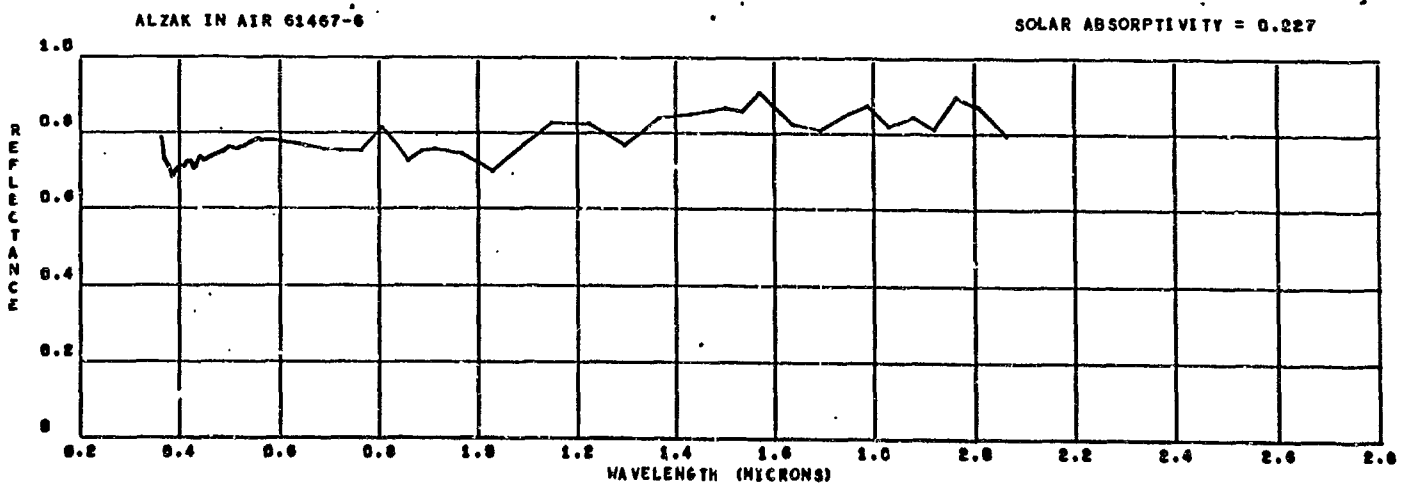
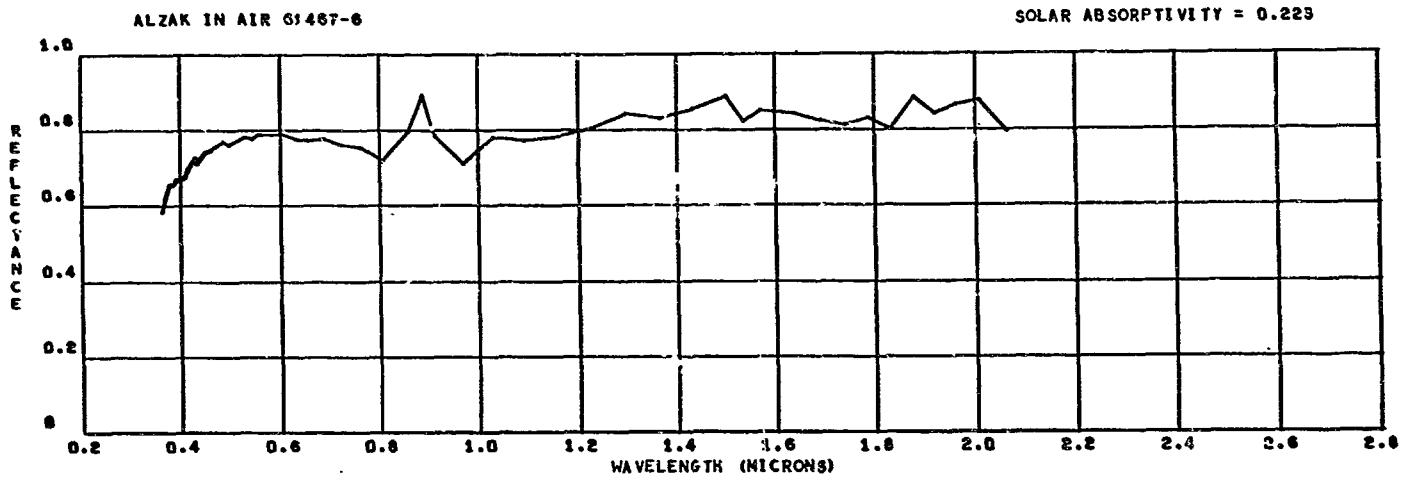
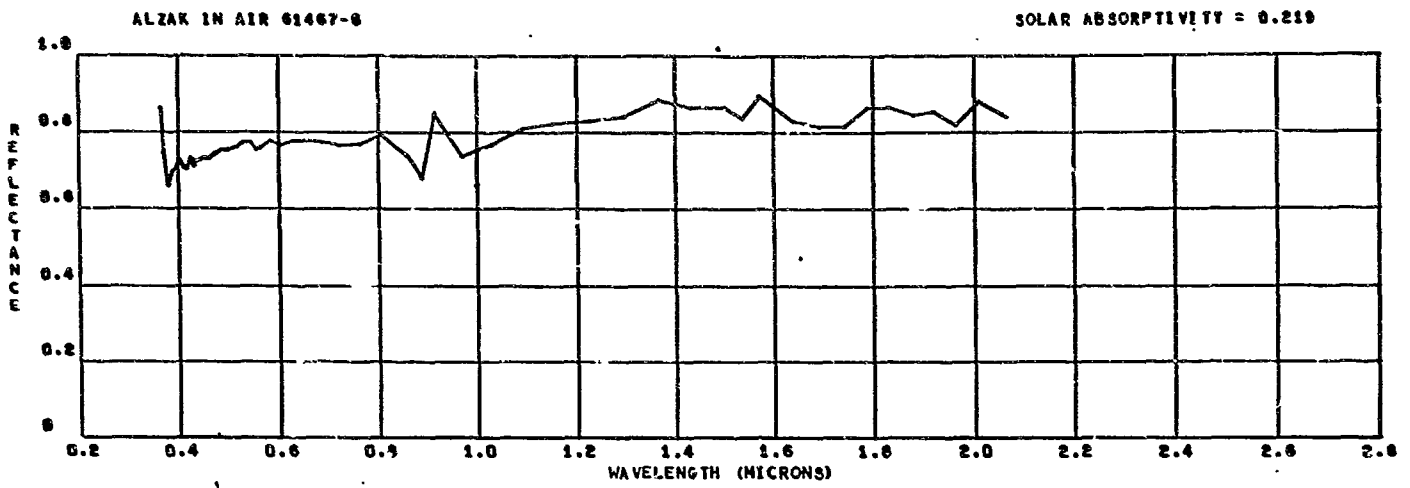
SOLAR ABSORPTIVITY = 0.229

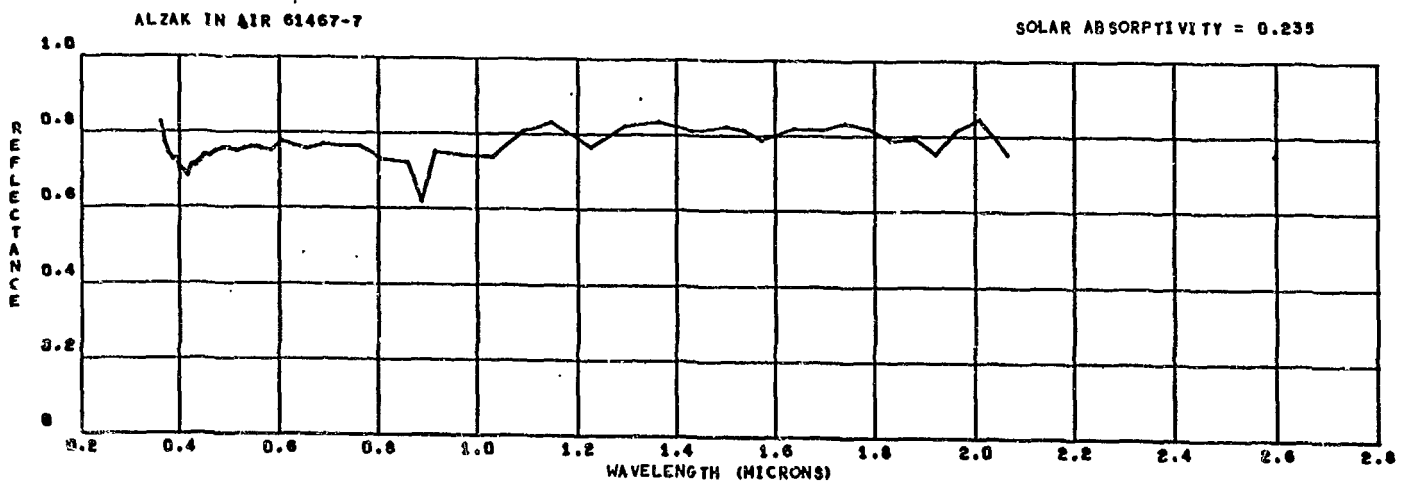
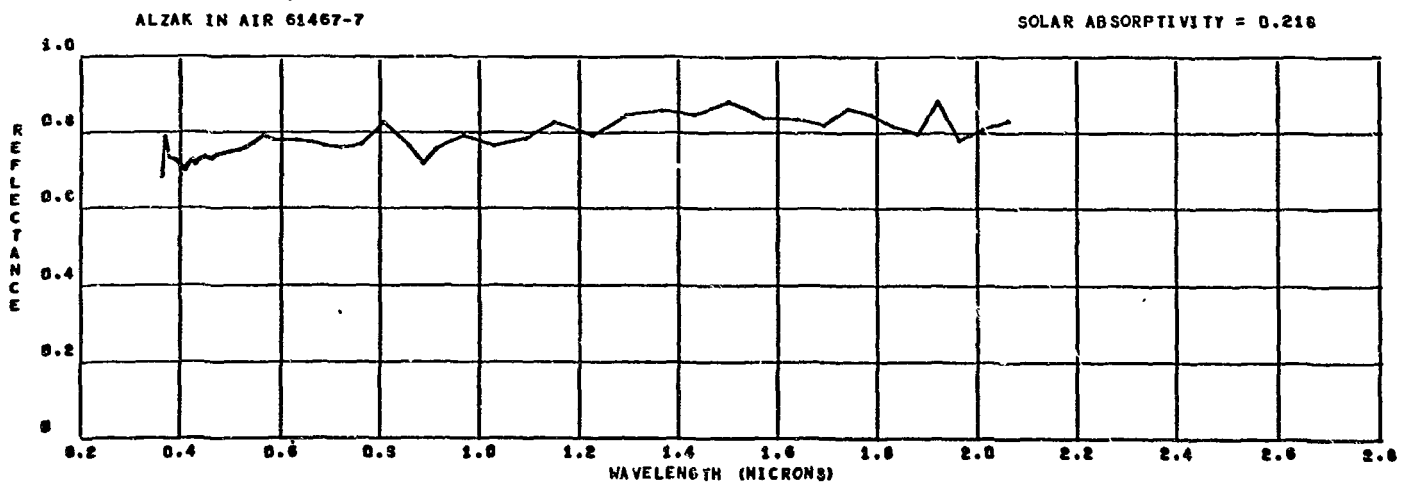
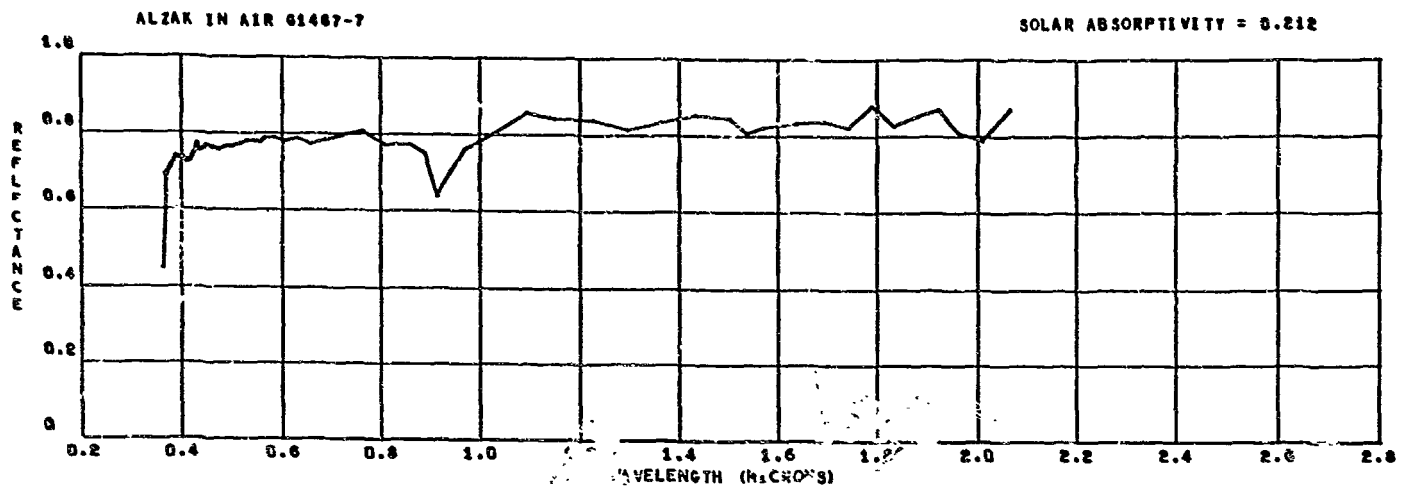


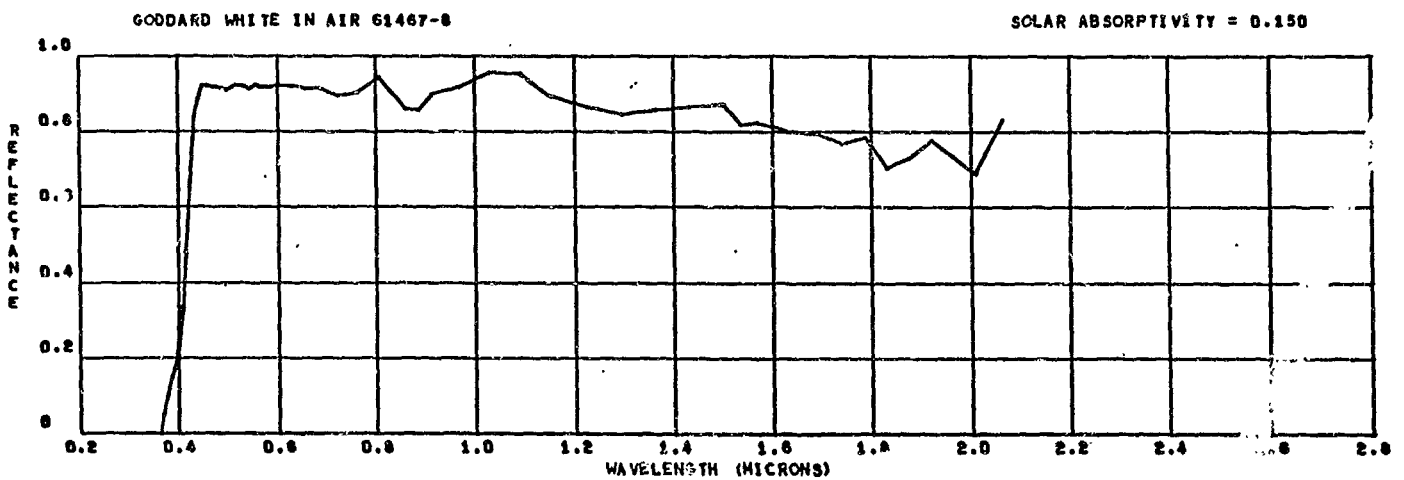
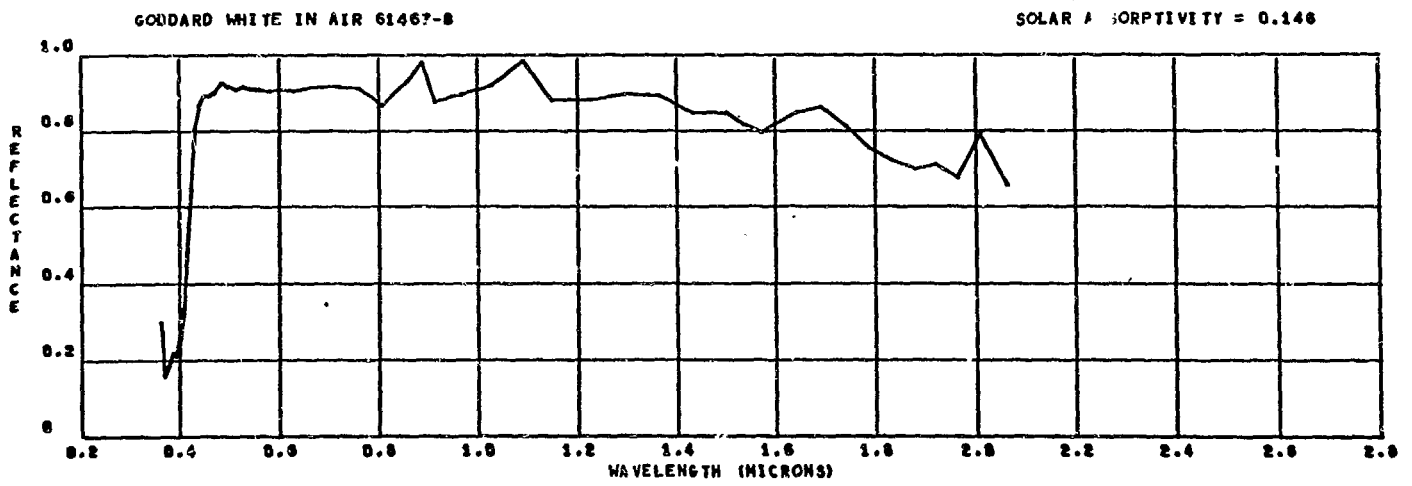
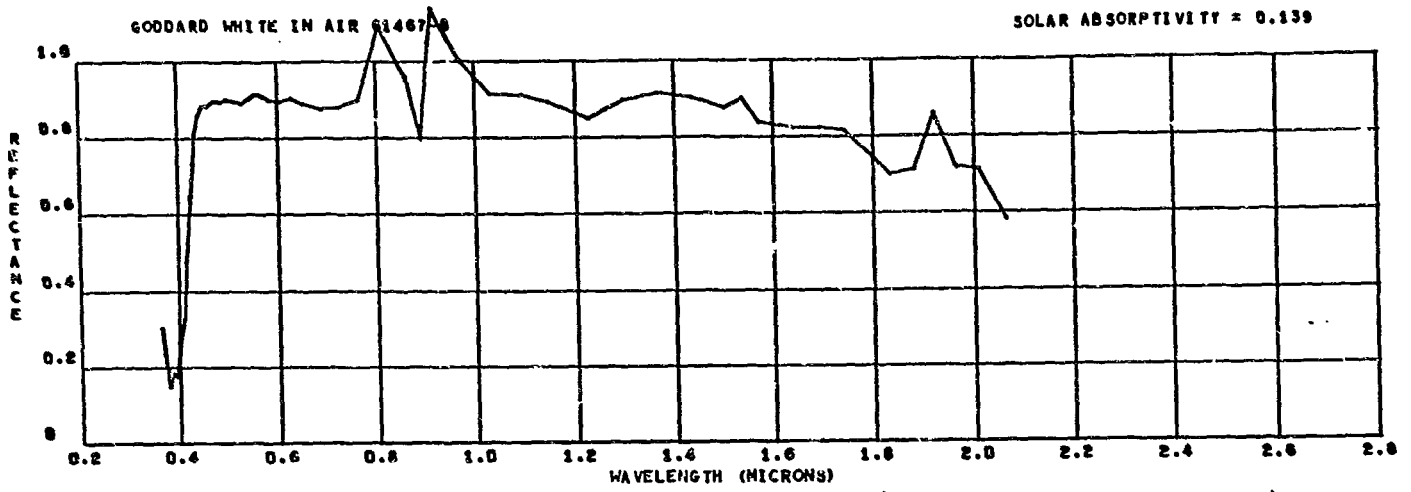
ALZAK (T1) 5X10E13E 5X10E14P 945 EUVSH IN AIR 61467-5

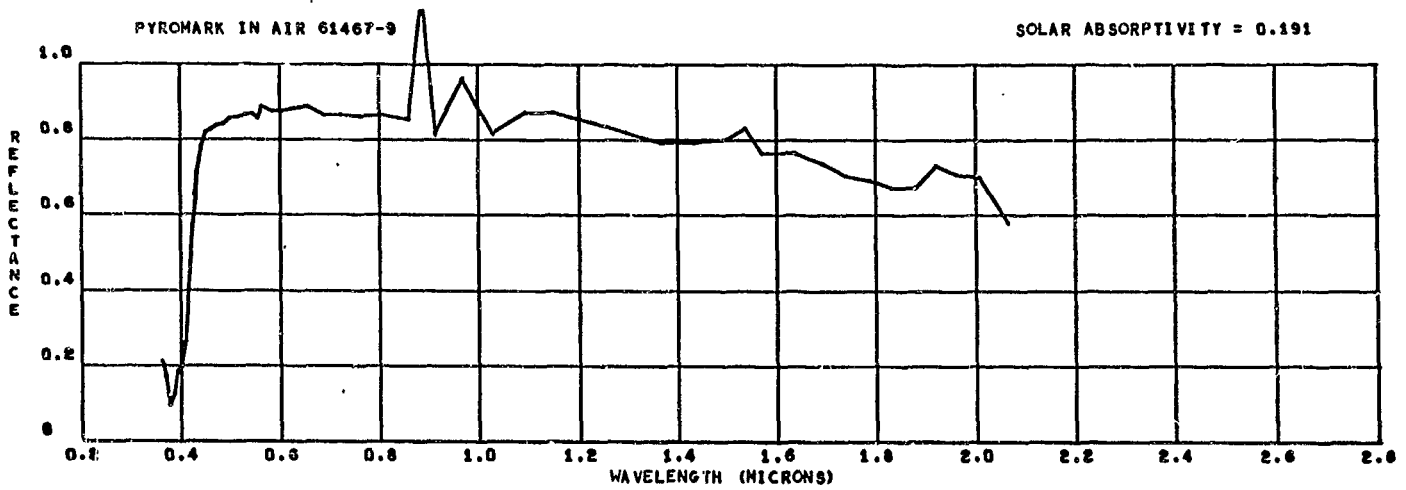
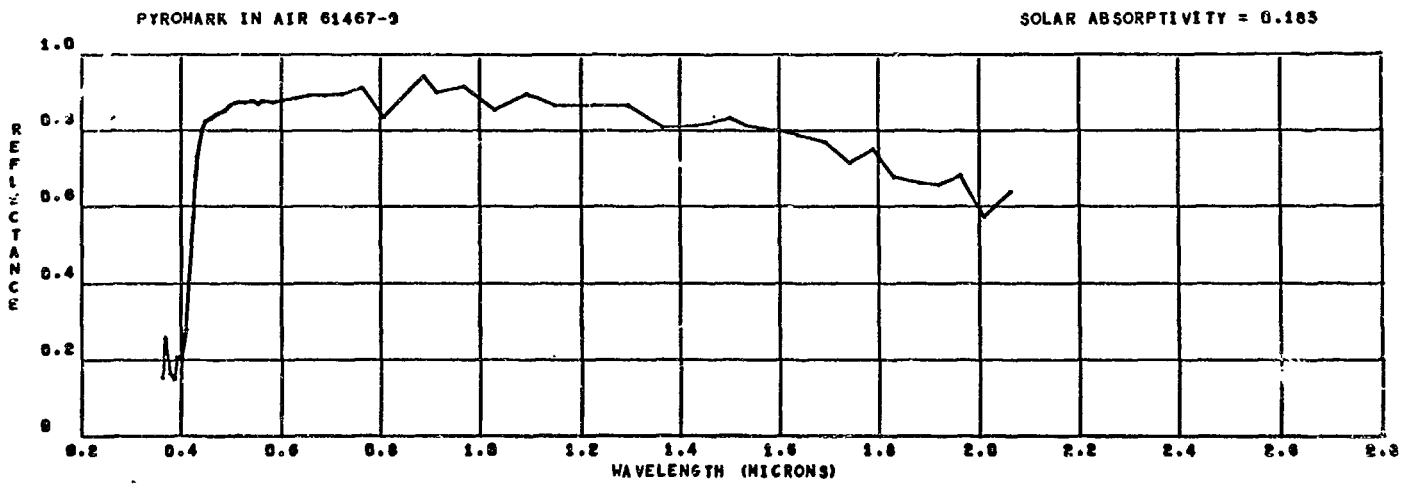
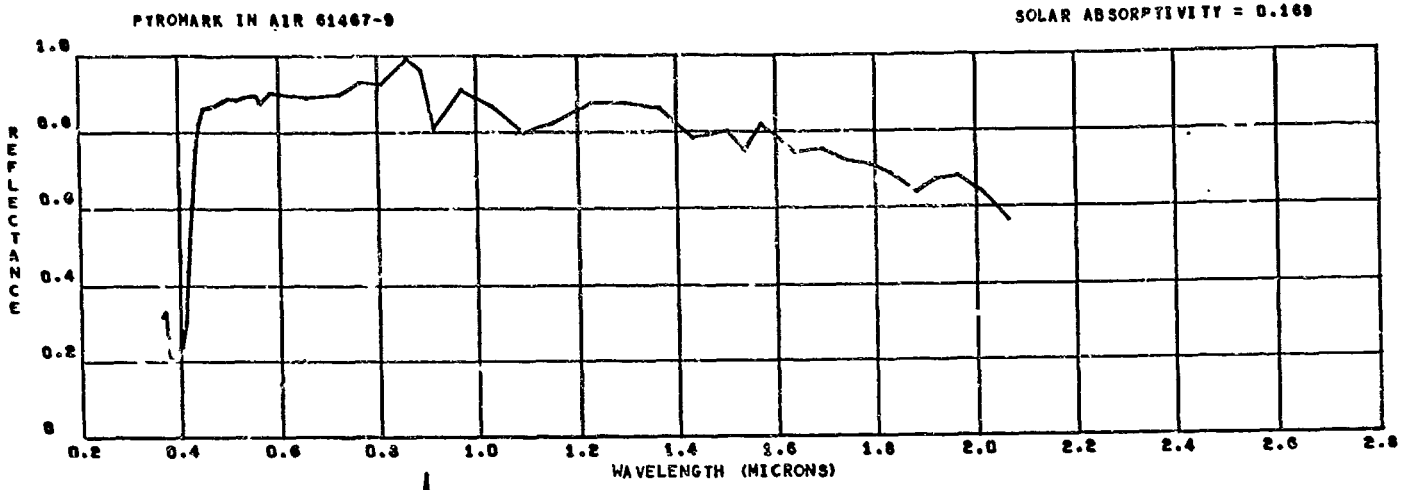
SOLAR ABSORPTIVITY = 0.238

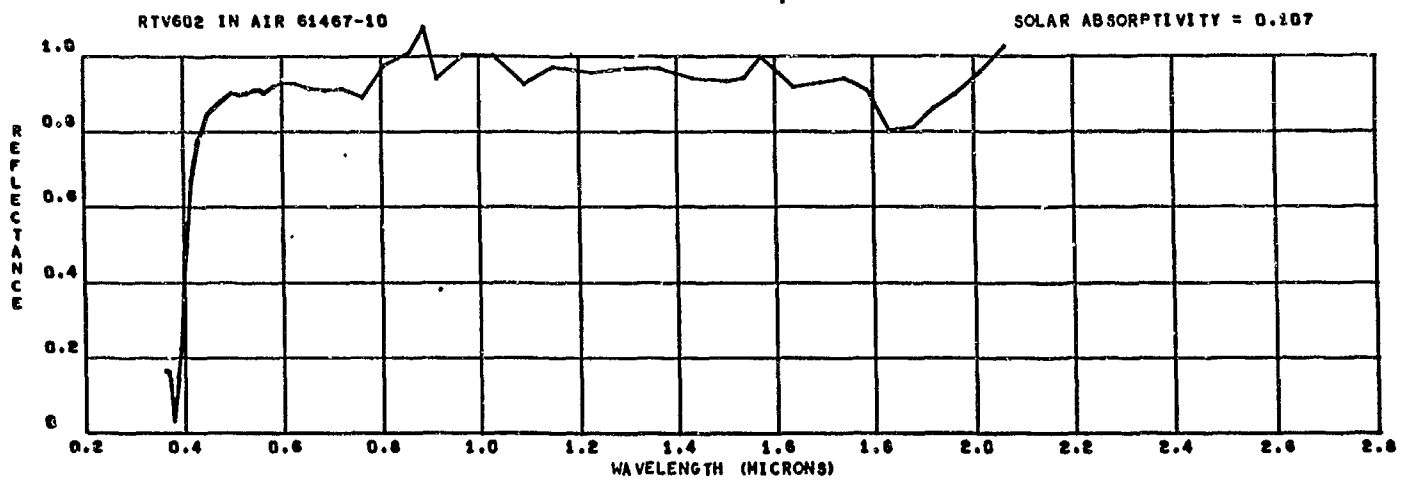
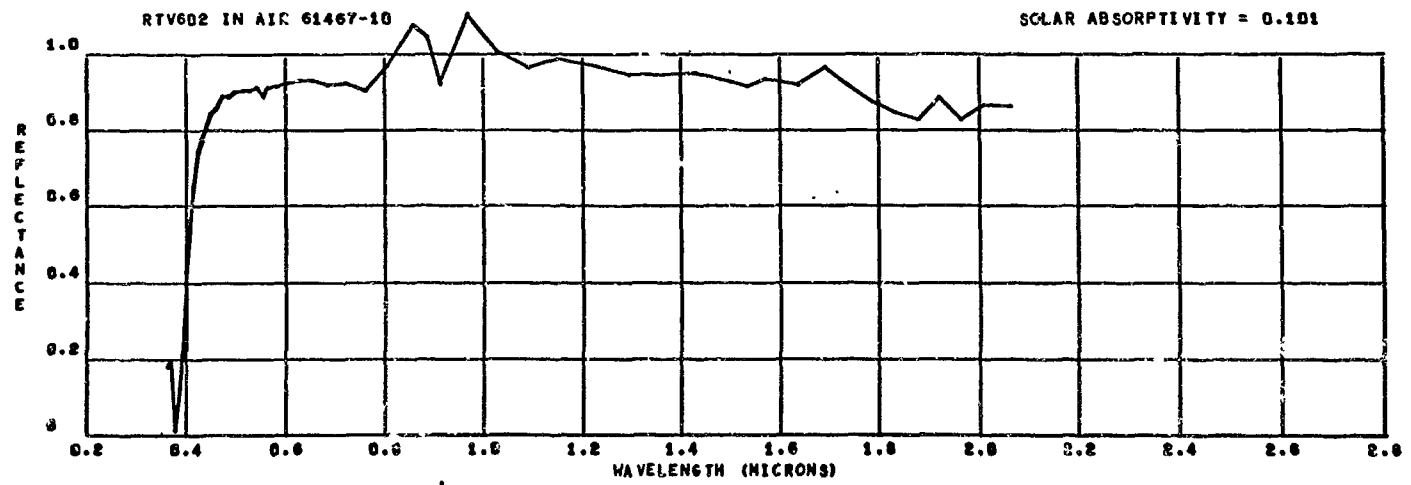
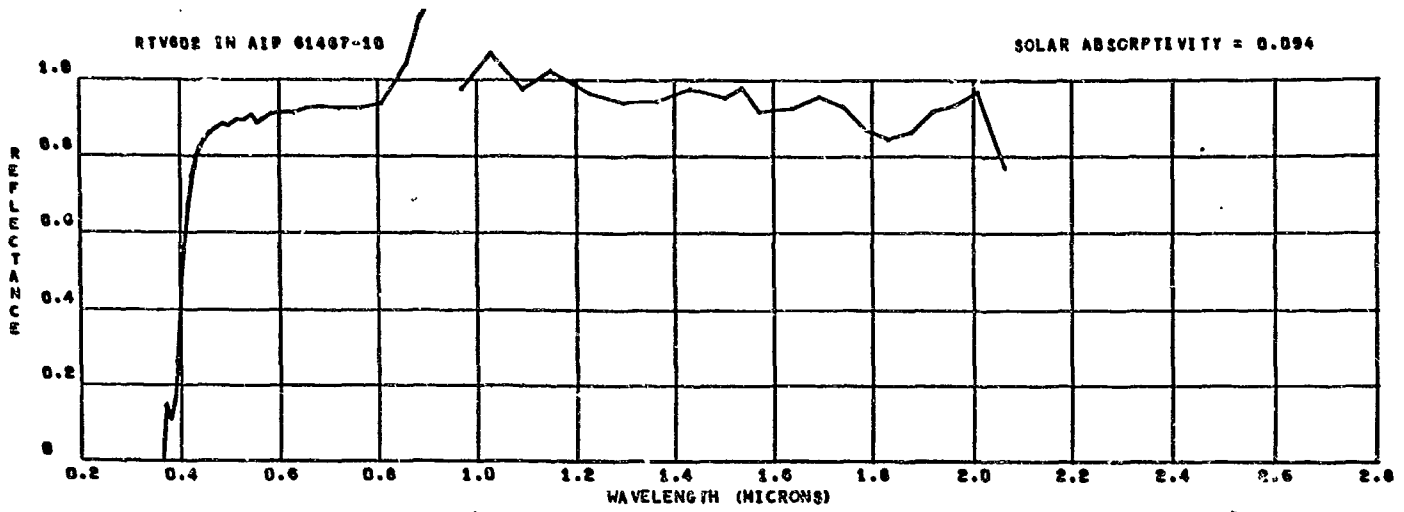


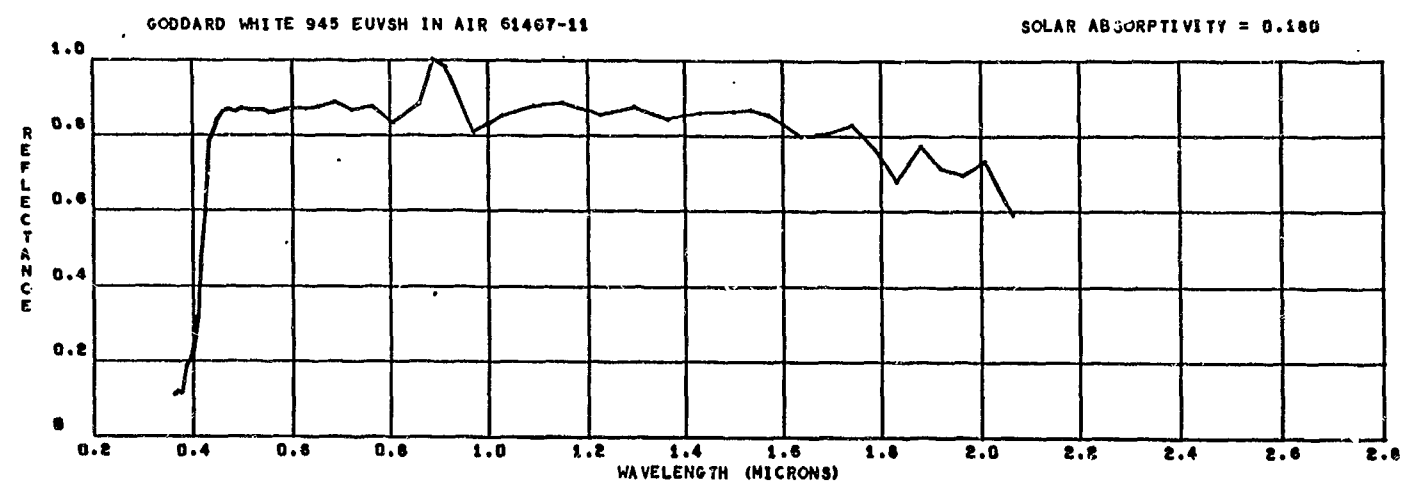
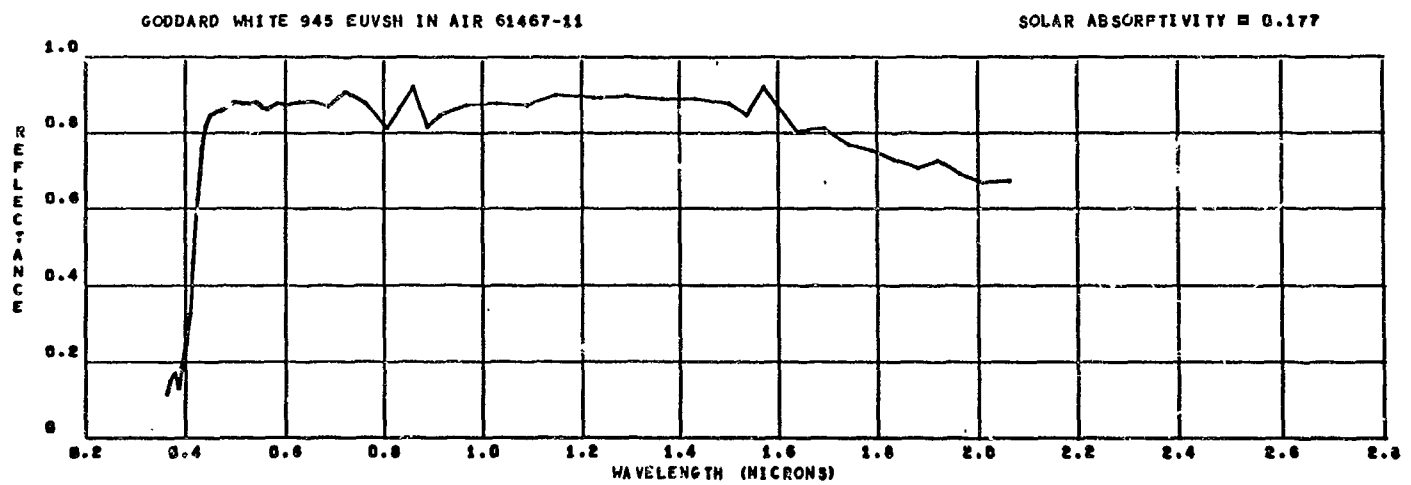
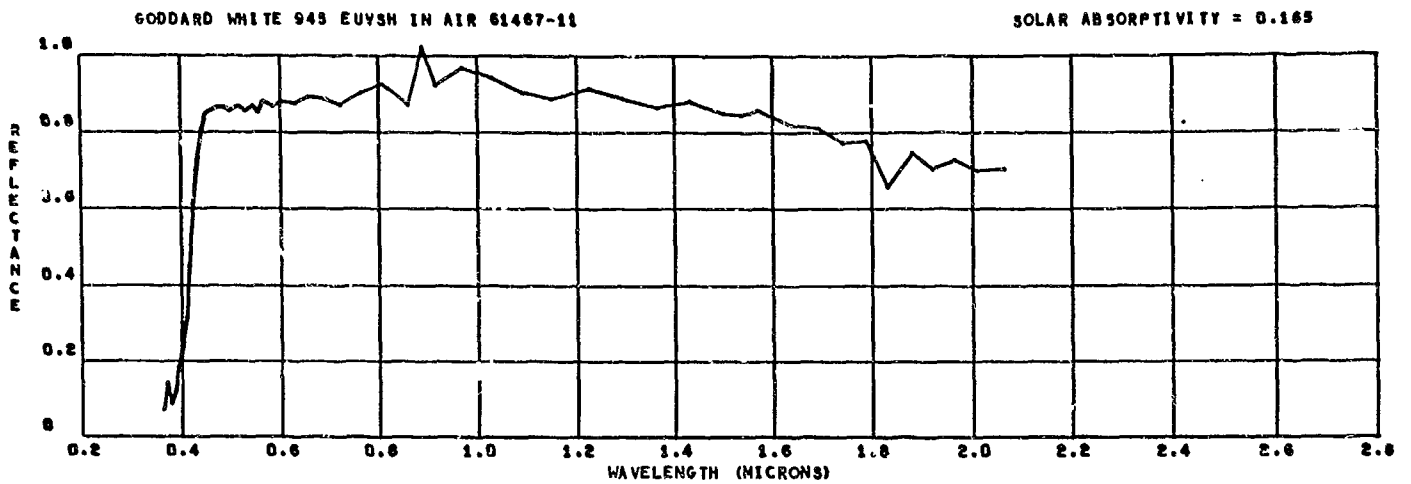


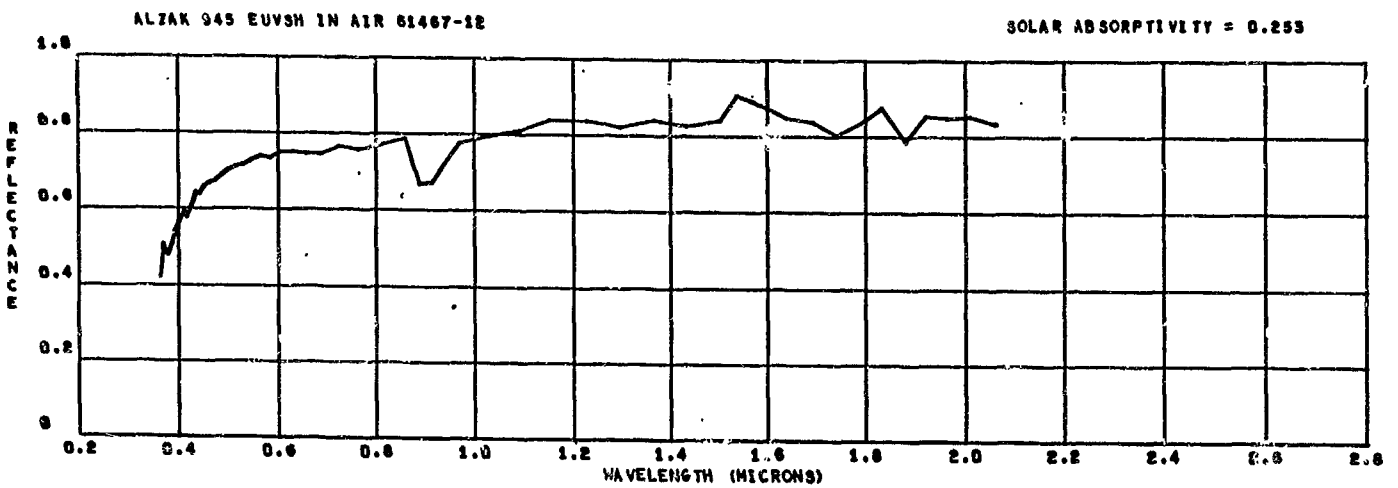
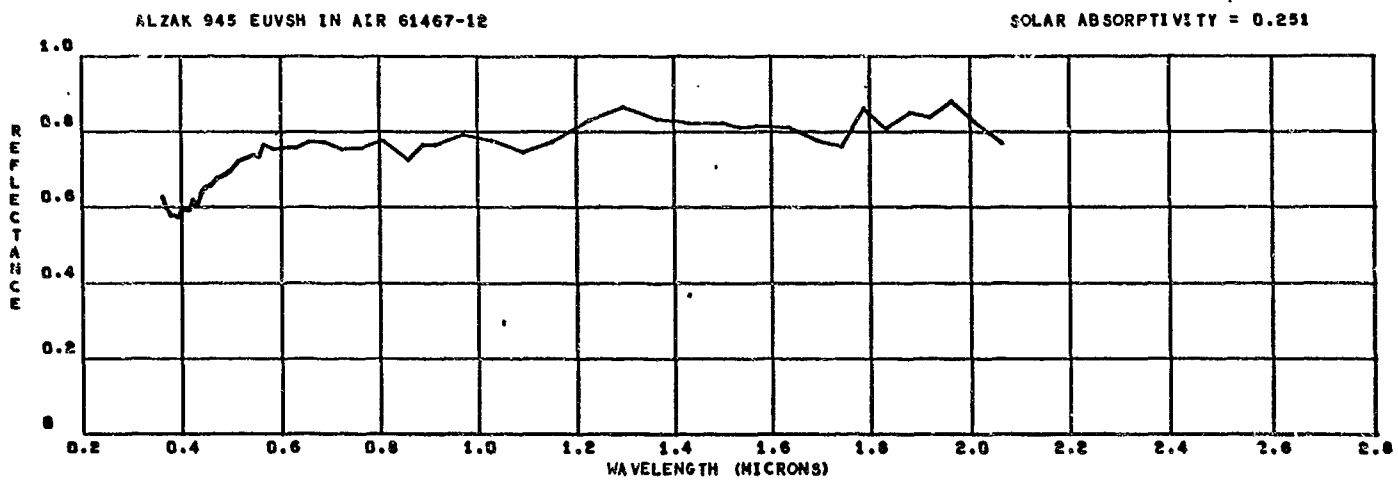
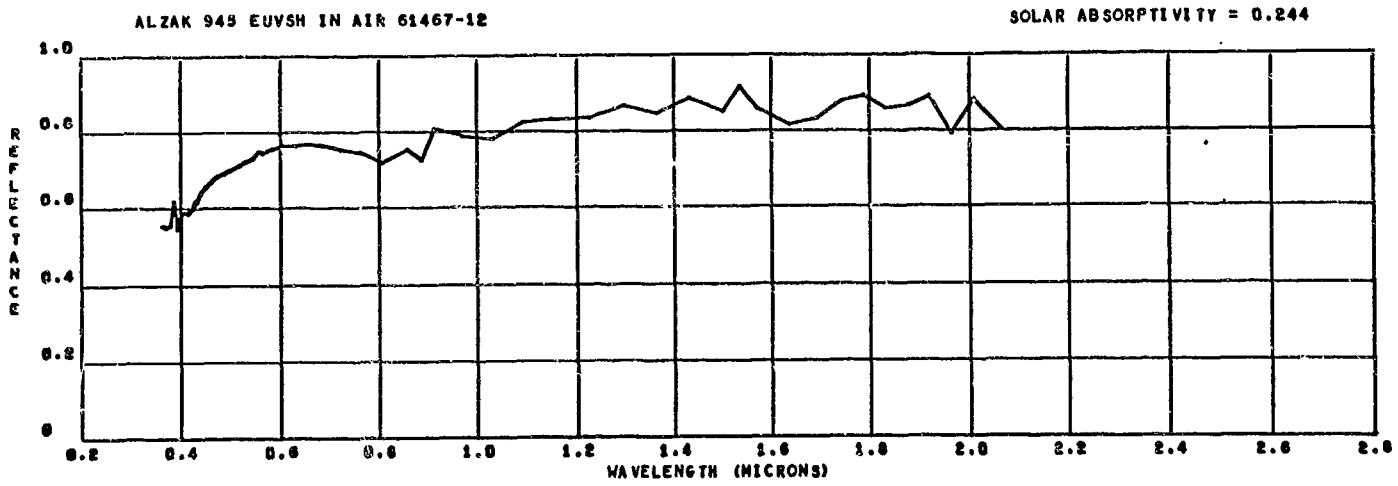


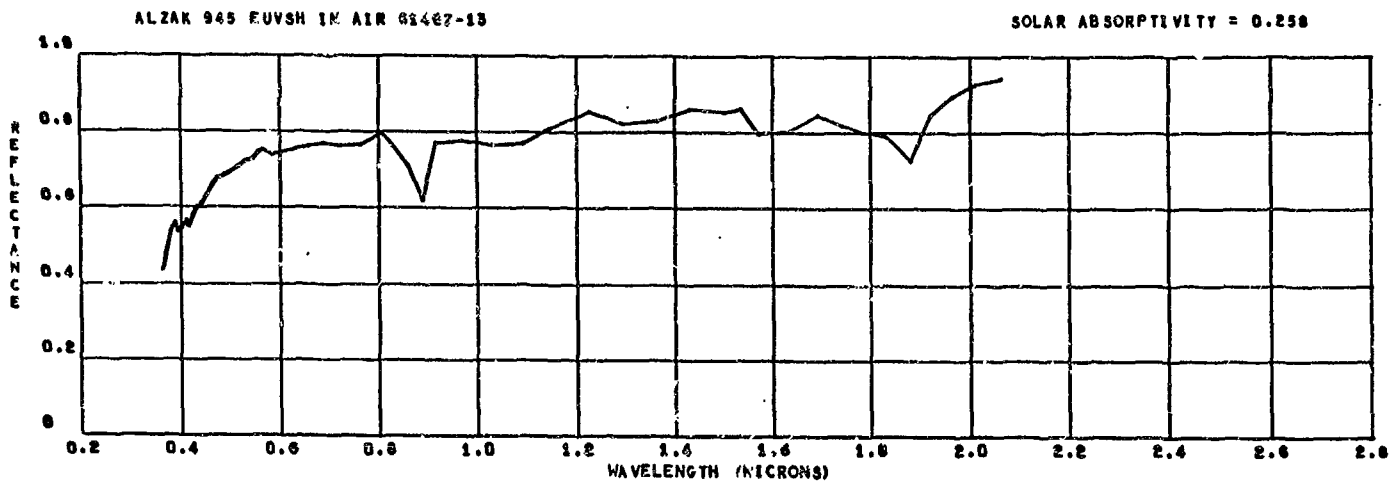
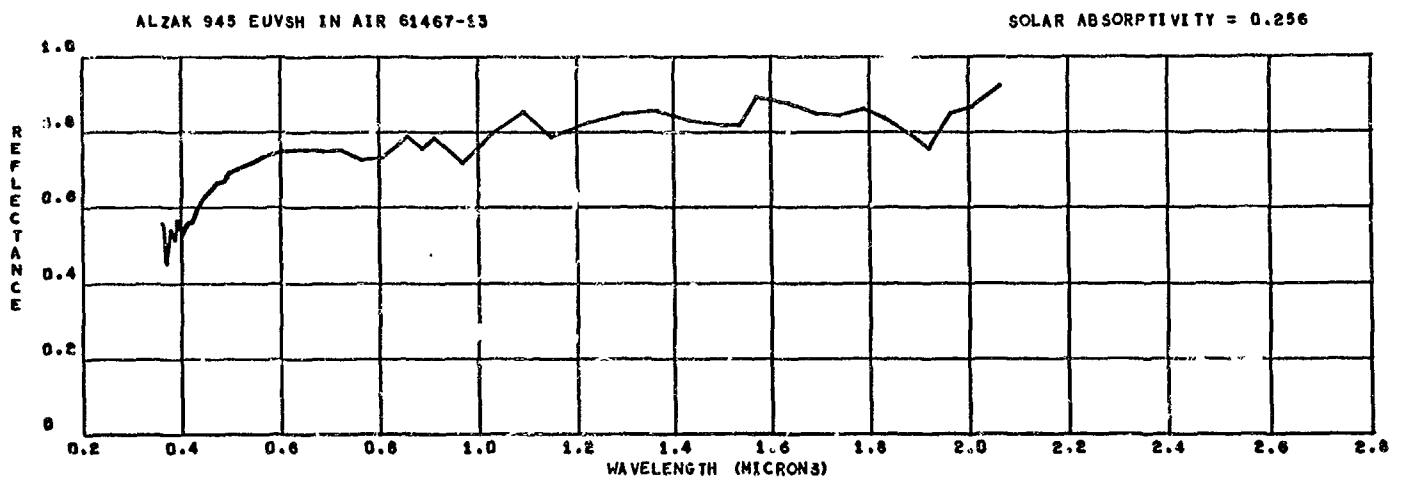
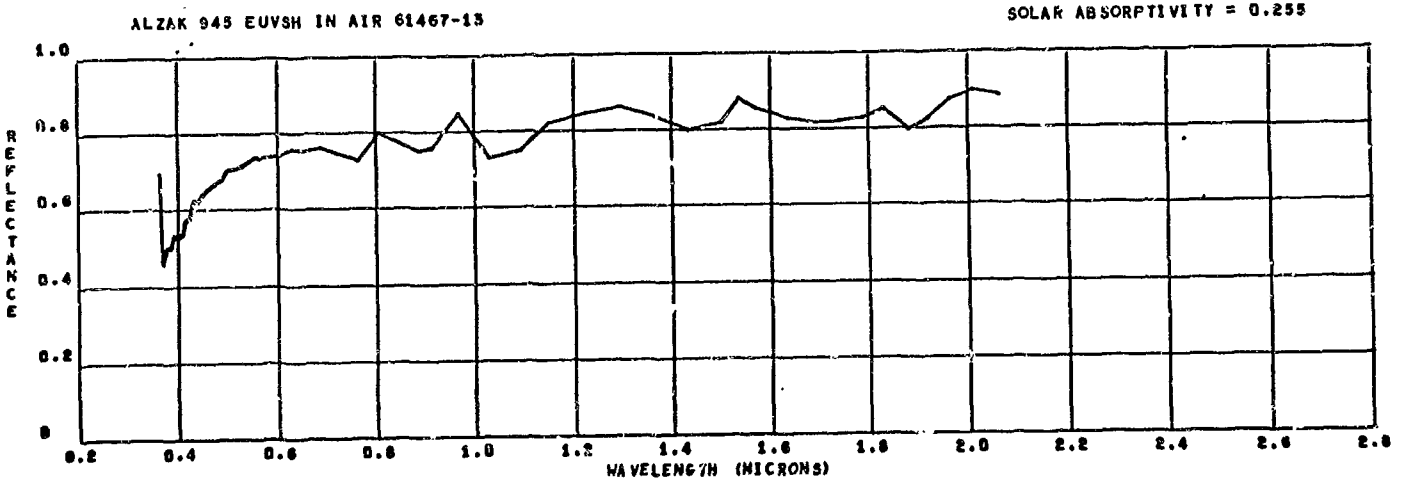






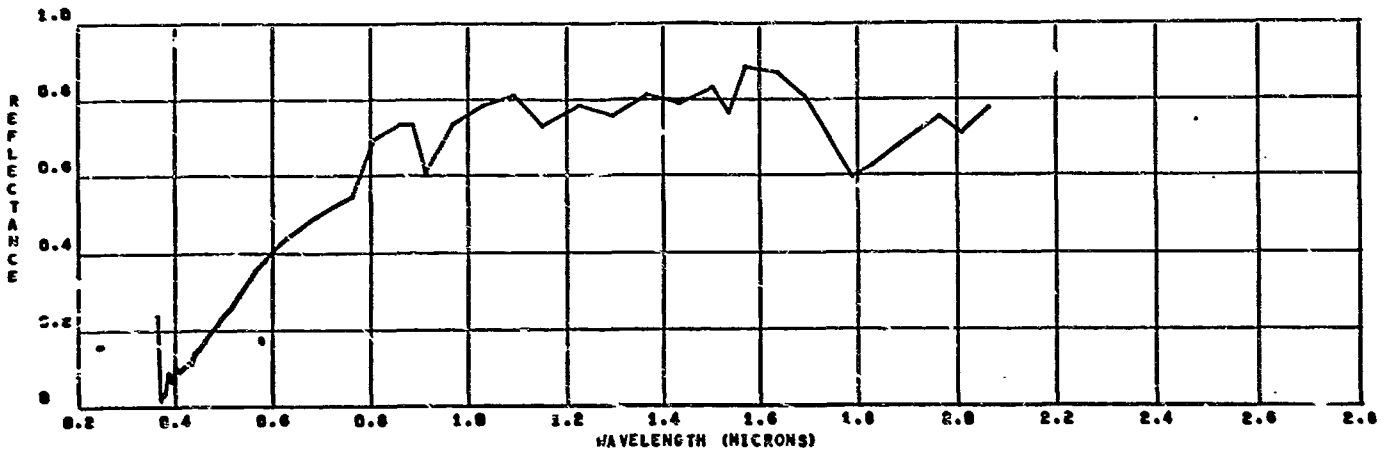






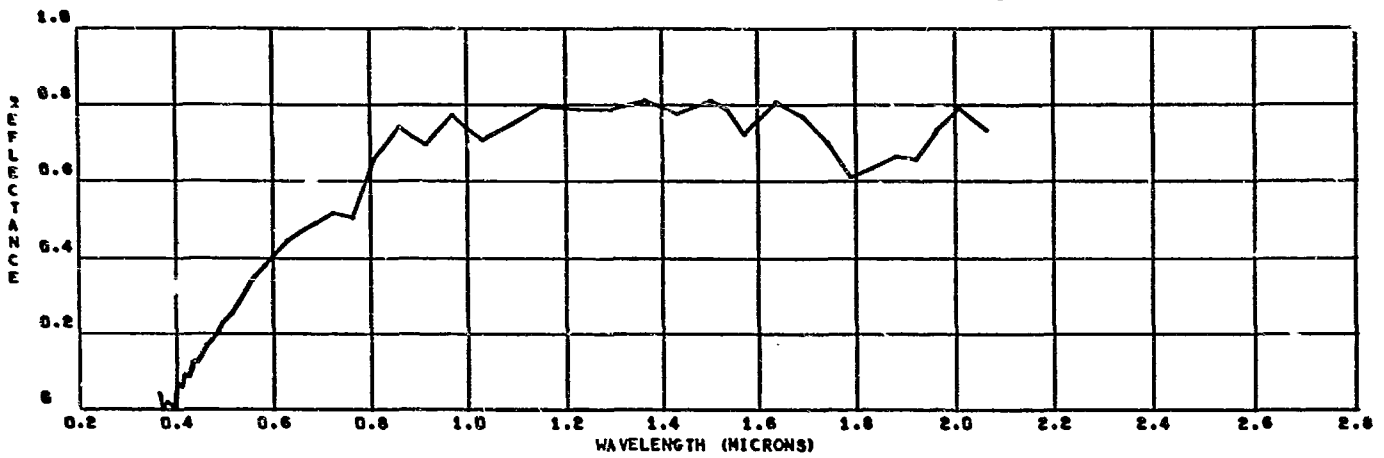
LEXAN (ETCHED) 5X10E13E 5X10E14P 945 EUVSH IN AIR 61467-14

SOLAR ABSORPTIVITY = 0.486



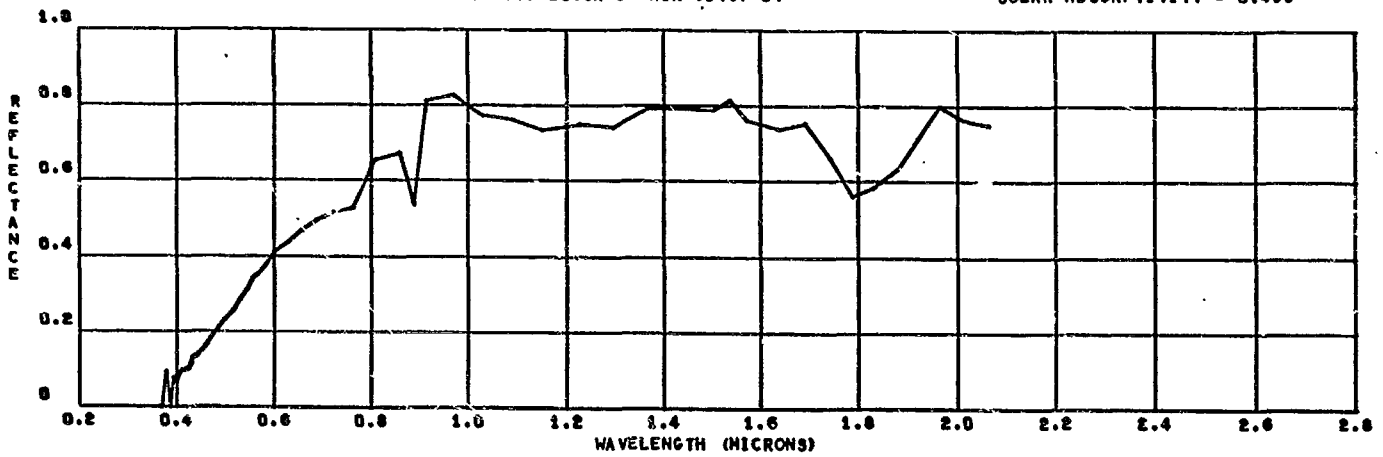
LEXAN (ETCHED) 5X10E13E 5X10E14P 945 EUVSH IN AIR 61467-14

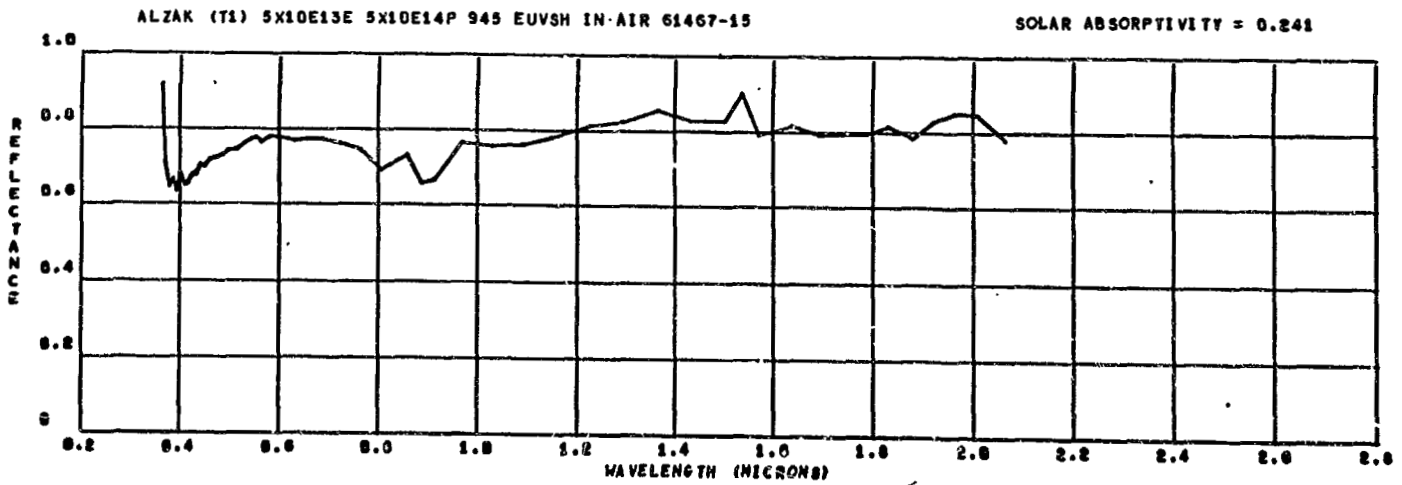
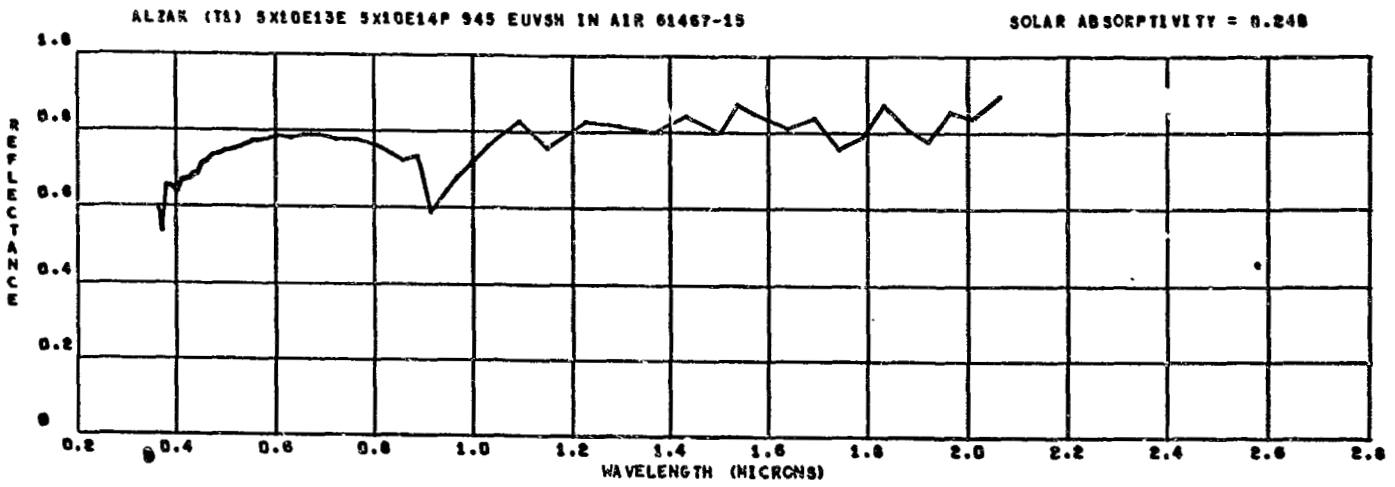
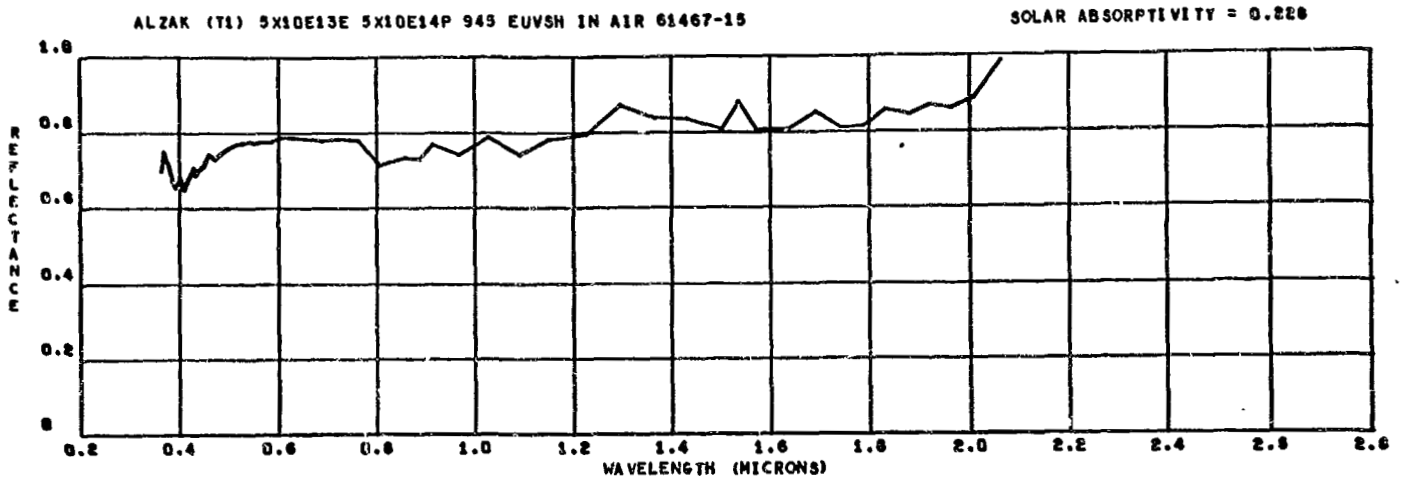
SOLAR ABSORPTIVITY = 0.495



LEXAN (ETCHED) 5X10E13E 5X10E14P 945 EUVSH IN AIR 61467-14

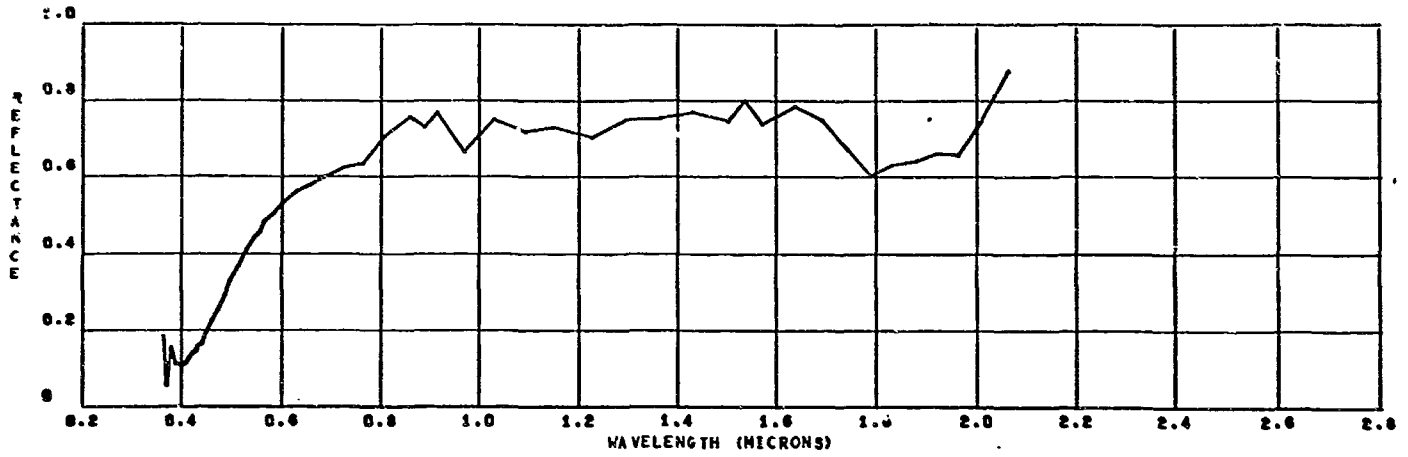
SOLAR ABSORPTIVITY = 0.499





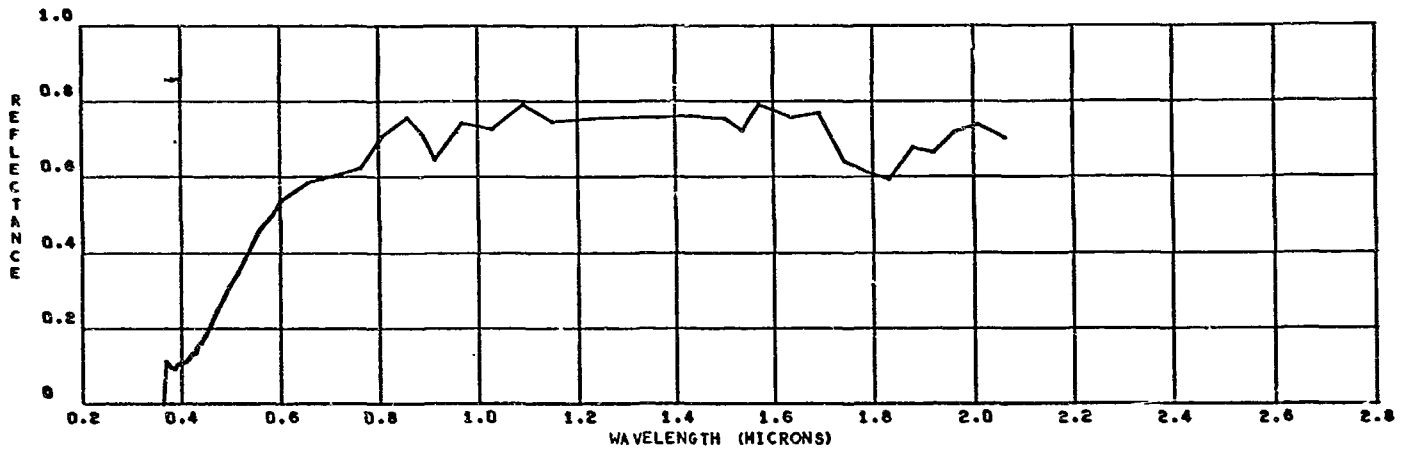
MYLAR 5X10E13E 5X10E14P 945 EUVSH IN AIR 61467-16

SOLAR ABSORPTIVITY = 0.145



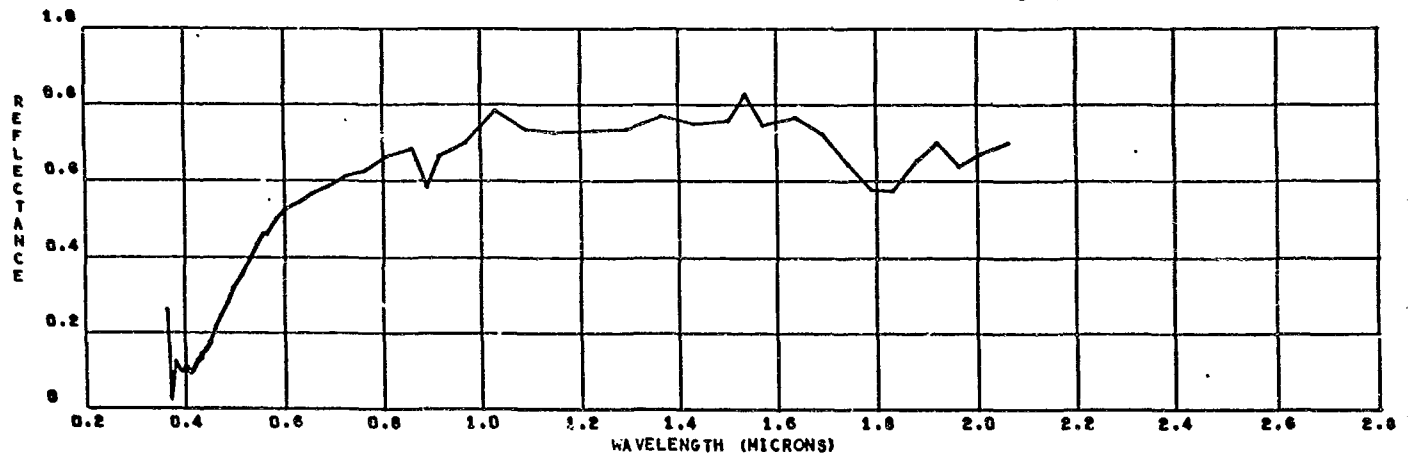
MYLAR 5X10E13E 5X10E14P 945 EUVSH IN AIR 61467-16

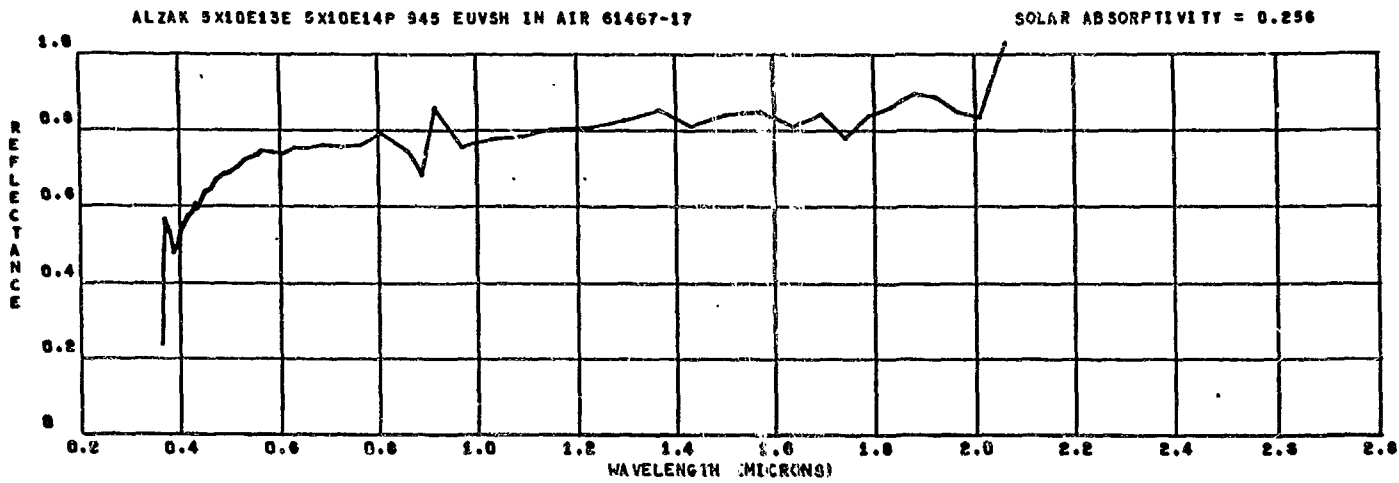
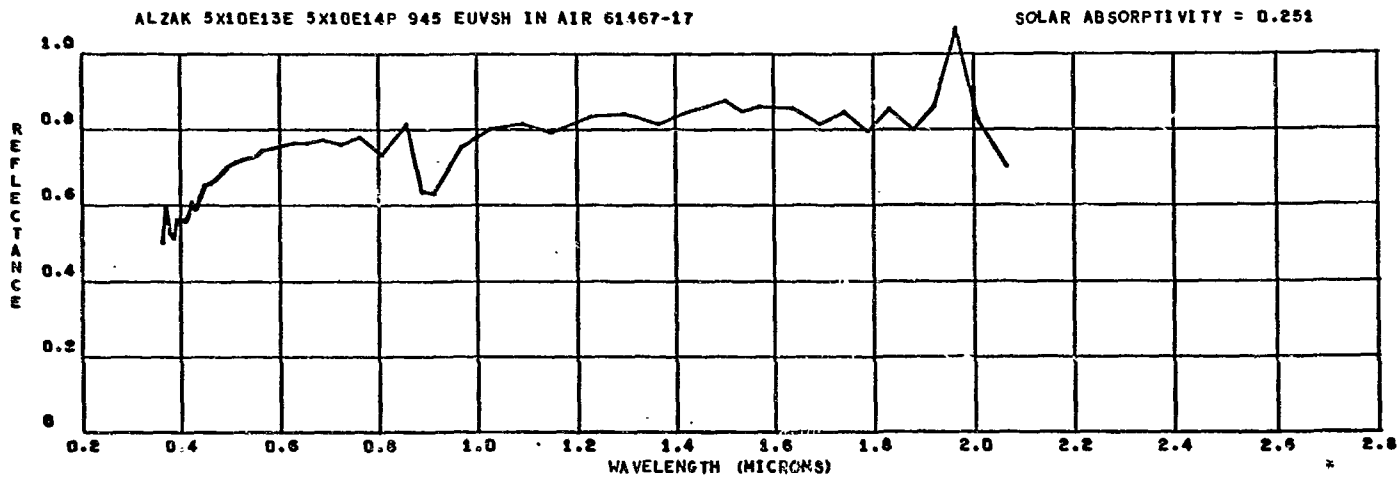
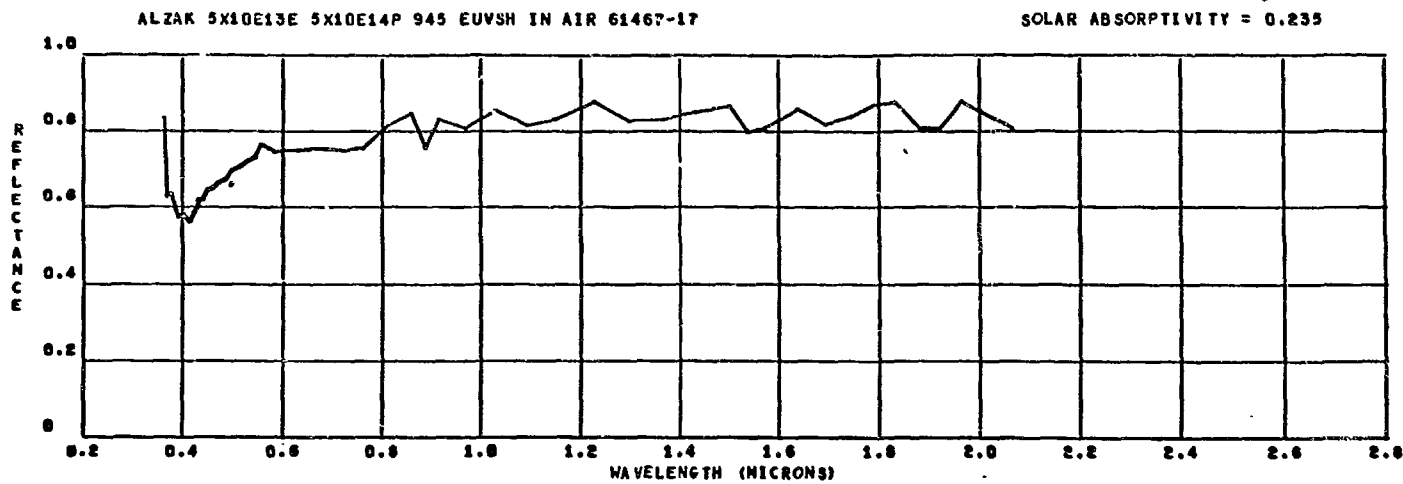
SOLAR ABSORPTIVITY = 0.449

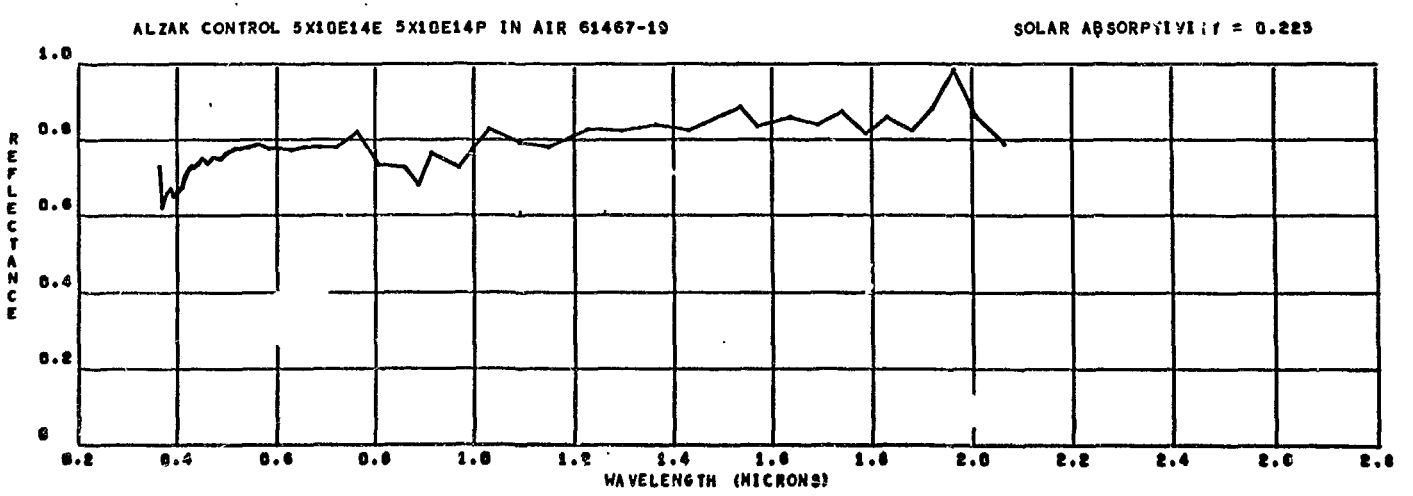
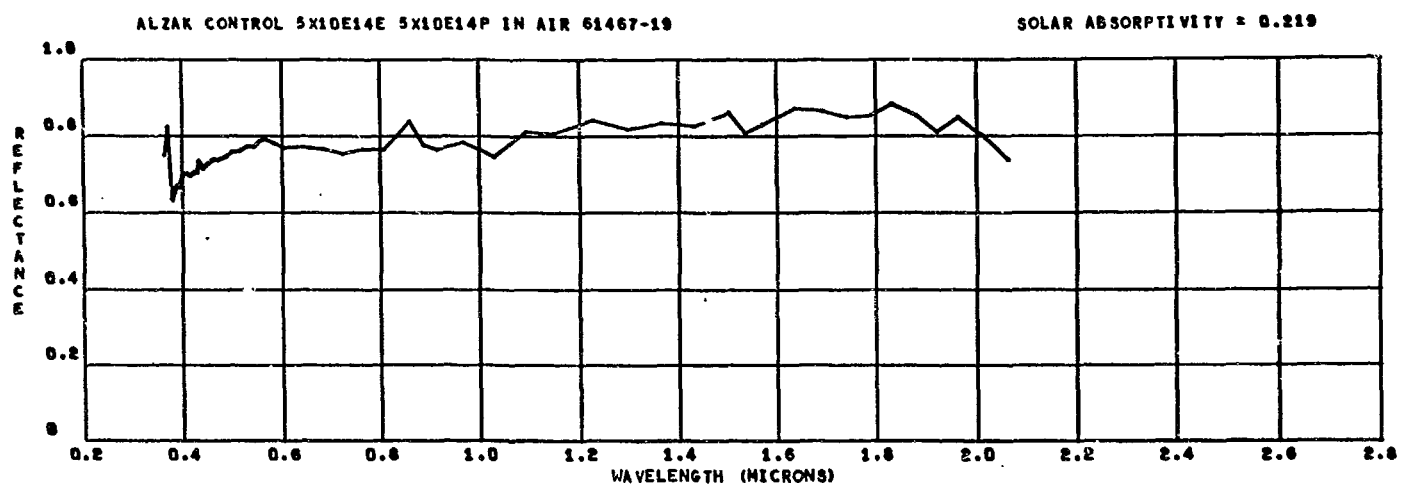
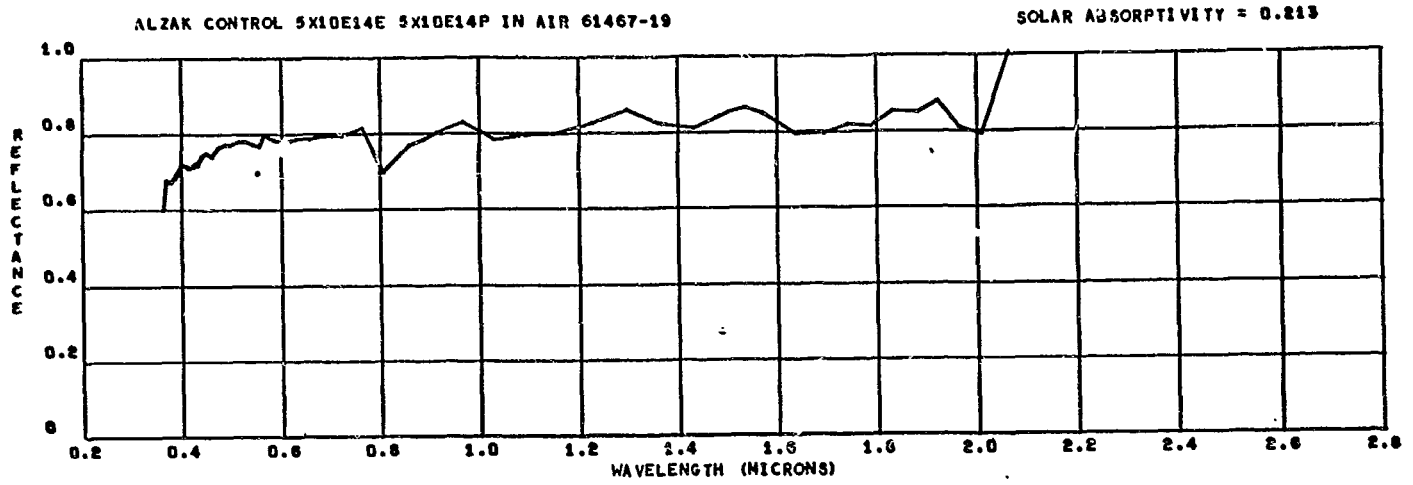


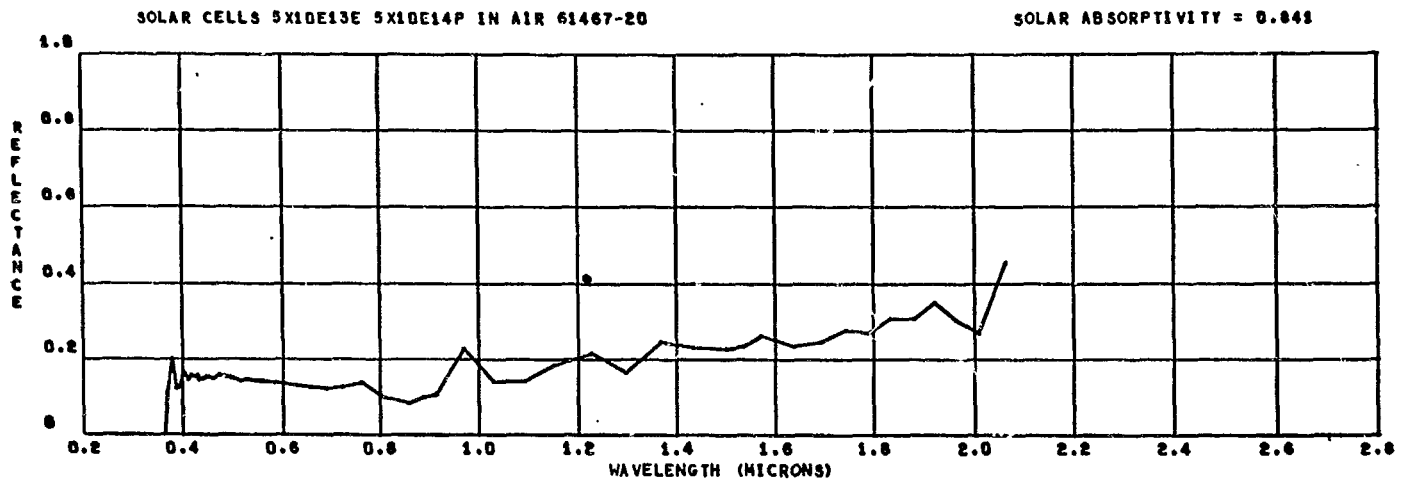
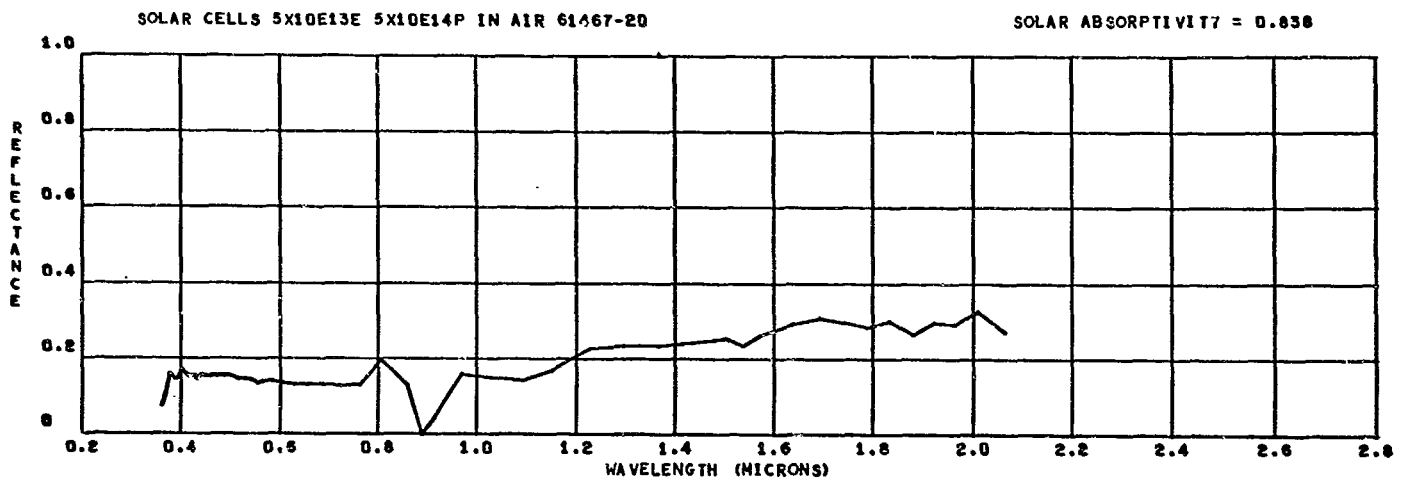
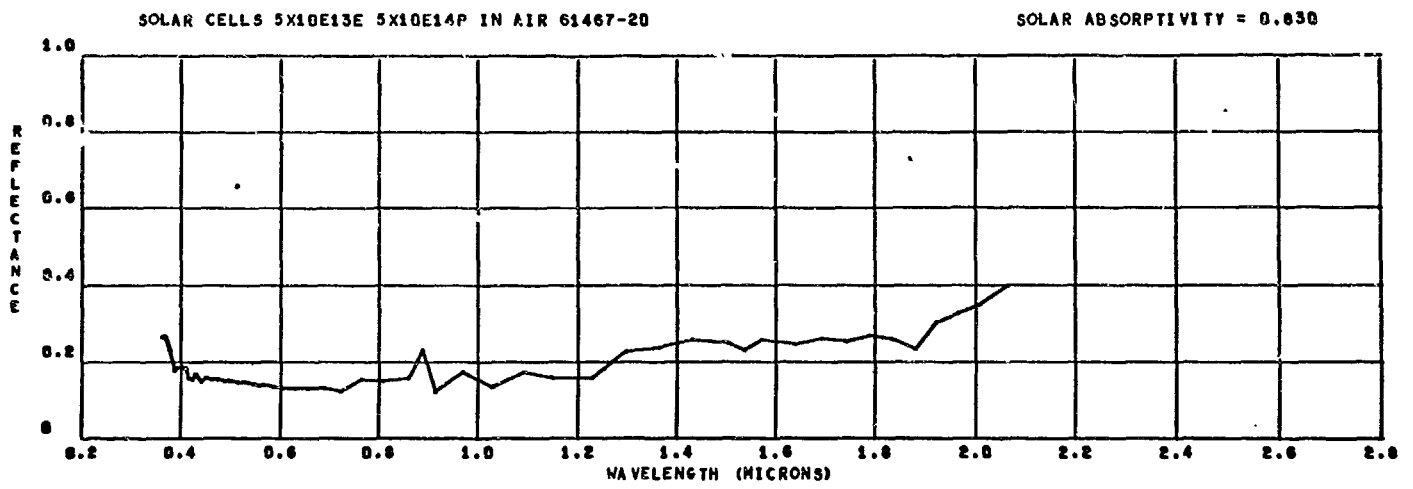
MYLAR 5X10E13E 5X10E14P 945 EUVSH IN AIR 61467-16

SOLAR ABSORPTIVITY = 0.460



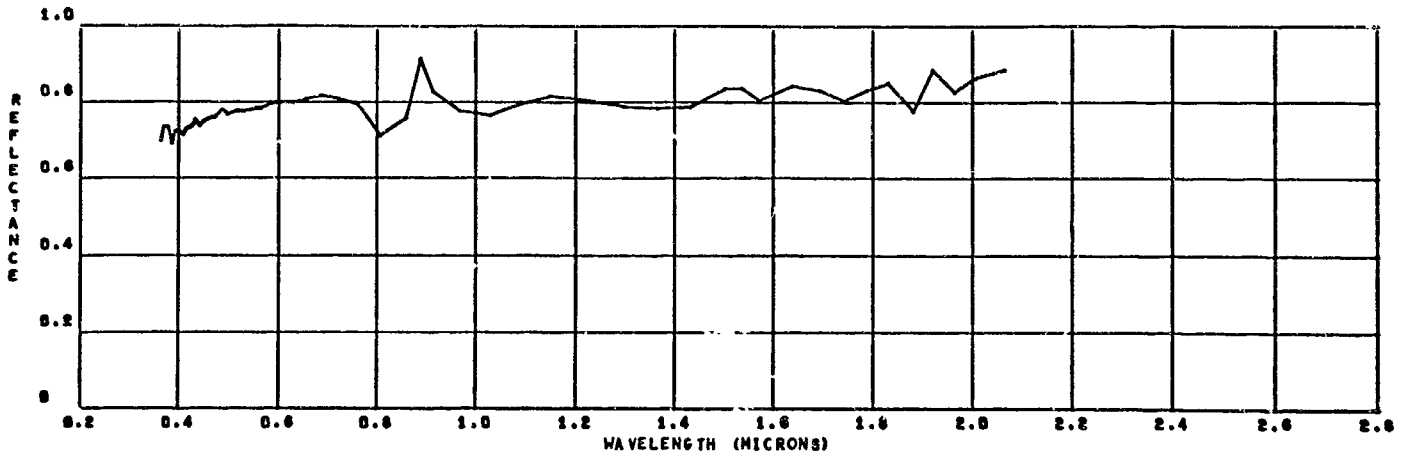






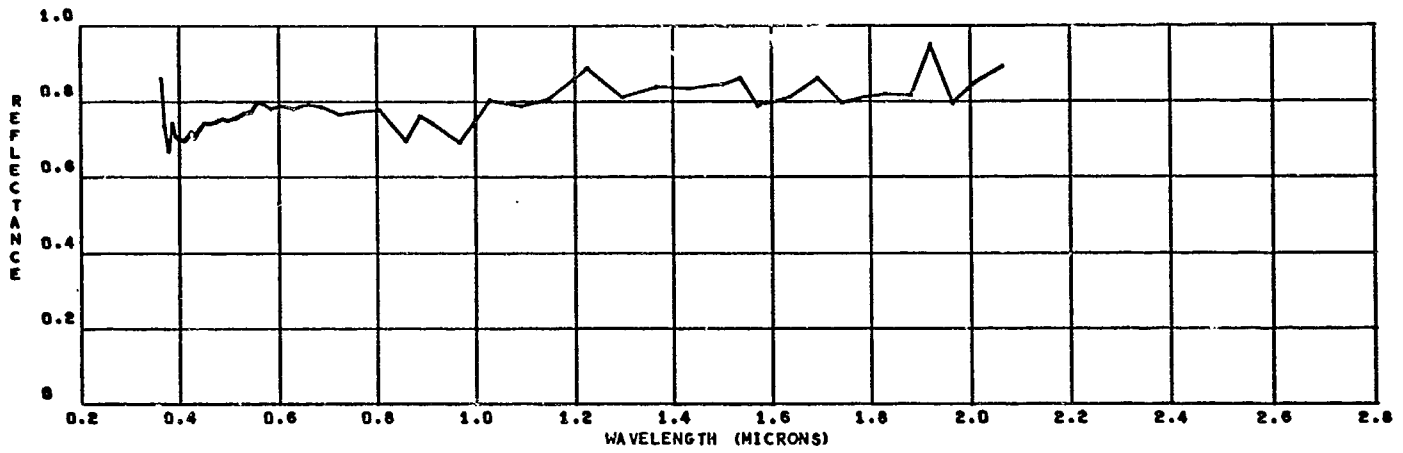
ALZAK (T1) 5X10E13E 5X10E14P IN AIR 61467-21

SOLAR ABSORPTIVITY = 0.211



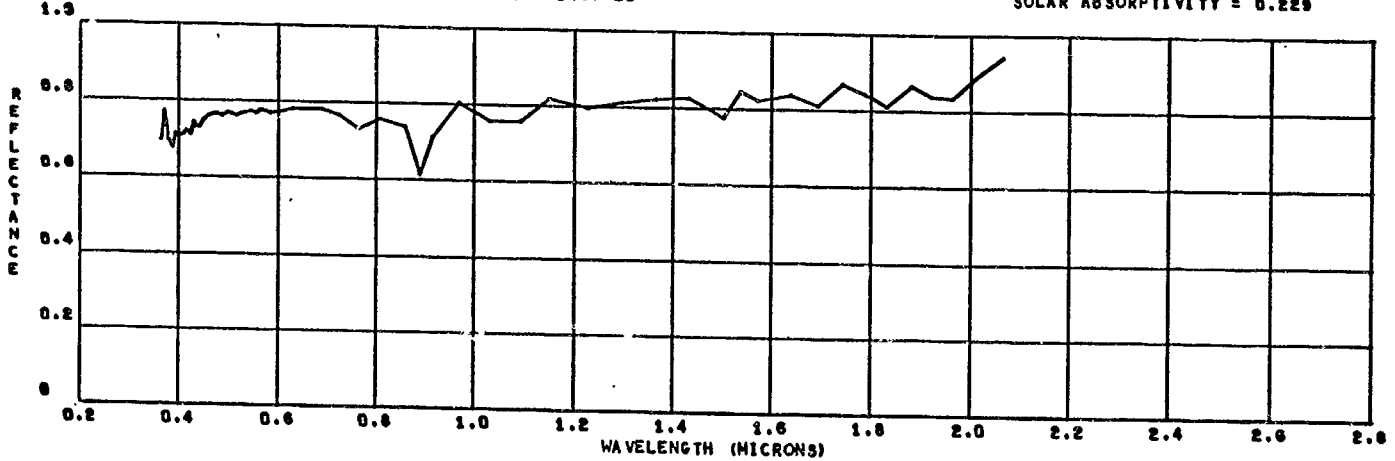
ALZAK (T1) 5X10E13E 5X10E14P IN AIR 61467-21

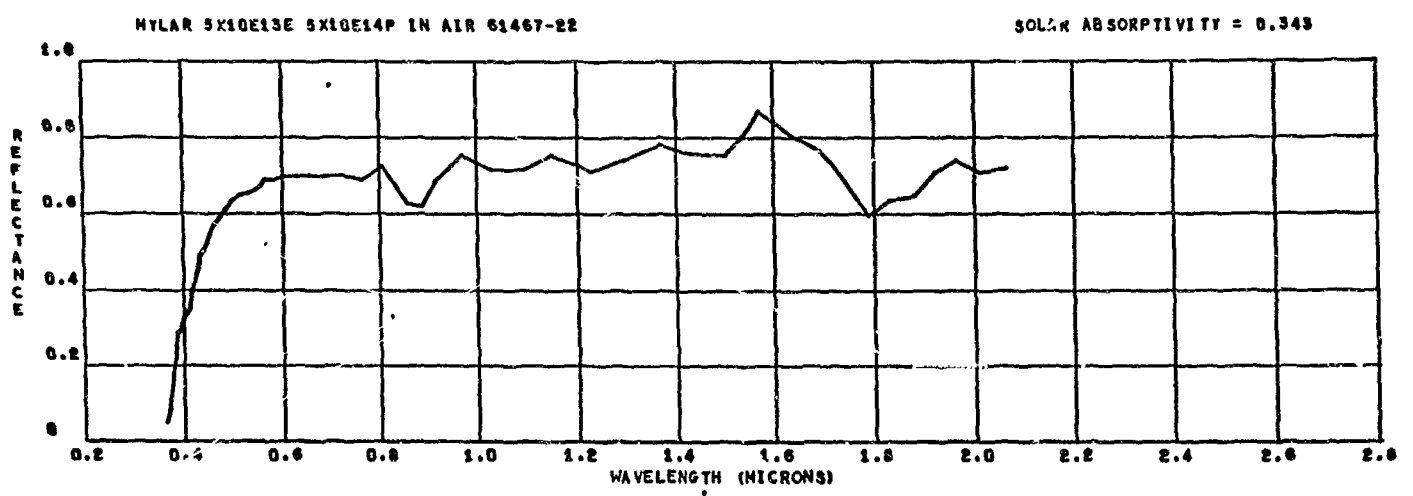
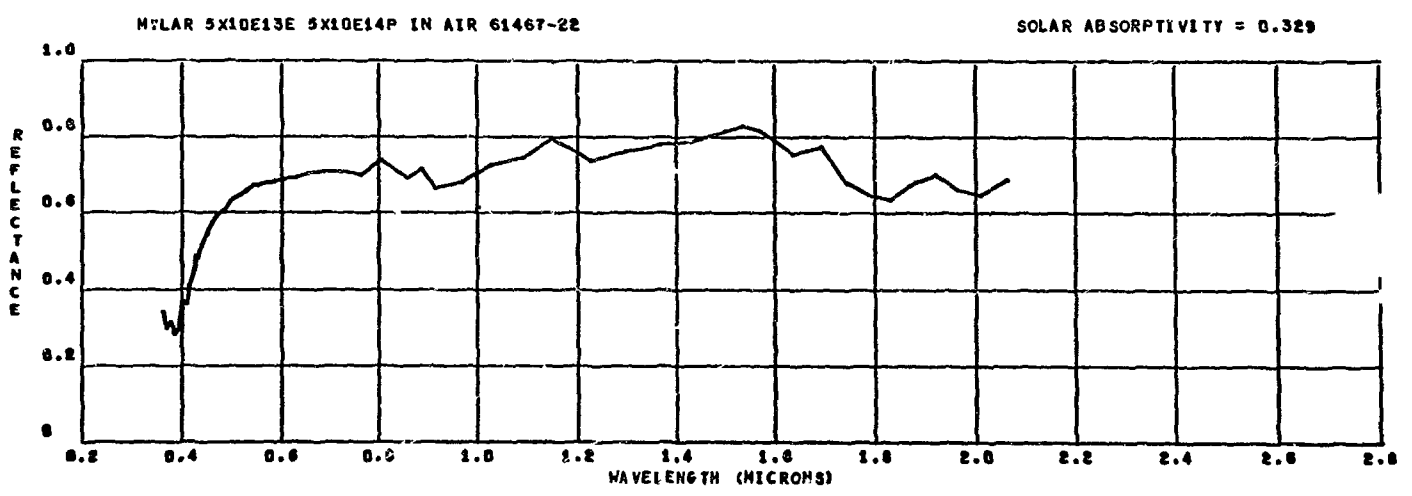
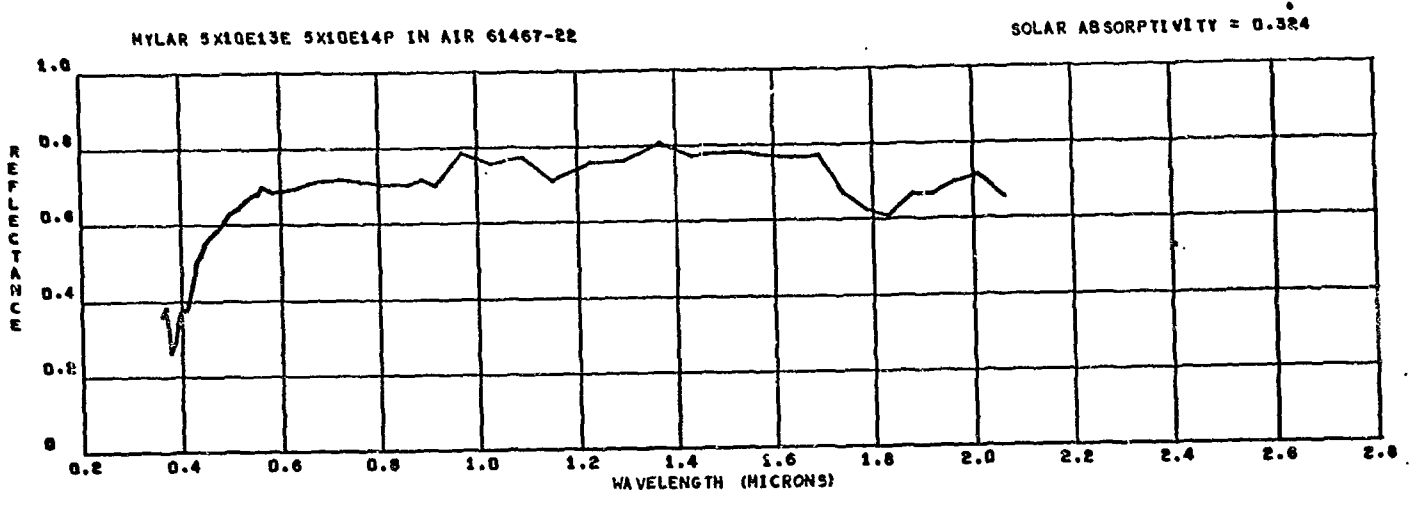
SOLAR ABSORPTIVITY = 0.222



ALZAK (T1) 5X10E13E 5X10E14P IN AIR 61467-21

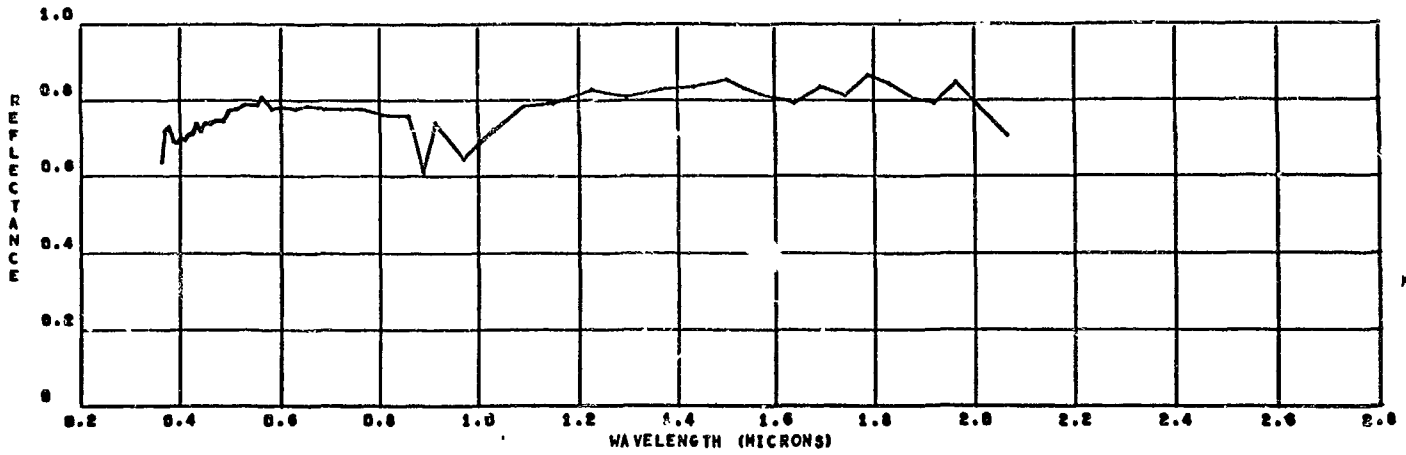
SOLAR ABSORPTIVITY = 0.229





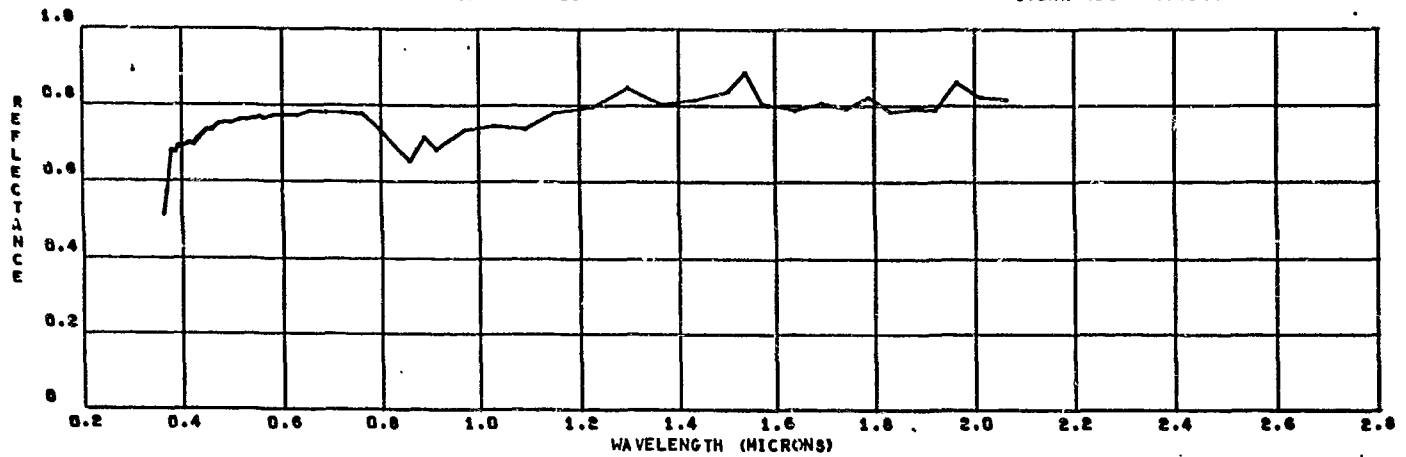
ALZAK 5X10E13E 5X10E14P IN AIR 61467-23

SOLAR ABSORPTIVITY = 0.232



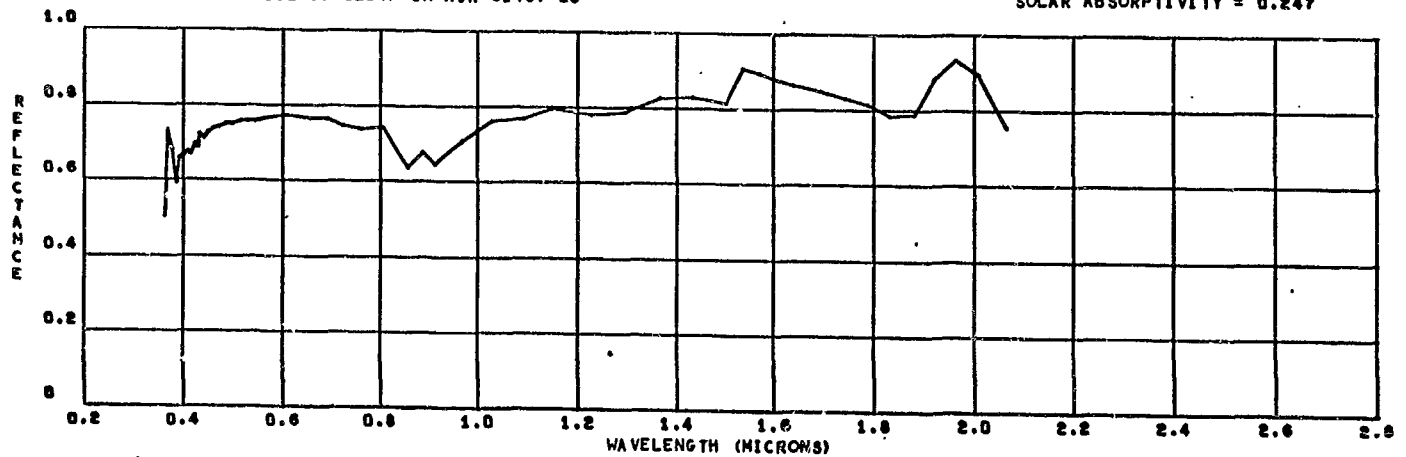
ALZAK 5X10E13E 5X10E14P IN AIR 61467-23

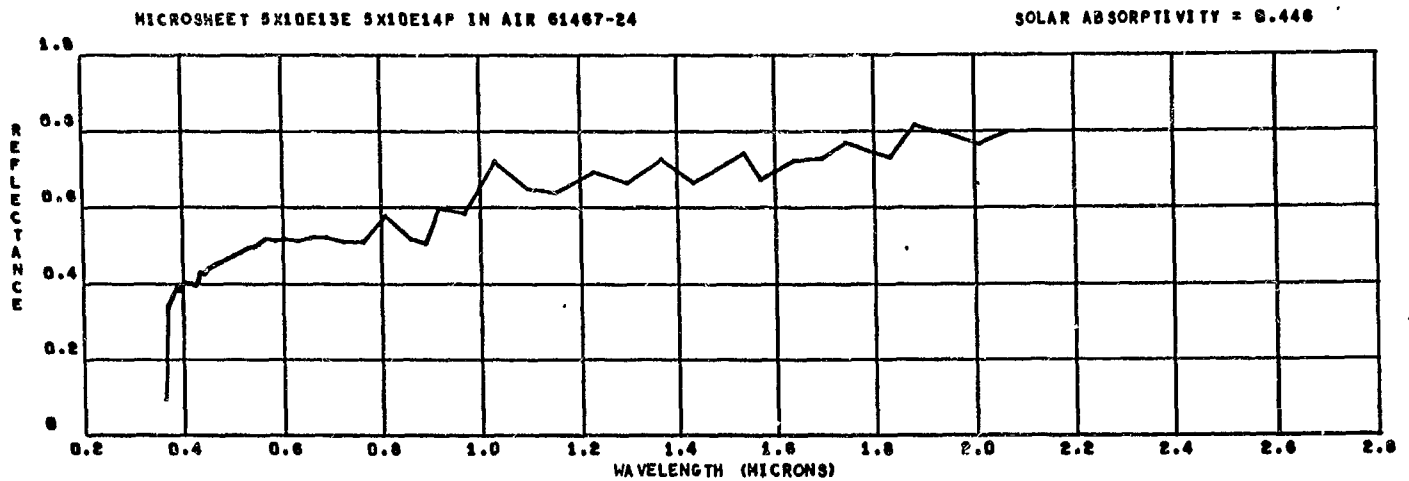
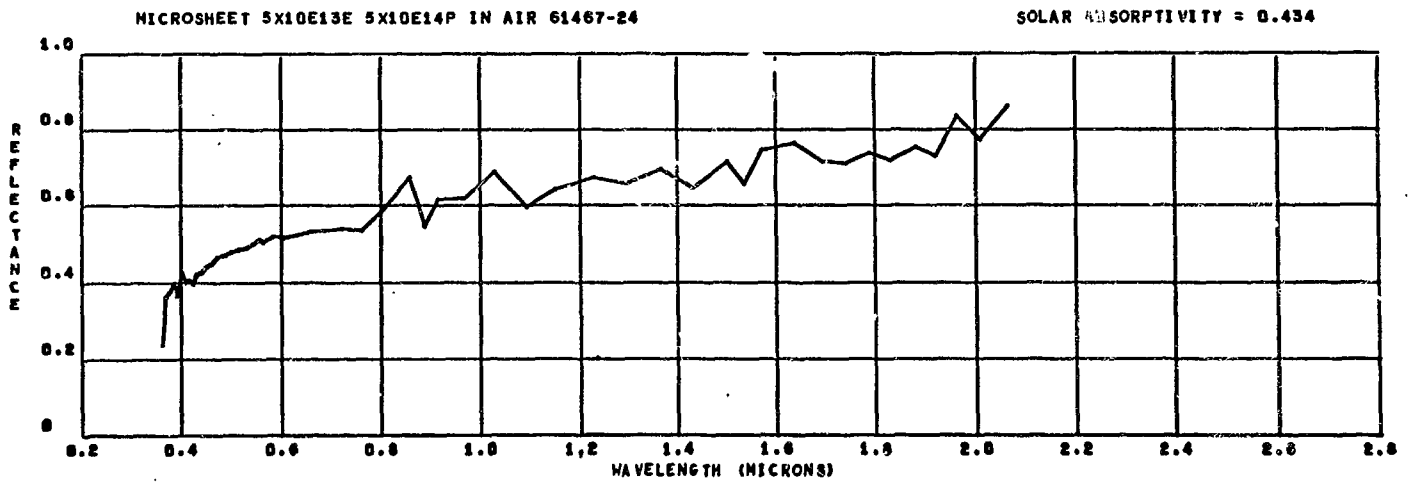
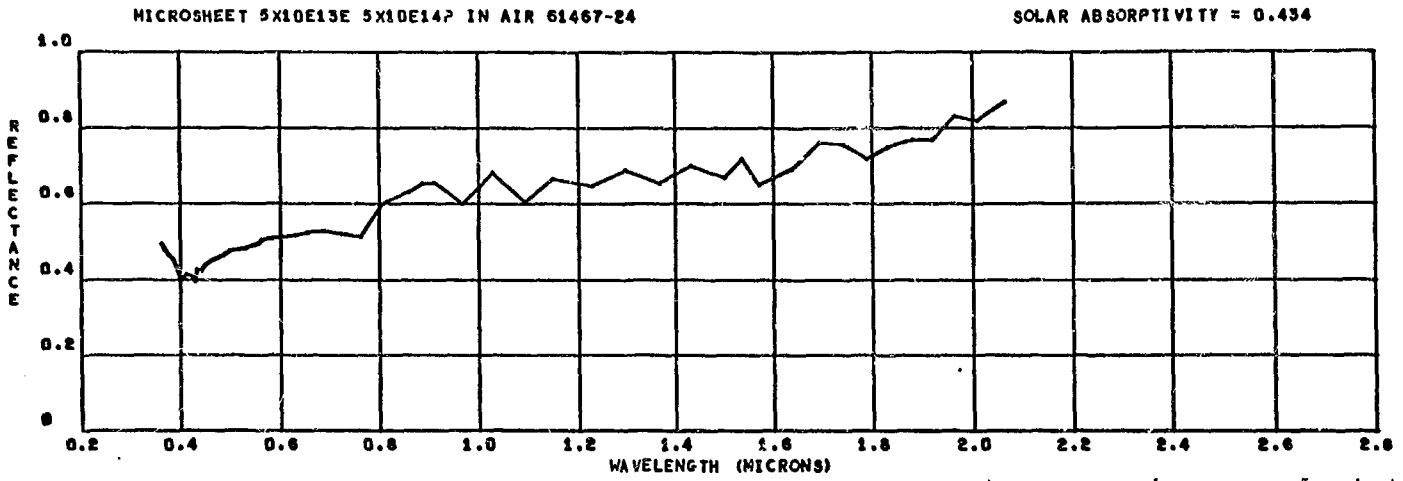
SOLAR ABSORPTIVITY = 0.242

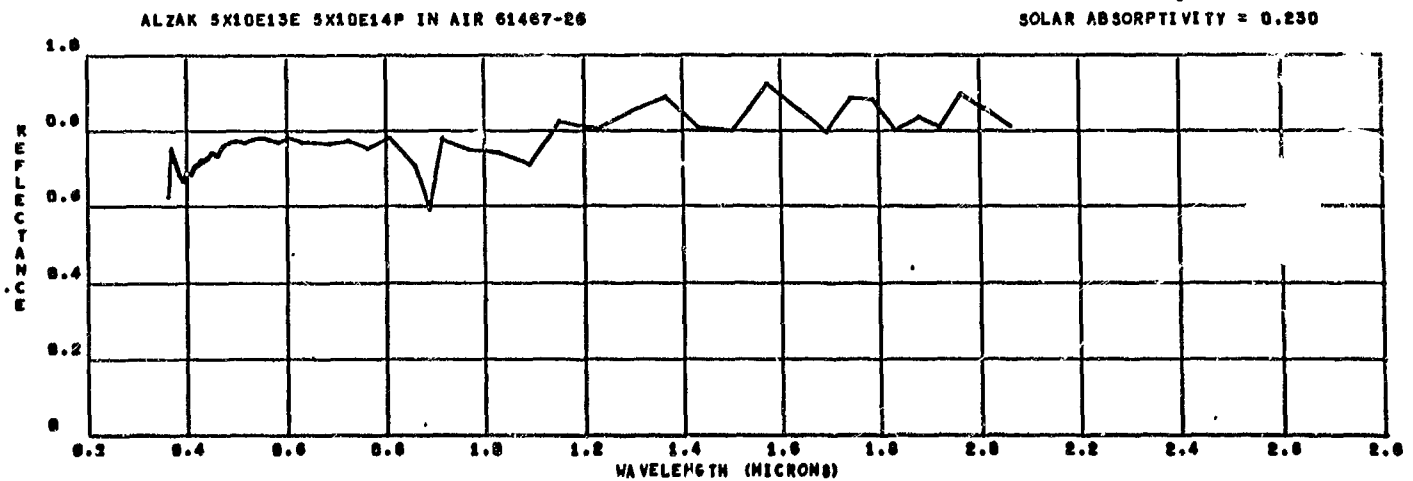
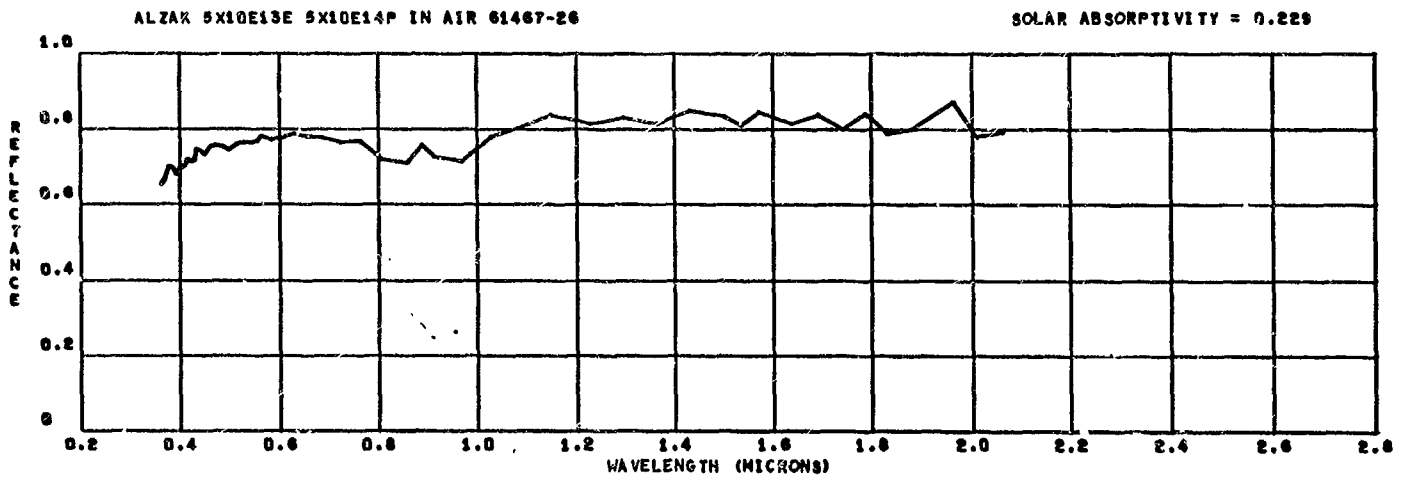
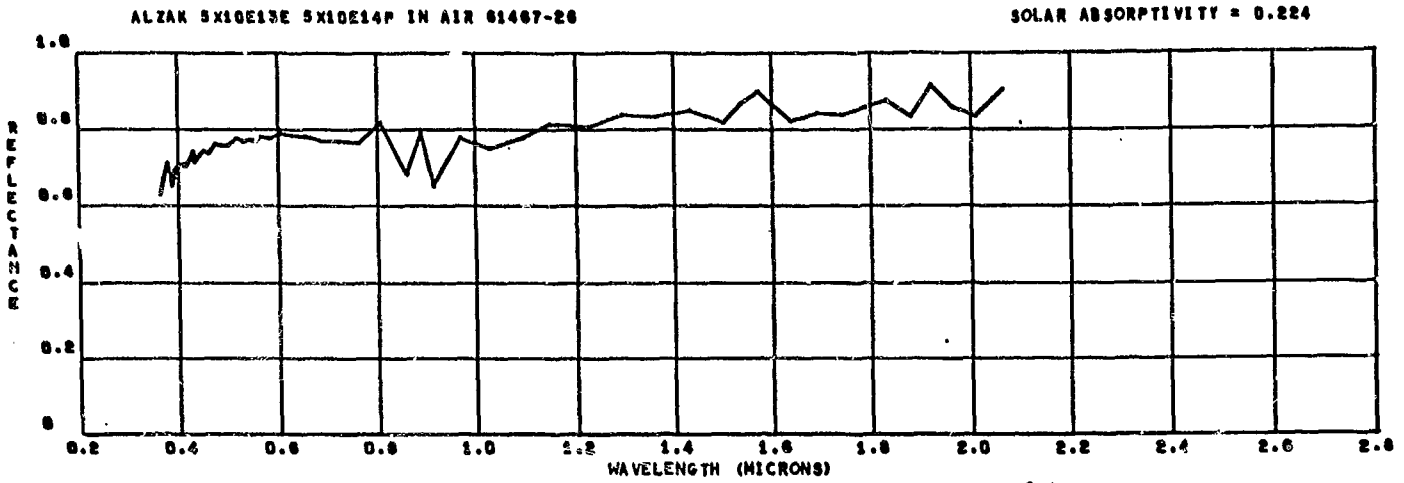


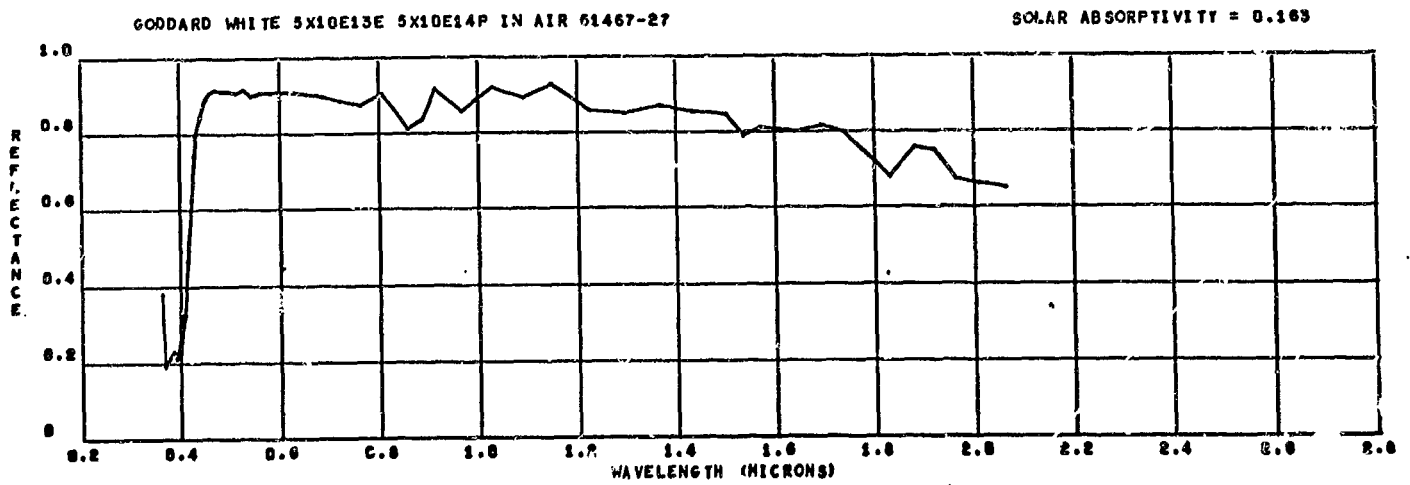
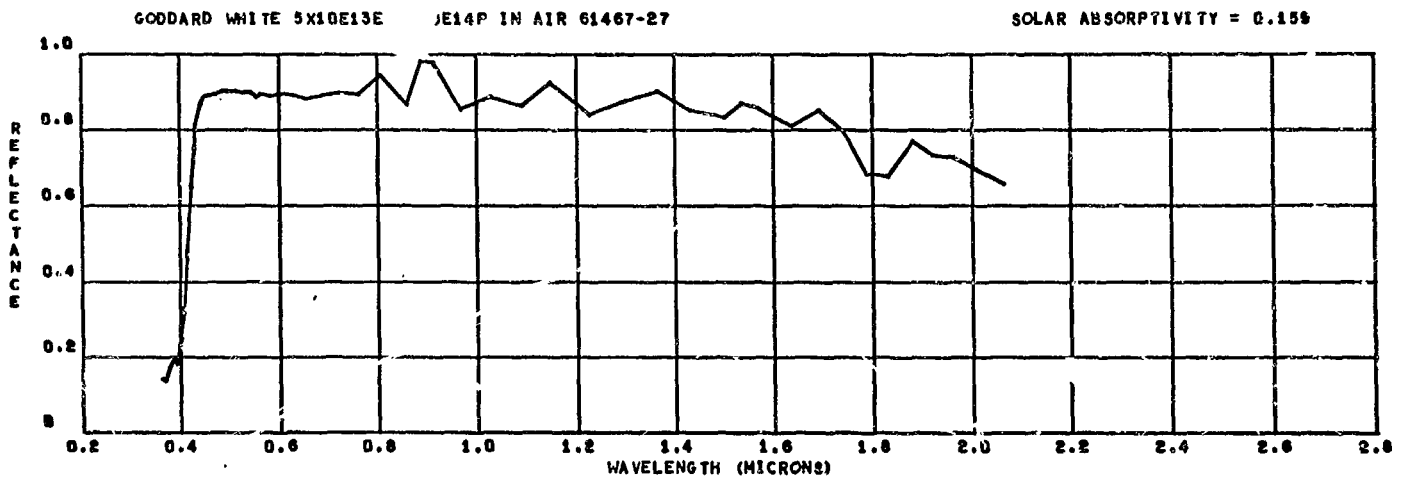
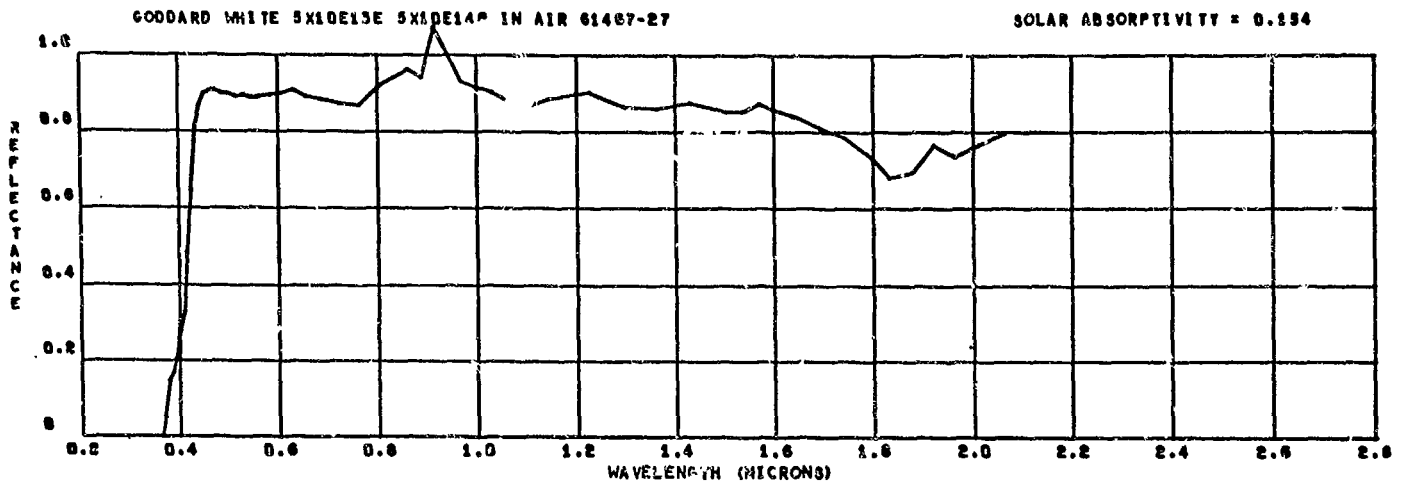
ALZAK 5X10E13E 5X10E14P IN AIR 61467-23

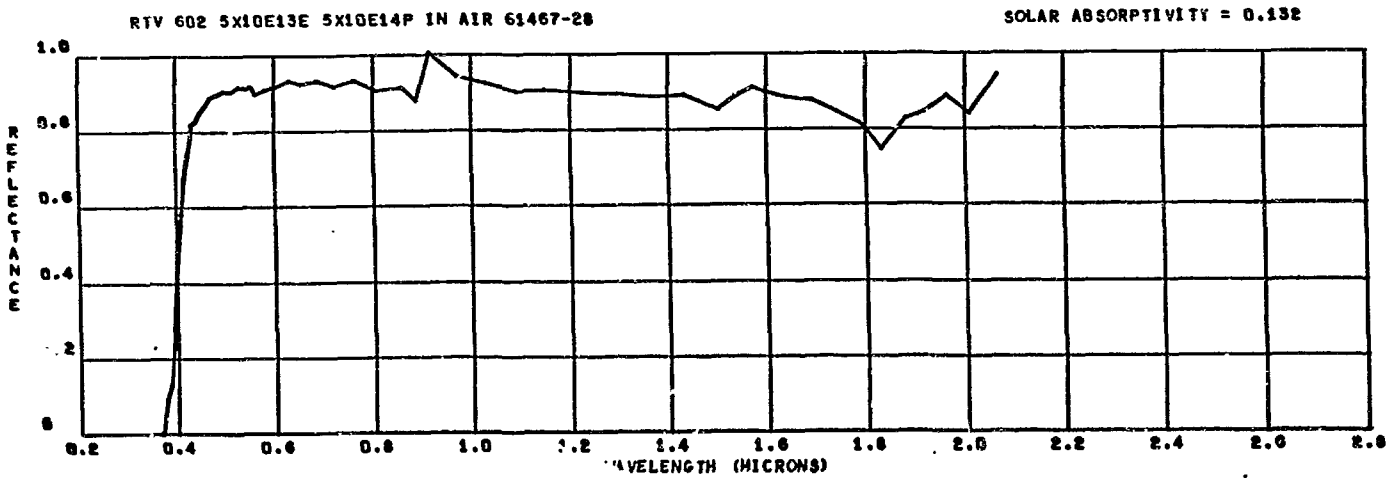
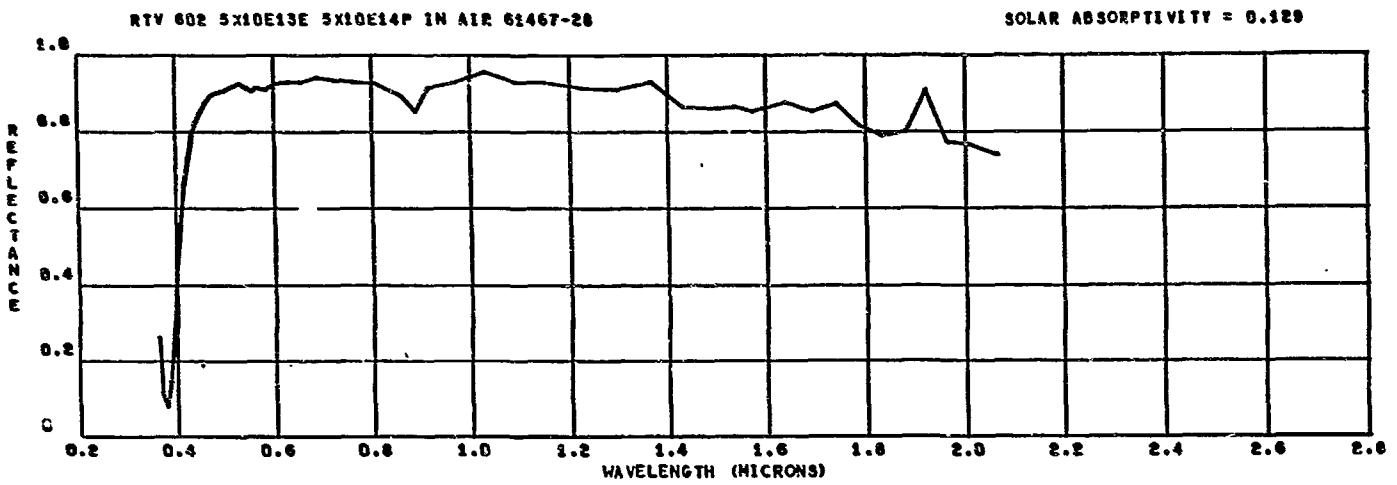
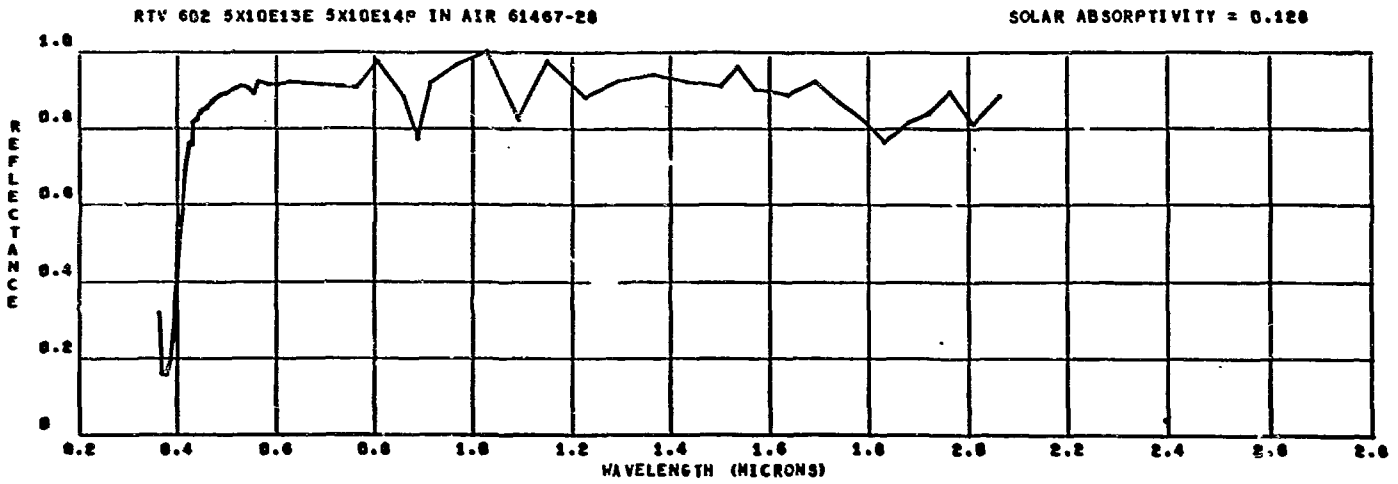
SOLAR ABSORPTIVITY = 0.247

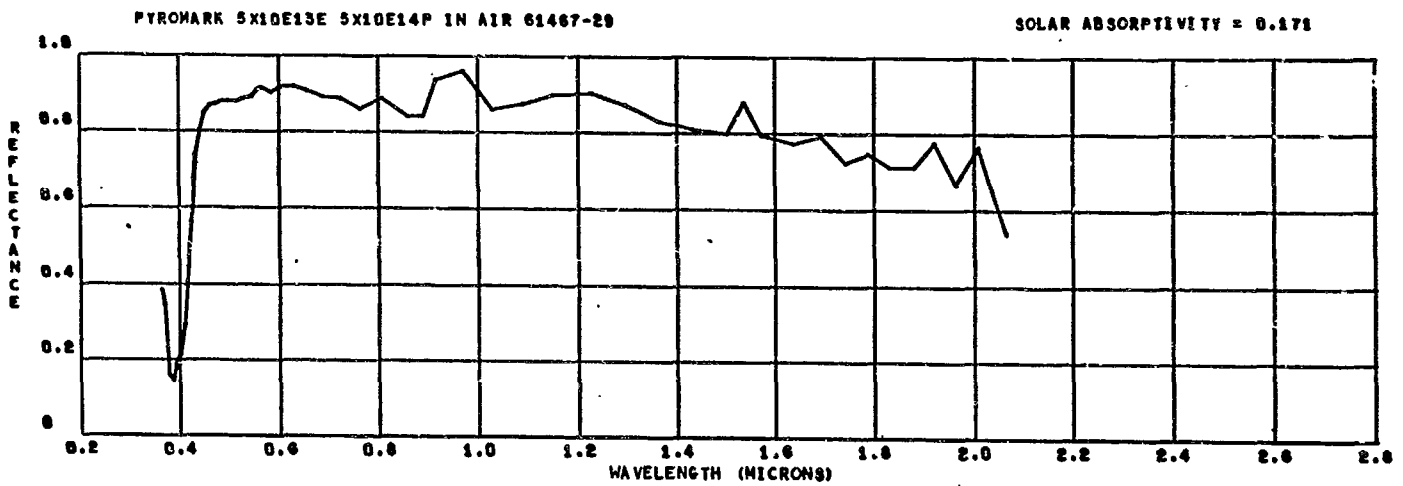
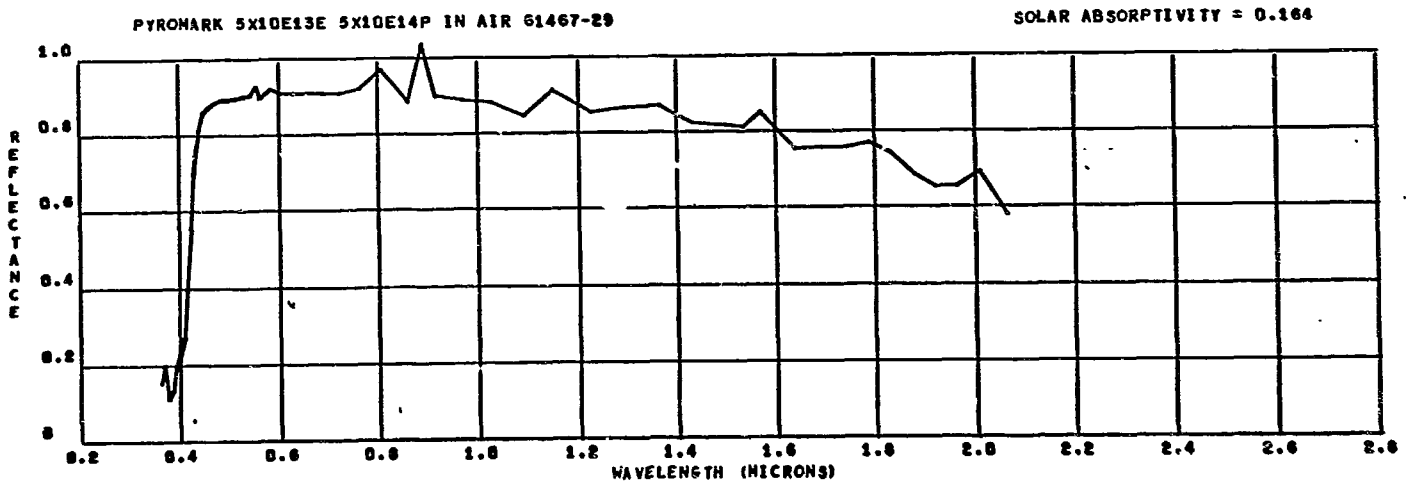
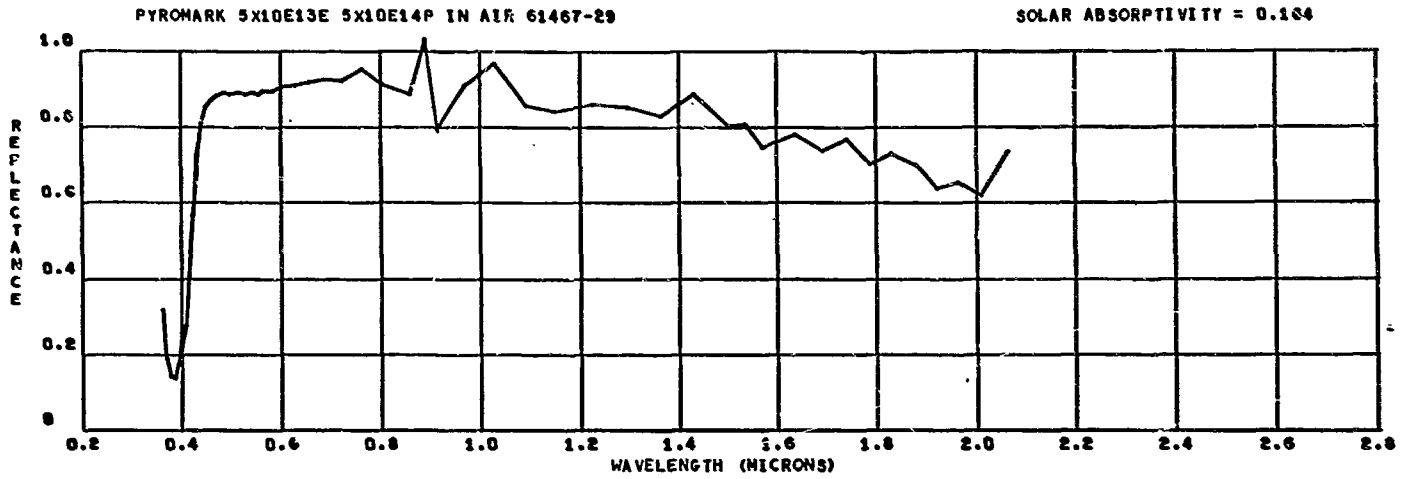


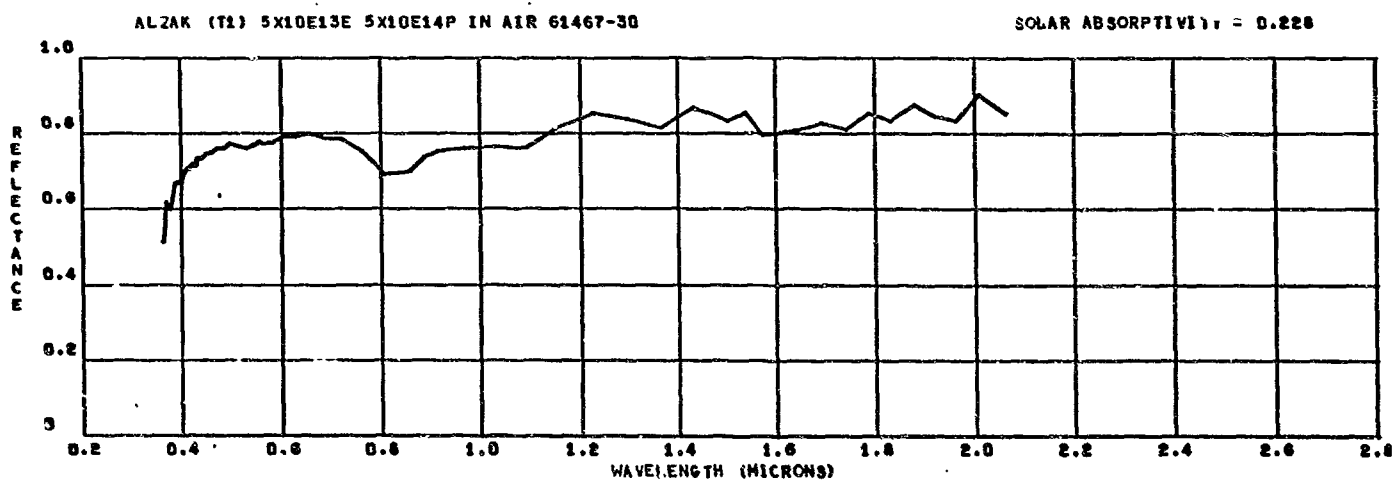
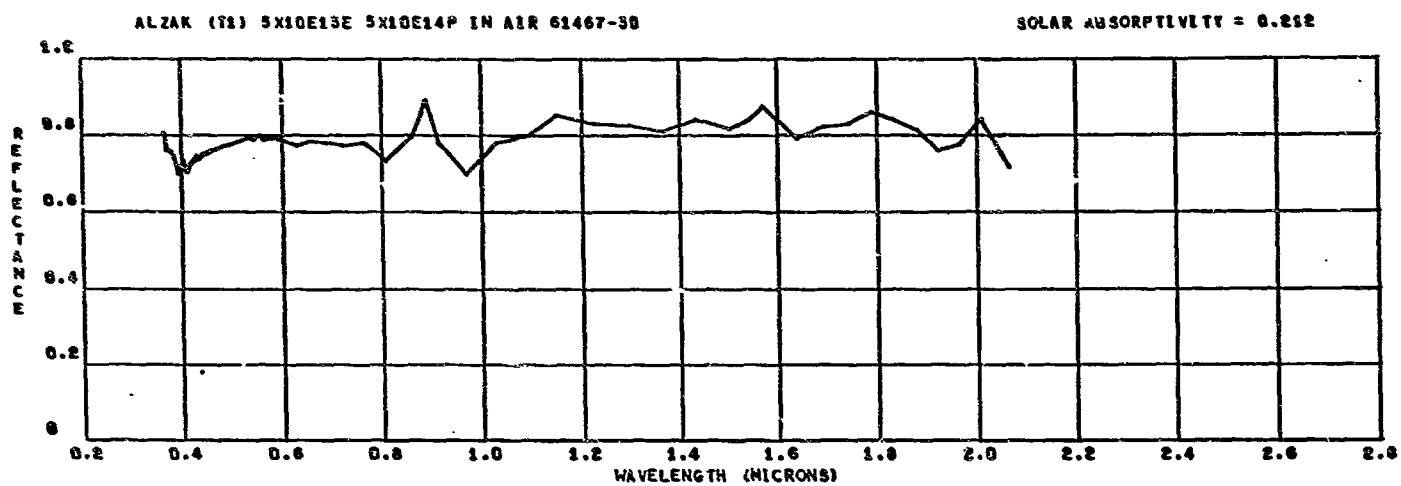
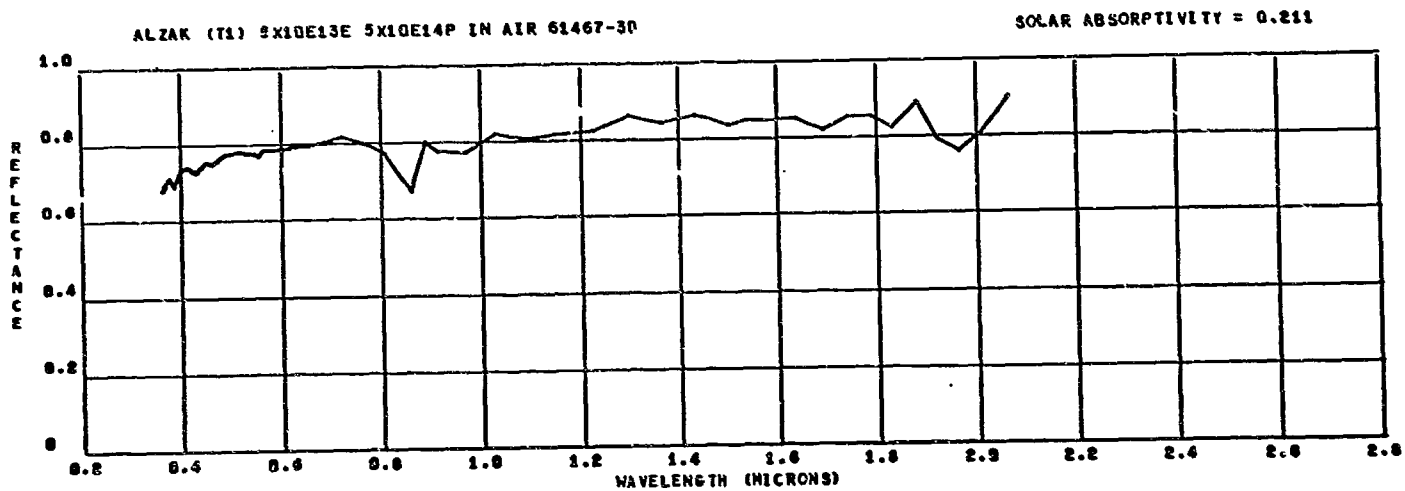












APPENDIX F

COMPILATION OF SPECTRAL REFLECTANCE DATA FROM THE BECKMAN DK-IL MEASUREMENTS AND FROM THE LEEDS AND NORTHEUP HOHLRAUM/13-2 PERKIN-ELMER MEASUREMENTS

Table F-1 lists the wavelength intervals, the reference values (MgO for diffuse and aluminum for the specular materials), and the energy in the intervals used for computation of solar absorptance values presented in this appendix. Table F-2 lists the reflectance of the three thicknesses of Alzak and the white coatings. Table F-3 lists the reflectance and transmission of both Lexan samples together with their reflectance over a polished aluminum substrate. Table F-4 lists the reflectance and transmission of the Mylar, the reflectance of Mylar over wrinkled aluminized Mylar, and the reflectance of the two solar cells and the microsheet.

Table F-5 lists the wavelength intervals, the average energy in the intervals, and the infrared reflectance of the Alzak and the white paints used to compute the total normal emittance values presented in this appendix.

Table F-1. Wavelength Intervals, Reference, and Energy Increments Used for Solar Absorptance Computation

Wavelength Interval (microns)	Reference Reflectance		Energy in the Interval
	MgO (diffuse)	Aluminum (specular)	
0 - 0.30	0.950	0.922	0.01
0.30 - 0.38	0.960	0.924	0.06
0.38 - 0.43	0.968	0.923	0.06
0.43 - 0.47	0.972	0.922	0.06
0.47 - 0.51	0.974	0.920	0.06
0.51 - 0.55	0.974	0.917	0.06
0.55 - 0.60	0.973	0.913	0.06
0.60 - 0.65	0.971	0.908	0.06
0.65 - 0.70	0.969	0.902	0.06
0.70 - 0.76	0.966	0.893	0.06
0.76 - 0.84	0.964	0.870	0.06
0.84 - 0.93	0.960	0.880	0.06
0.93 - 1.04	0.958	0.930	0.06
1.04 - 1.08	0.956	0.946	0.02
1.08 - 1.13	0.956	0.951	0.02
1.13 - 1.18	0.955	0.956	0.02
1.18 - 1.24	0.954	0.960	0.02
1.24 - 1.30	0.953	0.962	0.02
1.30 - 1.38	0.951	0.965	0.02
1.38 - 1.47	0.950	0.967	0.02
1.47 - 1.58	0.951	0.968	0.02
1.58 - 1.71	0.949	0.970	0.02
1.71 - 1.90	0.946	0.971	0.02
1.90 - 2.17	0.942	0.972	0.02
2.17 - 2.60	0.946	0.973	0.02
2.60 - 10.00	---	---	0.03

Table F-2. Reflectance of Alzak and White Paints

Wavelength Interval (microns)	Reflectance					
	Alzak			White Paints		
	0.100 mils	0.175 mils	0.290 mils	Goddard White	Pyromark Standard White	RTV-602 White
0 - 0.30	0.880	0.884	0.821	0.110	0.160	0.108
0.30 - 0.38	0.880	0.884	0.821	0.110	0.160	0.108
0.38 - 0.43	0.852	0.835	0.829	0.530	0.463	0.638
0.43 - 0.47	0.843	0.835	0.831	0.966	0.940	0.929
0.47 - 0.51	0.834	0.830	0.824	0.960	0.944	0.952
0.51 - 0.55	0.832	0.828	0.825	0.947	0.927	0.951
0.55 - 0.60	0.821	0.819	0.817	0.942	0.923	0.950
0.60 - 0.65	0.823	0.821	0.819	0.941	0.919	0.949
0.65 - 0.70	0.819	0.812	0.806	0.938	0.916	0.939
0.70 - 0.76	0.806	0.800	0.791	0.938	0.904	0.930
0.76 - 0.84	0.780	0.769	0.761	0.935	0.895	0.925
0.84 - 0.93	0.806	0.804	0.802	0.929	0.885	0.910
0.93 - 1.04	0.873	0.871	0.869	0.920	0.855	0.902
1.04 - 1.08	0.914	0.893	0.901	0.917	0.842	0.890
1.08 - 1.13	0.888	0.911	0.902	0.910	0.932	0.884
1.13 - 1.18	0.885	0.905	0.899	0.900	0.817	0.865
1.18 - 1.24	0.921	0.913	0.909	0.872	0.812	0.875
1.24 - 1.30	0.919	0.909	0.913	0.901	0.805	0.870
1.30 - 1.38	0.903	0.922	0.917	0.884	0.790	0.872
1.38 - 1.47	0.939	0.936	0.920	0.839	0.753	0.869
1.47 - 1.58	0.945	0.932	0.936	0.842	0.739	0.863
1.58 - 1.71	0.927	0.944	0.933	0.798	0.688	0.820
1.71 - 1.90	0.955	0.937	0.935	0.717	0.649	0.772
1.90 - 2.17	0.935	0.927	0.922	0.689	0.621	0.817
2.17 - 2.60	0.959	0.930	0.905	0.429	0.462	0.559
2.60 - 10.00	0.959	0.930	0.905	0.429	0.462	0.559
Solar Absorptance	0.142	0.150	0.157	0.189	0.224	0.178

Table F-3. Reflectance of Lexan Samples

Wavelength Interval (microns)	Reflectance of Lexan					
	Etched			Dull		
	Reflectance	Transmission	Over Aluminum	Reflectance	Transmission	Over Aluminum
0 - 0.30	0.135	0.008	0.138	0.095	0.008	0.117
0.30 - 0.38	0.135	0.008	0.138	0.095	0.008	0.117
0.38 - 0.43	0.442	0.172	0.457	0.448	0.170	0.462
0.43 - 0.47	0.639	0.315	0.737	0.642	0.311	0.786
0.47 - 0.51	0.618	0.345	0.749	0.620	0.340	0.788
0.51 - 0.55	0.588	0.365	0.727	0.592	0.361	0.779
0.55 - 0.60	0.554	0.380	0.715	0.556	0.375	0.761
0.60 - 0.65	0.540	0.419	0.720	0.539	0.422	0.769
0.65 - 0.70	0.538	0.442	0.736	0.539	0.445	0.780
0.70 - 0.76	0.512	0.454	0.740	0.513	0.455	0.788
0.76 - 0.84	0.492	0.485	0.736	0.493	0.487	0.786
0.84 - 0.93	0.461	0.518	0.738	0.462	0.520	0.785
0.93 - 1.04	0.438	0.548	0.762	0.437	0.550	0.814
1.04 - 1.08	0.410	0.578	0.782	0.408	0.581	0.825
1.08 - 1.13	0.380	0.572	0.752	0.378	0.582	0.805
1.13 - 1.18	0.354	0.582	0.726	0.352	0.591	0.766
1.18 - 1.24	0.354	0.613	0.760	0.352	0.628	0.809
1.24 - 1.30	0.342	0.642	0.795	0.340	0.650	0.852
1.30 - 1.38	0.310	0.658	0.775	0.289	0.667	0.823
1.38 - 1.47	0.272	0.680	0.762	0.262	0.692	0.809
1.47 - 1.58	0.253	0.720	0.793	0.242	0.730	0.842
1.58 - 1.71	0.165	0.670	0.619	0.162	0.678	0.651
1.71 - 1.90	0.140	0.728	0.676	0.132	0.735	0.712
1.90 - 2.17	0.122	0.735	0.642	0.110	0.749	0.623
2.17 - 2.60	0.065	0.581	0.403	0.062	0.593	0.417
2.60 - 10.00	0.065	0.581	0.403	0.060	0.593	0.417
Solar Absorptance	0.136		0.340	0.137		0.302

Table F-4. Reflectance of Mylar, Solar Cells and Microsheet

Wavelength Interval (microns)	Reflectance					
	Mylar (shiny side out)			Solar Cells		
	Reflectance	Transmission	Over Crinkled Aluminized Mylar	N/P	P/N	Microsheet (6.0 mils)
0 - 0.30	0.123	0.362	0.275	0.010	0.010	0.925
0.30 - 0.38	0.123	0.362	0.275	0.170	0.090	0.925
0.38 - 0.43	0.182	0.662	0.533	0.182	0.109	0.921
0.43 - 0.47	0.199	0.742	0.691	0.159	0.090	0.941
0.47 - 0.51	0.198	0.770	0.734	0.141	0.079	0.962
0.51 - 0.55	0.193	0.784	0.752	0.129	0.077	0.966
0.55 - 0.60	0.182	0.788	0.762	0.119	0.074	0.964
0.60 - 0.65	0.173	0.782	0.759	0.099	0.062	0.970
0.65 - 0.70	0.175	0.787	0.762	0.099	0.064	0.976
0.70 - 0.76	0.172	0.789	0.760	0.098	0.067	0.974
0.76 - 0.84	0.169	0.792	0.757	0.105	0.072	0.978
0.84 - 0.93	0.165	0.803	0.710	0.112	0.085	0.976
0.93 - 1.04	0.162	0.799	0.800	0.129	0.096	0.968
1.04 - 1.08	0.158	0.799	0.820	0.171	0.106	0.970
1.08 - 1.13	0.152	0.788	0.804	0.206	0.121	0.963
1.13 - 1.18	0.148	0.785	0.800	0.222	0.129	0.960
1.18 - 1.24	0.152	0.791	0.822	0.231	0.135	0.963
1.24 - 1.30	0.153	0.788	0.832	0.239	0.141	0.965
1.30 - 1.38	0.152	0.790	0.818	0.245	0.148	0.969
1.38 - 1.47	0.144	0.788	0.794	0.257	0.150	0.965
1.47 - 1.58	0.143	0.802	0.823	0.269	0.158	0.964
1.58 - 1.71	0.122	0.743	0.653	0.278	0.159	0.960
1.71 - 1.90	0.128	0.746	0.717	0.288	0.158	0.962
1.90 - 2.17	0.124	0.707	0.664	0.310	0.166	0.962
2.17 - 2.60	0.068	0.418	0.300	0.305	0.148	0.953
2.60 - 10.00	0.068	0.418	0.300	0.305	0.148	0.953
Solar Absorbance	0.115		0.314	0.838	0.903	0.040

Table F-5. Infrared Reflectance of Alzak and the White Paints

Wavelength Interval (microns)	Energy in Region (100°F)	Infrared Reflectance					
		Alzak			White Paints		
		0.100 mils	0.175 mils	0.290 mils	Goddard White	Pyromark Standard White	RTV-602 White
2 - 3	0.03	0.182	0.232	0.285	0.603	0.639	0.418
3 - 4	0.32	0.184	0.288	0.436	0.882	0.839	0.743
4 - 5	1.37	0.120	0.141	0.242	0.863	0.761	0.613
5 - 6	03.11	0.088	0.126	0.235	0.913	0.782	0.797
6 - 7	04.89	0.110	0.217	0.341	0.924	0.879	0.894
7 - 8	06.20	0.369	0.562	0.729	0.944	0.898	0.936
8 - 9	06.87	0.825	0.813	0.929	0.951	0.947	0.951
9 - 10	07.03	0.829	0.824	0.966	0.912	0.933	0.928
10 - 11	08.81	0.739	0.945	0.951	0.927	0.945	0.927
11 - 12	06.39	0.800	0.899	0.889	0.958	0.968	0.952
12 - 13	05.86	0.824	0.841	0.846	0.916	0.934	0.926
13 - 14	05.29	0.845	0.815	0.827	0.911	0.832	0.934
14 - 15	04.73	0.848	0.792	0.811	0.826	0.748	0.942
15 - 16	04.21	0.870	0.785	0.811	0.785	0.703	0.952
16 - 17	03.73	0.872	0.765	0.808	0.767	0.698	0.963
17 - 18	03.31	0.906	0.772	0.812	0.774	0.693	0.950
18 - 19	02.92	0.912	0.754	0.810	0.762	0.672	0.880
19 - 20	02.61	0.922	0.750	0.811	0.770	0.674	0.802
20 - 21	02.28	0.920	0.752	0.818	0.783	0.705	0.753
21 - 22	02.02	0.908	0.758	0.817	0.803	0.734	0.741
22 - 23	01.80	0.872	0.755	0.801	0.803	0.732	0.699
23 - 24	01.60	0.839	0.748	0.784	0.774	0.662	0.688
24 -	16.62	0.839	0.748	0.784	0.774	0.662	0.688
Total Normal Emittance		0.740	0.729	0.787	0.861	0.807	0.864